frontiers | Research Topics

Water and ecological system: response, management, and restoration, volume II

Edited by
Chunhui Li, Yujun Yi, Qiang Liu and Celso Santos

Published in
Frontiers in Earth Science
Frontiers in Ecology and Evolution
Frontiers in Environmental Science

ISSN 1664-8714
ISBN 978-2-8325-6389-2
DOI 10.3389/978-2-8325-6389-2

Generative AI statement
Any alternative text (Alt text) provided alongside figures in the articles in this ebook has been generated by Frontiers with the support of artificial intelligence and reasonable efforts have been made to ensure accuracy, including review by the authors wherever possible. If you identify any issues, please contact us.

About Frontiers

Frontiers is more than just an open access publisher of scholarly articles: it is a pioneering approach to the world of academia, radically improving the way scholarly research is managed. The grand vision of Frontiers is a world where all people have an equal opportunity to seek, share and generate knowledge. Frontiers provides immediate and permanent online open access to all its publications, but this alone is not enough to realize our grand goals.

Frontiers journal series

The Frontiers journal series is a multi-tier and interdisciplinary set of open-access, online journals, promising a paradigm shift from the current review, selection and dissemination processes in academic publishing. All Frontiers journals are driven by researchers for researchers; therefore, they constitute a service to the scholarly community. At the same time, the *Frontiers journal series* operates on a revolutionary invention, the tiered publishing system, initially addressing specific communities of scholars, and gradually climbing up to broader public understanding, thus serving the interests of the lay society, too.

Dedication to quality

Each Frontiers article is a landmark of the highest quality, thanks to genuinely collaborative interactions between authors and review editors, who include some of the world's best academicians. Research must be certified by peers before entering a stream of knowledge that may eventually reach the public - and shape society; therefore, Frontiers only applies the most rigorous and unbiased reviews. Frontiers revolutionizes research publishing by freely delivering the most outstanding research, evaluated with no bias from both the academic and social point of view. By applying the most advanced information technologies, Frontiers is catapulting scholarly publishing into a new generation.

What are Frontiers Research Topics?

Frontiers Research Topics are very popular trademarks of the *Frontiers journals series*: they are collections of at least ten articles, all centered on a particular subject. With their unique mix of varied contributions from Original Research to Review Articles, Frontiers Research Topics unify the most influential researchers, the latest key findings and historical advances in a hot research area.

Find out more on how to host your own Frontiers Research Topic or contribute to one as an author by contacting the Frontiers editorial office: frontiersin.org/about/contact

Water and ecological system: response, management, and restoration, volume II

Topic editors

Chunhui Li — Beijing Normal University, China
Yujun Yi — Beijing Normal University, China
Qiang Liu — Beijing Normal University, China
Celso Santos — Federal University of Paraíba, Brazil

Citation

Li, C., Yi, Y., Liu, Q., Santos, C., eds. (2025). *Water and ecological system: response, management, and restoration, volume II*. Lausanne: Frontiers Media SA.
doi: 10.3389/978-2-8325-6389-2

This work is supported by the National Key Research and Development Program of China (2022YFC3202001) and the Joint Funds of the National Natural Science Foundation of China (Grant No. U2243236).

Table of contents

frontiers | Frontiers in Earth Science

TYPE Editorial
PUBLISHED 15 May 2025
DOI 10.3389/feart.2025.1613976

OPEN ACCESS

EDITED AND REVIEWED BY
Wouter Buytaert,
Imperial College London, United Kingdom

*CORRESPONDENCE
Chunhui Li,
chunhuili@bnu.edu.cn

RECEIVED 18 April 2025
ACCEPTED 02 May 2025
PUBLISHED 15 May 2025

CITATION
Li C, Yi Y, Liu Q and Santos CAG (2025) Editorial: Water and ecological systems: responses, management, and restoration, volume II.
Front. Earth Sci. 13:1613976.
doi: 10.3389/feart.2025.1613976

Editorial: Water and ecological systems: responses, management, and restoration, volume II

Chunhui Li[1,2]*, Yujun Yi[1], Qiang Liu[1] and Celso Augusto Guimarães Santos[3]

[1]Key Lab of Water and Sediment Science of Ministry of Education, School of Environment, Beijing Normal University, Beijing, China, [2]State Key Laboratory of Wetland Conservation and Restoration, School of Environment, Beijing Normal University, Beijing, China, [3]Department of Civil and Environmental Engineering, Federal University of Paraíba, João Pessoa, Brazil

KEYWORDS

climate change, ecological effects, human activities, hydrological effects, water resources management

Editorial on the Research Topic
Water and ecological systems: responses, management, and restoration, volume II

1 Introduction

Climate change and the intensification of human activities can induce unprecedented alterations in global hydrological and ecological systems. These disruptions manifest in altered river flows, degraded water quality, biodiversity loss, and compromised ecosystem services. In a warming world, ecological systems have different hydrological responses to changes in climate and human activities and have different water demands in different basins or regions. However, the hydrological and ecological system response remains uncertain. Water resources management and ecological restoration in a changing world need to elucidate its hydrological and ecological response and then provide a suitable way to adapt to global change. Understanding the interactions between water cycles and ecological processes is critical for devising adaptive management strategies that reconcile socioeconomic development with environmental sustainability.

This Research Topic "Water and Ecological System: Response, Management, and Restoration-Volume II" aims to collect and present the latest research developments in hydrological and ecological response in different basins or regions and its implication for water resources management and ecological restoration. Articles published in this Research Topic would shed light on divergent evidence in hydrological and ecological response, explain it with new and deeper insight, and interpret its implication for ecological water demand, water resources management and planning, and ecological restoration. These articles are expected to benefit communities, basins, and government agencies in water and ecosystem management that deal with hydrological and ecological responses in a changing world.

This Research Topic collects 14 manuscripts that explore these interactions across varied geographic and climatic contexts. From the cascade reservoirs of the Yellow River to the coal mining regions of Huainan and the Karst landscapes of Guizhou, the articles investigate hydrological responses to environmental stressors, evaluate ecosystem health, and propose frameworks for r This synthesis consolidates their findings, identifies cross-cutting themes, and outlines future research priorities.

2 Main researches and contributions

2.1 Hydrological responses to climate change and human activities

Climate change including global warming and other related Research Topic profoundly affects hydrological processes such as precipitation and evaporation. Li et al. attribute streamflow reductions in the Daqing River Basin in the North China Plain, to a combination of climate change (35% contribution) and human activities (65%), notably afforestation and water conservancy projects. Hydrological simulations and elasticity coefficient analyses highlight the vulnerability of semi-arid regions to compounding stressors, urging adaptive strategies to mitigate water scarcity.

Human activity and climate change have significantly modified the hydrological processes of groundwater. In coal mining areas, dewatering operations have become more influential than climate change, making human activity the primary factor impacting groundwater systems. Zhou et al. investigate groundwater level fluctuations in the Pansan Coal Mine in Huainan, China, demonstrating that El Niño-Southern Oscillation (ENSO) signals persist despite over-exploitation. Wavelet analysis reveals interannual resonance between groundwater levels and precipitation, underscoring the dual pressures of climate variability and mining. The study highlights the need to integrate climate teleconnections into groundwater management, particularly in regions reliant on fossil fuel extraction. Quaternary aquifers showed 80 m declines in water tables, underscoring the need for managed aquifer recharge.

Cascade hydropower development significantly alters the structure and function of river ecosystems. Phytoplankton, as primary producers, are highly sensitive to environmental changes, and their diversity and community structure reflect the state of the water environment. Luo et al. examine the role of hydraulic residence time (HRT) in shaping phytoplankton communities in the Upper Yellow River cascade reservoirs. Their study reveals that HRT positively correlates with phytoplankton abundance and diversity, with deterministic processes (e.g., water temperature, nutrient availability) dominating community assembly. Annual regulation reservoirs (e.g., Liujiaxia) exhibited 30% higher species richness than runoff-dominated systems. Annual regulation hydropower stations, characterized by longer HRT, support higher species richness compared to runoff stations. These findings emphasize HRT as a critical factor in reservoir management to balance hydropower generation and aquatic ecosystem health. However, prolonged HRT amplified cyanobacterial dominance, raising concerns about eutrophication risks.

Rivers are critical to ecological and societal sustainability, yet human activities like urbanization, industrialization, and agricultural runoff increasingly threaten their ecological health. Bu et al. apply set pair analysis to assess Dalian's rivers, identifying S12 and S15 as healthy (Grade II) due to restored connectivity. In contrast, S7 (near a steel mill) ranked as severely polluted (Grade V), with macroinvertebrate assemblages dominated by pollution-tolerant Chironomidae.

2.2 Water resources, ecological system and environmental carrying capacity assessment

The agricultural water footprint (WF) is essential for understanding environmental impacts and managing water resources, especially in waterscarce regions. Wei et al. develop an integrated framework to assess agricultural water footprints (WF) in Beijing, combining blue, green, and grey water metrics with reliability-resilience-vulnerability (RRV) indices. WF were analysed using STIRPAT model. The overall WF decreased from 22.0×10^8 m^3 to 3.9×10^7 m^3, showing a significant downward trend from 1978 to 2018, and 25 out of 35 years exceed the water stress thresholds (WSI >1), They were driven by improved irrigation efficiency and crop restructuring. However, water stress indices (WSI >1) persist, underscoring the need for policies that enhance water-use efficiency and reduce nitrogen pollution.

Evaluating resource and environmental carrying capacity (RECC) within the framework of ecological civilization is essential for reconciling development with ecological preservation and optimizing land-use patterns. Yang et al. evaluate resource and environmental carrying capacity (RECC) in Guizhou's Karst regions using an obstacle degree model and Pearson's correlation analysis. They find significant medium-to-high positive correlations: resource carrying capacity with environmental capacity (0.61) and overall capacity (0.74). The environmental capacity correlates with the overall capacity (0.80). Conversely, the socioeconomic carrying capacity shows no significant correlations with the resource carrying capacity (−0.21), environmental capacity (−0.32), or overall capacity (0.23). These results indicate that resource and environmental capacities have a significantly greater influence on the overall carrying capacity than socioeconomic indicators. They identify delayed socioeconomic development and inadequate infrastructure as key constraints, advocating for industrial modernization and market-driven resource allocation to enhance RECC.

For urban river ecological health, Bu et al. and Zhang et al. advance bioassessment protocols for urban and undammed rivers. Bu's entropy-weighted set pair analysis identifies pH, dissolved oxygen, and ammonium nitrogen as critical determinants of river health in Dalian, while Zhang's multimetric index (MMI) for the Zaogang River integrates hydrologic, chemical, and biological indicators to guide restoration.

The Chishui River, as an important tributary of the upper Yangtze River without dams, the macroinvertebrate community structure and habitat suitability conditions holds significant implications for water ecological conservation and restoration. Li et al. identify taxa of *Ephemeroptera, Plecoptera*, and *Trichoptera* as

key bio-indicators in the pristine Chishui River. ANOSIM analysis revealed seasonal shifts in community composition, with dry-season dominance by *Baetis* and *Heptagenia*. Habitat suitability modeling prioritized riffle habitats with moderate flow velocities (0.3–0.6 m/s) and gravel substrates (D50 = 100–300 mm).

Liu et al. quantify the gross ecosystem product (GEP) of Shandong Mata Lake National Wetland Park, valuing its regulatory and cultural services at CNY 74.8 million annually. Regulation services (78.5% of total) dominated, with water purification (CNY 480,000) and flood regulation (CNY 220,000) as primary contributors. Scenario modeling suggests carbon sequestration could increase by 25% under afforestation.

2.3 Innovations in monitoring and modeling

In order to explore the relationship between groundwater levels and hydrometeorological factors in Fengnan District. Zhang et al. employ a PCA-CIWOABP neural network to predict groundwater levels in Fengnan District, achieving mean absolute errors (MAE) of 0.19–0.23. Their model, which integrates hydrological and meteorological data, demonstrates the potential of machine learning for real-time groundwater management in the North China Plain.

Large-scale afforestation projects on the Loess Plateau have resulted in significant vegetation greening, contributing to ecosystem restoration and enhanced soil conservation. Tan et al. identify the drivers of evapotranspiration (ET) changes, attributing long-term increases (80%) to vegetation greening and interannual variability to climate fluctuations. Their findings caution against afforestation in arid zones, where ET amplification exacerbates water deficits.

3 Other cross-cutting insights

Multiple studies highlight the growing frequency of droughts and floods under climate change. For instance, Li et al. note a 1.09–1.32 mm/year decline in precipitation across the Daqing River Basin, while Tan et al. report rising temperatures as a key driver of increasing ET on the Loess Plateau. These trends necessitate adaptive infrastructure, such as sponge cities and managed aquifer recharge, to buffer against hydrological extremes.

Anthropogenic pressures—overfishing, mining, urbanization—emerge as primary drivers of ecosystem decline. Du et al. document the recovery of fish populations in the Yangtze River following a 10-year fishing ban, noting a 91% increase in average body length for nine species (e.g., *Hemiculter leucisculus*). However, piscivores like *Pseudobagrus crassilabris* declined due to trophic cascades. Spatial heterogeneity was evident: Huangshi showed improved Margalef richness (from 4.55 to 4.78), while Jingzhou stagnated. yet stress that full biodiversity restoration requires decades. Similarly, Zhou et al. link groundwater depletion in Huainan to coal mining, advocating for stricter regulations on dewatering.

The studies collectively advocate for holistic approaches that bridge hydrology, ecology, and socioeconomics. Wei et al. and Yang et al. demonstrate how water footprint analysis and RECC evaluations can align agricultural practices and land-use planning with ecological limits. Meanwhile, Liu et al. and Bu et al. showcase the policy relevance of ecosystem service valuation and bioassessment.

4 Challenges and future directions

4.1 Data gaps and methodological limitations

Several studies identify limitations in data resolution and model accuracy. For example, Zhang et al. note the scarcity of long-term groundwater monitoring data, while Li et al. emphasize the need for high-temporal-resolution biodiversity surveys. Future research should leverage emerging technologies—remote sensing, IoT sensors, eDNA—to enhance data Research Topic.

4.2 Scaling local findings to regional policies

While case studies provide valuable insights, scaling local solutions (e.g., the Chishui River's undammed management) to regional or national levels remains challenging (Li et al.). Participatory modeling and decision-support systems could facilitate knowledge transfer, as demonstrated by Cui et al. in optimizing crop structures for water-energy-food nexus sustainability.

4.3 Balancing ecological and socioeconomic goals

The tension between conservation and development persists, particularly in rapidly urbanizing regions. Zhang et al. and Li et al. propose "happy river" frameworks that integrate ecological health with human wellbeing metrics (e.g., flood safety, cultural value). Such frameworks require robust stakeholder engagement and adaptive governance.

The studies in this Research Topic collectively advance our understanding of water-ecosystem interactions in a changing climate. Moving forward, interdisciplinary collaboration, technological innovation, and adaptive governance will be essential to navigate the complexities of water and ecosystem management. This synthesis underscores the urgency of translating scientific insights into actionable policies to safeguard water resources and ecological resilience for future generations.

Author contributions

CL: Writing – review and editing, Writing – original draft. YY: Writing – review and editing, Writing – original draft. QL: Writing – review and editing, Writing – original draft. CS: Writing – original draft, Writing – review and editing.

Funding

The author(s) declare that financial support was received for the research and/or publication of this article. This work is supported by the National Key Research and Development Program of China (2022YFC3202001) and the Joint Funds of the National Natural Science Foundation of China (Grant No. U2243236).

Acknowledgments

The editors thank all contributing authors, reviewers, and the Frontiers team for their support in producing this Research Topic.

Conflict of interest

The authors declare that the research was conducted in the absence of any commercial or financial relationships that could be construed as a potential conflict of interest.

The author(s) declared that they were an editorial board member of Frontiers, at the time of submission. This had no impact on the peer review process and the final decision.

Generative AI statement

The author(s) declare that no Generative AI was used in the creation of this manuscript.

Publisher's note

All claims expressed in this article are solely those of the authors and do not necessarily represent those of their affiliated organizations, or those of the publisher, the editors and the reviewers. Any product that may be evaluated in this article, or claim that may be made by its manufacturer, is not guaranteed or endorsed by the publisher.

frontiers | Frontiers in Ecology and Evolution

TYPE Original Research
PUBLISHED 10 October 2024
DOI 10.3389/fevo.2024.1478024

OPEN ACCESS

EDITED BY
Caihong Tang,
North China Electric Power University, China

REVIEWED BY
Peng Hu,
China Institute of Water Resources and Hydropower Research, China
Yuan Zhang,
Guangdong University of Technology, China

*CORRESPONDENCE
Chunhui Li
Chunhuili@bnu.edu.cn

RECEIVED 09 August 2024
ACCEPTED 20 September 2024
PUBLISHED 10 October 2024

CITATION
Zhang J, Xiang J, Ma Q, Li C and Xu X (2024) Water ecological health evaluation of urban river: a case study of Zaogang River, China. *Front. Ecol. Evol.* 12:1478024. doi: 10.3389/fevo.2024.1478024

Water ecological health evaluation of urban river: a case study of Zaogang River, China

Jiaqi Zhang[1], Jiaqi Xiang[1], Qiwen Ma[1], Chunhui Li[1]* and Xiangen Xu[2]

[1]Key Lab of Water and Sediment Science of Ministry of Education, School of Environment, Beijing Normal University, Beijing, China, [2]Changzhou Academy of Environmental Science, Changzhou, China

The ecological health of urban rivers serves as a critical indicator of the overall health of urban ecosystems. The water ecological health status of the Zaogang River in Changzhou City was evaluated; nine sections of the river and the Old Zaogang River were sampled, and an assessment system with 8 indexes for hydrologic integrity, physical structural integrity, chemical integrity, and biological integrity was set up. A comprehensive scoring system, based on index scores and their corresponding weights, was employed to evaluate the ecological health of the Zaogang River. The assessment revealed that most sections of the Zaogang River were in a healthy state, classified as second-class level. In contrast, the Old Zaogang River exhibited sub-health conditions in one section, indicating a need for comprehensive restoration measures. Water ecological health evaluation system constructed in this study is relatively complete and comprehensive, and provides a good example for the rapid evaluation of urban rivers. Additionally, the findings of the study offer guidance for managing rivers in Changzhou city.

KEYWORDS

water ecological health, water ecological health status, assessment indicators, biological integrity, Zaogang River

1 Introduction

In recent years, with the accelerated progress of industrialization and urbanization, a large amount of domestic sewage and industrial wastewater has been discharged into rivers, far exceeding the self-purification capacity of the rivers themselves. Rivers and lakes are increasingly facing ecological challenges. Preserving the health and vitality of rivers and lakes, while ensuring the sustainable use of water resources, has become a critical and urgent societal task.

The evaluation of water ecological health serves as a crucial basis for the scientific formulation of water resource allocation plans and river protection measures, providing a scientific basis for the rational utilization of water resources and ecological protection and

restoration in the river basin (Stoddard et al., 2006; Poikane et al., 2020; Brosed et al., 2022). Two primary methodologies currently dominate the study of water ecological health: the comprehensive index method and predictive modeling. The comprehensive index method employs a mathematical comprehensive assessment model and a set of biological, chemical, and physical indicators to determine the overall status of water ecological health. Common methods include the Index of Stream Condition (ISC) (European Commission, 2000), Riparian, Channel, and Environmental Inventory (RCE), and Rapid Bioassessment Protocols (RBPs) (Tang et al., 2002). Predictive modeling evaluates the status of water ecological health by comparing actual river species with the species that should exist without human interference. Common methods include the Index of Biological Integrity (IBI) (Wright et al., 1984) proposed by Karr and the River Invertebrate Prediction and Classification System (RIVPACS) (Thornbrugh et al., 2018) proposed by Wright. The rapid development of monitoring technology has facilitated the measurement of river biological characteristics, structural morphology, water quality, and quantity. The comprehensive evaluation index method MMI, developed in the 1990s, enables a holistic assessment of water ecosystems (Prudente et al., 2018). MMI has a wide range of applications and can be used in many types of water bodies, such as rivers, lakes, and reservoir areas (Zhou et al., 2019; Li et al., 2021). In recent years, the evaluation system for urban river health has been gradually improved and developed (Martinez-Haro et al., 2015; Díaz et al., 2019). While focusing on aquatic organisms, abiotic elements have been incorporated into the evaluation system, making the evaluation system more perfect and comprehensive. Deng et al. (2014) built an urban water ecological health evaluation index system containing 24 indicators from three aspects, including natural ecology, social economy, and landscape environment, and established a fuzzy comprehensive evaluation model based on the analytic hierarchy process. Su et al. (2019) developed a river ecosystem health evaluation index system focusing on integrity, stability, and sustainability to explore the impact of water transfer projects on the Yangtze River ecosystems' health. Under the guidance of the concept of resilience, Zhang et al. (2022) built an urban water ecological health evaluation index system based on the pressure-state-response model (PSR), evaluating and predicting water ecological health levels and development trends using combined weighting methods and matter-element extension models. Becker et al. (2022) used the River Ecosystem Service Index (RESI) to evaluate the service function of the ecosystem and to guide the restoration of the ecological service function of rivers to cities. Meanwhile, water ecological evaluation is to describe the physical structure, chemical state, and biological state of the water ecological system, thereby evaluating the health status of the system, identifying critical issues, and providing a basis for evaluating the effectiveness of ecological restoration measures and adjusting policies and regulations (Zhang et al., 2023). In this study, a rapid evaluation system for water ecological health was established by combining the predictive modeling method and comprehensive index method, integrating the advantages of both methods and aiming to identify the key issues of urban rivers in Changzhou, thereby providing guidance for relevant policies for water ecological health protection.

Changzhou, located in the Taihu Lake basin, boasts a well-developed plain river network. Changzhou has attached great importance to water ecological health in recent years. In 2014, the city established the water ecological health evaluation index system by referencing the Indicators, Standards, and Methods of River Health Assessment and the assessment report of important rivers in Jiangsu Province, and combining the specific conditions of the city. Based on the various characteristics and functions of rivers, a single-factor evaluation of water ecological health status is carried out using 14 indicators, including physical, chemical, ecological characteristics, and social service functions. On this basis, the natural and social attributes of rivers are further evaluated, and the health status of rivers is comprehensively evaluated. In 2019, Changzhou renamed "River and Lake Health Assessment" to "River and Lake Ecological Status Assessment," aligning with the local standard of Jiangsu Province, Ecological Assessment of River and Lake (Water Resources Department of Jiangsu Province, 2019). Based on the hydrological and ecological characteristics of the city rivers, the "phytoplankton" index in aquatic organisms has been adjusted to "zooplankton and benthic animals," and the original two indicators of "aquatic organisms" have been increased to three, while the total weight coefficient of "aquatic organisms" remains unchanged. It includes 13 indicators from 5 aspects: water security, aquatic organisms, aquatic habitat, water space, and public satisfaction (Ji et al., 2020).

As a multifunctional river in Changzhou, China, the Zaogang River plays a vital role in water transfer to the Yangtze River. Therefore, evaluating its water ecological health status is of utmost importance. In this study, the assessment of the water's ecological health status is conducted to establish a scientific understanding of the river's ecological condition and provide a basis for effective river management.

2 The research area and data

2.1 Overview of the research area

Changzhou is located in the northwest of the Taihu Lake Basin, bordering the Yangtze River in the north, Taihu Lake in the south, and the Jinli hills and mountains in the west. Reservoirs and dams are dotted all over the place, with plains and polders situated between the rivers in the north and the lakes in the south. The river system is highly developed, forming a complete network. Renowned as the "Jiangnan water town," Changzhou's Zaogang River is one of its significant backbone rivers, connecting with the Yangtze River in the north and the Guan River in the south, ultimately leading to the Dawanbang River. Stretching 20.2 kilometers in length, the Zaogang River serves multiple functions, including flood control, drainage, irrigation, water supply, ecological balance, and navigation in the west of the Wuchengxi region. There are many tributaries of the river, and the dredging project was completed in 1996. The upstream, in Yutang town, has been curved and straightened, and the downstream has been

diverted into two streams in Huzhuang, north of Longhutang. One stream flows southwest along the river through Changzhou High-tech Zone into the Guan River, while the other flows southeast along the east branch of the Old Zaogang River through the Yonghui River to the Beitang River, and ultimately reaches the Grand Canal through the tributaries such as the Hengtang River, Dingtang Port, and Sanshan Port. Some parts of the river flow into Jiangyin (Zhong, 2013). The locations of the Zaogang River and the Old Zaogang River are shown in Figure 1.

2.2 Data source and processing

River macrobenthos, ecological water level satisfaction degree, and phytoplankton double index of biotic integrity use the data from Changzhou Academy of Environmental Science. The data on vegetation cover, artificial disturbance of the riparian zone, and river connectivity are obtained through the interpretation of Orvital satellite images. More information can be found at https://www.ovital.com.

3 Methods

3.1 Set of sampling sites

The sampling and investigation of the water quality was conducted on September 23 and 24, 2023, for detailed ecological and environmental analysis of the Zaogang River in Xinbei District, Zhonglou District, and Tianyu District, Changzhou City, Jiangsu Province, China. As a key water resource in this region, the Zaogang River system is comprised of two main sections: the Zaogang River and the Old Zaogang River. The core objective of this survey is to obtain the latest and accurate data to ensure the typicality and timeliness of the analysis results. Therefore, in order to avoid that the local conventional monitoring points usually selected cannot represent the ecological status of the whole river, the local conventional monitoring points were avoided in the selection of sampling points, and multiple sampling sites were set up along the river, hoping to fully reflect the ecological status of the Zaogang River.

Sampling sites were strategically selected at critical points along the river, including its headwaters, midsection, and terminus, as well as at the confluences of tributaries and key dam locations. The sampling sites extend from the outer section of the Zaogang River Junction to the section after the intersection of the Dawanbang River and the Sanjing River. The Zaogang River is a smaller urban river, but multiple sampling sites were still set up, with the points spaced at an appropriate distance and having a certain degree of representativeness. The river length represented by the sampling sites is considered to be able to cover both the Zaogang River and the Old Zaogang River, so it is believed that the sampling sites can represent the ecological condition of the river. To minimize external interference factors, careful observations are carried out at least 500 meters upstream of each sampling site to avoid areas that may affect the physical and chemical properties of the river, such as industrial sewage outfalls, livestock manure accumulation points, and household garbage dumping areas. Taking into account the water quality, water quantity, and coastal discharge status of the Zaogang River, 9 sampling sites are selected (Figure 1), among which 6 are along the Zaogang River and 3 along the Old Zaogang River. The latitude and longitude coordinates and the basic description of each sampling site are shown in Table 1. The distance between S1 and S2 is relatively short; however, S1 is situated outside the Zaogang River junction while S2 lies within it. Analyzing the ecological conditions of S1 and S2 can provide insights into how the junction influences the river's ecological status to some extent. Meanwhile, S3 is positioned at the confluence of the Zaogang River and the Old Zaogang River, serving as a valuable reference for comparing

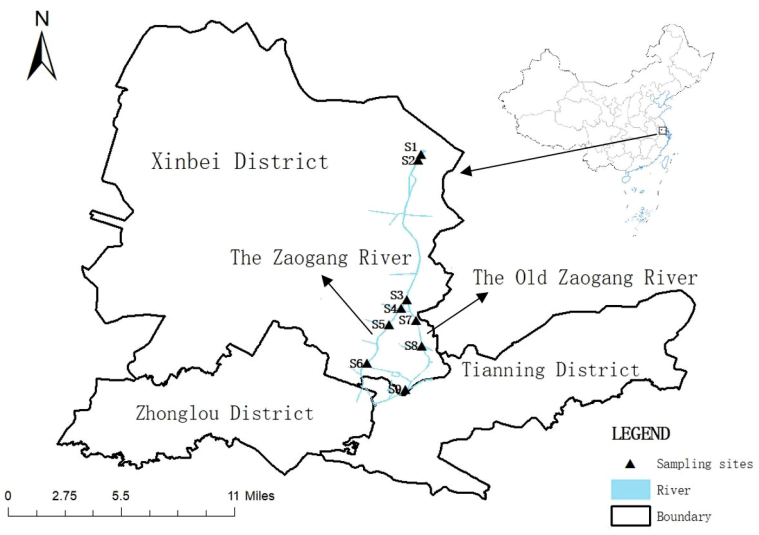

FIGURE 1
Sampling sites of the Zaogang River and the Old Zaogang River in Changzhou city.

TABLE 1 The basic situation of the sampling sites of the Zaogang River and the Old Zaogang River.

Sampling site	Name	Latitude and longitude		Basic situation
S1	Outer section of Zaogang River junction	E 119°59′33″	N 31°57′55″	Over the damn, and the river is turbid
S2	Inner section of Zaogang River junction	E 119°59′22″	N 31°57′43″	Inside the damn, the river is turbid with a small number of floating objects
S3	Honghe Road Bridge section of Zaogang River	E 119°58′59″	N 31°51′55″	The river is turbid, there are a few submerged plants in the water, and the vegetation in the riparian zone is rich
S4	Taojiawan Bridge section of Zaogang River	E 119°58′38”	N 31°51′27″	The river has a clear yellow-green dividing line, with a large number of submerged plants and some floating plants on the green side, and the vegetation in the riparian zone is rich
S5	Zaogang River ecological channel section	E 119°58′10”	N 31°50′50″	The river is a little green and the vegetation in the riparian zone is rich
S6	Section of the confluence of the Dawanbang River and the Sanjing River	E 119°57′11”	N 31°49′3″	The river is yellowish-green with a large number of floating and submerged plants
S7	Section of the confluence of Beitang River and Old Zaogang River	E 119°58′51”	N 31°48′1″	A few floating objects and a few floating plants in the river
S8	Xinxiaotang bridge section of Old Zaogang River	E 119°59′33”	N 31°50′1″	Factories along the riparian zone, and there are a few floating objects, a few floating plants, and a few submerged plants in the river
S9	Panlong Road section of Old Zaogang River	E 119°59′15”	N 31°51′8″	The river is clear and the riparian zone is sparsely vegetated

ecological conditions between these two rivers. The remaining sampling sites are located where both rivers converge, making them representative and significant.

Stainless steel water quality samplers are used for sampling. For sites S1, S2, S3, S7, and S8, the sampler is dropped vertically from the bridge, with sampling locations primarily in the middle of the river. The sampling locations for the remaining sites are 1-2 meters away from the riparian zone, and the depth of sampling is approximately 1 meter below the river's surface.

3.2 Sample analysis method

The indicators of water quality investigation are comprised entirely of indoor detection indicators, including COD (mg/L), NH3-N (mg/L), TP (mg/L), TN (mg/L), Pb (mg/L), and Electrical conductivity (μs/cm). The GW-2000E portable multi-parameter water quality tester is used for determination, while the DIS-1D portable digester facilitates the digestion process.

3.3 Evaluation methods

3.3.1 Evaluation principles

Based on the acquired data, an evaluation system is constructed to evaluate the water ecological health status of the Zaogang River, focusing on four criteria levels: hydrologic integrity, physical structural integrity, chemical integrity, and biological integrity. Considering the impact of dams on the Zaogang River, assessing its flow holds little significance. Dams have a relatively important impact on river connectivity to a certain extent, thus the indicators of hydrological integrity are selected as the ecological water level satisfaction degree and river connectivity. The Zaogang River is a typical urban river greatly affected by human activities, making it crucial to evaluate vegetation cover and artificial disturbance of the riparian zone. Benthic animals and phytoplankton are sensitive to environmental changes and can indicate the cleanliness and ecological status of water bodies to a certain extent. Fish, at the top of the nutrient level in the water ecosystem, play a vital role in representing the water environment's stability. Therefore, indicators of biological integrity such as Hilsenhoff index, phytoplankton double index, and fish retention index were selected for assessment purposes. The determination of index weights is based on the "Technical guidelines for river and lake health assessment" (Ministry of Water Resources of the People's Republic of China, 2020). Table 2 presents the specific indicators along with their respective weights.

3.3.2 Ecological water level satisfaction degree assessment methods

Urban rivers have varying degrees of ecological functions. The essence of river ecological levels and ecological discharge is that both water quantity and quality must be simultaneously satisfied to maintain the normal development of diverse ecological functions. However, because urban rivers are controlled by sluices and dams, they affect river connectivity and, consequently, river discharge. Therefore, the index of river ecological discharge satisfaction is used instead of the river ecological water level satisfaction. The scoring criteria are shown in Table 3.

TABLE 2 Evaluation index system, including 8 indices.

Target level	Criteria level	Indicator level	Weight of indicators
Water ecological health	Hydrologic integrity	Ecological water level satisfaction degree	0.2
	Physical structural integrity	River connectivity	0.1
		Vegetation cover of the riparian zone	0.1
		Artificial disturbance of the riparian zone	0.1
	Chemical integrity	Water quality	0.2
	Biological integrity	Macrobenthos Hilsenhoff index	0.1
		Phytoplankton double index of biotic integrity	0.1
		Fish retention index	0.1

3.3.3 River connectivity assessment methods

River connectivity is an important parameter to measure the degree of correlation among each part of the river (Amoros and Roux, 1988), and maintaining connectivity is of great significance and thus crucial for river integrity (Wang et al., 2019). As the Zaogang River is a typical urban river, its connectivity is vulnerable to human interference. Therefore, investigating the number of artificial dams and other blocking facilities along the river is crucially important for evaluating its hydrological integrity.:

$$A = \frac{NB}{L} \quad (1)$$

where A is the connectivity index of the river (pieces/10km), N_B is the number of facilities affecting river connectivity (pieces), and L is the length of the river (km).

The score is assigned according to A, and Table 4 presents the detailed scoring criteria used in the assessment.

TABLE 3 Ecological water level satisfaction degree scoring criteria.

Scoring criteria	Score	Grade
The average water level is not lower than the lowest ecological water level for 3 consecutive days	[80,100]	Excellent
The average water level was lower than the minimum ecological water level for 3 consecutive days, but the average water level was not lower than the minimum ecological water level for 7 consecutive days	[60,80)	Good
The average water level was lower than the minimum ecological water level for 7 consecutive days, but the average water level was not lower than the minimum ecological water level for 14 consecutive days	[40,60)	Average
The average water level was lower than the minimum ecological water level for 14 consecutive days, but the average water level was not lower than the minimum ecological water level for 30 consecutive days	[20,40)	Fair
The average water level was lower than the minimum ecological water level for 3 consecutive days, but the average water level was not lower than the minimum ecological water level for 60 consecutive days	(0,20)	Poor
The average water level is lower than the lowest ecological water level for 60 consecutive days	0	

3.3.4 Vegetation cover of the riparian zone assessment methods

According to the "Guidelines for River and Lake Health Assessment" (Department of River and Lake Management, 2020), two 10m×10m quadrates on both sides of the riparian zone of each site are selected to calculate the vegetation cover using the following calculation formula:

$$PC_r = \frac{A_{ci}}{A_{ai}} \times 100 \quad (2)$$

where PC_r is the vegetation cover of the riparian zone, A_{ci} is the vegetation coverage area (km^2) of the riparian zone i, and A_{ai} is the area (km^2) of the riparian zone i. Scoring is performed according to PC_r, and the scoring criteria and the description are shown in Table 5.

3.3.5 Artificial disturbance of the riparian zone assessment methods

Located in the main urban area of Changzhou City, the Zaogang River is closely intertwined with urban life and is susceptible to disturbance by human activities. Therefore, evaluating the degree of artificial disturbance is essential. Utilizing remote sensing maps and other tools, we conduct investigations to ascertain the presence of 15 typical human activities within the riparian zone and its adjacent land areas. Following this, the degree of artificial disturbance is assessed. The scoring criteria is based on the "Technical guidelines for river and lake health assessment" (Ministry of Water Resources of the People's Republic of China, 2020). The scoring criteria for this assessment are detailed in Table 6.

3.3.6 Water quality assessment methods

The single-factor evaluation method is employed for each water quality index. Afterward, these indices are synthesized to obtain a comprehensive evaluation of water quality at the sampling site. Measured concentrations of COD, ammonia nitrogen, total phosphorus, total nitrogen, and Pb are rated according to the standard values specified in the "Environmental Quality Standards for Surface Water" (Ministry of Ecology and Environment of the People's Republic of China, 2002). The water quality category of the worst-performing parameter is then taken as representative of the water quality category for each sampling site of the Zaogang River. A comprehensive evaluation of the water quality category is subsequently determined.

Each water quality index for each sampling site undergoes linear interpolation against the scoring threshold to derive the scoring value. The scoring criteria are detailed in Table 7. It is assumed that each

TABLE 4 River connectivity scoring criteria.

River connectivity(%)	>5	(4,5]	(2.5,4]	(1.5,2.5]	(1,1.5]	[0,1]
Score	0	[0,20]	[20,40]	[40,60]	[60,80]	[80,100]

index is of equal importance, so the water quality index for each sampling site is determined by calculating the average of the values.

3.3.7 River macrobenthos assessment methods

Macrobenthos are important components of water ecosystems. They are sensitive to environmental changes and have weaker migration abilities than other aquatic animals. Therefore, compared with fish and plankton, macrobenthos can better represent the level of pollution in the water environment (Riato et al., 2020). The assessment of river macrobenthos is based on data provided by the Changzhou Academy of Environmental Science, with the monitoring section designated as the No. 9 Bridge section. The Hilsenhoff index (HBI) can be briefly explained as a measure of the sensitivity of macrobenthos in rivers to organic pollution. The Hilsenhoff index is used to evaluate the water quality of these sections, leveraging the varying sensitivity or tolerance of different macrobenthos to organic pollution and the abundance of information on different groups. The evaluation formula is as follows:

$$\mathrm{HBI} = \frac{\Sigma_1^n n_i t_i}{N} \tag{3}$$

where n_i is the number of individuals of the I th taxon, N is the total number of sample individuals, and it is the tolerance value (TV) of the I th taxon.

The tolerance values of macrobenthos refer to the "aquatic organism monitoring and evaluation of rivers" (Ministry of Ecology and Environment of the People's Republic of China, 2023). The corresponding score table and description of HBI values are shown in Table 8.

3.3.8 Phytoplankton double index of biotic integrity assessment methods

Phytoplankton is sensitive to changes in environmental factors, and changes in its abundance and community composition can often represent changes in the water environment, especially for relatively static water bodies. The Zaogang River is an urban river, and its flow rate is relatively slow. The community structure of phytoplankton can well represent the quality of the water environment. The monitoring section is the No. 9 Bridge section. Biological indicators are evaluated by the percentage of cyanobacteria density and total phytoplankton density (Zhang et al., 2024). The evaluation formula is as follows:

$$P_{DIBI} = C_{PD} \times 0.7 + C_{CP} \times 0.3 \tag{4}$$

where C_{PD} is the standardized value of total phytoplankton density, C_{CP} is the standardized value of the percentage of cyanobacteria density, and P_{DIBI} is the phytoplankton biodiversity index. The standardization method of the P-DIBI index is shown in Table 9.

TABLE 5 Vegetation cover of the riparian zone scoring criteria.

Vegetation cover of the riparian zone (%)	Description	Score
0-5	Almost no vegetation	0
5-25	Sparse vegetation	25
25-50	Medium-density coverage	50
50-75	High-density coverage	75
>75	Extremely high-density coverage	100

3.3.9 Fish retention index assessment methods

Fish plays a crucial role in the water ecosystem, occupying the top position in the nutrient structure and contributing to its overall stability. Changes in fish species can serve as an indicator of the long-term ecological health of a river. The evaluation of the fish retention index is based on data provided by Changzhou Academy of Environmental Science. Due to the unavailability of historical data for Zaogang River, the Changzhou section of Jing-Hang Grand Canal was selected as a reference point for evaluation (Qin et al., 1988). The Jing-Hang Grand Canal and the Zaogang River are the main urban rivers in Changzhou city, sharing similar characteristics during this period. Therefore, it is considered that Jing-Hang Grand Canal can be used as a reference point for evaluating fish retention index to some extent. The calculation formula is as follows:

$$FOEI = \frac{FO}{FE} \times 100 \tag{5}$$

Where FOEI is fish retention index (%), FO is the number of fish species obtained from the river survey, and FE is the number of fish species in the 1980s.

3.3.10 Comprehensive assessment methods

Based on the corresponding weights and scores of each indicator at each sampling site, a comprehensive score for each site is obtained. The calculation formula is as follows:

$$\mathrm{RHI} = \sum_{i=1}^{n} a_i b_i \tag{6}$$

where RHI is the comprehensive score of each sampling site, as is the I index, and b_i is the score assigned to the I index.

According to the comprehensive scores of each sampling site, the water ecological health status of each sampling site is determined, and the water ecological health assessment classification table is shown in Table 10.

10.3389/fevo.2024.1478024

TABLE 6 Artificial disturbance of the riparian zone scoring criteria.

Human activity	Inside flowage line	Riparian zone (15m)	Riparian zone extending to the land (within 10 m)
Fortified by masonry		-5	
Sand mining	-30	-40	
Construction (building)	-15	-10	-5
Highway (railway)	-5	-10	-5
Landfill or dump of Garbage		-60	-40
Pipeline		-15	-5
Agricultural cultivation		-15	-5
Livestock breeding		-10	-5
Dig a well		-10	-5
Pit		-5	-2
Grave		-10	-5
Storage		-5	-2
Exploitation of underground resources		-10	-5
Archaeological excavation		-10	-5
Fairtrade		-10	-5

4 Results

4.1 Ecological water level satisfaction degree results

According to the "Water Ecological Protection Target Plan of Changzhou City", the lowest ecological water level at the main control section in Changzhou City is 3.44 meters. The average water levels of the Zaogang River, measured at 1.59 meters, 1.54 meters, 1.84 meters, and 1.72 meters on four consecutive days from February 19 to 22, were all below this threshold. Consequently, the Zaogang River received a score of 75 for ecological water level satisfaction, which indicates a good level of ecological water level satisfaction.

TABLE 7 Water quality scoring criteria.

Water quality category	I,II	III	IV	V	Below V
Score	[90, 100]	[75, 90]	[60, 75]	[40, 60]	[0, 40]

TABLE 8 HBI scoring criteria.

HBI	Description	Score
0~3.75	Extremely clean	[90, 100]
3.76~4.25	Very clean	[80, 90]
4.26~5.00	Clean	[70, 80]
5.01~5.07	General clean	[60, 70]
5.76~6.50	Slightly pollute	[40, 60]
6.51~7.25	Pollute	[20, 40]
7.26~10	Serious pollute	[0, 20]

4.2 River connectivity results

Utilizing remote sensing maps, we investigated the artificial facilities, such as dams, along the Zaogang River and the Old Zaogang River. The presence of two dams along the Zaogang River results in a connectivity index of 1.40, reflecting moderate disruption in river continuity. In contrast, there is only one artificial facility along the Old Zaogang River, yielding a higher connectivity index of 2.28, which suggests reduced river connectivity and, by extension, hydrological integrity compared to the Zaogang River. The evaluation and scoring of river connectivity were conducted using linear interpolation, with the detailed results presented in Table 11.

4.3 Vegetation cover of the riparian zone assessment results

The assessment included nine representative sites: the outer section of the Zaogang River junction (S1), the inner section (S2), the Honghe Road Bridge section (S3), the Taojiawan Bridge section (S4), the ecological channel section (S5), the section at the

TABLE 9 Standardization method of P-DIBI index.

Total phytoplankton density/(10^4 cells·L^{-1})	Percentage of cyanobacteria density	Score
≤20	≤20%	100
50	30%	90
200	40%	80
400	50%	70
600	60%	60
800	70%	50
1000	75%	40
3000	80%	30
4500	85%	20
5000	90%	10
≥5500	≥95%	0

TABLE 10 Water ecological health assessment classification table.

Classification	Status	Score
First-class river	Very healthy	80≤RHI ≤ 100
Second-class river	Healthy	60≤RHI ≤ 80
Third-class river	Sub-healthy	40≤RHI ≤ 60
Fourth-class river	Ill-healthy	20≤RHI ≤ 40
Fifth-class river	Sick	RHI<20

confluence of the Dawanbang and Sanjing Rivers (S6), and three sections along the Old Zaogang River, namely the section at the confluence with the Beitang River (S7), the Xinxiaotang Bridge section (S8), and the Panlong Road section (S9). These last three sites are part of the Old Zaogang River. The evaluation results for all sites are detailed in Table 12.

The riparian zone along the Zaogang River was characterized by high-density vegetation cover, with the Taojiawan Bridge section (S4) and the ecological channel section (S5) showing an exceptionally high level of 100% coverage. In contrast, the Old Zaogang River has significantly lower vegetation cover. The Xinxiaotang Bridge section (S8) and the Panlong Road section (S9) are notably below the 50% mark, indicating medium-density coverage. The vegetation cover at the confluence of the Beitang River and the Old Zaogang River (S7) slightly exceeds 50% and is considered high-density coverage. The overall vegetation cover of the riparian zone of the Old Zaogang River requires improvement.

4.4 Artificial disturbance of the riparian zone assessment results

Using remote sensing maps, we investigated the presence of various artificial disturbance activities in the riparian zone of the Zaogang River. Additionally, the degree of artificial disturbance for both the Zaogang River and the Old Zaogang River was evaluated. The findings of this assessment are detailed in Table 13.

The degree of artificial disturbance along the Zaogang River and the Old Zaogang River is as follows: all sections of the Zaogang River (S1, S2, S3, S4, S5, S6) feature masonry fortifications. Constructions extend into the riparian zone and land areas, particularly at the inner section of the Zaogang River junction (S2). The Honghe Road Bridge section (S3) includes coastal constructions and pipelines within the riparian zone. Along the ecological channel section of the Zaogang River (S5), constructions are present, and highways or railways are observed. Similarly, the riparian zone at the confluence of the Dawanbang River and the Sanjing River (S6) features highways or railways. In summary, the outer section at the Zaogang River junction (S1) and the Taojiawan Bridge section (S4) exhibit low levels of artificial disturbance. However, the Honghe Road Bridge section (S3) and the ecological channel section (S5) show high degrees of artificial disturbance, with typical human activities such as masonry fortifications, construction, and highways or railways in the riparian zone and adjacent land.

The Old Zaogang River exhibits a higher degree of artificial disturbance across all sections (S7, S8, S9), characterized by masonry fortifications and the presence of highways or railways. Notably, the riparian zone of the Xinxiaotang Bridge section (S8) also features coastal structures and pipelines. Overall, the Old Zaogang River, particularly section S8, experiences significant human activity interference, including masonry fortifications, construction, highways, railways, and pipelines.

Artificial disturbances are present to varying extents in both the Zaogang River and the Old Zaogang River, with each section showing different degrees of disturbance. Comparatively, the Zaogang River fares better in terms of lower disturbance levels. Nonetheless, enhanced management and protection measures are essential to mitigate the negative impacts on the riparian zones and the adjacent lands of both rivers.

4.5 Water quality assessment results

According to the results of water quality experiments, both the Zaogang River and the Old Zaogang River primarily fall within Class V, signifying poor water quality. The primary pollution factors include total nitrogen, lead (Pb), and chemical oxygen demand (COD). The COD levels across the sampling sites range from Class II to Class V, revealing notable variability. Among these, the more significant pollutants are COD and Pb. This may be attributed to the fact that the Zaogang River and the Old Zaogang River are typical urban rivers with a high level of human activity in their vicinity. Additionally, there are several factories and enterprises located nearby, leading to higher concentrations of COD and Pb in both the Zaogang River and the Old Zaogang River. The detailed assessment results, including these findings, are presented in Table 14.

Each water quality index is analyzed separately, with the results reflecting the changes in ammonia nitrogen concentration along each section of the Zaogang River. Notably, with the exception of the section of the confluence of Beitang River and Old Zaogang River (S7), which has a high ammonia nitrogen concentration of

TABLE 11 Results of river connectivity, showing that the situation of the Old Zaogang River is worse.

River	The length of the evaluated river(km)	The number of facilities (Pieces)	River connectivity (Pieces/10km)	Score
Zaogang River	14.33	2	1.40	64
Old Zaogang River	4.39	1	2.28	44.4

TABLE 12 Results of vegetation cover, indicating the vegetation cover performs great especially in the Zaogang River.

Sampling site	Name	Vegetation cover (%)	Score	Description
S1	Outer section of Zaogang River junction	57.5	75	High-density coverage
S2	Inner section of Zaogang River junction	86	100	Extremely high-density coverage
S3	Honghe Road Bridge section of Zaogang River	85	100	Extremely high-density coverage
S4	Taojiawan Bridge section of Zaogang River	75	75	High-density coverage
S5	Zaogang River ecological channel section	100	100	Extremely high-density coverage
S6	Section of the confluence of the Dawanbang River and the Sanjing River	100	100	Extremely high-density coverage
S7	Section of the confluence of Beitang River and Old Zaogang River	54	75	High-density coverage
S8	Xinxiaotang bridge section of Old Zaogang River	40	50	Medium-density coverage
S9	Panlong Road section of Old Zaogang River	37.5	50	Medium-density coverage

1.01 mg/L and is classified as Class IV, the water quality in other sections is classified as Class II.

Additionally, the COD concentration at Section S4, located at the Taojiawan Bridge (50.7 mg/L), significantly exceeds the standard, resulting in surface water quality that is classified below Class V. This may be due to the presence of tributaries in this section, which has a higher COD concentration, thus affecting the COD concentration of the river. Similarly, the COD concentrations in the outer section of the Zaogang River junction (S1) at 30.65 mg/L, the inner section of the Zaogang River junction (S2) at 38.8 mg/L, and the Honghe Road Bridge section (S3) at 31.75 mg/L, are also extremely high, all categorized as Class V water quality. In contrast, the COD concentration at the Xinxiaotang Bridge section of the Old Zaogang River (S8), while relatively high at 22.1 mg/L, corresponds to a Class IV water quality rating. However, the remaining sections adhere to Class II water quality standards.

TABLE 13 Results of artificial disturbance.

Sampling site	Name	Score
S1	Outer section of Zaogang River junction	95
S2	Inner section of Zaogang River junction	90
S3	Honghe Road Bridge section of Zaogang River	75
S4	Taojiawan Bridge section of Zaogang River	95
S5	Zaogang River ecological channel section	75
S6	Section of the confluence of the Dawanbang River and the Sanjing River	85
S7	Section of the confluence of Beitang River and Old Zaogang River	85
S8	Xinxiaotang bridge section of Old Zaogang River	60
S9	Panlong Road section of Old Zaogang River	85

It is evident that the concentration of total nitrogen at the Panlong Road section of the Old Zaogang River (S9) is alarmingly high at 2.11 mg/L, resulting in water quality worse than Class V. Additionally, the concentrations at the Zaogang River ecological channel section (S5) with 1.73 mg/L, the confluence of the Dawanbang River and the Sanjing River (S6) at 2 mg/L, and the confluence of the Beitang River and the Old Zaogang River (S7) at 1.87 mg/L, are also high, all classified as Class V water quality. Slightly high concentrations, corresponding to Class IV water quality, are found in the outer section of the Zaogang River junction (S1) at 1.3 mg/L, the Taojiawan Bridge section (S4) at 1.42 mg/L, and the Xinxiaotang Bridge section of the Old Zaogang River (S8) at 1.27 mg/L. The remaining sections have low total nitrogen concentrations, meeting Class III water quality standards.

On the other hand, in terms of total phosphorus concentration, that certain sections, specifically the inner section of the Zaogang River junction (S2) at 0.11 mg/L, the confluence of the Dawanbang River and the Sanjing River (S6) at 0.11 mg/L, the confluence of the Beitang River and the Old Zaogang River (S7) at 0.14 mg/L, and the Xinxiaotang Bridge section of the Old Zaogang River (S8) at 0.11 mg/L, all adhere to Class III water quality standards. The remaining sections perform better, meeting Class II water quality standards.

At the same time, the Pb concentrations in the Xinxiaotang Bridge section of the Old Zaogang River (S8) at 0.12 mg/L and the Panlong Road section of the Old Zaogang River (S9) at 0.15 mg/L seriously exceeds the standard, indicating water quality that is worse than Class V. The Pb concentration in the outer section of the Zaogang River junction (S1) at 0.09 mg/L and the confluence of the Beitang River and the Old Zaogang River (S7) at 0.09 mg/L is also extremely high, classified as Class V water quality. Other sections comply with Class III water quality standards.

Electrical conductivity, on the other hand, shows minimal variation, consistently ranging from 90 to 200 μs/cm. Notably, the sections at the confluence of the Dawanbang River the

10.3389/fevo.2024.1478024

TABLE 14 The main pollution indicators at each sampling point in the Zaogang and Old Zaogang rivers, highlighting the difference in COD and total nitrogen concentrations.

Sampling site	COD	Score	NH^3-N	Score	TP	Score	TN	Score	Pb	Score	Comprehensive level	Comprehensive score
S1	V	58.70	II	95.43	II	94.38	IV	66.00	V	44	V	71.70
S2	V	42.40	II	95.57	III	88.75	III	82.20	III	75.19	V	76.82
S3	V	56.50	II	90.14	II	92.5	III	75.75	III	85.69	V	80.12
S4	Below V	28	II	96.57	II	90	IV	55.2	III	88.88	Below V	71.73
S5	II	92.67	II	96	II	92.5	V	51.6	II	90	V	84.55
S6	II	91.53	II	97.43	III	88.5	V	38.4	II	90	V	81.17
S7	II	96.9	IV	96.9	III	81.75	V	54.8	V	55.2	V	77.11
S8	IV	63.15	II	63.15	III	76.5	IV	62.25	Below V	14.4	Below V	55.89
S9	II	95.2	II	95.2	II	100	Below V	8.8	Below V	35.6	Below V	66.96

Sanjing River, and the Panlong Road section of the Old Zaogang River, exhibit relatively high electrical conductivity, measuring 210.6 μs/cm and 188.9 μs/cm, respectively. Conversely, the Honghe Road Bridge section and the Taojiawan Bridge section of the Zaogang River show relatively low electrical conductivity, at 91.2 μs/cm and 90.6 μs/cm, respectively.

4.6 River macrobenthos assessment results

The macrobenthos in the Zaogang River mainly belong to Chironomidae, with a few specimens belonging to Monoculodes limnophilus, and some belonging to Limnoperna lacustris and Nephtys. The specific distribution is shown in Figure 2.

The Hilsenhoff index of the Zaogang River is 4.26, corresponding to clean water quality, and the linear interpolation score is 80.

4.7 Phytoplankton double index of biotic integrity assessment results

Phytoplankton in the Zaogang River include Bacillariophyta, Chlorophyta, Chrysophyta, Cryptophyta, and Cyanophyceae, with the majority being Cyanophyceae, which account for 92% of the total phytoplankton. Cyanobacteria, or Cyanophyceae, are common harmful algae known for producing the most algal toxins. Their dominance among the phytoplankton suggests a certain degree of eutrophication in the Zaogang River, indicating significant pollution. The specific distribution of phytoplankton is detailed in Figure 3. The standardized value for total phytoplankton density is 86.53, the standardized value for the percentage of Cyanophyceae density is 5.64, and the phytoplankton biodiversity index stands at 62.27.

4.8 Fish retention index results

Eight species of fish were monitored in the Zaogang River, with the dominant species being crucian carp, grass carp, and minnow. Additionally, five minor species including the flower loach, loach, Chinese paracobitis, triangular bream, and blunthead bream were also detected. Compared with the monitoring results from the 1980s, the number of species detected has significantly decreased, and some new species, such as minnow, blunthead bream, flower loach, and Chinese paracobitis, have been introduced. This indicates that the ecological condition of the river has undergone significant changes. Compared with the 1980s, the health status has declined significantly and new species have been introduced. The scoring result is 14.81 points. The extremely low score of the fish conservation index may be partly due to the significant changes in water quality of the Zaogang River compared to the reference point, with a noticeable decrease in cleanliness, and partly due to the slow flow rate of the Zaogang River and the impact of sluice dams on river connectivity, which are not conducive to fish reproduction.

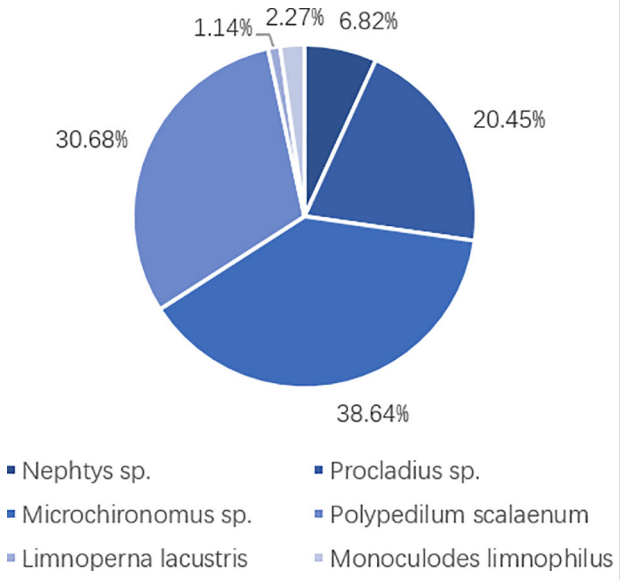

FIGURE 2
Show the distribution and dominant species of the macrobenthos.

4.9 Comprehensive assessment results

A comprehensive score is obtained by comprehensive evaluation of each index of each sampling site, and the results are shown in Table 15.

The analysis is based on the scores of various sections of the Zaogang River and the Old Zaogang River. The Zaogang River's overall condition is slightly better than that of the Old Zaogang River, yet neither is ideal. The comprehensive scores for all the sections (S1, S2, S3, S4, S5, S6) of the Zaogang River all fall within the inclusive range of 68 to 72. The "Technical guidelines for river and lake health assessment" (Ministry of Water Resources of the People's Republic of China, 2020), places the Zaogang River in the second-class level, indicating a healthy status in terms of morphological and structural integrity, water ecological integrity, resilience against disturbance, and biodiversity. However, defects are noted, particularly in the phytoplankton biotic integrity index, river connectivity, fish retention index, and water quality score. Strengthening daily management and water quality care is essential to further enhance the river's health status.

One sections of the Old Zaogang River are in a sub-healthy status, with unsatisfactory scores for vegetation cover, artificial disturbance, water quality, and fish retention index indicating a need for timely water environment repair to restore the Old Zaogang River to health. Among all indicators, the fish retention index performs the worst. Fish, being a vital component of the ecosystem, play a crucial role in maintaining its stability and deserve serious attention. Governance measures should be implemented to restore the diversity of fish populations and ensure the stability of aquatic ecosystems.

In 2015, the Zaogang River's water ecological health status was assessed with a comprehensive index of 0.67, graded as 'medium,' with a relatively low health index for natural attributes. The river's overall water quality was inferior, mainly due to high concentrations of ammonia nitrogen, averaging 2.27 mg/L, and 3.2% of the riparian zone was unstable. Compared to the health status in 2015, it has notably improved, transitioning from "medium" to "good". This improvement is particularly evident in the water quality and the status of the riparian zone condition.By 2019, the Zaogang River's overall water ecological health status had improved to 'good'. The macrobenthos diversity score was low, indicating a less diversified river ecosystem and lower aquatic biodiversity. The vegetation cover score of the riparian zone was also low. Despite a slight decrease in overall water quality compared to 2015, the macrobenthos assessment showed improvement, and there was a significant improvement in the riparian zone's vegetation cover. The results indicate that over the past decade, the ecological health status of the Zaogang River has significantly improved since 2019, demonstrating that comprehensive renovation efforts have had a lasting effect on the river's ecological status.

It is noteworthy that fish were previously excluded from the health assessment of the Zaogang River. Nonetheless, fish are a crucial component of the water ecosystem, and assessing them holds significant importance. The results of the fish assessment in this study are far from satisfactory, possibly due in part to the oversight of fish in prior evaluations of water ecological health. The preservation and enhancement of fish integrity and diversity should be accorded serious attention, aiming to establish a robust and stable water ecosystem and further advance river health.

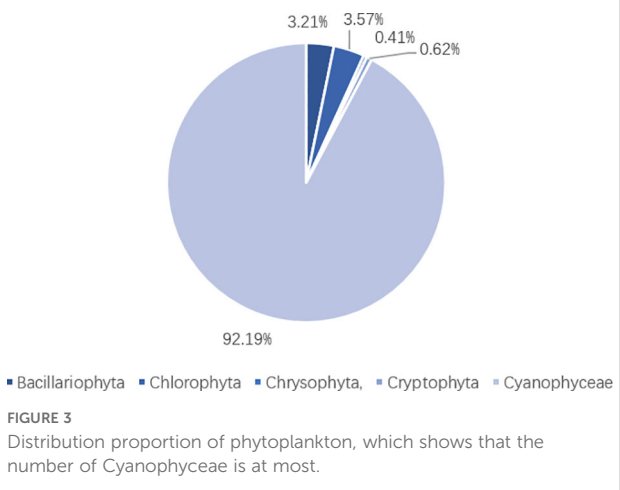

FIGURE 3
Distribution proportion of phytoplankton, which shows that the number of Cyanophyceae is at most.

5 Discussion

In this study, nine sections of the Zaogang River and the Old Zaogang River were sampled to assess water quality indices such as chemical oxygen demand (COD), ammonia nitrogen (NH3-N), total phosphorus (TP), total nitrogen (TN), and lead (Pb). These parameters were determined using established analytical methods, including the dichromate method for COD, Nessler's reagent spectrophotometry for NH3-N, ammonium molybdate

TABLE 15 Index scores and comprehensive scores of various points in Zaogang River.

Sampling site	Ecological water level satisfaction degree	River connectivity	Vegetation cover	Artificial disturbance	Water quality	Hilsenhoff index	Phytoplankton double index of biotic integrity	Fish retention index	Comprehensive score	Health status
S1	75	64	75	95	71.70	80	62.27	14.81	68.45	Healthy
S2	75	64	100	90	76.82	80	62.27	14.81	71.47	Healthy
S3	75	64	100	75	80.12	80	62.27	14.81	70.63	Heathy
S4	75	64	75	95	71.73	80	62.27	14.81	68.45	Healthy
S5	75	64	100	75	84.55	80	62.27	14.81	71.52	Healthy
S6	75	64	100	85	81.17	80	62.27	14.81	71.84	Healthy
S7	75	44.4	75	85	77.11	80	62.27	14.81	66.57	Healthy
S8	75	44.4	50	60	55.89	80	62.27	14.81	57.33	Sub-healthy
S9	75	44.4	50	85	66.96	80	62.27	14.81	62.04	Healthy

spectrophotometry for TP, alkaline potassium persulfate digestion UV spectrophotometry for TN, dithizone spectrophotometry for Pb, and the electrochemical probe method.

According to the 'Environmental Quality Standards for Surface Water,' the obtained indices were scored using linear interpolation. Additionally, the ecological water level satisfaction degree, Hilsenhoff index, fish retention index and phytoplankton biotic integrity index were calculated based on data provided by the Changzhou Academy of Environmental Science. Satellite maps and remote sensing data were employed to assess river connectivity, vegetation cover, and human interference levels, contributing to the establishment of an evaluation index system for assessing the ecological health status of the Zaogang River.

The results indicate that most sections of the river are in a healthy status, classified as second-class level, while the health condition of the Old Zaogang River is slightly poor, with one section in a sub-healthy status requiring comprehensive treatment.

This study assessed the aquatic ecological health of the Zaogang River across four dimensions: hydrological, biological, chemical, and physical structural integrity. Key indicators reflecting water ecological health were selected from multiple perspectives, establishing a comprehensive evaluation system for water ecological health. This system offers a scientific understanding of the Zaogang River's health, guides further comprehensive improvement measures, and enhances the river's ecological health across multiple dimensions. Additionally, this study provides a rapid yet rigorous framework for assessing the ecological health of urban rivers, significantly enhancing the health of urban river ecosystems.

However, as the data in this study relied solely on a single sampling, it may have been influenced by seasonal factors. Future research should involve multiple samplings across different seasons and times to gather more data, thereby minimizing the impact of seasonal factors on river health assessments, achieving more objective and comprehensive results, and providing more targeted guidance for integrated river management strategies.

Currently, the evaluation of water ecological health is gradually incorporating the assessment of water ecosystem services. These services encompass a variety of functions, including supply services that provide essential resources such as drinking water and irrigation; cultural services that offer recreational opportunities and aesthetic enjoyment; regulation services that help maintain environmental balance through processes like flood control and water purification; and support services that underpin other ecosystem functions, such as nutrient cycling and habitat provision (Cao et al., 2021).

Water ecosystem services serve as a crucial link between ecosystems and human society, highlighting the interdependence between natural systems and human well-being. The evaluation of these services can be achieved through various methodologies, including ecological modeling methods (Yang et al., 2019), which utilize mathematical representations to simulate complex interactions within ecosystems; survey questionnaires designed to gather data on public perceptions and usage patterns related to water resources; and value evaluation methods aimed at quantifying the economic benefits derived from these ecosystem functions.

The system for evaluating water ecosystem services established in this study acknowledges its limitations in comprehensiveness. It

is important to recognize that while it provides valuable insights into certain aspects of river ecosystems, there are numerous factors influencing their health that may not be fully captured by current models or assessments. Future research could benefit from integrating additional methodologies mentioned above—such as participatory approaches involving local communities—to build a more holistic understanding of river ecosystems.

By expanding upon existing frameworks for evaluation, researchers can enhance their ability to identify critical areas requiring conservation efforts or policy interventions. This comprehensive approach will ultimately contribute to more effective management strategies aimed at preserving both aquatic environments and the myriad benefits they provide to society. Such advancements in knowledge will facilitate informed decision-making processes among policymakers tasked with safeguarding natural resources while balancing societal needs.

Data availability statement

Publicly available datasets were analyzed in this study. This data can be found here: 10.6084/m9.figshare.27161688

Author contributions

JZ: Software, Writing – original draft, Methodology, Formal analysis, Writing – review & editing. JX: Data curation, Writing – original draft, Formal analysis. QM: Data curation, Formal analysis, Writing – review & editing. CL: Writing – review & editing. XX: Writing – review & editing.

Funding

The author(s) declare financial support was received for the research, authorship, and/or publication of this article. This work is supported by the National Key Research and Development Program of China (2022YFC3202001) and the National Natural Science Foundation China (52070023).

Conflict of interest

The authors declare the research was conducted in the absence of any commercial or financial relationships that could be construed as a potential conflict of interest.

Publisher's note

References

Amoros, C., and Roux, A. L. (1988). Interaction between water bodies within the floodplains of large rivers: Function and development of connectivity. *Münstersche Geographiseche Arbeiten* 29, 125–130.

Becker, I., Egger, G., Gerstner, L., Householder, J. E., and Damm, C. (2022). Using the River Ecosystem Service Index to evaluate "Free Moving Rivers" restoration measures: A case study on the Ammer river (Bavaria). *Int. Rev. Hydrobiol.* 107, 117–127. doi: 10.1002/iroh.202102088

Brosed, M., Jabiol, J., and Chauvet, E. (2022). Towards a functional assessment of stream integrity: A first large-scale application using leaf litter decomposition. *Ecol. Indic.* 143, 109403. doi: 10.1016/j.ecolind.2022.109403

Cao, T. G., Yi, Y. J., Liu, H. X., and Yang, Z. F. (2021). The relationship between ecosystem service supply and demand in plain areas undergoing urbanization: A case study of China's Baiyangdian Basin. *J. Environ. Management.* 289, 112492. doi: 10.1016/j.jenvman.2021.112492

Deng, X. J., Xu, Y. P., Zhai, L. X., and Liu, Y. (2014). Establishment and application of the index system for urban river health assessment. *Acta Ecologica Sin.* 34, 993–1001. doi: 10.5846/stxb201209221339

Department of River and Lake Management (2020). *Guidelines for river and lake health assessment* (Ministry of Water Resources of the People's Republic of China). Available online at: https://slj.sxxz.gov.cn/zwyw/gzdt/202011/t20201106_3572298.html.

Díaz, S., Settele, J., Brondízio, E. S., Ngo, H. T., Agard, J., Arneth, N., et al. (2019). Pervasive human-driven decline of life on Earth points to the need for transformative change. *Science* 366, eaax3100. doi: 10.1126/science.aax3100

European Commission (2000). *Water framework directive: directive 2000/60/EC of the European Parliament and of the Council establishing a framework for the community action in the field of water policy* (European Commission). Available at: https://environment.ec.europa.eu/topics/water/water-framework-directive_en.

Ji, H. T., Ma, L., Li, J., Zhang, X., Zhuang, M., and Yu, X. (2020). Assessment on the health status of rivers and lakes in Changzhou City ——a case study of Zaogang River. *Jiangsu Water Resources.* 05, 34–40. doi: 10.16310/j.cnki.jssl.2020.05.007

Li, D. M., Liu, B., Chen, S., Wu, N. C., and Guan, Y. Q. (2021). Improving biological condition assessment accuracy by multimetric index approach with microalgae in streams and lakes. *SCIENTIA Sin. Vitae* 51, 1287–1298. doi: 10.1360/SSV-2021-0236

Martinez-Haro, M., Beiras, R., Bellas, J., Capela, R., Coelho, J. P., Lopes, I., et al. (2015). A review on the ecological quality status assessment in aquatic systems using community based indicators and ecotoxicological tools: What might be the added value of their combination? *Ecol. Indic.* 48, 8–16. doi: 10.1016/j.ecolind.2014.07.024

Ministry of Ecology and Environment of the People's Republic of China (2002). *Environmental quality standards for surface water.GB 3838-2002* (Ministry of Ecology and Environment of the People's Republic of China). Available online at: https://www.mee.gov.cn/ywgz/fgbz/bz/bzwb/shjbh/shjzlbz/200206/t20020601_66497.shtml.

Ministry of Ecology and Environment of the People's Republic of China (2023). *Technical guidelines for water ecological monitoring—aquatic organism monitoring and evaluation of rivers(on trial).HJ 1295—2023* (Ministry of Ecology and Environment of the People's Republic of China). Available online at: https://www.mee.gov.cn/xxgk2018/xxgk/xxgk01/202305/t20230511_1029703.html.

Ministry of Water Resources of the People's Republic of China (2020). *Technical guidelines for river and lake health assessment.SL/T 793—2020* (Ministry of Water Resources of the People's Republic of China). Available online at: http://www.chinawater.com.cn/yw/202006/t20200609_999328.html.

Poikane, S., Herrero, F. S., Kelly, M. G., Borga, A., Birk, S., and Bund, W. (2020). European aquatic ecological assessment methods: A critical review of their sensitivity to key pressures. *Sci. Total Environ.* 740, 140075. doi: 10.1016/j.scitotenv.2020.140075

Prudente, B. D. S., Pompeu, P. S., and Montag, L. (2018). Using multimetric indices to assess the effect of reduced impact logging on ecological integrity of Amazonian streams. *Ecol. Indic.* 91, 315–323. doi: 10.1016/j.ecolind.2018.04.020

Qin, A. L., Yuan, C. M., and Zhou, Z. H. (1988). The influence of the contamination of water on the fish stock in the Jing-Hang Grand Canal (the section of Changzhou). *J. Nanjing University(Natural Science)* 01, 97–107.

Riato, L., Leibowitz, S. G., and Weber, M. H. (2020). The use of multiscale stressors with biological condition assessments: A framework to advance the assessment and management of streams. *Sci. Total Environ.* 737, 139699. doi: 10.1016/j.scitotenv.2020.139699

Stoddard, J. L., Larsen, D. P., Hawkins, C. P., Johnson, R. K., and Norris, R. H. (2006). Setting expectations for the ecological condition of streams: The concept of reference condition. *Ecol. Appl.* 16, 1267–1276. doi: 10.1890/1051-0761(2006)016[1267:SEFTEC]2.0.CO;2

Su, Y. F., Li, W. M., Ai, Z. Q., Liu, D. F., Zhu, C. H., Li, J. L., et al. (2019). Establishment and application of the index system for health assessment of the middle and lower reaches of the Hanjiang River. *Acta Ecologica Sin.* 39, 3895–3907. doi: 10.5846/stxb201807081484

Tang, T., Cai, Q. H., and Liu, J. K. (2002). River ecosystem health and its assessment. *Chin. J. Appl. Ecol.* 09, 1191–1194.

Thornbrugh, D. J., Leibowitz, S. G., Hill, R. A., Weber, M. H., Johnson, Z. C., Olsen, A. R., et al. (2018). Mapping watershed integrity for the conterminous United States. *Ecol. Indic.* 85, 1133–1148. doi: 10.1016/j.ecolind.2017.10.070

Wang, Q., Xu, P., Li, X. M., and Wang, Z. J. (2019). Assessment method for the influence of hydroelectric dams on the physical habitat quality and longitudinal connectivity of rivers: a case study of the Wubu and Zaodu rivers. *Acta Ecologica Sin.* 39, 5508–5516. doi: 10.5846/stxb201808261822

Water Resources Department of Jiangsu Province (2019). *Specification for ecological river and lake status assessment.DB32/T 3674-2019* (Market Supervisory Authority of Jiangsu Province).

Wright, J. F., Moss, D., Armitage, P. D., and Furse, M. T. (1984). A preliminary classification of running-water sites in Great Britain based on macro-invertebrate species and the prediction of community type using environmental data. *Freshw. Biol.* 14, 221–256. doi: 10.1111/j.1365-2427.1984.tb00039.x

Yang, D., Liu, W., Tang, L. Y., Chen, L., Li, X. Z., and Xu, X. L. (2019). Estimation of water provision service for monsoon catchments of South China: Applicability of the InVEST model. *Landscape Urban Plann.* 182, 133–143. doi: 10.1016/j.landurbplan.2018.10.011

Zhang, H. X., Nie, Q. H., Su, Y. P., Wang, X., Chen, Y. X., Weng, Y. X., et al. (2024). Constructing a new index of phytoplankton integrity for evaluating the health of reservoirs. *Acta Scientiae Circumstantiae* 44, 452–462. doi: 10.13671/j.hjkxxb.2023.0455

Zhang, Y. F., Zhu, Y. Y., Chen, Y. J., and Tian, G. X. (2022). Urban river health assessment based on concept of resilience -taking Jinshui River in Zhengzhou City as a case study. *Bull. Soil Water Conserv.* 42, 238–246+257. doi: 10.13961/j.cnki.stbctb.20220929.004

Zhang, Z. M., Fan, Y. G., and Jiao, Z. J. (2023). Wetland ecological index and assessment of spatial-temporal changes of wetland ecological integrity. *Sci. Total Environ.* 862, 160741. doi: 10.1016/j.scitotenv.2022.160741

Zhong, Z. L. (2013). Study on diversion ratio of river in Changzhou City. *Jiangsu Water Resour.* 29, 22–24. doi: 10.16310/j.cnki.jssl.2013.02.019

Zhou, X. D., Xu, M. Z., Wang, Z. Y., Yu, B. F., and Shao, X. J. (2019). Responses of macroinvertebrate assemblages to environmental variations in the river-oxbow lake system of the Zoige wetland (Bai River, Qinghai-Tibet Plateau). *Sci. Total Environ.* 659, 150–160. doi: 10.1016/j.scitotenv.2018.12.310

frontiers | Frontiers in Earth Science

TYPE Original Research
PUBLISHED 06 November 2024
DOI 10.3389/feart.2024.1488755

OPEN ACCESS

EDITED BY
Chunhui Li,
Beijing Normal University, China

REVIEWED BY
Yanli Liu,
Nanjing Hydraulic Research Institute, China
Cuishan Liu,
Nanjing Hydraulic Research Institute, China
Xuchun Ye,
Southwest University, China

*CORRESPONDENCE
Weifan Chen,
chenweifan_1999@163.com

RECEIVED 30 August 2024
ACCEPTED 16 October 2024
PUBLISHED 06 November 2024

CITATION
Li Z, Chen W and Wang L (2024) Quantification of streamflow response to climate change and human activities within upstream mountainous areas of the Daqing River Basin, Northern China.
Front. Earth Sci. 12:1488755.
doi: 10.3389/feart.2024.1488755

Quantification of streamflow response to climate change and human activities within upstream mountainous areas of the Daqing River Basin, Northern China

Zengyi Li[1], Weifan Chen[2]* and Linna Wang[2]

[1]School of Water Conservancy, North China University of Water Resources and Electric Power, Zhengzhou, China, [2]State Key Laboratory of Simulation and Regulation of Water Cycle in River Basin, China Institute of Water-Resources and Hydropower Research, Beijing, China

The Daqinghe River Basin is located in the North China Plain. In recent years, however, climate warming, drying, and intense human activities have led to declining ecosystem functions and shrinking wetlands in the region. Understanding streamflow changes in the upstream mountainous areas of the Daqinghe River Basin in this changing environment and identifying the driving factors can provide a scientific basis for water resources management and optimization in these areas. This study focuses on the Beihedian River watershed, the Xidayang Reservoir watershed, and the Wangkuai Reservoir watershed in the upstream mountainous areas of the Daqinghe River. It is based on hydro-meteorological data collected between 1963 and 2019. The methods used in the study include the linear tendency estimation method, the non-parametric Mann-Kendall trend test, the elasticity coefficient method, and hydrological simulation methods. The results of this study suggest that the streamflow, precipitation, and potential evapotranspiration (PET) in the three watersheds showed an overall decreasing trend. The minimum precipitation decrease rate ranged from −1.09 to −0.55 mm/a, and the minimum streamflow decreasing rate at the Beihedian Hydrological Station was −1.32 mm/a, with a minimum range of 0–176.03 mm. Change-point analysis revealed that the streamflow in the Beihedian River and Xidayang Reservoir watersheds experienced a significant change point around 1999, with a significant level of α=0.05. As for the Wangkuai Reservoir watershed, a significant change point was observed around 1980, which is likely attributable to land system reforms and protective forest projects. The attribution analysis which combined both climate change and human activities using the elasticity coefficient method and hydrological simulation methods indicated that climate change contributed an average of 32.93%, 34.50%, and 35.12% to the reduction in streamflow in the three watersheds, respectively. Human activities accounted for an average contribution of 67.07%, 65.50%, and 64.88%, respectively. Water conservancy projects, afforestation, and other human activities were identified as the primary factors contributing to streamflow decreases.

KEYWORDS

streamflow, land use change, climate change, human activities, hydrological simulation method

1 Introduction

On a global scale, climate change and human activities are affecting the water cycle in many watersheds (Chien et al., 2013; Liu et al., 2020). Climate change including global warming and other related issues profoundly affects hydrological processes such as precipitation and evaporation, which exhibit varying temporal and spatial distributions. It can also lead to an increased frequency of extreme weather events (Wu et al., 2021; Yang et al., 2019). In the past 40 years, significant human activities have had an undeniable impact on hydrological processes within the watershed (Lyu et al., 2024; Zhang et al., 2023). Human activities primarily influence hydrological cycling by altering the structure of underlying surfaces (Zhang and Yu, 2021). Therefore, human activities within the watershed are also one of the main causes of river evolution (Deng et al., 2024; Zheng et al., 2023). In this context, understanding the hydrological evolution under changing environments and quantifying the impact of various factors on streamflow is crucial for water resource management and sustainable development (Liu et al., 2020; Jiang et al., 2015; Liang et al., 2015; Zeng et al., 2020).

Baiyangdian Lake, situated within the Daqing River System in the Haihe River Basin, is of significant importance. The lake plays an irreplaceable role in maintaining the ecological balance of North China, regulating the climate in the Beijing-Tianjin-Hebei region, replenishing groundwater resources, alleviating floods and droughts, and preserving biodiversity and rare species (Moiwo et al., 2010; Song et al., 2018; Zerizghi et al., 2020). The upstream areas of the Daqing River Basin include eight rivers that flow into the lake, contributing an average annual streamflow volume of 2.23 billion m^3 and an average streamflow depth of 71.5 mm (Liu et al., 2022). The upstream mountainous areas in the western part of the basin are the primary catchment areas, accounting for 85% of the total streamflow. However, the water resources situation in the Daqing River Basin has become increasingly challenging due to the combined effects of climate warming, drying in North China, and intense human activities since the 1960s (Cheng et al., 2017; Wang et al., 2021; Yang and Cao, 2021). This has led to a growing conflict between water resource availability and economic development (Song et al., 2018; Dai et al., 2011; Xu et al., 2013). Given that the upstream mountainous areas are crucial as primary water sources in the Daqing River Basin (Hu et al., 2012), understanding the main causes of streamflow decline in these regions is essential for the rational development and effective allocation of water resources within the basin. It also supports the implementation of scientifically informed water resource management practices.

Numerous studies have investigated the evolution and causes of streamflow changes in the Daqing River Basin. Lei et al. used a process-based terrestrial model (version 4 of the Community Land Model, CLM4) to quantify the spatiotemporal variation in streamflow across the region due to climate factors and changes in carbon dioxide concentration. Their results indicate a decreasing trend in streamflow related to climate since 1960, with a limited impact from the rise in atmospheric CO_2 concentration (Lei et al., 2014). Du et al. developed a monthly ABCD model for the Yongding River Basin and two subbasins, the Yanghe and Sanggan Rivers, to assess the relative contributions of climate change and human activities to streamflow reduction. They found a significant decline in annual streamflow since the 1980s, with human activities being the predominant influencing factor, especially during the rainy season (Du et al., 2023). Li et al. employed the Statistical DownScaling Model (SDSM) to downscale predicted precipitation and temperature for the mountainous Yongding watershed under four SSP-RCP climate scenarios across four General Circulation Models (GCMs). The Bayesian Model Averaging (BMA) method was then used for multi-model integration to mitigate GCM uncertainty, and the multi-model ensemble data were adjusted using the Quantile Mapping (QM) method. Subsequently, the SWAT model was applied to simulate streamflow responses under future climate conditions (Li et al., 2023). Qiao et al. applied two methods, the watershed water-energy balance equation and the Geomorphology-Based Hydrological Model (GBHM), to study streamflow changes in a semiarid mountainous watershed. Their findings revealed a significant downward trend in streamflow and leaf area index (LAI) over the past 40 years, with different interdecadal quantitative results from the two methods. GBHM, in particular, struggled to accurately simulate reservoir scheduling and other processes (Qiao et al., 2023). Zhang et al. calculated multi-year averages of 17 environmental variables from 57 selected watersheds, including hydrological, meteorological, vegetation, land use, terrain, and soil data. They established a quantitative relationship between streamflow and watershed area for the first time and evaluated the correlation between environmental factors and the impact on streamflow scale (Zhang et al., 2019). Wang et al. used the Mann-Kendall test, double cumulative curve method, and streamflow sensitivity analysis to separate and quantify the relative effects of climate variability and land use changes on streamflow. Then they estimated the sensitivity of streamflow in North China from 1957 to 2000 to these factors (Wang et al., 2019). Huang et al. developed an extended Budyko framework incorporating Total Water Storage (TWS) from the Gravity Recovery and Climate Experiment (GRACE), and applied it to the Qinba Mountain area by four classic Budyko equations. Their results indicated that the extended Budyko framework more accurately represents the relationship between monthly water supply and demand compared to the original framework (Huang et al., 2021).

This study specifically targets three primary streamflow-producing areas located in the upstream mountainous regions of the Daqing River Basin. By comprehensively analyzing the trends in water cycle elements, the study employs both the elasticity coefficient method and the hydrological simulation method to determine the causes of water resource depletion within the basin. Additionally, it quantitatively examines the sensitivity of streamflow to variations in various driving factors and assesses the respective contribution rates of climate change and human activities to streamflow variation. The ultimate objective of this study is to provide scientific references for improving water resource management within the watershed and implementing effective measures for managing small watersheds.

2 Materials and methods

2.1 Study area

The study area is located in the upstream mountainous regions of the western Daqing River Basin and includes three hydrological

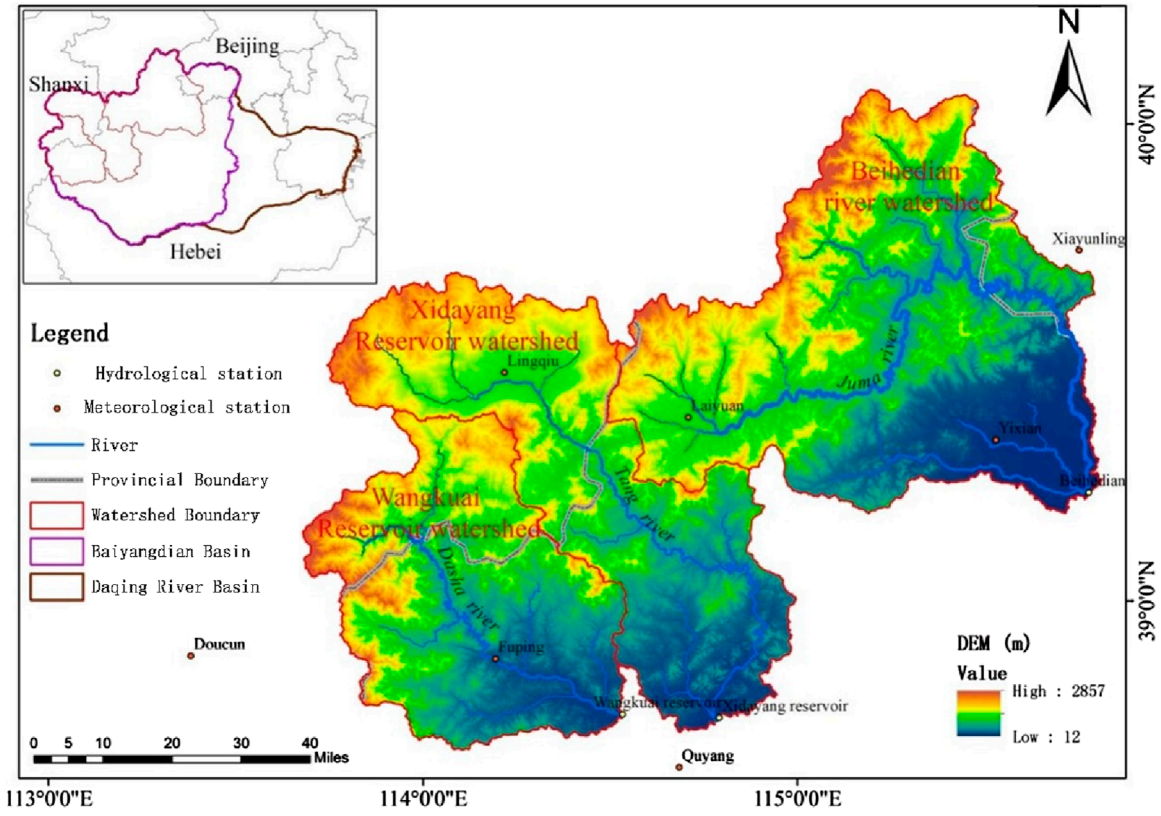

FIGURE 1
Location map of the study area.

stations: Beihedian Station, Xidayang Reservoir Station, and Wangkuai Reservoir Station (Figure 1). Geographically, it is located between 113°39′–115°48′E and 38°39′–40°03′N, covering a total area of 15,028 km^2. The terrain generally exhibits high elevation in the northwest and low elevation in the southeast, with an average altitude of 868.42 m and the highest point reaching 2,857 m (Figure 1). The study area experiences a temperate semiarid continental monsoon climate, characterized by four distinct seasons. Rain and heat often occur simultaneously. Spring is characterized by little rainfall and low humidity, while summer is hot and rainy. Autumn is typically clear with moderate temperatures, and winter is cold with little precipitation. The average annual precipitation in the study area is 533 mm, and the average annual PET is 817 mm. Precipitation is unevenly distributed throughout the year, with the majority of rainfall occurring from June to September. Additionally, there is significant interannual variability in rainfall, which can lead to both droughts and floods.

2.2 Data sources and Preprocessing

The data required for this study include meteorological and hydrological station observation data, Digital Elevation Model (DEM) data, land use type data, and Normalized Difference Vegetation Index (NDVI) data. Seven national meteorological stations located in the upstream mountainous areas of the Daqing River Basin were carefully selected for this study. Daily observation data covering the period from 1963 to 2019 were obtained from the China Meteorological Data Service Centre (http://data.cma.cn/). The dataset includes various meteorological parameters such as average temperature, maximum and minimum temperature, precipitation, wind speed, sunshine duration, relative humidity, and vapor pressure. To address missing data, temporal and spatial interpolation methods were applied. Spatial interpolation was used when nearby stations with similar natural conditions to the stations with missing data were available, while temporal interpolation was performed by data from the same period in adjacent years when spatial interpolation was not possible. The PET was estimated by the Penman-Monteith equation recommended by the Food and Agriculture Organization (FAO). The basin-scale precipitation and PET data were obtained through the inverse distance weighting (IDW) interpolation method. Daily streamflow observation data from Wangkuai Reservoir, Xidayang Reservoir, and Beihedian hydrological stations, spanning 1963 to 2019, were sourced from the Hebei Hydrological Survey and Research Center and the Baoding Hydrological Survey and Research Center. The DEM data were acquired from the Geospatial Data Cloud (http://www.gscloud.cn/). The land use type data and NDVI data used in the study were obtained from the Resource and Environment Science and Data Center of the Chinese Academy of Sciences (https://www.resdc.cn/).

2.3 Methodology

2.3.1 Trend analysis

The trend patterns of hydrometeorological variables in the Daqing River Basin were analyzed using the linear propensity estimation and the non-parametric Mann-Kendall trend test methods.

2.3.1.1 Linear propensity estimation method

The linear propensity estimation method was employed to establish a simple linear regression equation that reflects the changes in hydrometeorological variables over time. The formula is shown in Equation 1

$$y = ax + b \tag{1}$$

where x is the sequential value of years; y is the value of the hydrometeorological variable corresponding to the year x; a is the regression coefficient, with positive and negative signs indicating an upward or downward trend, respectively; and b is the regression constant.

2.3.1.2 Mann-Kendall trend test method

The Mann-Kendall (MK) test method is a widely used approach for testing trends in hydro-meteorological variables, including temperature, precipitation, and streamflow. This method does not require samples to follow a specific distribution and can directly assess change in the variables. When performing a trend test on a given sequence $X\{x_i, i = 1, 2, \ldots, n\}$ with n samples, the test statistic Z is calculated by the following formula 2:

$$Z = \begin{cases} \dfrac{S-1}{\sqrt{\mathrm{Var(s)}}} & S > 0 \\ 0 & S = 0 \\ \dfrac{S+1}{\sqrt{\mathrm{Var(s)}}} & S < 0 \end{cases} \tag{2}$$

where, n is the length of the hydrometeorological variable sequence. S is calculated by the following formula 3:

$$S = \sum_{i=1}^{n-1} \sum_{j=i+1}^{n} sgn\left(x_j - x_i\right) \quad (j = 2, 3, 4, \ldots, n) \tag{3}$$

where x_i and x_j are the hydrometeorological variable values for the i -th and $(i+1)$-th years, respectively. The function $sgn(\cdot)$ is calculated by the following formula 4:

$$sgn\left(x_j - x_i\right) = \begin{cases} 1, & x_j > x_i \\ 0, & x_j = x_i \\ -1, & x_j < x_i \end{cases} \tag{4}$$

When the sample size n is sufficiently large, the variance $Var(s)$ of the test statistic S is calculated by the following expression Equation 5:

$$Var(s) = \frac{n(n-1)(2n+5)}{18} \tag{5}$$

The Mann-Kendall method utilizes the test statistic Z to assess the trend of the hydro-meteorological variable sequence. A positive value of Z $(Z > 0)$ indicates an upward trend while a negative value $(Z < 0)$ indicates a downward trend. The magnitude of Z reflects the significance of the change in the sequence. When $|Z| > Z_{1-\frac{\alpha}{2}}$, the variable exhibits a significant upward or downward trend at the significance level α. The critical value required for the test, $\pm Z_{1-\frac{\alpha}{2}}$, can be obtained by referencing a table.

2.3.2 Abrupt change analysis

The Pettitt method is used for detecting abrupt change points by directly analyzing rank sequences. The change point k is identified at time t_0 if the following condition is satisfied as represented by the following formula 6:

$$k_{t_0} = Max\left|S_k\right| \quad (k = 2, 3, \cdots, n) \tag{6}$$

Then t_0 is considered as an abrupt change point. Here, the rank sequence S_k is the cumulative count of values at time i that is greater or less than the values at time j, where $j = 1, 2, \ldots, i$.

The statistical significance level of an abrupt change point is determined by the statistical quantity P, which is calculated according to the following formula 7:

$$P = 2\,exp\left[-6k_{t_0}^2\left(n^3 + n^2\right)\right] \tag{7}$$

If P is not larger than 0.5, then the detected abrupt change point is considered statistically significant.

2.3.3 Elasticity coefficient method

2.3.3.1 Budyko Hypothesis

The Budyko theory (Budyko, 1974) is based on the water balance equation, which can be expressed as Equation 8:

$$R = P - ET + \Delta S \tag{8}$$

where, R is the multi-year average streamflow depth, mm; P is the multi-year average precipitation, mm; ET is the multi-year average actual evapotranspiration, mm; and ΔS is the change in basin storage, mm.

After years of research, Budyko proposed that the multi-year evapotranspiration rate of a watershed is determined by PET and precipitation. Therefore, the Budyko Hypothesis can be simply expressed as Equation 9:

$$\frac{ET}{P} = f\left(\frac{ET_0}{P}\right) = f(\varphi) \tag{9}$$

where, ET_0 is the multi-year average PET, mm; P is the multi-year average precipitation, mm, and φ is the aridity index.

The original Budyko Hypothesis did not consider the effects of underlying surface conditions and watershed characteristics. Based on this, several studies have proposed a series of empirical Budyko formulas that incorporate parameters to represent underlying surface conditions (Milly and Dunne, 2002; Porporato et al., 2004). These formulas have been theoretically derived and validated. In this study, we selected the equations developed by Fu, Choudhury-Yang, and Zhang (Table 1) to attribute and identify the changes in watershed streamflow.

It is generally considered that the change in basin storage (ΔS) can be neglected when studying closed watersheds over long-term hydrological sequences. In other words, under the assumption of

TABLE 1 Three Commonly Used Formulas based on the Budyko Hypothesis.

Formula	Parameter	References
$ET/P = 1 + ET_0/P - \left[1 + (ET_0/P)^{\omega}\right]^{1/\omega}$	ω	Fu et al. (2007), Wu et al. (2016)
$ET/P = 1/\left[1 + (P/ET_0)^{n}\right]^{1/n}$	n	Choudhury (1999), Yang et al. (2008)
$ET/P = \left[1 + \omega(ET_0/P)\right]/\left[1 + \omega(ET_0/P) + (ET_0/P)^{-1}\right]$	ω	Zhang et al. (2001)

In the Fu formula, the parameter ω reflects the underlying surface conditions of the watershed, which is related to land use, vegetation, soil, etc. In the Choudhury-Yang formula, the parameter n has the same meaning as in the Fu formula. In the Zhang formula, the parameter ω represents the vegetation's effective water coefficient, indicating the relative differences in the way plants utilize soil moisture for transpiration. In this study, we use the unified notation "n" to represent these parameters.

constant basin storage, the water balance equation can be expressed as Equations 10–12:

$$R = P - \left(P + ET_0 - P\left(1 + \left(\frac{ET_0}{P}\right)^{n_{Fu}}\right)^{\frac{1}{n_{Fu}}}\right) \tag{10}$$

$$R = P - \frac{P \times ET_0}{\left(P^{n_{CY}} + {ET_0}^{n_{CY}}\right)^{\frac{1}{n_{CY}}}} \tag{11}$$

$$R = P - \frac{P + n_{Zh} ET_0}{1 + n_{Zh}\frac{ET_0}{P} + \left(\frac{ET_0}{P}\right)^{-1}} \tag{12}$$

2.3.3.2 Elasticity coefficients

Assuming that P, ET_0 and n are independent variables and combining them with the water balance equation, the annual streamflow volume can be expressed in the form of a total differential, given by Equation 13:

$$dR = \frac{\partial R}{\partial P}dP + \frac{\partial R}{\partial ET_0}dET_0 + \frac{\partial R}{\partial n}dn \tag{13}$$

The sensitivity of streamflow volume R to each influencing factor can be represented by the elasticity coefficient ε. The elasticity coefficient is defined as the degree of change in watershed streamflow resulting from a unit change in a climatic factor. It can be expressed as Equation 14:

$$\varepsilon_x = \frac{\partial R/R}{\partial x_i/x_i} \tag{14}$$

where, ε_x is the sensitivity of streamflow volume to the influencing factor x, where x can be P, ET_0, or n. Both P and ET_0 are multi-year average values of the watershed.

2.3.3.3 Contribution of climate and underlying surface to streamflow variation

To quantitatively differentiate the contributions of various factors to streamflow variation, a complementary method based on the Budyko Hypothesis is employed. Zhou et al. proposed a complementary equation to separate the contributions of climate change and underlying surface change to streamflow variation, based on the complementary relationship of elasticity coefficients and the assumption of independence between P and ET_0 (Zhou et al., 2015). This method eliminates theoretical calculation errors. The complementary relationship equation can be expressed as Equation 15:

$$\frac{\partial R/R}{\partial P/P} + \frac{\partial R/R}{\partial ET_0/ET_0} = 1 \tag{15}$$

Due to the uncertainty associated with climate and underlying surface conditions, the complementary relationship weighted factor method based on the Budyko Hypothesis introduces the weighting factors α to represent different pathways of change (Zhou et al., 2016). Through algebraic identity derivation, the complementary method for attributing streamflow variation is proposed. The expression can be given as Equation 16:

$$\Delta R = \alpha\left[\left(\frac{\partial R}{\partial P}\right)_1 \Delta P + \left(\frac{\partial R}{\partial ET_0}\right)_1 \Delta ET_0 + P_2\Delta\left(\frac{\partial R}{\partial P}\right) + E_{0,2}\Delta\left(\frac{\partial R}{\partial ET_0}\right)\right]$$

$$+(1-\alpha)\left[\left(\frac{\partial R}{\partial P}\right)_2 \Delta P + \left(\frac{\partial R}{\partial ET_0}\right)_2 \Delta ET_0 + P_1\Delta\left(\frac{\partial R}{\partial P}\right) + E_{0,1}\Delta\left(\frac{\partial R}{\partial ET_0}\right)\right] \tag{16}$$

where, ΔR is the change in streamflow volume, mm; α is the weighting factor ($0 \leq \alpha \leq 1$), which is the contribution of different pathways of climate change and human activities to the changes in streamflow volume. In this study, α is set to 0.5. Subscripts 1 and 2 are the baseline period and abrupt change period before and after the abrupt change point, respectively. The formulas for calculating the changes in precipitation, evapotranspiration, and underlying surface, denoted as ΔR_P, R_{ET_0} and ΔR_n are as Equations 17–19:

$$\Delta R_P = \alpha\left[\left(\frac{\partial R}{\partial P}\right)_1 \Delta P\right] + (1-\alpha)\left[\left(\frac{\partial R}{\partial P}\right)_2 \Delta P\right] \tag{17}$$

$$\Delta R_{ET_0} = \alpha\left[\left(\frac{\partial R}{\partial ET_0}\right)_1 \Delta ET_0\right] + (1-\alpha)\left[\left(\frac{\partial R}{\partial ET_0}\right)_2 \Delta ET_0\right] \tag{18}$$

$$\Delta R_n = \alpha\left[P_2\Delta\left(\frac{\partial R}{\partial P}\right) + E_{0,2}\Delta\left(\frac{\partial R}{\partial ET_0}\right)\right] + (1-\alpha)\left[P_1\Delta\left(\frac{\partial R}{\partial P}\right) + E_{0,1}\Delta\left(\frac{\partial R}{\partial ET_0}\right)\right] \tag{19}$$

2.3.4 Hydrological simulation method

The WATLAC hydrological model (Li et al., 2016; Li et al., 2021; Ren et al., 2017; Ye et al., 2011) is a distributed hydrological model that simulates the surface and subsurface streamflow processes in a watershed driven by rainfall and evaporation. It incorporates processes such as vegetation interception, soil water storage, surface streamflow, soil recharge to groundwater, and saturated groundwater movement. The model adopts spatial discretization based on grid cells to simulate surface streamflow and the flow paths are determined based on terrain elevation and the water network. Groundwater movement is simulated by MODFLOW with finite difference grid discretization in space and coupling with the surface streamflow model to facilitate data transfer within the program. The finite difference grid used for groundwater

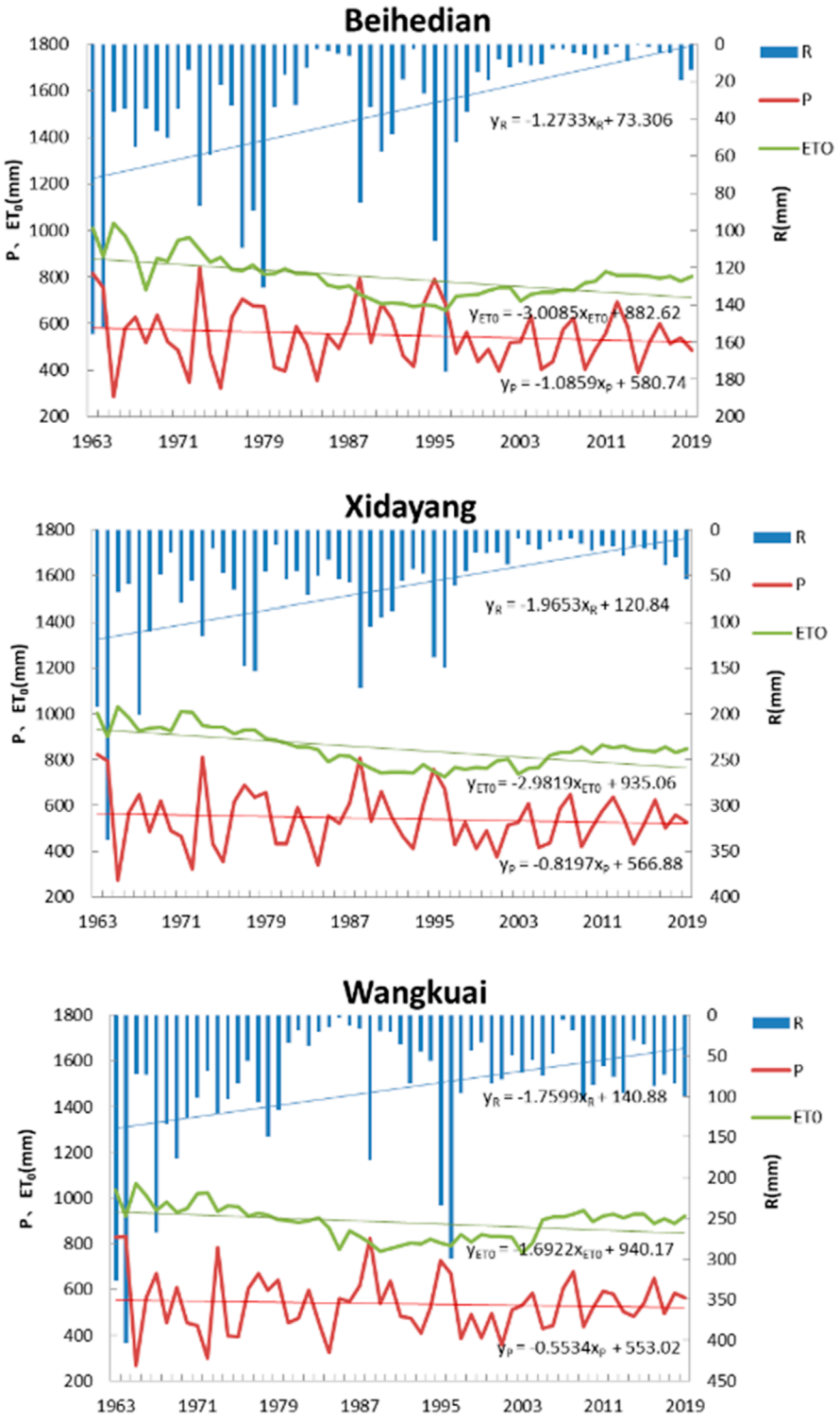

FIGURE 2
Analysis results of linear estimation method.

simulation matches the planar grid cells used for surface water simulation on the horizontal plane. The WATLAC hydrological model allows for variable time steps for surface and subsurface streamflow, considering the differences in flow velocity between the two components and reducing the computational workload for groundwater simulation. Moreover, the model enables the quantitative differentiation of different streamflow components and provides detailed water balance outputs.

TABLE 2 MK trend analysis statistical results table.

Small watershed	Meteorological stations	Area/km^2	MK trend test Z-value			Coefficient of variation Cv		
			R	P	ET_0	R	P	ET_0
Beihedian	Yixian, Laiyuan, Xiayunling	6,854	−4.91**	−0.99	−3.91**	1.21	0.96	0.96
Xidayang	Lingqiu, Quyang	4,413	−4.61**	−0.64	−3.94**	1.03	0.95	0.96
Wangkuai	Fuping, Wutaixian	3,761	−1.72*	−0.26	−2.70**	1.06	0.95	0.96

*and**indicate significance tests at the confidence levels of $p<0.05$ and $p<0.01$, respectively.

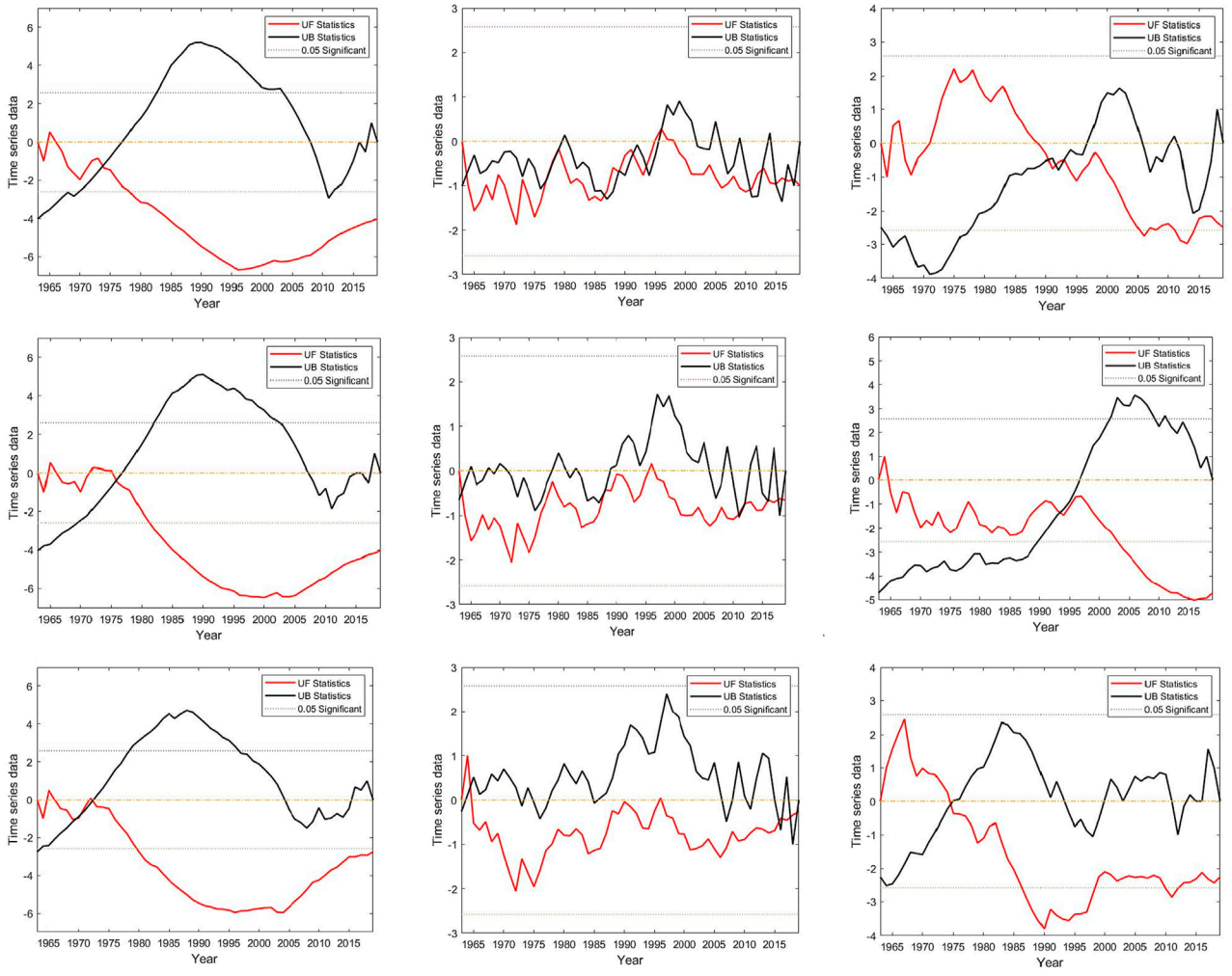

FIGURE 3
MK Trend Analysis Change Chart [Note: From top to bottom are Beihedian, Xidayang, and Wangkuai, and from left to right are evapotranspiration (ET_0), precipitation (P), and runoff depths (R)].

This paper employs the WATLAC hydrological model. Based on the change-point analysis of hydrometeorological data, the long-term data are divided into a baseline period and an abrupt change period. The meteorological data, soil data, and river data from the baseline period are used as inputs to simulate the watershed streamflow. The model parameters are calibrated by observed streamflow data. Using the well-calibrated model, the meteorological data from the abrupt change period are substituted for the original baseline period data to simulate the abrupt change period streamflow in the watershed. The quantitative relationship between the abrupt change in climate change and human activities is then analyzed.

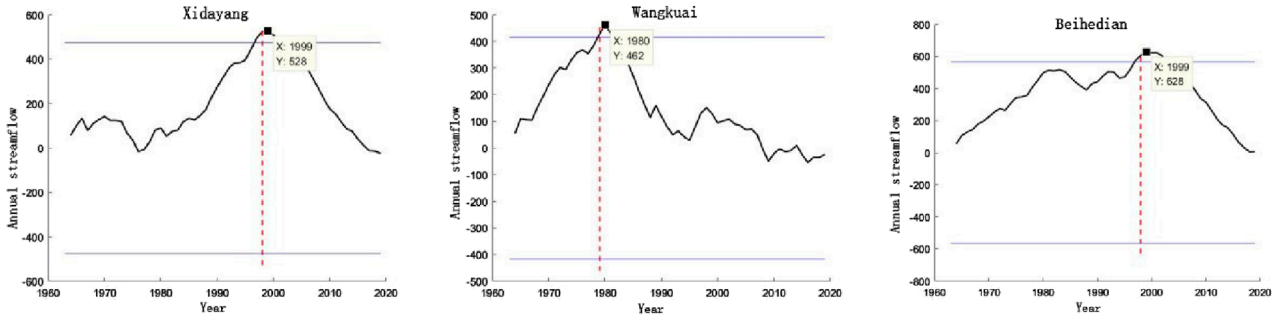

FIGURE 4
Results of abrupt change-point detection test.

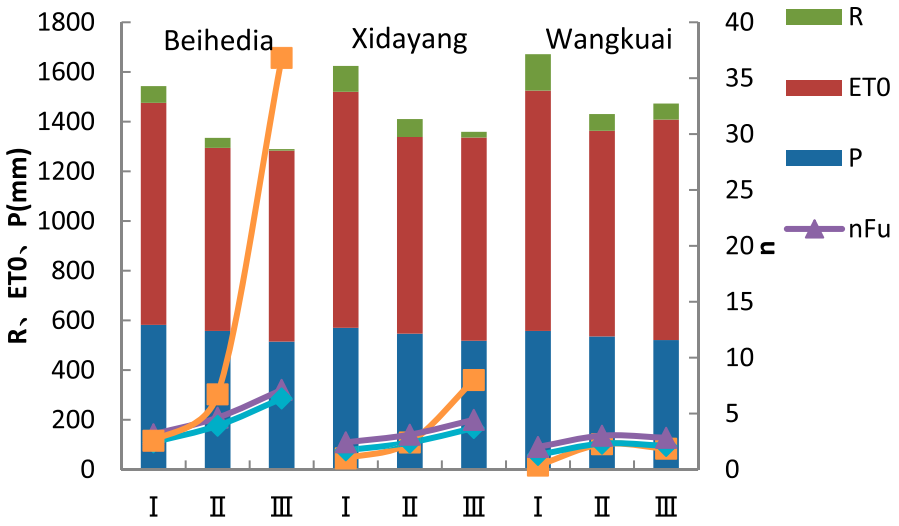

FIGURE 5
Values of hydrological elements and underlying surface parameters.

The Nash-Sutcliffe efficiency (NSE) is used as the objective function for parameter calibration. The calculation formula is as Equation 20:

$$NSE = 1 - \frac{\sum_{i=1}^{n}(Q_0 - Q_m)^2}{\sum_{i=1}^{n}(Q_0 - \overline{Q}_0)^2} \quad (20)$$

where Q_0 is the measured values; Q_m is the simulated values; $\overline{Q}_0$ is the average value of the measured values; and n is the length of the streamflow series.

The NSE quantitatively indicates the goodness-of-fit of the entire modeling process and serves as a dimensionless statistical parameter to assess the accuracy of the simulated values compared to the measured values. An NSE value of 1 indicates a perfect match between the simulated values and the measured values. If NSE is negative, it indicates that the credibility of the model's simulated values is lower than that of directly using the measured average value.

3 Results

3.1 Trend Analysis Results

An overall decreasing trend in streamflow depth, precipitation, and PET for the three watersheds over the past 60 years can be obtained in Figure 2. The decreasing trends for the three variables are consistent across the different watersheds, indicating a high degree of similarity. The interannual variation range of streamflow depth varies between 3.97 and 404.33 mm, 9.20–338.07 mm, and 0–176.03 mm, indicating significant fluctuations and differences between wet and dry seasons (Figure 2). For example, in the control watershed of Xidayang Reservoir Station, the maximum streamflow depth occurred in 1964 with a value of 338.07 mm, while the minimum streamflow depth was recorded in 2008 with a value of 9.20 mm (Figure 2). The overall decrease rate of precipitation was the lowest, ranging from −1.09 to −0.55 mm/a. The decrease in precipitation was smaller than the decrease in streamflow depth, indicating that variables other than precipitation changes also affect streamflow reduction. On the other hand, the decrease in PET did

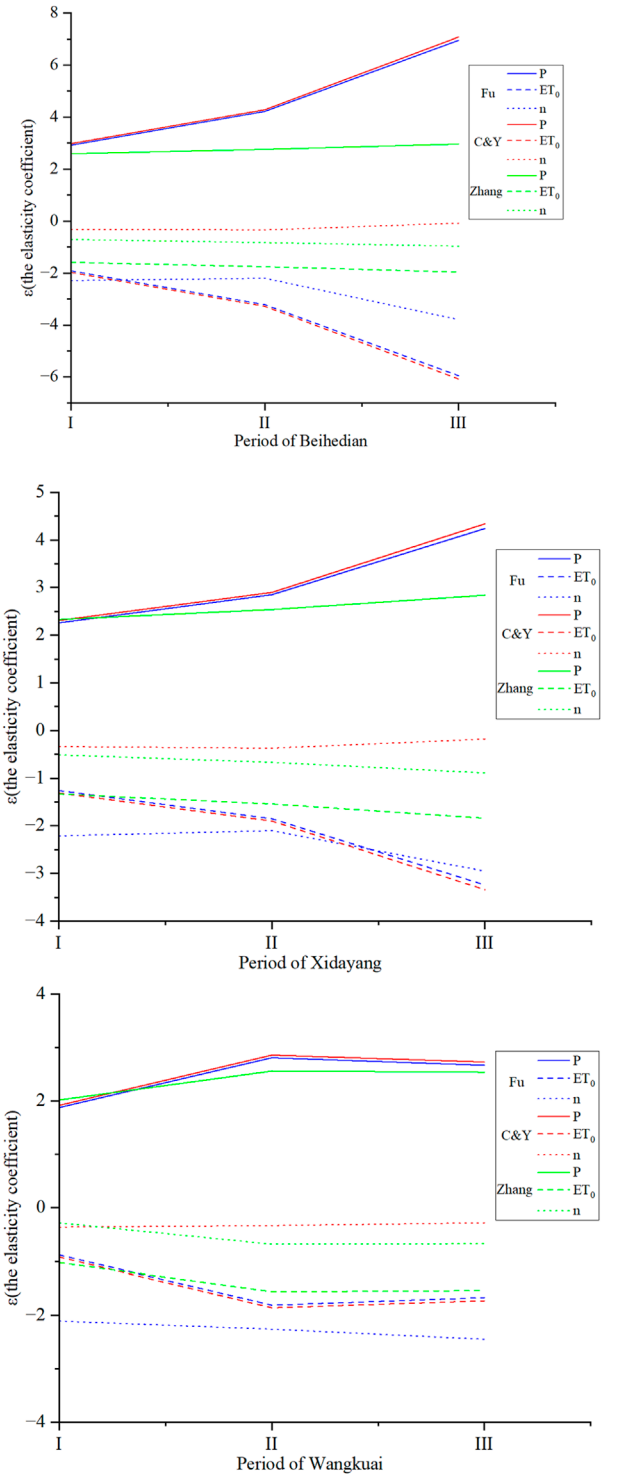

FIGURE 6
Result of sensitivity analysis.

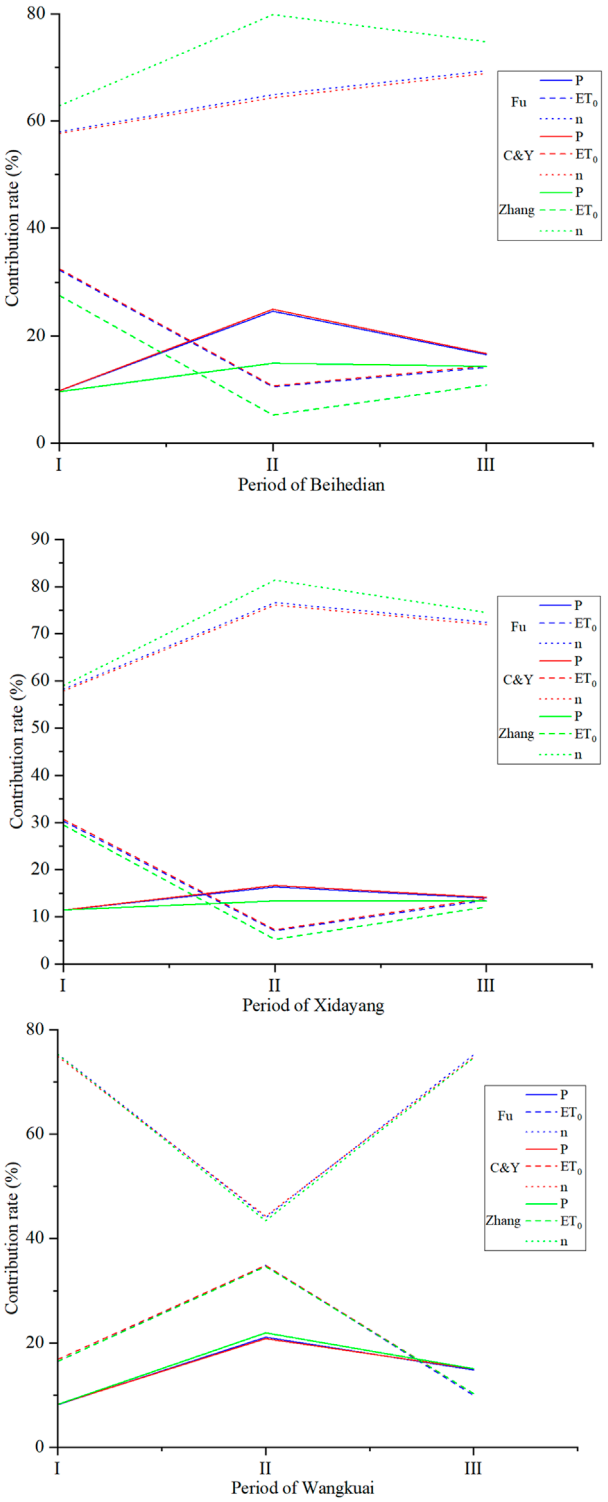

FIGURE 7
Result of quantitative analysis.

not lead to an increase in streamflow depth. This may be due to the moderate impact of a decrease in PET on streamflow when PET is greater than precipitation. The streamflow depth exhibited a decreasing trend in all three small watersheds, with decreasing rates of −1.76 mm/a, −1.97 mm/a, and −1.32 mm/a, respectively.

The Z-values obtained from the Mann-Kendall test for streamflow, precipitation, and PET in the three watersheds are all less than 0 (Table 2; Figure 3). This indicates that all variables exhibit a decreasing trend, which is consistent with the results

TABLE 3 Sensitivity of runoff to precipitation, PET, and underlying surface parameters.

Small watershed	Time interval	Fu			Choudhury&Yang			Zhang		
		ε_p	ε_{ET0}	ε_n	ε_p	ε_{ET0}	ε_n	ε_p	ε_{ET0}	ε_n
Beihedian	1963–1979	2.92	−1.92	−2.29	2.98	−1.98	−0.32	2.59	−1.59	−0.71
	1980–1998	4.22	−3.22	−2.20	4.28	−3.28	−0.34	2.76	−1.76	−0.83
	1999–2019	6.95	−5.95	−3.79	7.08	−6.08	−0.08	2.96	−1.96	−0.97
Xidayang	1963–1979	2.26	−1.26	−2.21	2.31	−1.31	−0.34	2.33	−1.33	−0.51
	1980–1998	2.85	−1.85	−2.10	2.90	−1.90	−0.37	2.54	−1.54	−0.67
	1999–2019	4.24	−3.24	−2.95	4.34	−3.34	−0.18	2.84	−1.84	−0.89
Wangkuai	1963–1979	1.88	−0.88	−2.11	1.92	−0.92	−0.36	2.02	−1.02	−0.28
	1980–1998	2.81	−1.81	−2.26	2.86	−1.86	−0.33	2.56	−1.56	−0.68
	1999–2019	2.67	−1.67	−2.45	2.73	−1.73	−0.28	2.54	−1.54	−0.67

TABLE 4 Contribution rates of climate change and human activities to runoff.

Study area	Base period	Mutation period	FU(%)			Choudhury&Yang (%)			Zhang (%)		
			ΔR_P	ΔR_{ET_0}	ΔR_n	ΔR_P	ΔR_{ET_0}	ΔR_n	ΔR_P	ΔR_{ET_0}	ΔR_n
Beihedian	1963–1979	1980–1998	9.75	32.27	57.98	9.77	32.53	57.70	9.59	27.55	62.86
	1980–1998	1999–2019	24.61	10.47	64.92	24.97	10.67	64.36	14.90	5.24	79.86
	1963–1979	1999–2019	16.51	14.12	69.38	16.70	14.40	68.90	14.33	10.85	74.81
Xidayang	1963–1979	1980–1998	11.43	30.31	58.26	11.43	30.68	57.88	11.49	29.47	59.03
	1980–1998	1999–2019	16.34	7.06	76.60	16.65	7.25	76.10	13.37	5.23	81.40
	1963–1979	1999–2019	13.99	13.55	72.46	14.17	13.89	71.95	13.34	12.12	74.54
Wangkuai	1963–1979	1980–1998	8.17	16.46	75.38	8.23	16.85	74.92	8.21	16.47	75.32
	1980–1998	1999–2019	21.09	34.87	44.04	20.83	34.87	44.30	21.93	34.66	43.41
	1963–1979	1999–2019	14.82	9.95	75.23	15.02	10.28	74.70	15.05	10.31	74.63

obtained from the linear propensity estimation method. At the same time, it further demonstrates that the results of linear propensity estimation are reasonable and reliable. Additionally, the PET in all three watersheds shows a significant decreasing trend and passes the significance test at a confidence level of 99% (Table 2). The decreasing trend in runoff depth in the Wangkuai River watershed is lower compared to the other two watersheds, only passing the significance test at a confidence level of $P < 0.05$ (Table 2). This indicates that the degree of runoff reduction in the Wangkuai Reservoir watershed during the study period was not as severe as the other two watersheds. However, the decreasing trend in annual precipitation is not significant and does not pass the significance test. Therefore, the annual precipitation in the three river basins did not decrease continuously during the study period, but instead showed alternating periods of high and low rainfall (Figure 3). Furthermore, the Cv of runoff depth, precipitation, and evapotranspiration are similar among the three basins. This also shows the fluctuation levels of the variables in the three watersheds are similar, indicating a high level of consistency among the watersheds.

3.2 Change-point Analysis Results

The Pettitt abrupt change-point detection test was applied to detect the abrupt change points in the annual streamflow series of the Xidayang Reservoir Hydrological Station, Wangkuai Reservoir

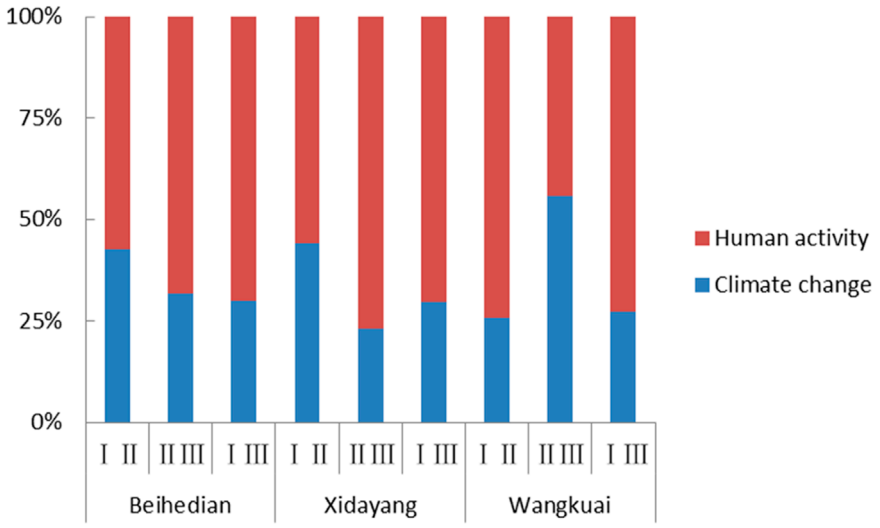

FIGURE 8
Proportion of climate change and human activities impact obtained by hydrological simulation method.

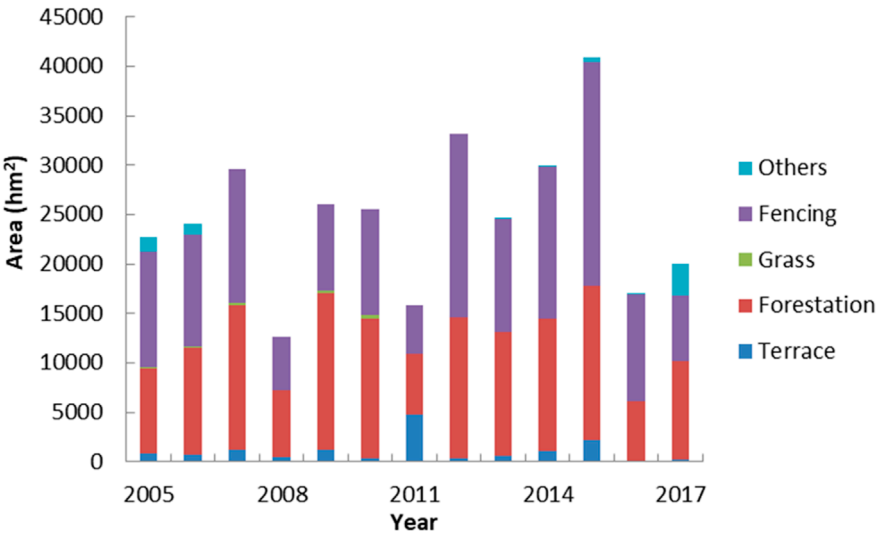

FIGURE 9
Completion status of various treatment measures.

Hydrological Station, and Beihedian Hydrological Station from 1963 to 2019. The Pettitt statistic for the Xidayang Reservoir Station and Beihedian Station fluctuated and increased before 1999 but decreased afterward, reaching a significant level of α=0.05 (Figure 4). This indicates that both stations experienced a significant change point around 1999. On the other hand, the streamflow series of the Wangkuai Reservoir Station showed a significant change point around 1980 (Figure 4). This could be attributed to the implementation of land system reforms and the construction of the Three-North Shelterbelt Forest Program in China during the mid to late 1970s (Huang, 2018). These initiatives led to improved forest quality in the watershed, significantly increased vegetation coverage, and enhanced plant transpiration. Combined with the effects of meteorological conditions such as precipitation and temperature, these factors contributed to the decrease in watershed streamflow. Therefore, the derived change points in the watershed streamflow are considered reasonable, and the results of the abrupt change-point detection test are consistent with those of relevant studies, confirming the reliability of the conclusions.

Based on the analysis of the change points in the three hydrological stations, the years 1980 and 1999 were selected as the change years. The period 1963–1979 (Period I) was designated as the natural baseline period. During this period, the hydrometeorological variables were relatively stable and there was minimal human interference that could impact streamflow. The period 1980–2019 represented the period of human activities'

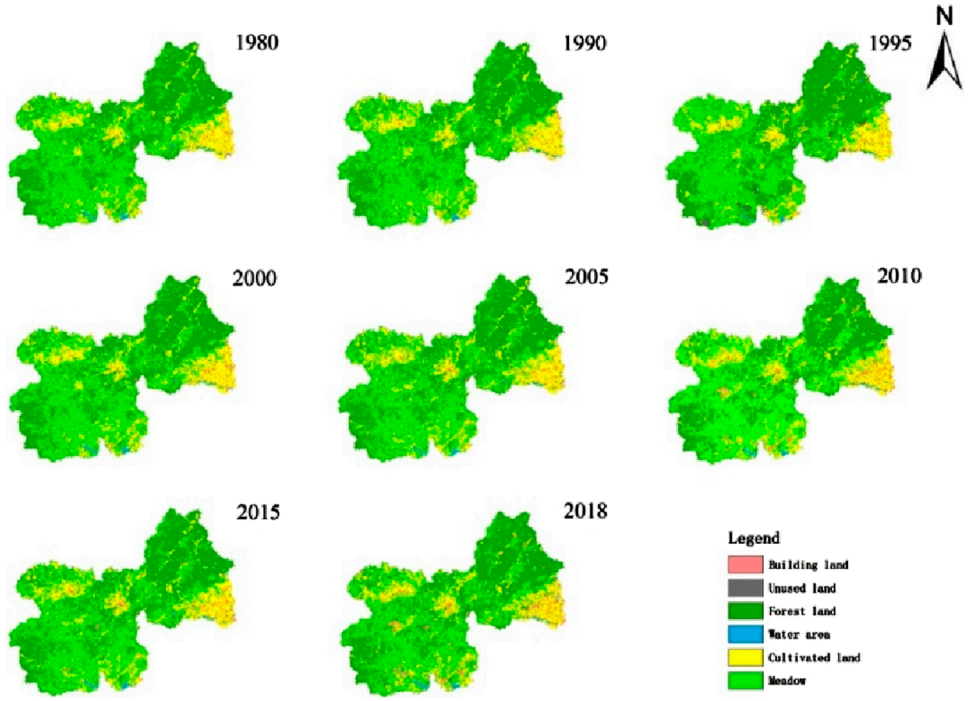

FIGURE 10
Completion status of various treatment measures.

influence on streamflow and was further divided into two periods: 1980–1998 (Period II) and 1999–2019 (Period III). These periods experienced intense human activities such as water conservancy construction, afforestation, and increased water consumption, which resulted in significant disturbances to the streamflow.

In this study, an analysis was conducted based on these three periods, and the values of hydro-meteorological variables within each period are shown in Figure 5. The results demonstrate a high level of consistency among the three methods. The parameter n, representing the underlying surface, shows an increasing trend in all three watersheds. This trend is particularly pronounced in the Beihedian River watershed, where the change from Period II to Period III is most significant. This indicates that the impacts of human activities such as water conservancy projects and afforestation on streamflow have been progressively intensifying year by year.

3.3 Calculation results from the elasticity coefficient method

3.3.1 Sensitivity analysis

The sensitivity of streamflow depth to precipitation, PET, and underlying surface parameters is analyzed by three methods based on the Budyko Hypothesis. In this study, the elasticity coefficient ε_x is employed to quantitatively characterize the sensitivity of streamflow depth to these variables.

It is evident that precipitation is positively correlated with streamflow, while PET and underlying surface parameters are negatively correlated with streamflow (Table 3, Figure 6). Taking the calculation results based on Zhang Lu's empirical formula as an example, for the Beihedian River watershed, a 10% increase in baseline precipitation corresponds to a 25.9% increase in streamflow depth, while a 10% decrease in PET and underlying surface parameters corresponds to a 15.9% and 7.1% increase in streamflow depth, respectively. Furthermore, the sensitivity of streamflow depth to both precipitation and PET in the Beihedian River watershed increases over time. The precipitation sensitivity coefficient increases from 2.92 to 6.95 and the PET sensitivity coefficient increases from 1.92 to 5.95. Similar patterns were observed in the Xidayang Reservoir watershed, where the sensitivity of streamflow depth to precipitation and Pet also increases over time. The precipitation sensitivity coefficient increases from 2.62 to 4.24 and the PET sensitivity coefficient increases from 1.26 to 3.24. In contrast to the above two watersheds, the Wangkuai Reservoir watershed exhibits an initially significant enhancement and then a slight weakening in the sensitivity of streamflow depth to precipitation and PET over time.

Regarding the elasticity coefficients of streamflow depth to underlying surface parameters in the three watersheds, there are discrepancies among the calculation results obtained from the three methods (Table 3, Figure 6). Notably, the calculation results based on the Choudhury-Yang Formula exhibit an opposite trend compared to the other methods. However, the overall observation of a weak increasing tendency in sensitivity indicates the increasing influence of human activities on streamflow variations.

3.3.2 Quantitative analysis

Based on the results of the abrupt change-point detection test for streamflow depth in the three watersheds, the study period is divided into three periods: before 1980, after 1999, and between 1980 and

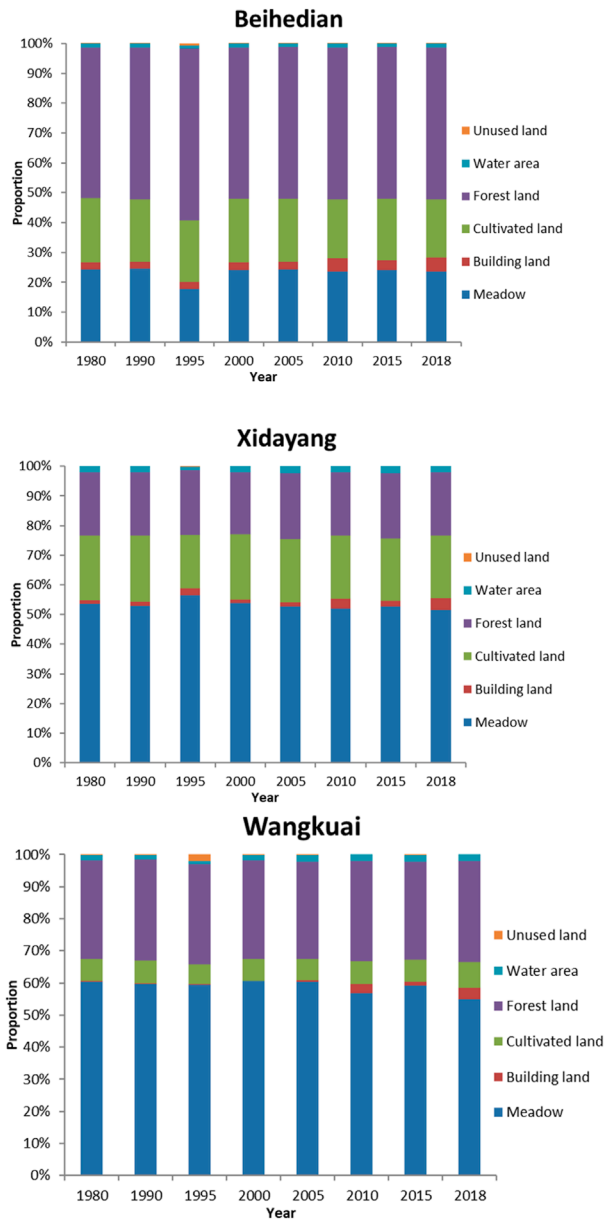

FIGURE 11
Proportion of land use types in different watersheds.

1999. Using formulas and three water balance equations based on the Budyko Hypothesis, the contribution rates of P, ET_0 and n to the changes in streamflow depth are calculated.

Analysis of the data in Table 4, Figure 7 indicates that the results obtained from the three methods are relatively consistent, demonstrating a certain level of reliability. The impact of human activities on streamflow in the Beihedian River watershed is found to be above 57% and shows an increasing trend overall. In the Xidayang Reservoir watershed, the impact of human activities is higher compared to the other two watersheds, with the contribution rates in the order of Periods II and III, I and III, and I and II (Table 4, Figure 7). Moreover, the impact of human activities is more pronounced in Period III compared to Period II. Since the year 2000, the intensification of human activities has led to a rapid decrease in streamflow. In contrast to the other two watersheds, the Wangkuai Reservoir watershed shows a lower contribution rate of human activities to streamflow, with the contribution rates in the order of Periods I and II, I and III, and II and III. The decreasing role of human activities in reducing streamflow has become weaker over time in this watershed.

3.4 Calculation results from the hydrological simulation method

In this study, the WATLAC hydrological model is employed to simulate three small watersheds within the study area at a spatial scale of 1 km and a daily time scale. Taking the Beihedian River watershed as an example for Periods I and II, the watershed data from Period I was used to build the model. The model was calibrated and parameterized using measured data, and the calibration results showed an NSE of 0.74 for this period, indicating a high accuracy and reliability of the model. To quantitatively assess the impacts of climate change and human activities on streamflow, the watershed data from Period II was used as input for the calibrated model to simulate the daily streamflow volume for that period. The difference between the simulated streamflow for Periods I and II was then calculated to represent the contribution of climate change to streamflow, and the contribution rate of human activities was determined accordingly.

Human activities have a significant influence in all three watersheds. Except for Periods II and III in the Wangkuai Reservoir watershed, human activities accounted for more than 50% of the influence on watershed streamflow in all three watersheds during the different periods. Particularly in the Xidayang Reservoir Basin during Periods II and III, human activities accounted for approximately 75% of the influence, far exceeding the 25% attributed to climate change's impact on watershed streamflow (Figure 8).

4 Discussion

4.1 Attribution analysis of precipitation runoff process

The formation and evolution of precipitation-streamflow processes are comprehensive processes influenced by a complex interplay between natural and human activities. These processes are affected by a multitude of factors. From the perspective of human activities, their impact on surface streamflow can be categorized into direct and indirect effects. The direct effects include activities such as water consumption, water induction projects, water diversion projects, and the construction of reservoirs (Shakarami et al., 2023).

The indirect effects primarily manifest in changes to the underlying surface of the watershed. Changes in land use types and alterations in vegetation cover can modify surface roughness (Bronstert et al., 2002; Zhang et al., 2007). These modifications can have profound effects on processes such as watershed streamflow yield, concentration, and evapotranspiration (Sterling et al., 2013; Xin et al., 2019). Such changes have significant implications for regional and even global water cycling processes and variations in water resources. Therefore, it is important to analyze

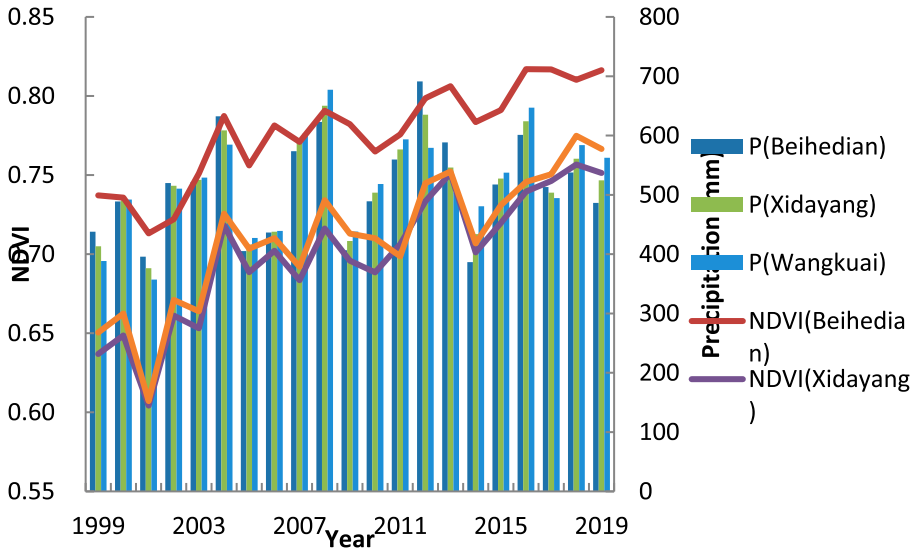

FIGURE 12
Changes in NDVI and precipitation in various watersheds.

the four aspects of human activities that have a significant impact on human activities: soil erosion control, changes in land use types, changes in the fraction of vegetation cover (FVC), and changes in water consumption. This analysis will help clarify the causes of variations in streamflow.

Due to the combined effects of natural factors and human socioeconomic activities, severe soil erosion occurs in the mountainous area of the Daqing River Basin. It results in damage to water and soil resources as well as loss of land productivity. The watershed experiences frequent disasters such as heavy rainstorms, floods, dust storms, and sandstorms. For example, in 2005, the city of Baoding had a total area of soil erosion of 6,180 km^2, with moderate to severe erosion accounting for 72% of this area. Soil erosion is severe in the region. To improve the current ecological environment, various soil and water conservation measures were implemented in the city, including terracing, afforestation, grass planting, and the closure and management of degraded land. The status of these treatment measures can be seen in Figure 9. In 2020, the area affected by soil erosion in Baoding decreased to 4,345.96 km^2, with moderate to severe erosion covering 3.6% of this area. The area of soil erosion decreased by 1.27% compared to 2019 and by 29.68% compared to 2005, indicating significant effectiveness in soil and water conservation efforts (Figure 9). On one hand, soil and water conservation measures improve soil structure and result in increased soil porosity. This allows for greater infiltration depth and prolonged infiltration time, which in turn can intercept streamflow. On the other hand, these measures enhance the watershed's flood control and water storage capacity, thus affecting the collection of surface streamflow and increasing effective evaporation, thereby reducing the volume of river streamflow.

In order to visually demonstrate the impact of soil and water conservation measures on land use and vegetation cover in the watershed, an analysis of land use types from 1980 to 2019 was conducted for the typical years. Figures 10, 11 illustrate the spatial distribution changes of different land use types in the watershed and their respective area proportions. It is evident that the main land use types in the study area are grassland, forestland, and farmland. Comparing Period III with Period II, there was a decrease in the area of farmland, grassland, and unused land, accompanied by an increase in forestland, which became the dominant land use type in the watershed. This change can be attributed to large-scale deforestation and cultivation on slopes that occurred from the late 1950s to the early 1960s, resulting in significant alternations to land use and damage to natural vegetation. Since the late 1970s, extensive soil and water conservation projects have been implemented in the watershed. In the early 1980s, largescale afforestation campaigns were carried out, leading to an increase in the forestland area within the watershed. The expansion of forestland played a significant role in water conservation by enhancing soil water retention capacity and reducing surface streamflow volume. In the rainy season, a portion of rainfall may be converted into underground streamflow. These measures had a positive effect on controlling flood and maintaining river flow during the dry season, increasing the low-flow volume and ensuring stable river discharge. However, it is important to note that the study area has deep soil layers and belongs to a semiarid region where vegetation transpiration consumes a significant amount of water. Therefore, the regulating effect of forest vegetation on river flow during the dry season is limited. In fact, during the dry season, vegetation can further intercept and retain streamflow by absorbing soil moisture through root growth. This can lead to drier soil conditions and increased storage of precipitation, further exacerbating the impact on streamflow.

Under the influence of human activities, changes occur in soil erosion, land use types, etc., thereby affecting the values of underlying surface parameters (Jiang et al., 2015). Among these parameters, the underlying surface parameter n is mainly influenced by factors such as vegetation, soil, and topography, while the variability of soil properties and topography within the watershed is relatively weak over a short period. Changes in the underlying surface parameters are mainly related to vegetation. Therefore, NDVI is selected as a

parameter to reflect vegetation growth status and analyze the impact of human activities and climate change on the underlying surface. It exhibits a linear relationship with chlorophyll density and vegetation productivity. And precipitation plays a very important role in the growth process of plants, so we simply consider precipitation as a factor in climate change. Figure 12 displays the changes in NDVI and precipitation. It can be observed that the overall NDVI values are relatively small with significant fluctuations but show an upward trend. Although both climate change and human activities can contribute to changes in underlying surface conditions, the increase in NDVI within the watershed is primarily influenced by human activities due to the insignificant changes in precipitation.

In the early 1980s, China implemented land reform policies, which encouraged farmers to increase agricultural activities to boost agricultural production. This resulted in a significant increase in grain output. However, water productivity remained relatively unchanged. As a consequence, there was an increase in agricultural water usage (Hu et al., 2012). Taking the city of Baoding as an example, the irrigated area was 6,573.33 km^2 in 2008, four times that of the early days of the People's Republic of China and twice that of 1957. Despite this expansion, large-scale flooding irrigation practices persist in the watershed, with a lack of water-saving measures. To meet irrigation needs, a large amount of groundwater is extracted, leading to the formation of extensive, deep underground cones of depression. This increases the extent of the unsaturated zone in the soil and its water storage capacity, thereby reducing streamflow formation. Furthermore, the significant decline in groundwater levels increases the hydraulic gradient between surface water and groundwater, leading to increased infiltration and further reducing the volume of surface streamflow.

The explosive growth of urban, industrial, mining, and residential land from 2000 to 2018 (Figure 11) indicates an accelerated pace of urbanization and rapid socioeconomic development. The proportion of industrial land is continuously rising, reflecting higher levels of urbanization. With the increase in population. and the demand for domestic and industrial water, the main water supply methods are through water diversion projects and groundwater extraction. However, engineering water induction directly reduces the flow in river channels, leading to a decline in surface streamflow. Moreover, the conversion of urban development land to impermeable hardened surfaces results in a rapid increase in surface streamflow and evaporation loss during heavy rainfall events, further reducing streamflow volume.

Based on the findings of this study, the following recommendations are proposed for the sustainable utilization and management of water resources in the watershed: In the field of agriculture, it is important to strengthen regulations on total water usage and efficiency, adjust planting structures, and actively promote water-saving technologies such as drip and sprinkler irrigation, while gradually advancing industrial upgrades. In the industrial sector, efforts should be closely aligned with industrial layout and urban planning, aiming to phase out high-water-consumption and heavily polluting enterprises, and to improve industrial water efficiency and recycling rates. In urban development, there should be a strong emphasis on promoting public water conservation initiatives, enhancing water quota management, and implementing water-saving measures for urban residents.

5 Conclusion

This study focuses on three small watersheds in the upstream mountainous areas of the Daqing River Basin. Attribution analysis of streamflow changes was conducted from the perspectives of climate change and human activities. The main factors influencing streamflow changes in the watershed were explored. The conclusions are as follows:

(1) From 1963 to 2019, a significant decreasing trend was observed in both the annual streamflow depth and PET across the Beihedian River, Xidayang Reservoir, and Wangkuai Reservoir watersheds. The magnitude of the decrease was similar among these watersheds, indicating a high level of consistency. However, the decreasing trend in annual precipitation was not significant and did not pass the significance test.

(2) The streamflow series in the Wangkuai Reservoir and Beihedian River watersheds exhibited significant change points in 1999, whereas the streamflow series in the Xidayang Reservoir watershed experienced a significant change point in 1980. These change points may be related to the implementation of land system reforms and the construction of the Three-North Shelterbelt Forest Program in the mid to late 1970s.

(3) Based on the elasticity coefficient method and hydrological simulation method, consistent results were obtained: the average contribution rates of climate change to streamflow reduction in the three small watersheds were 32.93%, 34.50%, and 35.12%, respectively, while the average contribution rates of human activities were 67.07%, 65.50%, and 64.88%, respectively. Climate change has led to a reduction in streamflow volume in the watershed to some extent, but the primary reason for water resource depletion in the watershed is still the excessive interference of human activities.

Data availability statement

The raw data supporting the conclusions of this article will be made available by the authors, without undue reservation.

Author contributions

ZL: Data curation, Formal Analysis, Validation, Visualization, Writing–original draft, Writing–review and editing. WC: Conceptualization, Data curation, Formal Analysis, Methodology, Writing–review and editing. LW: Conceptualization, Formal Analysis, Methodology, Writing–review and editing.

Funding

The author(s) declare that financial support was received for the research, authorship, and/or publication of this article. This study was funded by the National Natural Science Foundation of China Regional Innovation and Development Joint Fund (U23A2001) and the Major

Science and Technology Program for Water Pollution Control and Treatment (2018ZX07110001).

Conflict of interest

The authors declare that the research was conducted in the absence of any commercial or financial relationships that could be construed as a potential conflict of interest.

Publisher's note

References

Bronstert, A., Niehoff, D., and Bürger, G. (2002). Effects of climate and land-use change on storm runoff generation: present knowledge and modelling capabilities. *Hydrol. Process.* 16, 509–529. doi:10.1002/hyp.326

Budyko, M. (1974). *Climate and life*. New York, NY: Academic Press.

Cheng, D. M., Liu, X. H., Zhao, S. N., Cui, B. S., Bai, J. H., and Li, Z. j. (2017). Influence of the natural colloids on the multiphase distributions of antibiotics in the surface water from the largest lake in North China. *Sci. Total Environ.* 578, 649–659. doi:10.1016/j.scitotenv.2016.11.012

Chien, H. C., Yeh, P. J. F., and Knouft, J. H. (2013). Modeling the potential impacts of climate change on streamflow in agricultural watersheds of the Midwestern United States. *J. Hydrol.* 491 (1), 73–88. doi:10.1016/j.jhydrol.2013.03.026

Choudhury, B. (1999). Evaluation of an empirical equation for annual evaporation using field observations and results from a biophysical model. *J. Hydrol.* 216 (1-2), 99–110. doi:10.1016/S0022-1694(98)00293-5

Dai, G. H., Liu, X. H., Liang, G., Han, X., Shi, L., Cheng, D. M., et al. (2011). Distribution of organochlorine pesticides (OCPs) and polychlorinated biphenyls (PCBs) in surface water and sediments from Baiyangdian Lake in North China. *J. Environ. Sci.* 23 (10), 1640–1649. doi:10.1016/S1001-0742(10)60633-X

Deng, Q. H., Zhang, X. M., Zhang, L. Z., Shao, X., and Gu, T. S. (2024). The impact mechanism of human activities on the evolution of coastal wetlands in the Liaohe River Delta. *Front. Ecol. Evol.* 12. doi:10.3389/fevo.2024.1423234

Du, Y., Bao, A. M., Zhang, T., and Ding, W. (2023). Quantifying the impacts of climate change and human activities on seasonal runoff in the Yongding River basin. *Ecol. Indic.* 154, 110839. doi:10.1016/j.ecolind.2023.110839

Fu, G. B., Charles, S. P., and Chiew, F. H. S. (2007). A two-parameter climate elasticity of streamflow index to assess climate change effects on annual streamflow. *Water Resour. Res.* 43 (11), 2578–2584. doi:10.1029/2007WR005890

Hu, S. S., Liu, C. M., Zheng, H. X., Wang, Z. G., and Yu, J. J. (2012). Assessing the impacts of climate variability and human activities on streamflow in the water source area of Baiyangdian Lake. *J. Geog. Sci.* 22 (5), 895–905. doi:10.1007/s11442-012-0971-9

Huang, B. B. (2018). Drive factors of surface runoff changes between 1980-2010 in the mountainous areas of Haihe Basin. Master thesis *Adv. Meteorology*.

Huang, P., Song, J. X., Cheng, D. D., Sun, H. T., Kong, F. H., Jing, K. X., et al. (2021). Understanding the intraannual variability of streamflow by incorporating terrestrial water storage from GRACE into the Budyko framework in the Qinba Mountains. *J. Hydrol.* 603, 126988. doi:10.1016/j.jhydrol.2021.126988

Jiang, C., Xiong, L. H., Wang, D. B., Liu, P., Guo, S. L., and Xu, C. Y. (2015). Separating the impacts of climate change and human activities on runoff using the Budyko type equations with time-varying parameters. *J. Hydrol.* 522, 326–338. doi:10.1016/j.jhydrol.2014.12.060

Lei, H., Yang, D., and Huang, M. (2014). Impacts of climate change and vegetation dynamics on runoff in the mountainous region of the Haihe River basin in the past five decades. *J. Hydrol.* 511, 786–799. doi:10.1016/j.jhydrol.2014.02.029

Li, J. Z., Li, Y. P., Zhang, T., and Feng, P. (2023). Research on the future climate change and runoff response in the mountainous area of Yongding watershed. *J. Hydrol.* 625, 130108. doi:10.1016/j.jhydrol.2023.130108

Li, Y. L., Tao, H., Yao, J., and Zhang, Q. (2016). Application of a distributed catchment model to investigate hydrological impacts of climate change within Poyang Lake catchment (China). *Hydrol. Res.* 47, 120–135. doi:10.2166/nh.2016.234

Li, Y. L., Zhang, Q., Tao, H., and Yao, J. (2021). Integrated model projections of climate change impacts on water-level dynamics in the large Poyang Lake (China). *Hydrol. Res.* 52 (1), 43–60. doi:10.2166/nh.2019.064

Liang, W., Bai, D., Jin, Z., You, Y., Li, J., and Yang, Y. (2015). A study on the streamflow change and its relationship with climate change and ecological restoration measures in a sediment concentrated region in the loess plateau, China. *China. Water Resour. manage.* 29 (11), 4045–4060. doi:10.1007/s11269-015-1044-5

Liu, Q., Yang, D., and Cao, L. (2022). Evolution and prediction of the coupling coordination degree of production–living–ecological space based on land use dynamics in the Daqing River Basin, China. *Sustainability* 14, 10864. doi:10.3390/su141710864

Liu, T., Huang, H. Q., Shao, M. A., Cheng, J., Li, X. D., and Lu, J. H. (2020). Integrated assessment of climate and human contributions to variations in streamflow in the ten great gullies basin of the upper yellow river, China. *J. Hydrol. Hydromech.* 68, 249–259. doi:10.2478/johh-2020-0027

Lyu, X. L., Jia, Y. W., Qiu, Y. Q., Du, J. K., Hao, C. F., Dong, H., et al. (2024). Influence of human-induced land use change on hydrological processes in semi-humid and semi-arid region: a case in the Fenhe River Basin. *J. Hydrol-Reg Stud.* 51, 101605. doi:10.1016/j.ejrh.2023.101605

Milly, P. C. D., and Dunne, K. A. (2002). Macroscale water fluxes 2. Water and energy supply control of their interannual variability. *Water Resour. Res.* 38 (10), 24. doi:10.1029/2001WR000760

Moiwo, J. P., Yang, Y. H., Li, H. L., Han, S. M., and Yang, Y. M. (2010). Impact of water resource exploitation on the hydrology and water storage in Baiyangdian Lake. *Hydrol. Process* 24 (21), 3026–3039. doi:10.1002/hyp.7716

Porporato, A., Daly, E., and Rodriguez-Iturbe, I. (2004). Soil water balance and ecosystem response to climate change. *Am. Nat.* 164 (5), 625–632. doi:10.1086/424970

Qiao, Z. X., Ma, L., Xu, Y., Yang, D. W., Liu, T. X., and Sun, B. L. (2023). Runoff change and attribution analysis in a semiarid mountainous basin. *Ecol. Eng.* 195, 107075. doi:10.1016/j.ecoleng.2023.107075

Ren, L., Xiang, X. Y., and Liu, W. L. (2017). River runoff changes in the past millennium under extreme climatic conditions in China. *Appl. Ecol. Env. Res.* 15 (4), 1157–1166. doi:10.15666/aeer/1504_11571166

Shakarami, L., Ashofteh, P. S., and Singh, V. P. (2023). Disaggregating the effects of climatic variability and dam construction on river flow regime. *Water Resour. Manag.* 36 (10), 3813–3838. doi:10.1007/s11269-022-03235-9

Song, C. Q., Ke, L. H., Pan, H., Zhan, S. G., Liu, K., and Ma, R. H. (2018). Long-term surface water changes and driving cause in Xiong'an, China:from dense Landsat time series images and synthetic analysis. *Sci. Bull.* 63 (11), 708–716. doi:10.1016/j.scib.2018.05.002

Sterling, S. M., Ducharne, A., and Polcher, J. (2013). The impact of global land-cover change on the terrestrial water cycle. *Nat. Clim. Chang.* 3, 385–390. doi:10.1038/NCLIMATE1690

Wang, D. D., Yu, X. X., Jia, G. D., and Wang, H. N. (2019). Sensitivity analysis of runoff to climate variability and landuse changes in the Haihe Basin mountainous area of north China. *Agr Ecosyst. Environ.* 269, 193–203. doi:10.1016/j.agee.2018.09.025

Wang, H. N., Lv, X. Z., and Zhang, M. Y. (2021). Sensitivity and attribution analysis based on the Budyko hypothesis for streamflow change in the Baiyangdian catchment, China. *Ecol. Indic.* 121, 107221. doi:10.1016/j.ecolind.2020.107221

Wu, J. K., Li, H. Y., Zhou, J. X., Tai, S. Y., and Wang, X. L. (2021). Variation of runoff and runoff components of the upper shule river in the northeastern qinghai–tibet plateau under climate change. *Water* 13, 3357. doi:10.3390/w13233357

Wu, J. W., Miao, C. Y., Wang, Y. M., Duan, Q., and Zhang, X. (2016). Contribution analysis of the long-term changes in seasonal runoff on the Loess Plateau, China, using eight Budyko-based methods. *J. Hydrol.* 545, 263–275. doi:10.1016/j.jhydrol.2016.12.050

Xin, Z. H., Li, Y., Zhang, L., Ding, W., Ye, L., Wu, J., et al. (2019). Quantifying the relative contribution of climate and human impacts on seasonal streamflow. *J. Hydrol.* 574, 936–945. doi:10.1016/j.jhydrol.2019.04.095

Xu, F., Yang, Z. F., Chen, B., and Zhao, Y. W. (2013). Impact of submerged plants on ecosystem health of the plant-dominated Baiyangdian Lake, China. *Ecol. Modell.* 252, 167–175. doi:10.1016/j.ecolmodel.2012.07.013

Yang, H., and Cao, J. (2021). Analysis of basin morphologic characteristics and their influence on the water yield of mountain watersheds upstream of the xiongan new area, north China. *North China. Water* 13, 2903. doi:10.3390/w13202903

Yang, H. B., Yang, D. W., Lei, Z. D., and Sun, F. (2008). New analytical derivation of the mean annual water-energy balance equation. *Water Resour. Res.* 44 (3), W03410. doi:10.1029/2007WR006135

Yang, J., Chang, J. X., Yao, J., Wang, Y. M., Huang, Q., and Xu, G. X. (2019). Impact of natural climate variability on runoff based on Monte Carlo method. *Water Clim. Change.* 10, 344–359. doi:10.2166/wcc.2017.177

Ye, X. C., Zhang, Q., Bai, L., and Hu, Q. (2011). A modeling study of catchment discharge to Poyang Lake under future climate in China. *Quat. Int.* 244 (2), 221–229. doi:10.1016/j.quaint.2010.07.004

Zeng, F., Ma, M. G., Di, D. R., and Shi, W. Y. (2020). Separating the impacts of climate change and human activities on runoff: a review of method and application. *Water* 12, 2201. doi:10.3390/w12082201

Zerizghi, T., Yang, Y., Wang, W., Zhou, Y., Zhang, J., and Yi, Y. (2020). Ecological risk assessment of heavy metal concentrations in sediment and fish of a shallow lake: a case study of Baiyangdian Lake, North China Environ. *Monit. Assess.* 192, 1–16. doi:10.1007/s10661-020-8078-8

Zhang, J., and Yu, X. L. (2021). Analysis of land use change and its influence on runoff in the Puhe River Basin. *Environ. Sci. Pollut. R.* 28, 40116–40125. doi:10.1007/s11356-020-09798-7

Zhang, L., Dawes, W. R., and Walker, G. R. (2001). Response of mean annual evapotranspiration to vegetation changes at catchment scale. *Water Resour. Res.* 37 (3), 701–708. doi:10.1029/2000WR900325

Zhang, Q., Miao, C. Y., Guo, X. Y., Gou, J. J., and Su, T. (2023). Human activities impact the propagation from meteorological to hydrological drought in the Yellow River Basin, China. *J. Hydrol.* 623, 129752. doi:10.1016/j.jhydrol.2023.129752

Zhang, Q. F., Liu, J. K., Yu, X. X., and Chen, L. H. (2019). Scale effects on runoff and a decomposition analysis of the main driving factors in Haihe Basin mountainous area. *Sci. Total Environ.* 690, 1089–1099. doi:10.1016/j.scitotenv.2019.06.540

Zhang, X., Zwiers, F. W., Hegerl, G. C., Lambert, F. H., Gillett, N. P., Solomon, S., et al. (2007). Detection of human influence on twentieth-century precipitation trends. *Nature* 448, 461–465. doi:10.1038/nature06025

Zheng, D. D., Gui, Y. H., Kuang, J., and Bing, H. (2023). Downstream Channel evolution and its causes in the yuan river during the qing dynasty. *J. Earth Sci.* 34 (4), 1263–1271. doi:10.1007/s12583-021-1600-2

Zhou, S., Yu, B. F., Huang, Y. F., and Wang, G. (2015). The complementary relationship and generation of the Budyko functions. *Geophys. Res. Lett.* 42, 1781–1790. doi:10.1002/2015GL063511

Zhou, S., Yu, B. F., Zhang, L., Huang, Y., Pan, M., and Wang, G. (2016). A new method to partition climate and catchment effect on the mean annual runoff based on the Budyko complementary relationship. *Water Resour. Res.* 52 (9), 7163–7177. doi:10.1002/2016WR019046

frontiers | Frontiers in Environmental Science

TYPE Original Research
PUBLISHED 27 November 2024
DOI 10.3389/fenvs.2024.1499757

OPEN ACCESS

EDITED BY
Celso Santos,
Federal University of Paraíba, Brazil

REVIEWED BY
Ying Zhu,
Xi'an University of Architecture and Technology, China
Shanzhong Qi,
Shandong Normal University, China

*CORRESPONDENCE
Yuchi Yang,
yangyuchiplan@outlook.com

RECEIVED 21 September 2024
ACCEPTED 13 November 2024
PUBLISHED 27 November 2024

CITATION
Yang W, Li X and Yang Y (2024) Technical framework and empirical analysis of resource and environmental carrying capacity evaluation in karst regions under the constraint of ecological civilization.
Front. Environ. Sci. 12:1499757.
doi: 10.3389/fenvs.2024.1499757

Technical framework and empirical analysis of resource and environmental carrying capacity evaluation in karst regions under the constraint of ecological civilization

Wei Yang[1,2], Xiaohua Li[1,2] and Yuchi Yang[2,3]*

[1]College of Resources and Environmental Engineering, Anshun University, Anshun, China, [2]Rural Revitalization Research Center of Guizhou Universities, Anshun, Guizhou, China, [3]School of Architecture and Urban Planning, Tongji University, Shanghai, China

Evaluating resource and environmental carrying capacity (RECC) within the framework of ecological civilization is essential for reconciling development with ecological preservation and optimizing land-use patterns. This evaluation through the lens of ecological civilization is crucial for effective resource allocation. This article introduces a technical framework specifically designed for analyzing and evaluating resource and environmental carrying capacity in karst regions, focusing on Anshun City in Guizhou Province as a case study. The framework follows a structured approach, i.e., "problem identification, problem decomposition, and decision-making assessment," which proves effective for these evaluations. Furthermore, the integrated evaluation index system incorporating resources, environment, and socioeconomic factors under the principles of ecological civilization aligns with contemporary developmental requirements while reflecting the distinctive characteristics of the resources and environment in karst regions. This alignment enhances the specificity and relevance of the evaluation methodology. The application of the obstacle degree model strengthened the utility and depth of the evaluation results. Additionally, Pearson's correlation analysis clarified the complex interrelationships among various index factors, highlighting the significant role of unique local resources in the carrying capacity of karst regions. Additionally, the article reveals a delay in the socioeconomic development of karst regions, which adversely impacts their carrying capacity. Thus, promoting regional economic growth is crucial for enhancing the overall carrying capacity. In light of these findings, the article proposes practical strategies to enhance resource and environmental carrying capacity. These include establishing technical standards for evaluation, accelerating industrial transfers focused on technological innovation, and enhancing market mechanisms for resource allocation.

KEYWORDS

resource and environmental carrying capacity evaluation, ecological civilization, analytical framework, index system, karst regions, obstacle degree model, Pearson's correlation analysis

1 Introduction

Resource and environmental carrying capacity (RECC) is essential for advancing regional ecological civilization; conversely, the establishment of ecological civilization is crucial for enhancing this carrying capacity. The concept of ecological civilization represents a key path toward sustainable socioeconomic development in China, tackling challenges such as resource depletion, environmental pollution, and ecological imbalance stemming from rapid industrialization and urbanization. Promoting green development and fostering harmonious coexistence between humans and nature are pivotal strategies for China's socioeconomic progress in the contemporary era. Major initiatives include deepening ecological civilization, aiming for carbon neutrality and carbon peaking emissions, and refining the market allocation system for resource and environmental management. These initiatives serve as fundamental principles for national planning and sustainable development. Evaluating resource and environmental carrying capacity in the context of ecological civilization is essential for achieving sustainable and high-quality socioeconomic transformation in regions. This approach ensures the alignment of economic and social development with ecological protection and optimizes regional resource allocation while safeguarding natural and cultural heritage. In recent years, the evaluation of resource and environmental carrying capacity has increasingly become a fundamental consideration in regional development strategies (Huang and Song, 2019). The outcomes of these evaluations have been utilized in land planning, urban development, and regional economic strategies (Huang, 2017; Fan, 2007), providing valuable theoretical frameworks for optimizing regional land use and resource management.

The concept of RECC has significantly evolved since its inception. Initially, carrying capacity referred to biological populations, defined by Park and Burgess (1921) as the population size an environment can support under specific conditions. Malthus (1978) expanded this idea, proposing that unchecked population growth would outpace food production, causing famines. However, the RECC concept has since been expanded to include ecological, resource, and environmental capacities, referring to the sustainable population or activity level that an ecosystem can support while maintaining ecological balance (Sun et al., 2020). Recent studies have divided RECC into several subdomains: (1) resource carrying capacity (RCC), which focuses on land, water, and mineral resources. The RCC assesses resource availability to support human activity without degradation (Liu et al., 2023). (2) Environmental carrying capacity, which is the environment's capacity to absorb pollutants and waste while sustaining ecosystem health (Gao et al., 2020). (3) Ecological carrying capacity relates specifically to ecological system resilience and biodiversity maintenance capacity (Niu et al., 2020). These definitions underscore RECC as a multi-dimensional concept that integrates physical resource limitations with ecological resilience and environmental quality (Liu et al., 2020; Niu et al., 2020). Evaluating RECC necessitates moving from single-factor to multi-factor assessment models, incorporating land, water, climate, and ecological health metrics. Resource and environmental carrying capacity synthesizes these concepts (Sun et al., 2020) and indicates the maximum population that a region can support while preserving optimal natural conditions and ecological balance (Niu et al., 2018). Research in developing evaluation systems has shifted from single-factor to multi-factor assessments (Shen et al., 2022). Scholars have deepened the principles, content, and perspectives of indicators, resulting in studies focused on various factors such as land, water, and ecological conditions (Liu et al., 2023; Gao et al., 2020). Research has encompassed both single-factor (Yang and Wang, 2022) and comprehensive assessments of carrying capacity (Shao et al., 2013; Yang et al., 2016). Additionally, studies have also varied in spatial scale, addressing evaluations at national, provincial, and urban levels (Wang J. et al., 2023; Luo et al., 2022), contributing to the development of assessment systems that incorporate factors such as water, climate, and land (Feng et al., 2021; Zhang et al., 2018; Yang et al., 2015; Liu and Borthwick, 2011).

Various methodological approaches are key to evaluating RECC, each suited to specific ecological complexities, data availability, and geographic requirements. These methods offer unique advantages in understanding RECC, particularly in ecologically sensitive, resource-limited karst regions. Comprehensive assessments integrate resource, environmental, and ecological data into composite RECC scores, providing policymakers with a holistic view of carrying capacity (Wang and Wang, 2022). System dynamics models analyze interactions between ecological, economic, and social factors and are effective for long-term, predictive assessments (Wang M. et al., 2023; Ge et al., 2021). These models are suitable where complex feedback loops and time-dependent changes are vital for understanding sustainability trends in karst landscapes. The ecological footprint method quantifies natural resource demand relative to regional supply and is particularly valuable in high-stress areas like karst regions (Liu et al., 2022; Jia et al., 2020). This method allows researchers to determine whether a region's resource consumption aligns with its regenerative capacity, making it highly applicable for comparative studies in stressed environments. Fuzzy evaluation models incorporate qualitative data and account for uncertainties, making them suitable for RECC evaluation in ecologically complex regions with limited data (Min et al., 2022; Tan et al., 2021). Fuzzy models' adaptability is advantageous in karst areas, where data precision is often challenging and uncertainty requires effective management. Advances in remote sensing and GIS now provide high-precision spatial data, enabling the detailed mapping of resource distributions and environmental impact zones (Peng et al., 2020). The barrier degree model critically identifies and assesses primary factors limiting regional RECC. This model quantifies obstacle factors, pinpointing issues that hinder sustainable resource management and environmental protection, particularly under ecological civilization constraints (Zhang et al., 2018; Lin et al., 2023). The model uses a structured approach, using indicators like urbanization rate, wastewater discharge, and resource use efficiency to calculate an "obstacle degree." A high barrier degree suggests major challenges to sustainable RECC, while a low degree indicates fewer obstacles (Chen et al., 2023). By identifying these barriers, the model aids policymakers in targeted interventions to strengthen resource and environmental resilience in karst and other fragile regions. Pearson's correlation analysis determines linear relationships between key RECC indicators, providing insights into dependencies among resource, environmental, and socioeconomic factors. In karst regions, Pearson's analysis reveals

associations between land-use intensity and water resource availability, aiding in identifying leverage points for enhancing RECC (Wu and Hu, 2020). However, its linearity assumption limits it, potentially missing complex, non-linear relationships in ecological systems, suggesting a need for complementary analyses (Wei et al., 2019). These methodologies enable adaptive, region-specific RECC assessments, addressing unique geographic, ecological, and resource constraints. This variety of approaches supports sustainable policy formulation, allowing researchers to select the most suitable tools based on study requirements and regional ecological characteristics.

Scholars have delineated various terms such as resource carrying capacity, environmental carrying capacity, ecological carrying capacity, and land and water resource carrying capacities (Liu et al., 2020; Niu et al., 2020; Niu et al., 2018). The concept of carrying capacity was first articulated by Park in 1921, who defined it as the maximum number of biological individuals that an environment can sustain under specific conditions (Park and Burgess, 1921), laying the groundwork for further exploration. Malthus (1978) later proposed a population growth model that indicated that famines and poverty would arise when the population exceeded the limits of food supply. Resource and environmental carrying capacity is a comprehensive synthesis of these concepts (Sun et al., 2020) and indicates the maximum population that can be supported in a region while maintaining an optimal natural environment and ecological balance (Niu et al., 2018). Research in developing evaluation systems has shifted from single-factor to multi-factor assessments (Shen et al., 2022). Scholars have deepened the principles, content, and perspectives of indicators, resulting in studies focused on various factors such as land, water, and ecological conditions (Liu et al., 2023; Gao et al., 2020). Research has encompassed both single-factor (Yang and Wang, 2022) and comprehensive assessments of carrying capacity (Shao et al., 2013; Yang et al., 2016). Additionally, studies have also varied in spatial scale, addressing evaluations at national, provincial, and urban levels (Wang J. et al., 2023; Luo et al., 2022), contributing to the development of assessment systems that incorporate factors such as water, climate, and land (Feng et al., 2021; Zhang et al., 2018; Yang et al., 2015; Liu and Borthwick, 2011). Researchers have also adopted diverse evaluation methods and models to meet different objectives, including comprehensive assessments (Wang J. et al., 2023; Wang and Wang, 2022), system dynamics (Wang M. et al., 2023; Ge et al., 2021; Yang et al., 2015), ecological footprints (Liu et al., 2022; Jia et al., 2020), fuzzy evaluations (Min et al., 2022; Tan et al., 2021), and energy value analysis. Recent studies, including those by Peng et al. (2020), have utilized remote sensing and GIS technology to conduct comprehensive evaluations in the karst regions of Southwest China.

Existing research in the field encompasses a wide range of aspects, including concepts, frameworks, indicator systems, evaluation methods, and models, yet several challenges persist. Existing assessment indicator systems often lack specificity, especially for karst regions, where limited studies fail to sufficiently highlight the region's unique characteristics. Moreover, the presentation of evaluation results is often insufficient, and a deeper analysis of factors influencing the regional carrying capacity and their interrelationships requires further exploration. Additionally, there is also a disconnection between current analyses and the realities of modern societal development. This highlights the necessity for a comprehensive evaluation framework specifically tailored to the distinct attributes of karst regions as this is crucial for enhancing the theoretical and methodological foundations of resource and environmental carrying capacity evaluations. In summary, although a relatively comprehensive theoretical framework for resource and environmental carrying capacity has been established (Li et al., 2022), karst regions encounter distinct challenges in this evaluation due to their unique geological and ecological conditions. Future studies should further integrate the concept of ecological civilization and deepen theoretical and empirical investigations of resource and environmental carrying capacity in karst regions, with the aim of providing more scientifically grounded guidance for sustainable development in these regions.

Karst regions are characterized by expansive landscapes, unique geological environments, ecological sensitivity, and constrained resource endowments. Although industrialization, urbanization, transportation, and tourism contribute to regional economic growth, they also result in significant land-use disruptions, severe ecological degradation, and escalating resource constraints. The growing conflicts between ecological preservation, development needs, and the conservation of natural and cultural heritage expose the limitations of current human activities. Consequently, it is essential to establish an analytical framework that accurately captures the distinctive characteristics of karst regions. This article focuses on this important area, specifically examining Anshun City in Guizhou, which exemplifies a karst region. Utilizing 2019 as the evaluation timeframe and county units as the fundamental evaluation units, the article uses qualitative methods such as surveys and expert consultations to construct an evaluation framework for resource and environmental carrying capacity based on the principles of ecological civilization. This framework not only enhances the theoretical foundation and analytical methodologies of resource and environmental assessments but also provides practical guidelines for policymaking related to ecological civilization development, land-use planning, and sustainable resource management in karst regions.

2 Research area

The research area is located in the central–western part of Guizhou, China, at the watershed between the North Panjiang and Wujiang river systems. This accessible region is geographically defined between longitudes 105°15′ to 106°35′ E and latitudes 25°21′ to 26°37′ N. It experiences an average annual temperature of 14.8°C, receives an annual precipitation of 1,222 mm, and benefits from 1,238.80 h of sunshine each year. Rich in mineral and water resources, this region is also recognized for its biodiversity, making it a focal point for national initiatives in natural forest protection and ecological development. Notably, over 12% of the region consists of scenic areas, significantly higher than the national average of 1% and Guizhou's average of 4.2%. Despite these advantages, the region faces challenges, including significant land degradation and soil erosion, characterized by high elevations in the central region and lower terrain in the north and south, as well as higher elevations in the

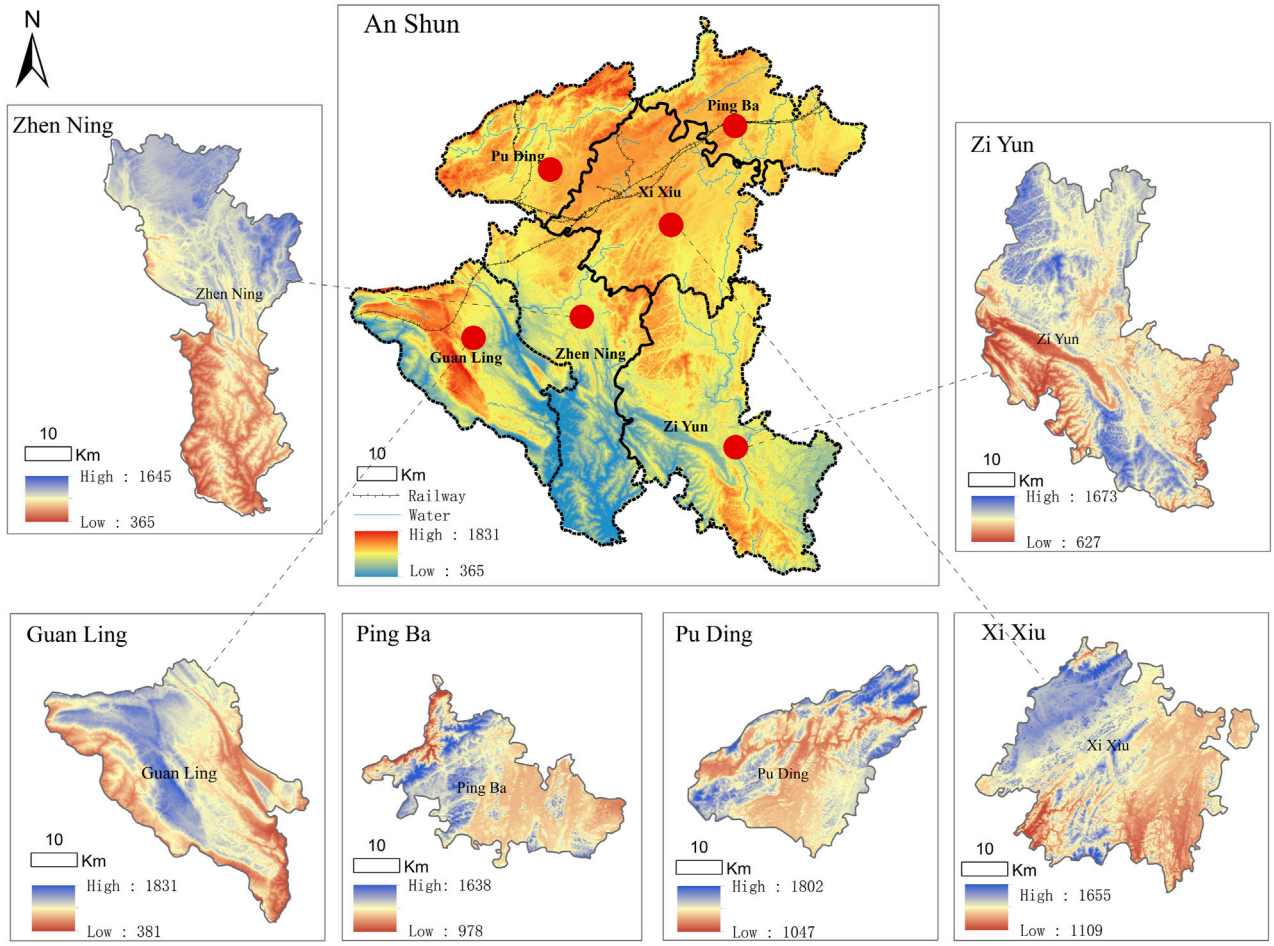

FIGURE 1
Overview of the research area [Approval Qian S (2023) No. 009], with simplified elements on the base map but no changes to the scope.

northwest and lower elevations in the southeast. This spatial differentiation showcases it as a quintessential region of concentrated karst topography (Figure 1).

In 2019, the total land area amounted to 9,267 km^2, with arable land covering 4.39 million acres. The forested cover reached 7.6194 million acres, resulting in a forest coverage rate of 59.03%. The region experienced an average annual runoff of 6.217 billion m^3, with a technical potential for hydropower generation estimated at 1.5929 million kilowatts, of which 1.5429 million kilowatts are economically viable. The resident population is approximately 2.3636 million, contributing to a regional gross domestic product (GDP) of 92.394 billion yuan with an annual growth rate of 8.1%. The industrial structure is divided into three sectors at a ratio of 17.0:31.7:51.3. The research area encompasses six districts and counties, Xi Xiu, Ping Ba, Pu Ding, Guanyin, Zi Yun, and Zhen Ning (Figure 1), supported by 2,003 healthcare institutions. Known as the "Mountain Park Province," Guizhou is characterized by striking landscapes, abundant water resources, beautiful valleys, impressive rock formations, and a wealth of natural resources, which contribute to its reputation as a "natural air conditioner," "green oxygen bar," and "summer resort." Under the province's expansive ecological strategy, the research area has actively pursued ecological civilization initiatives, including rocky desertification control, river management, and pollution reduction. These efforts, strongly supported by national policies, have resulted in gradual enhancements in resource and environmental endowments, as well as improvements in carrying capacity.

3 Research design

3.1 Data sources

This article derives data from various authoritative sources, encompassing land use, climate, water resources, socioeconomic factors, and ecological conditions. These sources include the results of the third national land resource survey, comprehensive land-use planning for the region from 2006 to 2020, and statistical yearbooks and public reports from 2015 to 2019. Additional data sources consist of environmental condition reports, plans for addressing stoniness in the region (2008–2015), water ecological civilization construction (2016–2030), soil and water conservation (2016–2030), government work reports, and various development plans related to industrial growth, transportation during the 13th Five-Year Plan, energy development, and wetland conservation. The evaluation

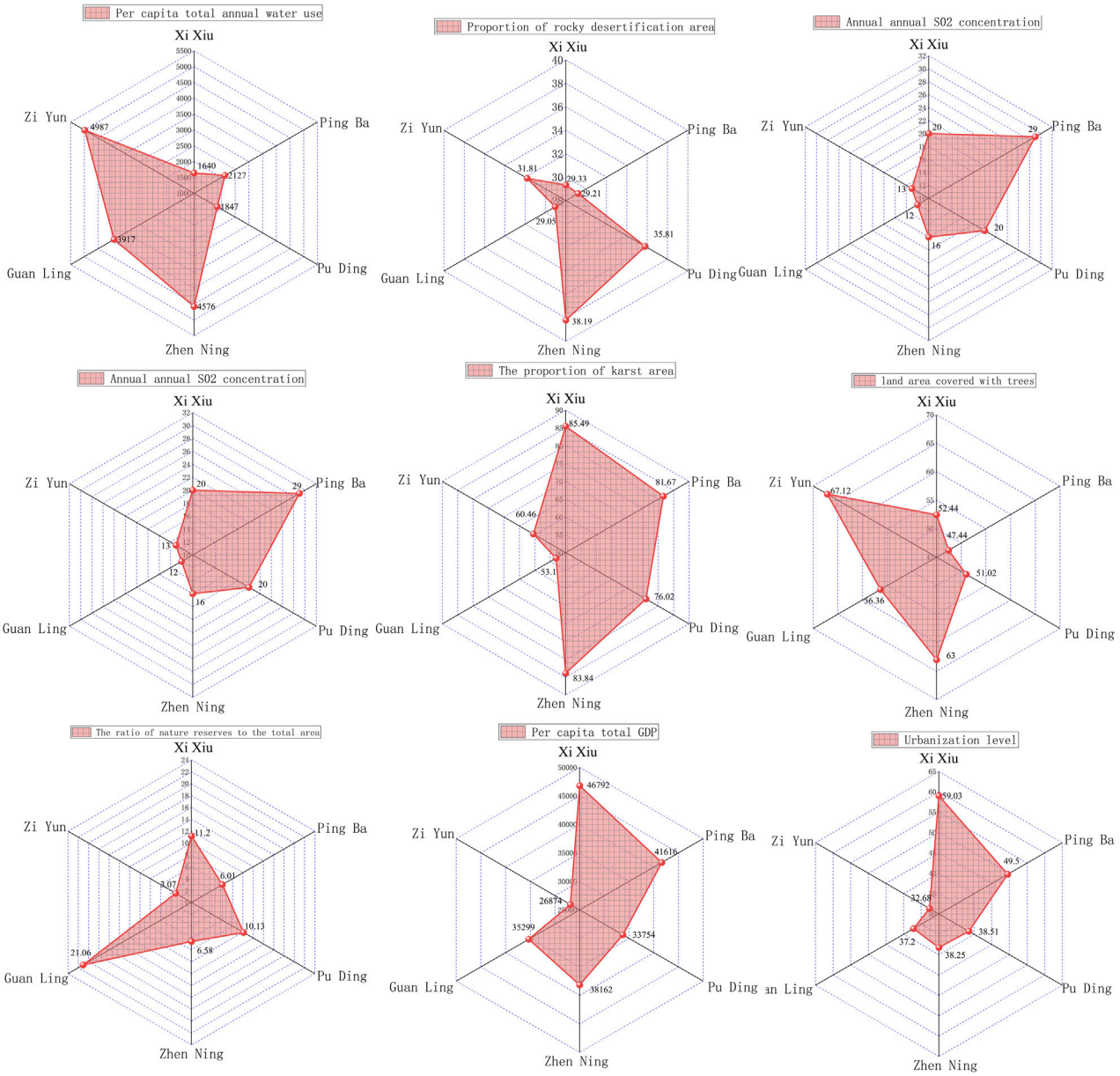

FIGURE 2
Radar chart presentation of typical indicators.

indicators for land, water, and air quality are illustrated by a single, representative baseline indicator for each category (Figure 2).

3.2 Research methods

3.2.1 Establishing the analysis framework for resource and environmental carrying capacity

This research addresses the distinct resource and environmental characteristics of karst regions, along with the characteristics of socioeconomic development. Through interviews, expert consultations, and empirical validation, we developed an analytical framework for evaluating resource and environmental carrying capacity, guided by the concept of ecological civilization (Figure 3). The framework consists of three logical phases: problem identification, analysis, and decision-making. When evaluating carrying capacity in karst regions, these phases are applied as follow:

(1) Problem identification: In this initial phase, we recognize critical issues such as widespread rocky desertification, severe soil erosion, ecological vulnerability, significant disturbances in land use, increasing resource constraints, and conflicts between development and conservation. The analysis is contextualized within national and regional commitments to green development, low-carbon initiatives, ecological protection, and high-quality growth, leading to the formulation of relevant research questions addressing the

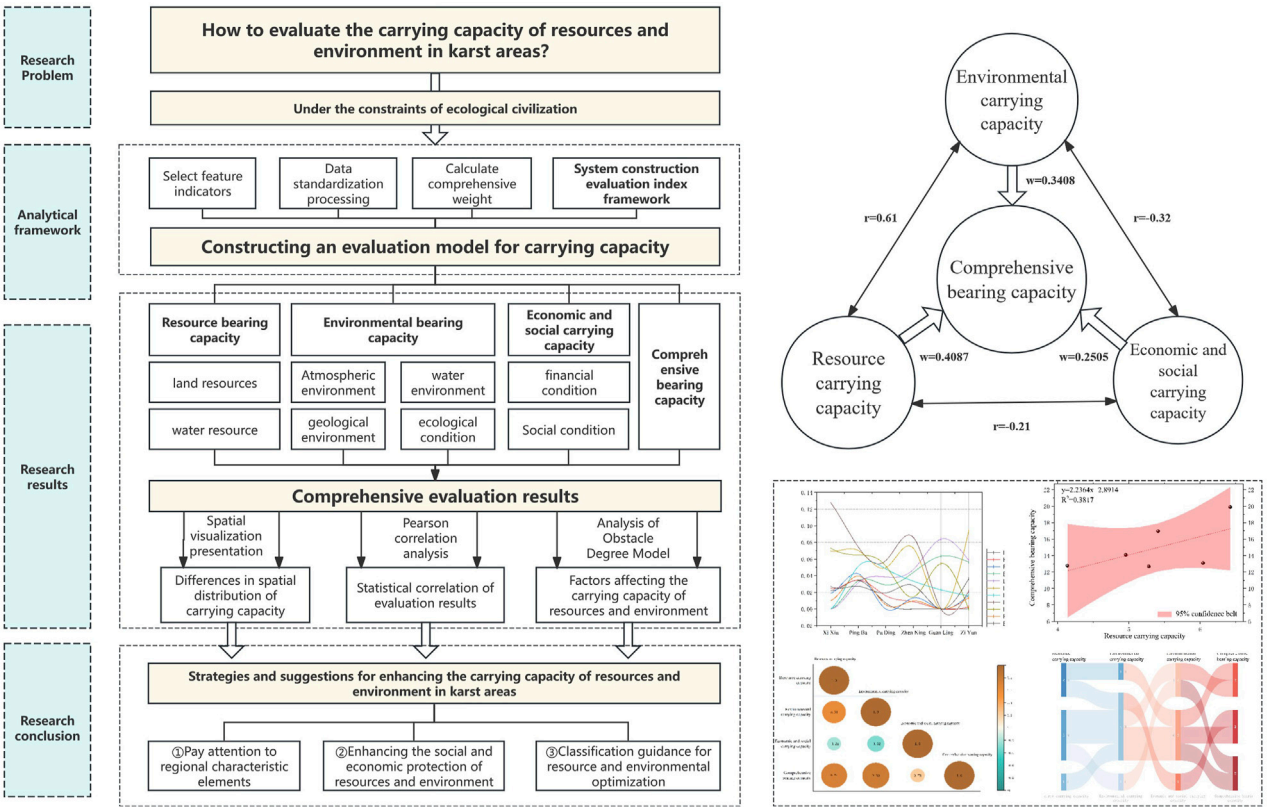

FIGURE 3
Research framework diagram for analyzing resource and environmental carrying capacity based on "problem design–problem deconstruction–decision evaluation."

carrying capacity of resources and the environment in karst regions.

(2) Problem analysis: Due to the distinct natural environment and resource endowments in karst regions, achieving sustainable development requires compliance with natural laws and customized approaches for local conditions. This phase constructs a comprehensive evaluation index system reflecting the region's unique features while examining resources, the environment, and socioeconomic dimensions. A mixed-method approach integrates interviews, expert consultations, comprehensive evaluation models, obstacle degree models, and Pearson's correlation analysis. It is used to assess the carrying capacity level, identify hindering factors, and explore the interrelations among these factors, with the results illustrated through spatial visualization.

(3) Decision-making: Utilizing the evaluation results as a foundation, this phase addresses current national macroeconomic strategies and urgent regional development needs. The focus is on identifying and mitigating obstacles to enhance resource and environmental carrying capacity, thereby promoting a harmonious human–environment relationship and achieving long-term sustainable development goals for the karst region. This process includes proposing scientifically grounded strategies and recommendations for improvements.

3.2.2 Technical process for evaluating resource and environmental carrying capacity

3.2.2.1 Development of an evaluation index system

Index selection principles: Adhering to the concept of ecological civilization, index selection emphasizes a systematic and locally relevant approach. Indicators must reflect the conditions of the research area, be easily interpretable, align with the basic theoretical framework for carrying capacity evaluation and national technical standards, and appropriately represent the carrying capacity status.

Selection of evaluation indexes: The research area, as a typical karst region, is abundant in mineral and tourism resources but also faces significant ecological challenges, including extensive rocky desertification, severe soil erosion, and inadequate vegetation cover. Although the economy is growing, its overall level remains relatively low. Drawing from existing research, technical standards, and expert consultations, we established an evaluation index system comprising three main criteria: resource, environmental, and socioeconomic carrying capacity. This system incorporates eight evaluation indexes, such as land resources and air quality, leading to a total of 30 specific indicators, including *per capita* arable land and *per capita* water usage (Table 1).

Setting weights for evaluation indexes: We applied a combination of the variance and Delphi methods to assign weights to the evaluation indexes. This process involved engaging experts from various fields, such as land planning, resource management, and ecological development, encompassing

TABLE 1 Construction of the evaluation indicator system and weight setting (Equations 1–3).

Evaluation standard layer	Evaluation index layer	Measurement index	Number	Measurement unit	Indicator attribute	Weight
Resource bearing capacity (0.4087)	Land resources (0.1934)	*Per capita* cultivated land area	R1	hm^2/human being	+	0.0522
		Proportion of the rocky desertification area	R2	%	-	0.0503
		Proportion of the effective irrigated area of cultivated land	R3	%	+	0.0282
		Proportion of unused land	R4	%	-	0.0184
		Proportion of regional soil erosion area	R5	%	-	0.0291
		Proportion of flooded area	R6	%	-	0.0152
	Water resource (0.2153)	*Per capita* total annual water use	R7	m^3/human being	-	0.0591
		Per capita water resources owned	R8	m^3/human being	+	0.0652
		Average annual rainfall	R9	mm	+	0.0518
		Utilization rate of water resource development	R10	%	+	0.0392
Environmental bearing capacity (0.3408)	Atmospheric environment (0.0662)	Annual nitrogen oxide concentration	E1	μg/m	-	0.0204
		Annual SO_2 concentration	E2	$\mu g/m^3$	-	0.0207
		Excellent rate of ambient air quality	E3	%	+	0.0251
	Water environment (0.1125)	Centralized treatment rate of wastewater and sewage	E4	%	+	0.0302
		Water resource contamination capacity (COD + NH_3-H)	E5	Ton	+	0.0324
		Area proportion of regional water ecological protection area	E6	%	+	0.0499
	Geological environment (0.0806)	Number of geological disaster points per unit area	E7	Individual/km	-	0.0304
		proportion of karst area	E8	%	-	0.0502
	Ecological condition (0.0815)	Land area covered with trees	E9	%	+	0.0385
		Forest area	E10	hm^2/100 km^2	+	0.0236
		Ratio of nature reserves to the total area	E11	%	+	0.0194
Economic and social carrying capacity (0.2505)	Financial condition (0.1721)	*Per capita* total GDP	S1	Yuan/person	+	0.0436
		Proportion of the tertiary industry in GDP	S2	%	+	0.0284
		Per capita fixed asset investment	S3	10,000 yuan/person	+	0.0411
		Per capita disposable income of urban residents	S4	Yuan/person	+	0.0289
		Per capita disposable income of rural residents	S5	Yuan/person	+	0.0301
	Social condition (0.0784)	Density of population	S6	Human being/km^2	-	0.0226
		Urbanization level	S7	%	+	0.0179
		Number of health institutions for 10,000 people	S8	10,000 people	+	0.0161
		Proportion of the number of residents with minimum living security	S9	%	+	0.0218

administrative officials, technical personnel, educators, and community representatives, to account for obstacles to regional ecological construction.

Variance-based weighting approach: The variance weighting method involves calculating the average values and variances of evaluation indicators, followed by normalizing the variance coefficients to derive the indicator weight values. The main steps are as follows:

① The average of each evaluation indicator is calculated:

$$\overline{M_j} = \frac{1}{n}\sum_{i=1}^{n} r_{ij},\ j = 1, 2, 3 \ldots\ldots, n, \tag{1}$$

where $\overline{M_j}$ is the average value of indicators, r_{ij} is the value of the jth evaluation indicator in the ith evaluation region, and n is the total number of indicators.

② The variance of the evaluation indicators is computed:

$$\sigma_j = \sqrt{\sum_{i=1}^{n}\left[r_{ij-\overline{M_j}}\right]^2}\ j = 1, 2, 3, \ldots.. n, \tag{2}$$

where σ_j is the mean square error of the indicators and n is the number of indicators.

③ The variance coefficients are normalized to derive the weight coefficients:

$$\omega_j = \frac{\sigma_j}{\sum_{i=1}^{n}\sigma_j},\ j = 1, 2, 3, \ldots\ldots n, \tag{3}$$

where ω_j is the normalized weight coefficient of the indicator and n is the total number of indicators.

Various indicators have diverse focuses and attributes, influencing the carrying capacity of the resources and environment differently. In the evaluation, the weight coefficients obtained through both the variance and Delphi methods are used to comprehensively determine the weight values of the indicators. The weights are assigned based on the significance of resource carrying capacity, environmental carrying capacity, and socioeconomic carrying capacity, as shown in Table 1.

Data standardization of evaluation indicators: This article encompasses a comprehensive system of indicators, featuring 3 criterion levels, 8 indicator levels, and 30 specific indicators. Indicators are categorized into positive and negative attributes to highlight their roles in evaluating resource and environmental capacities (Table 1). To eliminate dimensional disparities, we used the extreme value method for the standardization of the original data using the following formulas:

$$\text{Postive Indicators: } Z_{ij} = \frac{r_{ij} - min\, r_{ij}}{max\, r_{ij} - min\, r_{ij}},$$
$$(i = 1, 2, 3, \ldots.. m,\ j = 1, 2, 3, \ldots.. n), \tag{4}$$

$$\text{Negative Indicators: } Z_{ij} = \frac{max\, r_{ij} - r_{ij}}{max\, r_{ij} - min\, r_{ij}},$$
$$(i = 1, 2, 3, \ldots.. n,\ j = 1, 2, 3, \ldots.. n), \tag{5}$$

where Z_{ij} represents the standardized value of the jth evaluation indicator in the ith evaluation region, r_{ij} is the actual value of the jth evaluation indicator in the ith evaluation area, min r_{ij} and max r_{ij} denote the minimum and maximum values of the jth evaluation indicator in the ith evaluation region, respectively, m refers to the number of evaluation objects, and n is the total number of evaluation indicators.

Results and analysis of standardized indicators: In this article, we applied the extreme value method to standardize the indicators. The resource, environmental, and socioeconomic capacities of the research region include both positive and negative attributes. For positive indicators, the optimal value is the maximum observed in each district. Conversely, for negative indicators, the minimum value serves as the optimal baseline. The standardized values were computed using corresponding formulas, resulting in transformed indicator values ranging from 0 to 1, with 1 being the maximum and 0 being the minimum.

3.2.2.2 Selection of the evaluation model

After standardizing the indicators, we used a comprehensive evaluation model to calculate the index values for each criterion level pertaining to the resource and environmental carrying capacity in the research region. The model is expressed as follows:

$$K_i = \sum_{i=1}^{m} \omega_j \bullet Z_{ij},\ (i = 1, 2, 3, \ldots.. m,\ j = 1, 2, 3, \ldots.. n), \tag{6}$$

where K_i represents the index value for the ith criterion level, ω_j represents the weight coefficient for the jth indicator, and Z_{ij} represents the standardized value of the jth indicator in the ith evaluation region.

3.2.2.3 Introduction of the barrier model

The barrier degree model can be utilized to analyze the key factors contributing to disparities in the regional resource and environmental carrying capacity (Li et al., 2024; Ding et al., 2024). This model serves as a guiding tool to promote the efficient utilization of resources (Jia et al., 2017), such as land, within the research region by identifying and mitigating potential obstacles. By utilizing this model, we can effectively identify the primary barriers that impede the resource and environmental carrying capacity in the region. A higher barrier degree indicates a greater hindrance to achieving the region's overall resource and environmental capacity goals, while a barrier degree of 0 suggests no hindrances to these objectives. The barrier degree model incorporates several important variables, including factor contribution w_j, indicator deviation V_{ij}, and indicator barrier degree Z_{ij}. The overall barrier degree B_j assesses the impact of all identified obstacles on the resource and environmental carrying capacity in the research region.

$$V_{ij} = 1 - X_j, \tag{7}$$

$$Z_{ij} = \frac{\left(w_j \times V_{ij}\right)}{\sum_{j=1}^{n} w_j \times V_{ij}} \times 100\%, \tag{8}$$

$$B_j = \sum Z_{ij}. \tag{9}$$

In this model, the indicator deviation V_{ij} represents the difference between the standardized value of the jth indicator in the ith city and 1. The factor contribution w_j represents the weight of the jth indicator in that city. The barrier degree Z_{ij} represents how

10.3389/fenvs.2024.1499757

TABLE 2 Comprehensive evaluation results of the indicator level.

Region	Land resources	Water resources	Atmospheric environment	Water environment	Geological environment	Ecological environment	Economic condition	Social condition
Xi Xiu	0.1492	0.0773	0.0403	0.0851	0.0304	0.0382	0.1399	0.0467
Ping Ba	0.1216	0.0810	0.0000	0.0319	0.0059	0.0032	0.1029	0.0596
Pu Ding	0.0843	0.0713	0.0521	0.0411	0.0157	0.0351	0.0619	0.0285
Zhen ing	0.0727	0.1260	0.0539	0.0213	0.0144	0.0525	0.0650	0.0398
Guan Ling	0.1115	0.1593	0.0662	0.0557	0.0717	0.0605	0.0561	0.0333
Zi Yun	0.1012	0.1518	0.0561	0.0010	0.0607	0.0548	0.0168	0.0226

much the jth indicator impedes the resource and environmental carrying capacity, with higher values indicating greater hindrance. The barrier degree Z_{ij} for each indicator is expressed on a scale of 0% to 100%, where larger values signify a more significant impact on the carrying capacity.

3.2.2.4 Pearson's correlation analysis

Pearson's correlation analysis is utilized to evaluate the linear relationship between two sets of indicators. A higher correlation coefficient indicates a stronger relationship. This method calculates the correlation coefficient between two variables and determines its statistical significance. The introduction of Pearson's correlation analysis in this article aims to explore the linear associations among various evaluation indicators related to the resource and environmental carrying capacity in the research region. By examining these relationships, we can identify the critical factors that influence and determine the levels of resource and environmental carrying capacity in karst regions, as well as the primary obstacles. This comprehension enables targeted interventions to improve the area's resource and environmental carrying capacity, fostering high-quality and sustainable socioeconomic development in the region.

$$\rho(\mathrm{XY}) = \frac{\sum_{i=1}^{n}(X_i - E(X))(Y_i - E(Y))}{n \times (\sigma X)(\sigma Y)}, \tag{10}$$

$$\sigma(X) = \sqrt{\frac{\sum_{i=1}^{n}(X_i - E(X))^2}{n}}, \tag{11}$$

where $\rho(\mathrm{XY})$ represents the correlation coefficient (r), which illustrates the strength and direction of the relationship between two variables. The overall mean is denoted by $E(X)$, and the overall covariance is represented by $\sigma(X)$.

4 Empirical analysis and result interpretation

4.1 Evaluation results of resource and environmental carrying capacity and spatial disparities

4.1.1 Evaluation result analysis

The comprehensive evaluation of standardized indicator data (Equations 4, 5) generated an index for resource and environmental carrying capacity across different regions within the research region, as shown in Tables 2, 3 (Equation 6).

4.1.1.1 Analysis of resource carrying capacity results

The findings correspond well with the regional resource endowments; regions with higher water resource indexes demonstrate greater resource carrying capacities. The sequence of resource carrying capacity, from highest to lowest, is as follows: Guanling, Ziyun, Xixiu, Pingba, Zhenning, and Puding. Regions like Xi Xiu and Ping Ba, located near Gui'an New District, exhibit high land resource scores but low water resource scores, while Guan Ling and Zi Yun present high water resource scores and moderate land resource scores. Notably, Guan Ling has the lowest region of stoneland desertification and the least annual *per capita* water usage,

TABLE 3 Comprehensive evaluation results of the criterion level.

Region	Resource carrying capacity	Environmental carrying capacity	Economic and social carrying capacity	Comprehensive bearing capacity
Xi Xiu	0.2265	0.1941	0.1866	0.6072
Ping Ba	0.2026	0.0410	0.1625	0.4061
Pu Ding	0.1556	0.1439	0.0904	0.3900
Zhen Ning	0.1986	0.1421	0.1049	0.4456
Guan Ling	0.2707	0.2540	0.0894	0.6142
Zi Yun	0.2530	0.1727	0.0394	0.4651

coupled with high average annual rainfall, resulting in the highest resource carrying capacity. Conversely, Pu Ding consistently shows low values, and it ranks second-highest in stoneland desertification, soil erosion, and flooded land area, while its *per capita* water resources and average annual rainfall are fifth in the region, culminating in the lowest resource carrying capacity evaluation and reflecting the existing disparities in resource distribution.

4.1.1.2 Analysis of environmental carrying capacity results

The evaluation of the environmental carrying capacity effectively illustrates the ecological heterogeneity of the research region. There is a strong correlation between the evaluation indexes and actual conditions. The comprehensive evaluation ranks the regions from highest to lowest as follows: Guan Ling, Xi Xiu, Zi Yun, Pu Ding, Zhen Ning, and Ping Ba. A disparity of more than 6-fold exists between the highest and lowest values. In terms of the 11 measured indicators, Guan Ling excels in 7 indexes, including average annual SO_2 and NO_2 concentrations and the proportion of karst land region, although it scores lower in water pollution capacity and wastewater treatment rates. Conversely, Ping Ba ranks the lowest across six indicators, reflecting overall poor environmental quality.

4.1.1.3 Analysis of economic and social carrying capacity results

The evaluation results reveal significant disparities in local economic and social development. The research region displays markedly higher scores for economic conditions than for social conditions, with high and low values typically present in the same regions. The ranking from high to low is as follows: Xi Xiu, Ping Ba, Zhen Ning, Pu Ding, Guan Ling, and Zi Yun. A 4-fold difference exists between the highest and lowest values. Among nine measured indicators, Xi Xiu and Ping Ba showed the highest values for *per capita* GDP and fixed asset investment, whereas Zi Yun ranks lowest in six indicators for *per capita* GDP and investment. The regions of Pu Ding, Zhen Ning, and Guan Ling fall in the moderate range. Geographically adjacent Xi Xiu and Ping Ba present high economic and social carrying capacities, while Zi Yun demonstrates the lowest value, indicating a strong correlation with the current state of economic and social development.

4.1.1.4 Comprehensive evaluation of the resource and environmental carrying capacity

The cumulative results, representing the collective evaluation of resource, environmental, and socioeconomic carrying capacities, are ranked from high to low as follows: Guan Ling, Xi Xiu, Zi Yun, Zhen Ning, Ping Ba, and Pu Ding. Guan Ling boasts the highest overall scores, particularly in resource and environmental capacities, reflecting abundant availability and favorable conditions of land and water resources, albeit with weaker socioeconomic conditions. Conversely, Xi Xiu shows high resource and environmental carrying capacities, along with the highest socioeconomic capacity, attributed to advantageous spatial characteristics. Conversely, Pu Ding is characterized by its lowest resource carrying capacity and intermediate environmental and socioeconomic development capacities, culminating in the lowest comprehensive carrying capacity, highlighting the region's inadequate ecological and socioeconomic conditions.

4.1.2 Analysis of spatial disparities at the county level

Utilizing the spatial analysis capabilities of ArcGIS 10.8, we conducted a comprehensive evaluation of the resource and environmental carrying capacity in the research region. The results are visually represented at the county level (Figure 4), illustrating the diverse spatial heterogeneity of these capacities. To categorize these results effectively, we applied the natural breaks method, which focuses on minimal intra-group variation and maximal inter-group variation, dividing the groups into three defined categories: "high," "medium," and "low." Figures 4, 5 show that

(1) The overall evaluation of resource carrying capacity reveals a pronounced spatial distribution of "high in the south and low in the north," which closely correlates with the region's topographical features. Notably, high values are found in Zi Yun and Guan Ling, while Pu Ding reveals lower values. The spatial distribution of water and land resources demonstrates distinct disparities. Land resources generally follow a pattern of "low in the center, high at both ends," with Xi Xiu standing out as a high-value region. Conversely, water resources display a distribution pattern of "high in the south, low in the north," with significant values also shown in Zi Yun and Guan Ling.
(2) The comprehensive assessment scores for environmental carrying capacity exhibit a similar "high in the south, low in the north" distribution, closely linked to the region's topography. Guan Ling receives high scores, while Ping Ba presents lower and intermediate values. The differences between high and low scores highlight notable gaps in

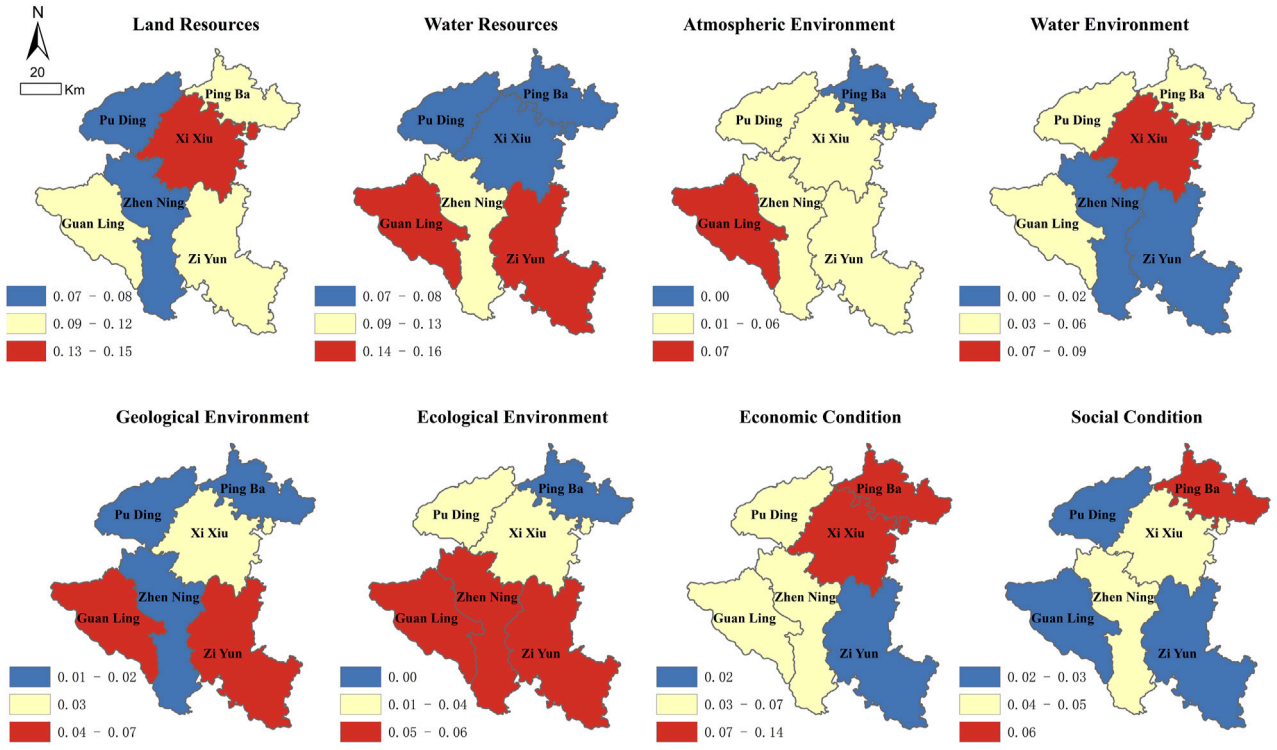

FIGURE 4
Spatial distribution map of comprehensive evaluation scores at the indicator level.

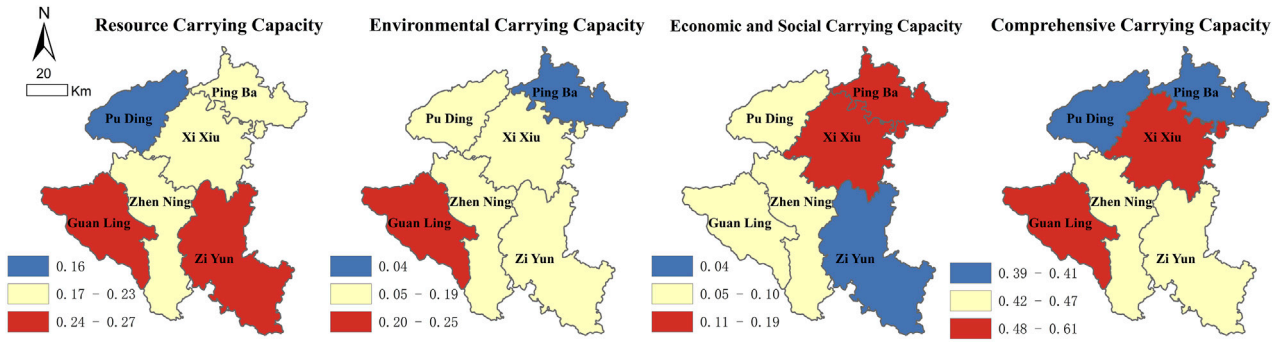

FIGURE 5
Spatial distribution map of comprehensive evaluation scores at the criterion level.

environmental capacity evaluations. Patterns in atmospheric, geological, and ecological environment scores are comparable, with mid–high values clustered in the southwestern regions, particularly in Guan Ling and Zhen Ning, as well as in southeastern Zi Yun. In contrast, water environment scores indicate a "high in the north, low in the south" trend, with Xi Xiu presenting a noteworthy high score across four evaluation indicators, emphasizing the substantial disparity between high and low values. Additionally, Ping Ba shows some indicators with a minimum score of 0, emphasizing the spatial heterogeneity in environmental capacity evaluations.

(3) The social and economic carrying capacity scores reveal a spatial pattern of "high in the northeast, low in the southeast, and mid-values in the central and western regions." Regions such as Xi Xiu and Ping Ba, which are adjacent to the Guian New District, exhibit higher values, whereas Zi Yun shows a lower score. Significant differences in economic and social conditions are evident in towns like Guan Ling and Pu Ding, reflecting a similar spatial distribution of high and low values, indicating a spatial homogeneity in socioeconomic carrying capacity assessments.

(4) Finally, the overall evaluation scores for carrying capacity consistently exhibit a "high in the south, low in the north"

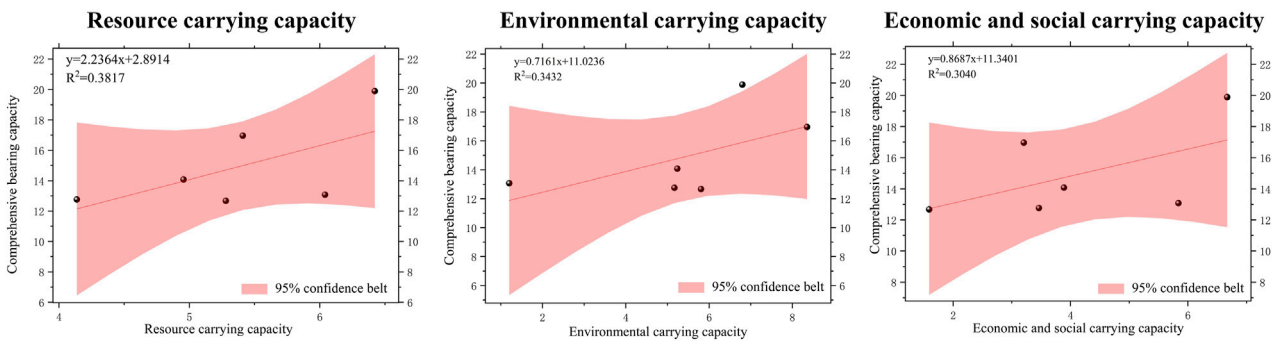

FIGURE 6
Linear fitting chart of resource carrying capacity, environmental carrying capacity, socioeconomic carrying capacity, and comprehensive carrying capacity (95% confidence interval).

FIGURE 7
Pearson's correlation coefficient chart of comprehensive evaluation scores at the criterion level.

distribution. This pattern is significantly influenced by environmental and resource carrying capacities rather than socioeconomic factors. The northern areas, particularly Ping Ba and Pu Ding, present lower values, while Xi Xiu and Guan Ling display higher scores, reinforcing the identified spatial disparities in the carrying capacity within the region.

4.2 Statistical correlation analysis

This section presents a statistical analysis of the relationships among the resource carrying capacity, environmental carrying capacity, socioeconomic carrying capacity, and overall carrying capacity in the research region. Utilizing univariate linear regression to fit the data and assessing the linear correlation coefficients (Figure 6), we find a strong linear relationship among the resource carrying capacity, environmental carrying capacity, and overall carrying capacity. To further elucidate the interdependencies among these indicators, we applied Pearson's correlation coefficient method for correlation analysis (Figures 7, 8) (Equations 10, 11).

The analysis of the standard layers (Figure 7) reveals significant medium-to-high positive correlations and resource carrying capacity, with environmental capacity (0.61) and overall capacity (0.74). The environmental capacity correlates with the overall capacity (0.80). Conversely, the socioeconomic carrying capacity shows no significant correlations with the resource carrying capacity (−0.21), environmental capacity (−0.32), or overall capacity (0.23). These results indicate that resource and environmental capacities have a significantly greater influence on the overall carrying capacity than socioeconomic indicators. A detailed statistical analysis of the indicator levels (Figure 8) reveals several key relationships:

(1) Land and water resources show differentiated correlations with other indicators, highlighting a strong connection

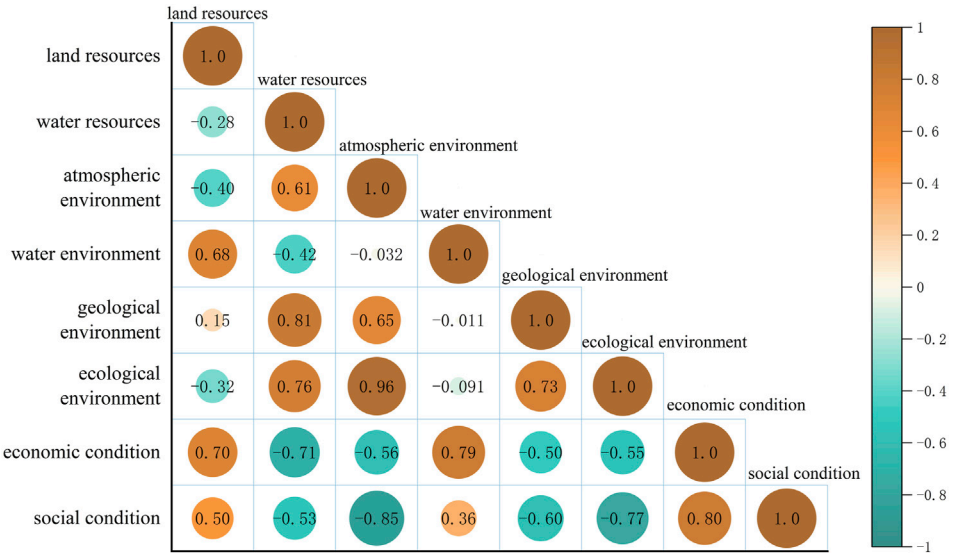

FIGURE 8
Pearson's correlation coefficient chart of comprehensive evaluation scores at the indicator level.

between land resources and socioeconomic factors, as well as a robust relationship between water resources and environmental elements. Specifically, land resources show medium-to-high positive correlations with the water environment (0.68), economic status (0.70), and social status (0.50). Water resources also show strong positive correlations with the atmospheric environment (0.61), ecological environment (0.81), and ecological environment (0.76). However, there are significant negative correlations between water resources and economic status (−0.71) and social status (−0.53).

(2) Within the environmental dimension, complex interdependencies exist among the indicators. Except for the water environment, there are notable negative correlations between environmental indicators and socioeconomic indicators. Significant positive correlations are evident between the atmospheric and geological environments (0.65), atmospheric and ecological environments (0.96), and geological and ecological environments (0.73). Other correlations within this dimension tend to be weaker, while the water environment positively correlates with economic status (0.79) and social status (0.36).

(3) The intricate relationships between resource carrying capacity and both environmental and socioeconomic capacities reveal that socioeconomic indicators significantly correlate with land resources, while environmental indicators strongly associate with water resources. Socioeconomic indicators show negative correlations with environmental indicators, despite having a high positive correlation (0.80) within their own dimension.

In addition, we categorized the comprehensive scores of the standard layers into "high, medium, and low" using the natural-breaks method. This classification is visualized through alluvial diagrams (Figure 9), illustrating the flow of scores among the different capacities. The diagrams reveal complex interrelations driven by the region's diverse resources, environments, and socioeconomic characteristics within the karst region. Notably, resource carrying capacity nodes primarily consolidate into an "M" category of environmental capacity, which then subsequently disperses into "H," "M," and "L" nodes for socioeconomic capacity. In turn, these socioeconomic nodes flow into overall capacity nodes. Notably, no cross-layer transitions occur between the resource and environmental capacities at an "H-L" level, indicating a stable relationship. However, socioeconomic capacity nodes exhibit cross-layer transitions, highlighting the intricate socioeconomic dynamics and their minor impact on the overall carrying capacity.

4.3 Analysis of obstacle factors

Given the extensive number of indicators, this article focuses on Equations 7–9 the top three obstacle factors ranked by their severity (Table 4).

4.3.1 Obstacle factors impacting the resource carrying capacity

Water resources pose a greater challenge than land resources regarding the overall carrying capacity (Figure 10). Notable spatial disparities exist between water and land resources. Important factors influencing the resource carrying capacity include *per capita* water availability (R8), average annual precipitation (R9), *per capita* arable land area (R1), water resource utilization rate (R10), and proportion of rocky desertification region (R2). Notably, R8, R9, and R10, which pertain to water resources, often rank as primary or secondary factors. This indicates that water scarcity is the primary impediment to resource carrying capacity in karst regions. The findings reveal a discrepancy between water availability and the overall resource carrying capacity, highlighting the need for improved

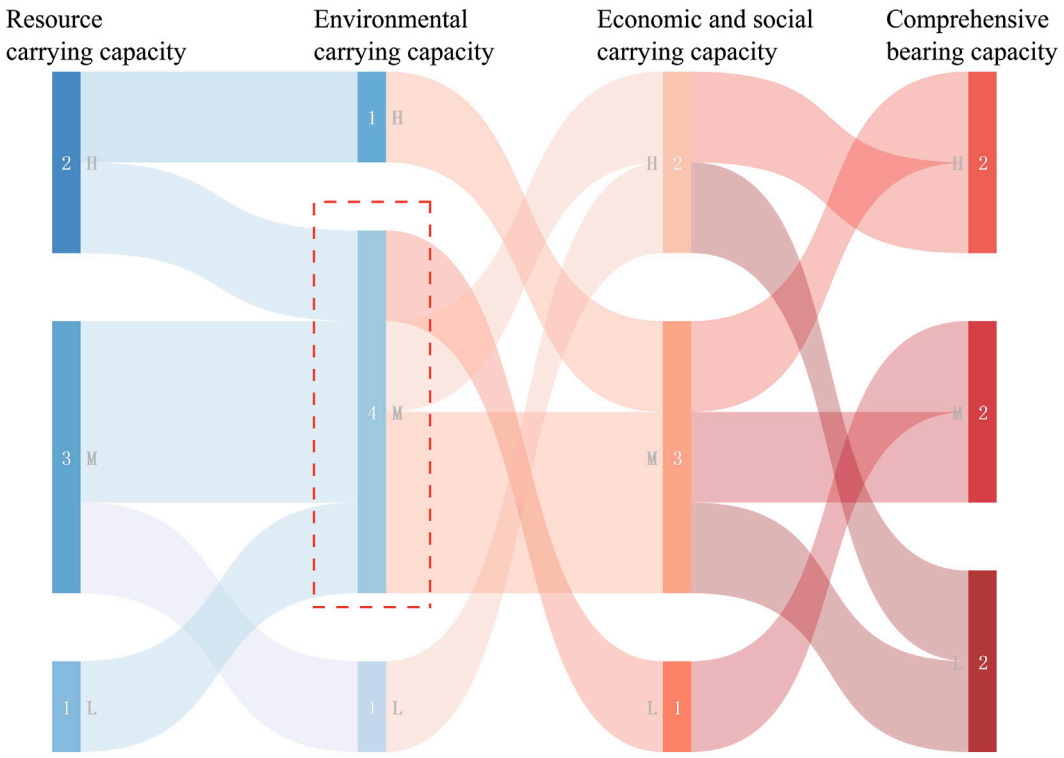

FIGURE 9
Alluvial diagram of comprehensive evaluation scores at the criterion level.

TABLE 4 Comprehensive analysis of obstacle factors at the indicator level.

Region	Resource carrying capacity			Environmental carrying capacity			Economic and social carrying capacity		
	First factor	Second factor	Third factor	First factor	Second factor	Third factor	First factor	Second factor	Third factor
Xi Xiu	R8 16.61%	R9 10.25%	R1 6.31%	E8 12.79%	E9 7.32%	E6 6.97%	S3 5.98%	S6 5.76%	S2 2.16%
Ping Ba	R7 9.95%	R8 9.38%	R1 8.79%	E8 7.46%	E6 7.03%	E9 6.48%	S2 4.78%	S5 2.74%	S4 2.20%
Pu Ding	R8 10.03%	R9 9.34%	R2 9.07%	E8 5.80%	E9 5.16%	E6 4.97%	S3 5.44%	S1 4.68%	S5 4.28%
Zhen Ning	R9 9.34%	R2 9.17%	R10 9.36%	E8 8.60%	E6 7.29%	E5 4.76%	S3 6.66%	S5 5.43%	S4 3.81%
Guan Ling	R10 9.13%	R8 5.39%	R1 5.16%	E5 8.40%	E4 6.34%	E9 5.46%	S3 8.32%	S5 7.68%	S1 6.52%
Zi Yun	R10 7.33%	R3 5.27%	R9 4.26%	E6 9.33%	E5 5.86%	E4 5.65%	S1 8.15%	S3 7.68%	S5 5.57%

coordinated management of water resources. Additionally, the abundance of *per capita* arable land area (R1) and the proportion of rocky desertification area (R2) further impede resource capacity. This contributes to significant regional disparities, with regions like Xi Xiu exhibiting strong land resource support, while regions such as Pu Ding and Zhen Ning show comparatively weak support. In terms of water resources, Zi Yun and Guan Ling have considerable support, whereas Pu Ding, Xi Xiu, and Ping Ba are notably weaker.

4.3.2 Obstacle factors impacting the environmental carrying capacity

The obstacle factors affecting environmental carrying capacity are more complex. Notably, key barriers include forest coverage and the proportion of karst areas, which are more significant than other elements (Figure 10). Factors such as the area proportion of ecological protection zones (E6), proportion of the karst area (E8), forest coverage (E9), water pollutant absorption capacity

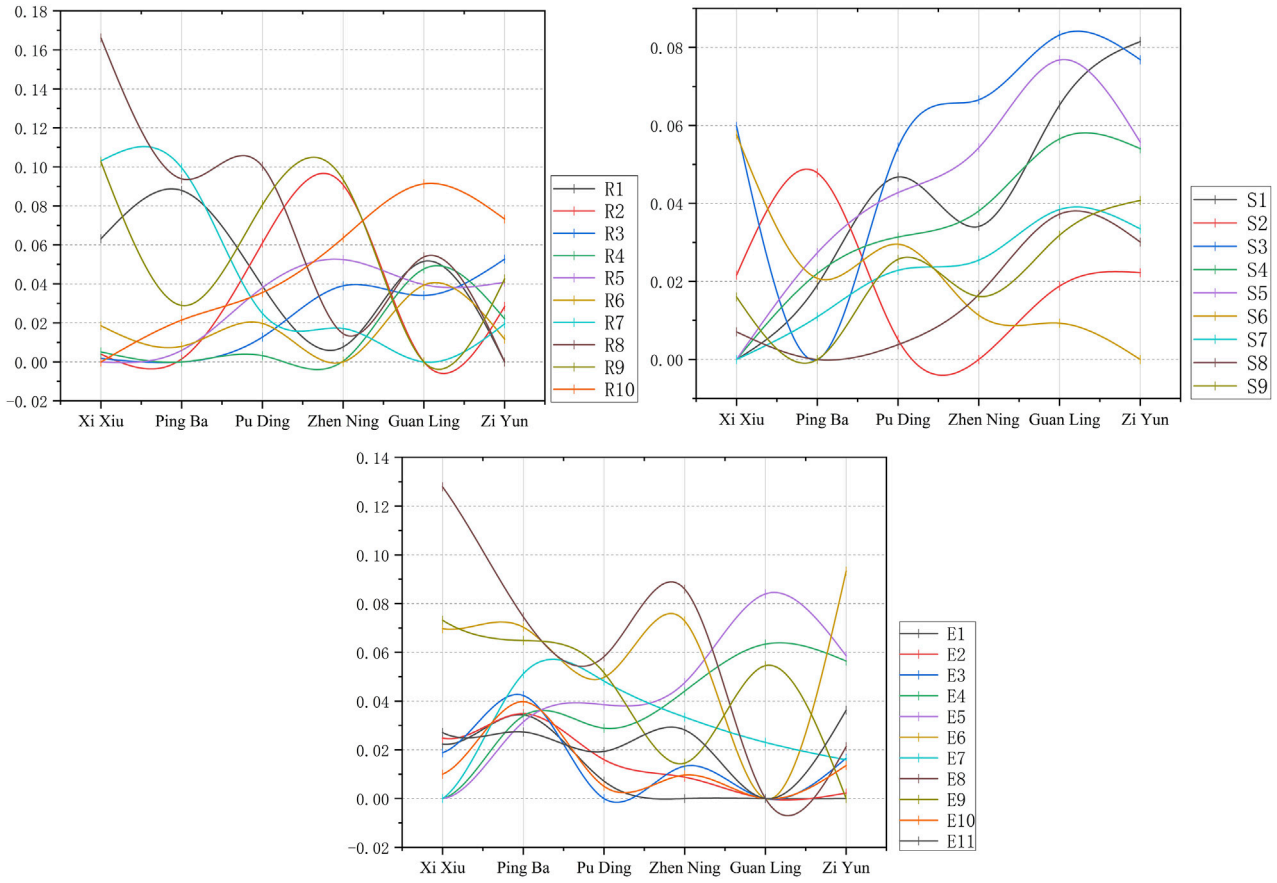

FIGURE 10
Statistical chart of different types of obstacle factors.

(E5), and centralized sewage treatment rate (E4) frequently emerge as key obstacles. The karst region proportion (E8) is particularly impactful, frequently ranking as a primary obstacle, thereby indicating its substantial restriction on enhancing environmental carrying capacity. The variables E6, E5, and E4 emphasize the strong influence of water environment factors on environmental capacity. Furthermore, forest coverage (E9), classified within the ecological environment dimension, significantly hinders the overall environmental carrying capacity.

4.3.3 Obstacle factors affecting the economic and social carrying capacity

The primary obstacle factors impacting the economic and social carrying capacity are predominantly economic in nature. The industrial development across the six counties lags behind population and social development (Figure 10). This disparity highlights the need for coordinated efforts to elevate economic levels and promote the mutual reinforcement of population dynamics and industrial growth. Key factors influencing economic and social carrying capacity include *per capita* fixed asset investment (S3), disposable income of rural residents (S5), *per capita* GDP (S1), the contribution of the tertiary sector to the GDP (S2), and disposable income of urban residents (S4). The indicators S3 and S5 illustrate how these economic factors constrain the development of the overall economic carrying capacity in the region. There is significant economic disparity among the regions, with Ping Ba and Xi Xiu performing better, while Zi Yun ranks lowest. This economic inequality closely correlates with resource and environmental factors, revealing a disconnection between industrial and social development in karst regions.

5 Discussion and conclusion

5.1 Discussion

In Southwest China, karst topography presents several challenges, including poor soil quality, rock desertification, and water scarcity, which profoundly affect the region's sustainable socioeconomic development. Therefore, constructing a technical framework and indicator system for analyzing resource and environmental carrying capacity aligned with ecological civilization principles is essential. The proposed evaluation index system for assessing resource and environmental carrying capacity is well-suited to challenges specific to karst regions, such as rocky desertification, water scarcity, and soil erosion. However, its applicability across regions with varied ecological types and developmental stages may be limited. Although the focus on karst-specific environmental factors enhances precision, broadening this framework's application would require

integrating flexible, region-specific indicators to capture diverse ecological and developmental characteristics.

(1) This technical framework is developed based on existing research to provide insights for specific regions' carrying capacity evaluation. The proposed framework entails a process of "problem design–problem decomposition–decision assessment," beginning with the identification of conflicts among resource, environmental, and socioeconomic factors. This framework aims to clearly define primary issues to ensure targeted decision-making. Moreover, its value extends beyond its theoretical application, offering practical guidance for spatial planning in karst regions through the integration of regional realities and optimization of resource, production, and ecological spaces while facilitating viable technical solutions.

(2) The comprehensive evaluation indicator system emphasizes regional characteristic elements.[1] The interplay of these factors demonstrates a system of mutual causality and interaction, reflecting the area's resource endowments and socioeconomic realities. Many current studies on carrying capacity indicator systems tend to overlook the significance of regional characteristics in indicator design and weight settings, often neglecting the ecological constraints on development initiatives. This article addresses this gap by proposing a comprehensive evaluation indicator system that combines the resource carrying capacity, environmental carrying capacity, and socioeconomic carrying capacity, aimed at effectively analyzing key issues and obstacles in the research area. The evaluation results reveal that the comprehensive carrying capacity is relatively high in the central region, especially in Xi Xiu and the southern area of Guan Ling, while the northern regions, like Ping Ba and Pu Ding, display lower capacities. The resource carrying capacity is highest in the southern counties, such as Guan Ling and Zi Yun, diminishing northward toward Ping Ba. Regarding the environmental carrying capacity, Guan Ling represents a high-value area compared to the lower-value zone in northeastern Ping Ba. Economic and social capacities show a more favorable profile in the central and northern regions, whereas the middle and southwest regions have lower ratings. Notably, these empirical findings correspond with the geographical economic realities of the research area. Furthermore, the analysis also highlights that critical resource and environmental deficiencies have not received adequate attention, underscoring the necessity for strengthened monitoring and assessment of these dynamic changes to effectively guide regional development in the future.

(3) This article thoroughly analyzes the key factors influencing resource and environmental carrying capacity through the integration of multiple data sources. It shifts the focus from a localized perspective to a holistic view, emphasizing the balance between resource utilization and conservation. By introducing an obstacle degree model, this article identifies primary constraints, such as water resources and rock desertification, assessing their significance in order to inform subsequent improvement measures. Challenges in karst regions are interconnected issues arising from a complex interplay of multi-dimensional factors. Future research should aim to distill the insights obtained from the model's results into practical regional development policies.

(4) The application of Pearson's correlation analysis provides a robust methodological tool for understanding the inherent relationships among various obstacle factors in karst regions, facilitating region-specific optimization strategies. Current research frequently fails to analyze these internal correlations adequately, which undermines the effectiveness of resource and environmental policy implementation. This article visually illustrates the associations among factors through Pearson's correlation coefficient diagrams and scatter plots, highlighting the importance of integrating quantitative analysis with systematic thinking. This approach will enhance the theoretical, methodological, and technical aspects of carrying capacity analysis and evaluation. Future research should concentrate on the diversity of factor characteristics and their dynamic interconnections, analyzing the intricate relationships underlying carrying capacity and reconsidering the networks of interaction between humans and nature, as well as between humans and society.

This article systematically constructs a technical framework and an indicator system for analyzing the resource and environmental carrying capacity in karst regions within the constraints of ecological civilization. It highlights the dialectical relationship among various environmental and social factors. Future research should prioritize the integration between qualitative and quantitative analyses, utilizing multi-dimensional, multi-method, and multi-spatial scale approaches to deeply examine the current characteristics and relational dynamics of resources, environment, ecology, and social development in karst regions. This approach will enable the implementation of targeted measures to improve resource and environmental quality while respecting natural systems.

5.2 Conclusion and policy implementation

5.2.1 Conclusion

This article provides a comprehensive analysis of the resource and environmental carrying capacity of Anshun City, a typical karst region in Guizhou Province, China, within the context of ecological civilization. It establishes a three-dimensional integrated evaluation framework that encompasses resource, environmental, and socioeconomic capacities, using quantitative research methods to better facilitate regional socioeconomic development. This article contributes a robust technical framework and case studies to support the advancement of ecological civilization while introducing new methodologies and theoretical insights.

The principal findings are summarized as follows: ① the novel technical framework for comprehensive evaluation effectively

1 Pay special attention to the regional characteristic elements such as rocky desertification, water and soil loss, water resources, economic level, and social development in the karst region.

addresses current research limitations by systematically examining regional resources, environmental factors, and socioeconomic characteristics within the framework of ecological civilization, which enables empirical assessments of karst regions. Subsequently, it provides practical policy recommendations to improve the resource and environmental carrying capacity in these regions, contributing to a deeper theoretical and technical foundation for conducting carrying capacity analyses in karst environments. ② The integrated index system, which combines resource, environmental, and socioeconomic factors, demonstrates strong adaptability to contemporary regional challenges and research demands. Unique indicators, such as the proportion of rock desertification and karst regions, effectively reflect the distinctive ecological characteristics of these regions. By systematically adjusting weights to reflect the diverse impacts of each indicator on the carrying capacity, the evaluations ensure objectivity and reliability. Higher weights are allocated to indicators representing the specific features and limitations of karst regions, while varied values are allocated to guiding indicators pertaining to the environmental carrying capacity, effectively integrating regional resource characteristics and development stages. This article enhances the relevance and practicality of the evaluation system, fostering a nuanced response to the specific conditions of karst regions. ③ The article also identifies critical factors that impede the resource and environmental carrying capacity in karst regions, providing a solid foundation for regional policy development. The implementation of an obstacle degree model enriches the analysis, providing increased usability and depth in assessing the carrying capacity related to resources, the environment, and socioeconomics. This model highlights significant obstacle factors that affect evaluations, granting insights that can improve regional resource and environmental carrying capacities. ④ Additionally, the intricate interrelations among various indicator factors were clarified, emphasizing the significant influence of characteristic resources on the carrying capacities in karst regions. Pearson's correlation analysis has elucidated these complex interactions, revealing that the impact of resource and environmental carrying capacities on the overall carrying capacity surpasses that of socioeconomic factors. The assessment portrays a distinctive environmental carrying capacity focused on water resources while indicating a strong correlation between land resources and socioeconomic capacities. Here, water resources reflect resource disparities, while land resources reveal variations in socioeconomic development. ⑤ Lastly, the delay in economic and social development notably restricts the advancement of comprehensive carrying capacities in the karst region. The region's inadequate resource endowment and low levels of economic development impede overall enhancements in carrying capacity. Socioeconomic factors play a notable obstructive role in bolstering socioeconomic capacities, as reflected in the underdevelopment of industrial sectors across the six counties compared to their population and social growth. Therefore, it is imperative to promote economic development indicators holistically across the region while tailoring support strategies to address the diverse developmental stages of different regions.

5.2.2 Policy implications

The main policy recommendations for enhancing the overall resource and environmental carrying capacity are as follows: ① lead by the natural resource management authorities to draft technical standards for assessing the carrying capacity in karst regions. This approach will ensure that evaluations are scientifically robust and tailored to the unique challenges of these regions. ② Focus on improving resource and environmental carrying capacity in the northern regions to promote high-quality and coordinated economic growth. The existing advantages of the southern counties should be utilized to support the northern regions' shift toward greener, low-carbon production through technological innovation. ③ Strengthen market-oriented resource allocation and environmental protection efforts by rigorously controlling pollution emissions from industrial and daily activities while reducing disparities between different regions. ④ Establish targeted regional initiatives for optimizing water resource management to improve the ecological status in karst regions. This approach should consider the distinct resource and environmental attributes of the region, guiding ecological civilization construction and development in a targeted manner. ⑤ Enhance the capacity for resource and environmental carrying, as well as high-quality development within the research area, by accelerating green technology innovations. The advantages of northern counties in funding, technology, and talent should be leveraged to implement energy-saving and emission-reduction initiatives and foster collaboration with the southern and southwestern counties.

Data availability statement

The original contributions presented in the study are included in the article/supplementary material; further inquiries can be directed to the corresponding author.

Author contributions

WY: conceptualization, data curation, formal analysis, funding acquisition, methodology, project administration, resources, software, supervision, validation, writing–original draft, and writing–review and editing. XL: data curation, formal analysis, investigation, methodology, resources, software, validation, and writing–original draft. YY: conceptualization, data curation, formal analysis, investigation, methodology, resources, software, validation, visualization, writing–original draft, and writing–review and editing.

Funding

The author(s) declare that financial support was received for the research, authorship, and/or publication of this article. This work was supported the Guizhou Province 2022 Philosophy and Social Sciences Planning Project (grant number 22GZYB54).

Conflict of interest

The authors declare that the research was conducted in the absence of any commercial or financial relationships that could be construed as a potential conflict of interest.

Publisher's note

References

Chen, Y., Liu, S., Ma, W., and Zhou, Q. (2023). Assessment of the carrying capacity and suitability of spatial resources and the environment and diagnosis of obstacle factors in the yellow river basin. *Int. J. Environ. Res. Public Health* 20, 3496. doi:10.3390/ijerph20043496

Ding, Y. L., Li, X. L., Liu, J., Song, J., and He, H. (2024). Sustainable development process and mechanism of urbanization in border cities in Northeast China: a case study of Dongning and Hunchun. *Sci. Geogr. Sin.* 44 (3), 474–482. doi:10.13249/j.cnki.sgs.20230573

Fan, J. (2007). Scientific basis for the zoning of principal functional areas in China. *Geogr. J.* 62 (4), 339–350. doi:10.11821/xb.2007.04.001

Feng, Z., You, Z., Yang, Y., and Shi, H. (2021). Comprehensive evaluation of resource and environment carrying capacity of Tibet based on a three-dimensional tetrahedron model. *Geogr. J.* 76 (3), 645–662. doi:10.11821/dlxb202103011

Gao, W., Chen, Y., Yan, C. A., and Li, J. C. (2020). Water environmental carrying capacity assessment based on ecosystem purification and human regulation coupling effect. *Acta Ecol. Sin.* 40 (14), 4803–4812. doi:10.5846/stxb201904190794

Ge, W., Chang, L., Qi, Z., Meng, F., and Liang, X. (2021). Development tendency analysis for the water resource carrying capacity based on system dynamics model and the improved fuzzy comprehensive evaluation method in the changchun city, China. *Ecol. Indic.* 122, 107232. doi:10.1016/j.ecolind.2020.107232

Huang, X. (2017). Strategic space construction of the yangtze river economic belt based on resources and environment carrying capacity. *Environ. Prot.* (15), 25–26. doi:10.14026/j.cnki.0253-9705.2017.15.004

Huang, X., and Song, Y. (2019). Evaluation model of regional resource and environment comprehensive carrying capacity based on the conjugation-wrestling mechanism. *J. Nat. Resour.* 34 (10), 2103–2112. doi:10.31497/zrzyxb.20191007

Jia, K. J., Zhang, H., Xu, X. L., 徐小黎, 祁帆, Hui, Z., et al. (2017). Evaluation techniques of land resources carrying capacity catering to land development and utilization. *Prog. Geogr.* 36 (3), 335–341. doi:10.18306/dlkxjz.2017.03.009

Jia, W., Xia, J., Gong, Z., and Cao, K. (2020). Dynamic assessment of tourism carrying capacity and its impacts on tourism economic growth in urban tourism destinations in China. *J. Destination Mark. and Manag.* 15, 100383. doi:10.1016/j.jdmm.2019.100383

Li, J. L., Pan, J. R., Feng, F., Peng, X., and Liu, C. (2024). Coupling coordination development of PWEE system and obstacle factors in nine provinces/regions of the Yellow River Basin. *J. Water Resour. and Water Eng.* 35 (01), 47–56. doi:10.11705/j.issn.1672-643X.2024.01.06

Li, Q., Wu, J., Su, Y., Zhang, C., Wu, X., Wen, X., et al. (2022). Estimating ecological sustainability in the guangdong-Hong Kong-Macao greater bay area, China: retrospective analysis and prospective trajectories. *J. Environ. Manag.* 303, 114167. doi:10.1016/j.jenvman.2021.114167

Lin, A., Liu, Y., Zhou, S., Zhang, Y., Wang, C., and Ding, H. (2023). Data-driven analysis and evaluation of regional resources and the environmental carrying capacity. *Sustainability* 15, 8372. doi:10.3390/su15108372

Liu, M. H., Xi, J. C., and Chen, S. H. (2020). Ecological carrying capacity accounting model and application in multi-type protected areas.Acta. *Ecol. Sin.* 40 (14), 4794–4802. doi:10.5846/stxb201905181028

Liu, R. Z., and Borthwick, A. G. L. (2011). Measurement and assessment of carrying capacity of the environment in Ningbo, China. *J. Environ. Manag.* 92 (8), 2047–2053. doi:10.1016/j.jenvman.2011.03.033

Liu, X., Tang, L., Sun, D., Li, Y., Xu, M., Kang, X., et al. (2023). Comprehensive evaluation of resources and environmental carrying capacity in guangdong coastal zone. *Trop. Geogr.* 43 (3), 459–473. doi:10.13284/j.cnki.rddl.003644

Liu, Y., Qu, Y., Cang, Y., and Ding, X. (2022). Ecological security assessment for megacities in the yangtze river basin: applying improved emergy-ecological footprint and dea-sbm model. *Ecol. Indic.* 134, 108481. doi:10.1016/j.ecolind.2021.108481

Luo, W., Shen, L., Zhang, L., Liao, X., Meng, C., and Jin, C. A. (2022). A load-carrier perspective method for evaluating land resources carrying capacity. *Int. J. Environ. Res. Public Health* 19, 5503. doi:10.3390/ijerph19095503

Malthus, T. R. (1978). *An essay on the principle of population*. London: Pickering.

Min, X., Wang, Y., and Chen, J. (2022). Resource carrying capacity evaluation based on fuzzy evaluation: validation using karst landscape region in southwest China. *Sustainability* 14, 16548. doi:10.3390/su142416548

Niu, F., Yang, X., and Sun, D. (2020). Water and soil carrying capacity and adjustment of industrial structure in hainan province tropical geography, 40(6), 1109–1116. doi:10.13284/j.cnki.rddl.003281

Niu, F. Q., Feng, Z. M., and Liu, H. (2018). A review on evaluating methods of regional resources and environment carrying capacity. *Resour. Sci.* 40 (4), 655–663. doi:10.18402/resci.2018.04.01

Park, R. E., and Burgess, E. W. (1921). *Introduction to the science of sociology*. Chicago: The University of Chicago Press.

Peng, T., Deng, H., Lin, Y., and Jin, Z. (2020). Assessment on water resources carrying capacity in karst areas by using an innovative DPESBRM concept model and cloud model. *Sci. total Environ.* 767, 144353. doi:10.1016/j.scitotenv.2020.144353

Shao, Y. S., Wang, H. F., and Yin, C. Y. (2013). Evaluation method of urban land population carrying capacity based on GIS-A case of Shanghai, China. *Comput. Environ. and Urban Syst.* 39, 27–38. doi:10.1016/j.compenvurbsys.2013.02.002

Shen, L., Cheng, G., Du, X., Meng, C., Ren, Y., and Wang, J. (2022). Can urban agglomeration bring "1 + 1 > 2Effect"? A perspective of land resource carrying capacity. *Land Use Policy* 117, 106094. doi:10.1016/j.landusepol.2022.106094

Sun, M., Wang, J., and He, K. (2020). Analysis on the urban land resources carrying capacity during urbanization:A case study of Chinese YRD. *Appl. Geogr.* 116 (2), 102170. doi:10.1016/j.apgeog.2020.102170

Tan, K., Yan, Z., Zhao, Z., Pu, J., Li, S., Miao, P., et al. (2020). Evaluation of resource and environmental carrying capacity of wenshan city in karst area based on fuzzy model. *Soil Water Conservation Res.* 28 (1), 218–227. doi:10.13869/j.cnki.rswc.2021.01.028

Wang, B., and Wang, X. (2022). Comprehensive evaluation of resources and environment carrying capacity in karst areas: take Guizhou as an example. *J. Hunan Univ. Sci. Technol. Nat. Sci. Ed.* 37 (1), 118–124. doi:10.13582/j.cnki.1672-9102.2022.01.016

Wang, J., Huang, Y., Wu, L., Jing, P., Li, J., Ouyang, S., et al. (2023a). Review on resource and environmental carrying capacity of mining areas in China. *Environ. Rev.* 31(2):218–228. doi:10.1139/er-2022-0093

Wang, M., Liu, M., Zhang, D., Qi, J., Fu, W., Zhang, Y., et al. (2023b). "Assessing and optimizing the hydrological performance of Grey-Green infrastructure systems in response to climate change and non-stationary time series," in *Water research*. United Kingdom: A journal of the international water association.

Wei, L., Jin, C., and Lu, Y. (2019). Exploring resources and environmental carrying capacities at the county level: a case study of China's Fengxian County. *PLoS ONE* 14, e0225683. doi:10.1371/journal.pone.0225683

Wu, X., and Hu, F. (2020). Analysis of ecological carrying capacity using a fuzzy comprehensive evaluation method. *Ecol. Indic.* 113, 106243. doi:10.1016/j.ecolind.2020.106243

Yang, J., Lei, K., Khu, S., and Meng, W. (2015). Assessment of water resources carrying capacity for sustainable development based on a system dynamics model:A case study of tieling city, China. *Water Resour. Manag.* 29 (3), 885–899. doi:10.1007/s11269-014-0849-y

Yang, L., and Wang, L. (2022). Comprehensive assessment of urban water resources carrying capacity based on basin unit: a case study of Qingdao, China. *Water supply* 22 (2), 1347–1359. doi:10.2166/ws.2021.351

Yang, Q., Zhang, F., Jiang, Z., Yuan, D., and Jiang, Y. (2016). Assessment of water resource carrying capacity in karst area of Southwest China. *Environ. earth Sci.* 75, 37. doi:10.1007/s12665-015-4816-6

Zhang, M., Liu, Y., Wu, J., and Wang, T. (2018). Index system of urban resource and environment carrying capacity based on ecological civilization. *Environ. Impact Assess. Rev.* 68, 90–97. doi:10.1016/J.EIAR.2017.11.002

frontiers | Frontiers in Earth Science

TYPE Original Research
PUBLISHED 28 November 2024
DOI 10.3389/feart.2024.1445241

OPEN ACCESS

EDITED BY
Qiang Liu,
Beijing Normal University, China

REVIEWED BY
Chengyu Xie,
Xiang Tan university, China
Jianwei Geng,
Chinese Academy of Sciences (CAS), China

*CORRESPONDENCE
Xiaolei Zhang,
zxl1334@163.com

RECEIVED 07 June 2024
ACCEPTED 04 November 2024
PUBLISHED 28 November 2024

CITATION
Zhang X, Guo X, Liu S, Shang X, Xu Z and Zhao J (2024) A study on groundwater level calculation based on PCA-CIWOABP.
Front. Earth Sci. 12:1445241.
doi: 10.3389/feart.2024.1445241

A study on groundwater level calculation based on PCA-CIWOABP

Xiaolei Zhang[1]*, Xiaoyi Guo[1], Shuyu Liu[1,2], Xiutang Shang[1], Zhiheng Xu[1] and Jiankun Zhao[3]

[1]School of Water Conservancy, North China University of Water Resources and Electric Power, Zhengzhou, China, [2]College of Water Conservancy and Hydropower Engineering, Hohai University, Nanjing, China, [3]Institute of Rural Hydropower and Water Conservation Engineering, Guangdong Research Institute of Water Resources and Hydropower, Guangzhou, China

In order to explore the relationship between groundwater levels and hydro-meteorological factors in Fengnan District, accurate estimation of groundwater levels in the area was undertaken. Real data on groundwater levels, water consumption, and rainfall from 2018 to 2021 in various townships within Fengnan District were selected. Utilizing the Principal Component Analysis method, the main influencing factors were extracted from the hydrological data of each township. Subsequently, a groundwater level calculation model was established using the CIWOABP(Cubic map - Intelligent weight adjustment - Whale Optimization Algorithm–Back Propagation) neural network in combination with these factors. The results indicate that: (1) Principal Component Analysis extracted a total of five principal components from various hydrological data in Fengnan District, namely, groundwater levels of monitoring wells #11 and #12, rainfall from rainfall station r1, and water consumption from Fengnan (FN) and Qianying (QY) towns. (2) The CIWOABP neural network was trained using 36 sets of actual measurement data and validated with 12 sets of simulated data. The mean absolute errors (MAE) for monitoring wells #11 and #12 were 0.19 and 0.23 respectively, and the mean squared errors (MSE) were 0.05 and 0.09 respectively. The model exhibited high computational accuracy and can be effectively employed to calculate actual groundwater levels. The research outcomes can provide theoretical and methodological insights for groundwater resource management in the North China Plain.

KEYWORDS

groundwater level, principal component analysis, intelligent weight adjustment, whale optimization algorithm, BP neutral network

1 Introduction

Groundwater resources play an irreplaceable role in various sectors such as production, daily life, and ecological environments (Chai et al., 2023; Stigter et al., 2023). However, persistent overexploitation and improper utilization of groundwater have led to various issues, including continual decline in groundwater levels (Costa et al., 2021) and deterioration of water quality (Hou et al., 2023). These problems pose threats to the sustainable utilization of water resources and ecological balance. Effectively addressing these potential risks necessitates the accurate prediction of groundwater level fluctuations, a challenging task. Groundwater level prediction is often hindered

by issues such as high-dimensional data, model complexity, and computational costs, posing significant challenges in practical applications (Zaghiyan et al., 2021). Therefore, the quest for a more efficient and precise groundwater level prediction method becomes especially crucial.

Subject to the comprehensive influences of various factors including rainfall, soil type, evapotranspiration, groundwater extraction, recharge, seasonal and climatic variations, land cover, and groundwater flow, the simulation and prediction of groundwater levels face substantial hindrances (Li et al., 2013; Deb, 2024). In order to mitigate the adverse impact of these complex factors on the simulation and prediction of groundwater level fluctuations, some researchers have employed the Principal Component Analysis (PCA) method to address the intricate relationships among influencing factors of groundwater levels. This approach involves dimensionality reduction to enhance the accuracy and stability of predictive models. Generally, there are two approaches to dimensionality reduction of original data concerning groundwater levels and their influencing factors using PCA: The first approach involves employing PCA to extract primary components from a multitude of factors that contribute to fluctuations in groundwater levels (Almanaseer and Sankarasubramanian, 2012; Chang et al., 2017). Jung et al. (2021) utilized Principal Component Analysis to perform dimensionality reduction on observed data including rainfall, evaporation, groundwater usage, tides, and more. Subsequently, they identified rainfall as a primary component, leading to a notable reduction in subsequent monitoring costs. The second approach involves Principal Component Analysis to extract composite data from a single factor that represents the original dataset (Naderianfar et al., 2017; Kim et al., 2021). Triki et al. (2014) applied Principal Component Analysis and cluster analysis to actual groundwater level data from 24 monitoring wells, categorizing them into three distinct groundwater fluctuation patterns. They further analyzed how these different patterns responded to variations in rainfall and temperature.

When dealing with accurate simulation and prediction of groundwater levels, traditional hydraulic calculations and big data-driven neural networks emerge as two primary methodologies. Traditional approaches build mathematical models for groundwater flow based on hydraulic motion equations. However, the complexity of groundwater systems and difficulties in data acquisition restrict their applicability and predictive capability (Matiatos et al., 2019; Li X. Q. et al., 2022). In recent years, neural network technology has emerged as a promising avenue for groundwater level prediction, offering new perspectives. Neural network types such as Convolutional Neural Networks (CNN), Recurrent Neural Networks (RNN), and Long Short-Term Memory Networks (LSTM) have been widely applied in groundwater level modeling. They can capture nonlinear relationships, enhancing model accuracy and generalization (Bowes et al., 2019; Xu et al., 2022; Yang and Zhang, 2022). Among these, the Backpropagation Neural Network (BPNN) stands out for its adaptability and generalization capabilities. BP neural networks adjust weights across multiple layers of neurons, learning groundwater level variation patterns from input data to achieve precise predictions (Zhang et al., 2022). Moreover, the incorporation of optimization algorithms further enhances the performance of the BP neural network. These algorithms adjust weights and biases to reduce prediction errors. Optimization techniques such as Artificial Bee Colony, Ant Colony, and Wavelet Decomposition have been introduced to improve model convergence speed, computational accuracy, and stability, resulting in improved predictive capabilities (Dash et al., 2010; Hosseini et al., 2016; Li et al., 2019; Zhang, 2022; Serravalle Reis Rodrigues et al., 2023).

The reviewed studies present advanced methodologies leveraging the Whale Optimization Algorithm (WOA) for improving water resource management. Notably, (Wang et al., 2023) introduces a robust monthly runoff interval prediction model combining WOA, Variational Modal Decomposition (VMD), LSTM networks, and non-parametric kernel density estimation. This innovative approach addresses the limitations of traditional point prediction by effectively capturing prediction uncertainty, thus aiding water management decisions. Other studies demonstrate the application of enhanced WOA variants in diverse contexts. For example, a multi-level scheduling method for mine water reuse utilizes opposition-based learning, Levy flight, nonlinear convergence factors, and adaptive inertia weight to enhance convergence speed, accuracy, and efficiency, significantly boosting reuse efficiency (Bo et al., 2022). Another study focuses on optimizing water resource allocation in Handan, China, using an ameliorative WOA with logistic mapping and inertia weighting, leading to more reliable water usage predictions (Yan et al., 2018). Further, an enhanced WOA for clustering incorporates elements from water wave optimization and tabu search, achieving superior performance compared to existing algorithms (Singh et al., 2023). Finally, the application of WOA and its enhancement at the Klang Gate Dam for reservoir operation optimization shows significant improvements in reducing water deficits and increasing reliability (Lai et al., 2021). Collectively, these studies highlight the versatility and efficacy of WOA and its variants in addressing complex water management challenges, providing valuable insights and tools for decision-makers.

In conclusion, the fluctuation of groundwater levels is influenced by complex factors, and traditional hydraulic calculation methods struggle to comprehensively account for various changing elements compared to neural network models. Therefore, this study aims to explore and enhance groundwater level prediction methods by combining principal component analysis for dimensionality reduction with an optimized BP neural network model. This approach seeks to elevate the accuracy and stability of groundwater level simulation.

2 Materials

2.1 Research area

The North China Plain is the world's largest area of groundwater funneling, with the majority of groundwater funnel zones concentrated in Hebei Province. Currently, over 20 groundwater funnel zones have merged into a vast interconnected area within Hebei Province, forming a super-sized groundwater funneling region. The study area (Fengnan District) is located in the eastern coastal plain of Hebei Province, in the southern part of Tangshan City, situated between 117°51′43″E and 118°25′28″E longitude, and 39°11′59″N and 39°39′28″N latitude. The study area is bordered

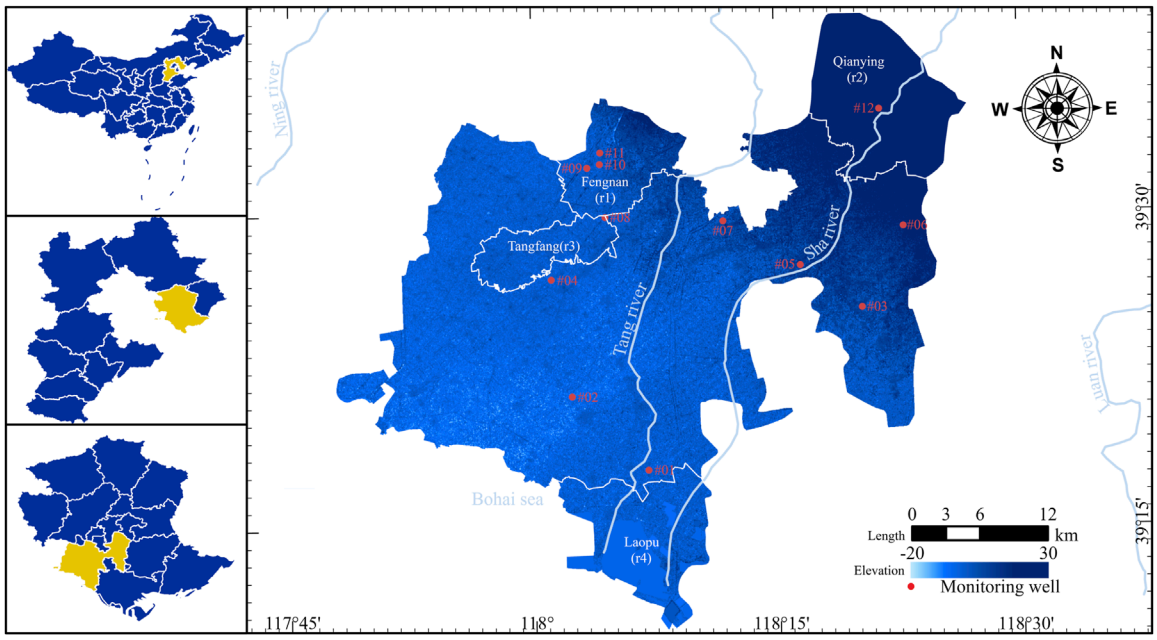

FIGURE 1
Map of research area. Created by ArcGIS 10.6 software (https://www.arcgis.com).

to the north by Fengrun District and Lutunan District of Tangshan City, to the south by the Bohai Sea, and is adjacent to Kaiping District, Luan Nan County, and Caofeidian New Area of Tangshan City to the east. To the west, it adjoins Binhai New Area and Ninghe District of Tianjin Municipality. Within the study area, there are two fifth-level rivers, Tang River and Sha River, and adjacent to it, there are two other rivers, Ning River and Luan River. The study area spans approximately 50 km from north to south and 48 km from east to west, covering a total area of 1288.4 square kilometers. The distribution of groundwater monitoring wells within Fengnan District and its surroundings is illustrated in Figure 1.

2.2 Data source

In the study area, the groundwater level experiences fluctuation due to both anthropogenic factors such as domestic and industrial water consumption, and natural factors including rainfall and infiltration. Currently, we have obtained water consumption data for major townships within the region from 2018 to 2021, rainfall data from rainfall stations, and groundwater level data from 12 monitoring wells. Detailed data information can be found in Table 1.

3 Methods

3.1 Combined PCA and CIWOABP neural network structures

The empirical dataset of this study exhibits the following characteristics: a relatively small variety of factors influencing groundwater level fluctuations, longer time series for the data records, but a relatively smaller number of data instances; within the same factor, multiple data categories are present, including 12 types of monitoring wells for groundwater levels, four rainfall stations for rainfall, and eight townships for water consumption. If the raw dataset is directly employed for training and prediction using the BP neural network, it is difficult to achieve highly desirable results.

Therefore, Dimensionality reduction was performed on water consumption, rainfall, and groundwater level data based on PCA. This process involved selecting mutually complementary townships, rainfall stations, and monitoring wells, as well as eliminating collinearity among variables. Principal components with cumulative variance contribution rates ranging from 85% to 100%, or eigenvalues greater than 1, were chosen as input and output data for the CIWOABP neural network (Wold et al., 1987; Jolliffe, 2022). Ultimately, a fitting study of the groundwater level calculation model for the Fengnan area was conducted. The technical roadmap of the study is illustrated in Figure 2.

3.2 Principal component analysis

The PCA method finds widespread application in data dimensionality reduction and denoising. PCA achieves this by linear transformation, converting high-dimensional data into a lower-dimensional space where the components are relatively independent. This approach maximizes the retention of essential key information from the original dataset, thereby achieving dimensionality reduction. The calculation steps of PCA are as follows (Demšar et al., 2013; Lin et al., 2022; Marukatat, 2023):

TABLE 1 Data attributes.

Data type	Rainfall	Water consumption	Groundwater level
Data source	Hydrological Data of the Haihe River Basin. Volume 1. Luanhe River Basin, Small Rivers along the Coast of Hebei Province. Hydrological Yearbook of the People's Republic of China	The water supply company's centralized management system	The water supply company's centralized management system
Collection method	Compiled by the Hydrological Bureau of the Haihe River Water Conservancy Committee of the Ministry of Water Resources, China, etc.	Monitor the user's water meter; Upload data to the management system in real-time	Monitor the water level gauge in the well; Upload data to the management system in real-time
Data composition	Fengnan (r1), Qianying (r2),Tangfang (r3), Laopu (r4)	FN, QY, DX, XJ, CH, XG, DO, HG	12 Wells (#1~#12)
Time period	2018–2021	2018–2021	2018–2021

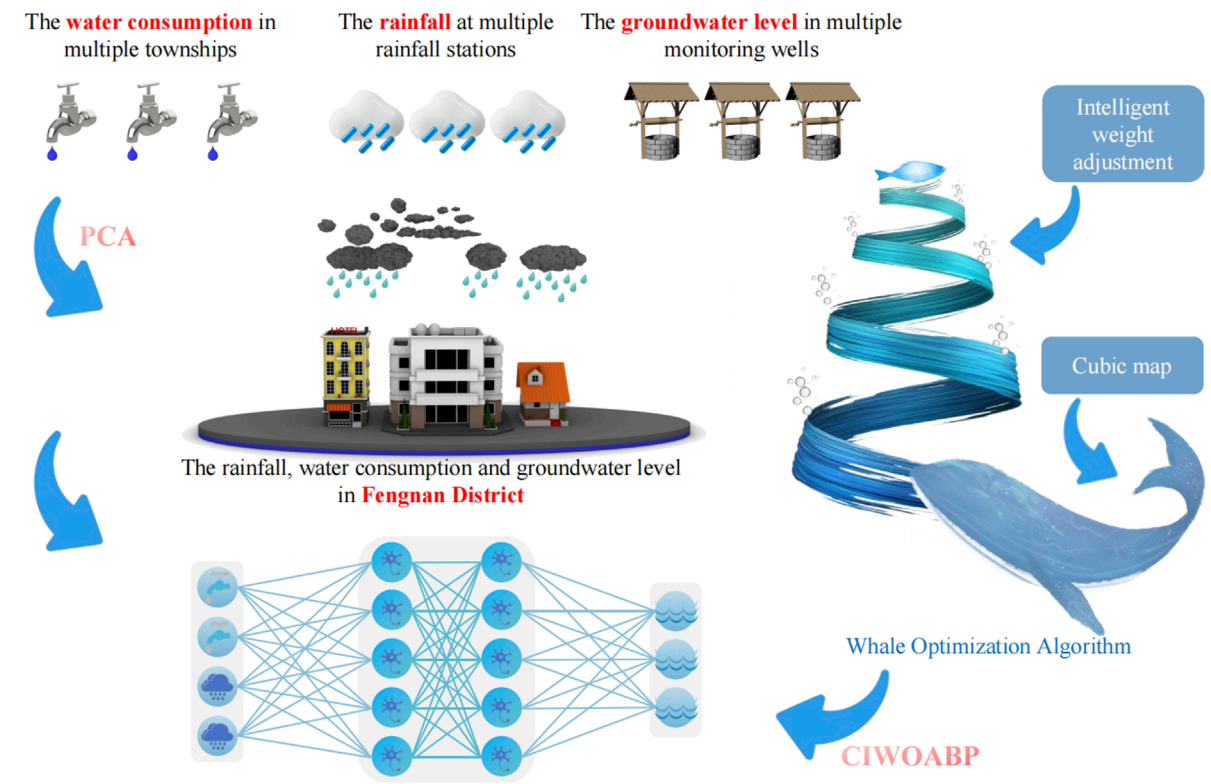

FIGURE 2
Technical flow chart.

The formula for calculating the covariance matrix is as Equation 1:

$$C = \frac{1}{m}\sum_{i=1}^{m}(x_i - \mu)(x_i - \mu)^T \quad (1)$$

where C represents the covariance matrix, m is the number of samples, x_i denotes the original data, and μ is the mean vector of the data.

The formula for eigenvalue decomposition is as Equation 2:

$$C = PDP^{-1} \quad (2)$$

where P is a matrix composed of eigenvectors, and D is a diagonal matrix consisting of eigenvalues arranged on the diagonal.

Selecting the eigenvectors corresponding to the k largest eigenvalues as principal components, the dimension-reduced data

can be calculated using Equation 3:

$$\bar{y} = \bar{x}(\overline{v_1}\ \ \overline{v_2}\cdots\overline{v_k}) \tag{3}$$

where $\bar{y}$ represents the data after dimensionality reduction, $\bar{x}$ is the data after subtracting the mean from the original data, and $\overline{v_i}$ represents the eigenvector of the ith principal component.

4 CIWOABP neural network

4.1 Whale optimization algorithm

In nature, whales form social groups and seek food based on interactions and foraging behaviors among individuals. Whales adjust their behavior to find more food by responding to changes in their surroundings and their own perception of the environment. The WOA applies this foraging strategy, treating the problem-solving process as a search for food (i.e., optimal solutions) in the solution space. In Figure 2, the basic structure of the BP neural network is 'input layer - neurons - output layer', which involves forward propagation calculation and backward feedback adjustment of weights and biases to optimize the solution. The whale optimization algorithm combines global and local search strategies to optimize the weights and biases of the BP neural network, thereby improving the performance and convergence speed of the neural network (Mirjalili and Lewis, 2016).

In the WOA, the current optimal individual is assumed to be the prey, while other individuals converge towards the optimal one. The mathematical model of this process is represented as follows:

$$\boldsymbol{X}(t_{i+1}) = \boldsymbol{X_p}(t_i) - \boldsymbol{A}\cdot\left|\boldsymbol{B}\cdot\boldsymbol{X_p}(t_i) - \boldsymbol{X}(t_i)\right| \tag{4}$$

where $\boldsymbol{X}$ is the individual's position vector, t_i represents the ith iteration or evolution count, $\boldsymbol{X_p}$ denotes the prey's position vector, and $\boldsymbol{A}$ and $\boldsymbol{B}$ are coefficient vectors, which can be defined as:

$$\boldsymbol{A} = 2ar_1 - a \tag{5}$$

$$\boldsymbol{B} = 2r_2 \tag{6}$$

where r_1 and r_2 are random numbers within the range [0, 1], a is known as the convergence factor, which linearly decreases from 2 to 0 as the iteration count increases, i.e.,:

$$a(t_i) = 2 - \frac{2t_i}{t_{max}} \tag{7}$$

where t_{max} represents the maximum number of iteration evolutions.

To mathematically describe the bubble-net feeding behavior of whales, this study incorporates two distinct approaches within the WOA algorithm: the Converging Encircling Mechanism and the Spiral Updating Position. The Converging Encircling Mechanism is implemented through Equations (4–7) as the convergence factor 'a' diminishes. In the Spiral Updating Position method, the simulated spiral motion of whales is employed to capture prey, and its mathematical model is represented as Equation 8:

$$\boldsymbol{X}(t_{i+1}) = \boldsymbol{D'}\cdot e^{bl}\cdot\cos(2\pi l) + \boldsymbol{X_p}(t_i) \tag{8}$$

where $\boldsymbol{D'} = \left|\boldsymbol{X_p}(t_i) - \boldsymbol{X}(t_i)\right|$ represents the distance between the current individual and the prey, b is a constant, and l is a random number within the range [-1, 1].

In addition to the bubble-net feeding behavior, whales can also search for food randomly. When $|\boldsymbol{A}| > 1$, individual whales perform random searches based on their positions relative to each other. The mathematical model for this is:

$$\boldsymbol{X}(t_{i+1}) = \boldsymbol{X_{rand}}(t_i) - \boldsymbol{A}\cdot\left|\boldsymbol{C}\cdot\boldsymbol{X_{rand}}(t_i) - \boldsymbol{X}(t_i)\right| \tag{9}$$

where $\boldsymbol{X_{rand}}$ represents the position vector of a randomly selected whale individual from the current population.

4.2 Cubic map

The initial whale population generated by random methods is unevenly distributed in the solution space, with poor diversity, which cannot effectively extract useful information from the solution space, thus affecting the search efficiency of the algorithm to some extent. Cubic mapping can be used to replace pseudo-random number generators, i.e., generating chaotic numbers between 0 and 1. Previous research has shown that using chaotic sequences for population initialization often yields better results (Wang et al., 2014; Kaur and Arora, 2018).

In this study, the Cubic map is employed to optimize the random approach for initializing the population in the WOA, with the following Equation 10:

$$z_{k+1} = c\left(1 - z_k^2\right) \tag{10}$$

where z_k represents the iteration value of the kth generation, and c is the adjusting coefficient.

4.3 Intelligent weight adjustment

From the previous Equation 7, it can be observed that in the basic WOA algorithm, the value of the control parameter "a" linearly decreases from 2 to 0 as the number of iterations increases. In fact, the optimization process of the WOA algorithm is highly complex, and the linear decrease strategy of the control parameter "a" cannot adapt well to the actual optimization process. It can easily lead to low convergence accuracy or getting stuck in local optima (Li M. et al., 2022). This study employs an adaptive algorithm to modify the weight values of the whale population during each evolution process, as Equation 11:

$$w = w_{min} + m\left(w_{max} - w_{min}\right)e^{\frac{-t_i}{t_{max}}} \tag{11}$$

where w is the weight coefficient, w_{min} and w_{max} are the initial and final values of the weight coefficient, and m is the adjustment coefficient.

4.4 Model evaluation

To validate the predictive results of the PCA-CIWOABP coupled model for groundwater levels in the Fengnan area, this

study employs the following six evaluation metrics as quantitative assessment criteria for evaluating the prediction results: Mean Absolute Error (MAE), Mean Squared Error (MSE), Root Mean Squared Error (RMSE), Mean Absolute Percentage Error (MAPE), Nash efficiency coefficient (NSE) and Pearson correlation coefficient (R), with the calculation formulas as Equations 12–17 (Zhang et al., 2023; Zhang et al., 2024a; Zhang et al., 2024b):

$$MAE = \sum_{i=1}^{n} |h_i - f_i|/n \tag{12}$$

$$MSE = \sum_{i=1}^{n} (h_i - f_i)^2/n \tag{13}$$

$$RMSE = \sum_{i=1}^{n} \left((h_i - f_i)^2/n\right)^{1/2} \tag{14}$$

$$MAPE = \sum_{i=1}^{n} |(h_i - f_i)/f_i|/n * 100\% \tag{15}$$

$$NSE = 1 - \sum_{i=1}^{n} (h_i - f_i)^2 / \sum_{i=1}^{n} \left(h_i - \overline{h}\right)^2 \tag{16}$$

$$R = \sum_{i=1}^{n} \left(h_i - \overline{h}\right)\left(f_i - \overline{f}\right) / \left[\sqrt{\sum_{i=1}^{n} \left(h_i - \overline{h}\right)^2} \sqrt{\sum_{i=1}^{n} \left(f_i - \overline{f}\right)^2}\right] \tag{17}$$

where h_i represents the actual measured values, f_i represents the predicted values, $\overline{h}$ and $\overline{f}$ are the average values of their respective datasets, and n denotes the number of data samples.

5 Result and discussion

5.1 Fluctuations in the distribution of groundwater levels

In this study, the fluctuation of groundwater level is primarily associated with residential water consumption and rainfall, while the distribution of groundwater level is correlated with the local water systems and elevation. Based on the annual average groundwater levels of monitoring wells within the region from 2018 to 2021, a contour map of groundwater levels was generated using the inverse distance weighted interpolation method, as shown in Figure 3.

To further investigate the seasonal fluctuation of groundwater levels within the Fengnan area, this study took monitoring wells #01, #05, #07, and #12 as examples and plotted the water level variations for each month. The specific results are depicted in Figure 4.

The groundwater levels at various monitoring wells exhibit a trend of "initial decrease followed by an increase," with the lowest levels typically occurring between May and July. Among them, the lowest water levels for each monitoring well were generally observed in May for the years 2018, 2019, and 2021. However, in 2020, the groundwater levels at all locations reached their nadir in July. For instance, monitoring well #12 reached its lowest levels in July 2020 and May 2021, with levels of 3.73 m and 4.45 m respectively.

The fluctuation of groundwater levels is not only influenced by local government water management measures but also related to the replenishment from nearby water systems. Combining with Figure 1, it can be observed that monitoring well #01 is located near the downstream of the Tang River, monitoring well #05 and #12 are situated in the middle and upper reaches of the Sha River respectively, and monitoring well #07 is positioned between the Tang River and the Sha River, receiving minimal replenishment from the river systems. Additionally, monitoring well #01 is closer to the Bohai Sea compared to other monitoring wells, and the rivers in Figure 1 all belong to the fifth-level river system, indicating relatively weak influence of river systems on groundwater levels. Therefore, monitoring well #01 steadily increased from 2018 to 2021, with a water level difference of 7.02 m between the beginning of 2018 and the end of 2021; monitoring well #05, #07, and #12 did not show significant changes in water levels compared to monitoring well #01, with differences in groundwater levels at the beginning and end of 2018 and 2021 being less than 1 m for monitoring well #05 and #07.

5.2 Principal component analysis results

In this study, due to the existence of multiple indicator factors for rainfall, water consumption, and groundwater levels, directly constructing a neural network would require a substantial amount of measured data. Consequently, the raw data was first standardized and then subjected to PCA using SPSS. The cumulative contribution rates and correlation coefficients of each component are illustrated in Figures 5, 6, respectively. In order to reduce data dimensionality, enhance data interpretability, filter out data noise, and prevent overfitting, this paper not only ranked and accumulated the variance contribution rates of each component one by one but also regarded components with cumulative variance contribution rates greater than 85% as the principal components of their respective datasets.

As shown in Figure 5, for groundwater levels, the variance contribution rates of monitoring wells #11 and #12 are 71.74% and 13.77%, respectively, with a cumulative contribution rate exceeding 85%. Hence, these two monitoring wells can be extracted as principal components and denoted as G_1 and G_2. Concerning residential water usage, the variance contribution rates for towns FN and QY are 78.78% and 14.23%, respectively, resulting in a cumulative contribution rate exceeding 90%. Therefore, these two towns can be extracted as principal components and labeled as W_1 and W_2. For rainfall, only rainfall station r1 achieves a contribution rate of 92.80%, leading to a cumulative contribution rate exceeding 90%. Thus, this rainfall station can be extracted as a principal component and denoted as R_1.

Considering the correlation coefficients in Figure 6, it's evident that the larger the absolute value of correlation coefficient between components, the closer the relationship between the original variables and that principal component. For groundwater levels, the first principal component G_1 shows higher correlation coefficients with monitoring wells #3 to #7, while the second principal component G_2 demonstrates higher correlations with monitoring wells #1 to #10, all exceeding 0.5. The linear combinations expressing the relationships between each principal component and the original variables are as Equations 18 and 19:

$$G_1 = 0.257G_{\#1} - 0.135G_{\#2} - 0.105G_{\#3} + 0.177G_{\#4} - 0.101G_{\#5} - 0.238G_{\#6} - 0.180G_{\#7} + 0.063G_{\#8} + 0.243G_{\#9} + 0.338G_{\#10} - 0.235G_{\#11} + 0.024G_{12} \tag{18}$$

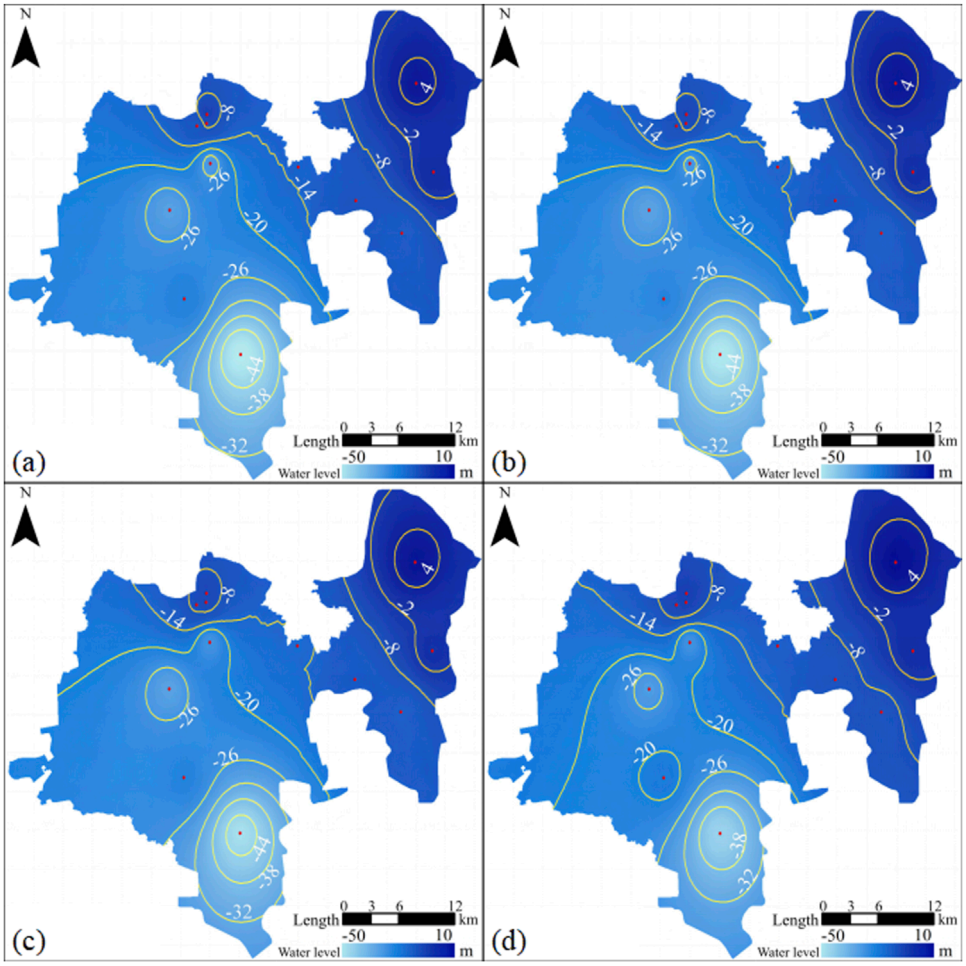

FIGURE 3
Distribution of annual average groundwater levels: **(A)** 2018, **(B)** 2019, **(C)** 2020, and **(D)** 2021.

$$G_2 = 0.102G_{\#1} + 0.120G_{\#2} + 0.128G_{\#3} + 0.100G_{\#4} + 0.095G_{\#5} + 0.102G_{\#6} + 0.119G_{\#7} + 0.118G_{\#8} + 0.092G_{\#9} + 0.078G_{\#10} + 0.078G_{\#11} + 0.127G_{12} \quad (19)$$

where G_i represents the standardized data of the original variables.

For residential water consumption, the first principal component W_1 has a strong correlation with DX, XJ, CH, HG, and XG, while the second principal component W_2. shows a significant correlation only with DQ, all with correlations above 0.5. The linear combination expressions between each principal component and the original variables are as Equations 20 and 21:

$$W_1 = 0.191W_{FN} + 0.067W_{QY} + 0.189W_{DX} + 0.186W_{XJ} + 0.158W_{CH} + 0.080W_{DQ} + 0.193W_{HG} + 0.152W_{XG} \quad (20)$$

$$W_2 = -0.063W_{FN} + 0.608W_{QY} - 0.096W_{DX} - 0.050W_{XJ} - 0.148W_{CH} + 0.576W_{DQ} - 0.041W_{HG} - 0.107W_{XG} \quad (21)$$

where W_i represents the standardized data of the original variables.

For rainfall, the primary component R_1 shows significant correlation coefficients with r2 to r4, all exceeding 0.8. The linear combination between the principal component and the original variables is expressed as Equation 22:

$$R_1 = 0.265R_{r1} + 0.261R_{r2} + 0.263R_{r3} + 0.248R_{r4} \quad (22)$$

where R_i represents the standardized data of the original variables.

5.3 Simulation results and analysis

The magnitude of calculation errors in the BP neural network model is not only related to the application of data mining techniques but also depends on the selection of input and output layer factors. To achieve a higher simulation accuracy model, this study utilizes principal component analysis to perform dimensionality reduction on the original data, thereby eliminating

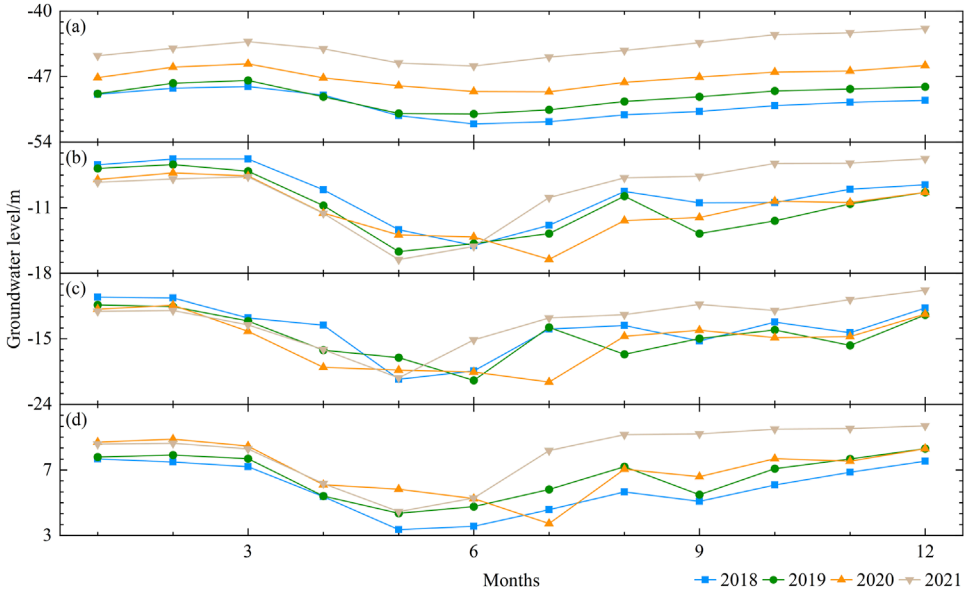

FIGURE 4
Fluctuations in monthly average groundwater levels: **(A)** #01, **(B)** #05, **(C)** #07, and **(D)** #12.

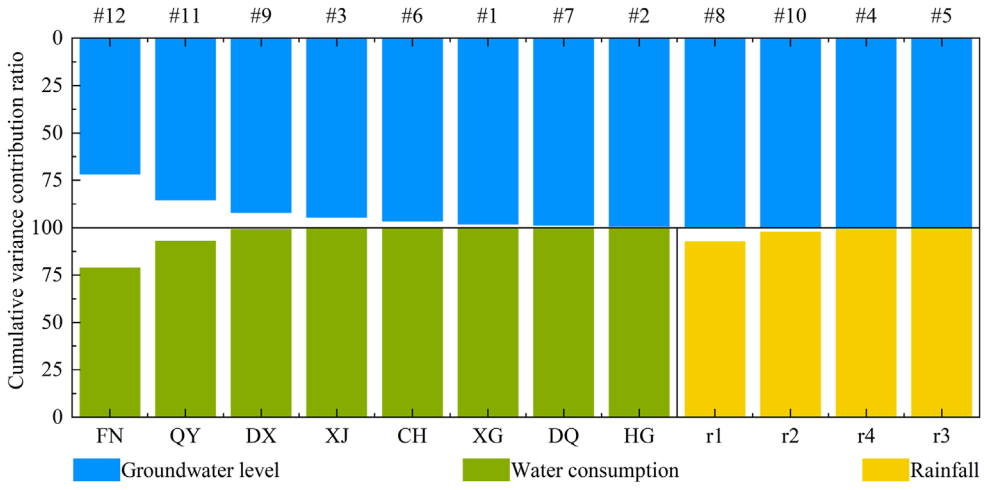

FIGURE 5
Cumulative variance contribution ratio.

the influence of collinearity. Ultimately, five principal components are obtained as the input and output layer factors for the neural network model.

The hydro-meteorological actual measurement data from 2018 to 2020 were selected to construct the groundwater level model for the Fengnan area. The actual measurement data from 2021 were used for model validation. The BP neural network was set up with the sigmoid activation function for the input layer and the tansig activation function for the output layer. The network was trained for 1000 iterations with a learning rate of 0.01 and a target minimum error of 0.00005. In the WOA, the initial population size and the maximum evolution generations were set to 30 and 50, respectively. The upper and lower limits of the independent variables were set to three and -3, respectively. For initializing the population using chaotic mapping, the adjustment coefficient c was set to 1. For updating the shrink-wrap mechanism using the adaptive weight method, the initial values w_{min} and w_{max} of the weight coefficients were set to 0 and 1, respectively, and the weight coefficient m was set to 1.

Furthermore, the neural structure in the BP neural network is a single layer with the number of neurons determined using a loop iteration in the Matlab algorithm. After evaluating the mean squared error, it was ultimately set to seven neurons. The neural network structure is 3-7-2. The comparison between different model training results and actual measurements is shown in Figure 7.

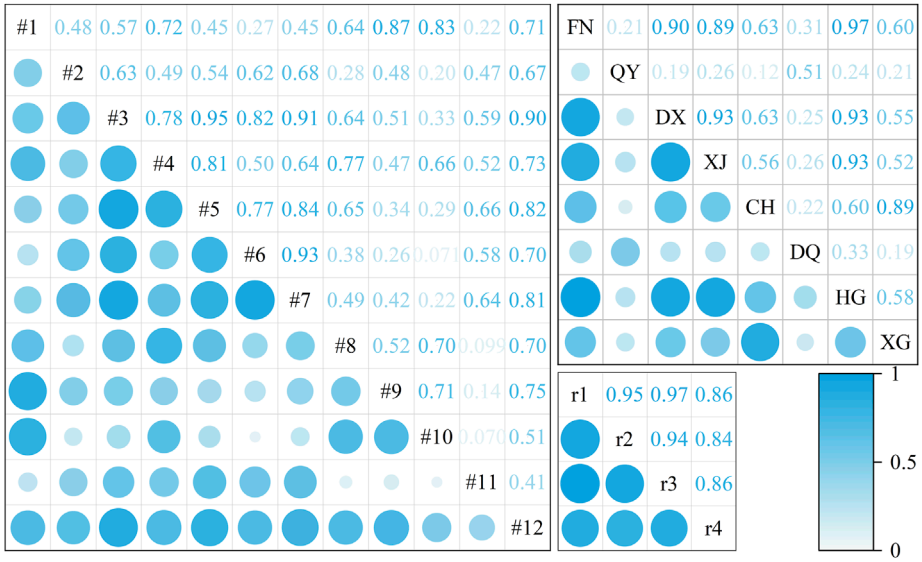

FIGURE 6
Correlation coefficient.

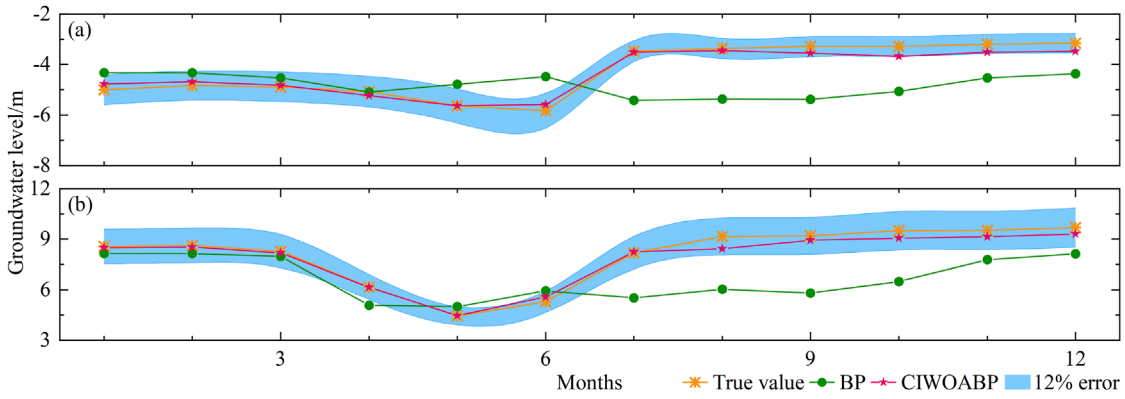

FIGURE 7
Comparison and analysis of different models: **(A)** The simulated prediction value of groundwater level in #11, and **(B)**: The simulated prediction value of groundwater level in #12.

The simulation and prediction values of the BP neural network and the CIWOABP neural network exhibit significant differences. Detailed data information can be found in Table 2. The overall error of the CIWOABP neural network's simulation prediction values is less than 12%. For monitoring wells #11 and #12, MAE is 0.19 and 0.23, MSE is 0.05 and 0.09, RMSE is 0.22 and 0.31, MAPE is 5.06% and 2.77%, NSE is 0.95 and 0.97, and R is 0.987 and 0.993, respectively. On the other hand, the BP neural network demonstrates lower prediction accuracy, with MAE values for monitoring wells #11 and #12 being 1.06 and 2.20, both exceeding 1. This indicates that the model's generalization ability is poor, and the credibility of the simulated results is low. Based on the validation results of the two models, it can be concluded that the PCA-CIWOABP neural network established for predicting groundwater levels in the Fengnan area has high prediction accuracy, good fitting performance, and can be used to calculate and predict actual groundwater levels effectively.

6 Discussion

The study area of this article is located in the North China Plain, the largest "groundwater funnel" area in China, where the local government has been continuously strengthening management measures in recent years. Measures include hydrogeological investigations, development of groundwater models, zoning protection of groundwater, and pollution control and remediation of groundwater (Kløve et al., 2014; Gleeson et al., 2020). The introduction of groundwater models and development,

TABLE 2 Comparison of simulations between BP and CIWOABP.

Model	PCA-BP		PCA-CIWOABP	
Wells	#11	#12	#11	#12
MAE	1.06	2.2	0.19	0.23
MSE	1.84	3.79	0.05	0.09
RMSE	4.08	5.49	0.22	0.31
MAPE	24.03%	25.43%	5.06%	2.77%
NSE	1.84	1.32	0.95	0.97
R	0.02	−0.29	0.99	0.99

as outlined in the introduction, primarily involve traditional hydrological models and neural network models under the drive of big data. Benefiting from local government regulations and monitoring, the availability of more hydrological information enables numerous researchers to conduct neural network research.

In this research work, it is noteworthy that although the neural network has five input and output elements, due to the limited training dataset, we introduced the PCA-CIWOA algorithm to meet the multi-input and multi-output requirements of the BP neural network. Other algorithms with similar capabilities include particle swarm optimization (Marini and Walczak, 2015), grey wolf optimization (Emary et al., 2016), and seagull optimization (Dhiman et al., 2021), each with some differences. For example, the whale optimization algorithm exhibits excellent global search capability and rapid convergence; particle swarm optimization involves information sharing and collaboration among individuals, making it suitable for continuous space optimization problems; the grey wolf algorithm combines competitive and cooperative characteristics, possessing good global search capability and convergence speed, applicable to continuous space optimization and multi-objective optimization problems. These algorithms require further comparative analysis, particularly for simulating and predicting groundwater levels in practical engineering applications.

Additionally, the interpolation methods can be used to generate images in regions with abundant water systems, and graph neural networks can be employed to achieve training and prediction results. Such as Bai and Tahmasebi (2023) represented each well as a node in a graph using a graph neural network (GNN) and utilized convolutional networks to obtain temporal features of sequences. The findings indicated that the model could achieve high simulation accuracy, even when spatial dependency relationships were completely unknown, through learning from the data. Nevertheless, the image interpolation methods are extremely important. The study employed the inverse distance interpolation method to generate groundwater level contour maps for the study area based on data from 12 monitoring wells. Xiao et al. (2016) examined seven interpolation methods, including inverse distance weighted interpolation, global polynomial interpolation, local polynomial interpolation, tension spline interpolation, ordinary Kriging interpolation, simple Kriging interpolation, and universal Kriging interpolation, to assess trends in groundwater level fluctuations in the study area. The effectiveness of these interpolation methods still needs to be further compared with actual engineering in future research work to determine their applicability.

Recently, deep learning algorithms have attracted significant attention in the field of water resources engineering. Although they are widely applicable, machine learning algorithms that rely on feature extraction still hold certain application value when the number of data samples is limited. However, when dealing with more complex multi-input and multi-output problems, the number of training samples required by deep learning algorithms far exceeds that of machine learning algorithms. Particularly in small-scale areas that urgently need remediation and have limited data samples, machine learning algorithms represented in this paper often demonstrate higher applicability than deep learning algorithms.

7 Conclusion

By reducing data dimensionality and incorporating optimization algorithms, the aim is to enhance the accuracy and stability of groundwater level simulations. The empirical research yields the following conclusions.

1. The resulting principal components (rainfall station r1, water consumption FN and QY, monitoring wells #11 and #12) still effectively represent the overall hydrological conditions in the study area, thus reducing the training complexity of the BP neural network.
2. In situations where the training samples are limited and there are multiple inputs and outputs, the BP neural network exhibits overall poor accuracy in simulating and predicting groundwater levels. The annual trend of water level changes in the simulation results may even be contrary to the actual situation.
3. The coupling of chaotic mapping and adaptive weight-based WOA significantly enhances the computational accuracy of groundwater level simulation in the BP neural network. The RMSE for monitoring wells #11 and #12 is 0.22 and 0.31, respectively, and the MAPE is 5.06% and 2.77%, respectively.

Data availability statement

The original contributions presented in the study are included in the article/supplementary material, further inquiries can be directed to the corresponding author.

Author contributions

XZ: Writing–review and editing. XG: Data curation, Writing–original draft. SL: Methodology, Writing–original draft. XS:

Software, Writing–review and editing. ZX: Writing–review and editing. JZ: Writing–review and editing.

Funding

The author(s) declare that financial support was received for the research, authorship, and/or publication of this article. This work was supported by The Key Research Project in Basic Research for Colleges and Universities in Henan Province (25A570005), North China University of Water Resources and Electric Power 15th Graduate Student Innovation Project (NCWUYC-202315005), the National Natural Science Foundation of China under contract No. 41930643, "Study on carbon and nitrogen process and its effect in the Lower Yellow River".

Conflict of interest

The authors declare that the research was conducted in the absence of any commercial or financial relationships that could be construed as a potential conflict of interest.

Publisher's note

References

Almanaseer, N., and Sankarasubramanian, A. (2012). Role of climate variability in modulating the surface water and groundwater interaction over the southeast United States. *J. Hydrol. Eng.* 17, 1001–1010. doi:10.1061/(ASCE)HE.1943-5584.0000536

Bai, T., and Tahmasebi, P. (2023). Graph neural network for groundwater level forecasting. *J. Hydrol.* 616, 128792. doi:10.1016/j.jhydrol.2022.128792

Bo, L., Li, Z., Liu, Y., Yue, Y., Zhang, Z., and Wang, Y. (2022). Research on multi-level scheduling of mine water reuse based on improved whale optimization algorithm. *Sensors* 22 (14), 5164. doi:10.3390/s22145164

Bowes, B. D., Sadler, J. M., Morsy, M. M., Behl, M., and Goodall, J. L. (2019). Forecasting groundwater table in a flood prone coastal city with Long short-term memory and recurrent neural networks. *Water* 11 (5), 1098. doi:10.3390/w11051098

Chai, Q., Han, W., Fang, W., Ding, Z., and Wu, F. (2023). Study on coordinated allocation of conventional and unconventional water resources in typical regions of North China. *Front. Earth Sci.* 11. doi:10.3389/feart.2023.1198431

Chang, F., Huang, C., Cheng, S., and Chang, L. (2017). Conservation of groundwater from over-exploitation—scientific analyses for groundwater resources management. *Sci. Total Environ.* 598, 828–838. doi:10.1016/j.scitotenv.2017.04.142

Costa, D., Zhang, H., and Levison, J. (2021). Impacts of climate change on groundwater in the Great Lakes Basin: a review. *J. Gt. Lakes Res.* 47 (6), 1613–1625. doi:10.1016/j.jglr.2021.10.011

Dash, N. B., Panda, S. N., Remesan, R., and Sahoo, N. (2010). Hybrid neural modeling for groundwater level prediction. *Neural comput. Appl.* 19 (8), 1251–1263. doi:10.1007/s00521-010-0360-1

Deb, S. (2024). Analyzing trends and change points in hydro-meteorological parameters and groundwater level in the Barak river basin in India. *Phys. Chem. Earth* 134, 103542. doi:10.1016/j.pce.2023.103542

Demšar, U., Harris, P., Brunsdon, C., Fotheringham, A. S., and McLoone, S. (2013). Principal component analysis on spatial data: an overview. *Ann. Assoc. Am. Geogr.* 103 (1), 106–128. doi:10.1080/00045608.2012.689236

Dhiman, G., Singh, K. K., Soni, M., Nagar, A., Dehghani, M., Slowik, A., et al. (2021). MOSOA: a new multi-objective seagull optimization algorithm. *Expert Syst. Appl.* 167, 114150. doi:10.1016/j.eswa.2020.114150

Emary, E., Zawbaa, H. M., and Hassanien, A. E. (2016). Binary grey wolf optimization approaches for feature selection. *Neurocomputing* 172, 371–381. doi:10.1016/j.neucom.2015.06.083

Gleeson, T., Cuthbert, M., Ferguson, G., and Perrone, D. (2020). Global groundwater sustainability, resources, and systems in the anthropocene. *Annu. Rev. Earth Planet. Sci.* 48, 431–463. doi:10.1146/annurev-earth-071719-055251

Hosseini, Z., Gharechelou, S., Nakhaei, M., and Gharechelou, S. (2016). Optimal design of BP algorithm by ACOR model for groundwater-level forecasting: a case study on Shabestar plain, Iran. *Arab. J. Geosci.* 9 (6), 436. doi:10.1007/s12517-016-2454-2

Hou, Q. Q., Pan, Y. J., Zeng, M., Wang, S., Shi, H. H., Huang, C. S., et al. (2023). Assessment of groundwater hydrochemistry, water quality, and health risk in Hainan Island, China. *Sci. Rep.* 13 (1), 12104. doi:10.1038/s41598-023-36621-3

Jolliffe, I. (2022). A 50-year personal journey through time with principal component analysis. *J. Multivar. Anal.* 188, 104820. doi:10.1016/j.jmva.2021.104820

Jung, H., Ha, K., Koh, D. C., Kim, Y., and Lee, J. (2021). Statistical analysis relating variations in groundwater level to droughts on Jeju Island, Korea. *J. Hydrol. Reg. Stud.* 36, 100879. doi:10.1016/j.ejrh.2021.100879

Kaur, G., and Arora, S. (2018). Chaotic whale optimization algorithm. *J. Comput. Des. Eng.* 5 (3), 275–284. doi:10.1016/j.jcde.2017.12.006

Kim, G. B., Hwang, C. I., and Choi, M. R. (2021). PCA-based multivariate LSTM model for predicting natural groundwater level variations in a time-series record affected by anthropogenic factors. *Environ. Earth Sci.* 80 (18), 657. doi:10.1007/s12665-021-09957-0

Kløve, B., Ala-Aho, P., Bertrand, G., Gurdak, J. J., Kupfersberger, H., Kværner, J., et al. (2014). Climate change impacts on groundwater and dependent ecosystems. *J. Hydrol.* 518, 250–266. doi:10.1016/j.jhydrol.2013.06.037

Lai, V., Huang, Y. F., Koo, C. H., Ahmed, A. N., and El-Shafie, A. (2021). Optimization of reservoir operation at Klang Gate Dam utilizing a whale optimization algorithm and a Lévy flight and distribution enhancement technique. *Eng. Appl. Comp. Fluid Mech.* 15 (1), 1682–1702. doi:10.1080/19942060.2021.1982777

Li, F., Feng, P., Zhang, W., and Zhang, T. (2013). An integrated groundwater management mode based on control indexes of groundwater quantity and level. *Water Resour. Manag.* 27 (9), 3273–3292. doi:10.1007/s11269-013-0346-8

Li, H. H., Lu, Y. D., Zheng, C., Yang, M., and Li, S. (2019). Groundwater level prediction for the arid oasis of northwest China based on the artificial bee Colony algorithm and a back-propagation neural network with double hidden layers. *Water* 11 (4), 860. doi:10.3390/w11040860

Li, M., Xu, G., Fu, Y., Zhang, T., and Du, L. (2022a). Improved whale optimization algorithm based on variable spiral position update strategy and adaptive inertia weight. *J. Intell. Fuzzy Syst.* 42, 1501–1517. doi:10.3233/JIFS-210842

Li, X. Q., Lin, Q. T., Chao, K. F., and li, D. X. (2022b). A simple numerical simulation method for unsaturated stratum under the water environmental load. *Comput. Geotech.* 154, 105177. doi:10.1016/j.compgeo.2022.105177

Lin, H. Y., Tseng, T. S., Wang, X., Fang, Z., Zea, A. H., Wang, L., et al. (2022). Intake patterns of specific alcoholic beverages by prostate cancer status. *Cancers* 14 (8), 1981. doi:10.3390/cancers14081981

Marini, F., and Walczak, B. (2015). Particle swarm optimization (PSO). A tutorial. *Chemom. Intell. Lab. Syst.* 149, 153–165. doi:10.1016/j.chemolab.2015.08.020

Marukatat, S. (2023). Tutorial on PCA and approximate PCA and approximate kernel PCA. *Artif. Intell. Rev.* 56 (6), 5445–5477. doi:10.1007/s10462-022-10297-z

Matiatos, I., Varouchakis, E. A., and Papadopoulou, M. P. (2019). Performance evaluation of multiple groundwater flow and nitrate mass transport numerical models. *Environ. Model. Assess.* 24 (6), 659–675. doi:10.1007/s10666-019-9653-7

Mirjalili, S., and Lewis, A. (2016). The whale optimization algorithm. *Adv. Eng. Softw.* 95, 51–67. doi:10.1016/j.advengsoft.2016.01.008

Naderianfar, M., Piri, J., and Kisi, O. (2017). Pre-processing data to predict groundwater levels using the fuzzy standardized evapotranspiration and precipitation index (SEPI). *Water Resour. Manag.* 31 (14), 4433–4448. doi:10.1007/s11269-017-1757-8

Serravalle Reis Rodrigues, V. H., de Melo Barros Junior, P. R., dos Santos Marinho, E. B., and Lima de Jesus Silva, J. L. (2023). Wavelet gated multiformer for groundwater time series forecasting. *Sci. Rep.* 13 (1), 12726. doi:10.1038/s41598-023-39688-0

Singh, H., Rai, V., Kumar, N., Dadheech, P., Kotecha, K., Selvachandran, G., et al. (2023). An enhanced whale optimization algorithm for clustering. *Multimed. Tools Appl.* 82 (3), 4599–4618. doi:10.1007/s11042-022-13453-3

Stigter, T. Y., Miller, J., Chen, J., and Re, V. (2023). Groundwater and climate change: threats and opportunities. *Hydrogeol. J.* 31 (1), 7–10. doi:10.1007/s10040-022-02554-w

Triki, I., Trabelsi, N., Hentati, I., and Zairi, M. (2014). Groundwater levels time series sensitivity to pluviometry and air temperature: a geostatistical approach to Sfax region, Tunisia. *Environ. Monit. Assess.* 186 (3), 1593–1608. doi:10.1007/s10661-013–8

Wang, G. G., Guo, L. H., Gandomi, A. H., Hao, G. S., and Wang, H. Q. (2014). Chaotic krill herd algorithm. *Inf. Sci.* 274, 17–34. doi:10.1016/j.ins.2014.02.123

Wang, W. C., Wang, B., Chau, K. W., and Xu, D. M. (2023). Monthly runoff time series interval prediction based on WOA-VMD-LSTM using non-parametric kernel density estimation. *Earth Sci. Inf.* 16 (3), 2373–2389. doi:10.1007/s12145-023-01038-z

Wold, S., Esbensen, K., and Geladi, P. (1987). Principal component analysis. *Chemom. Intell. Lab. Syst.* 2 (1), 37–52. doi:10.1016/0169-7439(87)80084-9

Xiao, Y., Gu, X. M., Yin, S. Y., Shao, J. L., Cui, Y. L., Zhang, Q. L., et al. (2016). Geostatistical interpolation model selection based on ArcGIS and spatio-temporal variability analysis of groundwater level in piedmont plains, northwest China. *SpringerPlus* 5 (1), 425. doi:10.1186/s40064-016-2073-0

Xu, H., Yang, X., Wang, D., Hu, Y., Shi, Y., Cheng, Z., et al. (2022). Predicting groundwater potential assessment in water-deficient islands based on convolutional neural networks. *Egypt. J. Remote Sens. Space Sci.* 25, 1013–1023. doi:10.1016/j.ejrs.2022.11.002

Yan, Z., Sha, J., Liu, B., Tian, W., and Lu, J. (2018). An ameliorative whale optimization algorithm for multi-objective optimal allocation of water resources in handan, China. *Water* 10 (1), 87. doi:10.3390/w10010087

Yang, X. Y., and Zhang, Z. R. (2022). A CNN-LSTM model based on a meta-learning algorithm to predict groundwater level in the middle and lower reaches of the heihe river, China. *Water* 14 (15), 2377. doi:10.3390/w14152377

Zaghiyan, M. R., Eslamian, S., Gohari, A., and Ebrahimi, M. S. (2021). Temporal correction of irregular observed intervals of groundwater level series using interpolation techniques. *Theor. Appl. Climatol.* 145 (3), 1027–1037. doi:10.1007/s00704-021-03666-1

Zhang, M. C. (2022). Prediction of rockburst hazard based on particle swarm algorithm and neural network. *Neural comput. Appl.* 34 (4), 2649–2659. doi:10.1007/s00521-021-06057-9

Zhang, R. T., Chen, S. Z., Zhang, Z. A., and Zhu, W. C. (2022). Genetic algorithm in multimedia dynamic prediction of groundwater in open-pit mine. *Comput. Intell. Neurosci.* 2022, 1–6. doi:10.1155/2022/8556103

Zhang, X. Q., Qi, Y., Li, H. Y., Wang, X., and Yin, Q. W. (2024a). Assessing the response of non-point source nitrogen pollution to land use change based on SWAT model. *Ecol. Indic.* 158, 111391. doi:10.1016/j.ecolind.2023.111391

Zhang, X. Q., Ren, H., Liu, J. W., Zhang, Y. H., and Cheng, W. H. (2024b). A monthly temperature prediction based on the CEEMDAN–BO–BiLSTM coupled model. *Sci. Rep.* 14 (1), 808. doi:10.1038/s41598-024-51524-7

Zhang, X. Q., Yin, Q. W., Liu, F., Li, H. Y., and Qi, Y. (2023). Comparative study of rainfall prediction based on different decomposition methods of VMD. *Sci. Rep.* 13 (1), 20127. doi:10.1038/s41598-023-47416-x

frontiers | Frontiers in Ecology and Evolution

TYPE Original Research
PUBLISHED 17 December 2024
DOI 10.3389/fevo.2024.1522066

OPEN ACCESS

EDITED BY
Qiang Liu,
Beijing Normal University, China

REVIEWED BY
Ying Zhu,
Xi'an University of Architecture and Technology, China
Bai Tao,
Xi'an University of Technology, China

*CORRESPONDENCE
Bonian Shui
shuibonian@163.com

RECEIVED 03 November 2024
ACCEPTED 02 December 2024
PUBLISHED 17 December 2024

CITATION
Li X, Cui C, Shui B, Hu C, Ye Z and Zhang Y (2024) Research on the evaluation index system for happy rivers and lakes: a case study of Xinchang County in Zhejiang Province, China. *Front. Ecol. Evol.* 12:1522066. doi: 10.3389/fevo.2024.1522066

Research on the evaluation index system for happy rivers and lakes: a case study of Xinchang County in Zhejiang Province, China

Xiaoyu Li[1], Chenxi Cui[1], Bonian Shui[1]*, Chengye Hu[1], Zhou Ye[2] and Yong Zhang[3]

[1]School of Fishery, Zhejiang Ocean University, Zhoushan, Zhejiang, China, [2]College of Water Resources and Environmental Engineering, Zhejiang University of Water Resources and Electric Power, Hangzhou, Zhejiang, China, [3]River Chief's Office, Xinchang County Water Resources and Hydropower Bureau, Shaoxing, Zhejiang, China

The "Happy Rivers and Lakes" initiative is an important measure to systematically address the complex water issues in China. It further highlights the effectiveness of constructing happy rivers and lakes based on river health assessments. This approach aims to identify typical practices and the effectiveness of river and lake management and protection at the local level, guiding for river and lake management and conservation work in the new era. This study focuses on county-level administrative units and develops a research framework for the evaluation index system of happy rivers and lakes. A total of 11 primary indicators and 22 secondary indicators are selected from aspects such as river and lake safety, water resources, water environment, biodiversity, and social services. The evaluation and analysis are conducted around the Chengtan River, Huangze River, and Xinchang River, as well as two large reservoirs in Xinchang County. The results show that the comprehensive evaluation score of happy rivers and lakes in Xinchang County is 92.66, categorizing it as a model of happy rivers and lakes. The evaluation results aim to provide references and guidance for similar regions inside and outside Zhejiang Province in their research and practical applications related to happy rivers and lakes.

KEYWORDS

happy rivers and lakes, evaluation index system, water management and conservation, rivers in mountainous area, Xinchang county

1 Introduction

Amid the intensifying global climate change and the accelerated pace of urbanization, the ecological integrity of rivers and lakes confronts increasingly formidable challenges (Vinna et al., 2018). The scarcity of freshwater resources has emerged as a significant impediment to China's economic advancement, with the country's per capita water resources amounting to merely one-quarter of the global average (Yang, 2021). In response, the Ministry of Water Resources of China promulgated the "Notice on the Construction of Happy Rivers and Lakes" in April 2022. Furthermore, in July 2023, a more methodical framework for the administration and protection of China's rivers was articulated with the publication of the "Work Plan for the Evaluation of the Effectiveness of Happy Rivers and Lakes Construction (Trial)." This plan encompasses the integrated stewardship of water resources, the aquatic environment, and water ecology, as well as stringent regulation of river and lake shoreline space management, and river sand mining oversight, with an emphasis on building and sustaining safe, healthy, beautiful, and blissful rivers and lakes. Zhejiang Province is spearheading the national endeavor to craft happy rivers and lakes. In 2023, it unveiled a five-year "Zhejiang Province Comprehensive Plan for Building Happy Rivers and Lakes" (2023-2027), aiming to establish an axis based on eight principal water systems (Statistics Bureau of Zhejiang Province. Water environment, 2023) and to create nearly a hundred distinctive county-level happy mother rivers. This initiative also aspires to establish over a thousand high-quality, aesthetically pleasing water villages and to revitalize waterfront corridors extending beyond ten thousand kilometers, forming a foundational pattern of "eight belts, a hundred corridors, a thousand pearls, ten thousand paths" ("Among the eight major water systems, a hundred ecological corridors of joyful rivers and lakes are formed, with numerous beautiful lakes and rivers scattered throughout the fluvial network, extending the reach of the happiness-inducing waterway network to thousands of miles (Voice of Zhejiang, 2023).")throughout the region.

Upon examining national and international research, the concept of happy rivers and lakes is unique to China. Related scholarly pursuits, such as river health and ecological restoration (HAN and XIA, 2020), are more prevalent elsewhere (Wang, 2020). The notion of river health traced back to the 1970s in the United States and saw further refinement in the 1990s (Faust et al., 2016; Gardner et al., 2019). Initially, research centered on the natural characteristics of rivers, but over time, it evolved to encompass the river itself, human requirements, and the societal functions of rivers. Scofield defines river health as a state wherein a river's biodiversity and ecosystem functions remain largely unimpaired (Schofield and Davies, 1996).

Rooted in the concept of healthy rivers and lakes, happy rivers and lakes prioritize a people-centric approach, fostering harmonious coexistence between humans and water. This paradigm takes into account human needs and perceptions as its starting point, undertaking comprehensive evaluations of aspects such as river safety, ecology, livability, intelligence, culture, development, and public satisfaction to establish a holistic, scientific, and actionable system for assessing the quality of river and lake ecological environments and integrated development. Research in the realm of happy rivers and lakes emphasizes not only the conservation of river ecosystems but also sustainably addressing human needs (Li and Huang, 2024). Wu (2024) encapsulates Xiangtan City's endeavors in constructing happy rivers and lakes from the perspectives of ecological restoration, soil and water conservation, environmental enhancement, and cultural preservation. He advocates that the construction of happy rivers and lakes should honor and adhere to natural principles by conserving water resources and optimizing river hydrological conditions while cultivating a wholesome and livable aquatic milieu. Several scholars have advanced management suggestions, recommending that the construction of happy rivers and lakes encompass aspects such as implementing the river and lake chief system (Wu et al., 2020; Zhang et al., 2022, 2023b), optimizing the allocation and scheduling of water resources, bolstering water ecological protection and restoration, enhancing comprehensive water environment management, promoting water culture, and invigorating green water economy pilots (Jiang, 2024; Song, 2024b; Tong, 2024). Yang Along (2024) evaluated the Songhua River, Nemur River, and Tongken River using the analytic hierarchy process grounded in understanding the essential connotations and system construction of happy rivers and lakes in Longjiang.

Since the concept of happy rivers and lakes was put forward, some scholars have explored research methods. Lv et al. (2024) employed the DPSIR model to construct a happy rivers and lakes evaluation index system for Heilongjiang Province, thereby overcame the pronounced subjectivity inherent in the priorly established indicator system and analyzed the main influencing factors that affect the happy rivers and lakes index. The evaluation framework for happy river and lakes is structured around the concept of "goal—criteria—indicator." The methodology employed for index calculation involves the "single index quantification—multiple indices synthesis—poly-criteria integration" approach (Zuo et al., 2021). The method verified that the proposed evaluation system accurately represented the happy river status of the Yellow River, and the evaluation system is therefore reliable and applicable. The role of the assessment framework for the happy rivers and lakes evaluation index system thus far has been to furnish policymakers with valuable insights integral to comprehensive river management (Zuo et al., 2020). The overall differences among various rivers and lakes in China are quite pronounced, ensuring the precision of self-assessment within river and lake evaluation systems remains a formidable challenge (Liu et al., 2021; Su et al., 2023; Zhang et al., 2023a); thus, the evaluation system for happy rivers and lakes needs further refinement. This paper endeavors to investigate the evaluation index system of happy rivers and lakes in Zhejiang Province, in alignment with Zhejiang's overarching objectives for happy rivers and lakes construction. Xinchang County was chosen as the pilot assessment area to offer decision support for advancing high-quality river and lake development in the new phase for Zhejiang Province, and to furnish scientific evidence for the preservation and management of river and lake ecological environments.

2 Materials and methods

2.1 Study area

Xinchang County falls under the administration of Shaoxing City in Zhejiang Province. Nestled in the eastern realm of Zhejiang and the southeastern part of Shaoxing, it lies between the longitudes of 120°41′34″E and 121°13′34″E, and latitudes of 29°13′55″N to 29°33′52″N. The climate is noted for its mild and humid conditions with pronounced seasons. During spring and early summer, there is a convergence of rain and warmth, followed by sunny and hot conditions in midsummer; autumn and winter offer a harmonious interplay of sunlight and temperature. The region is prone to frequent adverse weather conditions. It is endowed with ample water resources, with a generally balanced supply and demand. The county is laced with tributaries of streams, the landscape punctuated by towering mountains and steep inclines. The river courses are sinuous with substantial elevation changes, leading to swift water flows that are unsuitable for navigation yet fecund in water resources. The yearly average natural runoff is calculated at 947 million m3, with each square kilometer yielding 771,000 m3 of water, and a per capita provision of 2,370 m3, nearly matching the provincial average. Since the inception of the People's Republic of China, the industrious locals have constructed over 600 reservoirs of varying sizes. Xinchang County is situated in the upper reaches of the Cao'e River basin, populated with numerous streams and ravines that merge into three principal rivers: the Xinchang River, the Chengtan River, and the Huangze River. The total area of the basin spans 1,963 km², with Xinchang County encompassing 1,200.7 km². The average water quality at the confluence points of the "Three Rivers"—Xinchang River, Chengtan River, and Huangze River—attains the Class II surface water quality standard according to "Environmental quality standards for surface water" (GB 3838-2002) (Ministry of Ecology and Environment of the People's Republic of China, 2002) (Figure 1).

2.2 Establishment of an evaluation index system for happy rivers and lakes

The geographical landscape of Zhejiang Province can be succinctly described as "seven parts mountains, one part water, and two parts fields," with a predominance of mountainous and hilly terrain. In regions such as Quzhou, Jinhua, Lishui, Wenzhou, and Shaoxing, mountainous rivers are widely distributed. Xinchang County within Shaoxing City is characterized by numerous mountainous rivers, where the river sections are steep and the currents swift, with vast water areas. The ecological attributes of different rivers vary significantly, necessitating the creation of an evaluation index system tailored to the specific conditions of the region. This system will serve as a pivotal guide for the construction and assessment of happy rivers and lakes in Xinchang County and other similar areas (such as Quzhou, Jinhua, Lishui, and Wenzhou). In light of the characteristics of the rivers and lakes in Xinchang County, this index system emphasizes two key aspects: firstly, the

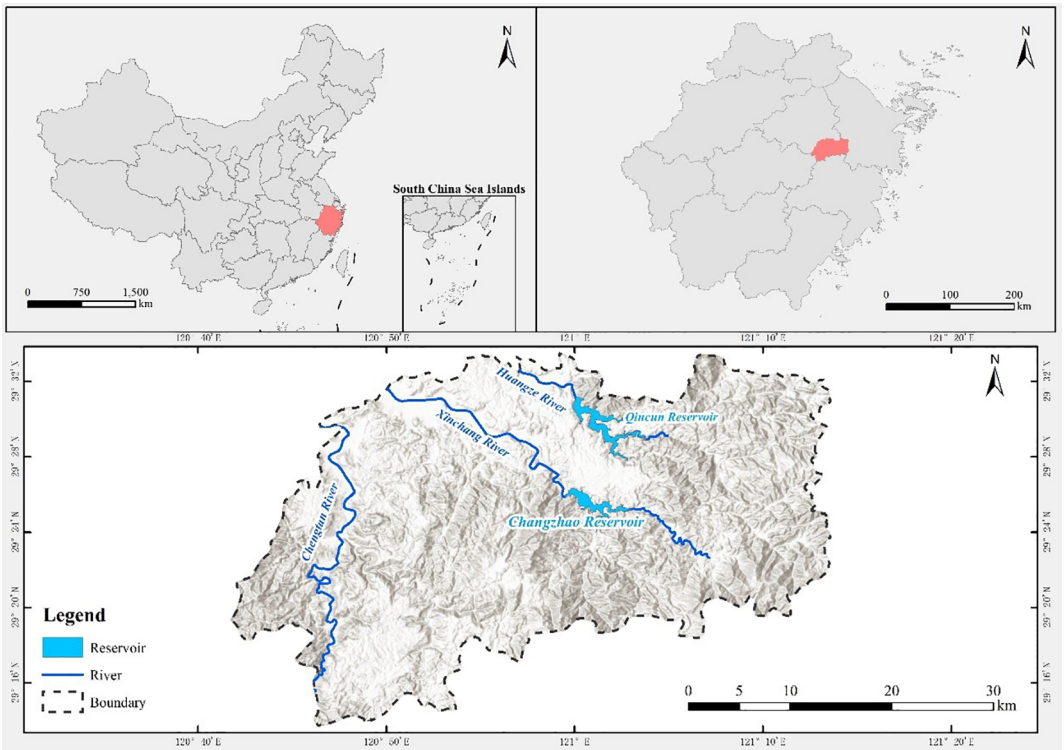

FIGURE 1
Study area, rivers, and reservoirs in Xinchang County.

principle of safeguarding biodiversity; and secondly, the principle of integrating production, ecology, and living (Figure 2).

Integrate the relevant standards from the "Guidelines for the Health Assessment of Rivers and Lakes in Zhejiang Province (Trial)" (August 2023) and the "Guidelines for the Assessment of Aquatic Ecosystem Health in Lakes and Reservoirs in Zhejiang Province (Trial)" (October 2023), while drawing on the technical documents such as the "Guidelines for Assessing the Happiness of Rivers and Lakes in Hangzhou" (2021), the "Guidelines for Assessing the Happiness of Rivers and Lakes in Nanjing (Trial)" (2021), the "Guidelines for Assessing the Happiness of Rivers and Lakes in Suzhou (Trial)" (2021), and the "Guidelines for the Assessment of the Happiness of Rivers and Lakes in the Nanhui District of Huzhou" (2020) to construct an indicator system.

Scope of application: This index system is applicable for assessing both the township-level (and above) and suburban rivers, lakes, and reservoirs within Xinchang County, as well as for the evaluation of "Happy Rivers and Lakes" within other mountainous river and lake networks in Zhejiang Province.

2.2.1 Index selection

The evaluation data is derived from a series of long-term monitoring and multifaceted surveys. The data for this study originates from the "Zhejiang Statistical Yearbook," "Zhejiang Water Resources Bulletin," "Chengtan River Health Assessment Report in Xinchang County," "Huangze River Health Assessment Report in Xinchang County," "Xinchangjiang River Health Assessment Report in Xinchang County," "Qincun Reservoir Aquatic Ecosystem Health Assessment Report in Xinchang County," "Changzhao Reservoir Aquatic Ecosystem Health Assessment Report in Xinchang County," as well as the spring and summer biodiversity investigations conducted in 2023 in Xinchang County.

In this study, the primary indicators encompass the safety of rivers and lakes, riparian vegetation, biodiversity of river and lake ecosystems, the aquatic environment of rivers and lakes, the economic development related to water, drinking water Sources, the management and protection mechanisms for rivers and lakes, the water culture, hydrophilic implementation, and public satisfaction.

Set varying weights for the 22 secondary indicators within the 11 primary indicators, according to the type of evaluation, as specified in Table 1.

According to the standard grading system of this evaluation framework for Happy Rivers and Lakes (with a maximum score of 100 and the highest level being Grade I): a comprehensive evaluation score of 90 (inclusive) ~ 100 qualifies as Grade I (Exemplary Happy River and Lake); a score of 80 (inclusive) ~ 90 qualifies as Grade II (Happy River and Lake); a score of 60 (inclusive) ~ 80 qualifies as Grade III (Ordinary Happy River and Lake); and a score below 60 qualifies as Grade IV, not meeting the standards.

2.2.2 Methodology for calculating metrics

2.2.2.1 The safety rivers and lakes

(1) Flood prevention and disaster mitigation compliance

The compliance rate for flood prevention and disaster mitigation in rivers and lakes has reached 90% or above; the dams of the reservoirs have undergone safety assessments.

The compliance rate for flood prevention and disaster mitigation in rivers and lakes refers to the percentage of shoreline length that meets the designed flood prevention and disaster mitigation standards out of the total shoreline length requiring flood prevention. A compliance rate of 90% or above (including) scores full marks, while a rate below 50% (including) scores no points. The formula for calculating the score is provided in Equation 1.

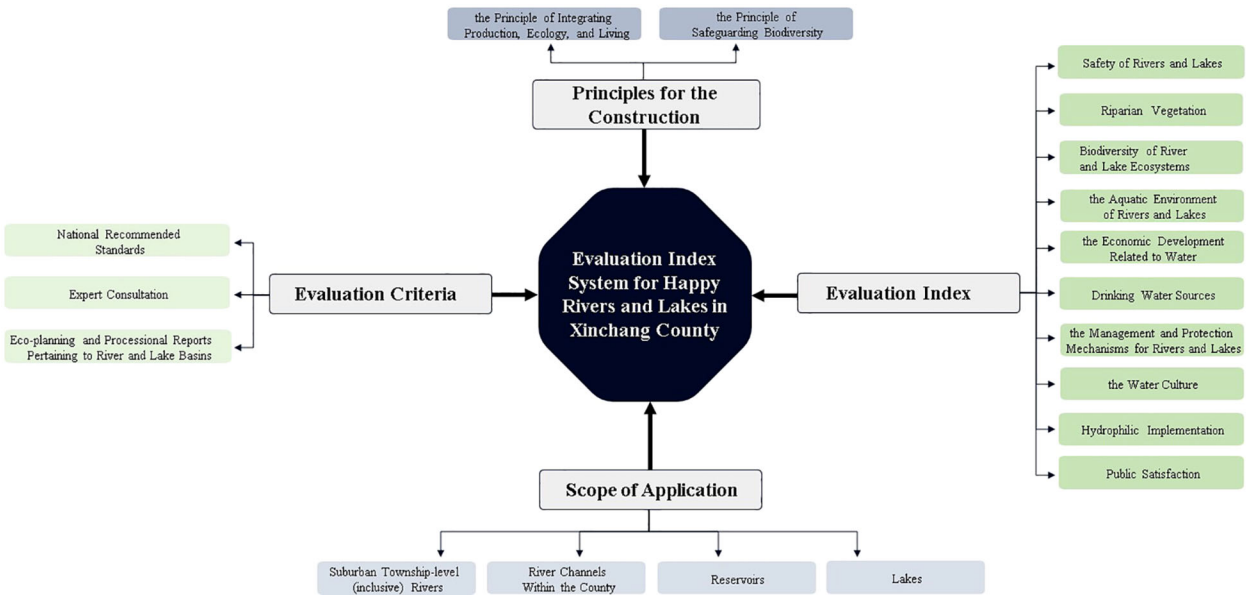

FIGURE 2
Framework for the evaluation of happy river systems in Xinchang County.

TABLE 1 Assessment indicator system for happy rivers and lakes in Xinchang.

Number	Primary Indicator	Primary Indicator Weight	Secondary Indicator	Secondary Indicator Weight
1	the Safety Rivers and Lakes	0.1	Flood Prevention and Disaster Mitigation Compliance	0.5
2			Operation Status of Hydraulic Engineering Projects	0.5
3	Riparian Vegetation	0.15	Shoreline vegetative cover	1
4	Biodiversity of River and Lake Ecosystems	0.25	Diversity of Fish	0.2
5			Diversity of Large Benthic Invertebrates	0.2
6			Diversity of Phytoplankton	0.2
7			Diversity of Zooplankton	0.2
8			Diversity of Periphytic Algae	0.2
9	The Aquatic Environment of Rivers and Lakes	0.15	the Quality of Water	0.5
10			the Assurance of Ecological Flow	0.5
11	the Economic Development Related to Water	0.1	Average annual growth in revenue from water-related tourism	0.3
12			The Annual Growth in the Output Value of Aquaculture	0.3
13			The Per Capita Income Growth Rate from Microhydropower	0.4
14	Drinking Water Sources	0.05	the Compliance Status of Potable Water Sources	1
15	the Management and Protection Mechanisms for Rivers and Lakes	0.1	The "River and Lake Chief System" Collaboration Mechanism Situation	0.5
16			Zoning and Classification Control Situation of River and Lake Water Areas and Shoreline Spaces	0.25
17			Supervision of the River-Related Projects	0.25
18	the Water Culture	0.03	Cultural Display	0.5
19			Development of Cultural, Physical, and Tourism Activities	0.5
20	Hydrophilic Implementation	0.04	The Status of Supporting Facilities for Urban and Rural Hydrophilic Structures	0.5
21			Riverside-waterfront Greenways	0.5
22	Public Satisfaction	0.03	Satisfaction Survey	1

The evaluation result will be "unsatisfactory" in the following situations. a) Public satisfaction survey score is below 60 points; b) The annual average water quality over the past year is below Level V; c) A significant or more serious safety production accident and water-related illegal incident occurred in the past year; d) The significant issues identified through superiors' undercover investigations, spot checks, and media scrutiny have not been resolved within the designated timeframe.

$$P_1 = \begin{cases} 100 & (L_{stdk} \geq 0.9L) \\ 250 \times \frac{L_{stdk}}{L} - 125 & (0.5L < L_{stdk} < 0.9L) \\ 0 & (L_{stdk} \leq 0.5L) \end{cases} \quad (1)$$

P_1 is the score assigned to flood prevention and disaster preparedness compliance in rivers and lakes; L_{stdk} is the length of dikes and revetments that meet the standards (km); and L is the total length of existing dikes or revetments (km).

(2) Operation status of hydraulic engineering projects

The quality of hydraulic engineering is compliant, and hydraulic structures meet design standards. Water conservancy facilities function optimally. Operation of the water project tasks are completed. Where there are no tasks, it is considered a reasonable exception.

This item is scored out of 100 points, with full marks awarded if evaluation criteria are met. For each of the three requirements not fulfilled according to the evaluation standards, 30 points are deducted.

2.2.2.2 Riparian vegetation

The riparian vegetation coverage is defined as the proportion of the vertical projected area of both natural and artificial vegetation along the river (or lake) banks to the total area of the riparian zone. Emphasis is placed on evaluating the coverage status of trees, shrubs, and herbaceous plants across the terrestrial span. Scores for riparian vegetation coverage are determined using both the coverage itself and the natural shoreline rate of the river (or lake), with the criteria for assigning points outlined in Table 2.

TABLE 2 Scoring standards for vegetation coverage of river (lake) riparian zones (natural shoreline method).

The riparian vegetation coverage(%)	(60,100]	(50,60]	(40,50]	(30,40]	(10,30]	[0,10]
score assignment	100	90	85	50	20	0

2.2.2.3 Biodiversity of river and lake ecosystems

(1) Diversity Index

The diversity index for fish, large benthic invertebrates, phytoplankton, zooplankton, and periphytic algae are calculated according to Equation 2. The score assignment criteria can be found in Table 3, with a linear interpolation method applied during the scoring process.

$$H' = -\sum P_i \log_2 P_i \quad (2)$$

In this formula, *H'* represents the Shannon-Wiener diversity index (Ortiz-Burgos, 2016). P_i is the proportion of the entire community made up of species i, excluding non-native species.

2.2.2.4 The aquatic environment of rivers and lakes

(1) The quality of water

The assessment of water quality must incorporate at least five indicators, including pH, dissolved oxygen, permanganate index, ammonia nitrogen, and total phosphorus. The collection of samples, sampling stations, the frequency of monitoring, and the processing of monitoring data should adhere to the relevant regulations outlined in the "Environmental quality standards for surface water" (GB 3838-2002) and the "Regulation for water environmental monitoring" (SL 219-2013) (Ministry of Water Resources of the PRC, 2013). Seasonal rivers during dry periods may be excluded from the monitoring evaluation. Should high baseline values of certain water quality indicators arise due to natural causes such as geological characteristics, soil conditions, or the nature of biological communities, a comparative analysis with corresponding water quality indicators from neighboring rivers and lakes should be conducted. If anthropogenic pollution is ruled out, it may be permissible not to evaluate that particular water quality indicator; however, this decision must be justified with an explanation.

Evaluate the water quality class of river segments (lake areas). According to the "Environmental quality standards for surface water" (GB 3838-2002) and the annual average value of each water quality indicator, use the single-factor evaluation method to assess the water quality class corresponding to each indicator. The overall water quality class of the river or lake is determined by the poorest water quality class among all indicators. Assign a score to the quality of water. The scoring criteria are shown in Table 4.

(2) The assurance of ecological flow

Evaluate the proportion of days on which the ecological flow (or water level) of rivers and lakes meets the control objectives. The formula for calculating the score is as follows:

$$\mathbf{S = D \times A \times 100} \quad (3)$$

S is the score for the satisfaction of ecological flow requirements; *D* is the days meeting the ecological flow (or water level) control objectives for rivers and lakes;*A* is the annual days.

TABLE 3 Diversity index scoring criteria.

Shannon diversity index (*H'*)	*H'*>3	2<*H'*≤3	1≤*H'*≤2	0<*H'*<1
Score assignment	90-100	80-90	70-80	0-70

2.2.2.5 The economic development related to water

The development of a water-based economy seeks to better satisfy the populace's demands for water resources, water environment, and water ecology. It aims to harness the ecological value of water resources while facilitating the conversion of ecological worth into economic value, thereby realizing the concept that lucid waters and lush mountains are indeed invaluable assets. The development of the water economy in Xinchang County is primarily manifested in the following aspects:

(1) Average annual growth in revenue from water-related tourism

The annual growth in the revenue of water-related tourism is expressed through the average annual growth rate of the revenue in this sector. The scoring criteria are detailed in Table 5.

(2) The annual growth in the output value of aquaculture

The growth in the annual output value of aquaculture is represented by the average growth rate of the total annual output value, with the scoring criteria outlined in Table 5.

(3) The per capita income growth rate from microhydropower

The return on investment for microhydropower projects is represented by the annual rate of return for microhydropower, with the scoring criteria outlined in Table 5.

2.2.2.6 Drinking water sources

(1) The compliance status of potable water sources

the construction of centralized drinking water sources has successfully passed inspection, and the compliance rate of water quality standards within the evaluation period is 100%. This item carries a full score of 100 points; meeting the evaluation criteria grants 100 points. If the construction of centralized drinking water sources fails to pass inspection, 50 points are deducted. For each instance of non-compliance within the evaluation period, 50 points are deducted.

2.2.2.7 The management and protection mechanisms for rivers and lakes

(1) The "River and Lake Chief System" collaboration mechanism situation

Evaluation Criteria for River (Lake) Chief System: The River (Lake) Chief must perform their duties effectively, addressing major issues of the river or lake; formulate and implement a "one river, one strategy"; properly install river and lake chief information boards; establish a joint prevention and control mechanism for transboundary waterways.

TABLE 4 Criteria for water quality assessment and scoring.

Water quality class	I	II	III	IV	V	Worse than class V
Score assignment	100	95	85	60	40	0

This item carries a full score of 100 points. Achieving the evaluation criteria awards 100 points; for each instance in which any of the four requirements is not met, 25 points will be deducted until the score is nullified. The formula for assigning points is as follows:

$$P_{hhz}=\begin{cases} 100-25\times N_{hh} & (N_{hh}<10) \\ 0 & (N_{hh}\geq 10) \end{cases} \quad (4)$$

In the formula: P_{hhz} represents the score assigned to the River (Lake) Chief System; N_{hh} denotes the number of problems identified during the implementation of the River (Lake) Chief System.

(2) Zoning and classification control situation of river and lake water areas and shoreline spaces

Standards for evaluation of river and lake shoreline spatial zoning and management: Completion of demarcation of protection or management boundary lines for rivers and lakes; absence of newly unauthorized constructions, indiscriminate stacking, encroachment, or illicit extraction activities within the protection control line and river management area; establishment of a "list database" for historical usage; the water area of rivers and lakes does not decrease within the year, and compensation for occupied projects is enforced.

This item carries a full score of 100 points. Achieving the evaluation criteria awards 100 points; for each instance in which any of the three requirements is not met, 30 points will be deducted until the score is nullified.

(3) Supervision of the river-related projects

Evaluation Criteria for River-Related Project Supervision: Regulatory norms for river-related projects, project licensing refinement, and Well-Maintained Records.

This section is worth 100 points. River-related projects encompass activities such as water extraction, drainage, and construction within river management boundaries. Meeting the evaluation criteria earns a full 100 points; for each identified problem within a project, 20 points are deducted until no points remain. The formula for assigning points is as follows:

$$P_{xm}=\begin{cases} 100-5\times N_{xm} & (N_{xm}<5) \\ 0 & (N_{xm}\geq 5) \end{cases} \quad (5)$$

In this context: P_{xm} is the score assigned to the regulatory status indicator of river-related projects; N_{xm} is the number of river-related projects with existing problems.

2.2.2.8 The water culture

(1) Cultural display

Criteria for Assessing the Presentation of Aquatic Culture: Through diverse media channels, including newspapers and magazines, radio and television, online platforms, brochures, WeChat public accounts, and TikTok, actively promote and disseminate the unique culture of rivers and lakes.

This item is awarded 100 points, contingent upon the number of water culture promotion activities undertaken within the evaluation period of the current year, as specified in Table 6.

(2) Development of cultural, physical, and tourism activities

Each year, a vibrant assortment of cultural and sports events related to water culture is organized, with a comprehensive evaluation determined by the scale, frequency, and impact of these activities; refer to Table 7 for the criteria-based scoring.

2.2.2.9 Hydrophilic implementation

(1) The status of supporting facilities for urban and rural hydrophilic structures

Criteria for Evaluating the Integration of Water-Friendly Public Amenities: ① The arrangement of water-friendly spaces, including parks, squares, riverside walkways, piers, and platforms, is logical; parks and squares are easily accessible, and pathways along urban rivers are unobstructed. ② The provision of user-oriented facilities such as seating, railings, trash receptacles, fitness equipment, lighting, rain shelters, safety warning signs, and directional signboards around rivers and lakes adequately fulfills public needs.

This segment is evaluated on a scale of 100 points, with scores allocated based on the configuration of waterfront recreational areas and the availability of supportive public amenities, as outlined in Table 8.

(2) Riverside-waterfront greenways

Evaluation Criterion for Waterfront Greenways: Length of Waterfront Greenways/the Total Shoreline Length within the Management Zone.

This section is assessed on a scale of 100 points, denoted by the ratio of waterfront greenways. It pertains to the proportion of river and lake waterfront greenways' shoreline length compared to the total shoreline length of rivers and lakes within the designated management area (excluding segments of natural shoreline). The formula for assigning points is as follows, and the scoring table is depicted in Table 9.

TABLE 5 Scoring standard for water economic development.

Average annual growth rate of revenue from water-related tourism(%)	≥15	[10,15)	[5,10)	[1,5)	<1
Average annual growth rate of total output value of aquaculture(%)	≥7%	[5,7)	[3,5)	[1,3)	<1
Annual returns from microhydropower(%)	≥6	[5,6)	[3,5)	[1,3)	<1
Score assignment	100	85	75	60	0

TABLE 6 Scoring standard for the exhibition of water culture.

The frequency of water culture exhibitions (times/year)	0	1	2	≥3
Score assignment	0	40	70	100

$$P_{bs}=\frac{N_{bs}}{N_{zc}} \quad (6)$$

P_{bs} represents the waterfront greenway ratio; N_{bs} is the length of the waterfront greenway; N_{zc} is the total length of river and lake shorelines within the management area.

2.2.2.10 Public Satisfaction

Public satisfaction pertains to the degree of contentment among individuals living near rivers and lakes, particularly regarding water safety, the aquatic environment, the ecosystem, and the cultural significance of these water bodies. This measure is scored on a scale of 100 and is assessed through the distribution of questionnaires or online surveys. Each evaluation unit is required to survey at least 50 individuals, with scores determined by the average of the public's ratings. Refer to Table 10 for further details. Please refer to Attachment 1 for the questionnaire.

3 Evaluation of the happiness of rivers and lakes in Xinchang county

3.1 The scope of evaluation

Xinchang County lies in the upper reaches of the Cao'e River basin, traversed by three chief rivers (Table 11): the Xinchang River, the Chengtan River, and the Huangze River. The Xinchang River meanders through the Changzhao Reservoir (large-scale projects (2) type projects), while the Huangze River courses through the Qincun Reservoir (large-scale projects (2) type projects).

3.2 Evaluation results

3.2.1 The safety rivers and lakes

(1) Flood prevention and disaster mitigation compliance

The compliance rate of the embankment along the Xinchang River stands at 92%, thereby achieving a perfect score of 100 points; the compliance rate along the Chengtan River is 84.5%, which translates to a score of 86.3 points; and the embankment compliance rate for the Huangze River is 100%, hence receiving a score of 100 points.

In alignment with the "Comprehensive Planning Revision for the Cao'e River Basin" (2008-2030), both Changzhao Reservoir and Qincun Reservoir are pivotal in ensuring flood security. As a result, it has been determined that the flood protection and disaster prevention compliance for Changzhao Reservoir is 100%, awarded with a score of 100 points; likewise, the compliance for Qincun Reservoir is 100%, also garnering a score of 100 points.

(2) Operation status of hydraulic engineering projects:

According to the "Xinchang County Chengtan River River Health Assessment Report," there are no regulated water conservancy projects in the upper reaches of the Chengtan River.

Based on the "Xinchang County Huangze River River Health Assessment Report" and the "Xinchang County Qincun Reservoir Water Ecological Health Assessment Report," the Qincun Reservoir project is large-scale projects (2) type reservoir, primarily engineered for water supply and flood control, with supplementary multifaceted applications in irrigation and power generation. Water conservancy facilities function optimally; operation of the water project tasks are completed, and as a result, has been awarded a perfect score of 100.

According to the "Xinchang County Xinchang River River Health Assessment Report" and the "Xinchang County Changzhao Reservoir Water Ecological Health Assessment Report," the Changzhao Reservoir, as a quintessential water conservancy project, is a large-scale project (2) type reservoir that harmoniously combines water supply, irrigation, power generation, fishery, and navigation. It stands as one of the pivotal projects for flood and drought mitigation in the Cao'e River basin. The water conservancy infrastructure operates flawlessly, meeting its designated tasks, and thus has been granted a full score of 100.

3.2.2 Riparian vegetation

According to the survey statistics of the shoreline types in the "Xinchang County Chengtan River Health Assessment Report, the vegetation coverage rate of the shoreline stands at 55.25%, having been awarded a score of 90 points.

According to the Report on the Health Assessment of Rivers, Lakes, and Reservoirs in Xinchang County—Huangze River Section 1, the average vegetation coverage along the Huangze River fluctuates between 72% and 78%, thereby meriting a perfect score of 100. The Report on the Health Assessment of Rivers, Lakes, and Reservoirs in Xinchang County—Xinchang River indicates that the average vegetation coverage of the Xinchang River stands at 78.30%, justifying a score of 100. Based on the Report on the Aquatic Ecological Health Assessment of Qincun Reservoir in Xinchang County, the average vegetation coverage of Qincun Reservoir is recorded at 58.43%, yielding a score of 90. Furthermore, the Report on the Aquatic Ecological Health Assessment of Changzhao Reservoir in Xinchang County reveals that the average vegetation coverage of Changzhao Reservoir is 68.50%, consequently earning a score of 100.

TABLE 7 Scoring standard for the development of cultural, physical, and tourism activities.

The influence of Cultural, Physical, and Tourism endeavors	Substandard	Mediocre	Superior	Outstanding
Score assignment	0	40	70	100

TABLE 8 Scoring standard for hydrophilic public amenities.

The convenience level of implementing hydrophilicity	Score assignment
The configuration of the waterside expanse is judicious, featuring convenient and easily accessible transport options that facilitate seamless pedestrian walkways adjacent to the water's edge; public facilities are thoroughly equipped and maintained in superb condition.	100
The configuration of the waterside expanse is a reasonable layout, featuring convenient and easily accessible transport options that facilitate seamless pedestrian walkways adjacent to the water's edge; public facilities are relatively equipped and maintained in superb condition.	[70,100)
The configuration of the waterfront area is mediocre, offering convenient transportation and largely unobstructed walkways. Fundamental amenities are available for ease, and the facilities are well-maintained.	[40,70)
The configuration of the waterside areas is inefficient, and accessibility proves difficult. The pedestrian pathways bordering the water are unfinished. Furthermore, the supply of public amenities is inadequate, with some of the existing facilities exhibiting signs of damage or neglect.	[0,40)

3.2.3 Biodiversity of river and lake ecosystems

(1) Diversity of fish

According to the results of fish diversity surveys undertaken in March and June of 2024 (Table 12), the diversity index for fish within the Chengtan River has been recorded at 75 points, the Huangze River at 76 points, the Xinchang River at 83 points, the Qinchun Reservoir at 69 points, and the Changzhao Reservoir at 74 points.

(2) Diversity of large benthic invertebrates

According to the comprehensive survey on benthic invertebrate diversity undertaken in March 2024 (Table 12), Chen Tan River was accorded a benthic diversity score of 77, and Huangze River, Xinchang River, Qincun Reservoir, Changzhao Reservoir were 81, 76, 84, and 67 respectively.

(3) Diversity of phytoplankton

According to the findings of the phytoplankton diversity investigation in March 2024 (Table 12), the diversity scores for phytoplankton in the Chengtan River, Huangze River, Xinchang, Qinzhun Reservoir, and Changzhao Reservoir are 84, 82, 84, 77, and 76, respectively.

(4) Diversity of zooplankton

According to the findings of the March 2024 investigation regarding zooplankton diversity (Table 12), the biodiversity scores for zooplankton in Chengtan River, Huangze River, Xinchang River, Qincun Reservoir, and Changzhao Reservoir were recorded at 66, 70, 71, 72, and 70, respectively.

(5) Diversity of periphytic algae

Based on the findings of the investigation regarding phytoplankton diversity conducted in March 2024 (Table 12), the biodiversity scores for periphytic algae in Chengtan River, Huangze River, Xinchang River, Qincun Reservoir, and Changzhao Reservoir were recorded at 84, 86, 81, 81, and 87, respectively.

3.2.4 The aquatic environment of rivers and lakes

(1) The quality of water

Based on the environmental quality levels of water as assessed in the reports titled "Health Assessment Report of Chengtan River and Lakes in Xinchang County," "Health Assessment Report of Huangze River and Lakes in Xinchang County," "Health Assessment Report of Xinchang River and Lakes in Xinchang County," "Ecological Health Assessment Report of Qinkun Reservoir in Xinchang County," and "Ecological Health Assessment Report of Changzhao Reservoir in Xinchang County," an average value was calculated. Accordingly, Chengtan River was awarded a score of 88.3, Huangze River achieved a score of 94.3, Xinchang River received 92.5, Qinkun Reservoir was granted 95, and Changzhao Reservoir also attained 95.

(2) The assurance of ecological flow

Based on the findings detailed in the "Xinchang County Chengtan River Lake Health Assessment Report," the "Xinchang County Huangze River Lake Health Assessment Report," the "Xinchang County Xinchang River Lake Health Assessment Report," the "Xinchang County Qin Cun Reservoir Ecological Health Assessment Report," and the "Xinchang County Zhang Zhao Reservoir Ecological Health Assessment Report," Combined with field visits, ground investigations, and expert consultations, it is evident that the water levels and ecological flow fluctuations of the three rivers and two reservoirs substantially comply with the requisites of the ecological environment. Consequently, it is deemed fitting to accord this criterion the maximum score, resulting in a standardized score of 100.

3.2.5 The economic development related to water

(1) Average annual growth in revenue from water-related tourism

Xinchang County has unveiled the "Top Ten Blissful Rivers and Lakes Waterfront Routes." During the May Day holiday, the premier waterfront tourism route attracted a remarkable influx of 141,500 visitors. In alignment with Xinchang County's fundamental goal of establishing an extensive network of blissful rivers and lakes, the annual growth rate of revenue from aquatic tourism has been set at a targeted 15%. As a result, this accomplishment merits a flawless score of 100.

TABLE 9 Scoring standard for riverside-waterfront greenways.

Waterfront greenway ratio	[30%,100%]	[20%,30%)	[10%,20%)	[0,10%)
Score assignment	100	80	70	30

TABLE 10 Scoring standard for public satisfaction indicators.

Public evaluation	Score assignment
[90,100)	100
[80,90)	90
[60,80)	70
[0,60)	50

(2) The Annual growth in the output value of aquaculture

In Xinchang County, the total output of aquatic products in 2021 attained a remarkable 3,855 tons, comprising 440 tons from freshwater capture and 3,415 tons from freshwater aquaculture; the annual total output value amounted to an impressive 130 million yuan. In 2022, the total aquatic product output witnessed a commendable increase to 3,979 tons, including 468 tons from freshwater capture and 3,511 tons from freshwater aquaculture; the annual total output value ascended to 140 million yuan. By 2023, the total aquatic product output further surged to 4,177 tons, with 498 tons from freshwater capture and 3,679 tons from freshwater aquaculture; the annual total output value ascended to 150 million yuan. The annual growth rate of total output value in aquaculture has consistently surpassed 7% for two consecutive years. In the Xinchang County, freshwater aquaculture focus on propagating species such as the *Acrossocheilus parallens* and the *Opsariichthys bidens*, while the primary species stocked in the reservoirs are *Hypophthalmichthys molitrix* and *Hypophthalmichthys nobilis*. In conclusion, this endeavor merits an outstanding score of 100 points.

(3) The per capita income growth rate from microhydropower

Xinchang is the first county in Zhejiang Province to achieve primary electrification in rural areas, earning the title of "Hometown of Microhydropower." Xinchang is guided by the principle of fostering the green and healthy development of the microhydropower industry, maximizing the value of its water resources, and has pioneered a development path centered on the consolidation of microhydropower assets for village revitalization and wealth generation. According to a report on the path to shared prosperity through microhydropower released by Xinchang County, village collectives can annually secure an annualized return of 6%, thus earning a full score of 100 points.

3.2.6 Drinking water sources

(1) The compliance status of potable water sources

In alignment with the findings presented in the "Report on the Water Quality Status of Urban Centralized Drinking Water Sources in Shaoxing City" (Third Quarter, 2023), the Qincun Reservoir and Changzhao Reservoir located in Xinchang County has been designated as Class II in terms of water quality, thereby fulfilling the requisite functional requirements. As a result, both reservoirs have been bestowed with an impeccable score of 100 points.

3.2.7 The management and protection mechanisms for rivers and lakes

(1) The "River and Lake Chief System" collaboration mechanism situation

Based on the reports entitled "Health Assessment Report of Chengtan River and Lakes in Xinchang County," "Health Assessment Report of Huangze River and Lakes in Xinchang County," "Health Assessment Report of Xinchang River and Lakes in Xinchang County," "Ecological Health Assessment Report of Qinkun Reservoir in Xinchang County," and "Ecological Health Assessment Report of Changzhao Reservoir in Xinchang County," and the county-level river and lake chief's performance report, it is observed that the boundary delimitation for the three rivers and two reservoirs has been accomplished, thereby establishing clear management boundaries and enforcing rigorous social management of activities involving the rivers and lakes. The implementation of the "one river, one strategy" governance plan is in progress, aimed at achieving compliance with river safety standards and enhancing the quality, alongside measures for the ecological protection and rehabilitation of rivers and lakes. Furthermore, the revisions of the "Comprehensive Happiness River and Lake Construction Plan for Xinchang County," "Modern Water Network Construction Plan for Xinchang County," and "Comprehensive Prevention and Control Plan for Mountain Flood Disasters in the Zuoyujiang River Basin of Xinchang County" have been initiated. In consideration of the aforementioned content, the total score for this item is 100 points.

(2) Zoning and classification control situation of river and lake water areas and shoreline spaces

Based on the reports entitled "Health Assessment Report of Chengtan River and Lakes in Xinchang County," "Health Assessment Report of Huangze River and Lakes in Xinchang County," "Health Assessment Report of Xinchang River and

TABLE 11 Evaluation of essential data on rivers and reservoirs.

Type	Name	Length within XinChang County (km)	Basin areas (km^2)
River	Xinchang River	48.9	440
	Huangze River	50.6	375
	Chengtan River	41.1	386.7
Type	Name	Capacity ($\times 10^8$ m^3)	Basin areas (km^2)
Large-scale projects (2) type projects	Changzhao Reservoir	1.86	8.38
	Qincun Reservoir	2.44	9.39

TABLE 12 diversity index in sampling area.

Sampling Area	Fish diversity index in the spring			Fish diversity index in the summer			Large benthic invertebrates diversity		
	D′	*J′*	*H′*	*D′*	*J′*	*H′*	*D′*	*J′*	*H′*
Huangze River	0.910	0.592	0.820	1.941	0.915	2.569	3.338	0.885	2.199
Chengtan River	0.962	0.819	0.900	1.603	0.913	2.167	2.435	0.787	1.795
Xinchang River	1.820	0.887	1.427	1.924	0.936	2.309	2.147	0.902	1.641
Changzhao Reservoir	1.610	0.840	1.352	1.970	0.747	2.368	1.362	0.404	0.785
Qincun Reservoir	1.895	0.831	1.489	0.582	0.258	0.410	4.091	0.933	2.463
Sampling Area	Phytoplankton diversity			Zooplankton diversity			Periphytic Algae diversity		
	D′	*J′*	*H′*	*D′*	*J′*	*H′*	*D′*	*J′*	*H′*
Huangze River	5.331	0.691	2.304	1.460	0.963	1.092	5.658	0.754	2.681
Chengtan River	6.825	0.682	2.474	1.443	1.000	0.693	6.173	0.689	2.453
Xinchang River	5.282	0.716	2.400	1.796	0.975	1.168	4.998	0.628	2.191
Changzhao Reservoir	2.997	0.589	1.669	1.388	0.915	1.004	5.689	0.782	2.721
Qincun Reservoir	3.784	0.526	1.708	1.830	0.971	1.203	5.419	0.599	2.187

Lakes in Xinchang County," "Ecological Health Assessment Report of Qinkun Reservoir in Xinchang County," and "Ecological Health Assessment Report of Changzhao Reservoir in Xinchang County," and field visits, on-site inspections, and expert consultations, the three rivers and two reservoirs have demonstrated the capacity to conduct annual special clean-up operations for river and lake "illegal occupation, unauthorized excavation, indiscriminate dumping, and unauthorized construction," achieving a 100% processing rate and establishing a regularized supervisory mechanism. Consequently, it is deemed appropriate to directly assign the maximum score to this indicator, thus awarding a score of 100 for all instances.

(3) Supervision of the river-related projects

In 2023, Xinchang County embarked upon nine projects related to its rivers, each of which complied with regulatory standards through the possession of comprehensive permits and complete archival documentation; therefore, this item scores 100 points.

3.2.8 The water culture

(1) Cultural display

Based on the reports entitled "Health Assessment Report of Chengtan River and Lakes in Xinchang County," "Health Assessment Report of Huangze River and Lakes in Xinchang County," "Health Assessment Report of Xinchang River and Lakes in Xinchang County," "Ecological Health Assessment Report of Qinkun Reservoir in Xinchang County," authorized departments can utilize a diverse array of platforms such as newspapers, magazines, radio programs, television broadcasts, internet media, flyers, brochures, WeChat official accounts, and Tiktok to promote the unique cultural heritage associated with the three rivers and two reservoirs. Consequently, they have been awarded a perfect score of 100.

(2) Development of cultural, physical, and tourism activities

Xinchang County is abundantly endowed with water resources, and the heritage of its river and lake culture extends back through the ages. The local government and the populace organize numerous historical and cultural activities related to water each year, such as the Garden Festival launched by the banks of Baiyun Lake, along with various family and couple tourism routes along the waterfront, giving rise to a flourishing scene. The water culture journey in Xinchang consistently leads within the province, with poetic routes of the Tang Dynasty, landscapes painted in verse, and numerous tourists drawn by repute to experience the picturesque charm of Xinchang's mountains and waters. Thus, this project is awarded a perfect score of 100.

3.2.9 Hydrophilic implementation

(1) The status of supporting facilities for urban and rural hydrophilic structures

According to the contents of the "Health Assessment Report of Chengtan River and Lakes in Xinchang County," "Health Assessment Report of Huangze River and Lakes in Xinchang County," "Health Assessment Report of Xinchang River and Lakes in Xinchang County," "Ecological Health Assessment Report of Qinkun Reservoir in Xinchang County," and through on-site visits, field surveys, and expert consultations, it has been concluded that the configuration of three rivers and two reservoirs within the waterside expanse was judicious, featuring convenient and easily accessible transport options that facilitate seamless pedestrian walkways adjacent to the water's edge; public facilities are thoroughly equipped and maintained in superb condition.

(2) Riverside-waterfront greenways

Xinchang County has integrated the scattered resources along its rivers and lakes to establish a "waterfront node" database for the

development of waterside tourism. This initiative aims to connect the county's main riverine slow-moving traffic systems, enhancing the open sharing of water spaces and creating a felicitous river-lake waterside route IP where "mountains are visible, water is in sight, and nostalgia is palpable." The coverage rate of the urban and rural 15-minute waterside circle has reached 92%.

In terms of waterside greenways, Xinchang Riverside Park features a 3.53-kilometer-long waterside greenway. The Jingling Riverside Greenway stretches 8.7 kilometers, linking the Nineteen Peaks Scenic Area with scenic villages along the route. The Qiaoying Reservoir ring-reservoir waterside greenway spans 13 kilometers, with observation decks and camping platforms as waterside amenities. The Huangze River Waterside Greenway extends 11.23 kilometers, and the Chengtan River Waterside Greenway covers 7.2 kilometers, resulting in a total waterside greenway length of 43.66 kilometers.

The primary course of the Xinchang River within the county stretches over 48.9 kilometers, the main course of the Chengtan River extends for 44.1 kilometers, and the principal course of the Huangze River measures 50.6 kilometers. Collectively, the aggregate river length totals 143.6 kilometers. Considering that the waterfront greenway encompasses more than 30% of the total river length, this criterion merits a score of 100 points.

3.2.10 Public satisfaction

A public satisfaction survey conducted in April 2024 along the banks of the Xinchang River, Huangze River, and Chengtang River, which engaged riverbank residents, riverway managers, and local citizens, encompassed a total of 50 participants, all of whom successfully returned their questionnaires. The analysis was performed based on the average scores derived from the three areas.

The average public satisfaction score for Chengtan River is 89.47, thus it is assigned a score of 90. Huangze River received an average satisfaction score of 76.67, leading to an assigned score of 70. Xinchang River boasts an impressive average satisfaction score of 95.79, resulting in a perfect score of 100. The overall composite average for the three regions stands at 86.67.

3.3 Comprehensive evaluation results

By the established evaluation index system for the Happiness River and Lake, the overall assessment score for Xinchang County's Happiness River and Lake stands at an impressive 92.66 points (Table 13), categorizing it as Grade I (Exemplary Happy River and Lake).

4 Discussion

Riverscapes function as an indispensable linchpin of ecological environments and human sustenance, embodying a pivotal role in the terrestrial material cycle and equilibrium, as well as in the nourishment and progress of humankind (Shao et al., 2024). The notion of the "River of Happiness" has surfaced amidst the contemporary era of our nation's river management initiatives. In contrast to previous understandings of rivers, the "River of Happiness" is rooted in significant national strategies, approaching the issue through a systemic and comprehensive lens, necessitating elevated standards and embodying more profound connotations (Song, 2024a). The resolution of our nation's complex water challenges demands institutional innovation; therefore, the creation of river and lake systems that serve the public good is of paramount importance. Throughout the country, the construction of Happiness Rivers and Lakes is gradually being initiated. Nonetheless, the scholarly exploration of felicitous rivers remains in its nascent stage (Zuo et al., 2021), characterized by diverse and fragmented perceptions among the populace. The pertinent accomplishments exhibit discrepancies in the selection of indicators, the determination of weights, the assignment of target values, and the evaluation methodologies (Research group of the happy river, 2020; Gong et al., 2022). Numerous mathematical methodologies, including the analytic hierarchy process (Ramanathan, 2001), multivariate analysis (Chau and Muttil, 2007), data envelopment analysis (Zhao et al., 2006), artificial neural network (Liu et al., 2023), fuzzy comprehensive assessment (Zhao and Yang, 2009), and grey correlation analysis (Liu et al., 2024) etc. are utilized in the happy rivers and lakes studies (Anwar Sadat et al., 2020). The evaluation system predominantly selects indicators from dimensions such as Flood Control Capacity, Water Resources Reliability, Water Environment Livability, Aquatic Ecosystem Health, and Water Culture Prosperity (Ju et al., 2022). However, some of these indicators and methodologies fall short in terms of operability and accuracy. It is essential to further delve into the research on the Happy Rivers and Lakes initiative, revising and refining the methodologies through extensive consultations with experts from the relevant regions and sectors, thereby progressively enhancing the adaptability and practicality of the methods.

Given the paramount importance placed on the protection of river and lake water ecosystems as well as hydrobiont in Xinchang County (Department of Water Resources of Zhejiang Province, 2023), this research places a special emphasis on evaluating aquatic biodiversity when constructing the evaluation index system. The assessment results of the "Happy River and Lake" initiative reveal a notable vulnerability in the aspect of river and lake biodiversity indices, attributable to objective issues and shortcomings that persist. As the socio-economic landscape has evolved, the extensive construction of dams along rivers has drastically disrupted natural water flow, resulting in profound, widespread, and severe anthropogenic impacts on riverine ecosystems. The erection of river barrages and other hydraulic structures has hindered the natural migratory paths of aquatic species, including the *Anguilla japonica*, *Anguilla marmorata*, *Coilia mystus*, *Coilia ectenus*, and crabs. Unfortunately, fishways have yet to be established in either the Xinchang River or the Huangze River, leading to fragmented habitat connectivity for aquatic organisms, which impedes their migration and contributes to a decline in both aquatic community numbers and biodiversity. Although a fishway has been installed in the middle section of the Chengtan River, its steep gradient and structural attributes do not facilitate the migration of small fish, necessitating further optimization and renovation.

TABLE 13 Comprehensive evaluation of happy rivers and lakes.

Number	Primary Indicator	Secondary indicators	Chengtan River	Huangze River	Xinchang River	Qincun Reservoir	Changzhao Reservoir	Summation
			Score assignment	Score assignment	Score assignment	Score assignment	Score assignment	
1	the Safety Rivers and Lakes	Flood Prevention and Disaster Mitigation Compliance	86.3	100	100	100	100	4.86
2		Operation Status of Hydraulic Engineering Projects	—	100	100	—	—	5.00
3	Riparian Vegetation	Shoreline vegetative cover	90	100	100	90	100	14.40
4	Biodiversity of River and Lake Ecosystems	Diversity of Fish	75	76	78	69	78	3.76
5		Diversity of Large Benthic Invertebrates	77	81	76	84	67	3.85
6		Diversity of Phytoplankton	84	82	84	77	76	4.03
7		Diversity of Zooplankton	66	70	71	72	70	3.49
8		Diversity of Periphytic Algae	84	86	81	81	87	4.19
9	The Aquatic Environment of Rivers and Lakes	the Quality of Water	88.3	94.3	92.5	95	95	6.98
10		the Assurance of Ecological Flow	100	100	100	100	100	7.50
11	the Economic Development Related to Water	Average annual growth in revenue from water-related tourism	—	—	—	—	—	3.00
12		The Annual Growth in the Output Value of Aquaculture	—	—	—	—	—	3.00
13		The Per Capita Income Growth Rate from Microhydropower	—	—	—	—	—	4.00
14	Drinking Water Sources	the Compliance Status of Potable Water Sources	100	100	100	100	100	5.00
15	the Management and Protection Mechanisms for Rivers and Lakes	The "River and Lake Chief System" Collaboration Mechanism Situation	100	100	100	100	100	5.00
16		Zoning and Classification Control Situation of River and Lake Water Areas and Shoreline Spaces	100	100	100	100	100	2.50
17		Supervision of the River-Related Projects	—	—	—	—	—	2.50
18	the Water Culture	Cultural Display	100	100	100	100	100	1.50
19		Development of Cultural, Physical, and Tourism Activities	—	—	—	—	—	1.50
20	Hydrophilic Implementation	The Status of Supporting Facilities for Urban and Rural Hydrophilic Structures	100	100	100	100	100	2.00
21		Riverside-waterfront Greenways	—	—	—	—	—	2.00
22	Public Satisfaction	Satisfaction Survey	90	70	100	—	—	2.60
Summation								92.66

"—" signifies that the corresponding data remains uncollected.

10.3389/fevo.2024.1522066

Along the upper reaches of the Huangze River, delicate reeds and cattail marshes gracefully undulate in the tender caress of the breeze, while submerged flora such as *Ceratophyllum demersum* purify the aqueous realm. In the distance, aquatic birds engage in playful antics, sketching a tranquil and harmonious tableau of the natural ecosystem. Since the inauguration of the "Happy Rivers and Lakes" initiative across Xinchang County, unwavering endeavors have been pursued to expedite the development of secure, ecologically sound, habitable, prosperous, and intelligent river systems. This encompasses enhancing flood control and disaster preparedness, nurturing cultural and tourism advancements, emphasizing ecological preservation, reinforcing water system governance, and establishing a "river network of shared prosperity, three rivers united in harmony" within the riparian expanse. Through the execution of a series of strategic measures, public consciousness regarding river preservation and care has markedly heightened, and individuals have acquired a deeper sense of accomplishment and felicity from the beautiful river and lake ecology.

5 Conclusion and suggestions

This article delineates a comprehensive evaluation index system for the Happy Rivers and Lakes, articulating a meticulous discourse on the foundational principles governing the assessment framework, methods of quantification, apportionment of weights, and the architectural design of the system. Given the intricate and varied nature of river and lake ecosystems, the development of this evaluation system necessitates further refinement and optimization. This study also has certain limitations, being applicable only to the assessment of mountainous river-lake systems. Moreover, variations in focus and research methodologies give rise to different evaluation outcomes. Additionally, varying focuses and methodologies can yield divergent evaluation outcomes. Consequently, a comprehensive evaluation of happy rivers and lakes necessitate a multi-faceted approach. Prospective research should concentrate on: augmenting the monitoring and forecasting of shifts within river and lake ecosystems; investigating more scientific and rational methodologies for quantification and weight distribution; and fostering the extensive implementation and acceptance of the evaluation system across a broader array of regions and disciplines.

Data availability statement

The original contributions presented in the study are included in the article/Supplementary Material. Further inquiries can be directed to the corresponding author.

Author contributions

XL: Conceptualization, Data curation, Investigation, Methodology, Software, Writing – original draft, Writing – review & editing. CC: Data curation, Investigation, Writing – original draft. BS: Funding acquisition, Resources, Writing – review & editing. CH: Formal analysis, Writing – review & editing. ZY: Writing – review & editing. YZ: Writing – review & editing.

Funding

The author(s) declare financial support was received for the research, authorship, and/or publication of this article. The author(s) declare financial support was received for the research, authorship, and/or publication of this article. This work is supported by the Research on the Evaluation of the Happiness River and Lakes in Xinchang County and the Restoration of Biodiversity China.

Conflict of interest

The authors declare the research was conducted in the absence of any commercial or financial relationships that could be construed as a potential conflict of interest.

Publisher's note

Generative AI statement

The author(s) declare that no Generative AI was used in the creation of this manuscript.

Supplementary material

The Supplementary Material for this article can be found online at: https://www.frontiersin.org/articles/10.3389/fevo.2024.1522066/full#supplementary-material

References

Anwar Sadat, M., Guan, Y., Zhang, D., Shao, G., Cheng, X., and Yang, Y. (2020). The associations between river health and water resources management lead to the assessment of river state. *Ecol. Indic.* 109, 105814. doi: 10.1016/j.ecolind.2019.105814

Chau, K., and Muttil, N. (2007). Data mining and multivariate statistical analysis for ecological system in coastal waters. *J. Hydroinformatics - J. HYDROINFORM* 9, 305–317. doi: 10.2166/hydro.2007.003

Department of Water Resources of Zhejiang Province (2023). *Xinchang: Catalyzing the Vitality of "Shared Prosperity along One River, Harmony across Three Rivers" to Promote the Development of Happy River Lakes throughout the Region*. Available online at: https://slt.zj.gov.cn/art/2023/11/10/art_1513110_59039411.html (accessed December 10, 2024).

Faust, D. R., Moore, M. T., Emison, G. A., and Rush, S. A. (2016). Potential implications of approaches to climate change on the clean water rule definition of "Waters of the United States. *Bull. Environ. Contam. Toxicol.* 96, 565–572. doi: 10.1007/s00128-016-1773-z

Gardner, R. C., Okuno, E., Tai, S., Fennessy, M. S., Johnston, C. A., Otte, M. L., et al. (2019). Advocating for science: amici curiae brief of wetland and water scientists in support of the clean water rule. *WETLANDS* 39, 403–414. doi: 10.1007/s13157-019-01160-z

Gong, L., Tian, J., and Jin, C. L. (2022). Comprehensive evaluation of Happy River based on ERG demand model. *Water Resources Prot.* 38, 25–33. Available at: https://kns.cnki.net/kcms2/article/abstract?v=-xbefZa1CdvK0s-Ms4msZRRs4R6wQ36n_ayOv-41yQxUP_kiPlsszOh9mXgvRroVb-CZVavXlKrXptTtBs9OACN037fCERk8Rx7NCvOmHWXMbrjhucUGRMN2SDYYBxRjCVhrDL63wRGqdiIf5r9sHEtWZNLaMpgSs22k41xSsm6ApKtLnuFcWkD9GCQgjYemZrrvR42S3LmN9XJ9A0xphg==&uniplatform=NZKPT.

HAN, Y. P., and XIA, F. (2020). Evaluation of Xingfu river based on demand level theory. *South–North Water Transf. Water Sci. Technol.* 6, 01–07,38. doi: 10.16747/j.cnki.cn61-1109/tv.2024.05.037

Jiang, C. L. (2024). Practice analysis for the construction of happy rivers and lakes in the Hanjiang River Basin of Guangdong Province and relevant measures. *Water Resour. Dev. Res.*, 1–7. Available at: https://kns.cnki.net/kcms2/article/abstract?v=KetWmXlLxlfJrdNvNd5UmKK45cXtmINfBQu0WmVjtlHZd9pOm4zCPqZRYff6XHF8K6LtirjB2PFYUTeFglOK97uU3UsuMe5TYNQxrOkusIx28CiB8JpmXvQ9MpXZqq0VhNGeLsvhnieKfJfTQih0mmV-L_p3MVvz3DT8P4DLe7aSGDBy3iWsRMh69MG3RScw&uniplatform=NZKPT&language=CHS.

Ju, Q., Liu, C., and Jiang, S. (2022). Integrated evaluation of rivers based upon the river happiness index (RHI): happy rivers in China. *Water* 14, 2568. doi: 10.3390/w14162568

Li, B. S., and Huang, F. (2024). Research on the construction of evaluation index system for happy rivers and lakes. *Harnessing Huaihe River* 7, 44–46. Available at: https://kns.cnki.net/kcms2/article/abstract?v=KetWmXlLxldY5uugq4diQGg2NL_Jp_XPo2THyoifbKtAi4IHE5T6XSnyn1VQjzJw57atPGIAMT_ujgkUEXeNu68jAJmgb9W7_L1i0NdGQnqq1SeaUnM9hDbZKxxTeFhLM1aSWRnwZonJo_VrCI4aLle2KH8pLL7ymv3KyEkKXmM_uZEFRZYl4C_tuczc2bW7&uniplatform=NZKPT&language=CHS (accessed December 10, 2024).

Liu, Y., Mu, Z., Dong, W., Huang, Q., Chai, F., and Fan, J. (2024). Establishment of an evaluation indicator system and evaluation criteria for the Weihe river ecological watersheds. *WATER* 16, 2393. doi: 10.3390/w16172393

Liu, C., Pang, Z., Ni, G., Mu, R., Shen, X., Gao, W., et al. (2023). A comprehensive methodology for assessing river ecological health based on subject matter knowledge and an artificial neural network. *Ecol. Inform.* 77, 102199. doi: 10.1016/j.ecoinf.2023.102199

Liu, Y., Su, H., Zhang, S., and Jin, T. (2021). Update of river health assessment indicator system, weight, and assignment criteria in China. *Water SUPPLY* 21, 3153–3167. doi: 10.2166/ws.2021.087

Lv, K., Si, Z. J., and Li, T. N. (2024). Evaluation system of happy rivers and lakes in Dulu River and its application. *Water Resour. Power* 42, 47–52. doi: 10.20040/j.cnki.1000-7709.2024.20231765

Ministry of Ecology and Environment of the People's Republic of China (2002). Environmental quality standards for surface water.GB 3838-2002. Available online at: https://www.mee.gov.cn/ywgz/fgbz/bz/bzwb/shjbh/shjzlbz/200206/t20020601_66497.shtml (accessed December 10, 2024).

Ministry of Water Resources of the PRC (2013). Regulation for water environmental monitoring. SL 219-2013. Available online at: https://std.samr.gov.cn/hb/search/stdHBDetailed?id=8B1827F1C849BB19E05397BE0A0AB44A (accessed December 10, 2024).

Ortiz-Burgos, S. (2016). "Shannon-weaver diversity index," in *Encyclopedia of Estuaries*. Ed. M. J. Kennish (Dordrecht, Springer Netherlands), 572–573. doi: 10.1007/978-94-017-8801-4_233

Ramanathan, R. (2001). A note on the use of the analytic hierarchy process for environmental impact assessment. *J. Environ. Manage.* 63, 27–35. doi: 10.1006/jema.2001.0455

Research group of the happy river (2020). Analysis of the connotation and index system for the Happy River. *China Water Resour.* 23, 1–4. Available at: https://kns.cnki.net/kcms2/article/abstract?v=KetWmXlLxlc7wHhzx8Yby1DYI-HFnQlKYbBEAwLAOX8zNtm0sy1gcfyjAzaRs4kAC8iidrAhvs_hFS_eeGovqAX1WWxDbFT4MXG3_Ex2d1JDk6f2AH-3VCEvp23BjKVRLqoDej3QPg_RWbAxQXLUmAmahoJL2SZGbZWgdqsylxW4CejExiKy-mEH6KHFBy3M&uniplatform=NZKPT&language=CHS (accessed December 10, 2024).

Schofield, N. J., and Davies, P. E. (1996). Measuring the health of our rivers. *Water* 23, 39–43.

Shao, W., Han, G., Li, J., Yang, Z., Liu, J., and Xu, T. (2024). Establishing a river health evaluation index system for seven rivers in Jiamusi City of China. *Water Sci. Technol.* 89, 2254–2272. doi: 10.2166/wst.2024.126

Song, H. T. (2024a). *). Evaluation of happy rivers and lakes in the main stream of Nenjiang River based on SMI-P model and entropy-weighted TOPSIS method* (Harbin: Heilongjiang University). doi: 10.27123/d.cnki.ghlju.2024.000863

Song, L. M. (2024b). Analysis of the overall plan for the construction of Xingfu River and lake in Nangang River, Guangzhou City. *Shaanxi Water Resour.* 5, 100–102. doi: 10.16747/j.cnki.cn61-1109/tv.2024.05.037

Statistics Bureau of Zhejiang Province. Water environment (2023). "Water environment, (2022)," in *Zhejiang Natural Resources Statistical Yearbook on Environment 2023* (China Statistical Publishing House, Beijing, China).

Su, Y., Fan, Z., Gan, L., Li, Y., Fei, G., Liu, Y., et al. (2023). Assessing lake health in China: Challenges due to multiple coexisting standards. *J. Hydrol.-Reg. Stud.* 46, 101351. doi: 10.1016/j.ejrh.2023.101351

Tong, T. (2024). Reflecting the harmony between people and water, creating a happy river and lake that showcases the characteristics of Longjiang. *Heilongjiang Hydraul. Sci. Technol.* 52, 132–135. doi: 10.14122/j.cnki.hskj.2024.04.025

Vinna, L. R., Wuest, A., Zappa, M., Fink, G., and Bouffard, D. (2018). Tributaries affect the thermal response of lakes to climate change. *Hydrol. Earth Syst. Sci.* 22, 31–51. doi: 10.5194/hess-22-31-2018

Voice of Zhejiang (2023). Report to the People: Zhejiang has taken the lead nationally in initiating the construction of comprehensive and happy rivers and lakes throughout its entire territory. Available online at: http://slt.zj.gov.cn/art/2023/8/15/art_1567479_59038599.html (accessed December 10, 2024).

Wang, H. (2020). The strategy and technology for ensuring water environment and ecological security provide support for building a happy river. *China Water Resour.* 884, 21,25. Available at: https://kns.cnki.net/kcms2/article/abstract?v=KetWmXlLxldTbSLjECpJwBWIOPEQTvwBljrxNpBEWtxXQsc3NTz8llaT57Our4JF9hiusE4L5MMlErlsPonrSbF9_B43_s46Rw6rElHTp7xX-Xda64X9GwXgC6H3a879JIou3uxY5MeGtQ2tBYX6IWJxMLjRhIqjhWmMHXkw2yrG-SynZ0yj3WrXO0zO_Bg0&uniplatform=NZKPT&language=CHS (accessed December 10, 2024).

Wu, Y. (2024). Analysis of the construction of happy river and lake - taking the construction of happy river and lake in Lianshui, Xiangtan City as an example. *Hunan Hydro Power* 3, 118–120. doi: 10.16052/j.cnki.hnslsd.2024.03.006

Wu, C., Ju, M., Wang, L., Gu, X., and Jiang, C. (2020). Public participation of the river chief system in China: current trends, problems, and perspectives. *Water* 12, 3496. doi: 10.3390/w12123496

Yang, Y. (2021). Evaluation of China's water-resource utilization efficiency based on a DEA-Tobit two-stage model. *Water Supply* 21, 1764–1777. doi: 10.2166/ws.2020.349

Zhang, Z., Xiong, C., Yang, Y., Liang, C., and Jiang, S. (2022). What makes the river chief system in China viable? Examples from the Huaihe river basin. *Sustainability* 14, 6329. doi: 10.3390/su14106329

Zhang, X., Zhou, Y., and Han, C. (2023a). Research on high-quality development evaluation and regulation model: A case study of the yellow river water supply area in Henan province. *WATER* 15, 261. doi: 10.3390/w15020261

Zhang, Z., Zou, X., Zhang, C., and Sharifi, S. (2023b). Has China's river chief system improved the quality of water environment? Take the yellow river basin as an example. *Pol. J. Environ. Stud.* 32, 4403–4416. doi: 10.15244/pjoes/168105

Zhao, M., Cheng, C., Chau, K., and Li, G. (2006). Multiple criteria data envelopment analysis for full ranking units associated to environment impact assessment. *Int. J. Environ. pollut.* 28 (3/4). doi: 10.1504/IJEP.2006.011222

Zhao, Y. W., and Yang, Z. F. (2009). Integrative fuzzy hierarchical model for river health assessment: A case study of Yong River in Ningbo City, China. *Commun. Nonlinear Sci. Numer. Simul.* 14, 1729–1736. doi: 10.1016/j.cnsns.2007.09.019

Zuo, Q. T., Hao, M. H., Jiang, L., and Zhang, Z. Z. (2021). Happy River evaluation system and its application. *Adv. Water Sci.* 32, 45–58. doi: 10.14042/j.cnki.32.1309.2021.01.005

Zuo, Q., Hao, M., Zhang, Z., and Jiang, L. (2020). Assessment of the happy river index as an integrated index of river health and human well-being: A case study of the Yellow river, China. *Water* 12, 3064. doi: 10.3390/w12113064

frontiers | Frontiers in Ecology and Evolution

TYPE Original Research
PUBLISHED 08 January 2025
DOI 10.3389/fevo.2024.1533380

OPEN ACCESS

EDITED BY
Celso Santos,
Federal University of Paraíba, Brazil

REVIEWED BY
Yakui Ding,
Jiangsu University, China
Huawei Li,
North China University of Water Resources and Electric Power, China

*CORRESPONDENCE
Jiuhe Bu
bujh@cwxu.edu.cn

RECEIVED 23 November 2024
ACCEPTED 18 December 2024
PUBLISHED 08 January 2025

CITATION
Bu J, Wang T and Xu T (2025) River health assessment based on set pair analysis model in typical Northern Chinese City.
Front. Ecol. Evol. 12:1533380.
doi: 10.3389/fevo.2024.1533380

River health assessment based on set pair analysis model in typical Northern Chinese City

Jiuhe Bu*, Tao Wang and Tian Xu

School of Environmental Science and Engineering, Wuxi University, Wuxi, Jiangsu, China

Rivers are critical to ecological and societal sustainability, yet human activities like urbanization, industrialization, and agricultural runoff increasingly threaten their ecological health. This study investigates the ecological health of six major rivers in Dalian City, China, focusing on the relationships between aquatic biological communities and environmental factors. A total of 168 phytoplankton species, 110 zooplankton species, and 102 macrozoobenthos species were identified. The key environmental factors influencing these communities included pH, dissolved oxygen, ammonium nitrogen, total phosphorus, and altitude. Using an entropy-weighted set pair analysis model, spatial variations in river ecosystem health were evaluated. Monitoring sites S12 and S15 exhibited good health conditions, while sites S4, S8, and S17 were rated as poor (Grade IV), and S7 was severely polluted (Grade V). Other sites showed borderline health (Grade III). This research provides valuable insights for improving river ecosystem management and biodiversity conservation in Dalian City, offering a scientific basis for addressing water quality and ecological challenges.

KEYWORDS

river health, biodiversity, aquatic ecosystems, Dalian City rivers, biodiversity conservation

Highlights

- The relationship between river biomes and environmental factors was studied by multivariate analysis;
- A river ecological health assessment model for Dalian City was established;
- Entropy weight method and set pair analysis method were used to assess river health.

1 Introduction

Rivers are essential components of the natural environment, acting as vital lifelines for both ecological systems and human societies (Chen et al., 2022a; Islam et al., 2024). In addition to these direct functions, rivers play a key role in nutrient cycling, sediment transport, and ecosystem services, such as flood regulation and water purification (Withers and Jarvie, 2008; Rattan et al., 2017). However, increasing human activities are placing escalating pressures on rivers, threatening their ecological health and sustainability. Urbanization, industrialization, agricultural runoff, and climate change have collectively led to habitat degradation, water quality decline, and biodiversity loss (Bryan et al., 2018; Wu et al., 2024). These challenges highlight the urgent need for effective strategies to assess and manage the health of river ecosystems. The concept of river ecological health has garnered significant attention in recent decades as researchers, policymakers, and conservationists work to balance development with environmental sustainability (Blue, 2018; Ding et al., 2022; Dong et al., 2022; Cai et al., 2023a). River health refers to the ability of a river system to maintain its ecological integrity and function while providing ecosystem services to both human and non-human communities. To assess river health, scientists utilize a combination of physical, chemical, and biological indicators. Although chemical and physical indicators provide valuable insights into river conditions, biological indicators are particularly effective in reflecting long-term ecological changes. Aquatic biological communities, such as phytoplankton, zooplankton, and macroinvertebrates, are highly sensitive to environmental disturbances and are considered reliable indicators of river health (Vugteveen et al., 2006; Stefanidis et al., 2023; Zhang et al., 2024).

Commonly used methods for assessing river health include the Analytic Hierarchy Process (AHP), Factor Analysis, Matter-Element Model, Grey Relational Analysis, Artificial Neural Networks (ANN), and Set Pair Analysis (SPA) (Vollmer et al., 2016; Yang et al., 2023; Kholodkevich, 2024). These methods are utilized to perform comprehensive evaluations of multi-indicator systems. The selection of indicators generally includes detailed metrics such as water quantity, water quality, aquatic organisms, physical structure, and riparian zone conditions. It is important to note that river health assessment methods are often customized to address the specific conditions of individual rivers. This tailoring ensures a more objective and accurate evaluation of the health status of each river type. As a result, the methods have distinct evaluation targets and defined scopes of applicability. In accordance with river management requirements, these methodologies are designed to account for the unique characteristics and management needs of particular river systems, allowing for precise and practical health assessments.

Despite significant advances in river health assessment methodologies, challenges persist, particularly in applying existing frameworks to urban rivers, which are shaped by distinct hydrological, ecological, and anthropogenic dynamics (Guimarães et al., 2021; Rowiński et al., 2022). Urban rivers are often under compounded pressures due to their proximity to human activities, making them highly vulnerable to pollution, flow alterations, and habitat fragmentation (Zhang et al., 2015, Zhang et al., 2023; Chen et al., 2022b). These challenges are particularly relevant in the context of rapidly urbanizing regions like Northern Chinese City. These rivers are shaped by the unique geographical and climatic conditions of Northern Chinese cities. Previous research on the region's rivers has largely focused on water quality and hydrology, with comparatively little attention given to the biological communities that support river ecosystem functions. This gap impedes the development of effective management strategies and limits our ability to accurately assess the ecological health of these rivers. Moreover, existing river health assessment methods often overlook the specific conditions of these rivers, highlighting the need for tailored evaluation frameworks.

This study aims to address these shortages by employing advanced analytical techniques to investigate the relationships between aquatic biological communities and environmental factors in rivers of a typical northern city. Specifically, the research utilizes multivariate analysis methods to explore the distribution patterns of phytoplankton, zooplankton, and macroinvertebrates, along with their interactions with environmental variables. These analyses provide insights into the ecological dynamics of river systems and deepen our understanding of the factors influencing river health. In addition to biological analysis, the study proposes a novel river health assessment framework that integrates multiple dimensions of river ecology, including water quality, quantity, and aquatic biodiversity. The framework also evaluates river health in the study area using set pair analysis.

2 Study area and data source

Dalian is located in the southern part of the Liaodong Peninsula, China (38°43'–40°10'N, 120°58'–123°31'E), covering an area of 12,573.85 km^2 and with a population of 7.54 million in 2023. It is bordered to the north by the Northeast China Plain and the Inner Mongolia Autonomous Region, and connects Bohai Bay to the Shandong Peninsula across the sea. Often referred to as the "gateway to Beijing and Tianjin" and the "window to Northeast China", Dalian plays a key role in the region's economic and cultural exchange. Dalian is a typical water-stressed coastal city in China, with an average annual water resource availability of about 3.1 billion m^3. In 2023, the per capita water resources were only 495 m^3, approximately 16.5% of the global average (3,000 m^3). The six major rivers are the primary surface water sources, accounting for over 90% of the total surface water supply in the city. The exploitation rates of these rivers are very high, with some approaching or exceeding 40%.

As the Northeast Asian International Shipping Center and the largest coastal port city in northeastern China, Dalian's economy is rapidly developing. However, with increasing water consumption driven by economic growth and decreasing runoff due to climate change and other factors, ensuring sufficient water for river ecosystems and maintaining their health has become an increasingly challenging issue.

In this study, the six main rivers were selected for investigation (Biliu river, Fuzhou river, Dasha river, Yingna river, Zhuang river, Dengsha river). For each river, three or four representative sample sites were chosen, covering the upstream, midstream, and downstream sections. A total of 19 sample sites were selected based

on water quality, water volume, and sewage outlets. Water quality and aquatic biodiversity data were collected in October 2023, while other data were obtained from the Dalian Statistical Yearbook. The location information and environmental conditions of 19 sampling points are shown in Figure 1 and Supplementary Table S1.

3 Methodology

This study evaluates the river health of the research area by integrating water quality and aquatic ecosystem monitoring data. A comprehensive river health assessment index system was developed, and the evaluation was conducted using multivariate statistical analysis, the entropy weight method, and set pair analysis. The detailed workflow is illustrated in Figure 2. It is important to note that the monitoring data presented in this paper primarily cover autumn, particularly October. As a result, the analysis does not account for variations in water ecological health and its influencing factors across different seasons. The results and discussions are based on the autumn scenario. However, some analyses that are not season-dependent will be further explored in the paper.

3.1 River health indicators

Considerable research has been conducted on river ecosystem health evaluation. However, due to the unique characteristics of the rivers in Dalian, existing index systems are not suitable for assessing river health in this region. Therefore, an index system tailored to the specific ecological and environmental conditions of Dalian's rivers needs to be developed.

Through investigation and analysis, the primary issues affecting the rivers in Dalian have been identified as water quality deterioration, reduced water quantity, and a decline in biological diversity. Considering the independence and clarity of the indicators, data availability, and findings from other studies, factors such as water quality, water quantity, and aquatic biodiversity were selected to reflect the overall health of the rivers (Table 1).

3.2 Evaluation standard

On the basis of The surface water environment quality standards GB3838-2002, the water quality pollution classification standard is shown in Table 2.

The threshold of the exploitation degree of rivers should be determined based on the theory of human-water harmony, this approach ensures that the exploitation can meet the reasonable demands of the economy and society, while also promoting the sustainable development of water resources and river ecosystems (Meng et al., 2009; Wang et al., 2022; Liu et al., 2024). An exploitation degree that is either too high or too low does not align with the requirements for river health. Internationally, the generally accepted reasonable limit for river exploitation is between 30% and 40%. Even with optimal use of rain and flood resources, the exploitation degree should not exceed 60%.

The conceptual model for evaluating river exploitation degree is shown in Figure 3. The model follows a parabolic structure, with the optimal exploitation range set at 30–40%. Exploitation levels above 60% or below 0% receive a score of 0. Based on this scoring system, river health is categorized as follows: 100–80 corresponds to Grade I; 80–60 to Grade II; 60–40 to Grade III; 40–20 to Grade IV; and 20–

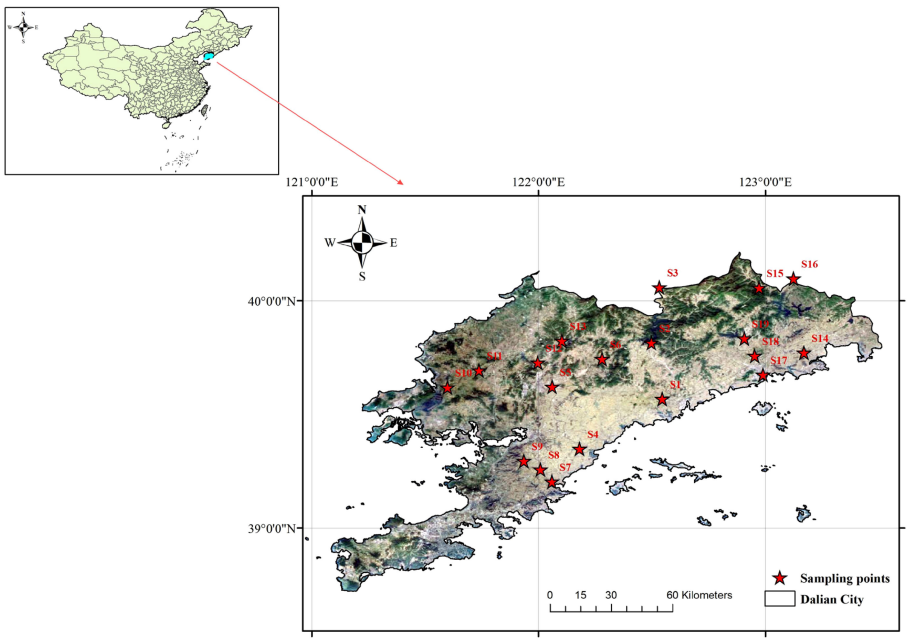

FIGURE 1
Geographic location of Dalian city.

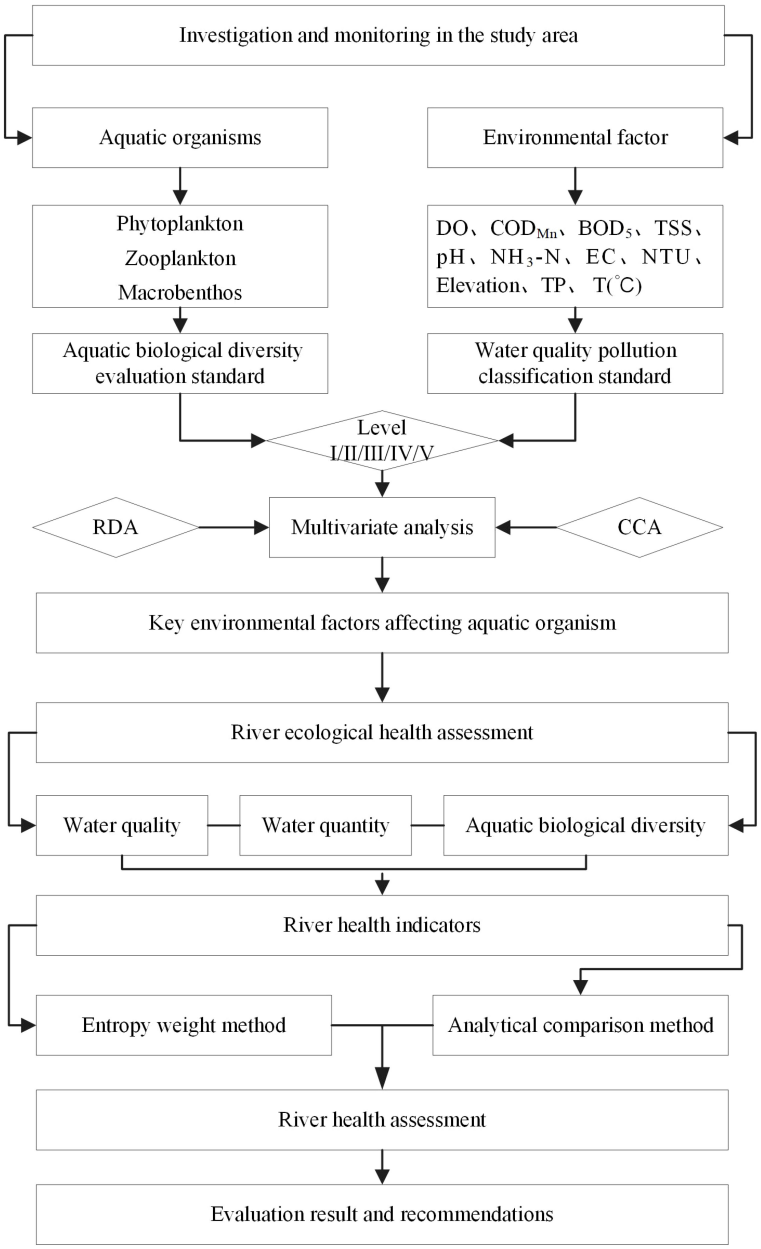

FIGURE 2
The technical flowchart.

0 to Grade V. This classification enables a detailed assessment of river health, aligning with management goals.

The health status of the river is evaluated by calculating the biological diversity index, using established evaluation standards for the index. The diversity indices include the Shannon-Wiener diversity index (H), Pielou evenness index (E), and Margalef index (M). The calculation formulas for each index are shown below:

$$H = -\sum_{i=1}^{S} \frac{n_i}{N} \log 2 \frac{n_i}{N} \quad (1)$$

$$E = -\sum_{i=1}^{S\sum} \frac{\frac{n_i}{N} log2 \frac{n_i}{N}}{log2S} \quad (2)$$

$$M = \frac{S-1}{lnN} \quad (3)$$

where S is the total number of species appeared in each sample point; N is the total number of individuals in each point; n_i is the number of i specie.

The evaluation standard of each aquatic biological diversity index is shown on Table 3.

3.3 Evaluation methodology

Assessing river ecological health is inherently complex due to the ambiguous nature of river health and the often conflicting

TABLE 1 Assessment indicator system of river health.

Factor	Detailed indicators
Water quality	DO
	COD_{Mn}
	BOD_5
	NH_3-N
	TP
	Escherichia coli
Water quantity	Exploitation degree of the evaluated river
	Amount of regional water resources
Aquatic biological diversity	Diversity index of phytoplankton
	Diversity index of zooplankton
	Diversity index of macrobenthos

interactions among its various components. To address these challenges, this study combines set pair analysis and entropy methods, offering a robust framework for analyzing and resolving the complexities of river health evaluation.

3.3.1 Set pair analysis method of river ecosystem health evaluation

When using set pair analysis to evaluate river ecosystem health, based on the river ecosystem health evaluation index system constructed by the researcher, the river's health can be categorized into five grades. Assume that there are A evaluated indices in Grade I, B1, B2, B3 evaluated indices in Grades II, III, and IV, respectively, and C evaluated indices in Grade V. According to set pair analysis theory, the connection degree of each evaluated sample is calculated as:

$$\mu_m = \frac{A}{5} + \frac{B_1}{5} i_1 + \frac{B_2}{5} i_2 + \frac{B_3}{5} i_3 + \frac{C}{5} j = a + b_1 i_1 + b_2 i_2 + b_3 i_3 + cj \quad (4)$$

By comparing the connection degree of a, b_1, b_2, b_3 and c, the preliminary difference level of the evaluated samples can be determined. Further set pair analysis is then conducted to identify the similarities, differences, and oppositions of evaluation index values compared to the evaluation standards, for indicators that correlates positively with standard, the connection degree μ_{mn} is determined as:

$$\mu_{mn} = \begin{cases} 1 + 0i_1 + 0i_2 + 0i_3 + 0j, & x_j \in [S_1, +\infty) \\ \frac{x-S_2}{S_2-S_1} + \frac{S_1-x}{S_2-S_1} i_1 + 0i_2 + 0i_3 + 0j, & x_j \in [S_2, S_1) \\ 0 + \frac{x-S_3}{S_3-S_2} i_1 + \frac{S_2-x}{S_3-S_2} i_2 + 0i_3 + 0j, & x_j \in [S_3, S_2) \\ 0 + 0i_1 + \frac{x-S_4}{S_4-S_3} i_2 + \frac{S_3-x}{S_4-S_3} i_3 + 0j, & x_j \in [S_4, S_3) \\ 0 + 0i_1 + 0i_2 + \frac{x-S_5}{S_5-S_4} i_3 + \frac{S_4-x}{S_5-S_4} j, & x_j \in [S_5, S_4) \\ 0 + 0i_1 + 0i_2 + 0i_3 + 1j, & x_j \in [0, S_5) \end{cases} \quad (5)$$

For indicators that correlates negatively with standard, the connection degree μ_{mn} is determined as:

$$\mu_{mn} = \begin{cases} 1 + 0i_1 + 0i_2 + 0i_3 + 0j, & x_j \in [0, S_1] \\ \frac{S_2-x}{S_2-S_1} + \frac{x-S_1}{S_2-S_1} i_1 + 0i_2 + 0i_3 + 0j, & x_j \in (S_1, S_2] \\ 0 + \frac{S_3-x}{S_3-S_2} i_1 + \frac{x-S_2}{S_3-S_2} i_2 + 0i_3 + 0j, & x_j \in (S_2, S_3] \\ 0 + 0i_1 + \frac{S_4-x}{S_4-S_3} i_2 + \frac{x-S_3}{S_4-S_3} i_3 + 0j, & x_j \in (S_3, S_4] \\ 0 + 0i_1 + 0i_2 + \frac{S_5-x}{S_5-S_4} i_3 + \frac{x-S_4}{S_5-S_4} j, & x_j \in (S_4, S_5] \\ 0 + 0i_1 + 0i_2 + 0i_3 + 1j, & x_j \in (S_5, +\infty) \end{cases} \quad (6)$$

where m is the number of evaluation sample; n is the number of evaluation index; x is the measured value; S_1、S_2、S_3、S_4、S_5 represent the upper limit of I~V level standard respectively.

3.3.2 The entropy weight method to determine the weight coefficient of the evaluation indexes

The weight of an index reflects its influence on the overall river ecosystem health. In this study, the entropy weight method was used to determine the weight coefficients of the evaluation indices. In information theory, entropy measures the degree of disorder or uncertainty in a system, and can quantify the amount of information. An index providing more information has a smaller entropy value, indicating lower disorder and a greater role in the final decision. Therefore, the entropy weight method is applied to calculate the weight coefficients of the evaluation indices. The main computational steps are as follows:

1. Assuming there are m evaluation objects, each evaluation objects have n evaluation indexes, the judgment matrix R is:

$$R = (r_{st})_{m\times n}, (s = 1, 2, \ldots, m; t = 1, 2, \ldots, n) \quad (7)$$

where m is the number of evaluation sample; n is the number of evaluation index; r_{st} is the measured value.

2. Normalize the judgment matrix R, the element of the normalized matrix B is:

$$b_{st} = \frac{r_{st} - r_{min}}{r_{max} - r_{min}} \quad (8)$$

where r_{max}、r_{min} are the most satisfying and the most dissatisfied value respectively (the bigger the better or the smaller the better) of different things in the same assessment index.

TABLE 2 Water quality pollution classification standard.

Level	DO (mg/L) ≥	NH_3-N (mg/L) ≤	TP (mg/L) ≤	COD_{Mn} (mg/L) ≤	BOD_5 (mg/L) ≤	E.coli (MPN/L) ≤
I	7.5	0.15	0.02	2	3	200
II	6	0.5	0.1	4	3	2000
III	5	1	0.2	6	4	10000
IV	3	1.5	0.3	10	6	20000
V	2	2	0.4	15	10	40000

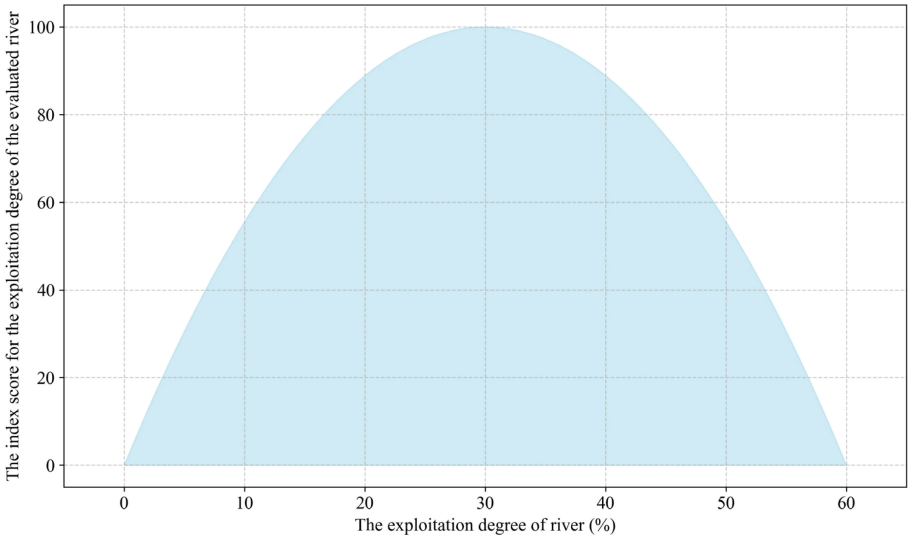

FIGURE 3
The conceptual model of index score for the exploitation degree of the evaluated river.

3. According to the traditional conception of entropy, the entropy value of each evaluation index is:

$$e_t = -(\sum_{s=1}^{m} f_{st} ln f_{st})/lnm, (s = 1, 2, \ldots, m; t = 1, 2, \ldots, n) \quad (9)$$

where $f_{st} = b_{st}/\sum_{s=1}^{m} b_{st}$, When f_{st}=0, $e_t = 0$.

4. The entropy weight of each evaluation index is:

$$W = (w_t)_{1\times n}, \quad w_t = (1 - e_t)/(n - \sum_{t=1}^{n} e_t), \sum_{t=1}^{n} w_t = 1 \quad (10)$$

where W is entropy weight, e_t is the entropy value of each evaluation index.

3.3.3 River ecosystem health evaluation model based on entropy weight and set pair analysis

According to the index weight vector W and the connection degree μ_m and μ_{mn}, the evaluation model based on entropy weight and set pair analysis is:

$$\overline{\mu_m} = \mu_m \times \sum_{t=1}^{n} (w_t \times \mu_{mt}) \quad (11)$$

where $\overline{\mu_m}$ is the comprehensive connection degree of evaluation sample m, t is the number of evaluation index.

Normalize all components in each $\overline{\mu_m}$, the final connection degree of each evaluated sample can be get.

Finally the evaluated sample level can be get according to the following formula, the evaluated sample belong to l level based on h_l.

$$h_1 = y_1 + y_2 + \ldots + y_l > \lambda, l = 1, 2, \ldots, 5. \quad (12)$$

where y_1=a, y_2=b_1, y_3=b_2, y_4=b_3, y_5=c;λ is confidence coefficient, the general value is in [0.5, 0.7]. The evaluate result is more reliable if λ is bigger.

4 Results

4.1 Analysis of river water ecological status

4.1.1 River water quality condition

Based on water quality monitoring results and the "Environmental Quality Standards for Surface Water" (GB3838-

TABLE 3 Evaluation standard of aquatic biological diversity index.

Diversity index Health level	Phytoplankton diversity index			Zooplankton diversity index		Macrobenthos diversity index		
	H	*E*	*M*	*H*	*M*	*H*	*E*	*M*
	≥	≥	≥	≥	≥	≥	≥	≥
I	3.0	0.8	4.0	3.0	4.0	3.0	0.8	3.0
II	2.5	0.6	3.0	2.0	3.0	2.5	0.5	2.5
III	2.0	0.4	2.0	1.5	2.0	2.0	0.3	2.0
IV	1.0	0.2	1.0	1.0	1.0	1.0	0.2	1.0
V	0	0	0	0	0	0	0	0

2002), the water quality of major rivers in Dalian was assessed using a single-factor evaluation method. The analysis of the results, presented in Table 4, shows that most rivers in Dalian fall within Class III or below. The primary pollutants are ammonia nitrogen and total phosphorus. BOD_5 levels at various sampling points range from Class I to Class IV, while COD_{Mn} levels also vary between Class I and Class IV, indicating significant differences across the sites. Additionally, the water quality at sampling points S5, S8, S9, and S10 is classified as Class V.

4.1.2 River biological condition

Phytoplankton: A total of 168 phytoplankton species were identified during the aquatic ecological survey of six major rivers in Dalian, encompassing 19 sampling sites. These included 91 species of Bacillariophyta (54.17%), 39 species of Chlorophyta (23.21%), 13 species of Euglenophyta (7.74%), 3 species each of Cryptophyta, Xanthophyta, and Chrysophyta (1.79% each), 15 species of Cyanophyta (8.93%), and 1 species of Pyrrophyta (0.60%). The spatial distribution of phytoplankton, illustrated in Figure 4, demonstrates significant spatial variability. Overall, Bacillariophyta and Chlorophyta were dominant in most sampling sites, while Cyanophyta dominated in specific locations such as S1 and S17.

Zooplankton: A total of 110 zooplankton species were identified, comprising 35 species of Protozoa (47.8%), 42 species of Rotifera (40.3%), 20 species of Cladocera (10.4%), and 13 species of Copepoda (16.4%). As shown in Figure 4, zooplankton displayed evident spatial distribution differences. Protozoa were predominant in most sampling sites, while Copepoda were mainly found near coastal sampling sites, such as S4, S10, and S17.

Macrozoobenthos: The survey identified 102 species of macrozoobenthos, including 70 species of aquatic insects (68.63%), 6 species of crustaceans (5.88%), 10 species of annelids (9.8%), and 16 species of mollusks (15.69%). The spatial distribution of macrozoobenthos, depicted in Figure 4, also exhibited significant spatial differences.

Table 5 presents the species count of phytoplankton, along with the Shannon-Wiener diversity index (*H*), Pielou's evenness index (*E*), Margalef richness index (*M*), and their evaluations as per diversity index standards for each sampling site. The highest phytoplankton species count was recorded at S4 with 27 species, whereas the lowest counts, of 11 species each, were at S18 and S19. The diversity indices closely mirrored species richness, with cleaner sites demonstrating higher richness. For instance, the indices at S3 —*H* (2.62), *E* (0.93), *M* (3.84)—were the highest among all sites, indicating the best water quality when assessed via phytoplankton. Conversely, the lowest values for these indices (*H*: 1.02; *E*: 0.38; *M*: 1.78) were observed at S1, where Xanthophyta was the predominant group.

The species number, density, biomass, Shannon-Wiener diversity index (*H*), and Margalef richness index (*M*) of zooplankton at each sampling point are shown in Table 5. The

TABLE 4 Results of single factor and comprehensive evaluation of river water quality.

Sampling point	DO	COD_{Mn}	BOD_5	NH_3-N	TP	Comprehensive assessment
S1	I	III	III	I	II	III
S2	I	II	I	II	II	II
S3	I	I	II	II	II	II
S4	II	II	II	IV	I	IV
S5	V	II	IV	V	III	V
S6	I	II	III	II	II	III
S7	IV	III	II	IV	III	IV
S8	II	III	II	V	III	V
S9	I	IV	IV	V	III	V
S10	I	II	IV	V	II	V
S11	I	III	III	IV	II	IV
S12	II	II	I	III	II	III
S13	I	II	III	II	II	III
S14	III	II	III	II	II	III
S15	I	I	I	II	I	II
S16	I	I	III	II	I	III
S17	I	I	III	II	I	III
S18	IV	III	II	IV	IV	IV
S19	I	I	I	II	I	I

In order to better distinguish the assessment results, green is Class I, blue is Class II, yellow is Class III, orange is a Class IV, and red is Class V.

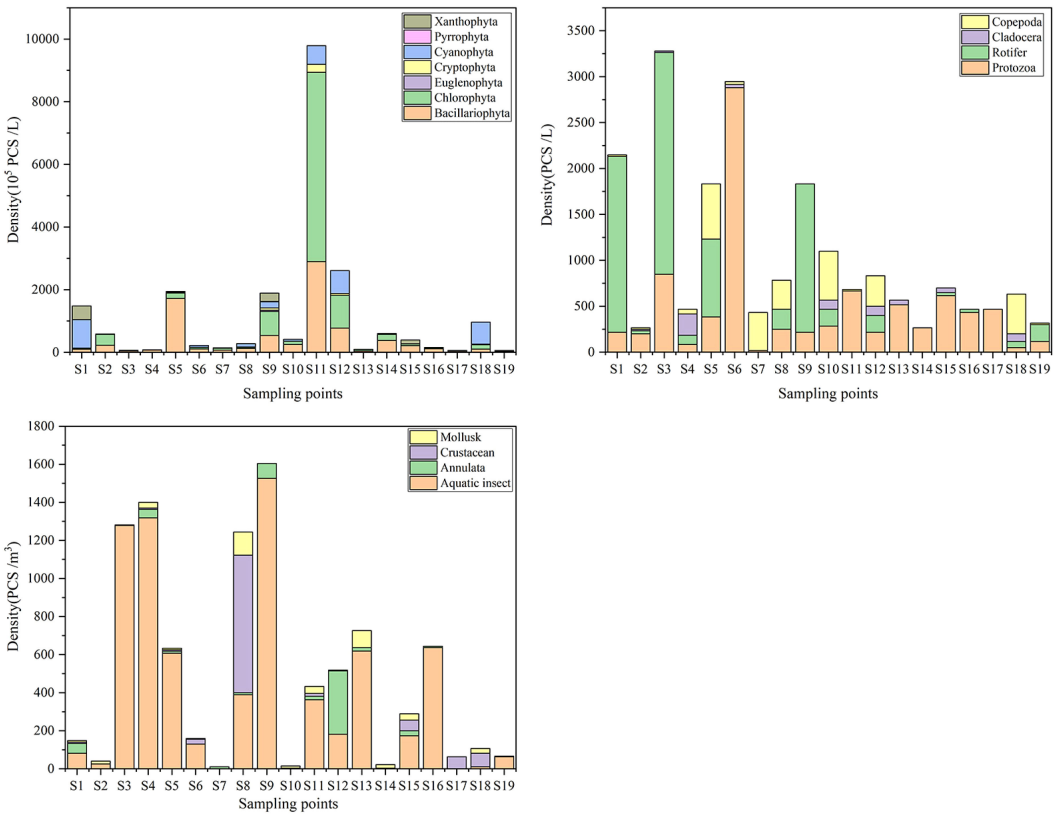

FIGURE 4
The aquatic organisms density at sampling sites.

zooplankton species number was highest at S11, with 11 species, and lowest at S14 and S7, with only 3 species each. The diversity indices generally reflected a pattern similar to species richness, with cleaner sites exhibiting higher species richness. For example, S11 had the highest *H* value (2.31) and *M* value (10.11), with 12 species identified, indicating that S11's water quality, based on zooplankton evaluation, was the best in the study area. In contrast, S7 exhibited the lowest biodiversity indices (*H*: 0.43; *M*: 10.87), with just three species observed.

Table 5 presents the species number, Shannon-Wiener diversity index (H), Pielou evenness index (E), Margalef richness index (M), and evaluation results for benthic macroinvertebrates at each sampling site. The results indicate that sites S1 and S15 were lightly polluted. However, the dominant species at these sites were not sensitive, with only a few Ephemeroptera species observed. At S1, the most abundant species were Glyptotendipes cauliginellus and Limnodrilus hoffmeisteri, while Cardina denticulata sinensis dominated at S15. Sites with moderate pollution had the highest species diversity, with dominant species appearing more frequently and abundantly. These species were primarily moderately pollution-tolerant taxa, including Limnodrilus hoffmeisteri. Sites with heavy or severe pollution, mainly near river mouths, were dominated by highly pollution-tolerant species such as Chironomidae larvae and oligochaetes, as well as moderately tolerant species like Radix ovata. Notably, only one species was recorded at S7, where the proximity to a steel mill discharge resulted in high conductivity, negatively affecting benthic macroinvertebrate survival.

4.2 Relationship between river biomes and environmental factors

Figure 5 presents the results of the redundancy analysis (RDA), illustrating the relationships between phytoplankton or sampling sites and environmental factors. The horizontal and vertical axes represent the first and second ordination axes, respectively. The correlation coefficient between the first and second axes is zero, indicating that the ordination results are reliable.

From the left panel, species in the upper-left corner (species types are listed in Appendix), including (2), (7), (10), (11), (12), (16), (22), and (34), are positively correlated with ammonia nitrogen (E2), BOD_5 (E5), and total phosphorus (E3), while negatively correlated with dissolved oxygen (E1). Other environmental factors have minimal impact on these species. In contrast, species near the horizontal axis on the right, such as (3), (8), (24), (25), (26), (29), (36), and (38), show positive correlations with dissolved oxygen (E1) and pH (E7). Altitude (E11) significantly affects species like (6), (17), and (20). From the right panel, sampling sites in the first quadrant show high similarity and are mainly influenced by altitude (E11), while those in the third quadrant are strongly correlated with pH (E7).

10.3389/fevo.2024.1533380

TABLE 5 Assessment results of aquatic biodiversity index at different sampling sites.

Sampling point	Phytoplankton diversity index				Zooplankton diversity index			Macrobenthos diversity index			
	Species Count	H	E	M	Species Count	H	M	Species Count	H	E	M
S1	14	IV	IV	IV	10	IV	I	13	II	II	I
S2	20	III	II	III	6	V	I	6	III	I	III
S3	17	II	I	II	7	III	I	14	IV	III	III
S4	27	IV	III	II	10	III	I	13	IV	IV	III
S5	16	III	II	III	8	V	I	16	III	II	II
S6	12	III	I	III	9	III	I	10	II	I	III
S7	18	III	I	II	3	V	I	1	—	—	—
S8	25	II	II	II	7	IV	I	17	II	II	II
S9	16	III	I	III	10	II	I	13	III	II	IV
S10	19	III	I	III	10	III	I	2	V	I	V
S11	20	IV	III	III	11	II	I	10	IV	II	IV
S12	23	II	I	II	10	III	I	9	III	II	IV
S13	16	III	I	II	9	III	I	7	IV	III	IV
S14	22	III	II	II	3	V	I	3	IV	II	IV
S15	22	III	II	II	10	II	I	14	I	I	II
S16	22	II	I	II	6	IV	I	13	IV	II	III
S17	19	IV	III	III	7	III	I	1	—	—	—
S18	11	III	I	III	4	IV	I	5	IV	II	IV
S19	11	III	I	III	7	III	I	7	II	I	III

In order to better distinguish the assessment results, green is Class I, blue is Class II, yellow is Class III, orange is a Class IV, and red is Class V.

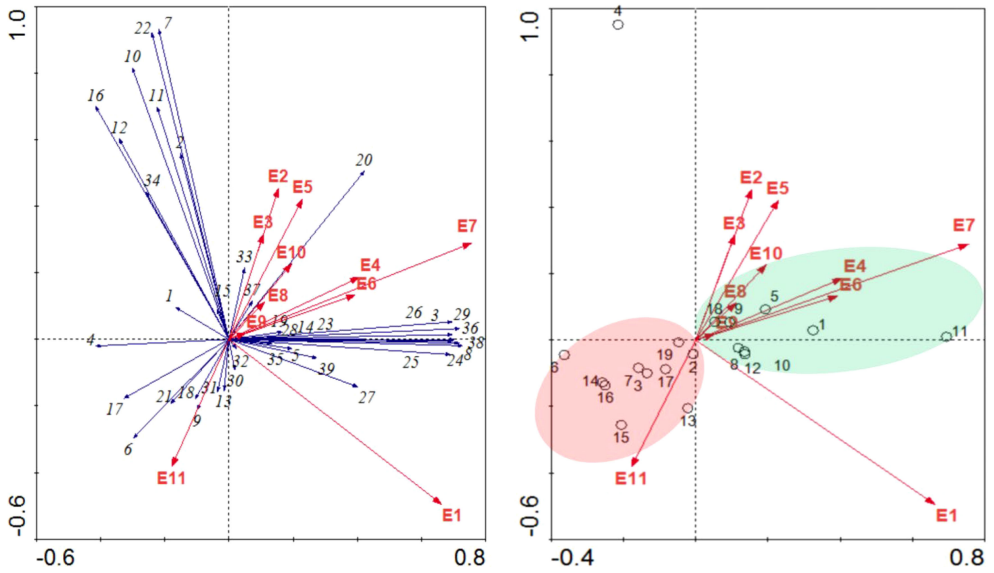

FIGURE 5
RDA analysis of phytoplankton species density and environmental factors in major rivers of Dalian City (Red arrow represents environmental factors, blue arrow represents species, and circle represents sampling point E1: DO; E2: NH_3-N; E3: TP; E4: COD_{Mn}; E5: BOD_5; E6: T(℃); E7: pH; E8: EC; E9: TDS; E10: Turbidity; E11: Altitude).

The RDA analysis results indicate that the correlation between the first axis and pH (r = 0.537) is the highest, while the second axis correlates most strongly with dissolved oxygen (r = 0.4498). This suggests that pH and dissolved oxygen are the primary factors influencing the phytoplankton community structure in major rivers of Dalian. Additionally, ammonia nitrogen, total phosphorus, BOD_5, and altitude also exert significant influence on the phytoplankton community.

Figure 6 presents the results of the canonical correspondence analysis (CCA), illustrating the relationships between zooplankton species, sampling sites, and environmental factors (species details are listed in Appendix). The left panel shows that species within the red circle, including (4), (8), (9), (10), (12), (13), (14), are closely associated with altitude (E11). In contrast, species in the green circle, such as (1), (2), (3), (5), (6), and (7), are positively correlated with ammonia nitrogen (E2) and conductivity (E8), indicating minimal distributional variation. Species like (11) are sensitive to pH (E7).

The right panel reveals that sampling sites in the red circle are mainly influenced by altitude (E11), while those in the green circle are primarily affected by ammonia nitrogen (E2). Sites in the yellow circle are most influenced by pH (E7).

The CCA analysis results reveal that the first ordination axis is most strongly correlated with dissolved oxygen (r = -0.7291) and ammonia nitrogen (r = 0.6702), while the second axis is primarily associated with COD (r = -0.6386). These findings suggest that dissolved oxygen, ammonia nitrogen, and COD are the key environmental factors shaping the zooplankton community structure in the major rivers of Dalian.

Figure 7 presents the canonical correspondence analysis (CCA) results, elucidating the relationships between macroinvertebrate communities, sampling sites, and environmental factors. The analysis confirms the reliability of the ordination results, as the correlation coefficient between the first and second axes is zero.

The CCA results indicate that the first ordination axis shows strong correlations with dissolved oxygen (r = 0.7432), ammonia nitrogen (r = -0.7084), and total phosphorus (r = -0.6259). Meanwhile, the second axis is most significantly correlated with ammonia nitrogen (r = 0.5314). These findings highlight that dissolved oxygen, ammonia nitrogen, and total phosphorus are the primary environmental factors influencing the community structure of macroinvertebrates in the major rivers of Dalian.

4.3 Comprehensive assessment of river ecological health

Using the entropy weighting method, the weights of various evaluation indicators are determined (Table 6):

The ecological health of six rivers in Dalian was assessed using river health evaluation methods and an established indicator system. First, the evaluation indicator values from various monitoring sections were compared to river health classification standards to preliminarily assess the health status of each section through set pair analysis correlation degrees. Based on the confidence criterion formula with a λ value of 0.7, the health grades of river sections were determined. The results, presented in Table 7, show that sections S12 and S15 have relatively good health conditions. In contrast, sections S4, S8, and S17 are classified as Grade IV, indicating poor health, while section S7 is categorized as Grade V, representing severe pollution. Other sections fall under Grade III, indicating a critical health state.

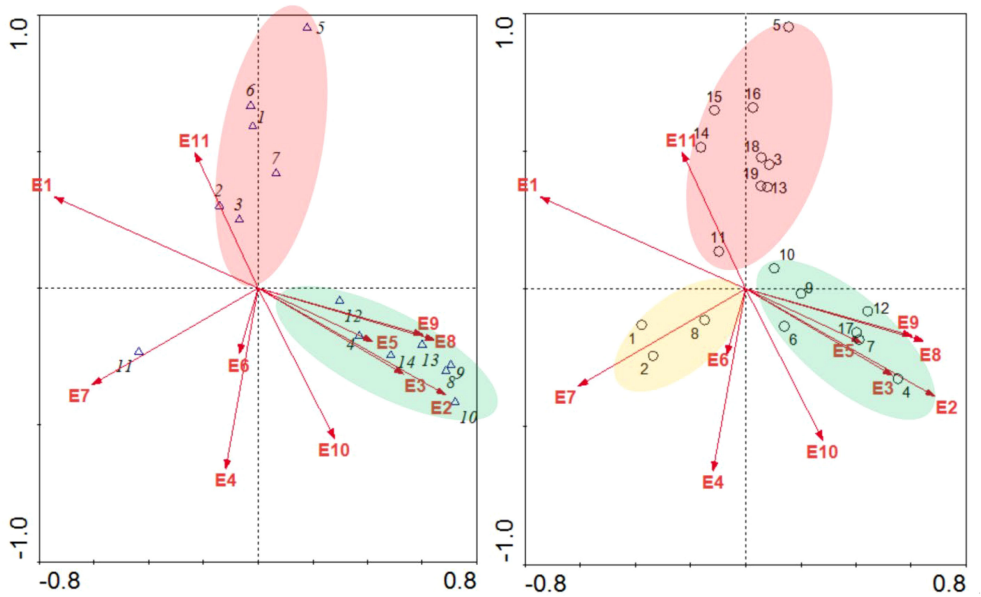

FIGURE 6
CCA analysis of zooplankton species density and environmental factors in major rivers of Dalian City.

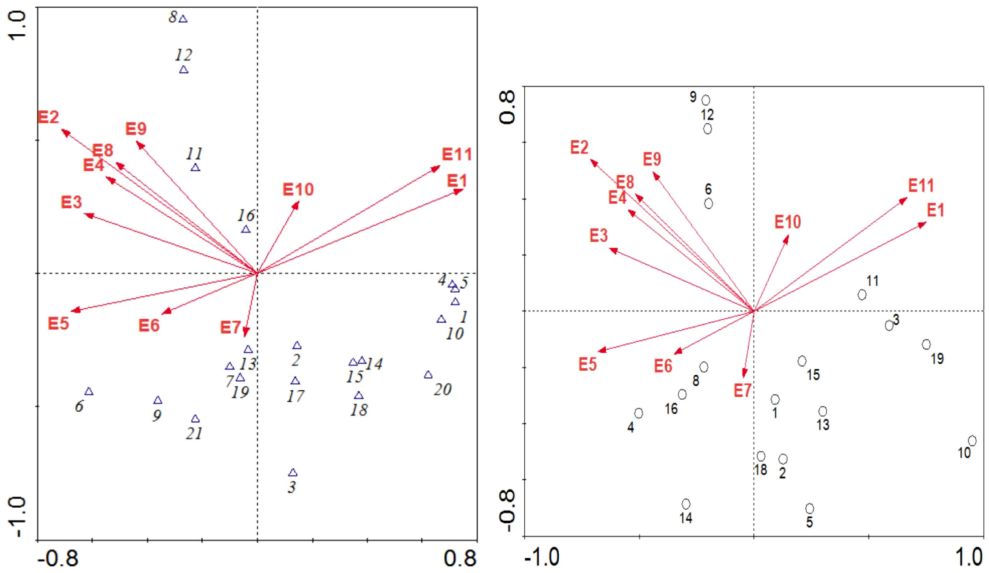

FIGURE 7
CCA analysis of macrobenthic species density and environmental factors in major rivers of Dalian City.

5 Discussion

The study revealed that pH and dissolved oxygen are the primary factors influencing phytoplankton communities in the major rivers of Dalian. Previous research has demonstrated a significant positive correlation between algal primary productivity and pH levels (Yu et al., 2022), with pH variations influencing the growth and distribution of phytoplankton (Raven and Beardall, 2021). Nitrogen and phosphorus, essential nutrients in aquatic ecosystems, serve as fundamental elements for phytoplankton growth and play critical roles in the development of aquatic organisms. Studies have identified nitrogen and phosphorus as key limiting factors for the structure and distribution of phytoplankton communities (Liu et al., 2021; Lin, 2023).

Dissolved oxygen and BOD_5 are effective indicators of organic pollution in water bodies, while dissolved oxygen, ammonia nitrogen, and COD significantly impact zooplankton communities in Dalian's major rivers. Zooplankton communities are also influenced by conductivity and altitude, where conductivity reflects ion concentrations and salinity levels—factors that affect individual growth and the spatial-temporal distribution of zooplankton (Bandara et al., 2021; Yi et al., 2024). Furthermore, factors such as pH, dissolved oxygen, ammonia nitrogen, total phosphorus, BOD_5, and altitude indirectly affect zooplankton communities through trophic interactions, as zooplankton feed on phytoplankton.

Multivariate analysis reveals that, in comparison to phytoplankton and zooplankton, the correlations between macrozoobenthos and environmental factors are weaker. This difference can likely be attributed to the distinct habitat characteristics of macrozoobenthos, which reside in benthic environments where sediment conditions play a more prominent role than water quality parameters. Unlike planktonic organisms, whose distributions are primarily influenced by water column properties such as temperature, nutrient concentrations, and light availability, benthic organisms are more closely tied to the physical and chemical conditions of the substrate. These conditions, such as sediment texture, organic matter content, and redox potential, are critical in shaping the health and distribution of macrozoobenthos.

The research primarily focuses on the natural ecological factors that influence river health, yet it does not fully account for the profound impact of human societal activities. For river ecosystems to thrive sustainably, both natural ecological conditions and external anthropogenic pressures must be considered. Human activities, particularly land-use changes, urbanization, and industrialization, can

TABLE 6 Indicator weight.

Evaluation Indicator	Weight	Evaluation Indicator	Evaluation Indicator	Evaluation Indicator	Weight
DO	0.06	Phytoplankton *H*	0.03	Macroinvertebrates *H*	0.06
NH_3-N	0.04	Phytoplankton *E*	0.04	Macroinvertebrates *E*	0.05
TP	0.04	Phytoplankton *M*	0.06	Macroinvertebrates *M*	0.06
COD	0.05	Zooplankton *H*	0.06	Utilization rate of water resources development	0.2
BOD	0.07	Zooplankton *M*	0.08	Ecological water demand guarantee rate	0.1

TABLE 7 Comprehensive correlation degree and health grade of river samples.

Sampling Site	Comprehensive correlation degree	Health level
S1	$\mu_1 = 0.311 + 0.130i_1 + 0.375i_2 + 0.184i_3 + 0j$	III
S2	$\mu_2 = 0.338 + 0.246i_1 + 0.408i_2 + 0i_3 + 0.008j$	III
S3	$\mu_3 = 0.301 + 0.286i_1 + 0.388i_2 + 0.025i_3 + 0j$	III
S4	$\mu_4 = 0.0925 + 0.162i_1 + 0.307i_2 + 0.277i_3 + 0.161j$	IV
S5	$\mu_5 = 0.210 + 0.444i_1 + 0.229i_2 + 0.050i_3 + 0.067j$	III
S6	$\mu_6 = 0.344 + 0.323i_1 + 0.296i_2 + 0.037i_3 + 0j$	III
S7	$\mu_7 = 0.091 + 0.063i_1 + 0.132i_2 + 0.306i_3 + 0.408j$	V
S8	$\mu_8 = 0.195 + 0.474i_1 + 0.006i_2 + 0.314i_3 + 0.010j$	IV
S9	$\mu_9 = 0.143 + 0.395i_1 + 0.258i_2 + 0.179i_3 + 0.025j$	III
S10	$\mu_{10} = 0.422 + 0.109i_1 + 0.435i_2 + 0i_3 + 0.035j$	III
S11	$\mu_{11} = 0.347 + 0.128i_1 + 0.428i_2 + 0.097i_3 + 0j$	III
S12	$\mu_{12} = 0.580 + 0.166i_1 + 0.208i_2 + 0.046i_3 + 0j$	I
S13	$\mu_{13} = 0.425 + 0.211i_1 + 0.274i_2 + 0.090i_3 + 0j$	III
S14	$\mu_{14} = 0.057 + 0.371i_1 + 0.276i_2 + 0.282i_3 + 0.014j$	III
S15	$\mu_{15} = 0.684 + 0.190i_1 + 0.089i_2 + 0.036i_3 + 0j$	II
S16	$\mu_{16} = 0.360 + 0.226i_1 + 0.225i_2 + 0.189i_3 + 0j$	III
S17	$\mu_{17} = 0.032 + 0.086i_1 + 0.365i_2 + 0.306i_3 + 0.211j$	IV
S18	$\mu_{18} = 0.412 + 0.167i_1 + 0.186i_2 + 0.235i_3 + 0j$	III
S19	$\mu_{19} = 0.453 + 0.195i_1 + 0.312i_2 + 0.039i_3 + 0j$	III

lead to increased pollution, altered hydrological regimes, and habitat degradation, all of which exacerbate the challenges faced by river ecosystems. Thus, achieving a harmonious balance between environmental protection and socio-economic development is paramount. In Dalian, several challenges, such as high pollutant loads, water scarcity, and sedimentation problems, hinder the health of river ecosystems. To address these issues, the following countermeasures and recommendations are proposed, incorporating both ecological restoration and human-centered solutions:

Developing Alternative Water Sources: To reduce the dependency on river water and ensure the maintenance of ecological water requirements, the development of alternative water sources is critical (Cai et al., 2023b). Unconventional water resources, such as rainwater harvesting and seawater desalination, can supplement the existing water supply. By integrating rainwater collection systems into urban infrastructure and promoting seawater desalination for non-potable uses, Dalian can diversify its water supply sources, thus reducing stress on river systems.

Enhancing Water Resource Efficiency: Increasing the efficiency of water resource use is another crucial strategy for reducing the pressure on river ecosystems (Yasmeen et al., 2023). This can be achieved by improving sewage treatment infrastructure, advancing wastewater recycling technologies, and promoting industrial water reuse. For example, municipal wastewater treatment plants should be upgraded to higher treatment standards, enabling the safe reuse of treated wastewater for irrigation and industrial processes. Furthermore, industries should be encouraged to implement closed-loop water recycling systems to minimize freshwater consumption and reduce pollutant discharge.

Scientific Pollution Management: Effective pollution management requires a data-driven approach that incorporates the ecological carrying capacity of different regions (Li et al., 2023). Implementing rational pollution discharge allocations, based on scientific research into the water environmental carrying capacity of Dalian's rivers, can help balance ecological protection with industrial and municipal growth. This approach involves identifying the maximum pollutant load each river segment can support without compromising its ecological health. Additionally, research on the sources, types, and impacts of pollutants (e.g., nutrients, heavy metals, and microplastics) will be critical in developing targeted pollution control strategies.

In conclusion, sustainable management of river ecosystems in Dalian requires a multifaceted approach that integrates ecological, technological, and policy solutions. By focusing on both natural ecological restoration and human-centered interventions, Dalian can improve its river health while also supporting continued urban and industrial development. Through the development of alternative water sources, the promotion of water-use efficiency, and scientific pollution management, the city can address the pressing challenges facing its rivers and foster long-term ecological sustainability. Future research should continue to explore the dynamic relationship between human activities and river health, incorporating both natural and social science perspectives to inform more effective environmental management strategies.

6 Conclusion

This study investigates the health of six major rivers in Dalian City by analyzing aquatic biodiversity and key environmental factors. The research utilized multivariate analysis to identify critical factors influencing phytoplankton, zooplankton, and macrozoobenthos communities. Additionally, a comprehensive river ecosystem health evaluation system was developed, integrating baseline data and relevant research. Using entropy-weighted set pair analysis, we assessed ecological health variations across different monitoring sites, offering valuable insights into river management and biodiversity conservation.

The main conclusions are as follows:

1. A total of 168 phytoplankton species were identified in Dalian's rivers, with Bacillariophyta (diatoms) and Chlorophyta (green algae) as the dominant taxa. The primary factors influencing phytoplankton communities were pH and dissolved oxygen, with additional effects from ammonium nitrogen, total phosphorus, biochemical oxygen demand (BOD_5), and altitude.
2. A total of 110 zooplankton species were recorded, with protozoa and freshwater rotifers as the dominant groups. Key factors affecting zooplankton communities included dissolved oxygen, ammonium nitrogen, and COD_{Mn}, alongside notable influences from conductivity and altitude.

3. A total of 102 macrozoobenthos species were identified, with Tubificidae (oligochaetes) and moderately pollution-tolerant aquatic insects as dominant taxa. Dissolved oxygen, ammonium nitrogen, and total phosphorus were the main factors influencing macrozoobenthos communities.
4. Rivers at monitoring sites S12 and S15 exhibited relatively good ecological health, while sites S4, S8, and S17 were classified as Grade IV, indicating poor ecological health. Site S7 was classified as Grade V, reflecting severe pollution. Other sites were classified as Grade III, indicating borderline health status.

Despite these findings, several limitations highlight the need for further research. The study was based on a single survey, which did not account for seasonal variations. Future research should include long-term monitoring to better understand temporal dynamics. Moreover, the river health assessment model focused primarily on hydrological and environment factors and did not fully incorporate socio-economic aspects, suggesting a need for a more holistic approach in future evaluations.

Data availability statement

The original contributions presented in the study are included in the article/Supplementary Material. Further inquiries can be directed to the corresponding author.

Author contributions

JB: Writing – original draft, Writing – review & editing, Conceptualization, Funding acquisition, Methodology. TW: Data curation, Software, Validation, Writing – review & editing. TX: Data curation, Software, Validation, Writing – review & editing.

Funding

The author(s) declare financial support was received for the research, authorship, and/or publication of this article. This research was funded by the Natural Science Foundation of Jiangsu Province (BK20230174), the Foundation of Basic Science (Natural Science) research in Jiangsu Province (22KJB570008), and Wuxi University Research Start-up Fund for Introduced Talents (552424056).

Acknowledgments

We would like to extend special thanks to the editor and the reviewers for their valuable comments in greatly improving the quality of this research.

Conflict of interest

The authors declare that the research was conducted in the absence of any commercial or financial relationships that could be construed as a potential conflict of interest.

Generative AI statement

The author(s) declare that no Generative AI was used in the creation of this manuscript.

Publisher's note

All claims expressed in this article are solely those of the authors and do not necessarily represent those of their affiliated organizations, or those of the publisher, the editors and the reviewers. Any product that may be evaluated in this article, or claim that may be made by its manufacturer, is not guaranteed or endorsed by the publisher.

Supplementary material

The Supplementary Material for this article can be found online at: https://www.frontiersin.org/articles/10.3389/fevo.2024.1533380/full#supplementary-material

References

Bandara, K., Varpe, Ø., Wijewardene, L., Tverberg, V., and Eiane, K. (2021). Two hundred years of zooplankton vertical migration research. *Biol. Rev.* 96, 1547–1589. doi: 10.1111/brv.12715

Blue, B. (2018). What's wrong with healthy rivers? Promise and practice in the search for a guiding ideal for freshwater management. *Prog. Phys. Geography: Earth Environ.* 42, 462–477. doi: 10.1177/0309133318783148

Bryan, B. A., Gao, L., Ye, Y., Sun, X., Connor, J. D., Crossman, N. D., et al. (2018). China's response to a national land-system sustainability emergency. *Nature* 559, 193–204. doi: 10.1038/s41586-018-0280-2

Cai, F., Hu, Z., Jiang, B., Ruan, W., Cai, S., and Zou, H. (2023a). Ecological health assessment with the combination weight method for the river reach after the retirement and renovation of small hydropower stations. *Water* 15, 355. doi: 10.3390/w15020355

Cai, Y., Wu, J., Shi, S. Q., Li, J., and Kim, K.-H. (2023b). Advances in desalination technology and its environmental and economic assessment. *J. Cleaner Production* 397, 136498. doi: 10.1016/j.jclepro.2023.136498

Chen, D., Zhao, Q., Jiang, P., and Li, M. (2022a). Incorporating ecosystem services to assess progress towards sustainable development goals: A case study of the Yangtze River Economic Belt, China. *Sci. Total Environ.* 806, 151277. doi: 10.1016/j.scitotenv.2021.151277

Chen, S. S., Kimirei, I. A., Yu, C., Shen, Q., and Gao, Q. (2022b). Assessment of urban river water pollution with urbanization in East Africa. *Environ. Sci. pollut. Res.* 29, 40812–40825. doi: 10.1007/s11356-021-18082-1

Ding, R., Yu, K., Fan, Z., and Liu, J. (2022). Study and application of urban aquatic ecosystem health evaluation index system in river network plain area. *IJERPH* 19, 16545. doi: 10.3390/ijerph192416545

Dong, M., Liu, M., Yin, L., Zhou, J., and Sun, D. (2022). Concept and practices involved in comprehensive river control based on the synergy among flood control, ecological restoration, and urban development: A case study on a valley reach of luanhe river in a semiarid region in north China. *Water* 14, 1413. doi: 10.3390/w14091413

Guimarães, L. F., Teixeira, F. C., Pereira, J. N., Becker, B. R., Oliveira, A. K. B., Lima, A. F., et al. (2021). The challenges of urban river restoration and the proposition of a framework towards river restoration goals. *J. Cleaner Production* 316, 128330. doi: 10.1016/j.jclepro.2021.128330

Islam, S. T., Rahman, S. H., Matin, M. A., Dey, A., Talukder, B., Sanyal, N., et al. (2024). State of the world's rivers. *Annu. Rev. Environ. Resour.* 49, 137–162. doi: 10.1146/annurev-environ-111022-020951

Kholodkevich, S. V. (2024). Brief overview of methods for assessing the health of aquatic ecosystems. Problems and prospects of development. *Inland Water Biol.* 17, 830–844. doi: 10.1134/S1995082924700500

Li, X., Meng, X., Ji, X., Zhou, J., Pan, C., and Gao, N. (2023). Zoning technology for the management of ecological and clean small-watersheds via k-means clustering and entropy-weighted TOPSIS: A case study in Beijing. *J. Cleaner Production* 397, 136449. doi: 10.1016/j.jclepro.2023.136449

Lin, S. (2023). Phosphate limitation and ocean acidification co-shape phytoplankton physiology and community structure. *Nat. Commun.* 14, 2699. doi: 10.1038/s41467-023-38381-0

Liu, G.-W., Dai, C.-L., Shao, Z.-X., Xiao, R.-H., and Guo, H.-C. (2024). Assessment of ecological flow in hulan river basin utilizing SWAT model and diverse hydrological approaches. *Sustainability* 16, 2513. doi: 10.3390/su16062513

Liu, X., Chen, L., Zhang, G., Zhang, J., Wu, Y., and Ju, H. (2021). Spatiotemporal dynamics of succession and growth limitation of phytoplankton for nutrients and light in a large shallow lake. *Water Res.* 194, 116910. doi: 10.1016/j.watres.2021.116910

Meng, L., Chen, Y., Li, W., and Zhao, R. (2009). Fuzzy comprehensive evaluation model for water resources carrying capacity in Tarim River Basin, Xinjiang, China. *Chin. Geogr. Sci.* 19, 89–95. doi: 10.1007/s11769-009-0089-x

Rattan, K. J., Corriveau, J. C., Brua, R. B., Culp, J. M., Yates, A. G., and chambers, P. A. (2017). Quantifying seasonal variation in total phosphorus and nitrogen from prairie streams in the Red River Basin, Manitoba Canada. *Sci. Total Environ.* 575, 649–659. doi: 10.1016/j.scitotenv.2016.09.073

Raven, J. A., and Beardall, J. (2021). Influence of global environmental Change on plankton. *J. Plankton Res.* 43, 779–800. doi: 10.1093/plankt/fbab075

Rowiński, P. M., Okruszko, T., and Radecki-Pawlik, A. (2022). Environmental hydraulics research for river health: recent advances and challenges. *Ecohydrology Hydrobiology* 22, 213–225. doi: 10.1016/j.ecohyd.2021.12.003

Stefanidis, K., Karaouzas, I., Oikonomou, A., Smeti, E., Kouvarda, T., Latsiou, A., et al. (2023). Geodiversity as a potential indicator of stream health in ecological quality assessment systems. *Ecohydrology* 16, e2551. doi: 10.1002/eco.2551

Vollmer, D., Regan, H. M., and Andelman, S. J. (2016). Assessing the sustainability of freshwater systems: A critical review of composite indicators. *Ambio* 45, 765–780. doi: 10.1007/s13280-016-0792-7

Vugteveen, P., Leuven, R. S. E. W., Huijbregts, M. A. J., and Lenders, H. J. R. (2006). Redefinition and elaboration of river ecosystem health: perspective for river management. *Hydrobiologia* 565, 289–308. doi: 10.1007/s10750-005-1920-8

Wang, G., Xiao, C., Qi, Z., Lai, Q., Meng, F., and Liang, X. (2022). Research on the exploitation and utilization degree of mineral water based on ecological base flow in the Changbai Mountain basalt area, northeast China. *Environ. Geochem Health* 44, 1995–2007. doi: 10.1007/s10653-021-00865-7

Withers, P. J. A., and Jarvie, H. P. (2008). Delivery and cycling of phosphorus in rivers: A review. *Sci. Total Environ.* 400, 379–395. doi: 10.1016/j.scitotenv.2008.08.002

Wu, C., Gao, P., Zhou, J., Fan, X., Xu, R., and Mu, X. (2024). Fuzzy evaluation and obstacle factors of urban ecological health changes in the Wei River Basin, northwest China. *Ecol. Processes* 13, 50. doi: 10.1186/s13717-024-00529-1

Yang, R., Chen, Y., Qiu, Y., Lu, K., Wang, X., Sun, G., et al. (2023). Assessing the Landscape Ecological Health (LEH) of Wetlands: Research Content and Evaluation Methods (2000–2022). *Water* 15, 2410. doi: 10.3390/w15132410

Yasmeen, R., Hao, G., Ye, Y., Shah, W. U. H., and Tang, C. (2023). The synergy of water resource agglomeration and innovative conservation technologies on provincial and regional water usage efficiency in China: A super SBM-DEA approach. *Water* 15, 3524. doi: 10.3390/w15193524

Yi, M., Li, L., Li, H., Liu, C., Deng, Y., Wu, Z., et al. (2024). Spatiotemporal variations of plankton communities in different water bodies of the Yellow River: Structural characteristics, biogeographic patterns, environmental responses, and community assembly. *J. Hydrology* 640, 131702. doi: 10.1016/j.jhydrol.2024.131702

Yu, H., Shi, X., Zhao, S., Sun, B., Liu, Y., Arvola, L., et al. (2022). Primary productivity of phytoplankton and its influencing factors in cold and arid regions: A case study of Wuliangsuhai Lake, China. *Ecol. Indic.* 144, 109545. doi: 10.1016/j.ecolind.2022.109545

Zhang, S., Han, G., and Gao, X. (2023). The urbanization impacts on potentially toxic metals: the distribution, sources and contamination risks in river situated in typical megacity, China. *Sustain. Cities Soc.* 97, 104784. doi: 10.1016/j.scs.2023.104784

Zhang, J., Xiang, J., Ma, Q., Li, C., and Xu, X. (2024). Water ecological health evaluation of urban river: a case study of Zaogang River, China. *Front. Ecol. Evol.* 12. doi: 10.3389/fevo.2024.1478024

Zhang, X., Wu, Y., and Gu, B. (2015). Urban rivers as hotspots of regional nitrogen pollution. *Environ. pollut.* 205, 139–144. doi: 10.1016/j.envpol.2015.05.031

frontiers | Frontiers in Environmental Science

TYPE Original Research
PUBLISHED 09 January 2025
DOI 10.3389/fenvs.2024.1530716

OPEN ACCESS

EDITED BY
Chunhui Li,
Beijing Normal University, China

REVIEWED BY
Huan Zhang,
Nanchang University, China
Fei Xiong,
Jianghan University, China

*CORRESPONDENCE
Jun Xu,
xujun@ihb.ac.cn
Mingdian Liu,
liumd@yfi.ac.cn

†These authors have contributed equally to this work

RECEIVED 19 November 2024
ACCEPTED 23 December 2024
PUBLISHED 09 January 2025

CITATION
Du J, Tian H, Xiang Z, Zhao K, Yu L, Duan X, Chen D, Xu J and Liu M (2025) Impact of the fishing ban on fish diversity and population structure in the middle reaches of the Yangtze River, China.
Front. Environ. Sci. 12:1530716.
doi: 10.3389/fenvs.2024.1530716

Impact of the fishing ban on fish diversity and population structure in the middle reaches of the Yangtze River, China

Juan Du[1,2†], Huiwu Tian[1†], Zhiyuan Xiang[1†], Kangshun Zhao[2,3], Lixiong Yu[1], Xinbin Duan[1], Daqing Chen[1], Jun Xu[2,3*] and Mingdian Liu[1*]

[1]National Agricultural Science Observing and Experimental Station of Chongqing, Yangtze River Fisheries Research Institute, Chinese Academy of Fishery Sciences, Wuhan, China, [2]Key Laboratory of Breeding Biotechnology and Sustainable Aquaculture (CAS), Institute of Hydrobiology, Chinese Academy of Sciences, Wuhan, China, [3]Key Laboratory of Lake and Watershed Science for Water Security, Nanjing Institute of Geography and Limnology, Chinese Academy of Sciences, Nanjing, China

The Yangtze River has experienced severe ecological degradation due to intensive human activities, including dam construction, land reclamation, and overfishing. These disturbances have disrupted the natural habitats of the Yangtze River, leading to a sharp decline in fish biodiversity and fishery resources. To address this ecological crisis, the Chinese government implemented a 10-year fishing ban in January 2021 to mitigate pressures on fish populations, restore aquatic habitats, and promote biodiversity recovery. The middle reaches of the Yangtze River are characterized by diverse fish species and a critical habitat for aquatic life, this study seeks to assess the effects of the fishing ban on fish diversity, body structure, population and community dynamics in this region. Fish monitoring data collected from 2017–2019 (pre-ban) and 2021–2023 (post-ban) were analyzed to evaluate changes in fish body size, species diversity, and community structure. The analysis results using the PSD method indicate that fish body size has increased following the fishing ban, suggesting the improvement of population structures, and a change in the complexity of food web structure. Species diversity indices showed partial recovery, but the recovery was uneven across different sampling sites. While fish populations showed signs of improvement, particularly in terms of body size and community stability, species diversity remained at relatively low levels in some areas, indicating that full recovery in biodiversity and resource levels may require extended conservation efforts. These findings suggest that while the fishing ban has had a positive initial impact on fish populations and ecological conditions, continued and long-term conservation measures are essential for fully recovering the river's biodiversity and restoring its fishery resources. The study also highlights the importance of monitoring fish species diversity, body structure, and community dynamics as part of ongoing efforts to evaluate the effectiveness of the fishing ban and refine resource management strategies for the middle reaches of the Yangtze River.

KEYWORDS

fish diversity, body length, food web, fishing ban, Yangtze River

1 Introduction

The Yangtze River, the third-largest river in the world, has undergone significant ecological changes over the last 50 years due to intensive human activities such as dam construction, land reclamation, overfishing, and bustling shipping (Chen et al., 2024; Liu et al., 2019). These activities have profoundly disrupted the river's biogeographic patterns and severely threatened its hydrobiology biodiversity (Feng et al., 2023; Höckendorff et al., 2017). The most notable consequence of this degradation was the functional extinction of the Chinese River Dolphin (*Lipotes vexillifer*) in 2017, and a significant decline in the population of the Yangtze finless porpoise (*Neophocaena asiaeorientalis)* (Wang et al., 2020; Zhang et al., 2020a). A survey from 2017 to 2021 recorded only 323 fish species in the Yangtze River basin, of which 35% are listed in the International Union for Conservation of Nature (IUCN) Red List, highlighting the critical extinction risks faced by freshwater species (IUCN, 2017; Yang et al., 2023). Compared to 1960, fishery resources in the Yangtze have decreased by 85% (Wang H. et al., 2022).

In response to this ecological crisis, the Chinese government initiated a 10-year fishing ban in January 2021, covering the mainstream, seven tributaries, and several connected lakes, including Dongting and Poyang lakes (Wang R. L. et al., 2022). Preliminary results following the implementation of the fishing ban indicate positive changes in the ecological conditions of the Yangtze River (Lei et al., 2023). Notably, the population of the Yangtze finless porpoise increased from 1,012 individuals in 2017 to 1,249 individuals in 2022 (Lei et al., 2023). This species tends to inhabit areas with high fish diversity (Wang et al., 2024), indicating the potential recovery of fish species diversity in the Yangtze River basin. In Poyang Lake, 93 fish species have been recorded after the fishing ban, with a noticeable increase in the resources of the four major Chinese carp species (Zhang et al., 2024). In the Chishui River, 11 endemic fish species have reappeared, further demonstrating the initial effectiveness of the 10-year fishing ban (Liu et al., 2023).

The Yangtze River is China's most important freshwater fishery resource area, typically divided into three regions—the upper, middle, and lower reaches—based on river characteristics and topography (Fang et al., 2023; Liu et al., 2019). The length of the middle reaches of the Yangtze River is about 955 km from Yichang (Hubei province) to Hukou (Jiangxi province), with a drainage area of 680,000 km^2 (Liu and Cao, 1992). The combination of meandering river courses, slow-flowing waters, and extensive lake-river networks in this region creates favorable hydrological conditions and abundant forage, which serve as critical feeding, wintering, and spawning grounds for a wide variety of aquatic species (Fang et al., 2023). Previous studies have recorded 215 fish species in the middle reaches, including 42 endemic (Yu, 2005). The middle reaches of the Yangtze River are spawning grounds and habitats for many economic fishes, such as the four major Chinese carps and bream (*Parabramis pekinensis*), as well as important migration routes for migratory fishes. Fish species are vital indicators of the health of freshwater ecosystems, as they occupy a crucial role in assessing the biodiversity and ecological integrity of these ecosystems (Qian et al., 2023). Studies on other regions, such as the Chishui River and Liangzi Lake, suggest that while the fishing ban has not led to dramatic changes in species diversity, it has alleviated the trend of decreasing fish body sizes and improved community structure to some extent. However, the full recovery of fish diversity, community structure, and ecosystem functionality in the Yangtze River will require substantial time and effort (Feng et al., 2023; Liu et al., 2023). Despite the fishing ban being in effect for 3 years as of 2023, there is still a lack of comprehensive and long-term studies on its impacts on fish species diversity, body size, resource recovery, population and community structure in the mainstream of the Yangtze River.

This study aims to fill this gap by analyzing fish monitoring data from 3 years before (2017–2019) and 3 years following (2021–2023) the implementation of the fishing ban. The objectives are to assess changes in fish body size, species diversity, population and community structure, and to evaluate the actual effects of the fishing ban on the recovery of fish resources in the middle reaches of the Yangtze River. By examining these trends, this study will provide a reference for fish conservation and the restoration of fishery resources in the region, as well as a baseline for future evaluations of the fishing ban's effectiveness. Furthermore, the findings will offer scientific support for refining fishing regulations and improving resource management strategies. Based on prior research, we hypothesize that while the reduction in individual fish body size will be mitigated, the recovery of species diversity, which rapidly declined during overfishing, will be low and remain at low levels (Fang et al., 2023; Feng et al., 2023; Liu et al., 2023). Fish abundance and biomass, which sharply decreased during overfishing, are expected to rise rapidly post-ban before stabilizing. Additionally, community structure in habitat utilization is expected to become more homogeneous (Petsch, 2016; Van der Sleen and Albert, 2022; Villéger et al., 2011), with an increase in the dominance of midwater fish species and a reduction in species preferring other habitats, such as benthic organisms, the three dominant species (IRI>1000) after the fishing ban, *Hypophthalmichthys molitrix*, *Hypophthalmichthys nobilis* and *Xenocypris macrolepis,* all belong to the upper middle layer of fish (Supplementary Table S1).

2 Methods

2.1 Sampling location and sampling collection

The sampling sites for this study were selected based on their accessibility and the representativeness of habitat types. The selection was further guided by consultation with prior surveys and local ecological knowledge. Three geographical sites were chosen: Jingzhou-JZ (30.3° N, 112.2° E) with broad waters and relatively stable hydrological conditions, Jianli-JL (29.8° N, 112.9° E) with relatively good water quality and minimal human disturbance, and Huangshi-HS (30.2° N,115.0° E) with diverse distribution of river channels and high fluidity of water bodies, respectively (Figure 1). Sample collections were conducted in June and October over the period from 2017 to 2019 and from 2021 to 2022. It needs to be stated that data from 2020 was excluded from the analysis due to limited monitoring during the pandemic period. Local fishermen were employed to collect the fish samples by using different types of products since the study area's water depth exceeded 1 m. At each site, fishing was done with

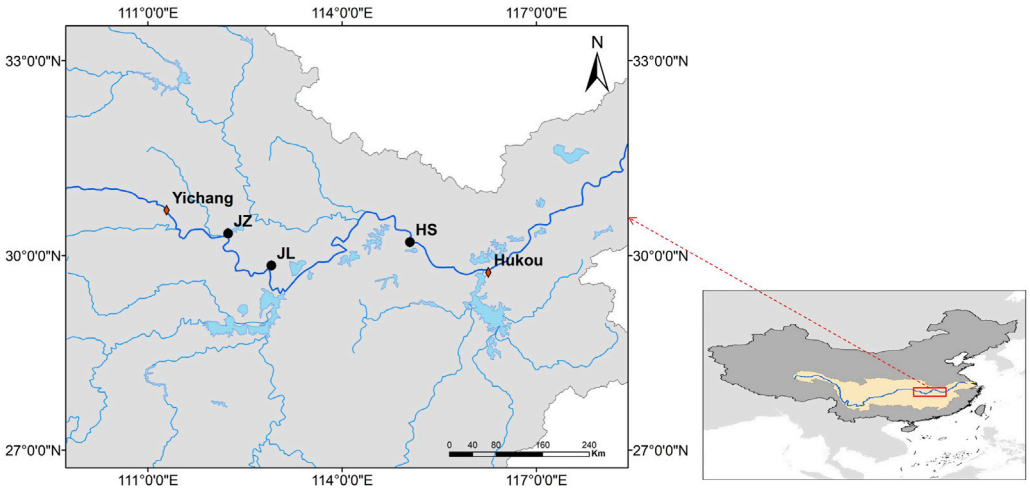

FIGURE 1
Distribution of sampling sites in the middle reaches of the Yangtze River, China.

fixed gill nets (mesh: height: length, 6 cm: 2 m: 100 m), drift nets (mesh: height: length, 2.5 cm: 2 m:230 m), ground cages (mesh: height: length, 1 cm: 0.4 m: 7 m). Ground cages were mainly placed in shallow water areas along the shore. Fishing was conducted daily for approximately 16 h from 4:00 p.m. to 8:00 a.m. Fish were identified when collected and released when practicable. Some fish samples that could not be identified were kept in formalin (5%–10%) and brought back to the laboratory for further identification. For biological measurements, fish body lengths were recorded accurately to 1 mm and body weights were measured accurately to 0.1 g.

2.2 Population body length analysis

Fish length data were statistically analyzed to determine the average length of species before the fishing ban (2017–2019) and during the post-ban period (2021–2023). A t-test was performed to analyze statistical differences, and results are presented as mean ± standard deviation (mean ± SD). Fish length categories were based on Gabelhouse's five-unit classification system, which includes Stock-Length (20% of the species' maximum recorded length), Quality Length (36%), Preferred Length (45%), Memorable Length (59%), and Trophy Length (74%). Proportional Size Distribution (PSD) was then calculated for each category, with PSD-Q representing the proportion of Quality Length, PSD-P for Preferred Length, PSD-M for Memorable Length, and PSD-T for Trophy Length (Gabelhouse, 1984). The formula follows: PSD = Proportion of individuals exceeding a specific body length/ Proportion of individuals exceeding a basic (Stock-Length) body length*100. In accordance with the regional growth conditions, standard length categories for species in the middle reaches of the Yangtze River were established using maximum recorded lengths from the Fishbase (Froese and Pauly, 2018). The maximum body length Linf was calculated by FiSAT II (version 12.2). The drawing was implemented by software of Originpro (version 2022b). The statistical significance of PSD values was determined using a t-test.

The representative 19 species of each site were selected through the index of relative importance (IRI) (Equation 1) in this study. IRI was based on the frequency of occurrence, number percentage and weight percentage, was used to determine the dominance of fish in each site (Pinkas et al., 1970).

$$IRI = (\%Ni + \%Wi) \times \%Fi \quad (1)$$

Where %Ni and %Wi are the proportion of species number and weight in the overall catch, respectively, and %Fi is the occurrence frequency. IRI values above 10% indicated that the species was dominant, while IRI values below 10% indicated that the species was common.

2.3 Species diversity and biomass analysis

Species diversity at a specific location during a defined temporal period is referred to as species diversity. In this study, fish species diversity at each sampling site was assessed based on spatial and temporal variations by using four established diversity indices: the Simpson dominance index, the Shannon-Wiener diversity index (H′), the Pielou evenness index (J′), and the Margalef richness index (D). Please refer to the relevant literature for detailed definitions and formulas about these indices (Magurran, 2013; Peet, 1974). Biomass was expressed as the catch per unit effort (CPUE), which was calculated by dividing the daily catch by the number of boats and the operating time (kg/boat*day) (Zhang et al., 2020b).

2.4 Food web inference

To investigate the structure of the fish food web, we constructed a meta-web using an adjacency matrix W, where the element $W_{ij} = 1$ indicates that species i can consume species j, and $W_{ij} = 0$ otherwise. This matrix was derived based on a niche model developed by (Gravel et al., 2013), which establishes a linear relationship between log body size and the centroid of the feeding niche. The linear model can be expressed as follows:

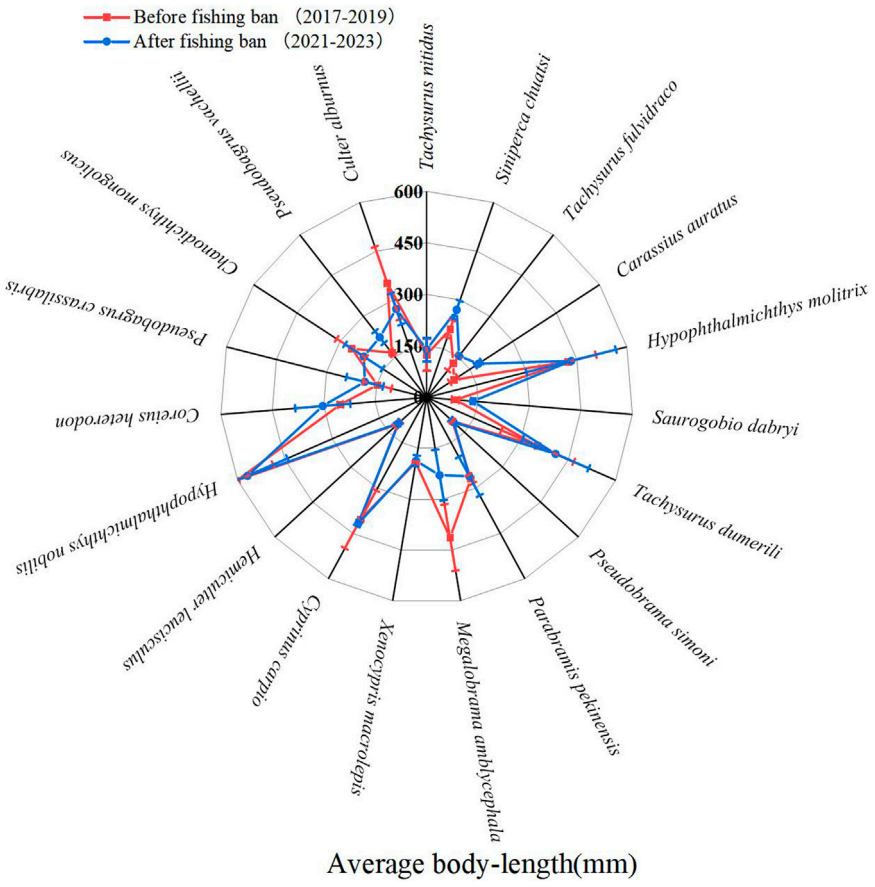

FIGURE 2
Changes in mean body length of 19 dominant fish species in the middle reaches of the Yangtze River before and after the fishing ban.

$$c = \log_{10}\left(M_{prey}\right) = \alpha_0 + \alpha_1 \times \log_{10}\left(M_{pred}\right) \quad (2)$$

Where M_{prey} and M_{pred} represent the body sizes of prey and predators, respectively. Coefficients for the model were obtained from literature values on predator-prey body size interactions (Albouy et al., 2019). Using these coefficients, niche parameters such as niche position n_i, feeding niche optimum c_i, and niche range r_i were inferred for each species. An interaction between species i and j was identified if the niche position n_j of species j falls within the interval (c_i-r_i/2, c_i + r_i/2). For each meta-web, corresponding to a particular site and year, 3 common food web metrics were computed: average clustering coefficient, average path length, and connectance.

Clustering coefficient (CC) reflects the degree of interconnectedness among nodes in the network; higher values indicate stronger local connectivity and potential network stability due to tighter relationships among neighboring nodes. Average path length (ChPath) is the mean shortest path between any two nodes in the network, with shorter values indicating higher information propagation efficiency within the network. Connectance describes the level of generalism in the network and is calculated as the ratio of actual links in the food web to the maximum possible links ($C = L/N^2$ (Equation 2), where L is the number of links and N is the number of nodes) (Danet et al., 2021). The topological network of the food web was visualized using Gephi 0.10.

2.5 Statistics

All data analyses were performed using standard statistical software (e.g., R or Origin). Differential analysis was conducted using t-tests and other appropriate statistical tests (using R package "stats" version 4.3.2). Results were considered statistically significant at a P-value of less than 0.05. The analysis also included normality tests and assumptions validation to ensure the robustness of the statistical models used. Traditional PSD calculation and its 95% confidence interval calculation were performed using R package FSA (Version 0.9.4) (Ogle, 2018).

3 Results

3.1 Changes in average body length

Before the fishing ban, the average body length of 19 dominant fish populations in the middle reaches of the Yangtze River ranged from 84.2 mm to 602.6 mm, with a median of 201.1 mm (Figure 2). After the fishing ban, the average body length of these populations ranged from 106.8 mm to 648.3 mm, with a median of 208.2 mm. Among them, the average body length of nine fish species remarkably increased by 2.4%–91.0% ($P < 0.05$). Conversely, five species

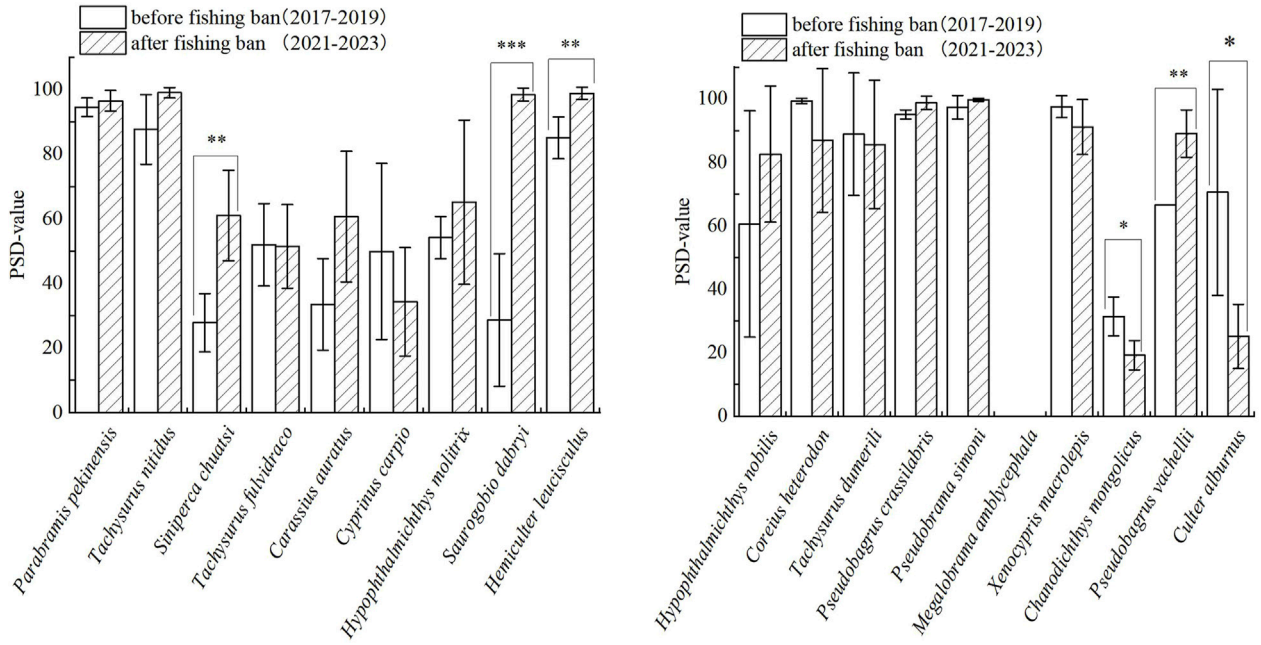

FIGURE 3
Changes in PSD of 19 dominant fish species in the middle reaches of the Yangtze River before and after the fishing ban.

exhibited no significant change in body length. In comparison, other five species—*P. pekinensis*, *Megalobrama amblycephala*, *X. macrolepis*, *Chanodichthys mongolicus*, and *Culter alburnus* showed significant decreases in body length ranging from 2.8% to 44.5% ($P < 0.05$).

3.2 Changes in PSD of 19 dominant fish species

The PSD values of these 19 dominant fish species exhibited marked changes before and after the fishing ban. Before the ban, PSD values ranged from 28 to 99, with a median of 73 and an average of 66. After the fishing ban, these values ranged from 34 to 100, with a median of 86 and an average of 76. Three species showed significant increases in their PSD values by 14–70 ($P < 0.05$). Four species exhibited an increase in PSD values, while three showed a decrease, though these changes were not statistically significant ($P > 0.05$). Additionally, six species did not show any significant changes in PSD values (Figure 3).

For three species with notable increases in PSD values, trends in the PSD-Q (Quality Length), PSD-P (Preferred Length), and PSD-T (Trophy Length) values were similar (Figure 4). As illustrated in Figure 4, these species exhibited increases in both PSD-Q and PSD-P values, ranging from 14 to 70 and 6 to 75, respectively. However, the PSD-M (Memorable Length) values of *Saurogobio dabryi* and *Hemiculter leucisculus* decreased by 11 and 8 respectively, while the PSD-M value of *Siniperca chuatsi* increased by 9. Futhermore, the PSD-T values of *S. dabryi* and *H. leucisculus* decreased by 1 and 7, respectively, while the PSD-T of *S. chuatsi* increased by 4.

3.3 Changes in species diversity and biomass

Regarding the diversity indices (Figure 5), the Margalef richness index of fish species at the three sampling sites ranged from 6.65 to 7.70 before the fishing ban (2017–2019), with a mean value of 7.14. After the fishing ban (2021–2023), this index ranged from 5.64 to 6.69, with a mean value of 6.25. The Pielou evenness index ranged from 0.55 to 0.74 before the ban (mean = 0.66) and from 0.58 to 0.71 after the ban (mean = 0.63). The Shannon-Wiener diversity index ranged from 2.23 to 3.14 before the ban (mean = 2.78), and from 2.00 to 3.14 after the ban (mean = 2.48). The Simpson dominance index ranged from 0.71 to 0.93 before the ban (mean = 0.85), and from 0.72 to 0.94 after the ban (mean = 0.81). Overall, the average values of these four diversity indices were higher before the fishing ban than post-ban. However, slight recoveries were observed in the Shannon-Wiener diversity index and Margalef richness index over the 3-year post-ban period. In contrast, the Pielou evenness index and Simpson dominance index showed no significant changes ($P > 0.05$).

Examining spatial heterogeneity across the three sampling sites, the diversity indices for Huangshi (HS) showed significant improvements after the fishing ban. Before the ban, the Margalef richness index, Pielou evenness index, Shannon-Wiener diversity index, and Simpson dominance index at HS had mean values of 4.55, 0.48, 1.74, and 0.60, respectively. After the ban, these four diversity indices increased to 4.78, 0.80, 2.69 and 0.90, respectively. For Jianli (JL) and Jingzhou (JZ), however, the mean values of the diversity indices did not show a significant increase following the fishing ban ($P > 0.05$, Table 1). On the other hand, catch per unit effort (CPUE) significantly increased after the fishing ban across all sampling sites, with the JZ site showing the highest increase compared to JL and HS ($P < 0.05$, Table 1).

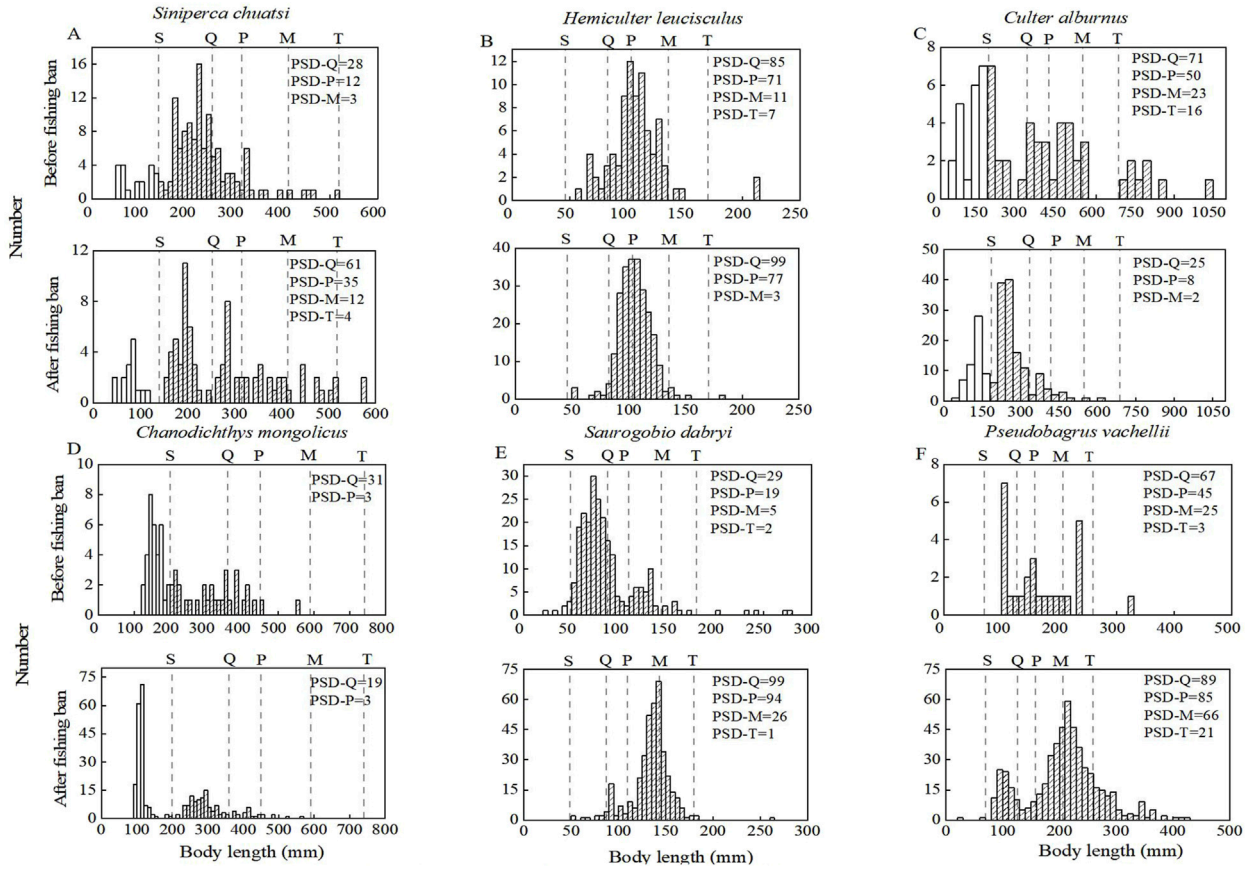

FIGURE 4
Changes in PSD of 6 dominant fish species **(A–F)** in the middle reaches of the Yangtze River before and after the fishing ban.

3.4 Changes in the food web

From Figure 6, we observed that all four indicators (nodes, connectance, CC, and ChPath) showed an increasing trend relative to the values in 2019 and 2021, which serve as key time points for assessing community recovery. Notably, the response pattern of node numbers exhibited a "delayed response" pattern (Figure 6A). In 2021, the number of nodes declined compared to 2019 before beginning a steady increase. Connectance, which represents the proportion of potential interactions within the food web, fluctuated only slightly over the study period, maintaining a consistent value of 0.12 between 2021 and 2023, consistent with the levels recorded from 2017 to 2019 (Figure 6B). However, the average clustering coefficient (CC) and average path length (ChPath) exhibited greater variability (Figures 6C, D). The topological network of 2017 has tighter local connections (high CC values) than in 2023. Notably, there was no substantial change in ChPath during the pre-ban period from 2017 to 2019, while CC steadily declined, indicating weakening connections between network nodes. In the early years of the fishing ban, CC followed an 'instant response' pattern in 2021, reflecting rapid changes in the food web structure, while ChPath showed a slight increase in 2023 compared to 2021. This suggests interactions among network nodes strengthened and the overall complexity of the network began to recover.

Across the three sampling sites, the connectance index exhibited a significant increase trend after the fishing ban (2021–2023) compared to pre-ban (2017–2019), with the JL sampling site recording the highest increase of 25% (Table 2). On the contrary, the other two indicators, ChPath and CC, showed varying degrees of decline following the fishing ban. Similarly, the JL monitoring point experienced the most significant decrease when compared to the other two locations, JL and HS sites. Regarding node indicator values, both JL and HS exhibited a downward trend post-fishing ban compared to the pre-ban period, apart from an increase at the JL station.

4 Discussion

4.1 The effect of the fishing ban on the body size and biomass

In fishery population assessments, body length structure is one of the most easily obtainable and commonly used indicators for understanding the status of fish populations (Phelps and Willis, 2013). Anderson's 5-unit body length proportional distribution (PSD) model has been widely adopted to quantitatively describe the distribution of individuals across various body length categories within a population (Anderson, 1976). By comparing PSD values at

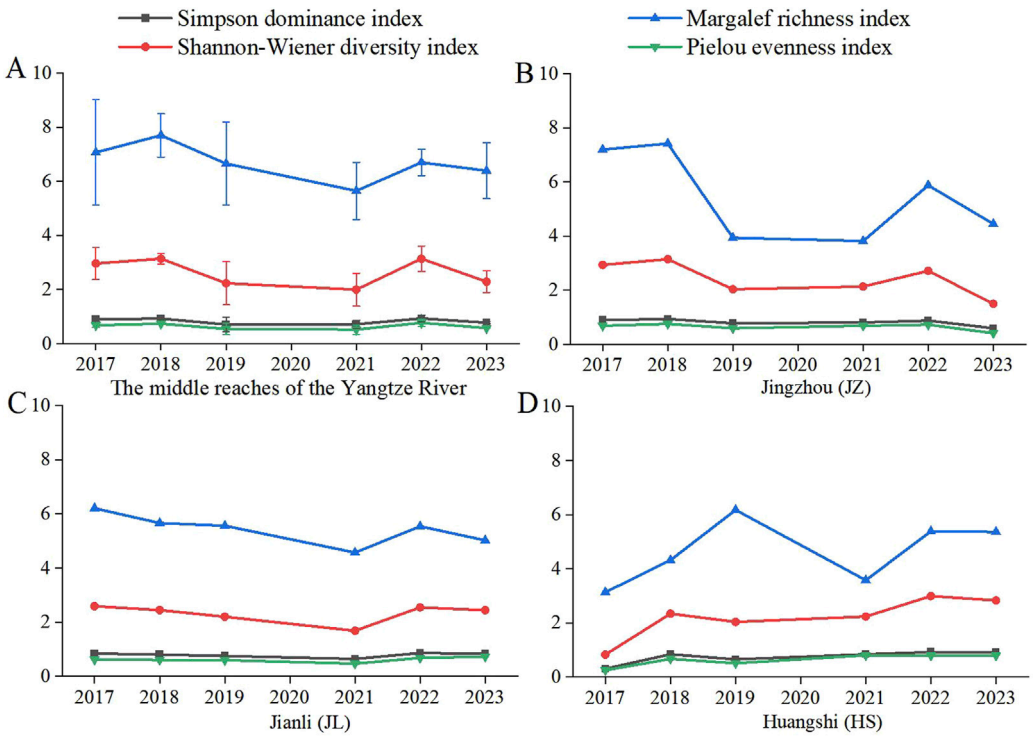

FIGURE 5
Changes in species diversity in the middle reaches of the Yangtze River **(A)** and three sampling sites [**(B–D)**, Jingzhou-JZ, Jianli-JL, Huangshi-HS] before and after the fishing ban.

TABLE 1 Spatial variation in diversity indexes and CPUE in the middle reaches of the Yangtze River.

Sites Index	Jingzhou (JZ)		Jianli (JL)		Huangshi (HS)		The middle reach of the Yangtze river (MYR)	
	Before fishing ban	After fishing ban	Before fishing ban	After fishing ban	Before fishing ban	After fishing ban	Before fishing ban	After fishing ban
Simpson	0.87 ± 0.08	0.77 ± 0.15	0.80 ± 0.05	0.78 ± 0.12	0.60 ± 0.27	0.90 ± 0.05	0.85 ± 0.12	0.81 ± 0.11
Shannon-Wiener	2.71 ± 0.59	2.12 ± 0.61	2.41 ± 0.2	2.23 ± 0.47	1.74 ± 0.80	2.69 ± 0.4	2.78 ± 0.48	2.48 ± 0.59
Margalef	6.19 ± 1.95	4.71 ± 1.05	5.81 ± 0.35	5.05 ± 0.49	4.55 ± 1.53	4.78 ± 1.04	7.14 ± 0.53	6.25 ± 0.54
Pielou	0.68 ± 0.08	0.61 ± 0.17	0.61 ± 0.01	0.63 ± 0.14	0.48 ± 0.21	0.80 ± 0.01	0.66 ± 0.10	0.63 ± 0.13
CPUE (kg/boat*day)	8.86 ± 2.39	21.04 ± 5.96	13.96 ± 1.06	27.64 ± 5.12	14.98 ± 1.86	20.22 ± 6.32	13.6 ± 3.28	21.85 ± 3.46

different time points, it is possible to access not only changes in fish population structure but also the dynamics of fish population health (Gabelhouse, 1984). Previous research has shown that fishing activities tend to favor larger individuals, thereby reducing the average body length and skewing the population structure toward smaller individuals (Allan et al., 2005; Feng et al., 2023). Prior to the comprehensive fishing ban, fish species in the Yangtze River were already showing signs of individual miniaturization, and population structure had been severely disrupted (Feng et al., 2023; Wang R. L. et al., 2022). Fishing pressure may exacerbate this trend by altering genetic factors that regulate fish size, reducing the frequency of fast-growing genotypes, and diminishing energy allocation to growth (Kokkonen et al., 2015; Morbey and Mema, 2018; van Wijk et al., 2013).

This study shows that after a 3-year fishing ban, the average body length and PSD values of 16 major fish populations in the middle reaches of the Yangtze River significantly increased. This indicates that the long-standing trend of individual miniaturization in these species has been partially alleviated. The growth of certain species PSD-P, PSD-M, and PSD-T indicates that the number of individuals in each length unit of the population has been restored orderly, and the proportion distribution of individuals in each unit

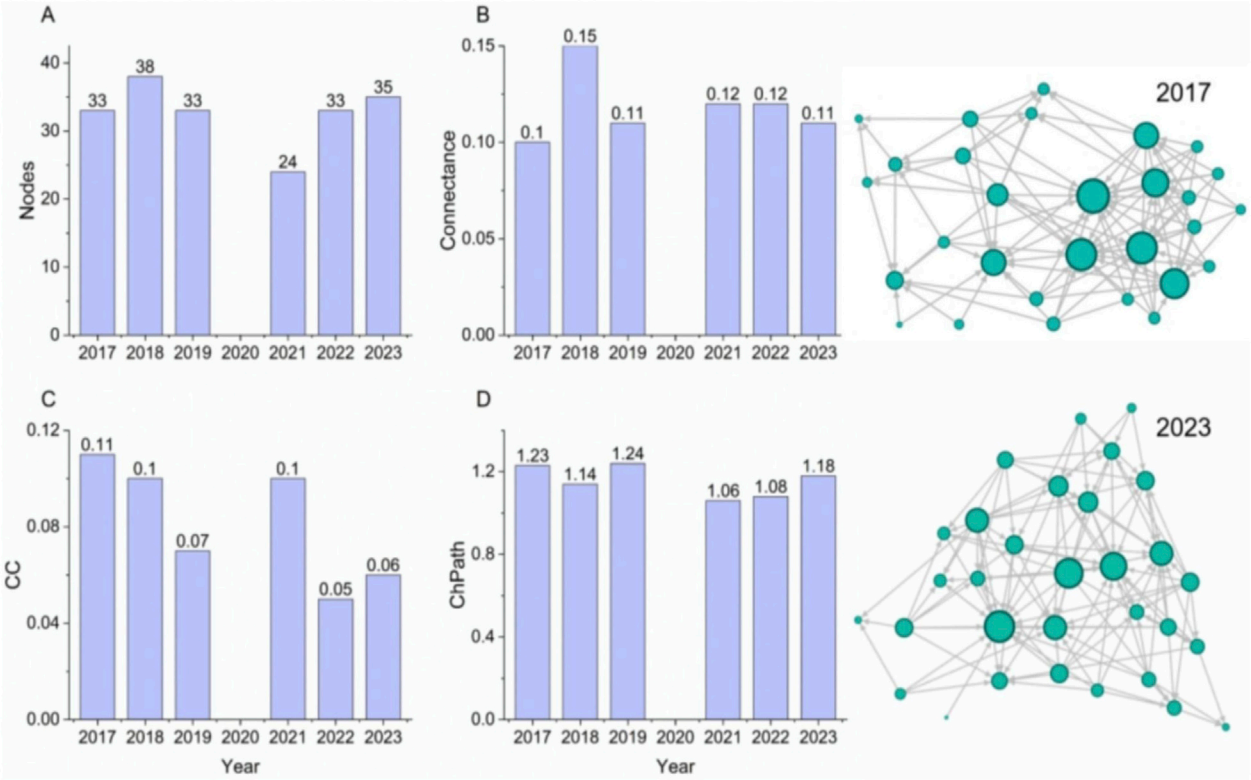

FIGURE 6
Four indexes of the food web and topological structure of fish communities between 2017 and 2023. The changes in **(A)** nodes, **(B)** Connectance, **(C)** average clustering coefficient (CC), and **(D)** average path length (ChPath) from 2017 to 2023.

TABLE 2 The average values of four indicators of the meta-network topology structure of fish communities at various sites in the middle reaches of the Yangtze River before (2017–2019) and after (2021–2023) the fishing ban.

Sites	Huangshi (HS)		Jingzhou (JZ)		Jianli (JL)	
Index	2017–2019	2021–2023	2017–2019	2021–2023	2017–2019	2021–2023
Nodes	22	20	29	16	18	23
Connectance	0.12	0.15	0.12	0.17	0.09	0.12
CC	0.08	0.06	0.09	0.05	0.13	0.06
ChPath	1.22	1.04	1.20	1.10	1.34	1.09

has gradually become complete and balanced. The population structure destroyed by overfishing has been optimized to a certain extent, and the effect of fishing bans has begun to emerge. Previous studies have also highlighted similar recovery trends, with significant increases in body size and PSD following a reduction in fishing pressure (Allen and Pine, 2000). For instance, in Lake Michigan, United States, yellow bass (*Diplophoron bifasciatum*) experienced a 2–5 cm increase in average body length after fishing pressure was reduced (Feiner et al., 2015). Similarly, the Clark salmon (*Oncorhynchus clavki*) in 19 lakes in North America showed a significant increase in both average body length and PSD after a decrease in fishing effort (Feiner et al., 2015).

Despite these positive trends, not all fish populations in the middle reaches of the Yangtze River experienced significant recovery. Some species showed either minimal improvement or even a decrease in average body length and PSD values. For example, *Culter mongolicus* and *Culter alburnus*—large, carnivorous fish that inhabit the upper and middle layers of slow-moving water bodies—experienced a decrease in body size following the fishing ban. This can be attributed to the restoration of their feed resources, such as annual bream-*P. pekinensis* (unpublished data), which increased the availability of smaller fish and led to a higher proportion of young fish being caught. Similarly, although *P. pekinensis* and *X. macrolepis* which inhabit slow-moving waters, had no noticeable changes in diet or size, the significant increase in resource availability did not translate into a noticeable shift in their body length structure. Research suggests that small fish with shorter life cycles tend to recover more rapidly after fishing pressure is

removed (Cheng et al., 2020). Species such as *H. leucisculus* and *Pseudobagrus crassilabris*, which are annual fish species preferring slow-moving water bodies, did not show significant changes in body length structure, likely due to their short lifespan and relatively stable body sizes (Fang et al., 2023).

Selective fishing targeting larger individuals may truncate the body length distribution of populations, leading to structural and dynamic instability (Hixon et al., 2014). Fish populations with lower PSD values (<50) are generally characterized by a greater proportion of smaller individuals and slower growth, whereas populations with higher PSD values (<80) exhibit faster average growth rates, larger body sizes, and more stable mortality, birth rates, and overall population structure (Phelps and Willis, 2013; Shin et al., 2005; Willis et al., 2008). Therefore, PSD values serve as a reliable metric for evaluating the structural condition of fish populations. Gabelhouse and Donald's study showed that a population's PSD value exceeds a certain threshold indicating a healthy, well-balanced population (Gabelhouse, 1984). Before the fishing ban, the PSD values of 8 out of 19 major fish species in the middle reaches of the Yangtze River were below 50, with only 3 fish species having PSD values between 50 and 80, indicating significant damage to the population structure. After the ban, PSD values of 5 fish populations remained below 50, while 5 fish populations showed PSD values between 50 and 80, suggesting partial recovery. This indicates that some populations are returning to a more balanced and healthy state. Overfishing, especially the depletion of mature female fish, reduces breeding capacity and population stability, leading to the decline or depletion of fish stocks (Barneche D R et al., 2018). Overfishing is responsible for 30% of the decline in fishery resources (Wang et al., 2024). After the fishing ban, the overall fish catch has also increased, reflecting positive ecological recovery.

4.2 The effect of the fishing ban on fish species diversity

Three years after the fishing ban in the middle reaches of the Yangtze River, our study observed increases in the Margalef and Shannon-Wiener indices (Figure 5A), which indicate a recovery in species richness and ecosystem diversity. However, these indices have not yet returned to pre-ban levels (2017–2019), suggesting that recovery is still underway. Similar trends have been documented in other freshwater systems. For instance, studies in Liangzi Lake and Chishui River showed partial recovery of species in Chishui River and some restoration of ecosystem functions in Liangzi Lake following fishing restrictions (Feng et al., 2023; Liu et al., 2023; Zhang et al., 2024). Despite these improvements, the food web and community dynamics in these ecosystems still face challenges, as evidenced by the relatively low stability of the Pielou and Simpson indices. These indices reflect the uneven distribution of species, with certain species continuing to dominate the ecosystem, contributing to an imbalance in community structure (Fang et al., 2023). This imbalance suggests that ecological recovery, though ongoing, remains incomplete. The persistence of such imbalances may be attributed to a combination of long-term environmental pressures and habitat degradation (Leclerc et al., 2023; Van der Sleen and Albert, 2022). Similar findings have been reported in marine ecosystems, where fish populations can take up to 15 years to fully recover after reductions in fishing pressure (Höckendorff et al., 2017; Hutchings, 2000). Importantly, the degree of recovery has been found to be more strongly related to species-specific traits—such as age at maturity, reproductive capacity, and the extent of population depletion—rather than to the taxonomic family (Feiner et al., 2015; Hixon et al., 2014; Morbey and Mema, 2018). The uneven distribution of species, as seen in this study, can undermine the stability of the ecosystem, making it more vulnerable to external shocks and disturbances.

Overall, although some species have started to reproduce again, the overall vulnerability of the ecosystem remains a concern, especially given that the interactions between predators and prey have not fundamentally changed (Feng et al., 2023; Wang R. L. et al., 2022). This continued imbalance in species distribution is a critical issue for the stability of the ecosystem in the long term. As such, while the fishing ban has contributed to partial species recovery, the ecosystem's overall health still requires significant improvement. The ecosystem's vulnerability and imbalance in species distribution underscore the need for targeted management and restoration efforts (Wang et al., 2024; Zhang et al., 2024). By addressing habitat degradation and promoting balanced species distributions, it will be possible to enhance the long-term sustainability of the Yangtze River ecosystem (Wang H. et al., 2022; Wang R. L. et al., 2022).

From a spatial perspective, we found significant variation in species diversity across different sampling sites of the middle reaches of the Yangtze River (Figures 5B–D). The Jingzhou-JZ site exhibited the highest diversity indices, followed by the Jianli-JL site, while the Huangshi-HS site had the lowest. The JZ site, with its broad waters and relatively stable hydrological conditions, supports complex aquatic structures and abundant vegetation, creating favorable habitats for diverse fish species (Fang et al., 2023). Similarly, the JL site benefits from relatively good water quality and minimal human disturbance, contributing to its higher fish species diversity (Yang et al., 2023). In contrast, the HS site, which has been heavily impacted by urbanization and industrialization, faces declining water quality and habitat degradation, leading to lower fish diversity (Liu and Cao, 1992). These findings highlight the need for focused conservation efforts in the HS site to restore habitat conditions and improve water quality, which are essential for enhancing fish diversity in this area.

4.3 The effect of the fishing ban on the food web

Theoretical frameworks suggest that both species richness and food web structure affect community biomass and its stability (Danet et al., 2021). In particular, high food web connectivity can enhance the strength of species interactions, which may amplify population variability and potentially reduce the stabilizing effect of species richness (Thébault and Loreau, 2006). Predators can also have cascading effects on population variability and synchronicity at lower trophic levels (Shanafelt and Loreau, 2018; Teng and McCann, 2004). These theoretical insights highlight the need to consider species richness and food web structure simultaneously, as their effects may conflict or interact in complex ways (Danet et al., 2021). In this study, we employed food-web structure metrics to examine

how the fish community in the middle reaches of the Yangtze River under a fishing ban policy. We measured food web complexity using four key metrics: nodes, connectance, CC, and ChPath. The number of nodes and connectance are positively correlated with food-web complexity (Montoya and Solé, 2003), providing insights into the overall structure and functioning of the ecosystem.

Our results suggest a slight increase in food web complexity following the fishing ban, although the current structure has not yet returned to pre-ban levels observed from 2017 to 2019. Notably, the connectance values in our study were lower than those reported in other aquatic ecosystems, where connectance is typically around 0.2 (Danet et al., 2021; Leclerc et al., 2023). This suggests that the food web in the middle Yangtze River is characterized by relatively weak interspecies connections (Brose, 2010; Marina et al., 2018), which may partly explain the food web's lower stability during the early recovery period (2021–2023). Weak interspecies interactions can impede the natural flow of energy through the system, potentially limiting the overall resilience of the ecosystem during recovery. Across the three sampling sites, the JL site is the most complex in the food web structure compared to JZ and HS, which may be attributed to its proximity to Dongting Lake and the advantages of slow water flow, abundant aquatic plants, and sufficient bait (Fang et al., 2023). Meanwhile, it is far from the Three Gorges Dam compared to JZ, avoiding severe erosion and having better sediment (Li et al., 2021). All of these are beneficial for the reproduction and recovery of fish, promoting the complexity of the food web structure.

Furthermore, although the taxonomic richness showed considerable variation, we observed relatively low changes in the average path length (ChPath) and a slight increase in the average clustering coefficient (CC) and the number of links during the initial recovery period (2021–2023). However, these values have not yet returned to the pre-ban levels observed in 2017–2019. This indicates that, although recovery is underway, the food web structure remains unstable compared to the period before the fishing ban. It is important to recognize that the stability and complexity of the food web are influenced by various factors, including habitat quality and ecosystem productivity (Leclerc et al., 2023). While fish communities in the Yangtze River are beginning to recover, habitat restoration is a slower process that will likely take longer (Wang H. et al., 2022; Zhang et al., 2024). This ongoing dynamic suggests that the fish populations and community structures have not yet reached a stable equilibrium. These findings indicate that the food web in the middle reaches of the Yangtze River remained relatively unstable in the early years following the fishing ban. The interspecies connections within the food web are weak, and the overall complexity of the food web has not increased significantly. Given that food web complexity typically increases with species richness and interaction strength (Marina et al., 2018), future research should focus on long-term monitoring to better understand the dynamic changes in the food web. Such research will provide crucial insights into the conservation and management of the Yangtze River ecosystem, particularly during the ongoing fishing ban.

4.4 Suggestions for fish conservation

Our research underscores the complexity of fishery resource management and highlights the necessity of a more comprehensive, multi-faceted conservation approach. Although beneficial in reducing immediate threats from overfishing, the current fishing ban policy does not sufficiently address the degradation of key aquatic habitats and the disruption of riverine connectivity (Zhang et al., 2020b; Zhang, 2022). Habitat destruction, pollution, and infrastructure development continue to fragment habitats, hindering the migration and reproduction of fish species (Höckendorff et al., 2017). Therefore, relying exclusively on the fishing ban policy is unlikely to provide the long-term ecological resilience needed for sustainable fish populations in the Yangtze River (Wang H. et al., 2022). Considering these considerations, we recommend the continued enforcement of the fishing ban, with a focus on its long-term implementation and continuous monitoring. However, this should be complemented by measures aimed at improving the connectivity between rivers and lakes, as well as enhancing the quality of aquatic habitats (Cheng et al., 2020; Wang R. L. et al., 2022). Restoring ecological corridors and mitigating habitat fragmentation would provide aquatic organisms with more extensive and more suitable living spaces (Chen et al., 2024), thereby increasing the overall effectiveness of the fishing ban and supporting the recovery of biodiversity.

Additionally, the experiences from regions such as Liangzi Lake and Chishui River, where fishing bans have been implemented, underscore the necessity of adopting a holistic approach to aquatic conservation (Feng et al., 2023; Liu et al., 2023). These case studies reveal that while fishing bans have led to some positive outcomes, they alone are insufficient to fully restore aquatic biodiversity. Future conservation strategies must involve integrated resource management, which includes habitat restoration, pollution control, and sustainable fisheries management (Barneche D R et al., 2018; Brose, 2010; Chen et al., 2024). Only through such comprehensive measures can we ensure the long-term sustainability of the Yangtze River ecosystem and the conservation of its biodiversity. In conclusion, while the fishing ban represents a crucial first step in reversing the decline of fish populations, it must be seen as part of a broader, integrated conservation strategy that includes habitat restoration, improved connectivity, and ecosystem management. The successful recovery of aquatic biodiversity in the Yangtze River requires a long-term commitment to both ecological restoration and sustainable resource management.

Data availability statement

The original contributions presented in the study are included in the article/Supplementary Material, further inquiries can be directed to the corresponding authors.

Author contributions

JD: Conceptualization, Data curation, Funding acquisition, Investigation, Methodology, Visualization, Writing–original draft, Writing–review and editing. HT: Data curation, Writing–review and editing. ZX: Writing–review and editing, Data curation. KZ: Writing–review and editing, Funding acquisition. LY: Supervision, Writing–review and editing. XD: Supervision, Writing–review and editing. DC: Supervision, Writing–review

and editing. JX: Supervision, Writing–review and editing. ML: Supervision, Writing–review and editing.

Funding

The author(s) declare that financial support was received for the research, authorship, and/or publication of this article. This work was supported by grants from the National Key R&D Program of China (2022YFC3202001), the National Natural Science Foundation of China (Grant No. 32401388), the Postdoctoral Fellowship Program of CPSF (grant no. GZC20241874) and the China Postdoctoral Science Foundation (grant nos 2024M763654 and 2024M753437).

Conflict of interest

The authors declare that the research was conducted in the absence of any commercial or financial relationships that could be construed as a potential conflict of interest.

Generative AI statement

The author(s) declare that no Generative AI was used in the creation of this manuscript.

Publisher's note

Supplementary material

The Supplementary Material for this article can be found online at: https://www.frontiersin.org/articles/10.3389/fenvs.2024.1530716/full#supplementary-material

References

Albouy, C., Archambault, P., Appeltans, W., Araujo, M. B., Beauchesne, D., Cazelles, K., et al. (2019). The marine fish food web is globally connected. *Nat. Ecol. Evol.* 3 (8), 1153–1161. doi:10.1038/s41559-019-0950-y

Allan, J. D., Abell, R., Hogan, Z. E. B., Revenga, C., Taylor, B. W., Welcomme, R. L., et al. (2005). Overfishing of inland waters. *Bioscience* 55 (12), 1041–1051. doi:10.1641/0006-3568(2005)055[1041:ooiw]2.0.co;2

Allen, M. S., and Pine, W. E. (2000). Detecting fish population responses to a minimum length limit: effects of variable recruitment and duration of evaluation. *North Am. J. Fish. Manag.* 20 (3), 672–682. doi:10.1577/1548-8675(2000)020<0672:dfprta>2.3.co;2

Anderson, R. O. (1976). Management of small warm water impoundments. *Fish. Manag. Ecol.* 1, 5–7.

Barneche, D. R., Robertson, D. R., R, W. C., and Marshall, D. J. (2018). Fish reproductive-energy output increases disproportionately with body size. *Science* 360 (6389), 642–645. doi:10.1126/science.aao6868

Brose, U. (2010). Improving nature conservancy strategies by ecological network theory. *Basic Appl. Ecol.* 11 (1), 1–5. doi:10.1016/j.baae.2009.11.003

Chen, J., Wang, H., Zhang, L., Jeppesen, E., and Xie, P. (2024). A new window for conservation biogeography. *Innovation Geoscience* 2 (1), 100052. doi:10.59717/j.xinn-geo.2024.100052

Cheng, F., Schmidt, B., Qin, J., Xie, S., and Li, W. (2020). Short-term distribution patterns of young-of-the-year fish assemblages between the main stem and affiliated lakes in the middle reaches of the Yangtze River, China. *North Am. J. Fish. Manag.* 41 (4), 904–915. doi:10.1002/nafm.10406

Danet, A., Mouchet, M., Bonnaffé, W., Thébault, E., and Fontaine, C. (2021). Species richness and food-web structure jointly drive community biomass and its temporal stability in fish communities. *Ecol. Lett.* 24 (24), 2364–2377. doi:10.1111/ele.13857

Fang, D. D., Yang, H. L., Zhang, H., Wu, J. M., and Wei, Q. W. (2023). Fish community structure and diversity in the middle reaches of the Yangtze River. *J. Fish. China in Chin.* 47 (2), 154–170.

Feiner, Z. S., Chong, S. C., Knight, C. T., Lauer, T. E., Thomas, M. V., Tyson, J. T., et al. (2015). Rapidly shifting maturation schedules following reduced commercial harvest in a freshwater fish. *Evol. Appl.* 8 (7), 724–737. doi:10.1111/eva.12285

Feng, K., Deng, W., Li, H., Guo, Q., Tao, K., Yuan, J., et al. (2023). Direct and indirect effects of a fishing ban on lacustrine fish community do not result in a full recovery. *J. Appl. Ecol.* 60 (10), 2210–2222. doi:10.1111/1365-2664.14491

Froese, R., and Pauly, D. (2018). FishBase. Available at: www.fishbase.org.

Gabelhouse, D. W. (1984). A length-categorization system to assess fish stocks. *North Am. J. Fish. Manag.* 4 (3), 273–285. doi:10.1577/1548-8659(1984)4<273:alstaf>2.0.co;2

Gravel, D., Poisot, T., Albouy, C., Velez, L., Mouillot, D., and Freckleton, R. (2013). Inferring food web structure from predator–prey body size relationships. *Methods Ecol. Evol.* 4 (11), 1083–1090. doi:10.1111/2041-210x.12103

Hixon, M. A., Johnson, D. W., and Sogard, S. M. (2014). BOFFFFs: on the importance of conserving old-growth age structure in fishery populations. *ICES J. Mar. Sci.* 71 (8), 2171–2185. doi:10.1093/icesjms/fst200

Höckendorff, S., Tonkin, J. D., Haase, P., Bunzel-Drüke, M., Zimball, O., Scharf, M., et al. (2017). Characterizing fish responses to a river restoration over 21 years based on species' traits. *Conserv. Biol.* 31 (5), 1098–1108. doi:10.1111/cobi.12908

Hutchings, J. A. (2000). Collapse and recovery of marine fishes. *Nature* 406 (6798), 882–885. doi:10.1038/35022565

IUCN (2017). *The IUCN red list of threatened species*. Version 2016-3.

Kokkonen, E., Vainikka, A., and Heikinheimo, O. (2015). Probabilistic maturation reaction norm trends reveal decreased size and age at maturation in an intensively harvested stock of pikeperch *Sander lucioperca*. *Fish. Res.* 167, 1–12. doi:10.1016/j.fishres.2015.01.009

Leclerc, C., Reynaud, N., Danis, P. A., Moatar, F., Daufresne, M., Argillier, C., et al. (2023). Temperature, productivity, and habitat characteristics collectively drive lake food web structure. *Glob. Chang. Biol.* 29 (9), 2450–2465. doi:10.1111/gcb.16642

Lei, G., Xinbin, D., and Daqing, C. (2023) *Bulletin on aquatic biological resources and habitat status in the Yangtze River basin*.

Li, S. X., Yang, Y., Zhang, H., Zhu, L., Zhu, Y., and Mingjin, Z. (2021). The scouring and siltation in river channels of the middle reaches of the Yangtze River (1975-2017) before/after the Three Gorges Project. *J. Lake Sci.* 33 (5), 1520–1531. doi:10.18307/2021.0520

Liu, F., Wang, Z., Xia, Z., Wang, J., and Liu, H. (2023). Changes in fish resources 5 years after implementation of the 10-year fishing ban in the Chishui River, the first river with a complete fishing ban in the Yangtze River Basin. *Ecol. Process.* 12 (1), 51. doi:10.1186/s13717-023-00465-6

Liu, J. K., and Cao, W. X. (1992). Fish resources of the Yangtze River Basin and the tactics for their conservation. *Resour. Environ. Yangtze Basin in Chin.* 1 (1), 17–23.

Liu, X., Qin, J., Xu, Y., Ouyang, S., and Wu, X. (2019). Biodiversity decline of fish assemblages after the impoundment of the three Gorges dam in the Yangtze River basin, China. *Rev. Fish Biol. Fish.* 29 (1), 177–195. doi:10.1007/s11160-019-09548-0

Magurran, A. E. (2013). *Ecological diversity and its measurement*. Springer Science and Business Media.

Marina, T. I., Salinas, V., Cordone, G., Campana, G., Moreira, M. E., Deregibus, D., et al. (2018). The food web of Potter Cove (Antarctica): complexity, structure and function. *Estuar. Coast. Shelf Sci.* 200, 141–151. doi:10.1016/j.ecss.2017.10.015

Montoya, J. M., and Solé, R. V. (2003). Topological properties of food webs: from real data to community assembly models. *Oikos* 102, 614–622. doi:10.1034/j.1600-0706.2003.12031.x

Morbey, Y. E., and Mema, M. (2018). Size-selective fishing and the potential for fisheries-induced evolution in lake whitefish. *Evol. Appl.* 11 (8), 1412–1424. doi:10.1111/eva.12635

Ogle, D. H. (2018). *Introductory fisheries analyses with R*. Chapman and Hall/CRC.

Peet, R. K. (1974). The measurement of species diversity. *Annu. Rev. Ecol. Syst.* 5, 285–307. doi:10.1146/annurev.es.05.110174.001441

Petsch, K. D. (2016). Causes and consequences of biotic homogenization in freshwater ecosystems. *Int. Rev. Hydrobiology* 101, 113–122. doi:10.1002/iroh.201601850

Phelps, Q. E., and Willis, D. W. (2013). Development of an asian carp size structure index and application through demonstration. *North Am. J. Fish. Manag.* 33 (2), 338–343. doi:10.1080/02755947.2012.760506

Pinkas, L., Oliphant, M. S., and Iverson, I. L. (1970). Food habits of albacore, bluefin tuna, and bonito in California waters. *Fish. Bull.* 152, 1–105.

Qian, M.-M., Wang, Z.-Y., Zhou, Q., Wang, J., Shao, Y., Qiao, Q., et al. (2023). Environmental DNA unveiling the fish community structure and diversity features in the Yangtze River basin. *Environ. Res.* 239, 117198. doi:10.1016/j.envres.2023.117198

Shanafelt, D. W., and Loreau, M. (2018). Stability trophic cascades in food chains. *R. Soc. Open Sci.* 5 (11), 180995. doi:10.1098/rsos.180995

Shin, Y.-J., Rochet, M.-J., Jennings, S., Field, J. G., and Gislason, H. (2005). Using size-based indicators to evaluate the ecosystem effects of fishing. *ICES J. Mar. Sci.* 62 (3), 384–396. doi:10.1016/j.icesjms.2005.01.004

Teng, J., and McCann, K. S. (2004). Dynamics of compartmented and reticulate food webs in relation to energetic flows. *Am. Nat.* 164 (1), 85–100. doi:10.1086/421723

Thébault, E., and Loreau, M. (2006). Trophic interactions and the relationship between species diversity and ecosystem stability. *Am. Nat.* 166, E95–E114. doi:10.1086/444403

Van der Sleen, P., and Albert, J. S. (2022). *Encyclopedia of inland waters*, 243–255.

van Wijk, S. J., Taylor, M. I., Creer, S., Dreyer, C., Rodrigues, F. M., Ramnarine, I. W., et al. (2013). Experimental harvesting of fish populations drives genetically based shifts in body size and maturation. *Front. Ecol. Environ.* 11 (4), 181–187. doi:10.1890/120229

Villéger, S., Blanchet, S., Beauchard, O., Oberdorff, T., and Brosse, S. (2011). Homogenization patterns of the world's freshwater fish faunas. *Proc. Natl. Acad. Sci.* 108 (44), 18003–18008. doi:10.1073/pnas.1107614108

Wang, H., Chen, J., Wang, P., Jeppesen, E., and Xie, P. (2024). How to manage fish within and after the 10-year fishing ban. *Innov. (Camb)* 5 (6), 100694. doi:10.1016/j.xinn.2024.100694

Wang, H., Wang, P., Xu, C., Sun, Y., Shi, L., Zhou, L., et al. (2022a). Can the "10-year fishing ban" rescue biodiversity of the Yangtze River? *Innov. (Camb)* 3 (3), 100235. doi:10.1016/j.xinn.2022.100235

Wang, R. L., Han, Y., Fan, F., Molinos, J. G., Xu, J., Wang, K. X., et al. (2022b). Need to shift in river-lake connection scheme under the "ten-year fishing ban" in the Yangtze River, China. *Ecol. Indic.* 143, 109434. doi:10.1016/j.ecolind.2022.109434

Wang, Z. T., Akamatsu, T., Duan, P. X., Zhou, L., Yuan, J., Li, J., et al. (2020). Underwater noise pollution in China's Yangtze River critically endangers Yangtze finless porpoises (*Neophocaena asiaeorientalis asiaeorientalis*). *Environ. Pollut.* 262, 114310. doi:10.1016/j.envpol.2020.114310

Willis, D. W., Murphy, B. R., and Guy, C. S. (2008). Stock density indices: development, use, and limitations. *Rev. Fish. Sci.* 1 (3), 203–222. doi:10.1080/10641269309388542

Yang, H., Shen, L., He, Y., Tian, H., Gao, L., Wu, J., et al. (2023). Status of aquatic organisms resources and their environments in Yangtze River system (2017–2021). *Aquac. Fish.* 9, 833–850. doi:10.1016/j.aaf.2023.06.004

Yu, X. (2005). Large-scale patterns in species diversity of fishes in the Yangtze River Basin. *Biodivers. Sci.* 13 (6), 473. doi:10.1360/biodiv.050121

Zhang, H., Jarić, I., Roberts, D. L., He, Y., Du, H., Wu, J., et al. (2020a). Extinction of one of the world's largest freshwater fishes: lessons for conserving the endangered Yangtze fauna. *Sci. Total Environ.* 710, 136242. doi:10.1016/j.scitotenv.2019.136242

Zhang, H., Kang, M., Shen, L., Wu, J., Li, J., Du, H., et al. (2020b). Rapid change in Yangtze fisheries and its implications for global freshwater ecosystem management. *Fish Fish.* 21 (3), 601–620. doi:10.1111/faf.12449

Zhang, Y. (2022). Freshwater biodiversity conservation in China: progress in the Yangtze River basin. *Aquatic Conservation Mar. Freshw. Ecosyst.* 32 (10), 1565–1570. doi:10.1002/aqc.3861

Zhang, Y., Zhang, H., Wu, Z., Zhao, M., and Feng, G. (2024). Community structure characteristics and changes in fish species at Poyang Lake after the Yangtze River fishing ban. *Fishes* 9 (7), 281. doi:10.3390/fishes9070281

frontiers | Frontiers in Ecology and Evolution

TYPE Original Research
PUBLISHED 22 January 2025
DOI 10.3389/fevo.2024.1459468

OPEN ACCESS

EDITED BY
Yujun Yi,
Beijing Normal University, China

REVIEWED BY
Yongjiu Cai,
Chinese Academy of Sciences (CAS), China
Atul Kabra,
Chandigarh University, India

*CORRESPONDENCE
Long Yan
yanlong@iwhr.com
Peng Hu
hp5426@126.com

RECEIVED 04 July 2024
ACCEPTED 23 December 2024
PUBLISHED 22 January 2025

CITATION
Li X, Yan L, Zhi X, Hu P, Shang C and Zhao B (2025) Characteristics of the macroinvertebrate community structure and their habitat suitability conditions in the Chishui River.
Front. Ecol. Evol. 12:1459468.
doi: 10.3389/fevo.2024.1459468

Characteristics of the macroinvertebrate community structure and their habitat suitability conditions in the Chishui River

Xinyu Li[1], Long Yan[1]*, Xu Zhi[2], Peng Hu[1]*, Chongju Shang[3] and Baolong Zhao[1]

[1]State Key Laboratory of Simulation and Regulation of Water Cycle in River Basin, China Institute of Water Resource and Hydropower Research, Beijing, China, [2]China Three Gorges Corporation, Wuhan, Hubei, China, [3]Institute of Disaster Prevention and Water Conservation, Guizhou Institute of Water Conservancy Science, Guizhou, Guiyang, China

Introduction: As an important tributary of the upper Yangtze River without dams, the study of the macroinvertebrate community structure and habitat suitability conditions in the Chishui River holds significant implications for water ecological conservation and restoration.

Methods: In order to explore the species composition, community characteristics and their ecological needs of macroinvertebrates in the Chishui River, 26 sampling sites were deployed in the Chishui River in this study in March (dry season), July (wet season), and November (normal season) of 2023 and performed community structure analysis.

Results: A total of 153 macroinvertebrate taxa were identified, with 62 taxa recorded in the dry season, 46 in the wet season and 115 in the normal season. The assemblage was predominantly composed of aquatic insects from the EPT group (*Ephemeroptera, Plecoptera* and *Trichoptera*). The results of ANOSIM analysis indicate that the species composition of macroinvertebrates varies significantly across different water periods. The Shannon-Wiener diversity index and Margalef index were significantly higher during the normal season compared to the dry and wet seasons. In contrast, the Pielou index and Simpson index remained relatively stable, suggesting a higher level of evenness in community structure across the different water periods. Based on the habitat suitability curves, *Corbicula fluminea* and *Heptagenia* prefer environments with high flow velocities and substrate particle sizes (D50) smaller than 300 mm. *Hydropsyche* sp.*1* and *Baetis* thrive in environments with medium to low water depths, high flow velocities, and D50 ranging from 100 to 300 mm. *Caridina* favor deeper waters, low flow velocities, and larger substrate particles. The GAM fitting results revealed that the number of macroinvertebrate taxa increased with rising pondus hydrogenii (pH) and electrical conductivity (EC) levels. Species richness initially declined and then rose within certain thresholds of total nitrogen (TN) and total phosphorus (TP) concentrations. The optimal conditions for macroinvertebrate communities in the Chishui River were determined to be a DO concentration of 9.8 mg/L and an NH3-N concentration of 0.12 mg/L.

Discussion: Overall, the macroinvertebrate community structure in the Chishui River is significantly influenced by factors such as water quality, flow velocity, and substrate particle size, and it demonstrates strong adaptability to seasonal variations.

KEYWORDS

undamed river, Chishui River, macroinvertebrates, community structure, habitat suitability

1 Introduction

Macroinvertebrates are primarily aquatic invertebrates that inhabit the riverbed for all or most of their life cycle and are visible to the naked eye (retained by a 500 μm mesh sieve) (Chen et al., 2021). As one of the most widely distributed biological groups in river ecosystems, macroinvertebrates play a crucial role in the food chain by facilitating organic matter decomposition, promoting self-purification of water, and serving as a vital link in the material cycle and energy flow within river ecosystems (Barbour et al., 1999; Qu et al., 2007; Zhang K. et al., 2023). Characterized by their species richness, broad distribution, limited migratory capacity, large size, and ease of collection and identification, macroinvertebrates are effective indicators of river ecosystem health. They reflect the impacts of multiple stressors, including hydrological, physical, chemical, and biological factors (Zhang et al., 2017; Wang et al., 2018). With the intensification of climate change and the deepening of human activities, the hydrological processes of rivers worldwide have undergone significant changes. This has not only disrupted the stability of river ecosystems but has also led to the degradation of ecosystem services and a decline in biodiversity (Schmitt et al., 2018; Chen et al., 2020). In this context, studying the spatiotemporal distribution, biodiversity, and community structure of macroinvertebrates is of significant scientific value and practical importance for comprehensively understanding changes in riverine ecosystems (Fu et al., 2024). By establishing the relationship between macroinvertebrates and habitat factors, such research can provide a theoretical basis for the formulation and implementation of ecological restoration measures in river basins, thereby effectively promoting the recovery and maintenance of river ecosystem health (Hu et al., 2021).

In the Yangtze River Basin of China, although water quality has improved in recent years, issues such as the imbalance of aquatic ecosystems and the decline in aquatic biodiversity remain prominent challenges, hindering the high-quality development of the Yangtze River Economic Belt (Yu et al., 2022).The Chishui River, a vital first-order tributary of the upper Yangtze River, remains free from dam construction and sustains its natural flow regime. The Chishui River exhibits typical characteristics of a mountainous river, with numerous tributaries and a complex river network. The intricate hydrological conditions and high habitat heterogeneity contribute to its uniqueness in terms of species diversity, evolutionary history among species, and ecosystem structure. This complex ecological environment not only provides rich habitats for aquatic organisms in the basin but also makes the Chishui River a region of significant scientific research value (Zhang D. et al., 2023). Therefore, conducting research on the biodiversity of the Chishui River basin is of significant importance. Understanding the ecological requirements and survival conditions of macroinvertebrates in this river can provide critical insights for basin authorities to develop and implement targeted ecological restoration strategies. Such efforts are essential for rehabilitating degraded river ecosystems, safeguarding aquatic biodiversity, and supporting the sustainable development and utilization of resources throughout the Yangtze River basin.

Previous studies on macroinvertebrates have often focused on the influence of water quality factors on their community structure (Jiang et al., 2024). For example, Liao et al. (2024) and Li et al. (2023) investigated the benthic macroinvertebrate community structure and its response to physico-chemical water properties in typical rivers of Xi'an and urban rivers in Dongguan, respectively. In recent years, with the deepening research on the community characteristics of large benthic invertebrates, an increasing number of scholars have recognized that, in addition to water quality factors, physical environmental factors of rivers, such as water depth (h), flow velocity (v), and the median particle size of the substrate (D50) also play a decisive role in shaping the community structure of large macroinvertebrates. Different macroinvertebrate taxa exhibit varying responses to these physical factors (Zhou et al., 2022). Therefore, understanding the impact of these environmental factors on benthic communities is of significant ecological importance, as different taxa respond differently to these environmental variables.

In response to the current state of research, this study aims to explore the primary factors influencing the habitat suitability of macroinvertebrates in the Chishui River by modeling the relationships between the macroinvertebrate community and environmental factors (including both water quality and physical environmental factors). Hypothesis 1: Water quality factors (such as dissolved oxygen and nutrient concentrations) have a significant seasonal impact on the macroinvertebrate community. Hypothesis 2: Physical environmental factors (such as flow velocity and

substrate particle size) affect the suitable habitats of different taxa in varying degrees, and taxa exhibit different response patterns. Through these analyses, this study seeks to provide theoretical support for ecological protection and water resource management in the Chishui River basin, as well as offer valuable insights and data to inform the ecological restoration and biodiversity conservation of similar rivers.

2 Materials and methods

2.1 Overview of the study area and sampling sites

The Chishui River (E104°45′–106°51′, N27°20′–28°50′), historically known as the Chihui River, Anle Water, and Dashe Water, is now often referred to as the "River of Fine Liquor" and the "River of Heroes." It is a significant first-order tributary on the right bank of the upper Yangtze River, the longest river in China. The Chishui River originates in Yinchuang Village, Chishuiyuan Town, Zhenxiong County, Yunnan Province. It flows eastward to Maotai Town in Renhuai City, where it turns northwest before continuing to Hejiang County, ultimately joining the Yangtze River. The main stream stretches 436.5 km, with a total elevation drop of 1,475 meters and an average gradient of 3.38‰. The Chishui River basin lies at the intersection of the Yunnan-Guizhou Plateau and the Sichuan Basin, featuring higher terrain in the south and lower terrain in the north. It is flanked by the Wumeng Mountains to the southwest, the Dalou Mountains to the east, and the Sichuan Basin to the north, forming a distinct and varied topographical region. The basin is located in the monsoon region of the subtropical zone, with an average annual temperature ranging from 12.7 to 18.1°C and an average annual precipitation of 1020.6 mm. Forests and cultivated land are the primary land use types in the Chishui River basin. The region is rich in forest resources, characterized by typical subtropical evergreen broadleaf forests, and is an important area for the production of species such as Nan bamboo, pine, and fir. Cultivated land is scattered, with more concentrated areas primarily in the headwaters of the Chishui River, the river valley, and the gentle slopes along its tributaries.

2.2 Sample collection and identification

26 sampling sites were deployed for this study, as shown in Figure 1. The selection of these sites was informed by prior research on aquatic organisms in the Chishui River, supplemented by site visits to assess local conditions. Sampling sites were strategically chosen to reflect varying pollution levels, land use patterns along the riverbanks, and habitat complexity, ensuring comprehensive coverage of environmental conditions. Data collection was conducted in March 2023 (dry season), July 2023 (wet season), and November 2023 (normal season). However, during the wet season, a significant rise in water level at sampling site 14 within a

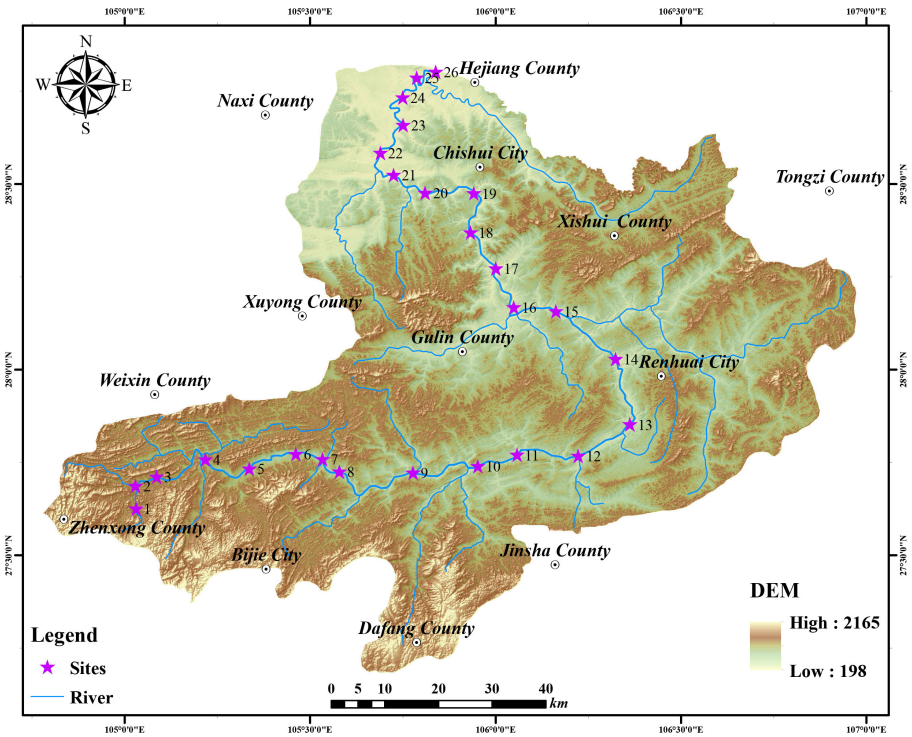

FIGURE 1
Overview of the study area and distribution of sampling sites.

single day prevented the collection of benthic samples. Additionally, no dominant taxa characteristic of the wet season were recorded at sampling site 19.

In this study, a Surber net with a sampling area of 0.25 m^2 (0.5m×0.5m) and a mesh size of 40 meshes (The pore size is 0.425 millimeters) was used to quantitatively collect macroinvertebrates. At each sampling site, samples were collected four times across different habitat types. The collected specimens were sorted in white porcelain trays and preserved in 100 ml sample bottles containing 37% formaldehyde solution. The samples were then transported to the laboratory for identification to the lowest feasible taxonomic level, following deployed taxonomic references for macroinvertebrates. Specimens were weighed using an electronic balance with a precision of 0.0001 g. For mollusks, the weight was recorded with shells intact, after blotting excess water from their mantle cavities using absorbent paper, in accordance with the Technical Requirements for Freshwater Macroinvertebrate Monitoring (Trial) (China National Environmental Monitoring Centre, 2021) issued by the China National Environmental Monitoring Center. The results were subsequently converted into density (ind./m^2) and biomass (g/m^2).

At the sampling sites, water temperature (T), pH, dissolved oxygen (DO) and electrical conductivity (EC) were measured *in situ* using a HACHHQ30d multi-parameter water quality analyzer. Additionally, 500 ml water samples were collected with a water sampler, stored in plastic bottles, and refrigerated for laboratory analysis of ammonia nitrogen (NH_3-N), total nitrogen (TN), and total phosphorus (TP).

All sample collection and measurement procedures followed the guidelines outlined in the Water and Wastewater Monitoring and Analysis Methods (State Environmental Protection Administration, 2002).

2.3 Data processing

2.3.1 Biodiversity

The biodiversity of macroinvertebrates was assessed using the Shannon-Wiener Diversity Index (H'), the Pielou Index (J') and the Margalef Richness Index (Dm). The specific formulas are as follows:

Shannon-Wiener Diversity Index:.

$$H' = -\sum_{i=1}^{S} p_i ln p_i \quad (1)$$

Where S is the total number of taxa, $p_i = n_i/N$, p_i is the proportion of the i-th taxa in the total abundance, n_i is the abundance of the i-th taxa, and N is the total abundance.

Pielou Evenness Index:

$$J' = \frac{H'}{log_2 S} \quad (2)$$

Where H' is the Shannon-Wiener Diversity Index, and S is the total number of taxa.

Margalef Richness Index:

$$Dm = \frac{(S-1)}{ln N} \quad (3)$$

Where S is the total number of taxa, and N is the total abundance.

2.3.2 Species turnover rate

The species turnover rate (Du et al., 2011) (R) is calculated using the following formula:

$$R = \frac{a+b-2c}{a+b-c} \times 100\,\% \quad (4)$$

Where a and b represent the number of taxa in two sampling events, and c is the number of taxa common to both samples.

2.3.3 ABC curve

The stability of the macroinvertebrate community in the Chishui River was assessed using the Abundance-Biomass Comparison (ABC) curve (Warwick, 1986). The W-value, representing the difference in area between the biomass and abundance curves and the coordinate axis, serves as the key statistic for the ABC analysis. When W>0, the biomass cumulative percentage curve consistently lies above the abundance cumulative percentage curve, indicating a stable community dominated by large, slow-growing taxa. In contrast, when W<0 and the curves intersect, the community is considered disturbed, with an increase in small, fast-growing taxa. If W<0 and the abundance cumulative percentage curve is above the biomass curve, the community is severely disturbed, characterized by a dominance of small, fast-growing taxa (Yemane et al., 2005; Yang et al., 2022).

$$W = \sum_{i=1}^{S} \frac{(B_i - A_i)}{50(S-1)} \quad (5)$$

Where A_i is the cumulative percentage of the i-th taxon's abundance, B_i is the cumulative percentage of the i-th taxon's biomass, and S is the total number of taxa.

2.3.4 Index of relative importance

The Index of Relative Importance (IRI) (Cortes, 1997) was employed to identify the dominant taxa within the macroinvertebrate community of the Chishui River. This index incorporates the abundance, biomass, and distribution of each taxon. In this study, taxa with an IRI ≥ 500 were considered dominant, while those with an IRI ≥ 1000 were classified as absolutely dominant taxa (Dou et al., 2023).

$$IRI = (N + W) \times F \times 10^4 \quad (6)$$

Where N is the abundance percentage of a taxon, W i is the biomass percentage of a taxon, and F is the frequency of occurrence of a taxon as a proportion of the total samples.

2.3.5 Community structure

One-way Similarity Analysis (ANOSIM) was employed to test for significant differences in macroinvertebrate communities across different hydrological periods of the Chishui River. The *R*-value, which ranges from -1 to 1, reflects the relative differences between within-group and between-group variations. An *R*-value close to 1 indicates substantial between-group differences, while a value close to 0 suggests that within-group and between-group differences are similar. A value approaching -1 signifies greater within-group variability and poor grouping effectiveness. *P*-values are used to assess whether observed differences are attributable to the grouping, with $P< 0.05$ indicating statistically significant differences due to the grouping.

Cluster Analysis and SIMPER (Clarke et al., 2014) Analysis: After standardizing the abundance data of macroinvertebrates from the Chishui River, the Bray-Curtis dissimilarity matrix was employed to assess the similarity among sampling sites. Cluster analysis was conducted using the group average method. Similarity Percentage (SIMPER) analysis was then applied to identify the main contributing taxa within each group and their average contribution rates.

DCA and RDA Analysis: Ordination analysis methods were applied to examine the response relationships between dominant macroinvertebrate taxa and environmental factors. Detrended Correspondence Analysis (DCA) was conducted on the macroinvertebrate abundance data. If the first axis length in the DCA results exceeded 4.0, Canonical Correspondence Analysis (CCA) was used. If the length was between 3.0 and 4.0, either RDA or CCA could be applied. If the length was less than 3.0, Redundancy Analysis (RDA) was preferred over CCA.

2.3.6 Habitat suitability curve

The physical environmental factors were normalized to derive the corresponding Habitat Suitability Index (HSI). These factors were plotted on the x-axis, while the taxa' preference for each factor was represented on the y-axis, creating a continuous curve that illustrates the relationship between the target taxa' preferences and the physical environmental variables. This curve quantitatively describes the taxa' response to changes in various habitat conditions. A value between 0 and 1 is assigned to indicate the taxa' preference for a given physical environmental factor, where 0 denotes an unsuitable condition and 1 represents an optimal condition. The closer the value is to 1, the stronger the taxa' preference for that particular environmental factor.

2.3.7 Generalized additive models

Generalized Additive Models (GAM) were employed to model the relationship between macroinvertebrate community structure and environmental factors, with a 95% confidence interval. The R^2 (coefficient of determination) and P-values are key statistics in the GAM model, used to assess the model's goodness of fit and the significance of predictor variables. R^2 represents the proportion of the total variation in the response variable explained by the predictor variables, ranging from 0 to 1, with values closer to 1 indicating stronger explanatory power. *P*-values evaluate the significance of predictor variables on the response variable, where $P \geq 0.05$ suggests no significant effect, $P< 0.05$ indicates a significant effect, and $P< 0.01$ denotes a highly significant effect.

3 Results

3.1 Species composition

In 2023, a total of 153 taxa of macroinvertebrates were collected and identified from the main stream of the Chishui River, as shown in Figure 2. These taxa belong to 5 phyla, 8 classes, 21 orders, and 79 families. Aquatic insects were the most numerous group, with 120 taxa, accounting for 77.9% of the total taxa. Among these, EPT (*Ephemeroptera*, *Plecoptera*, and *Trichoptera*) aquatic insects were the dominant group, comprising 36.4% of the total taxa, indicating that the water quality of the Chishui River is relatively clean (Wang, 2003). The species composition of macroinvertebrates exhibited significant differences across different hydrological periods. The number of taxa in the dry, wet, and normal periods was 62, 46, and 115, respectively, with the highest species richness observed during the normal period. In this period, species diversity was most prominent across all sampling sites. The species turnover rate showed considerable fluctuations, with a turnover rate of 80% between the dry and wet periods, and a turnover rate of 70.2% between the wet and normal periods. A total of 17 taxa, accounting for 11% of the total taxa, were present in all three sampling periods, mainly consisting of aquatic insects. There were 102 taxa that appeared only in one sampling period, with 30 taxa in the dry period, 8 taxa in the wet period, and 64 taxa in the normal period. Overall, the total number of taxa of macroinvertebrates decreased gradually from upstream to downstream, with EPT taxa being dominant throughout. Spatial analysis revealed a decreasing trend in taxa numbers from upstream to downstream, with upstream areas predominantly inhabited by aquatic insects, indicating better water quality, whereas downstream areas had fewer taxa, lower diversity, and a higher abundance of mollusks. In general, the benthic macroinvertebrate community in the Chishui River exhibited significant temporal and spatial taxa variations, with notable taxa turnover, reflecting the seasonal and spatial changes in water quality and their influence on community structure.

In 2023, the abundance of macroinvertebrates in the main stream of the Chishui River ranged from 18 to 430 individuals per square meter (ind./m^2) across different sampling sites, with an average abundance of 137.3 ind./m^2. Among the various sampling sites, the EPT group of aquatic insects accounted for the highest proportion of macroinvertebrate abundance. The average abundance was 166.9 ind./m^2 during the dry season, 57.75 ind./m^2 during the wet season, and 184.31 ind./m^2 during the normal flow period. From a temporal perspective, the abundance composition of macroinvertebrates during both the dry and normal flow periods was dominated by EPT taxa, which accounted for 68.5% and 73.3%, respectively. During the wet season, EPT taxa still represented the highest abundance composition at 44.2%, followed by Malacostraca at 23.5% and Mollusca at 16.5%. The abundance of macroinvertebrates was significantly higher during the dry and normal flow periods

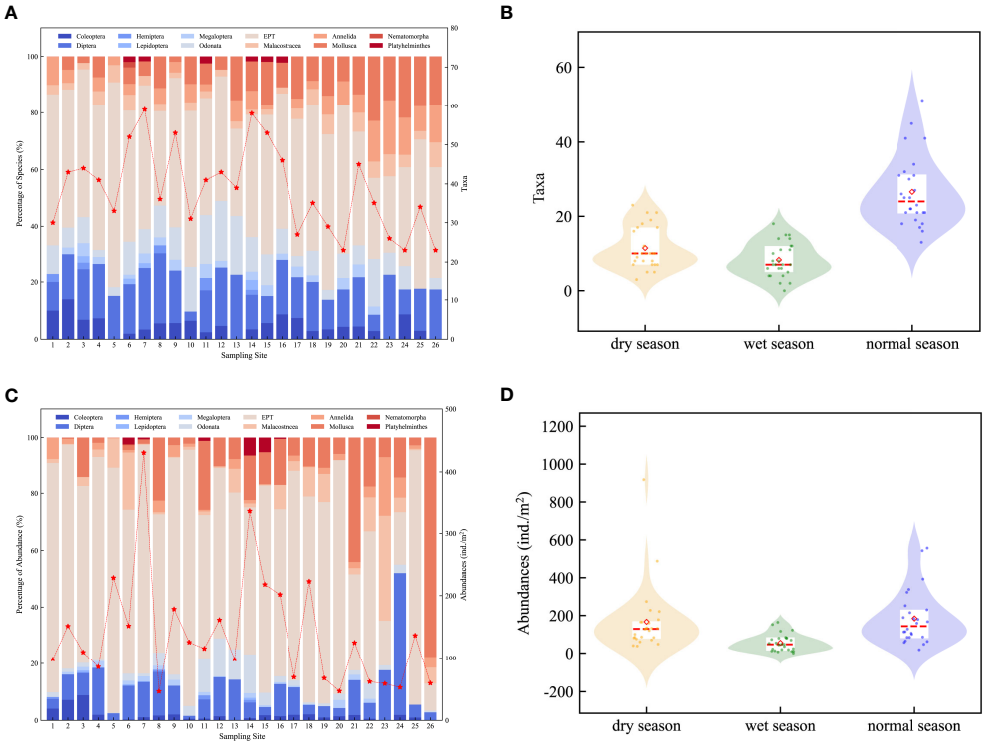

FIGURE 2
Species composition of macrobenthos. **(A, C)** Taxa; **(B, D)** Abundances.

compared to the wet season. According to the ANOSIM results, with R = 0.48 and P = 0.001, the seasonal differences in macroinvertebrate taxa abundance composition were significant. These results highlight the seasonal variability in macroinvertebrate abundance, with notable differences between dry, wet, and normal flow periods, emphasizing the influence of hydrological conditions on the composition of macroinvertebrate communities in the Chishui River. In the upstream areas, the abundance of macroinvertebrates was relatively high, with aquatic insect taxa being dominant and their abundance significantly greater than in the downstream areas. In contrast, the downstream regions exhibited lower species richness, with an increased proportion of mollusks, suggesting that water quality degradation may be affecting the community structure. Overall, the macroinvertebrate community structure in the Chishui River showed significant temporal and spatial variations, with species composition changing according to seasonal and spatial differences. Seasonal fluctuations and spatial heterogeneity to some extent determined the distribution patterns and species diversity of the benthic macroinvertebrates.

3.2 Biodiversity

The results for the Shannon-Wiener diversity index, Margalef richness index, Pielou evenness index, and Simpson evenness index for different water periods at each sampling site are shown in Figure 3. During the dry season, the indices ranged as follows: Shannon-Wiener (0.42-2.65), Margalef (0.47-4.05), Pielou (0.37-0.97), and Simpson (0.19-0.77). During the wet season, the indices ranged: Shannon-Wiener (0.49-2.61), Margalef (0.39-3.89), Pielou (0.28-1), and Simpson (0.12-1). During the normal flow period, the indices ranged: Shannon-Wiener (1.53-3.27), Margalef (3.5-7.94), Pielou (0.54-0.98), and Simpson (0.13-0.89). Overall, the median and average values of the Shannon-Wiener diversity index and Margalef richness index during the normal flow period were significantly higher than those during the dry and wet periods, which is consistent with the distribution of macroinvertebrate taxa numbers. The differences in the Pielou evenness index and Simpson evenness index among different water periods were relatively small, with the Pielou evenness index being more concentrated during the normal flow period. According to ANOSIM results, the Shannon-Wiener diversity index had an R value of 0.29 and a p-value of 0.001; the Margalef richness index had an R value of 0.41 and a p-value of 0.001; the Pielou evenness index had an R value of 0.06 and a p-value of 0.004; and the Simpson evenness index had an R value of 0.03 and a p-value of 0.095. These results indicate that the differences between groups for the Shannon-Wiener diversity index and Margalef richness index were greater than the differences within groups, and the group differences were significant. For the Pielou evenness index and Simpson evenness index, the within-group and between-group differences were similar, and the seasonal differences in the Simpson evenness index were not significant.

3.3 ABC curves

The ABC (Abundance-Biomass Comparison) curves for macroinvertebrates in the Chishui River during the dry, wet, and

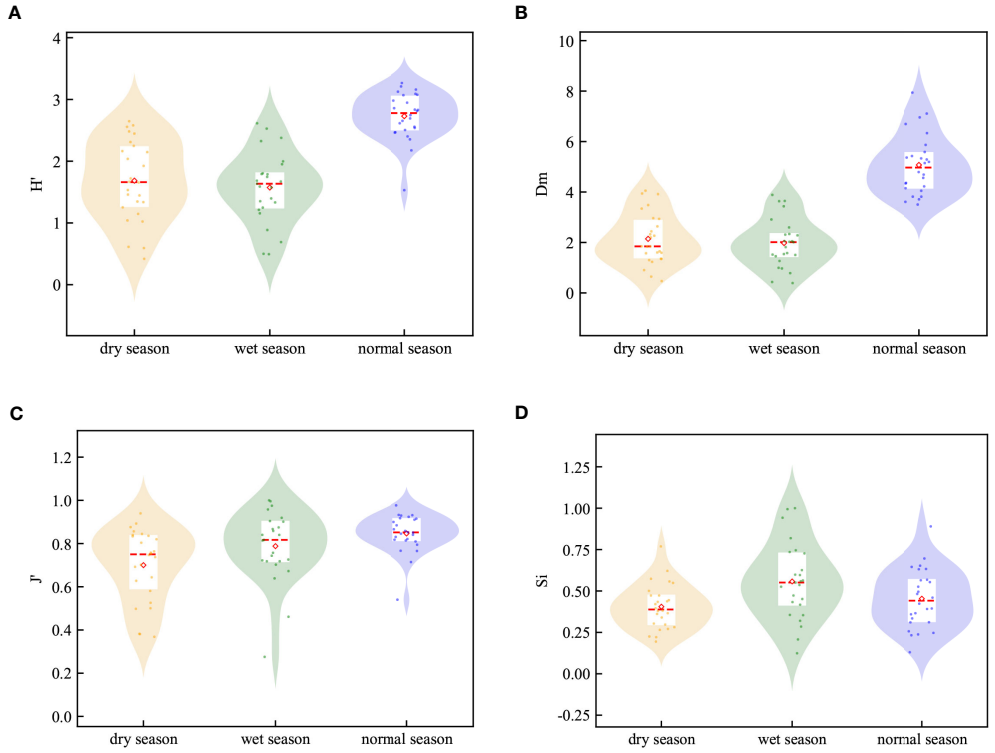

FIGURE 3
Index of macrobenthic diversity. **(A)** Shannon-Wiener diversity index; **(B)** Marglef richness index; **(C)** Pielou uniformity index; **(D)** Simpson's uniformity index.

normal flow periods in 2023 are shown in Figure 4(a - dry season; b - wet season; c - normal season). These curves visually represent the relationship between the cumulative abundance and cumulative biomass of macroinvertebrates during each hydrological period. The analysis of these curves provides insights into the stability and community structure of macroinvertebrates under different flow conditions in the Chishui River.

The results indicate the following, in the dry Season, the top three taxa in terms of abundance were *Heptagenia* (18.46%), *Baetis* (17.92%), and *Hydropsyche* sp.*1* (8.65%). The top three taxa in terms of biomass were *Heptagenia* (9.43%), *Corbicula fluminea* (9.05%), and *Semisulcospira cancellata* (8.52%).In the wet Season, the top three taxa in terms of abundance were *Caridina* (22.83%), *Hydropsyche* sp.*1*(15.06%), and *Semisulcospira cancellata* (11.88%). The top three taxa in terms of biomass were *Semisulcospira cancellata* (30.31%), *Radix ovata* (17.86%), and *Bellamya* (10.71%).In the normal Season, the top three taxa in terms of abundance were *Hydropsyche* sp.*1* (13.04%), *Baetis* (6.45%), and *Cinygmina* (6.03%). The top three taxa in terms of biomass were *Corbicula fluminea* (29.25%), *Limnoperna lacustris* (5.89%), and *Alainites* (5.41%).

Overall, during the dry season, the abundance curve initially exceeded the biomass curve, but eventually, the biomass curve

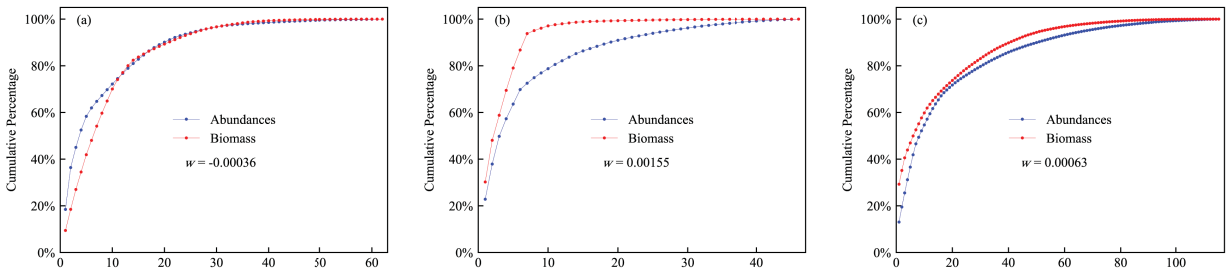

FIGURE 4
ABC curves and *W*-values of macrobenthos in different water periods. **(A)** dry season; **(B)** wet season; **(C)** normal season.

overtook it, causing both curves to intersect. With $W<0$, this indicated that the macroinvertebrate community experienced a certain level of disturbance, leading to reduced stability. This period was characterized by smaller-bodied taxa. In contrast, during the wet and normal flow periods, the biomass curve consistently remained above the abundance curve, with $W>0$. This suggested that the macroinvertebrate community structure was more stable and resilient during these periods.

3.4 Cluster analysis

Cluster analysis of the macroinvertebrate communities in the Chishui River was performed for different hydrological periods, resulting in three distinct clusters for each season, as illustrated in Figure 5 (a - dry season; b - wet season; c - normal season). During the dry season, Group 1 included sites 1, 2, 3, 4, 6, 7, 9, 11, 12, and 16; Group 2 included sites 5, 10, 13, 15, 17, 18, 19, 20, 21, 23, 24, 25, and 26; and Group 3 included sites 8, 14, and 22. During the wet season, Group 1 included sites 1, 2, 3, 4, 5, 6, 7, 8, 9, 10, 11, 12, 13, 15, 16, 18, 19, 20, 22, 23, 25, and 26; Group 2 included site 17; and Group 3 included sites 21 and 24. During the normal season, Group 1 included sites 1, 2, 3, 5, 6, 7, 9, 10, 11, 12, 13, 14, 15, 16, 17, 18, 19, 21, 22, and 25; Group 2 included sites 4 and 8; and Group 3 included sites 20, 23, 24, and 26. Subsequent SIMPER analysis was conducted to identify the main contributing taxa in each group, helping to understand the composition and the main factors driving the similarities within each cluster.

In the dry season, the main contributing taxa in Group 1 were *Hydropsyche* sp.*1* (8.15%), *Baetis* (6.64%), and *Ephemera* (6.54%); in Group 2, they were *Heptagenia* (19.16%), *Baetis* (16.17%), and *Leptophlebia* (11.7%); and in Group 3, they were *Dugesia japonica* (15.4%), *Ephemera* (10.63%), and *Heptagenia* (8.15%).In the wet season, the main contributing taxa in Group 1 were *Caridina* (15.87%), *Hydropsyche* sp.*1* (11.8%), and *Ephemera* (5.83%); in Group 2, *Caridina* accounted for 53.85%; and in Group 3, *Semisulcospira cancellata* accounted for 88.89%. In the normal season, the main contributing taxa in Group 1 were *Hydropsyche* sp.*1* (7.75%), *Corbicula fluminea* (4.07%), and *Cinygmina* (3.99%); in Group 2, they were *Hydropsyche* sp.*1* (36.54%), *Cinygmina* (17.3%), and *Heptagenia* (13.46%); and in Group 3, they were *Bellamya aeruginosa* (21.7%), *Palaemon* (9.59%), and *Caridina* (5.13%).

The results highlight clear distinctions in the macroinvertebrate community structure across different hydrological periods, with each group exhibiting unique characteristics. The taxa contributing significantly to the differentiation within each group provide insight into how the macroinvertebrate communities are influenced by environmental and ecological factors specific to each period. These groupings reflect the adaptability and dynamic nature of the macroinvertebrate communities, demonstrating their response to the seasonal changes in water flow and associated environmental conditions at the sampling sites.

3.5 Dominant taxa

The results of the relative importance index (IRI) are presented in Table 1. These results indicate that the dominant macroinvertebrate taxa in the Chishui River during the dry season are primarily *Heptagenia*, *Baetis*, and *Corbicula fluminea*, with *Baetis* and *Heptagenia* being the absolute dominant taxa during this period. During the wet season, the dominant taxa include *Caridina*, *Hydropsyche* sp.*1*, *Semisulcospira cancellata*, and *Ephemera*, with *Caridina*, *Hydropsyche* sp.*1* and *Semisulcospira cancellata* being the absolute dominant taxa. In the normal season, the dominant taxa are *Corbicula fluminea*, *Hydropsyche* sp.*1*, *Heptagenia*, *Cloeon*, and *Cinygmina*, with *Corbicula fluminea* and *Hydropsyche* sp.*1* being the absolute dominant taxa. The dominant taxa throughout the year

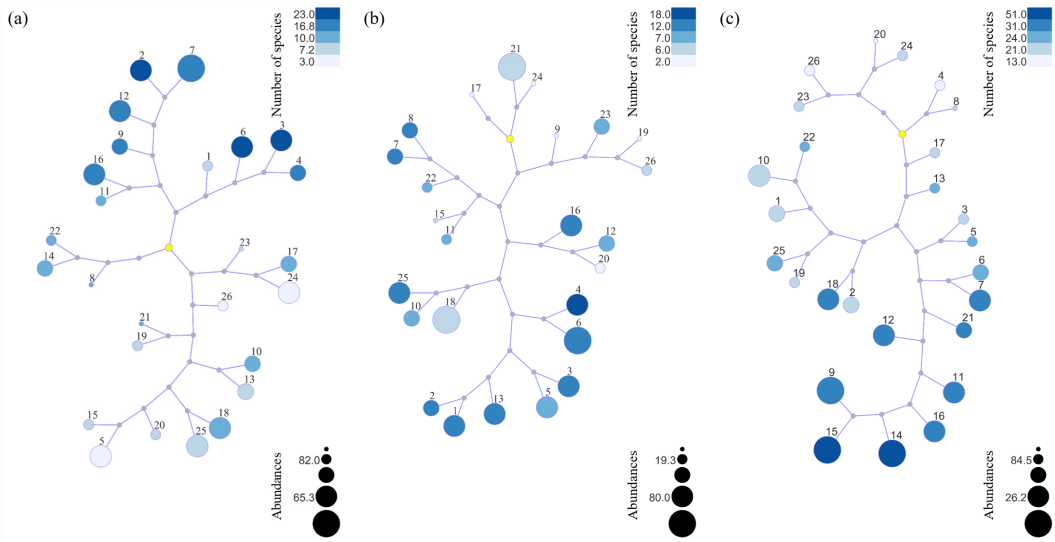

FIGURE 5
Cluster analysis of macrobenthic communities. **(A)** dry season; **(B)** wet season; **(C)** normal season.

TABLE 1 Dominant taxa of macrobenthos in Chishui River.

Dry Season		Wet Season		Normal Season		All year	
Taxa	IRI	Taxa	IRI	Taxa	IRI	Taxa	IRI
Heptagenia	2575	*Caridina*	2681	*Corbicula fluminea*	2014	*Corbicula fluminea*	1756
Baetis	1524	*Hydropsyche* sp.*1*	1576	*Hydropsyche* sp.*1*	1419	*Hydropsyche* sp.*1*	1636
Corbicula fluminea	622	*Semisulcospira cancellata*	1010	*Heptagenia*	632	*Heptagenia*	1162
		Ephemera	613	*Cloeon*	553	*Baetis*	1097
				Cinygmina	546	*Caridina*	713

include *Caridina*, *Hydropsyche* sp.*1*, *Heptagenia*, *Baetis*, and *Caridina*, with *Caridina*, *Hydropsyche* sp.*1*, *Heptagenia* and *Baetis* being the absolute dominant taxa.

3.6 Relationship between dominant taxa and water quality factors

Detrended Correspondence Analysis (DCA) was conducted on the abundance of macroinvertebrates at each sampling site. The results revealed that the first axis lengths during the dry, wet, and normal seasons were 0.46, 0.36, and 0.52, respectively, all of which were less than 3. As a result, redundancy analysis (RDA) was employed to explore the relationship between the dominant taxa and environmental factors (Figure 6: a - dry season; b - wet season; c - normal season). The RDA ordination results indicated that the dominant macroinvertebrate taxa in the Chishui River exhibited varying responses to environmental factors across different seasons.

During the dry season, TN and TP was strongly positively correlated with the first axis, while DO exhibited a strong positive correlation with the second axis. The taxa *Baetis* and *Heptagenia* was strongly positively correlated with DO, but strongly negatively correlated with NH_3-N and *Corbicula fluminea* was strongly positively correlated with TN and TP. Overall, the upstream sites showed a positive correlation with EC and DO, and a negative correlation with NH_3-N, whereas the downstream sites exhibited the opposite trend.

During the wet season, DO was strongly positively correlated with the first axis, while TP、TN was strongly negatively correlated with the second axis. *Caridina* and *Semisulcospira cancellata* was strongly positively correlated with TN and TP and strongly negatively correlated with NH_3-N. *Ephemera* was strongly positively correlated with DO and strongly negatively correlated with EC and *Hydropsyche* sp.*1* had weak correlations with various environmental factors. Overall, the upstream sites showed a positive correlation with DO and a negative correlation with EC, whereas the downstream sites exhibited the opposite trend.

During the normal season, EC was strongly positively correlated with the first axis, while pH and DO was strongly negatively correlated with the second axis. *Corbicula fluminea*, *Hydropsyche* sp.*1* and *Baetis* were strongly positively correlated with EC, *Cinygmina* was strongly negatively correlated with DO and *Cloeon* was strongly positively correlated with NH_3-N. Overall, the upstream sites showed a positive correlation with pH and DO, and a negative correlation with NH_3-N, whereas the downstream sites exhibited the opposite trend.

The comprehensive results showed that *Corbicula fluminea*, *Semisulcospira cancellata* and *Caridina* preferred environments with high phosphorus and nitrogen levels, while *Ephemera*, *Heptagenia*, *Baetis* and *Cinygmina* exhibited a strong correlation with DO. Overall, upstream sites were positively correlated with and DO, and negatively correlated with NH_3-N, whereas downstream sites showed the opposite trend. Upstream areas are typically shallower, which allows for greater exposure to sunlight, promoting photosynthesis by algae and

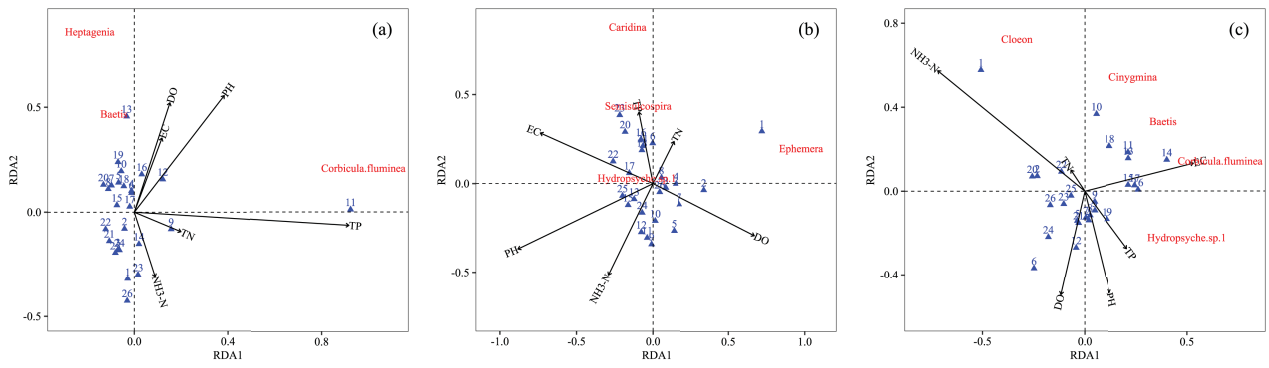

FIGURE 6
CCA ranking of dominant taxa and environmental factors. **(A)** dry season; **(B)** wet season; **(C)** normal season.

phytoplankton. This process leads to an increase in oxygen production, directly raising DO levels in the water. Furthermore, upstream sites generally experience fewer human activities and pollution sources, resulting in lower organic matter content and minimal oxygen consumption by microorganisms. As a result, DO levels remain high, favoring aerobic taxa like mayflies in these areas. Therefore, upstream sites are positively correlated with DO levels. In contrast, downstream areas are more affected by pollution and eutrophication, leading to shifts in the benthic community composition. These areas tend to favor taxa that feed on organic detritus, such as mollusks and oligochaetes, as well as pollution-tolerant taxa like chironomids and tubificid worms. The abundance of these taxa is positively correlated with NH_3-N and TP levels, reflecting the environmental stress and altered conditions typical of downstream regions.

3.7 Relationship between dominant taxa and physical environmental factors

During the benthic macroinvertebrate sampling in the Chishui River basin, water depth, flow velocity, and the median particle size of the substrate (D50) were measured at each sampling site. A frequency histogram was constructed to illustrate the distribution of the absolute dominant taxa throughout the year in the Chishui River basin. The ratio of the abundance of dominant taxa within each interval to the total abundance of the samples was calculated. Using the suitability univariate method, the relative abundance values corresponding to each physical environmental factor were normalized. Habitat suitability for each range was then established, with the habitat suitability for each dominant taxon defined as the ratio of the relative abundance value corresponding to each variable range to the maximum relative abundance value.

The suitability curves for water depth, flow velocity, and substrate composition for each of the absolute dominant taxa are shown in Figures 7–11 (Figure 7: *Corbicula fluminea;* Figure 8: *Hydropsyche* sp.*1*; Figure 9: *Heptagenia*; Figure 10: *Baetis*; Figure 11: *Caridina*). From these figures, it is evident that Corbicula fluminea and Ephemera prefer environments with high flow velocities and substrates with a D50 smaller than 300 mm. *Hydropsyche* sp.*1* and *Baetis* taxa prefer environments with medium to low water depth, high flow velocity, and substrates with a D50 between 100-300 mm. Macrobrachium taxa favor environments with deeper water, low flow velocity, and larger substrate particle sizes.

4 Discussion

4.1 Macroinvertebrate community structure in the Chishui River

The survey results indicate that in 2023, a total of 153 taxa of macroinvertebrates were collected from the Chishui River, with 62

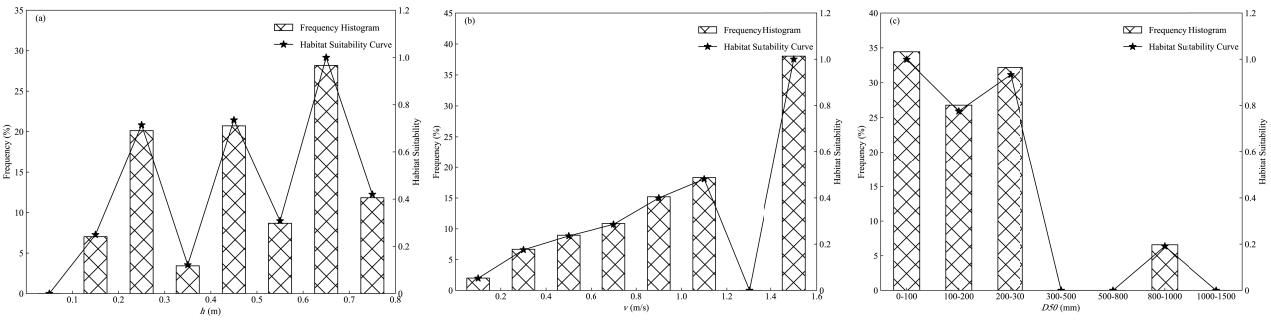

FIGURE 7
Habitat Suitability Curves for *Corbicula fluminea.* **(A)** water depth; **(B)** flow velocity; **(C)** D50.

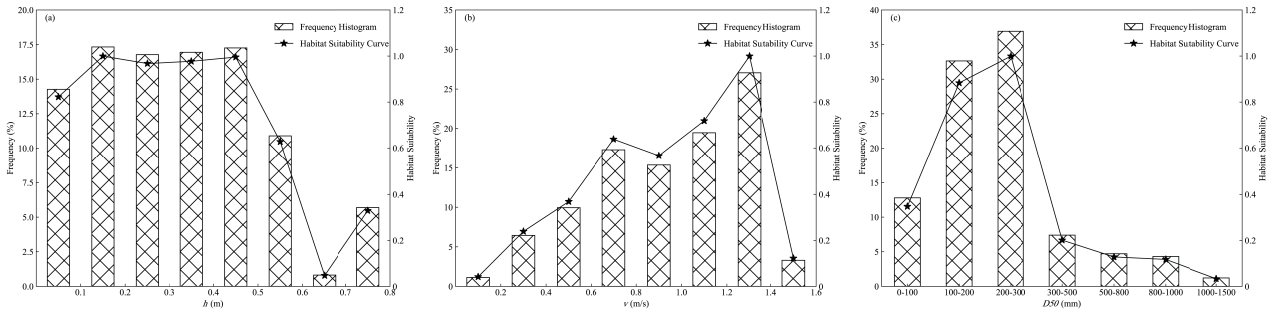

FIGURE 8
Habitat Suitability Curves for *Hydropsyche* sp.*1.* **(A)** water depth; **(B)** flow velocity; **(C)** D50.

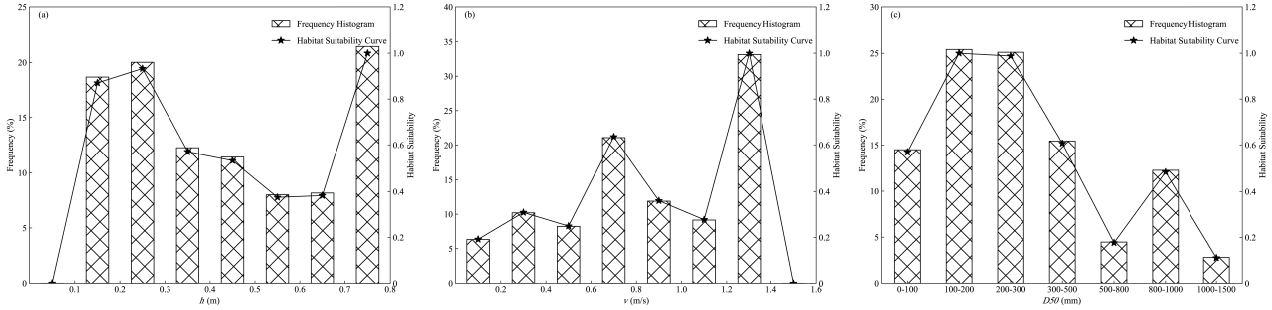

FIGURE 9
Habitat Suitability Curves for *Heptagenia*. **(A)** water depth; **(B)** flow velocity; **(C)** D50.

taxa identified in the dry season, 46 taxa in the wet season, and 115 taxa in the normal season. The community was predominantly composed of aquatic insect EPT groups. Compared to other rivers of similar scale (Sun et al., 2023; Zhang K. et al., 2023; Wang et al., 2024), the Chishui River basin exhibits relatively high macroinvertebrate diversity. This richness is linked to its significant role in the Yangtze River basin. The Chishui River, as a major undammed tributary of the upper Yangtze and a core area of the national nature reserve for rare and endemic fish species in the upper Yangtze, maintains natural river flow, lush vegetation, and low pollution levels. The absence of hydraulic engineering projects and near-natural ecosystem conditions provide a solid foundation for the biodiversity of aquatic organisms within the basin (Cao, 2000; Ja et al., 2020; Min et al., 2021). Additionally, the Chishui River displays typical characteristics of a mountainous river, with numerous tributaries and a complex river network. The distinct environmental variations along different river sections and the high habitat heterogeneity created by the complex hydrological conditions contribute to the rich diversity of macroinvertebrates in the Chishui River (Zhai and Qiu, 2011; Zhou and Gao, 2023).However, compared to past studies (Jiang, 2012; Wang, 2018; Zhang D. et al., 2023), the species richness of macroinvertebrates in the Chishui River has been gradually declined. This decline is primarily attributed to human activities

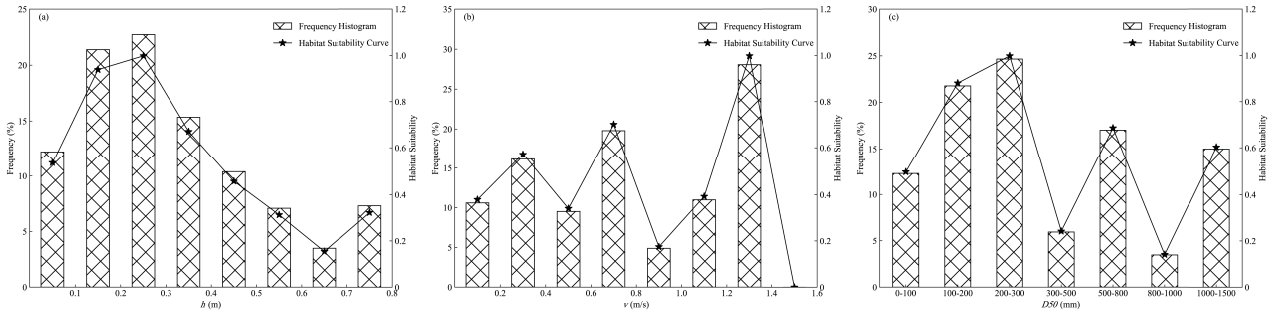

FIGURE 10
Habitat Suitability Curves for *Baetis*. **(A)** water depth; **(B)** flow velocity; **(C)** D50.

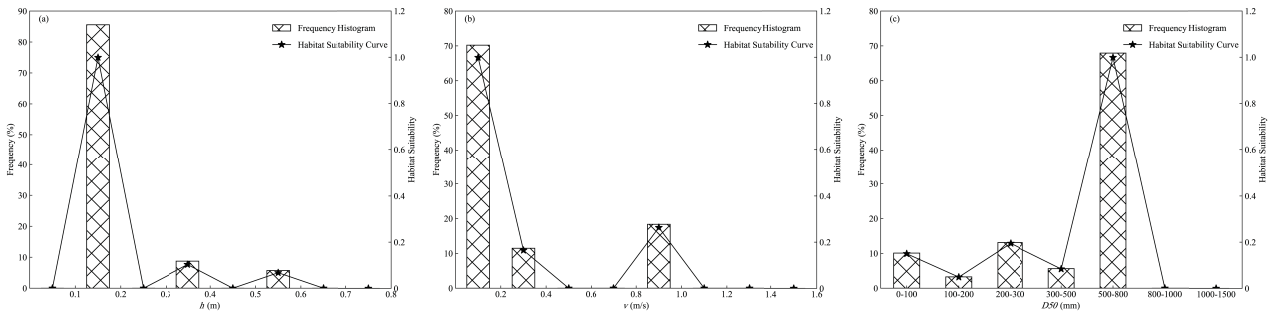

FIGURE 11
Habitat Suitability Curves for *Caridina*. **(A)** water depth; **(B)** flow velocity; **(C)** D50.

and changes in the natural environment, which have destroyed suitable habitats and altered the conditions of habitats for benthic taxa.

The macroinvertebrate community in the Chishui River is significantly shaped by different hydrological periods, with temporal changes influencing hydrological characteristics, hydrodynamic conditions, physicochemical factors, and riparian vegetation. In the dry season, *Ephemeroptera* (*Heptagenia* and *Baetis*) and *Mollusca* (*Corbicula fluminea*) are relatively abundant. In the wet season, *Decapoda* (*Caridina*), *Trichoptera* (*Hydropsyche* sp.*1*), *Mollusca* (*Semisulcospira cancellata*) and *Ephemeroptera* (*Ephemera*) dominate. During the normal season, *Hydropsyche* sp.*1*, *Corbicula fluminea* and *Ephemeroptera* (*Baetis*, *Cloeon*, *Cinygmina*) are more prevalent. The dominance of more sensitive taxa such as *Ephemeroptera* and *Trichoptera* in the dry and normal seasons contrasts with the prevalence of more pollution-tolerant taxa like *Caridina* and mollusks during the wet season. Through the combined analysis with water quality factors, we hypothesize that in the wet season, the concentrations of water pollutants such as NH_3-N, TN, and TP are higher, while DO levels are lower. These water conditions may lead to the disappearance of sensitive taxa, such as mayflies (*Ephemeroptera*), and be replaced by more pollution-tolerant taxa, such as taxa of *Caridina* and mollusks. Furthermore, the number of taxa observed during the normal season surpasses that of the dry season, which in turn exceeds the wet season. This trend may be attributed to the fact that during the normal season, aquatic insects like mayflies are in the juvenile stage of their life cycle, making them easier to collect and leading to higher diversity. In contrast, the wet season coincides with frequent rainfall and high water flow, which results in greater disturbance to benthic communities. Floods and the influx of pollutants, including agricultural fertilizers, often reduce or eliminate some macroinvertebrate taxa, leading to decreased diversity.

Additionally, spatial analysis results revealed significant differences in species abundance and diversity along the main stem of the Chishui River. The upstream areas exhibited higher abundance, with aquatic insects predominating, indicating relatively clean water quality and a diverse macroinvertebrate community. In contrast, the downstream areas had lower species richness, with a notable increase in the abundance and diversity of mollusks, suggesting possible water quality degradation and environmental changes. These spatial differences may be closely related to variations in pollution levels, flow velocity, substrate composition, and physicochemical factors in the water.

Overall, the macroinvertebrate community structure in the Chishui River exhibited significant temporal and spatial variations. Seasonal changes and spatial heterogeneity jointly determined the distribution patterns and species diversity of benthic macroinvertebrates, reflecting the impact of environmental changes on the community. Therefore, protecting the water quality and ecological environment of the Chishui River, particularly across different seasons and spatial regions, is of crucial ecological significance.

4.2 Relationship between macroinvertebrate communities and water quality factors

Using GAMs, we explored the relationship between macroinvertebrate communities and environmental factors. The model fitting results are illustrated in Figure 12. The R^2 values for pH, DO, EC, NH_3-N, TN and TP were 0.449, 0.182, 0.144, 0.148, 0.222,

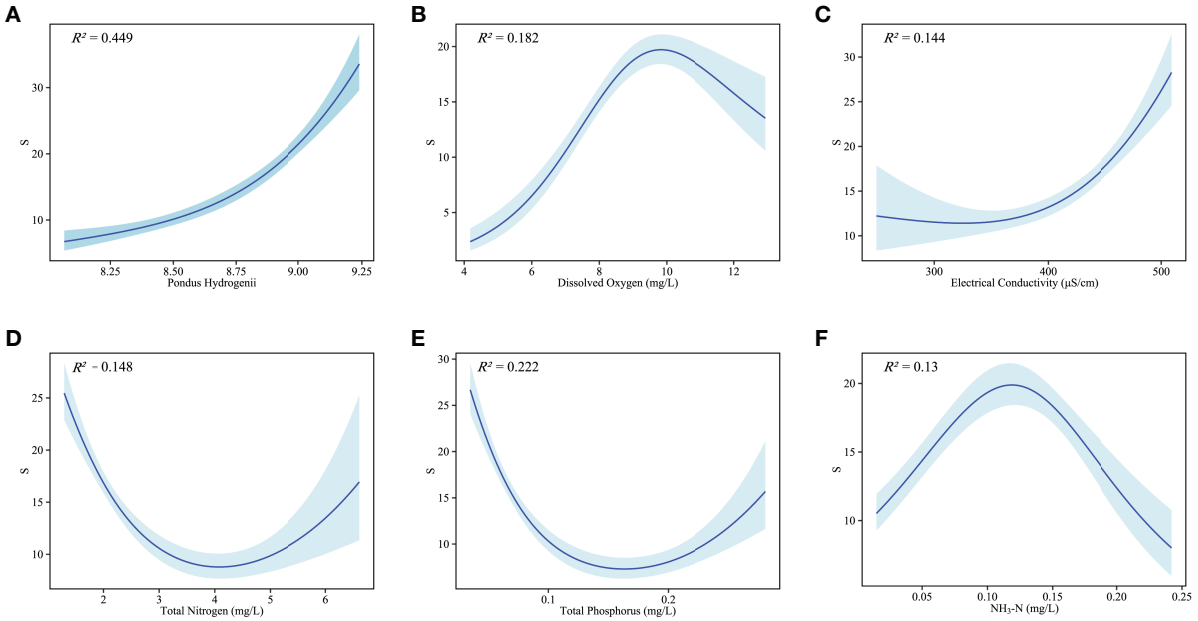

FIGURE 12
Response curve of macrobenthic community to environmental factors. **(A)** pH; **(B)** DO; **(C)** EC; **(D)** TN; **(E)** TP; **(F)** NH_3-N.

and 0.13, respectively, with all *p*-values being less than 0.01. Macroinvertebrates predominantly thrive in water environments with appropriate pH levels. In our study, we observed that as pH and EC increased, the diversity of macroinvertebrate species in the Chishui River also increased, until a threshold was reached (pH = 9.24).

Previous studies (Zhu et al., 2019; Su et al., 2020) have shown that DO levels significantly influence the feeding, reproduction, and overall life processes of aquatic organisms, with varying tolerances to DO among different taxa. Based on the GAM results, the optimal DO concentration for macroinvertebrate survival in the Chishui River was found to be 9.8 mg/L. According to the "Environmental Quality Standards for Surface Water" in China, Class I water quality is defined as having DO levels > 7.5 mg/L (State Environmental Protection Administration and General Administration of Quality Supervision, 2002). In our study, 77.9% of the sampling sites met this Class I standard, further reinforcing the conclusion that the Chishui River maintains relatively low pollution levels and high water quality.

TN and TP are critical factors in evaluating river eutrophication and act as reliable indicators of macroinvertebrate biodiversity and taxa richness (Yu et al., 2019; Zhang et al., 2021). The GAM analysis indicates a sharp decline in macroinvertebrate taxa richness as TN and TP concentrations rise. Interestingly, once TN reaches 0.41 mg/L and TP reaches 0.163 mg/L, a slight increase in taxa richness is observed. This trend reflects the varying tolerances of macroinvertebrate taxa to nutrient levels. In nutrient-rich environments, taxa such as *Corbicula fluminea*, *Semisulcospira cancellata*, and *Caridina* were identified as dominant, supporting findings by Zhang Y. et al. (2023). In contrast, taxa associated with cleaner waters, such as *Ephemeroptera*, declined significantly or even disappeared under high-nitrogen and high-phosphorus conditions, consistent with observations by Gong et al. (2001). These results highlight the differential responses of pollution-tolerant and sensitive taxa to changes in nutrient levels, emphasizing the ecological impact of eutrophication on macroinvertebrate communities.

Research indicates that NH_3-N serves as a vital nutrient for the growth of aquatic plants and algae, which can indirectly enhance macroinvertebrate productivity by supporting the base of the food web (Johnson et al., 2013). However, NH_3-N also has direct physiological effects on macroinvertebrates, influencing their immune responses and damaging tissues, with excessive concentrations proving lethal. The GAM fitting results reveal a nonlinear relationship between NH_3-N concentration and macroinvertebrate taxa richness in the Chishui River. As NH_3-N levels increase, taxa richness initially rises but subsequently declines. The analysis identifies 0.12 mg/L as the optimal NH_3-N concentration for macroinvertebrate survival, aligning with findings from Hong et al. (2007). This highlights the dual role of NH_3-N as both a nutrient and a potential stressor, emphasizing the need for balanced nutrient levels to support macroinvertebrate biodiversity.

5 Conclusions

Based on the analysis of macroinvertebrate community structure in the Chishui River and its relationship with environmental factors, the following conclusions were drawn:

1. A total of 153 taxa of benthic macroinvertebrates were identified in the Chishui River basin during this survey, predominantly aquatic insects from the EPT group. The composition and diversity of macroinvertebrates varied significantly across different hydrological periods. Compared to other rivers of similar scale, the Chishui River exhibits relatively high macroinvertebrate diversity. However, the species richness of macroinvertebrates is gradually declining due to anthropogenic activities and changes in the natural environment.
2. Macroinvertebrate communities at upstream sampling sites were positively correlated with DO and negatively correlated with NH_3-N, while downstream sites exhibited the opposite trends. These spatial differences reflect the influence of hydrological and environmental gradients along the river.
3. According to the GAM fitting results, the number of macroinvertebrate taxa in the Chishui River increased with increasing pH and EC; decreased initially and then increased to some extent with increasing TN and TP concentrations; and increased initially and then decreased with increasing DO and NH_3-N concentrations.
4. Based on this study, we suggest implementing pollution control measures targeting NH_3-N to protect sensitive taxa such as mayflies. Firstly, the efficiency of nitrogen removal in sewage treatment plants should be enhanced to reduce NH_3-N emissions from domestic and industrial wastewater. Secondly, given the large amount of farmland along the Chishui River, measures such as planting buffer strips and optimizing fertilization timing and dosage should be implemented to reduce agricultural nitrogen runoff.
5. This study relies on short-term monitoring data, which may not fully capture the long-term responses of benthic communities to environmental changes. Future research should include long-term monitoring and interannual variability analysis to evaluate the time-scale effects of community dynamics and identify delayed or cumulative impacts of environmental changes.
6. Given the multivariate nature of the relationships between taxa and environmental factors, causal relationships remain difficult to establish based on observational data alone. Future studies could incorporate experimental approaches, such as substrate preference or pollution simulation experiments, to directly assess the effects of key environmental variables on community structure, thereby advancing our understanding of these interactions.

Data availability statement

The original contributions presented in the study are included in the article/supplementary material. Further inquiries can be directed to the corresponding author.

Author contributions

XL: Data curation, Investigation, Software, Visualization, Writing – original draft, Writing – review & editing. LY: Investigation, Methodology, Project administration, Resources, Supervision, Writing – review & editing. XZ: Funding acquisition, Supervision, Writing – review & editing. PH: Funding acquisition, Investigation, Resources, Supervision, Writing – review & editing. CS: Funding acquisition, Investigation, Supervision, Writing – review & editing. BZ: Investigation, Software, Writing – review & editing.

Funding

The author(s) declare that financial support was received for the research, authorship, and/or publication of this article. This study was supported by the National Key Research and Development Program of China (2022YFC3202003, 2022YFC3205000); the National Natural Science Foundation of China (51809288); the National Key Research and Development Program of China (52122902, U240202, 52394233).

Conflict of interest

Author XZ was employed by China Three Gorges Corporation.

The remaining authors declare that the research was conducted in the absence of any commercial or financial relationships that could be construed as a potential conflict of interest.

Publisher's note

Supplementary material

The Supplementary Material for this article can be found online at: https://www.frontiersin.org/articles/10.3389/fevo.2024.1459468/full#supplementary-material

References

Barbour, M. T., Gerritsen, J., Snyder, B. D., and Stribling, J. B. (1999). Rapid bioassessment protocols foruse in streams and wadable rivers: Periphyton, benthic macroinvertebrates and fish. United States Environmental Protection Agency..

Cao, W. (2000). Thoughts on the construction of nature reserve for endemic fish in the upper reaches of the Yangtze River and related issues. *Resour. Environ. Yangtze Basin* 9, 131–132.

Chen, Z., Wang, Y., Qiao, W., Fu, J., and Pei, Y. (2021).). Restoration of macrozoobenthos community in Baiyangdian lake based on habit and food web. *Asian J. Ecotoxicol.* 5), 136–147. doi: 10.7524/AJE.1673-5897.20201117001

Chen, Q., Zhang, J., Mo, K., Chen, Y., Guan, T., Wang, G., et al. (2020). Effects of hydropower development on aquatic eco-environment and adaptive managements. *Adv. Water Sci.* 31, 793–810. doi: 10.14042/j.cnki.32.1309.2020.05.015

China National Environmental Monitoring Centre (2021). *Technical specifications for aquatic ecological monitoring-freshwater benthic macroinvertebrates (Trial)* (Beijing: China Environmental Science Press).

Clarke, K. R., Gorley, R. N., Somerfield, P. J., and Warwick, R. M. (2014). Change in marine communities: an approach to statistical analysis and interpretation (Primer-E Ltd: Plymouth, UK).

Cortes, E. (1997). A critical review of methods of studying fish feeding based on analysis of stomach contents: application to elasmobranch fishes. *Can. J. fish. Aquat. Sci.* 54, 726–738. doi: 10.1139/f96-316

Dou, Q., Wang, H., Song, D., Du, X., Wang, L., Huang, X., et al. (2023). Community structure of macrozoobenthos and biological evaluation of water quality in Huma River. *Chin. J. Fish.* 36, 52–60. doi: 10.3969/j.issn.1005-3832.2023.06.008

Du, F., Wang, X., Jia, X., Yang, S., Ma, S., Chen, H., et al. (2011). Species composition and characteristics of macrobenthic faunain Daya Bay, South China Sea. *J. Fish. Sci. China* 18, 877–892. doi: 10.3724/SP.J.1118.2011.00877

Fu, H., Zhang, Y., Huang, S., Chu, L., Yan, Y., and Gr, Y. (2024). Seasonal dynamics and assembly mechanism of macroinvertebrate community in Huishui River. *Resour. Environ. Yangtze Basin* 33, 1239–1249. doi: 10.11870/cjlyzyyhj20240

Gong, Z., Xie, P., Tang, H., and Wang, S. (2001). The influence of eutrophication upon community structure and biodiversity of macrozoob-enthos. *Acta Hydrobiol. Sin.* 25, 210–216. doi: 10.3321/j.issn:1000-3207.2001.03.002

Hong, M., Chen, L., Gu, S., Liu, C., Long, Z., and Zhang, W. (2007). Effects of ammonia exposure on immunity indicators of haemolymph and histological structure of hepatopancreas in Chinese mitten crab(Eriocheir sinensis). *J. Fish. Sci. China* 14, 412–418. doi: 10.3321/j.issn:1005-8737.2007.03.010

Hu, W., Wang, L., Mo, K., Li, W., and Chen, Q. (2021). Community structure and habitat characteristics of macrobenthos in river network of Yangzhou City. *Acta Scientiae Circumstantiae* 41, 1440–1448. doi: 10.13671/j.hjkxxb.2020.0432

Ja, W., Wu, S., Wang, W., and Chen, A. (2020). Research on evaluation of ecosystem services in chishui river basin based on InVEST. *J. China Inst. Water Resour. Hydropower Res.* 18, 313–320. doi: 10.13244/i.cnki.jiwhr.20190030

Jiang, X. (2012). *Macroinvertebrate Diversity Patterns in Midwestern Rivers and Their Environmental Assessment* (China(Hubei: Institute of Hydrobiology, Chinese Academy of Sciences).

Jiang, W., Zhang, M., and Liu, X. (2024). Effects of different pollution stresses on macrofaunal communities in the adjacent waters of Dongjiakou, Qingdao, China. *Acta Ecol. Sin.* 44, 7830–7843. doi: 10.20103/j.stxb.202312292871

Johnson, R. C., JIN, H. S., Carreiro, M. M., and Jack, J. D. (2013). Macroinvertebrate community structure, secondary production and trophic-level dynamics in urban streams affected by non-point-source pollution. *Freshw. Biol.* 58, 843–857. doi: 10.1111/fwb.12090

Li, Q., Zhang, M., Yu, M., Li, X., Chang, M., and Chen, L. (2023). Community structure and influencing factors of macroinvertebrate in urban rivers of Dongguan. *Ecol. Environ. Sci.* 33, 101–110. doi: 10.16258/j.cnki.1674-5906.2024.01.011

Liao, Y., Yang, X., Yang, T., Li, H., and Qu, Y. (2024). Community structure of benthic organisms in typical rivers of Xi'an and influencing factors. *J. Arid Land Resour. Environ.* 38, 101–110. doi: 10.13448/j.cnki.jalre.2024.209

Min, W., Huang, F., and Wang, W. (2021). Situation of water environment and evaluation of water quality in Chishui river basin. *Acta Agricult. Jiangxi* 33, 87–91. doi: 10.19386/j.cnki.jxnyxb.2021.08.015

Qu, X. D., Cao, M., Shao, M. L., Li, D. F., and Cai, Q. H. (2007). Macrobenthos in Jinping reach of Yalongjiang River and its main tributaries. *Chin. J. Appl. Ecol.* 18, 158–162. doi: 10.3321/j.issn:1001-9332.2007.01.027

Schmitt, R. J., Bizzi, S., Castelletti, A., and Kondolf, G. M. (2018). Improved trade-offs of hydropower and sand connectivity by strategic dam planning in the Mekong. *Nat. Sustain.* 1, 96–104. doi: 10.1038/s41893-018-0022-3

State Environmental Protection Administration (2002). *Analytical Methods for Water and Waste Water Monitoring* (Beijing: China Environmental Science Press).

State Environmental Protection Administration and General Administration of Quality Supervision (2002). *Environmental quality standards for surface water* (Beijing: China Environmental Science Press).

Su, Y., Li, W., Li, J., Sun, X., and Hu, W. (2020). Habitat suitability of macroinvertebrates: A case study in Qiaobian River, atributary of Yangtze River, China. *Acta Ecol. Sin.* 40, 5844–5854. doi: 10.5846/stxb201909201973

Sun, J., Xu, G., Chi, J., and Yang, Y. (2023). River health assessment of Qingyi river based on benthic macroinvertebrates. *Resour. Environ. Yangtze Basin* 32, 1254–1266. doi: 10.11870/cjlyzyyhj202306013

Wang, B. (2003). Water quality bioassess-ment using benthic macroinvertebrates. Nanjing Agricultural University, China (Zhejiang.

Wang, J. (2018). Macroinvertebrate diversity and its application in health bioassessment in the Chishui River. Institute of Hydrobiology, Chinese Academy of Sciences, China(Hubei.

Wang, J., Huang, Z., Li, H., Jang, X., Li, Z., Meng, X., et al. (2018). Construction of macroinvertebrate integrity-based health assessment framework for the Chishui river. *Environ. Monit. China* 34, 62–72. doi: 10.19316/j.issn.1002-6002.2018.06.07

Wang, F., Li, W., Yan, K., Zhang, X., Liu, Z., Li, Y., et al. (2024). Effects of watershed management process on functional feeding groups of macrobenthos and water environment in Huangbai River,a primary tributary of the middle reaches of Yangtze River. *Acta Scientiae Circumstantiae* 44, 376–389. doi: 10.13671/j.hjkxxb.2024.0160

Warwick, R. (1986). A new method for detecting pollution effects on marine macrobenthic communities. *Mar. Biol.* 92, 557–562. doi: 10.1007/BF00392515

Yang, Q., Xu, G., Zhang, P., and Chi, J. (2022). Macroinvertebrate community structure and water quality assessment in the Qingyi River Watershed. *Acta Ecol. Sin.* 42, 4169–4180. doi: 10.5846/stxb202101240247

Yemane, D., Field, J. G., and Leslie, R. W. (2005). Exploring the effects of fishing on fish assemblages using Abundance Biomass Comparison (ABC) curves. *ICES J. Mar. Sci.* 62, 374–379. doi: 10.1016/j.icesjms.2005.01.009

Yu, C., Huang, X., Chen, H., Godfray, H. C. J., Wright, J. S., Hall, J. W., et al. (2019). Managing nitrogen to restore water quality in China. *Nature* 567, 516–520. doi: 10.1038/s41586-019-1001-1

Yu, F., Liu, F., Xia, Z., Lin, P., Xu, C., Wang, J., et al. (2022). Classification and assessment methods for mountain channel habitats in the Chishui River basin, China. *Water* 14, 515. doi: 10.3390/w14040515

Zhai, H., and Qiu, L. (2011). Water resources protection and development of Chishui river region. *Environmental Science and Management* 36, 38–40. doi: 10.3969/j.issn.1673-1212.2011.08.012

Zhang, M., Cai, Q., and Qu, X. (2017). Macroinvertebrate succession and longitudinal zonation dynamics in Xiangxi Bay, after impoundment of the Three Gorges Reservoir. *Acta Ecol. Sin.* 37, 4483–4494. doi: 10.5846/stxb201601130086

Zhang, Y., Cai, Y., Zhang, Y., Gao, J., and Li, K. (2021). The response of benthic macroinvertebrate communities to environmental pressures in streams and rivers:A case study of Taihu and Chaohu Basins. *J. Lake Sci.* 33, 204–217. doi: 10.18307/2021.0111

Zhang, D., Liu, Y., Li, Z., Ge, Y., Zhang, J., and Xie, Z. (2023). Species diversity and recommended rehabilitative strategies of benthic macroinvertebrate in the Chishui River, a tributary of the Upper Yangtze River. *Biodivers. Sci.* 31, 60–72. doi: 10.17520/biods.2022674

Zhang, Y., Wen, S., Zhang, Q., Zhao, Z., Wang, X., Duan, X., et al. (2023). Macrozoobenthos community structure and biological evaluation of water quality in littoral zone of middle and lower reaches of Yangtze river. *Resour. Environ. Yangtze Basin* 32, 1417–1432. doi: 10.11870/cjlyzyyhj202307006

Zhang, K., Zhou, L., Chen, W., Shao, K., Wu, W., Chen, Y., et al. (2023). Macroinvertebrates community structure in relation to environmental variables in the lower reaches of the Yalong River. *China Environ. Sci.* 43, 1857–1186. doi: 10.19674/j.cnki.issn1000-6923.20230106.007

Zhou, W., and Gao, J. (2023). Runoff characteristics and change trends of the Chishuihe river watershed in recent 10 years. *Environ. Sci. Survey* 42, 73–78. doi: 10.13623/j.cnki.hkdk.2023.03.001

Zhou, X., Xu, M., Lei, F., Zhang, J., Wang, Z., and Luo, Y. (2022). Responses of macroinvertebrate assemblages to flow in the Qinghai-Tibet Plateau: Establishment and application of a multi-metric habitat suitability model. *Water Resour. Res.* 58, e2021WR030909. doi: 10.1029/2021WR030909

Zhu, L., Xiao, W., Zhou, D., Zhang, W., Wang, L., and Zhang, R. (2019). Macrozoobenthos community structure and its relationship with environmental factors in Dianshan Lake. *J. Hydroecol.* 40, 55–65. doi: 10.15928/j.1674-3075.2019.02.009

frontiers | Frontiers in Environmental Science

TYPE Original Research
PUBLISHED 27 January 2025
DOI 10.3389/fenvs.2025.1500075

OPEN ACCESS

EDITED BY
Celso Santos,
Federal University of Paraíba, Brazil

REVIEWED BY
Chunhui Li,
Beijing Normal University, China
Aiping Pang,
Nanjing Academy of Administration, China

*CORRESPONDENCE
Ailing Wang,
ailingwang@sdau.edu.cn
Tianxu Sun,
suntianxu1981@163.com

†These authors have contributed equally to this work and share first authorship

RECEIVED 23 September 2024
ACCEPTED 07 January 2025
PUBLISHED 27 January 2025

CITATION
Liu J, Xu M, Wang A, Sun T, Zhang C, Chen X and Zhang P (2025) Quantifying the human wellbeing of the national wetland park: gross ecosystem product accounting of Shandong Mata Lake National Wetland Park.
Front. Environ. Sci. 13:1500075.
doi: 10.3389/fenvs.2025.1500075

Quantifying the human wellbeing of the national wetland park: gross ecosystem product accounting of Shandong Mata Lake National Wetland Park

Jian Liu[1†], Meng Xu[1†], Ailing Wang[1*], Tianxu Sun[2*], Chuntao Zhang[3], Xue Chen[2] and Peng Zhang[1]

[1]College of Resources and Environment, Shandong Agricultural University, Taian, China, [2]Shandong Institute of Territorial and Spatial Planning, Jinan, China, [3]Shandong Deyun Land Real Estate Appraisal Consulting Co., Ltd., Zibo, China

National wetland parks, characterized by robust ecological functions, distinctive natural landscapes, and abundant cultural resources significantly enhance human wellbeing, serve as crucial providers of ecosystem products, and exert substantial influence on local socioeconomic development and ecological conservation. There is an urgent need to carry out the Gross Ecosystem Product (GEP) accounting and monetize the value of ecosystem products. Taking the Shandong Mata Lake National Wetland Park (SMTNWP) in China as the example, and considering the characteristics of wetland parks, this research constructed the GEP accounting index system comprising 11 secondary subjects from the perspectives of regulation and socio-cultural functions. Taking the year 2021 as the research period, the monetary value was assessed based on biophysical value accounting, and the GEP level was determined. The results showed that the GEP of SMTNWP in 2021 is CNY 74.8317 million, with a unit area GEP of 73,200 CNY/hm^2. Regulating ecosystem products constitute the core component of GEP, facilitating the sustainable development of wetland conservation and restoration, as well as eco-cultural tourism. Moving forward, efforts in wetland protection, restoration and maintenance should be sustained, and the platforms for promotion, education and scientific research should be proactively established. The research results can offer support and references for the establishment of unified accounting subjects and systems for similar ecosystems and national wetland parks, and translate the human wellbeing of national wetland parks into visual monetization, providing theoretical basis for the government to realize the value of ecosystem products, and further promoting the conversion of ecological value into economic benefits.

KEYWORDS

national wetland park, human wellbeing, gross ecosystem product (GEP), the Mata Lake, biophysical value, monetary value

1 Introduction

Since the Industrial Revolution, people's development of land resources has been continuously increasing, and the demand for ecosystem supply and service is excessive (Li, Y. and Xie, H., 2024). The importance of natural resource assets that provide ecosystem services, the accurate and detailed assessment of ecosystem service functions (Jiang and Dong, 2024), and the scientific and reasonable assessment of the contribution of ecosystems to people have become the focus of scholars' attention. Since the reform and opening up, China's urbanization and industrialization have developed rapidly, while the contradiction between humans and the natural ecological environment has gradually become prominent. Since the 18th CPC National Congress convened in 2012, China continues to promote the construction of ecological civilization, adhering to the ecological civilization ideology and concept of "clear waters and green mountains are as valuable as mountains of gold and silver." Ecosystem products refer to the goods and services provided by ecosystems and used for economic and other human activities (Hui et al., 2024). Gross Ecosystem Product (GEP, equivalent to the value of ecosystem products) accounting is an important task in evaluating the value of products or services that the ecological environment itself can provide for human and benefit humanity, and it measures the monetary value of products and services related to the ecosystem in a specific region during a certain accounting period (Zheng et al., 2023). GEP has become an accounting system that corresponds to Gross Domestic Product (GDP) and a new indicator for measuring total output, thereby better promoting the implementation of green development performance assessment and changing the economic and social development evaluation system that is solely dominated by GDP (Wang L. Y. et al., 2022).

In 2016, the Chinese Government issued *"the Guiding Opinions on the Reform of the System of Paid Use of Natural Resource Assets owned by the Whole People,"* which pointed out the need to carry out the inventory and accounting of natural resource assets owned by the whole people, and to clarify the quantity of natural resource assets owned by the whole people in China. In 2021, the Chinese Government issued *"the Opinions on Establishing and Improving the Mechanism for Realizing the Value of Ecosystem Products,"* which pointed out the need to evaluate the effectiveness of ecological protection and GEP, publish GEP accounting results, establish the GEP evaluation system, and explore GEP accounting methods for administrative and specific regional units. The implementation of the series of documents indicates that GEP accounting based on biophysical value and monetary value accounting is a necessity for realizing the value of ecosystem products, and the basis for ecological protection compensation and ecological environment damage compensation (Hui et al., 2024).

Wetlands are important natural resource assets and suppliers of ecosystem products, and the ecosystem services value of wetlands in China contributes the most to various ecosystems (Chen and Zhang, 2000), but there are also problems such as low conversion rate and low degree of marketization of wetland resource ecosystem products. It is urgent to protect, transform, and increase the value of wetland resource ecosystem products (Chen et al., 2023). National wetland parks have typical wetland ecological functions such as ecological environment restoration and living environment improvement, which can greatly satisfy people's demand for a better ecological environment and bring human wellbeing to the neighboring human beings. National wetland parks are also an important carrier for the development of cultural tourism industry and the provision of ecosystem products, which in turn have important impacts on the local socioeconomic development and ecological conservation. In August 2024, the Chinese Government issued the "*Implementation Opinions on Solidly Promoting the Construction of a Beautiful China through the Protection and Sustainable Utilization of Natural Resources*," proposing to promote the construction of national parks, improve the mechanism for realizing the value of ecosystem products, and enhance the ability of natural ecosystems to provide ecosystem products.

The concepts of "Ecosystem Product Value," "GEP," and "Gross Ecosystem Production" all originate from "Ecosystem Service Value (ESV)." In 2022, "*the Standard for the GEP Accounting (Trial)*" issued by the Chinese Government has defined the GEP refers to the sum of the monetary value of all ecosystem products provided by various ecosystems within a certain administrative region during the accounting period. At present, the academic community generally equates "Ecosystem Product Value," "GEP," "Gross Ecosystem Production," and "ESV," and the accounting indicator system mostly includes material product value, regulation service value, and cultural service value (Zhang et al., 2023).

In 1997, "*Nature's Services: Societal Dependence on Natural Ecosystems*" edited by Daily (Ouyang et al., 2013) and "*The Value of the World's Ecosystem Services and Natural Capital*" published by Costanza et al. (1997) became classic works, and the concept of ESV was proposed. The United Nations Millennium Ecosystem Assessment (MA) project aims to assess the relationship between ecosystem change and human wellbeing (Hui et al., 2024). "*The System of Environmental-Economic Accounting-Ecosystem Accounting 2012-Central Framework*" (*SEEA-EA 2012*) combines ecosystem accounting with economic accounting (Hui et al., 2024). Based on Costanza's unit value equivalent factor table in 1997 (Costanza et al., 1997) and combined with China's actual situation, Xie Gaodi, a Chinese scholar, has proposed the improved unit value equivalent factor table (Xie et al., 2008) to guide subsequent related research (Li X. K. et al., 2023).

At the academic research level, China started quantitative researches on ESV studies in the late 1990s. After the year 2012, relevant scholars (Ouyang et al., 2013) explored the concept, accounting methods, and applications of GEP. With the advancement of the national GEP accounting process, relevant research has accounted the GEP of different typical regions and ecosystems, such as typical soil desertification areas (Li, Y. Y. et al., 2023), typical reservoir areas (Cheng et al., 2024), Yangtze River Delta areas (Ji et al., 2024), and Beijing-Tianjin-Hebei region (Fan et al., 2024), which are national key strategic areas, and the research scale includes different regions such as global-level (Jiang et al., 2021), provincial-level (Hu et al., 2023; Ouyang et al., 2020), prefecture-level (Pema et al., 2017), and county-level (Shen et al., 2024; Li, Y.H. et al., 2024), as well as some specific wetland areas such as typical wetlands in large cities (Wang et al., 2024), urban scenic wetlands (Sun et al., 2024), and lake wetlands (Wang, F. et al., 2019). With the deepening of researches, current GEP research has

gradually expanded from value accounting to coupling and coordinating relationship with systems such as new urbanization (Zhang et al., 2024) and regional economy (Li, A. L. et al., 2024), exploring value realization paths and driving mechanisms (Gao and Zhu, 2024). At the practical level in various regions of China, Zhejiang Province, Shenzhen City, Wuyishan County and some other cities have carried out GEP accounting pilot exploration.

Based on scientific researches and local practice, national and local governments of China have formulated GEP accounting technical regulations. The Chinese Government issued the "*Technical Guidelines for the Accounting of Gross Ecosystem Product (GEP) of Terrestrial Ecosystems*" in 2020, and issued "*the Standard for the GEP Accounting (Trial)*" in 2022. In Shandong Province, Shenzhen City, etc., corresponding GEP accounting regulations have been formulated and issued based on their own actual conditions. The relevant regulations and guidance further improved the scientificity, normative approach and operability of GEP accounting results, promoting the verifiability and comparability of GEP accounting results.

In summary, current researches on GEP accounting focuses on different types of ecosystems, functional areas, and administrative regions at different scales, and the accounting subjects generally refer to relevant regulations and mostly focus on product supply services and ecological regulation services. However, Currently, GEP accounting researches are mostly carried out at the scale of administrative units, and GEP accounting cases based on national wetland parks as research units are relatively weak. Wetland parks, as important carriers of ecosystem products, have become a research gap in their GEP accounting, which cannot meet the urgent needs and practical exploration of GEP accounting for specific regional units. In previous studies, there were still some cases where the selection of evaluation indicators did not take into account the actual situation of the accounting area, the values of relevant accounting parameters were mechanically applied, and the accounting results did not conform to reality. In addition, the construction of national wetland parks also requires the provision of corresponding facilities for promotion, education and scientific research, and promotional materials, and the accounting index system should consider the value of promotion, education and scientific research. In addition, the management and operation of wetland parks require a certain amount of labor costs and require social labor to engage in relevant work, which can provide certain employment opportunities and generate certain social value. However, current accounting researches have relatively weak consideration for the values of social and cultural functions such as promotion, education and scientific research, and employment promotion, resulting in inaccurate value accounting results.

Conducting research on the GEP accounting of national wetland parks, constructing the GEP accounting system for national wetland parks, exploring suitable accounting methods and data sources, and applying accounting results reasonably can not only improve the GEP accounting system and methods for specific regional units, but also explore the role of national wetland parks in socioeconomic development and ecological conservation, expand the value realization models of wetland parks such as franchising, realize the economic and market-oriented development of ecosystem products, and assist the government in building the green performance concept that integrates ecological protection, restoration, and management, and plays an important role in providing theoretical support and practical basis for exploring the value realization mechanism of GEP in national wetland parks.

Shandong Mata Lake National Wetland Park (SMTNWP), as a national ecological civilization demonstration zone of China, has a rich variety of ecosystem product types, and it is significant to clarify various ecosystem types and distribution status in the region, study and construct the GEP accounting index system for SMTNWP, determine accounting models, methods and parameters, completes ecosystem product value accounting based on biophysical value and monetary value accounting, calculate the GEP of SMTNWP, and attach the "price tag" to ecosystem products, which can provide references for exploring new paths for promoting the management and development of public and commercial ecosystem products in SMTNWP, and is of great significance for realizing the value of ecosystem products, building the unified accounting subject and system, selecting suitable evaluation methods, models and parameters for similar ecosystems, similar regions and other wetland parks in GEP accounting practice, and translating the human wellbeing of national wetland parks into quantifiable and visualized monetary value.

2 Overview of the study area and data sources

2.1 Overview of the study area

2.1.1 Natural resources conditions

SMTNWP (118°2′56.65″-118°6′47.34″E, 37°3′56.46″-37°5′37.66″N) is a scenic area of AAA level in China, located in Qifeng Town, northeast of Huantai County, Zibo City (see Figure 1). The total area of SMTNWP spans 1,021.78 ha, with a north-south span of 3.13 km and an east-west span of 5.74 km, and is part of the Xiaoqing River system in the Yellow River Basin. The overall terrain of SMTNWP is relatively flat, with fertile soil. SMTNWP receives ample sunshine, and exhibits significant seasonal variations in precipitation. Specifically, the rainfall is the most concentrated from July to October, and the dry and abundant season is more obvious. The ecosystem pattern of SMTNWP is dominated by the wetland ecosystem, with relatively rich animal and plant resources, complex plant species and high diversity.

2.1.2 Development and utilization status

SMTNWP is an important wetland and lake ecosystem in the inland regions of Shandong Province, and is one of the top ten key ecological function protection areas in Shandong Province. The park features reed marshes and lotus ponds, and along with rich cultural relics such as the Five Sages Temple, Xu Ye Bookstore, Iceberg Site, Huicheng Site, Lulian Well, and Jinqiu Pavilion in SMTNWP. The unique natural landscapes contribute to diverse cultural landscapes and folk characteristics. SMTNWP focuses on the protection and restoration of wetland ecosystems and biological habitats, adhering to the fundamental principles of "protection priority, scientific restoration, rational utilization, and sustainable development." It carries out construction projects such as protection engineering, restoration engineering, promotion, education and scientific Research,

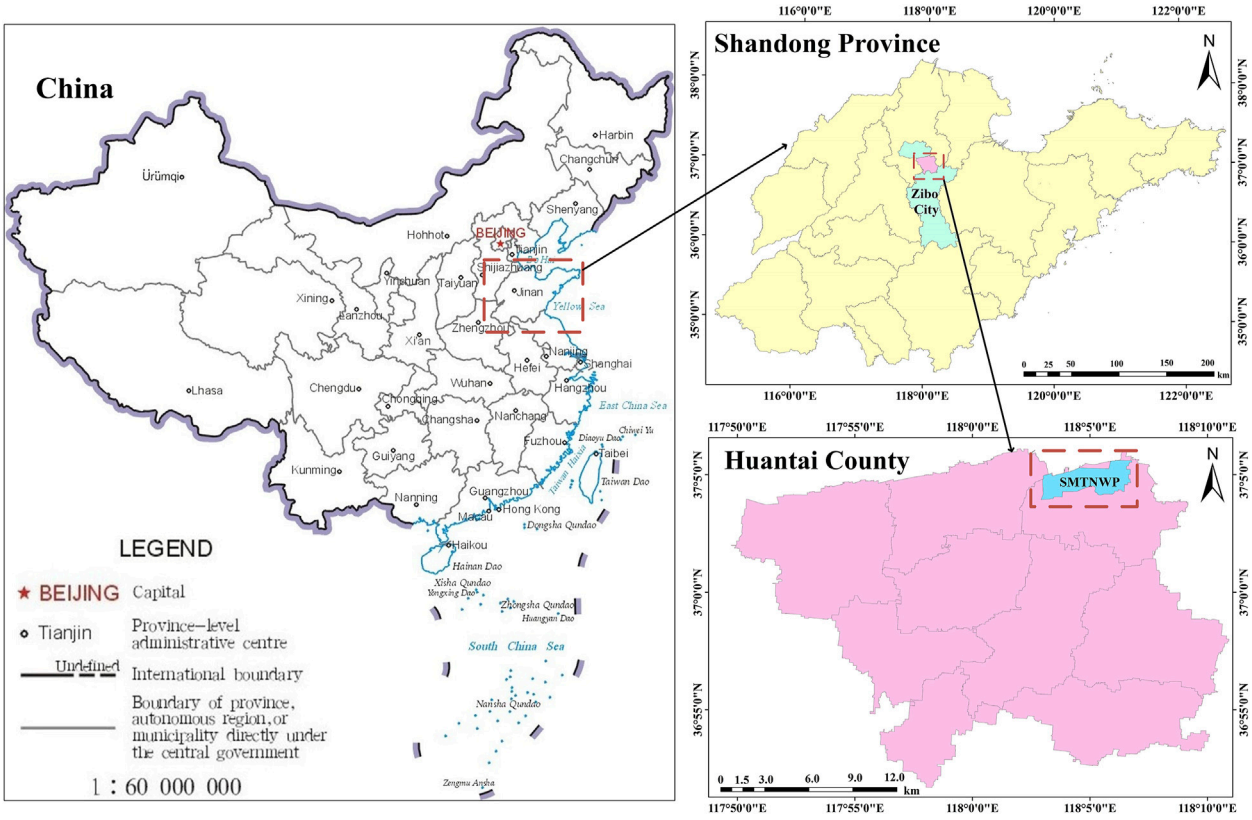

FIGURE 1
Overview of the study area (where the map of China on the left is a standard map, downloaded from the Standard Map Service System of the Ministry of Natural Resources, PRC, http://bzdt.ch.mnr.gov.cn/index.html).

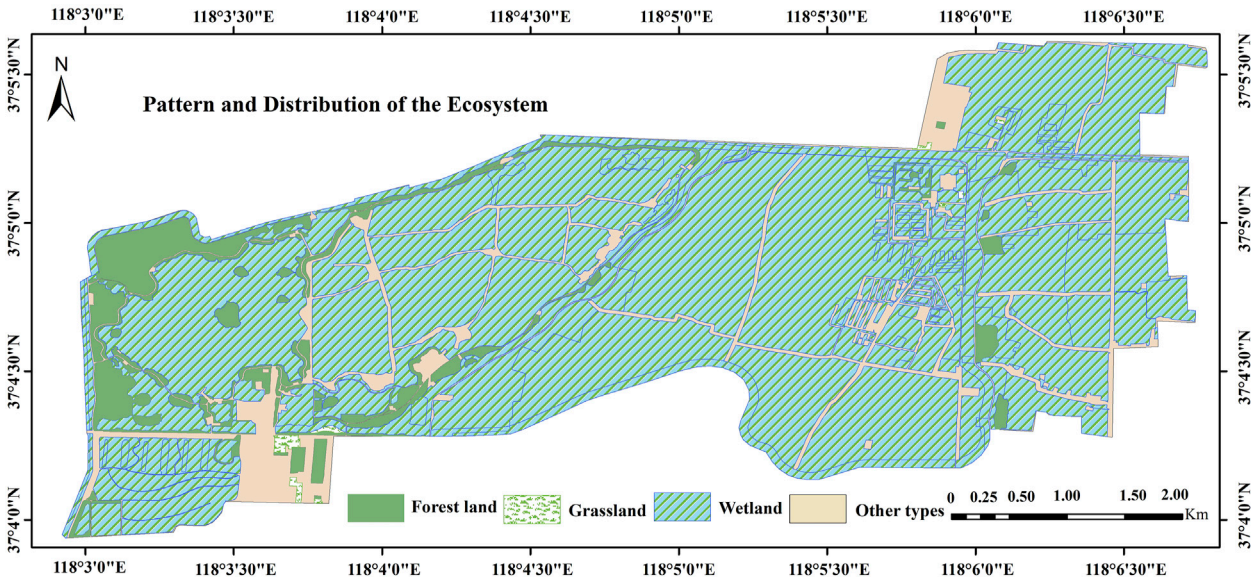

FIGURE 2
Spatial pattern of ecosystem in SMTNWP.

TABLE 1 Statistics of spatial pattern of ecosystem in SMTNWP.

Ecosystem category	Types of land use included	Area (hm^2)	Percent (%)
Grassland	Other grassland	2.78	0.27
Forest land	Other forest land	71.59	7.01
Wetland	River water surface	72.36	7.08
	Pond water surface	150.61	14.74
	Inland mudflat	613.43	60.03
Others	Other types of land use	111.02	10.87
Sum		1,021.78	100.00

infrastructure and service facilities, fully tapping into the natural and cultural landscape of SMTNWP, developing wetland ecological and cultural tourism, and attracting numerous tourists during its operation. In August 2015, SMTNWP became a member of the Yellow River Basin Wetland Protection Network. Currently, SMTNWP has been designated as the national wetland park, the national agricultural tourism demonstration site, the national water conservancy scenic area, the national ecological civilization demonstration area, the provincial-level scenic spot, the provincial-level geological park, and one of the first excellent cases of "Beautiful Rivers and Lakes" in China.

2.1.3 Spatial pattern of ecosystem

The ecosystem of SMTNWP encompasses grassland, forest land, wetland, and other types (see Figure 2; Table 1), among which the wetland ecosystem accounts for the largest proportion, with an area of 836.39 hm^2, which represents over 80% of the total area, and the inland mudflat and ponds account for a large proportion, forming an important wetland lake ecosystem. The forest ecosystem is mainly distributed in the northwest of the park, while the grassland ecosystem is mainly distributed in the southwest of the park, with sporadic distribution in the northeast. SMTNWP plays an important role in conserving regional water sources, purifying water quality, regulating regional microclimates, protecting regional ecological stability, and diluting atmospheric pollutants, in addition, it also attracts many tourists to relax, playing important natural, ecological, and social functions. Consequently, the rich and diverse ecosystem within the park provides a wide range of ecosystem services, including conservation of water sources, pollutant purification, carbon dioxide fixation and oxygen release, soil conservation, temperature regulation, flood regulation and storage, leisure and recreation, playing a significant role in ecosystem services and generating substantial potential ESV.

2.2 Data and sources

Land use data, including ecosystem spatial pattern data, are from the Natural Resources and Planning Bureau of Zibo City and the Natural Resources and Planning Bureau of Huantai County.

Meteorological data, including annual precipitation, monthly precipitation, temperature and rainstorm in the region, are from Meteorological Bureau of Huantai County, Statistics Bureau of Huantai County, National Climate Data Center (NCDC), Shandong Mata Lake Wetland Conservation Center, Shandong Mata Lake Tourism Development Co., Ltd., etc.

Field investigation data, including crown density, average depth of reservoirs, slope, expenditure on educational activities, number of tourists, ticket revenue, number of park employees and salary levels, are obtained from field research and interviews with the Shandong Mata Lake Wetland Conservation Center and Shandong Mata Lake Tourism Development Co., Ltd.

Data selected for biophysical value evaluation parameters, including pollutant purification model, carbon fixation mechanism model, oxygen release mechanism model, water quantity balance method, flood regulation and storage model, and Revised Universal Soil Loss Equation (RUSLE) used in biophysical value evaluation. The above models and methods required data including purification amount per unit area of various atmospheric and water pollutants by different ecosystems, carbon fixation rate of ecosystems, surface runoff coefficient of various ecosystems, daily rainstorm standard, rainstorm runoff regression equation of different ecosystems, soil erodibility factor and other relevant parameters. The values for these parameters are derived from the GEP accounting regulations and guidelines issued by China's national and local governments, such as the "*the Standard for the GEP Accounting (Trial)*," "*the Technical Specification for Gross Ecosystem Product (GEP) Accounting of Shandong Province of Terrestrial Ecosystem (Trial)*," "*the Technical Guidelines for the Accounting of Gross Ecosystem Product (GEP) of Terrestrial Ecosystems*," "*the Guidelines for Soil Loss Calculation of Production and Construction Projects (SL773-2018)*," and relevant literature.

Data selected for monetary value accounting parameters, including the values of pollutant treatment costs required for partial value accounting, carbon dioxide market prices, industrial oxygen production prices, reservoir unit capacity engineering costs, reservoir unit dredging engineering costs, sediment deposition coefficient, soil bulk density, and conversion coefficients for soil conservation nutrients (nitrogen, phosphorus, potassium) to urea, superphosphate, potassium chloride, etc. refer to relevant regulations such as "*the Technical Guidelines for the Accounting of Gross Ecosystem Product (GEP) of Terrestrial Ecosystems*" and literature.

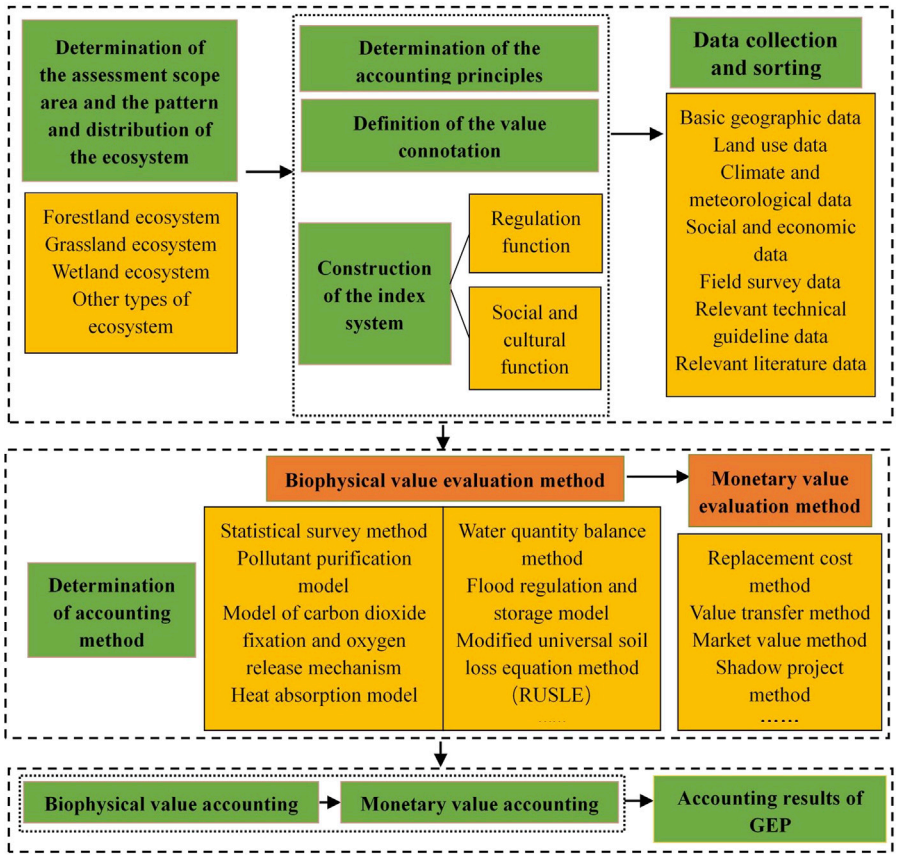

FIGURE 3
GEP accounting approach of SMTNWP.

Other data, including socio-economic data, major soil types, local electricity prices, prices of fertilizers such as urea, superphosphate, and potassium chloride, and prices of organic fertilizers, are primarily sourced from the Statistical Yearbook of Zibo City, Statistical Yearbook of Huantai County, Statistics Bureau of Huantai County, and the official website of Huantai County People's Government (http://www.huantai.gov.cn/art/2015/8/19/art_4883_928665.htm), State Grid Shandong Electric Power Company Huantai County Power Supply Company, and the website of China Report Hall (https://www.chinabgao.com/).

3 Research methods

3.1 GEP accounting approach

Firstly, determine the scope of the evaluation area and the ecosystem pattern, clarify the accounting principles, define the value connotation, construct the indicator system, and collect and organize data. The spatial scope for GEP accounting of the study is defined as SMTNWP, which encompasses an evaluation area of 1,021.78 hm^2 comprising ecosystems such as grasslands, forests, and wetlands. According to the needs of accounting, determine the accounting principles, define the timing and period of the calculated value, and clarify the connotation of the calculated value. Construct the accounting indicator system, and determine accounting subjects from the aspects of regulation function, and social and cultural function. Collect the necessary data for research in order to select appropriate localization accounting parameters.

Then, determine the methods for biophysical and monetary value evaluation. Select reasonable biophysical value accounting methods and parameters, and use models and methods including statistical survey methods, pollutant purification models, carbon dioxide fixation and oxygen release mechanism models, heat absorption models, water quantity balance methods, flood regulation and storage model, and RUSLE to evaluate the biophysical value of ecosystem products and services. Then, select reasonable value accounting methods and parameters, and use ecological economic evaluation methods such as replacement cost method, value transfer method, market value method, and shadow project method to account for the monetary value of ecosystem products and services.

Finally, calculate the GEP of SMTNWP. Calculate the biophysical value of ecosystem products and services of SMTNWP, and then calculate the monetary value based on the biophysical value accounting results, and analyze the calculation results.

The GEP accounting approach of SMTNWP is shown in Figure 3.

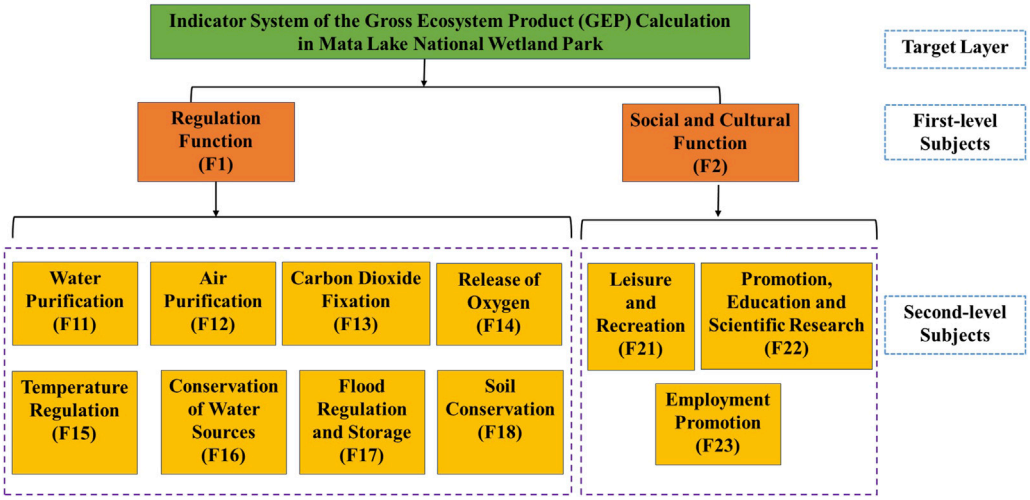

FIGURE 4
GEP accounting index system of SMTNWP.

3.2 Construction of accounting indicator system

National wetland parks, wetland nature reserves, protected communities, wetland wildlife habitats, and wetland multi-purpose management areas jointly constitute the wetland protection and management system. Different from the general meaning of protected areas, national wetland parks refer to wetland areas with wetland landscapes as the main body, wetland ecosystem protection and restoration as the core, and taking into account promotion, education and scientific research, ecological tourism and other activities of wetland ecosystem, and they contain certain cultural and aesthetic values and are artificially protected and managed, so their connotation is richer than that of general protected areas. As a result, national wetland parks not only provide supply and regulation value for wetland ecosystems, but also offer cultural values such as leisure and recreation, and promotion, education and scientific research. Additionally, the operation, maintenance and management of national wetland parks can also provide employment opportunities and generate certain social value.

SMTNWP has geological and geomorphological relics such as lakes, swamps, gullies, and hilly areas, as well as various natural ecological landscapes such as hydrology, celestial phenomena, reed marshes, lotus ponds, and bird habitats. The natural landscape is unique, the biodiversity is rich, and it has the charm of fishermen and historical and cultural relics. It integrates natural scenery, water landscape, historical sites, architectural sites, and water town charm. Therefore, it has important regulation, and social and cultural functions. Considering that SMTNWP is currently a profitable ecotourism park with limited material resources, the supply service function is not currently being considered.

On the basis of the systematic review of more than 10 GEP accounting technical specifications and guidelines issued in China and various cities both within and outside Shandong Province, this study follows the principles of objectivity, scientificity, practicability, systemization, step by step, based on exchange value, openness, etc., and comprehensively considers the consensus degree of accounting subjects to construct the GEP accounting index system of SMTNWP (see Figure 4). Due to SMTNWP being a wetland park, mainly consisting of grasslands, forests, and wetlands, ecological functions closely related to grasslands, forests, and wetlands were selected as the secondary accounting subjects for regulation functions. Considering that SMTNWP has carried out promotion, education and scientific research, and eco-tourism activities related to wetland ecosystems, providing certain employment opportunities, so the leisure and recreation indicators, etc., have been selected as the corresponding secondary accounting subjects for social and cultural functions. The final accounting index system consists of two first-level subjects of regulation function, and Social and cultural function, and 11 second-level subjects such as water purification, air purification, etc. The index system aims to reflect the real, specific and relatively stable value of the functional attributes of each ecosystem in the study area, and defines the connotation of each second-level accounting subject (see Table 2).

3.3 Determination of biophysical and monetary value accounting indicators

Based on the construction of first-level and second-level subjects, clarify the biophysical and monetary value accounting indicators and their units for GEP accounting of SMTNWP (see Table 3).

4 Accounting methods and result analysis

4.1 Accounting methods

4.1.1 Definition of GEP connotation

In the study, the GEP accounting period of SMTNWP is 2021, with a cycle of 1 year. The GEP connotation refers to the total value of various final products and services provided by various ecosystems within SMTNWP for human wellbeing and sustainable economic and

TABLE 2 Definition of GEP accounting subject connotations based on human wellbeing of SMTNWP.

Second-level Subjects		Connotation
F11	Water Purification	Wetland ecosystems including rivers, lakes, and swamps absorb, degrade, biologically transform, and transform water pollutants through physical and biochemical processes, thereby reducing the concentration of water pollutants and purifying the water environment (Wu et al., 2020)
F12	Air Purification	Ecological systems, such as forests, grasslands, and wetlands absorb, filter, block, and decompose atmospheric pollutants, thereby reducing the concentration of air pollutants, and enhancing air quality (Kong et al., 2023)
F13	Carbon Dioxide Fixation	Forests, grasslands, wetlands, and other ecosystems utilize organisms to synthesize organic matter from carbon dioxide or dissolve carbon dioxide in water bodies, thereby reducing concentration of carbon dioxide in the atmosphere (Wang, J. M. et al., 2019)
F14	Release of Oxygen	Forests, grasslands, wetlands, and other ecosystems release oxygen through plant photosynthesis, to maintain stable oxygen concentration in the atmosphere (Wang, J. M. et al., 2019)
F15	Temperature Regulation	Ecosystems such as forests and grasslands absorb energy through vegetation transpiration, occlusion, and evaporation, thereby regulating temperature and enhancing the comfort of human living environments (Zhao et al., 2019)
F16	Conservation of Water Sources	Ecosystems such as forests, grasslands, and wetlands intercept and store precipitation, enhance soil infiltration and accumulation, thereby achieving the goal of conserving soil moisture, replenishing groundwater, regulating surface runoff and river flow, and effectively redistributing precipitation (Hu et al., 2021)
F17	Flood Regulation and Storage	Forests, grasslands, reservoirs, lakes, and other ecosystems absorb and store precipitation, regulate stormwater runoff, reduce flood peak during rainstorm, to mitigate the threat and loss caused by flood peak in flood season and mitigate flood hazards (Ping and Zeng, 2023)
F18	Soil Conservation	Ecosystems such as forests and grasslands slow down the erosion of topsoil by rainwater, and increase soil resistance by retaining soil through root systems, thereby reducing sedimentation and soil loss, and maintaining soil nutrients (Wang W. J. et al., 2022)
F21	Leisure and Recreation	Wetland parks provide services such as recreation, sightseeing, entertainment, and landscape appreciation, allowing visitors to relax mentally and achieve non-material benefits such as emotional pleasure (Liu et al., 2023)
F22	Promotion, Education and Scientific Research	Wetland parks provide public education and promotion of wetland functions and values to the public, while universities and research institutions can conduct comprehensive studies on wetland ecology, and provide venues and services for educational and scientific research activities (Liu et al., 2023)
F23	Employment Promotion	Wetland parks require social labor for their daily management and operation, providing employment opportunities for relevant groups (Li et al., 2020)

social development in 2021, including the monetary value of natural elements and final services provided by various ecosystems such as grasslands, forests, and wetlands in the region related to their regulatory and socio-cultural functions. The GEP accounting process involves both biophysical and monetary value assessments.

4.1.2 Biophysical value accounting methods

4.1.2.1 Biophysical value of regulation function accounting methods

The wetland ecosystem area of SMTNWP comprises more than 80% of the total park area, and can play a role in adsorbing, degrading, and converting water pollutants such as COD, total nitrogen, and total phosphorus. This study calculates the water purification capacity of the ecosystem to characterize the amount of pollutants purified by the wetland ecosystem.

The ecosystems of SMTNWP, including grassland, forest, and wetland comprise nearly 90% of the entire park, and can absorb, filter, block, decompose, and reduce atmospheric pollutants such as SO_2, NO_2, and dust, playing a role in air purification. This study calculates the air purification capacity of ecosystems to characterize the amount of pollutants purified by ecosystems.

The ecosystems of SMTNWP, including forest, grassland, and wetland utilize photosynthesis to absorb carbon dioxide and mitigate greenhouse effects. This study quantifies the total amount of carbon dioxide fixation through the carbon sequestration mechanism model.

Plant photosynthesis facilitates the release of 1 mol of O_2 for every 1 mol of CO_2 absorbed. SMTNWP is abundant in plant resources, enabling significant oxygen release, which is beneficial for maintaining the stability of oxygen in the atmosphere and improving the living environment. This study calculates total amount of oxygen supply through the oxygen release mechanism model.

The ecosystems of SMTNWP, including forest and grassland absorb solar energy through transpiration and evaporation to regulate temperature and improve living environment comfort. This study calculates the total heat absorbed by ecosystems through the heat absorption model.

The ecosystems of SMTNWP, including forest, grassland, and wetland can conserve soil moisture, regulate rainstorm runoff, supplement groundwater, supplement water resources, and play the role of water conservation. This study uses the water quantity balance method and flood regulation model to separately calculate the flood regulation and storage capacity of vegetation, reservoirs, and rivers and lakes.

The forests and grasslands of SMTNWP can reduce soil erosion and sediment deposition through the role of ecosystems, while maintaining soil nutrients and playing a role in soil conservation.

TABLE 3 Biophysical and monetary value accounting indicators and units of SMTNWP's GEP.

First-level subjects	Second-level subjects	Biophysical value indicators		Monetary value indicators	
		Indicator description	Unit	Indicator description	Unit
F1	F11	Total amount of COD, total phosphorus, and total nitrogen for purifying water pollutants	t/a	Water purification value	CNY
	F12	Total amount of SO_2, NO_2, and dust for purifying air pollutants	t/a	Air purification value	
	F13	Total amount of carbon dioxide fixation	t·CO_2/a	Carbon dioxide fixation value	
	F14	Total amount of oxygen supply	t·O_2/a	Oxygen release value	
	F15	The total heat absorbed by ecosystems	kW·h	Temperature regulation value	
	F16	Total amount of water sources conservation	m^3/a	Conservation of water sources value	
	F17	Total amount of flood regulation and storage	m^3/a	Flood regulation and storage value	
	F18	Total amount of ecosystem's soil conservation	t/a	Sediment accumulation reduction value	
				Soil fertility preservation value	
F2	F21	Total amount of leisure and recreation personnel	person/a	Leisure and recreation value	
	F22	Activities carried out for promotion, education and scientific research	—	Promotion, education and scientific research value	
	F23	The total number of social labor engaged in wetland park related work	person/a	Employment promotion value	

This study uses the RUSLE method to calculate biophysical value of soil conservation function.

The accounting methods of the biophysical value of regulation functions are shown in Supplementary Table S1.

4.1.2.2 Biophysical value of social and cultural function accounting methods

4.1.2.2.1 Biophysical value accounting of leisure and recreation function. SMTNWP not only boasts a unique ecological and geographical environment, but also possesses a rich historical and cultural heritage, wetland landscapes, and cultural resources. According to surveys, there are more than 2,100 boat lanes of various sizes in the lake area of the park, interconnected both vertically and horizontally, forming a complex network. There are 30 bridges of different shapes and colors, 7 pavilions, 5 islands in the lake, 16 docks, and 10 boardwalks. The ecological and cultural landscapes have attracted many tourists to visit and have certain leisure and recreational functions. This study uses the total number of leisure and recreation people in the accounting year, namely the park pedestrian flow (ESQ_9), as the biophysical value accounting indicator of leisure and recreation function, and it was about 740,000 people in the year 2021.

4.1.2.2.2 Biophysical value accounting of promotion, education and scientific research function. SMTNWP has also carried out multiple publicity and popularization activities on wetland functions and values for the public, providing a comprehensive knowledge research and practical platform for wetland ecology for college students, and has certain promotion, education and scientific research functions.

4.1.2.2.3 Biophysical value accounting of employment promotion function. SMTNWP provides employment opportunities for surrounding residents through its daily management and operation process, and thereby promoting local employment. This study employs the number of social laborers engaged in related work of the wetland park throughout the accounting year (ESQ_{11}) as biophysical value accounting indicator of employment promotion function. In 2021, there were 67 social laborers engaged in related work of the wetland park.

The above data related to the biophysical value accounting of social and cultural function are all collected from on-site data by the Shandong Mata Lake Wetland Conservation Center and Shandong Mata Lake Tourism Development Co., Ltd.

4.1.3 Monetary value accounting methods

Based on biophysical value accounting, ecological economics methods, including replacement cost method, value transfer method, market value method, and shadow project method are employed to assess the monetary value of the regulation function, and statistical survey method, travel expense method, and other methods are used to calculate the monetary value of social and cultural function (see Supplementary Table S2).

4.2 Analysis of accounting results

4.2.1 Comprehensive analysis of GEP total value

The monetary value accounting for was conducted based on the biophysical value accounting of various ecological functions of SMTNWP in 2021, and subsequently, the proportion of the value

TABLE 4 Biophysical and monetary value accounting results of various ecosystem products in SMTNWP.

First-level Subjects	Second-level Subjects	Biophysical Value Indicators	Biophysical Value	Monetary Value Indicators	Monetary Value ($\times10^4$ CNY)	Percent (%)	Total Monetary Value ($\times10^4$ CNY)	Total proportion (%)
F1	F11	COD purification capacity/(t/a)	923.63	COD purification	480.29	6.42	587.68	7.85
		Total phosphorus purification capacity/(t/a)	71.59	Total phosphorus purification	35.80	0.48		
		Total nitrogen purification capacity/(t/a)	71.59	Total nitrogen purification	71.59	0.96		
	F12	SO_2 purification capacity/(t/a)	61.55	SO_2 purification	18.47	0.25	20.70	0.28
		NO_2 purification capacity/(t/a)	1.73	NO_2 purification	0.69	0.01		
		Dust purification capacity/(t/a)	90.56	Dust purification	1.54	0.02		
	F13	Total amount of carbon dioxide fixation/(t/a)	2098.81	Carbon dioxide fixation	12.42	0.17	12.42	0.17
	F14	Total amount of oxygen supply/(t/a)	1,526.41	Oxygen release	152.64	2.04	152.64	2.04
	F15	Total heat absorbed by ecosystems/(kW·h)	319,522.19	Temperature regulation	17.47	0.23	17.47	0.23
	F16	Total water sources conservation capacity/ ($\times10^4$ m^3/a)	198.04	Conservation of water sources	1,210.14	16.17	1,210.14	16.17
	F17	Total flood regulation and storage capacity/ ($\times10^4$ m^3/a)	600.21	Flood regulation and storage	3,667.68	49.01	3,667.68	49.01
	F18	Total ecosystem's soil conservation capacity/(t/a)	9,211.83	Sediment accumulation reduction	2.99	0.04	143.15	1.91
				Soil fertility preservation	140.16	1.87		
F2	F21	Total amount of leisure and recreation personnel/ ($\times10^4$ person/a)	74.00	Leisure and recreation	968.73	12.95	968.73	12.95
	F22	Activities carried out for promotion, education and scientific research	—	Promotion, education and scientific research	166.56	2.23	166.56	2.23
	F23	Total number of social labor engaged in wetland park related work/ (person/a)	67.00	Employment promotion	536.00	7.16	536.00	7.16
Total					7,483.17	100.00	7,483.17	100.00

of each second-level subject to the total GEP value was calculated (see Table 4). It is evident that in 2021, SMTNWP fully realized its regulation and socio-cultural functions of ecosystem products, with a total GEP of CNY 74.8317 million and a unit area GEP of 73,200 CNY/hm^2. Specifically, the value of regulation function, and social and cultural function were CNY 58.1188 and 16.7129 million, respectively.

The ranking of the value of first-level subjects in GEP accounting is as follows: regulation function > social and cultural function. The ranking of the value of second-level subjects in GEP accounting is as follows: flood regulation and storage > conservation of water sources > leisure and recreation > water purification > employment promotion > promotion, education, and scientific research > release of oxygen > soil conservation > air purification > temperature regulation > carbon dioxide fixation. From the perspective of some lowest-level indicators, in terms of water purification function, the ranking of the value is as follows: the purification of COD > the purification of total nitrogen > the purification of total phosphorus water pollutants; in terms of air purification function, the ranking of the value is as follows: the purification of SO_2 > the purification of dust > the purification of NO_2; in terms of soil conservation function, the ranking of the value is as follows: the maintaining of soil fertility > the reducing of sediment deposition.

Overall, the flood regulation and storage function holds the highest value, accounting for nearly 50%; the values of conservation of water sources, and leisure and recreation are both relatively high, each exceeding 10% of the total; the values of promotion, education and scientific research, release of oxygen, and soil conservation are average, with significant room for improvement; the values of air purification, temperature regulation, and carbon dioxide fixation are relatively low, offering the greatest potential for exploration.

In recent years, SMTNWP has intensified its investment in technology and engineering. By implementing water system connectivity projects, dredging of the river channel, and seasonal diversion of the Yellow River project, the water use of wetlands in the park have been effectively regulated, ensuring abundant water supply throughout the year and enhancing the function of the conservation of water sources. By implementing sewage control and interception projects, and the artificial wetland project such as artificial wetlands at the entrance of Zhulong River and Wuhe River, and based on the existing natural wetlands, the SMTNWP has aimed to improve the biodiversity and system stability of the wetland ecosystem through ecological restoration or moderate artificial reinforcement measures, enhance the level of water purification function, and sewage has been turned into "treasures." The projects not only ensured the daily supply of water to the wetlands in the park, but also improved water quality and enhanced the water resources situation. In addition, the constructions of vegetation restoration projects and bird habitat improvement projects have made the regional microclimate in the park increasingly prominent, and the temperature regulation function has become more prominent. The increase in the number of wild animals and plants, particularly bird populations, has not only created a high-quality environment for their growth and reproduction, but also transformed the park into a wintering ground and migration hub for various bird species.

"The Overall Plan of Shandong Mata Lake National Wetland Park" proposes to carry out the construction of wetland promotion, education and exhibition facilities and activities, to show the natural landscape, cultural landscape, wetland culture, and wetland functions of SMTNWP to the public. The plan includes constructing the Mata Lake Wetland Experience Hall, Reed Sculpture Garden, Artificial Wetland Water Purification Exhibition Area, Wetland Resources Exhibition Area, Bird Watching Pavilion and other facilities. The construction of these facilities will not only promote wetland education, but also attract more tourists to come and watch, enhancing the value of leisure, and recreation, and promotion, education and scientific research. At present, SMTNWP is conducting scientific research cooperation with some universities in Shandong Province. The university research teams has taken SMTNWP as the study area to investigate and study wetland soil, hydrology, water quality, wildlife and plants, aquatic organisms, and other wetland resources. Researches on the planting of aquatic plants in artificial wetlands is carried out, and plans are proposed to establish wetland water quality monitoring points, plant observation points, bird observation points, management centers, comprehensive monitoring rooms, research centers, etc. The above constructions of wetland monitoring facilities are conducive to enhancing the value of promotion, education and scientific research.

It is evident that after years of implementing a series of wetland protection, restoration technologies and engineering measures in the park, as well as investing in publicity, education, scientific research and service facilities projects, the ecosystem functions and ecological environment of SMTNWP have been significantly optimized. The value of social and cultural function, including leisure and recreation, promotion, education and scientific research, and employment promotion has also been fully demonstrated, and especially the value of regulating ecosystem products has been fully realized. Due to the decrease in the number of tourism and employment during the COVID-19 epidemic in 2021, the value of social and cultural function accounting is not high. Wetland protection and economic development need to be coordinated. The development of tourism formats and the increase in the number of tourists will bring challenges to wetland ecosystem protection and rational utilization of wetland resources. Balancing economic and social development and sustainable utilization of wetlands, and balancing regulation function and enhancement of social and cultural function value represented by leisure and recreation function are of great significance to promote the GEP enhancement and value realization of SMTNWP.

4.2.2 Analysis of each GEP value component

4.2.2.1 Analysis of regulation function value

The value of SMTNWP's regulation function ecosystem products is CNY 58.1188 million, accounting for 84.91% of the total GEP. The main value components are values of flood regulation and storage, and conservation of water sources, which are CNY 36.6768 million and 12.1014 million, respectively, accounting for 49.01% and 16.17% of the total GEP. The wetland ecosystem of the park covers an area of 836.39 hm^2, accounting for more than 80%. There are also grassland, woodland and other types of ecosystems, which rely on its unique hydrological and physical properties, the park absorbs and accumulates precipitation during rainstorm, mitigating potential flood peak losses, and can also regulate storm runoff, reduce flood peak, mitigate flood hazards, conserve

water and increase available water resources. At the same time, ecosystems such as forests and grasslands also account for a large proportion in SMTNWP, and they rely on the structure and processes of the canopy layer, litter layer, root system, and soil layer to intercept and store precipitation, enhance soil infiltration and accumulation, conserve soil moisture, supplement groundwater, fully regulate surface runoff and river discharge, play the function of accumulation and redistribution of precipitation, and also alleviate the threat and loss caused by flood peaks during the flood season, reduce flood hazards, and effectively play the ecological regulatory role of precipitation accumulation and redistribution. In addition, the abundant water resources of SMTNWP enable the full adsorption, degradation, biological absorption or transformation of water pollutants such as COD, total nitrogen, and total phosphorus, reducing pollutant concentrations and purifying the water environment, playing an important role in water quality purification, especially in purifying COD. Therefore, the value of COD purification is also significant.

However, other ecosystem products of regulation function such as air purification, carbon sequestration, oxygen release, temperature regulation, and soil conservation have also improved local microclimates, optimized the air environment, and enhanced the comfort of the park environment. However, the value of their ecosystem products is not relatively high, and their effectiveness requires further enhancement. Affected by factors such as increased use of fertilizers and pesticides on surrounding farmland and increased human activities in cities, the water quality and ecological environment of SMTNWP need to be protected, and pollution control should be the key focus. Otherwise, it will affect the enhancement of the functional values such as air purification, carbon dioxide sequestration, and release of oxygen.

4.2.2.2 Analysis of social and cultural function value

The value of social and cultural ecosystem products is CNY 16.7129 million, accounting for 15.09% of the total. The primary components are the values of leisure and recreation, and employment promotion, which are CNY 9.6873 million and 5.36 million respectively, representing 12.95% and 7.16% of the total GEP. Leisure and recreation are important cultural and ecosystem products of SMTNWP. The SMTNWP boasts a unique ecological environment, advantageous geographical location, and a rich historical and cultural heritage, featuring diverse wetland landscapes and cultural resources. There are numerous boat lanes of different sizes in the lakes of the park, connected vertically and horizontally, interweaving into a network. There are also bridges, pavilions, islands in the lake, docks, and boardwalks of various shapes and colors, with "Jiangnan in the North" as the tourism feature. The lake water in the park is rippling with blue waves, and plant landscapes such as reed marshes, lotus ponds, roadside lotus trees, and willows are distributed, and the poetic and wild charm is strong, and the rich cultural relics such as the Five Sages Temple, Xu Ye Bookstore, and Iceberg Site in the park enhance the cultural heritage. Ecotourism is conducted with a focus on natural ecology and regional cultural characteristics. Adhering to the principles of environmental protection and sustainable development. While ensuring ecological benefits, it also creates huge economic benefits and plays a significant role in value generation. In addition, SMTNWP is operated and managed by Shandong Mata Lake Tourism Development Co., Ltd., providing employment opportunities such as promotion, planning and tourism service management for surrounding residents, increasing employment opportunities for residents, maintaining social stability, and playing a certain social function. However, affected by the COVID-19 in the year 2021, the number of tourists and employees has decreased, the value of ecosystem products for leisure and recreation, and employment promotion was relatively low, and the value of social and cultural function still have greater room for improvement.

SMTNWP has also played a notable role in promotion, education and scientific research value, actively distributing promotional materials, setting up exhibition boards, carrying out publicity activities such as World Wetland Day, World Wildlife Day, and laws related to wetland conservation, conducting research activities related to water resources protection, organizing publicity activities such as the Wetland Photography Competition, Knowledge Competition of SMTNWP, and Style Painting and Calligraphy Exhibition, which have been reported by mainstream media multiple times. SMTNWP has actively provided publicity and science popularization lectures on wetland functions and values to the public, while also invested in the development and construction of a wetland experience hall, which is open to the public, aiming to promote wetland functions and wetland protection knowledge. Additionally, Shandong Mata Lake Tourism Development Co., Ltd. has collaborated with two universities to provide social practice, curriculum practice, and research platforms for university students, supporting teaching and research activities, and playing a crucial role in scientific research. However, the implementation of wetland science popularization and education activities and the fulfillment of wetland park social responsibility require a certain period. It is understood that the number of educational activities currently carried out in SMTNWP are still relatively small, and there is a relative lack of professional activity planning and wetland protection personnel. The facilities and equipment for wetland monitoring and protection are not advanced enough. Therefore, the value of promotion, education and scientific research is only 1.6656 million yuan, indicating significant potential for further exploration and improvement.

5 Discussion and conclusion

5.1 Discussion

5.1.1 Study value

In the context of the current government performance evaluation model, which primarily focuses on GDP as the core indicator, the introduction of GEP accounting adds a critical layer of insurance for local ecological protection, evaluates the contribution of natural ecosystems to human wellbeing, improve the evaluation system of composite ecosystems including the aspects of social, economic, and natural, and help decision-makers recognize the monetary value and importance of ecosystem products. GEP accounting provides essential references for government asset management, enabling local governments to seek economic development from the perspective of harmonious coexistence

between humans and nature, transforms the erroneous behaviors of neglecting any aspect in economic development and ecological protection, and makes GEP accounting results a hard constraint and direction guide for government decision-making. It transforms the "GDP only" performance view, achieving balanced accounting, operation, and dual improvement of GDP and GEP. China is constantly improving the value accounting scheme of ecosystem products, promoting the realization of the value of ecosystem products, and taking the development path of ecological protection and economic development that complement each other, and the behaviors are all beneficial explorations of ecological civilization construction, and important practices of implementing the concept of green development, promoting high-quality development, and can help to realize Chinese modernization.

National wetland parks in China serve as key specific geographical units for natural resource protection and ecological security, providing robust ecosystem products and services for economic and social development, and containing enormous value of ecosystem products. In the conservation practice of national wetland parks, faced with the trade-off between the interests of resource development and construction, and park production and operation, it is necessary to transform the human wellbeing of national wetland parks into quantifiable and visualized monetary values, and to fully understand the potential value of wetland parks for ecological conservation and socioeconomic development. GEP accounting at the scale of national wetland parks is a fundamental component of the value realization mechanism for ecosystem products. It is imperative to conduct accounting studies, develop an evaluation index system, clarify accounting process standards and parameter selection, and enhance the application of value accounting results. Efforts should be made to integrate accounting results into the evaluation system of national wetland park contributions and performance, promote accounting results into planning, projects, decision-making, and policies, provide a basis for government green performance and ecological protection effectiveness assessment, and promote the overall value realization of ecosystem products through the value realization of national wetland parks' ecosystem products.

5.1.2 Study characteristics

This study aims to address the practical needs of GEP accounting at the specific regional unit scale of national wetland parks, as well as the relatively weak status of related studies. By constructing the GEP accounting index system of SMTNWP and using ecological economics methods to account for the monetary value based on biophysical value accounting, the GEP of SMTNWP has been calculated. Prior to GEP accounting, this study considered the provision of educational facilities and promotional activities in the development, construction, and daily operation of national wetland parks, and incorporated the value of promotion, education and scientific research into the GEP accounting indicator system. Given that the management and operation of wetland parks require social labor engaged in related work, providing certain employment opportunities and exerting certain social value, the employment promotion value has been included in the GEP accounting indicator system. In the process of GEP accounting, giving the characteristics of specific regional unit scale of the study area, utilizing small-scale statistical data and monitoring data obtained from field investigations, combining with accurate land use data provided by relevant government departments, this study has scientifically selected evaluation models and methods to form the GEP accounting parameter database of SMTNWP by referring to several GEP accounting procedures and guidelines issued at the national and local levels in China, and relevant researches at home and abroad, and efforts have been made to achieve scientific GEP accounting as much as possible.

5.1.3 Study suggestions

The GEP accounting results indicate that after years of development, construction, and specialized management, SMTNWP has achieved significant progress in ecological security, ecological tourism development, park operation and management, publicity and market promotion, and the values of regulation and socio-cultural functions are relatively high. In the future, it is recommended to continue to strengthen professional, scientific, and standardized operation and management, strengthen supervision of park operation companies' activities related to wetland park construction and management, ensure that SMTNWP enhances and fully utilizes its ecological functions on the basis of water quality safety and ecological safety, prevent the value of ecosystem products from decreasing, and promote the improvement of SMTNWP's ecosystem product values, such as air purification, temperature regulation, and carbon dioxide fixation. Additionally, the brand value and comprehensive benefits of national wetland parks should be enhanced, and teaching and research academic exchange platforms should be established to continuously improve their value of promotion, education and scientific research. It is necessary to ensure the protection and benign utilization of wetland parks, guarantee the virtuous cycle and sustainable development of their ecological functions, to achieve the unity of ecological, social and economic benefits, and a favorable situation of coordinated and win-win protection and development.

The goal of conducting GEP accounting for national wetland parks is to establish a mechanism for realizing the value of ecosystem products of national wetland parks. Propose the following policy recommendations to promote the realization of ESV for national wetland parks. Firstly, clarify the wetland ecosystem product system and accurately evaluate the ESV of various ecosystem functions. National wetland parks should have a clear understanding of the ecological resources, gradually form a list and database of ecosystem products, accurately calculate the GEP level, clarify the ownership, utilization, and contracted management rights of ecological resources on the premise of protecting ecological functions, free up management rights, vigorously develop ecological industries, such as weaving reeds, grass, wood, willows, and cattails within the wetland area into various storage products and decorative items, gradually forming an ecological industry chain, and promoting the green transformation of the industry. Secondly, innovate the ecological compensation and trading modes of wetland carbon sinks based on the value of wetland carbon dioxide sequestration and oxygen release functions. Establish a diversified ecological protection and restoration investment mechanism, coordinate wetland resources within the region, utilize wetland parks for "wetland carbon dioxide sequestration," unify storage and

collection through the "Two Mountains Bank," build a wetland carbon trading platform, and encourage market entities to actively participate in the purchase of carbon dioxide sequestration indicators. Thirdly, encourage multi-party participation in the operation and management of national wetland parks, and improve the market operation mechanism. Under the main responsibility of the government to build the national wetland parks, enterprises and other social capital should be properly introduced to create franchised ecological products, and multiple entities should participate in the operation, investment, development and construction, so as to jointly build and share the value of ecosystem products, support the surrounding residents to actively participate in the operation and management of the wetland park tourism industry, and promote the realization of the common prosperity goal. Fourthly, actively develop and broaden the new tourism formats of the wetland parks. Relying on the natural and cultural landscape of wetlands, develop wetland ecological culture tourism, improve infrastructure, layout wetland related tourist attractions, plan tourist routes, actively carry out wetland ecological protection science popularization and public welfare activities, promote the value transformation and appreciation of ecosystem products, and guard against tourism damaging the ecological environment around the wetland parks. Fifthly, strengthen the construction of wetland related research platforms. Forming think tank resources in the fields of ecological function enhancement, GEP accounting, ecological protection and restoration management, realization and appreciation of the ESV, and development and utilization of ecological resources for wetland parks.

5.1.4 Study prospects

SMTNWP, as a special regional unit, differs from a complete administrative unit. In terms of obtaining localized parameters, SMTNWP lacks relevant small-scale statistical yearbook data for direct reference, which makes the calculation relatively challenging. For example, data such as the number of lake water changes, the average content of nitrogen, phosphorus, potassium, and organic matter in soil are difficult to collect and investigate in the field. The selection of universal parameters will affect the accuracy of accounting results and increase the uncertainty of accounting results. In this study, the GEP accounting index system was established according to the characteristics of the study area and the collection of data. However, SMTNWP is not limited to the GEP accounting subjects quantified in this study, for example, in the accounting process, the quantification and expression of characteristic cultural services and products have not fully been considered, especially in terms of the more scientific and accurate quantification methods for social and cultural functional values such as promotion, education, and scientific research, and employment promotion, and the pertinence of the accounting results needs to be improved. Therefore, in the future, in-depth studies will be strengthened in the selection of accounting indicators and precision determination of parameters, and according to the characteristics of the study area, accounting subjects that can reflect the characteristics of ecosystem products will be selected to achieve the comprehensive GEP characteristic expression of specific regional units; various models, methods and parameters should be applied to conduct GEP accounting, and the optimal models, methods and parameters should be screened to achieve accurate GEP accounting for specific regional units, and the GEP accounting results for different years will be timely updated, the accounting results will be compared to analyze the temporal evolution characteristics of GEP for specific regional units.

5.2 Conclusion

This study selected SMTNWP as the research area, analyzed the spatial pattern of ecosystems, constructed the GEP accounting index system that included regulation, and social and cultural functions, determined biophysical and monetary value accounting indicators, methods and models, and used ecological economics related methods to calculate the total GEP of SMTNWP in the year 2021 as CNY 74.8317 million and a unit area GEP of 73,200 CNY/hm^2. A comprehensive analysis of the total GEP value and each GEP value component was conducted. The study aims to provide support and references for the construction of unified accounting subjects and systems for similar ecosystems and national wetland parks, and provide theoretical basis for quantifying the human wellbeing of national wetland parks, better utilizing the overall ecosystem value of wetlands, helping to realize the value of ecosystem products, and further promoting the transformation of ecological value and economic benefits, and the following conclusions were drawn:

(1) In terms of ecosystem spatial pattern, the SMTNWP encompasses grassland, forest land, and wetlands, with wetlands constituting the predominant type, covering more than 80% of the park's total area. Wetland and lake ecosystems play an important role in conserving water sources, purifying water quality, regulating regional microclimates, protecting regional ecological stability, and diluting atmospheric pollutants.
(2) In terms of constructing the GEP accounting indicator system and its results, the system comprises 2 first-level subjects, including regulation function, and social and cultural function, and 11 second-level subjects such as water purification and air purification. Based on biophysical value accounting, ecological economics methods are used to calculate the monetary value. Overall, the flood regulation and storage function holds the highest value, followed by water conservation and leisure and recreation, which have relatively high values., the values of promotion, education and scientific research, release of oxygen, and soil conservation are all average, while those for air purification, temperature regulation, and carbon dioxide fixation are relatively low.
(3) In terms of regulation function value, due to the natural background ecological conditions of SMTNWP and the construction of wetland protection and restoration engineering measures in the later stage, the value of ecosystem products related to park regulation functions is high, which is the core part of ecosystem product supply. Due to the extensive coverage of the wetland ecosystem in SMTNWP, the values of flood regulation, and conservation of water sources account for more than 60% of the total. The

value of the ecological function that the wetland plays the major role is relatively high, which fully reflects that the wetland ecosystem, as a "natural sponge" and "kidney of the earth," plays an important role in accumulating and redistributing precipitation, absorbing and storing precipitation, regulating rainstorm runoff, reducing flood peaks, conserving water sources, and improving water quality.

(4) In terms of social and cultural functional value, leisure and recreation, and employment promotion values are the main components of SMTNWP's social and cultural ecosystem product value. Since the park's development and construction, Shandong Mata Lake Wetland Conservation Center and Shandong Mata Lake Tourism Development Co., Ltd. have actively developed cultural tourism while ensuring ecological stability. On the basis of protecting and restoring the wetland ecosystem of the park, they have fully explored the natural and cultural landscapes, developed ecological and cultural tourism of the wetland, carried out wetland park sightseeing experience activities, provided certain employment opportunities, and generated substantial ecological and social benefits.

(5) In terms of future GEP improvement, among SMTNWP's regulating ecosystem products, the values of air purification, temperature regulation, and carbon dioxide fixation functions are relatively low and have the greatest potential for exploration. There is significant room for improvement in the value of promotion, education and scientific research of social and cultural ecosystem products. Relevant wetland management departments should continue to implement wetland protection, restoration technologies and engineering measures, continuously improve the ecosystem and ecological environment of the park, enhance the comfort of the environment, and promote the value improvement of air purification, temperature regulation, and carbon dioxide fixation. Simultaneously, these departments can accelerate the scientific research work related to the wetland ecosystem of the park, actively build the platform for scientific research and academic exchanges, strengthen cooperation with relevant colleges and social groups, continue to carry out investigation and monitoring of wetland resources, make full utilization of wetland investigation and monitoring results to guide the protection, management and operation of the park, thereby promoting the continuous improvement of the value of SMTNWP's promotion, education and scientific research functions.

Data availability statement

The original contributions presented in the study are included in the article/Supplementary Material, further inquiries can be directed to the corresponding authors.

Author contributions

JL: Conceptualization, Data curation, Formal Analysis, Methodology, Software, Validation, Writing–original draft, Writing–review and editing. MX: Conceptualization, Data curation, Formal Analysis, Investigation, Methodology, Software, Visualization, Writing–original draft. AW: Conceptualization, Data curation, Funding acquisition, Investigation, Project administration, Resources, Supervision, Validation, Writing–review and editing. TS: Conceptualization, Data curation, Funding acquisition, Investigation, Project administration, Resources, Supervision, Writing–review and editing. CZ: Investigation, Resources, Supervision, Writing–review and editing. XC: Investigation, Resources, Supervision, Writing–review and editing. PZ: Data curation, Investigation, Supervision, Writing–review and editing.

Funding

The author(s) declare that financial support was received for the research, authorship, and/or publication of this article. This research was funded by Shandong Natural Science Foundation (grant number: ZR2019MD014), and the Pilot Technical Service Inventory Project of Natural Resource Assets Inventory of the Whole People of Shandong Province—Research on the Technical Method of Typical Wetland Replacement Price Estimation (grant number: SDGP370000000202202001746F_001).

Acknowledgments

We thank the reviewers for their useful comments and suggestions. We thank the Shandong Agricultural University for the assistance with equipment. Some field investigation data are obtained from field research and interviews with the Shandong Mata Lake Wetland Conservation Center and Shandong Mata Lake Tourism Development Co., Ltd., and we thank them for some necessary data. We thank the Shandong Institute of Territorial and Spatial Planning for the support of the project.

Conflict of interest

Author CZ was employed by Shandong Deyun Land Real Estate Appraisal Consulting Co., Ltd.

The remaining authors declare that the research was conducted in the absence of any commercial or financial relationships that could be construed as a potential conflict of interest.

Publisher's note

Supplementary material

The Supplementary Material for this article can be found online at: https://www.frontiersin.org/articles/10.3389/fenvs.2025.1500075/full#supplementary-material

References

Chen, Q. R., Wu, M. Y., and Xie, H. L. (2023). Value realization of ecological products of wetland resources: basic logic, core mechanism and mode. *J. Nat. Resour.* 38, 2490–2503. doi:10.31497/zrzyxb.20231005

Chen, Z. X., and Zhang, X. S. (2000). The value of ecosystem benefits in China. *Chin. Sci. Bull.* 45, 17–22+113.

Cheng, J., Liu, S. S., Huang, C. B., Wang, L. C., Liu, Z. L., and Peng, C. H. (2024). Impacts of environmental and socioeconomic factors on gross ecosystem product of the Three Gorges reservoir area, China. *Land Degrad. Dev.* 35, 2824–2839. doi:10.1002/ldr.5098

Costanza, R., d'Arge, R., de Groot, R., Farber, S., Grasso, M., Hannon, B., et al. (1997). The value of the world's ecosystem services and natural capital. *Nature* 387, 253–260. doi:10.1038/387253a0

Fan, Y., Zheng, Y., Jia, C. G., and Song, Y. T. (2024). The impact of China's urbanization on ecosystem service value from the perspective of gross ecosystem product: a case study of Beijing-Tianjin-Hebei region. *Sci. Rep.* 14, 15954. doi:10.1038/s41598-024-64655-8

Gao, P., and Zhu, P. X. (2024). Research on the driving mechanism of ecological product value realization: a fsQCA analysis of 37 typical cases. *China Land Sci.* 38, 114–124. doi:10.11994/zgtdkx.20240507.105536

Hu, Q. P., Lu, C. Y., Chen, T. T., Chen, W. T., Yuan, H. M., Zhou, M. X., et al. (2023). Evaluation and analysis of the gross ecosystem product towards the sustainable development goals: a case study of Fujian Province, China. *Sustainability* 15, 3925. doi:10.3390/su15053925

Hu, W. M., Li, G., and Li, Z. N. (2021). Spatial and temporal evolution characteristics of the Water conservation function and its driving factors in regional lake wetlands—two types of Homogeneous Lakes as examples. *Ecol. Indic.* 130, 108069. doi:10.1016/j.ecolind.2021.108069

Hui, X. X., Xu, X. C., and Zhu, L. (2024). Ecological product value accounting: review, problems and countermeasures. *Stat. Res.* 41, 13–28. doi:10.19343/j.cnki.11-1302/c.2024.07.001

Ji, L., Qi, Y. J., Jiang, Q. O., and Zhao, C. H. (2024). Spatial–temporal variations of the gross ecosystem product under the influence of the spatial spillover effect of urbanization and ecological construction in the Yangtze River Delta region of China. *Land* 13, 778. doi:10.3390/land13060778

Jiang, H. Q., Wu, W. J., Wang, J. N., Yang, W. S., Gao, Y. M., Duan, Y., et al. (2021). Mapping global value of terrestrial ecosystem services by countries. *Ecosyst. Serv.* 52, 101361. doi:10.1016/j.ecoser.2021.101361

Jiang, X. W., and Dong, C. (2024). Fine evaluation of ecological service functions in alpine and deep valley regions: a case study of the southeast Tibetan Plateau. *Ecol. Indic.* 163, 112047. doi:10.1016/j.ecolind.2024.112047

Kong, F. B., Wang, N., Xu, C. Y., Lu, Y., and Shen, Y. Q. (2023). Impact of value realization of forest ecological products on urban-rural income gap in 26 mountainous counties of Zhejiang Province. *Sci. Silvae Sin.* 59, 44–58. doi:10.11707/j.1001-7488.LYKX20220776

Li, A. L., Yang, Y. H., Niu, L. D., Luo, H. C., and Chi, H. X. (2024). Discriminating the non-coordination between ecosystem service value and economic development and its spatial characteristics in central Yunnan urban agglomeration in the recent 30 years. *Front. Ecol. Evol.* 12, 1366458. doi:10.3389/fevo.2024.1366458

Li, M. Q., Liu, F. L., and Huang, D. L. (2020). Study on employment of indigenous residents in national park from the perspective of ecological civilization—based on field investigation in Shennongjia National Park. *Saf. Environ. Eng.* 27, 1–5+25. doi:10.13578/j.cnki.issn.1671-1556.2020.01.001

Li, X. K., Lei, L., and Li, J. T. (2023). Integrating ecosystem service value into the evaluation of sustainable land use in fast-growing cities: a case study of Qingdao, China. *Ecol. Indic.* 153, 110434. doi:10.1016/j.ecolind.2023.110434

Li, Y., and Xie, H. (2024). Spatial–temporal variation and correlation analysis of ecosystem service values and ecological risks in winter city Shenyang, China. *Sci. Rep.* 14, 18182. doi:10.1038/s41598-024-67651-0

Li, Y. H., Wang, H. R., Liu, C. J., Sun, J. H., and Ran, Q. C. (2024). Optimizing the valuation and implementation path of the gross ecosystem product: a case study of Tonglu County, Hangzhou City. *Sustainability* 16, 1408. doi:10.3390/su16041408

Li, Y. Y., Xiong, K. N., Zhang, W. F., Song, S. Z., and Luo, L. (2023). Analyzing characteristics of grassland gross ecosystem product to inform decision making in the karst desertification control. *Agronomy* 13, 1861. doi:10.3390/agronomy13071861

Liu, J., Chen, X., Chen, W. F., Zhang, Y., Wang, A. L., and Zheng, Y. F. (2023). Ecosystem service value evaluation of saline-alkali land development in the Yellow River Delta—the example of the Huanghe Island. *Water* 15, 477. doi:10.3390/w15030477

Ouyang, Z. Y., Song, C. S., Zheng, H., Polasky, S., Xiao, Y., Batemane, I. J., et al. (2020). Using gross ecosystem product (GEP) to value nature in decision making. *Proc. Natl. Acad. Sci. U. S. A.* 117, 14593–14601. doi:10.1073/pnas.1911439117

Ouyang, Z. Y., Zhu, C. Q., Yang, G. B., Xu, W. H., Zheng, H., Zhang, Y., et al. (2013). Gross ecosystem product: concept,accounting framework and case study. *Acta Ecol. Sin.* 33, 6747–6761. doi:10.5846/stxb201310092428

Pema, D., Xiao, Y., Ouyang, Z. Y., and Wang, L. Y. (2017). Gross ecosystem product accounting for the garzê Tibetan autonomous prefecture. *Acta Ecol. Sin.* 37, 6302–6312. doi:10.5846/stxb201607011362

Ping, W. Y., and Zeng, K. (2023). Study on value accounting of ecological products from the perspective of national accounting: a case study of Jiangxi Province. *Stat. Decis.* 39, 17–22. doi:10.13546/j.cnki.tjyjc.2023.23.003

Shen, Y. Q., Yi, X., Chen, M., and Ouyang, Z. Y. (2024). Gross ecosystem product accounting in Miyun County: the supply and use of ecosystem services. *Front. Ecol. Evol.* 12, 1367768. doi:10.3389/fevo.2024.1367768

Sun, Z. H., Xue, W., Kang, D. Z., and Peng, Z. H. (2024). Assessment of ecosystem service values of urban wetland: taking east lake scenic area in wuhan as an example. *Land* 13, 1013. doi:10.3390/land13071013

Wang, F., Zhang, S. L., Hou, H. P., Yang, Y. J., and Gong, Y. L. (2019). Assessing the changes of ecosystem services in the Nansi Lake wetland, China. *Water* 11, 788. doi:10.3390/w11040788

Wang, J. M., Wu, S. Q., Cui, P., and Lei, J. C. (2019). Assessment on forest ecosystem service value in Wuma River Basin. *J. Guizhou Norm. Univ. Nat. Sci. Ed.* 37, 49–55. doi:10.16614/j.gznuj.zrb.2019.04.009

Wang, L. Y., Su, K., Jiang, X. B., Zhou, X. B., Yu, Z., Chen, Z. C., et al. (2022). Measuring gross ecosystem product (GEP) in Guangxi, China, from 2005 to 2020. *Land* 11, 1213. doi:10.3390/land11081213

Wang, W. J., Lu, F., and Ouyang, Z. Y. (2022). Spatial identification of territory space ecological conservation and restoration: a case study of Beijing. *Acta Ecol. Sin.* 42, 2074–2085. doi:10.5846/stxb202103150692

Wang, W. L., Xu, J., Luan, X. F., and Zhang, Z. M. (2024). Wetland ecosystem service values in Beijing significantly increased from 1984 to 2020: trend changes, type evolution, and driving factor. *Ecol. Indic.* 166, 112235. doi:10.1016/j.ecolind.2024.112235

Wu, B., Li, Y. L., Zhao, Q. Y., Zhang, W. Z., and Lu, R. C. (2020). The service value and driving mechanism of coastal wetland ecosystem in Beibu Gulf of Guangxi. *Ecol. Econ.* 36, 151–157.

Xie, G. D., Zhen, L., Lu, C. X., Xiao, Y., and Chen, C. (2008). Expert knowledge based valuation method of ecosystem services in China. *J. Nat. Resour.* 23, 911–919.

Zhang, L. B., Chen, X., Liang, T., Wang, H., Hao, C. Z., Ren, Y. F., et al. (2023). Research progress, problems and prospects of ecosystem products value accounting in China. *Res. Environ. Sci.* 36, 743–756. doi:10.13198/j.issn.1001-6929.2023.02.01

Zhang, S. W., Huang, C. Q., Li, X. S., and Song, M. L. (2024). The spatial–temporal evolution and influencing factors of the coupling coordination of new-type urbanization and ecosystem services value in the Yellow River Basin. *Ecol. Indic.* 166, 112300. doi:10.1016/j.ecolind.2024.112300

Zhao, W., Wen, F. P., Zhang, L. B., Gao, Y. N., and He, Y. L. (2019). Quantifying the cooling effects of the green vegetation in Xiamen City and its dynamics. *Res. Environ. Sci.* 32, 85–94. doi:10.13198/j.issn.1001-6929.2018.06.20

Zheng, H., Wu, T., Ouyang, Z. Y., Polasky, S., Ruckelshaus, M., Wang, L. J., et al. (2023). Gross ecosystem product (GEP): quantifying nature for environmental and economic policy innovation. *Ambio* 52, 1952–1967. doi:10.1007/s13280-023-01948-8

frontiers | Frontiers in Environmental Science

TYPE Original Research
PUBLISHED 30 January 2025
DOI 10.3389/fenvs.2024.1530694

OPEN ACCESS

EDITED BY
Chunhui Li,
Beijing Normal University, China

REVIEWED BY
琳琳 夏,
Guangdong University of Technology, China
Rui Wang,
Chinese Academy of Sciences (CAS), China

*CORRESPONDENCE
Liming Dong,
donglm@btbu.edu.cn

RECEIVED 19 November 2024
ACCEPTED 30 December 2024
PUBLISHED 30 January 2025

CITATION
Cui G, Wang H, Li X, Li W, Li H and Dong L (2025) Agricultural structure management based on water–energy–food and carbon sink scenarios in typical fuel ethanol raw material planting areas—a case study of the Hulan River Basin, Northeast China.
Front. Environ. Sci. 12:1530694.
doi: 10.3389/fenvs.2024.1530694

Agricultural structure management based on water–energy–food and carbon sink scenarios in typical fuel ethanol raw material planting areas—a case study of the Hulan River Basin, Northeast China

Guannan Cui[1,2,3], Haitao Wang[1,2,3], Xiaofei Li[1,2,3], Wenchao Li[1,2,3], Huijie Li[4] and Liming Dong[1,2,3]*

[1]Department of Environmental Science and Engineering, Beijing Technology and Business University, Beijing, China, [2]State Environmental Protection Key Laboratory of Food Chain Pollution Control, Beijing Technology and Business University, Beijing, China, [3]Key Laboratory of Cleaner Production and Integrated Resource Utilization of China National Light Industry, Beijing Technology and Business University, Beijing, China, [4]School of Public Administration, Jilin University, Changchun, China

The implementation of Chinese policies promoting fuel ethanol has significantly influenced the land use structure, water resources, and soil environment in ethanol raw material planting areas. This paper focuses on the Hulan River Basin, a benchmark region for maize cultivation, to investigate the specific crop allocation issues in relation to the impact of land use changes on water quality. The study projects an environmentally and economically sustainable structure for the cultivation of fuel ethanol raw materials using the CLUE-S model and multiple linear programming. Additionally, the carbon sequestration potential is assessed under different scenarios. Throughout the study period, the net ecosystem productivity (NEP) in the Hulan River Basin demonstrated variability, evidenced by a decrease of 33.96 $gC{\cdot}m^{-2}{\cdot}a^{-1}$ from 2010 to 2015 and a subsequent augmentation of 55.64 $gC{\cdot}m^{-2}{\cdot}a^{-1}$ from 2015 to 2020. Furthermore, the three scenarios (Grain Crop Priority Policy, Fuel Ethanol Crop Priority Policy, and Carbon Storage Priority Policy) effectively addressed the requirements for land use/cover types and enhanced carbon sequestration within the study area. Consequently, the outcomes provide a conceptual foundation for regional policymakers, providing insights into the refinement of land use within ethanol crop zones and fostering the advancement of the fuel ethanol industry, thus undergirding prospective land use strategies and refinement from the water, energy, food, and carbon perspectives.

KEYWORDS

agricultural crop structures, non-point source pollution, land use/cover, maize, CLUE-S

Abbreviations: NEP, net ecosystem productivity; ET, evapotranspiration; TN, total nitrogen; TP, total phosphorus; ROC, receiver operating characteristic; NPP, net primary productivity; RH, fraction of photosynthetic products consumed by soil heterotrophic respiration.

Highlights

- The variation in crop water demand within the Hulan River Basin is relatively small, indicating a limited disparity in water requirements among different agricultural crops.
- The carbon sink exhibits distinct seasonal fluctuations, with the winter season experiencing a comparatively lower level.
- The scenario simulation not only reduces regional non-point source pollution and increases water storage capacity but also enhances the regional carbon sink, providing a theoretical basis for optimizing the structure of ethanol raw material cultivation.

1 Introduction

In September 2017, following approval from the State Council, a coalition of 15 ministries, including the National Development and Reform Commission, unveiled the "Plan for the Expansion of Biofuel Ethanol Manufacturing and the Advancement of Vehicle Ethanol Gasoline Use." This plan emphasized the need for a robust expansion of advanced bioliquid fuels, such as cellulosic ethanol, to accommodate the market's ongoing demand. The strategy also set ambitious targets to ensure that ethanol-blended gasoline is universally available for vehicles by 2020 and to scale up the production of cellulosic ethanol by 2025. The aim is to position the technology, equipment, and industry at the forefront globally while establishing a more comprehensive, market-driven operational framework. However, in 2017, China's biofuel ethanol output was a modest 33.12×10^6 m^3, representing just 3% of the global output. With an annual gasoline production surpassing 104 million tons, biofuel ethanol constituted a mere 2% of the total gasoline production (Mao et al., 2018). This indicates that the potential for biofuel ethanol growth in China is vast. Yet, the bioenergy policy's backing could result in the preferential cultivation of energy crops like corn, cassava, and sugarcane, potentially impacting the planting areas for other crops and altering the internal structure of arable land. The extensive influence of human activities on land use has become a pivotal factor in the non-point source pollution of regional water environments. At present, China predominantly utilizes first-generation biofuel ethanol, predominantly derived from corn. Consequently, this study has chosen to focus on the corn cultivation base in Heilongjiang Province, China.

China, a nation with scarce water reserves, must prioritize the strategic planning and rational distribution of water resources to ensure sustainable agricultural water conservation (Yue et al., 2018). Research on agricultural water-saving in typical biological ethanol fuel planting areas should start with understanding the water requirement of crops. Evapotranspiration (ET) of plants refers to the total amount of water required by plants throughout their entire growth cycle (Wei et al., 2018). The water demand at different stages of crop growth is related to the transpiration and growth coefficient of crops, and the calculation of transpiration requires the Penman–Monteith formula (Schmidt and Zinkernagel, 2017). The growth coefficient is not only related to crop types, but it is also influenced by the geographical location of crops. Therefore, many studies have used remote sensing (Hassan et al., 2022) technology to study crop water demand on a large scale. In addition to the issue of agricultural water-saving, the control of agricultural non-point source pollution is also a current hot topic. Xu et al. (2022) pointed out that agricultural non-point source pollution is the most significant obstacle to the green development of agriculture and the ecological protection of planting areas. Agricultural non-point source pollution is characterized by significant randomness in its formation process, complex influencing factors, a wide distribution range, and a profound impact. The formation process is complex, and the mechanism is vague. Due to its long incubation period and significant harm (Chen and Fu, 2000), its pollutants can enter the water system from the soil through irrigation, resulting in excessive nitrogen and phosphorus content in rivers (Wang et al., 2019). In the field of agricultural non-point source pollution, research by He et al. (2022) has proved that the main pollutants of agricultural non-point source pollution are total nitrogen (TN) and total phosphorus (TP), which are also the main governance objects in the control of agricultural non-point source pollution. China's growing population and urbanization highlight the need for sustainable management of water, energy, food, and carbon resources. A multi-objective optimization model incorporating carbon emissions and sequestration was developed to optimize crop structure and water allocation (Li et al., 2024; Wu et al., 2025). This model provides scientific support for regional green development and sustainable resource allocation strategies applicable to similar areas.

To achieve the two major goals of agricultural water-saving and non-point source pollution control mentioned above, it is necessary to optimize the allocation of land use. Land use/cover layout refers to the spatial distribution of different types of land use and is an important basis for spatial regulation in land use planning. A large amount of research has proven that changes in land use, especially in a short period of time, can greatly affect the ecosystem of a certain region, thereby changing the environmental level of the region (Ndegwa Mundia and Murayama, 2009). Therefore, analyzing the environment from the perspective of land use change is one of the mainstream entry points for the current large-scale regional environment (Wu et al., 2024). In order to better regulate various types of land use within the research area, mainstream researchers have used many software programs to assist (Zhang et al., 2013) in establishing data models to better evaluate watershed ecological issues from a macro perspective (Li and Zhang, 2019), including SWAT (Liu et al., 2014; Ahmed et al., 2022) and InVEST (Liang et al., 2017; Zhao et al., 2019). In this experiment, another small-scale land use change model (CLUE-S) is used, which offers the advantages of simple model principles and high accuracy. Many current studies have used this model (Peng et al., 2020; Liu and Wang, 2021; Zhao et al., 2019). Based on the CLUE-S model and combined with SPSS, a known study area is predicted and simulated using the method of multi-objective linear programming to obtain the optimal balance between ecological environment protection and economic development (Zhou et al., 2021; Su et al., 2024). This study calculates the water demand for the entire growth cycle of crops in typical fuel ethanol raw material crop planting areas. It analyzes the land use changes in the research area in recent years, combining social and economic factors such as policy restrictions and economic benefits, as well as natural factors such as geographical characteristics and crop characteristics, to find the optimal land

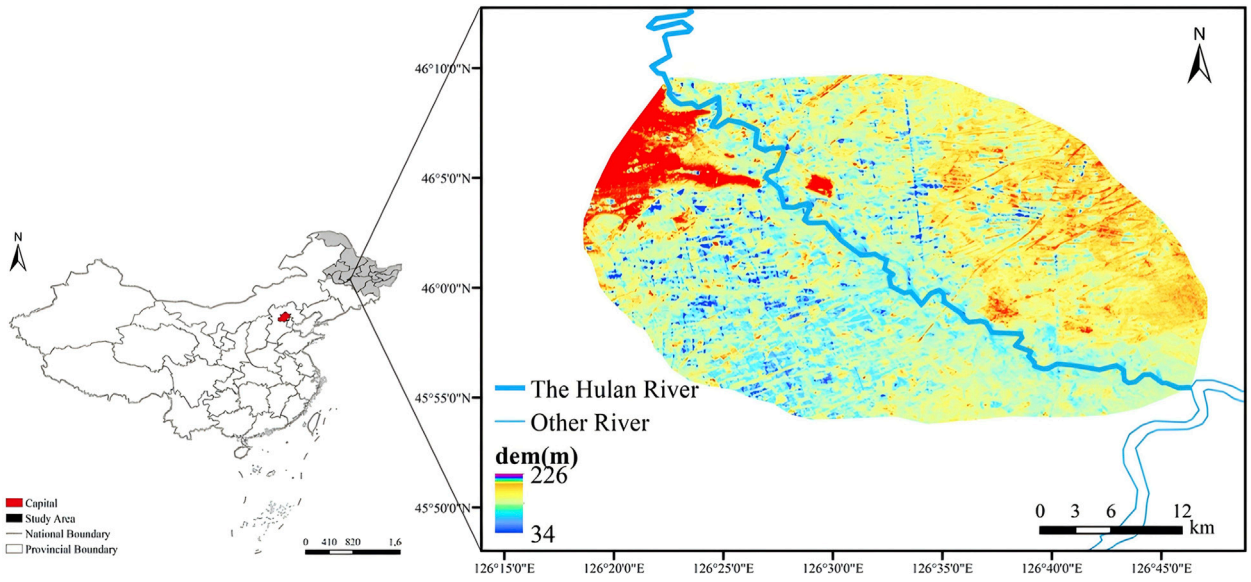

FIGURE 1
Overview of the maize planting area in the Hulan River Basin.

use method that meets policy and environmental quality requirements. It provides a reference basis for the ecological environment protection and economic development of fuel ethanol crop planting areas in the future. The research content is mainly divided into the following three parts:

(1) Analysis of the water demand of main crops in the Harbin section of the Hulan River Basin.
(2) According to the policy requirements, hydrological constraints, environmental requirements, and social and economic benefits, objectives and constraints are established through multi-objective linear programming, and the carbon storage of various crops in the study area is quantified under different scenario assumptions to determine the optimal land use allocation in the study area.
(3) Using the CLUE-S model, the land use situation in 2015 is simulated based on the land use situation in 2010. When the Kappa coefficient verifies the effectiveness of the model simulation, the obtained optimal land use situation in the study area is substituted to obtain a visualized land use optimization design for the 2030 study area.

This study divides cultivated land into crop levels to provide a scientific basis and more detailed management suggestions for local agricultural land planning and soil management.

2 Materials and methods

2.1 Overview of the study area

The Harbin section of the Hulan River Basin is located in the middle of Heilongjiang Province, covering an area of 856 km^2. The Hulan River is a tributary of the Songhua River and flows from northwest to southeast in the study area, with a total length of approximately 35 km. The region is located between 45°50′–46°10′ and between 126°15′–126°50′ (Figure 1) (Wang et al., 2021). The selected area is a typical maize-growing area. The wet season in Heilongjiang is from June to September; therefore, the main planting period for crops in this research area is from May to October. The main land use in the Hulan River Basin was cultivated land. The percentage area of farmland was 75.6%, and the irrigated farmland was 3.8%. The occupied areas of construction land and river land were 7.9% and 5.6%, respectively. The topography of the research area was plain, and the soil fertility was higher. The main soil types in the maize-growing area were black soil and meadow soil. There were several maize alcohol producers in the research area.

Based on the distinct characteristics of the wet season in the region, the Penman–Monteith formula (ElNesr and Alazba, 2012) was used to calculate the water demand of the main crops in the region, and the results were used for subsequent land use/cover planning in Equation 1:

$$ET_0 = \frac{0.408\Delta(R_n - G) + \gamma\, 900u_2\,(e_s - e_a)/(T_{mean} + 273)}{\Delta + \gamma\,(1.034u_2)}, \quad (1)$$

where ET_0 is reference crop evapotranspiration, mm/d; R_n is net surface radiation, MJ/(m^2·d); G is the soil heat flux MJ/(m^2·d); T_{mean} is the daily average temperature, °C; U_2 is the wind speed at a height of 2 m, m/s; e_s is the saturated water pressure, kPa; e_a is the actual water pressure, kPa; Δ is the slope of the saturated water pressure curve, kPa/°C; and γ is the constant of hygrometer, kPa/°C.

According to the different stages of crop growth (initial, mid-growth, maturity, etc.), K_c for different growth periods was obtained by referring to the crop coefficient table provided by FAO, and the actual crop evapotranspiration (ET_c) was then calculated using Equation 2:

$$ET_c = ET_0 \times K_c, \quad (2)$$

where ET_c is actual crop evapotranspiration, mm/d.

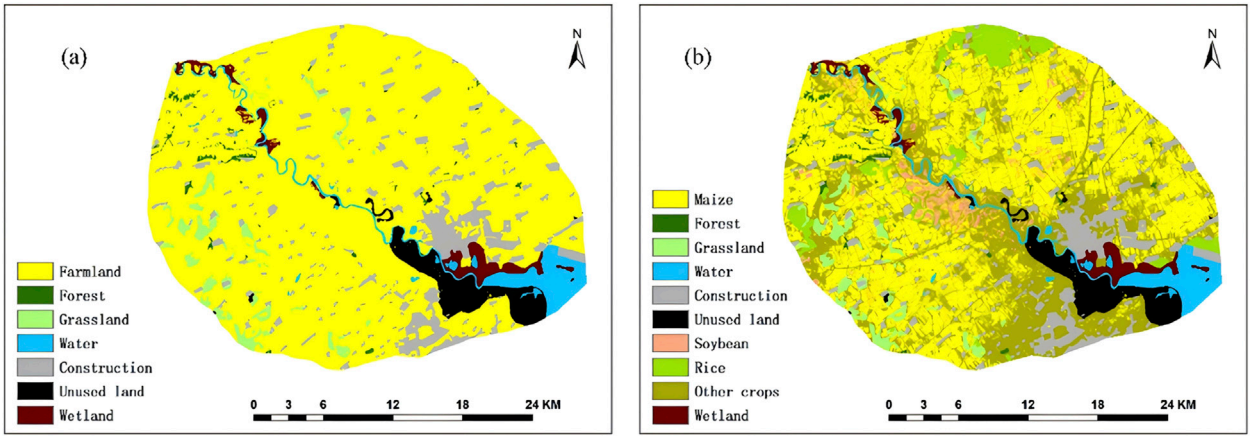

FIGURE 2
Land use/cover situation of the Hulan River research area in 2020. **(A)** The first-level classification, **(B)** The second-level classification.

The deduction of effective precipitation (P_e) was calculated using Equation 3:

$$P_e = P \times \text{Utilisation factor}, \quad (3)$$

where P is the total precipitation, mm. The utilization factor is determined by factors such as soil type and topography.

Based on P_e obtained from the abovementioned calculation, the irrigation water requirement (IWR) was calculated using Equation 4:

$$IWR = ET_c - P_e, \quad (4)$$

where the irrigation water requirement is recorded as 0 (no irrigation required) when $P_e > ET_c$.

2.2 Interpretation of land use

Landsat-TM remote sensing image data with cloud volume ≤5% from 2010 to 2020 were downloaded from the official website of NASA. The downloaded remote sensing image data were preprocessed by radiometric calibration, atmospheric correction, band synthesis, and image clipping. According to the classification system of the Chinese Academy of Sciences (CAS), land use was divided into farmland, forest, grassland, water, construction, unused land, and wetland (the first-level classification). Because of the different crop phenology information, the farmland in the Hulan River Basin was further divided into maize, soybean, rice, and other crops (the second-level classification). The spatial distribution maps of land use types were visualized using ArcGIS.

Due to the construction of a wetland park at the Hulan River Estuary in the Hulan River research area in 2018, there was a significant error in constructing the model using the 2020 land use/cover situation. Therefore, the actual model was constructed using the land use/cover change situation from 2010 to 2015, and the 2020 land use/cover situation was selected as the initial state for future simulation. Figure 2A shows the land use/cover situation under the first-level classification of the Hulan River research area in 2020, and Figure 2B shows the land use/cover situation under the second-level classification of the same area in 2020.

2.3 CLUE-S model construction

The CLUE-S framework is designed to analyze transformations in land use and land cover within a defined geographical area. It integrates physical and environmental factors with socio-economic influences to provide a comprehensive understanding of the spatial and temporal dynamics of land use and land cover. Developed by a team of researchers from Wageningen University in the Netherlands, led by P.H. Verburg, the CLUE-S builds upon the foundational work of its predecessor, the CLUE model. The model posits that regional shifts in land use and land cover are propelled by the demand for these uses and covers, with their distribution in equilibrium with regional land demand, as well as the natural and socio-economic context. Utilizing systems theory, the CLUE-S model manages the competitive interactions between various types of land use and land cover, enabling the concurrent simulation of their changes. The theoretical underpinnings of the CLUE-S model encompass the interconnectivity, stratification, rivalry, and relative stability inherent in land use and land cover transitions.

2.3.1 Selection and testing of driving factors

The driving factor is an important part of the CLUE-S model. Selecting driving factors that are highly correlated with the research area for simulation can provide a more accurate analysis of land use change in the region. The research area for land use/cover simulation should have no less than seven driving factors, including two categories: natural driving factors and humanistic driving factors. The determination of seven driving factors in the Hulan River research area is shown in Table 1.

The receiver operating characteristic (ROC) curves are instrumental in assessing the precision of selected drivers in simulating land use transitions within a study region. Figure 3 illustrates the ROC curves for various land uses in the Hulan River study area, with values spanning from 0.5 to 1, indicating their fitness for evaluation. A higher value signifies a greater capacity to explain the data. The figure reveals seven distinct land use/cover categories in the area, with water and construction land uses exhibiting perfect explanatory power, as indicated by an ROC value of 1. Wetlands have an ROC value of 0.94, indicating a strong explanatory capacity, while unused land and

TABLE 1 Selection of driving factors for the research area.

Hulan River research area	Natural driving factors			
	DEM	Slope	Slope direction	Distance from water
	Social driving factors			
	Distance from road	Distance from construction		Gross agricultural product

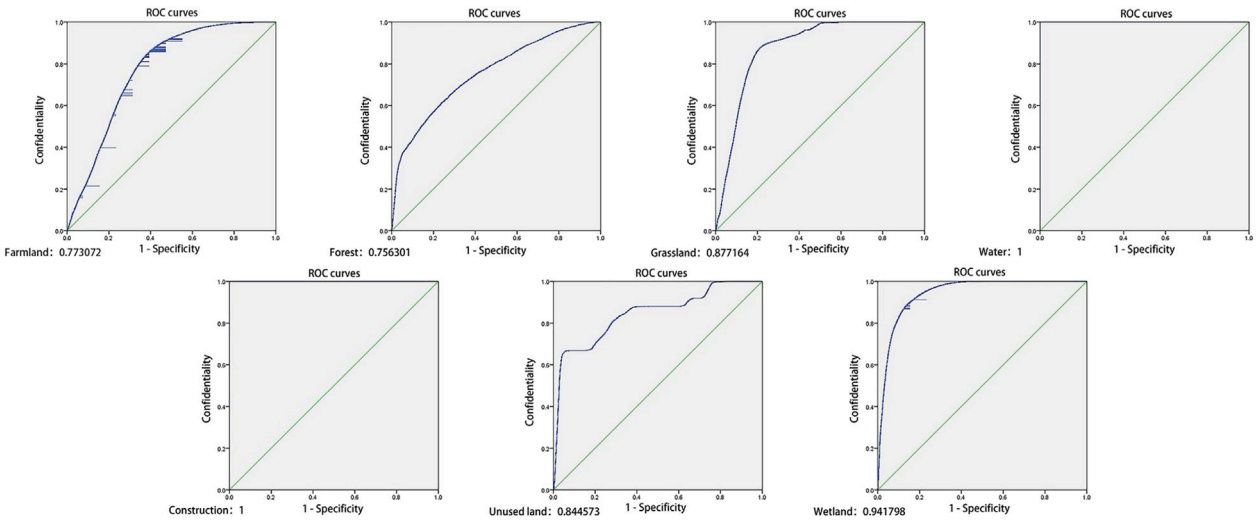

FIGURE 3
ROC curves of each land use type in the Hulan River research area.

TABLE 2 Various documents required to build the CLUE-S model.

File name	Document content
cov.x.x	Land use/cover in the initial year
demand.in	Various land demands year by year
region.fil	Restricted area
sclgr.fil	Driving factor
allow.txt	Land transfer matrix
allocl.reg	Logistic regression coefficient
main.txt	Main parameter file

grasslands have values of 0.84 and 0.88, respectively, also demonstrating robust explanatory power. The ROC values for arable land and forests are comparatively lower, at 0.77 and 0.76, yet they still surpass the commonly accepted threshold of 0.75 for strong explanatory power. Consequently, a thorough analysis indicates that the model developed in this study possesses commendable explanatory capabilities.

2.3.2 Model file settings

The CLUE-S model includes a non-spatial analysis module and a space allocation module. The non-spatial analysis module is used to calculate the demand quantity of each category in the study area in the target year, which needs to be calculated by external models or mathematical methods. The spatial allocation module is based on the input of land demand parameters and the spatial distribution characteristics of driving factors and iteratively allocates the land category ownership of grid units, thereby achieving spatiotemporal simulations of land categories for each year. Table 2 shows all the space allocation module files required for the CLUE-S model.

By comparing the land transfer situation in the Hulan River research area between 2010 and 2015, combined with other existing studies, the conversion elasticity of the Hulan River research area is set as shown in Table 3.

2.4 Estimation of Net ecosystem productivity

Net ecosystem productivity (NEP) is the difference between the net primary productivity (NPP) of vegetation in an ecosystem and the fraction of photosynthetic products consumed by soil heterotrophic respiration (R_H), which was used as a measure of the carbon sink in Equation 5:

$$NEP = NPP\text{-}R_H. \quad (5)$$

2.4.1 Estimation of NPP based on the CASA model

This study used ArcGIS 10.4 for data processing to estimate the NPP for the study area based on the CASA model. The CASA model is based on light energy utilization. It was developed by Potter et al. (1993). The model was subsequently refined by Potter and Klooster

TABLE 3 Conversion elasticity of land use/cover types.

Farmland	Forest	Grassland	Water	Construction	Unused land	Wetland
0.6	0.8	0.3	0.9	0.9	0.2	0.3

et al. It is applied in the studies of the carbon cycle and vegetation NPP (Potter et al., 1993).

NPP is calculated from the absorbed light and effective radiation available to the plant, along with the actual light utilization rate. The expression of NPP is shown in Equations 6–11:

$$NPP(x,t) = APAR(x,t) \times \varepsilon(x,t), \quad (6)$$

where APAR(x, t) is the photosynthetic effective radiation absorbed by pixel x during month t (g C·m^{-2}·month^{-1}) and ε(x, t) represents the actual light energy utilization by pixel x during month t (g C·m^{-2}·month^{-1}).

$$APAR(x,t) = SOL(x,t) \times FPAR(x,t) \times 0.5, \quad (7)$$

$$FPAR(x,t) = \alpha FPAR_{NDVI} + (1-\alpha)FPAR_{SR}, \quad (8)$$

$$FPAR_{NDVI} = \frac{NDVI_{(x,t)} - NDVI_{(i,min)}}{NDVI_{(i,max)} - NDVI_{(i,min)}} \times (FPAR_{max} - FPAR_{min}) + FPAR_{min}, \quad (9)$$

$$FPAR_{SR} = \frac{SR_{(x,t)} - SR_{(i,min)}}{SR_{(i,max)} - SR_{(i,min)}} \times (FPAR_{max} - FPAR_{min}) + FPAR_{min}, \quad (10)$$

$$SR(x,t) = \frac{1 + NDVI_{(x,t)}}{1 - NDVI_{(x,t)}}, \quad (11)$$

where SOL(x, t) represents the total solar radiation of pixel x in month t (MJ C·m^{-2}·month^{-1}); FPAR(x, t) represents the proportion of photosynthetically active radiation absorbed by the vegetation of pixel x in month t; the constant 0.5 indicates the proportion of the effective solar radiation (the wavelength is 0.38–0.71 μm) that the vegetation can use to the total solar radiation; NDVI (i, max) and NDVI (i, min) correspond to the maximum and minimum values of NDVI for vegetation type I, respectively, while SRmax and SRmin correspond to the percentage quantile at 5% and 95% of NDVI for vegetation type i, respectively. α is the adjustment factor for both methods of calculating FPAR, which is generally taken as 0.5. FPARmax is taken as 0.95, and FPARmin is taken as 0.001.

The expression of ε(x, t) is shown in Equations 12–15:

$$\varepsilon(x,t) = T_{\varepsilon_1}(x,t) \times T_{\varepsilon_2}(x,t) \times W_{\varepsilon}(x,t) \times \varepsilon_{max}, \quad (12)$$

where $T_{\varepsilon1}$(x, t) and $T_{\varepsilon2}$(x, t) are the stress effects of low and high temperatures on light energy utilization, respectively; $W_ε$(x, t) refers to the water stress effect coefficient; and $ε_{max}$ is the maximum light energy utilization of vegetation under ideal conditions.

$T_{\varepsilon1}$ is the reduction in vegetation first productivity due to the limitation of photosynthesis by the intrinsic biochemical action of the plant at low or high temperatures. It is calculated using Equation 13:

$$T_{\varepsilon_1}(x,t) = 0.8 + 0.02 \times T_{opt}(x) - 0.0005 \times \left[T_{opt}(x)\right]^2, \quad (13)$$

where T_{opt}(x) is the mean monthly temperature (°C) at which the vegetation NDVI value reaches its maximum.

$T_{\varepsilon2}$ represents the trend of gradually decreasing plant light energy utilization as the ambient temperature changes from T_{opt}(x) to high or low temperatures. It is calculated using Equation 14:

$$T_{\varepsilon_2} = \frac{1.184}{1 + \exp\left\{0.2 \times \left[T_{opt}(x) - 10 - T(x,t)\right]\right\}} \times \frac{1}{1 + \{1 + \exp\left[0.3 \times (-T_{opt} - 10 + T(x,t)\right]}, \quad (14)$$

where T(x, t) is the average monthly temperature. When the average monthly temperature is 10°C higher or 13°C lower than the optimum temperature T_{opt}(x), the value of $T_{\varepsilon2}$ (x, t) for that month is equal to half the value of $T_{\varepsilon2}$(x, t) when the average monthly temperature T(x, t) was the optimum temperature T_{opt}(x). The expression of Wε(x, t) is shown in Equation 15:

$$W_{\varepsilon}(x,t) = 0.5 + 0.5 \times E(x,t) \Big/ E_p(x,t), \quad (15)$$

where regional actual evapotranspiration E(x, t) is obtained according to the regional actual evapotranspiration model established by Zhou et al. (2002) and regional potential evapotranspiration E_p(x, t) is obtained according to the complementary relationship.

2.4.2 Estimation of R_H

R_H is calculated by referring to the empirical equation studied by Pei et al. (2009). It is calculated using Equation 16:

$$R_H = 0.22 \times \left[\exp(0.0912T) + \ln(0.3145R + 1)\right] \times 30 \times 46.5\%, \quad (16)$$

where R_H's unit is g C·m^{-2}·a^{-1}; T is the temperature (°C); and R is precipitation (mm).

2.5 Multi-objective linear programming

In addition to the spatial analysis module, other software applications or programs shall be used to complete the non-spatial analysis module. In this paper, the non-spatial analysis module used LINGO 18.0 for multi-objective linear programming (Yang et al., 2013). Interpreted data is used to create a land use transfer matrix for the study area. Considering local policies, agricultural water-saving, non-point source pollution control, and socio-economic benefits, equations are established from environmental and policy requirements; objective functions and constraint equations are established; and optimal land use/cover planning that meets all constraint conditions in the research area is analyzed.

Based on the carbon storage data of the study area obtained above, three assumptions are made for the possible future situation of the study area, namely, the priority scenario of grain crops (maximizing the planting area of grain crops), the priority

TABLE 4 Regression equation codes and initial year area of the research area.

Land use/cover	Code	Allocation in 2020 (hectare)
Maize	X1	35,719.2
Forest	X2	602.91
Grassland	X3	2,209.32
Water	X4	3,168.36
Construction	X5	7,486.11
Unused land	X6	3,322.35
Soybean	X7	2,226.51
Rice	X8	3,276.18
Other crops	X9	25,944.93
Wetland	X10	1,700.01
Farmland	X1+X7+X8+X9	67,166.82
Total	—	85,655.88

scenario of ethanol fuel crops (maximizing the planting area of ethanol fuel crops), and the priority scenario of carbon storage (maximizing the total carbon storage of the research area).

According to the secondary land use/cover classification, all the land in the research area will be fully divided. The Hulan River research area included 10 categories, namely, maize, forest, grassland, water, construction, unused land, soybean, rice, other crops, and wetland. Among them, maize, soybean, rice, and other crops were integrated into the first-level classification of farmland. Table 4 shows the land use/cover equation codes and initial year (2020) allocation of the Hulan River research area.

The setting of constraint equations for the research area should include the following three aspects:

(1) Land area constraints

The total area of the study area should remain unchanged during the total research period.

$$X1 + X2 + X3 + X4 + X5 + X6 + X7 + X8 + X9 + X10 = 85655.88.$$

(2) Indicator constraints

① Based on the purpose and practical requirements of minimizing pollutants, following a literature review and research by the same research group, it can be concluded that the main pollutants in farmland are total nitrogen and total phosphorus. Therefore, this paper integrates the existing research on soil nitrogen and phosphorus loads in the research area conducted by our research group and calculates the average nitrogen and phosphorus loads of soil under different land use/cover types. These values are used to represent the average nitrogen and phosphorus load caused by this type of land use/cover, with constraints aimed at minimizing nitrogen and phosphorus loads. Figure 4 shows the spatial distribution of nitrogen and phosphorus loads based on field studies and validated with published data.

Total nitrogen minimization:

$$MIN_{TN} = X1*2035 + X7*1864 + X8*2027 + X9*1946.$$

Total phosphorus minimization:

$$MIN_{TP} = X1*710 + X7*687 + X8*774 + X9*672.$$

② To achieve the goal of minimizing water consumption, hypothesis constraints were applied to reduce water demand. This study utilizes the ET_0 calculator, a specialized program developed by the FAO (Food and Agriculture Organization of the United Nations). The software program integrates multiple calculation methods and is based on the Penman–Monteith equation, as mentioned in Equation (1). The irrigation water demand for the study area is determined by subtracting the effective precipitation, which is presented in Table 6 of Section 3.1.

$MIN\ F(x) = \sum_{x=i}^{t} b_i m_i$, where b_i refers to the unit water consumption of the land use/cover type i and m_i refers to the area of the land use/cover type i.

$$MIN_W = X1*252.95 + X7*121.90 + X8*201.512 + X9*192.92.$$

③ To achieve the goal of maximizing economic benefits, the agricultural product wholesale website was consulted to obtain the purchase prices of the main agricultural products in the research area. Assuming the goal was to maximize economic benefits, an equation was constructed for this purpose. Economic benefits are embodied in the average purchase price of crops and total theoretical maximum output within a 1-year cycle (Table 5).

$MAX\ F(x) = \sum_{x=i}^{t} a_i m_i$, where a_i refers to the output efficiency per unit area of the land use/cover type i and m_i refers to the area of the land use/cover type i.

$$MAX_Y = X1*260000 + X7*140000 + X8*210000 + X9*300000.$$

(3) Assumption scenario constraints

Under the three set scenario assumptions, constraints were established under different hypothetical conditions. The order of priority was to maximize the planting area of grain, fuel ethanol crops, and carbon sequestration.

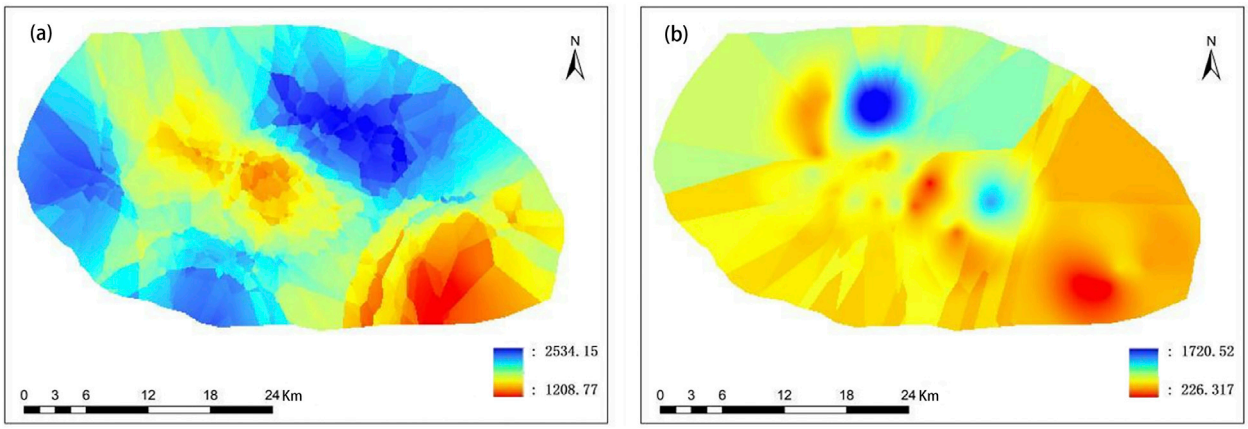

FIGURE 4
Nitrogen and phosphorus content of soil of the Hulan River Basin [**(A)** TN; **(B)** TP].

TABLE 5 Economic factors for the main crop types of the study area.

Average purchase price of crops (yuan/kg)				
Maize	Soybean	Rice	Cabbage	Potato
4	7	3.5	1	1.2
Theoretical maximum output (kg/ha)				
65,000	20,000	60,000	300,000	250,000

① Maximizing the planting area of grain: ensuring the maximization of the planting area of grain crops (rice and maize).

$$MAX_R = X1 + X8.$$

② Maximizing the planting area of fuel ethanol crops: ensuring the maximization of the planting area of fuel ethanol crops (maize).

$$MAX_R = X1.$$

③ Maximizing carbon sequestration: ensuring the maximization of land use/cover types with significant carbon sequestration. The calculation process is detailed in Section 2.4 of this paper. The carbon sink results are shown in Table 7 of Section 3.3. The carbon sink capacity of each land use type is considered the key indicator for the equation as follows:

$$MAX_C = X1^* 352.78 + X2^* 733.14 + X3^* 339.02 + X6^* 293.68 + X7^* 374.78 + X8^* 247.85 + X9^* 337.33.$$

The overall technical route of the study is shown in Figure 5.

3 Results and discussion

3.1 Water demand of the main crops

The ET_0 calculator, a specialized program developed by the Food and Agriculture Organization of the United Nations (FAO), is used to assist in the calculation of ET_0. The water demand calculation results are shown in Table 6. In the Hulan River Basin, there is no significant variation in the overall irrigation water demand. Notably, maize cultivation exhibits the highest irrigation water demand (252.77 mm) because of a higher K_c factor, while soybean cultivation has the lowest irrigation water demand (121.90 mm), representing a minimal difference of 130.87 mm between the two crops.

3.2 Land use interpretation results

The land use types of the Hulan River Basin included farmland, forest, grassland, water, construction, unused land, and wetland. Among them, the unused land was mainly swamp. According to the actual crop structures, farmland was subdivided into maize, rice, soybean, and other crops. The interpretation results of the three terms are displayed in Figure 6. The river channel at the outlet into the Songhua River was gentle and had abundant water. From 2010 to 2015, construction land was mostly distributed on the north bank. After 2015, the area of construction land increased across the river.

Figures 7, 8 depict the dynamics of land use transfers in the Hulan River Basin over 2010–2020. During the period of 2010–2015, the most prominent alteration in land use, in terms of area modification, was observed with the conversion of other cultivated land to maize cultivation. This transformation covered an extensive area of approximately 6704.46 ha, primarily concentrated in the northern and northwestern sectors of the study area. Furthermore, a significant land area of approximately 4644.27 ha underwent a transition from maize to other crops, with the main concentration observed in the southern and western sectors of the study area. Additionally, in the western part of the study area, an area of approximately 1392 ha, previously dominated by soybean, was predominantly converted to maize. Among the land use transfers involving forest, grassland, water, construction, and wetland, the transition toward maize exhibited the most pronounced spatial change. Consequently, there was a significant expansion in the extent of maize from 2010 to 2015. Notably, approximately 78% of the region remained unaffected by any alterations in land use types.

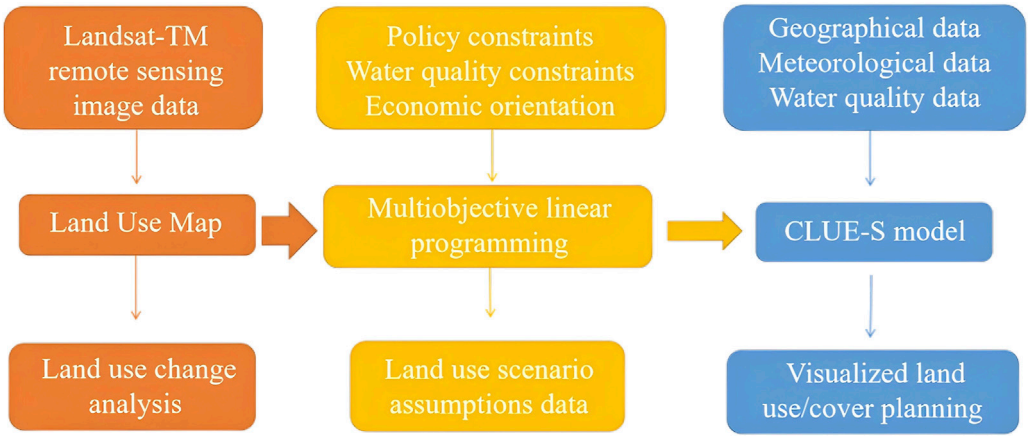

FIGURE 5
Technical route of the study.

TABLE 6 Water demand data of different crops and irrigation water demand calculated using the Penman–Monteith formula in the study area (mm).

	Crop type	K_c	Water demand	Effective precipitation	Irrigation water consumption
Hulan River Basin	Maize	1.2	467.11	214.34	252.77
	Soybean	0.5	336.25	214.34	121.90
	Rice	1.2	390.08	188.57	201.51
	Others (cabbage and potato)	1.1	369.01	176.09	192.92

From 2015 to 2020, the most prominent land use change in the Hulan River Basin was the conversion of maize to other crops, encompassing approximately 9161.64 ha. It exhibited a wide distribution, albeit with relatively lower occurrences observed in the southeastern direction. The second noteworthy land use change involved the conversion of beach land to unused land, amounting to approximately 1953.36 ha, primarily concentrated near the riverbanks in midstream and downstream of the river. Additionally, there was a significant and widespread transformation of approximately 2918.61 ha of other crops into maize.

3.3 Distribution characteristics of carbon sink in the Hulan River basin

The Hulan River Basin's carbon sink was estimated using the CASA model. According to the results, the carbon sink was estimated to be 329.35 $gC{\cdot}m^{-2}{\cdot}a^{-1}$ in 2010, but it decreased to 295.59 $gC{\cdot}m^{-2}{\cdot}a^{-1}$ in 2015. In 2020, 350.76 $gC{\cdot}m^{-2}{\cdot}a^{-1}$ of the carbon sink was achieved. According to Zhou et al. (2023), which covered the Heilongjiang Province from 2010 to 2020, the average yearly NEP was 329.77 $gC{\cdot}m^{-2}{\cdot}a^{-1}$. The NEP ranged from 281.38 $gC{\cdot}m^{-2}{\cdot}a^{-1}$ to 380.07 $gC{\cdot}m^{-2}{\cdot}a^{-1}$, suggesting a consistent trend with this paper. Specifically, between 2010 and 2015, NEP in the Hulan River Basin decreased by 33.96 $gC{\cdot}m^{-2}{\cdot}a^{-1}$. However, from 2015 to 2020, NEP increased by 55.64 $gC{\cdot}m^{-2}{\cdot}a^{-1}$. For each land use type, the carbon sink capacity is shown in Table 7.

Figure 9A illustrates the temporal distribution pattern of the Hulan River Basin's NEP, with an initial increase followed by a decrease. In 2010, the highest NEP was observed in July, reaching 107.08 $gC{\cdot}m^{-2}{\cdot}a^{-1}$. The NEP levels in January, February, and December were comparatively lower, ranging from roughly 0.5 to 0.6 $gC{\cdot}m^{-2}{\cdot}a^{-1}$. The peak of NEP in 2015 was measured in August at 78.67 $gC{\cdot}m^{-2}{\cdot}a^{-1}$, which was less than the maximum values documented for 2020 and 2010. In addition, there was a slight decrease in NEP in April, and the lowest monthly average value, 0.44 $gC{\cdot}m^{-2}{\cdot}a^{-1}$, appeared in December. In 2020, the carbon sink in the Hulan River Basin exhibited its highest monthly average value in July, reaching 114.51 $gC{\cdot}m^{-2}{\cdot}a^{-1}$. Conversely, the lowest monthly average value was observed in January, amounting to 0.35 $gC{\cdot}m^{-2}{\cdot}a^{-1}$.

According to Figure 9B, variations in land use types and their per unit area carbon sink capacities were observed in 2010, 2015, and 2020. Notably, forests showed higher NEP values due to their higher vegetation cover and carbon sequestration capabilities, while grassland and farmland showed varying performance. As the main crop in the area, soybean obtained relatively higher carbon sequestration than maize and rice. Noppol et al. (2022) found that the conversion of forest to agricultural land significantly reduced carbon stocks, while some conversions to grassland increased carbon stocks. Soil erodibility varied with the type of land use, with lower erodibility in grasslands due to higher organic carbon content and lower silt concentration. In contrast, chernozem soil, commonly found in Heilongjiang Province, typically has higher silt and clay concentrations, which benefits the fertile agricultural

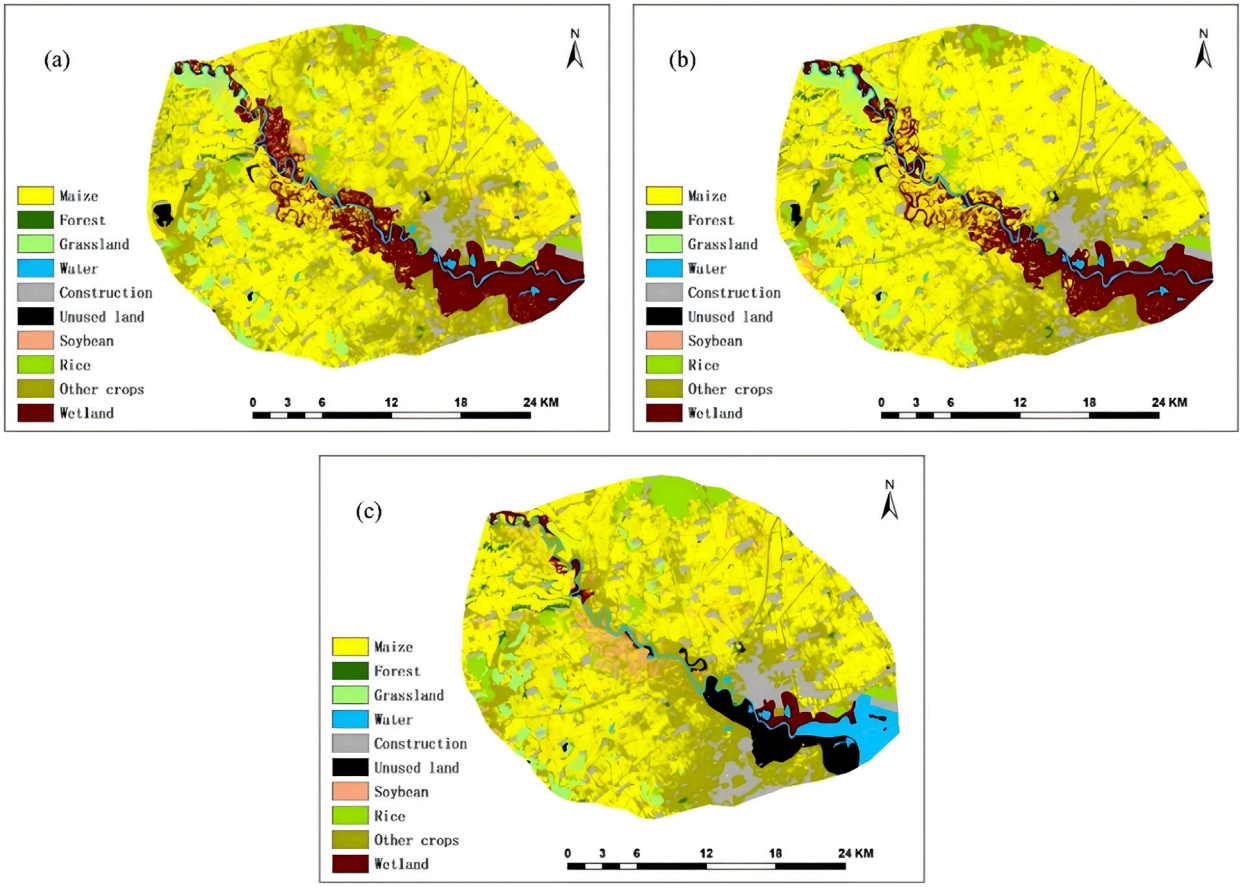

FIGURE 6
Land use/cover of the Hulan River Basin [**(A)** 2010; **(B)** 2015; and **(C)** 2020].

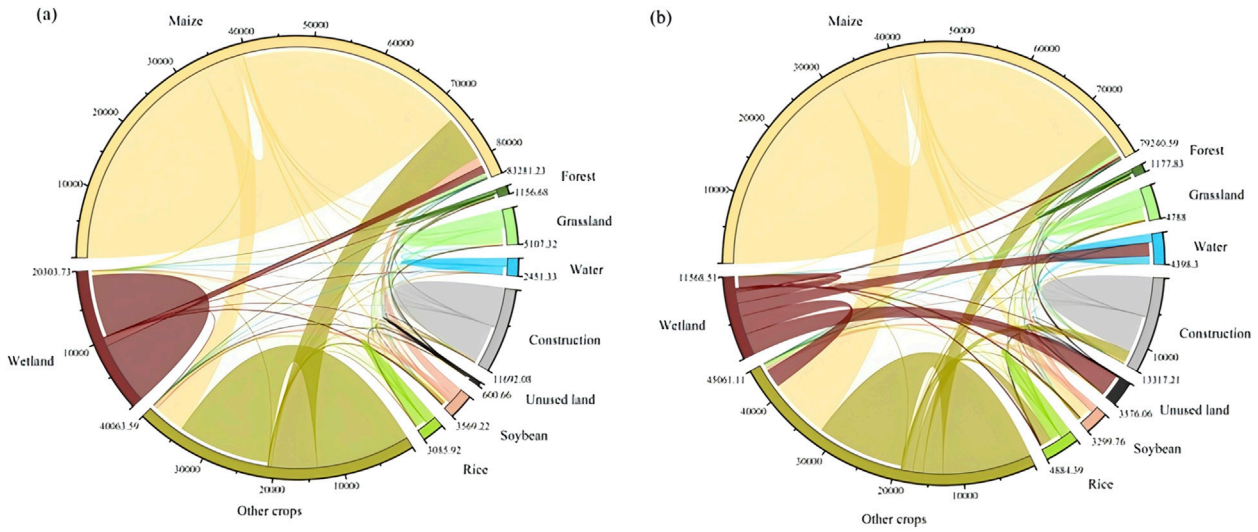

FIGURE 7
Chords of land use transfer in the Hulan River Basin [**(A)** 2010–2015 and **(B)** 2015–2020].

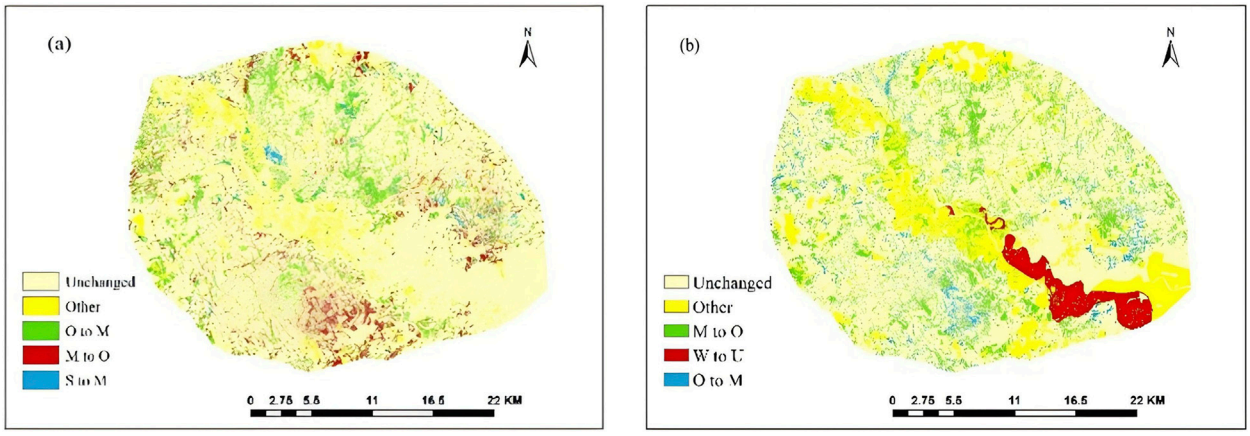

FIGURE 8
Spatial distribution of land use transfer in the Hulan River Basin [**(A)** 2010–2015 and **(B)** 2015–2020].

TABLE 7 Carbon sequestration of various land use types in the study area (g/m^2).

Grassland	Forest	Rice	Maize	Unused land	Soybean	Other crops
339.02	733.14	247.85	352.78	293.68	374.78	337.33

practices of maize and soybean cultivation. Therefore, unlike the grassland ecosystems of northern China (Li et al., 2023), policies aimed at returning forest or grassland grazing to grassland areas are not suitable for the Hulan River Basin.

Previous papers have indicated that climate change has certain influences on carbon sinks (Wang et al., 2021; Xu et al., 2023). Temperature and precipitation changes are factors directly influencing vegetation photosynthetic activity and soil respiration. Higher temperatures can enhance photosynthesis up to a threshold, while extreme precipitation variability may disrupt carbon sequestration (Wang et al., 2023; Arunrat et al., 2018). The stimulation of vegetation's photosynthetic activity and subsequent vegetation growth are facilitated by the elevated temperatures (Yuan et al., 2023). Moderate precipitation plays a critical role in facilitating optimal vegetation growth. Inadequate or excessive rainfall can exert deleterious impacts on vegetation growth, thereby significantly influencing the magnitude of NEP (Li et al., 2021). The crucial developmental phase for vegetation, wherein it grows from initiation to maturity, typically occurs during June and July each year. NEP for all 3 years peaks between June and September, indicating that the carbon absorption capacity of ecosystems is the strongest in the warm seasons. After the peak, NEP rapidly decreases by November, showing a clear seasonal pattern. The seasonal variations in temperature and precipitation directly influence NEP, resulting in increased NEP during these months. In 2020, the Hulan River Basin experienced relatively high levels of temperature and precipitation from June to August, ensuring optimal water-thermal conditions for vegetation and effectively enhancing vegetation's photosynthetic capacity. Consequently, land use types such as grassland and soybean exhibited the highest carbon sink per unit area among the 3 years. Conversely, lower precipitation levels were recorded from June to August 2015, contributing to regional aridity and restricted vegetation growth. Hence, grassland, soybean, and other land use types demonstrated the lowest carbon sink per unit area in that particular year.

The Hulan River Basin is in Heilongjiang Province, which is characterized by a cold temperate and temperate continental monsoon climate. Summers are hot, while winters are frigid and dry, with temperatures dropping below 0°C. There were discernible seasonal fluctuations in NEP. The carbon sink per unit area underwent a substantial increase during the months of April and May, whereas a rapid decrease was observed after July and August. Previous studies have provided substantial evidence to support the notion that precipitation exerts primary control over the NEP of China's terrestrial systems (Zhang et al., 2023). Hence, the carbon sink per unit area in July 2015 exhibited a notable decrease compared to the peak values observed in July 2010 and 2020. In both 2015 and 2020, a discernible decrease in monthly NEP was observed. This decrease can be attributed to agricultural activities and the significant reduction in April precipitation levels, especially when compared to those of 2010. The observed decrease in monthly NEP during these periods can be attributed to unfavorable hydrothermal conditions.

The carbon sink classification in the Hulan River Basin used the natural breakpoint method, where the range of 0–253 $gC{\cdot}m^{-2}{\cdot}a^{-1}$ was designated as the low carbon sink zone, 253–426 $gC{\cdot}m^{-2}{\cdot}a^{-1}$ was designated as the medium carbon sink zone, and 426–1,075 $gC{\cdot}m^{-2}{\cdot}a^{-1}$ was designated as the high carbon sink zone. As depicted in Figure 10, in 2010, the low carbon sink regions were predominantly located near the southeastern floodplains and riverbanks, with a substantial portion classified as medium carbon sink zones. Conversely, the high carbon sink regions are primarily concentrated in the northwestern area of the study area.

From 2010 to 2015, there was a noticeable decrease in the carbon sink. The low carbon sink areas remained concentrated near the

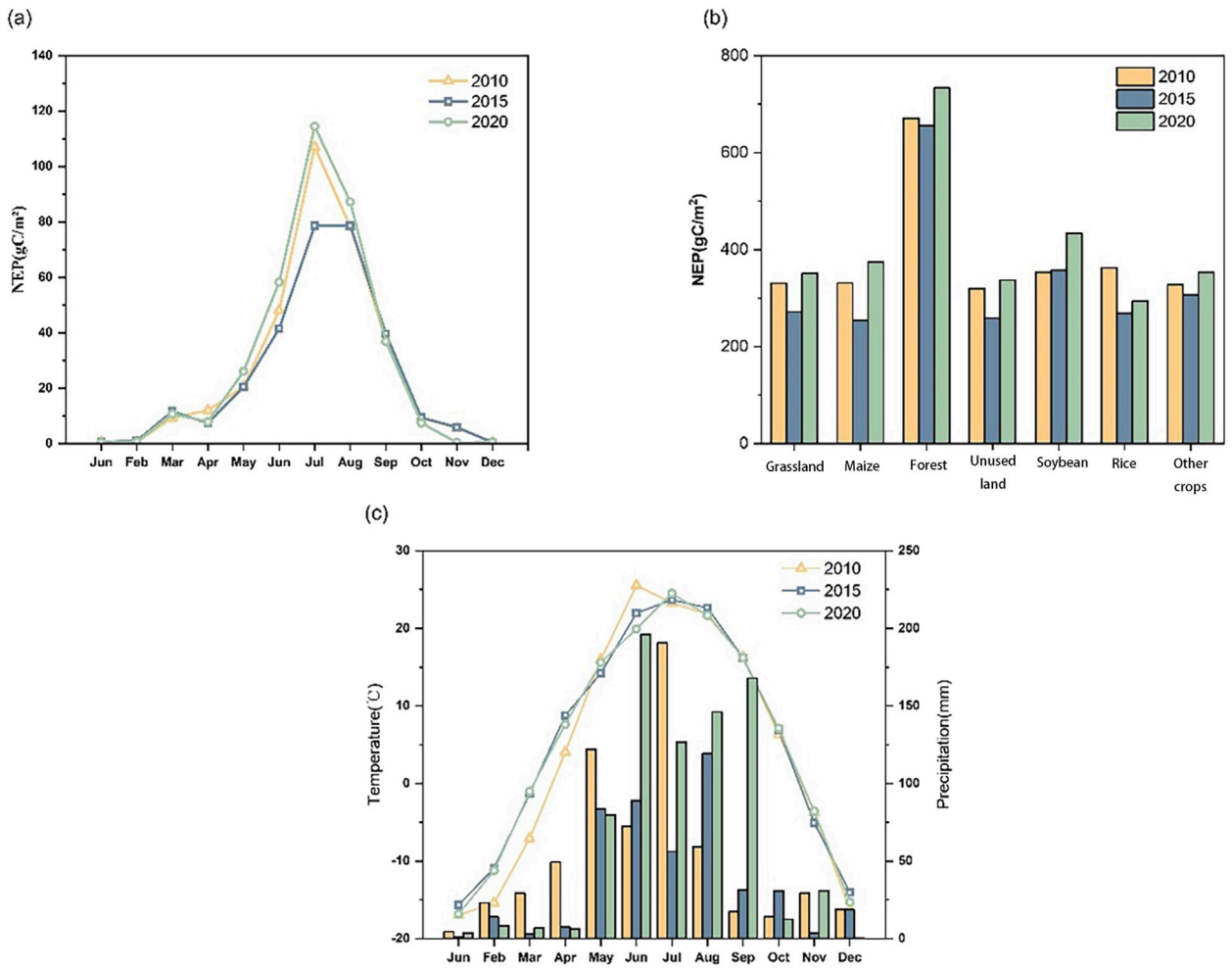

FIGURE 9
(A) Monthly average NEP of the Hulan River Basin. **(B)** NEP values for different land use types in the Hulan River Basin. **(C)** Monthly average temperature and precipitation of the Hulan River Basin.

southeastern floodplains and riverbanks, while the medium carbon sink zones showed a more extensive distribution. Notably, the high carbon sink areas experienced a significant reduction in the northwestern part of the study area.

However, in 2020, there was a marked increase in carbon sink. The low carbon sink areas persisted near the southeastern floodplains, albeit with a diminished spatial extent. The medium carbon sink zones demonstrated a pronounced increase and wider distribution. The high carbon sink regions were concentrated in the northwestern and northern parts of the study area. Over the period from 2010 to 2020, the Hulan River Basin witnessed an overall increase in NEP. The northwest had a discernible decrease in NEP and an increase in carbon sinks close to the water.

3.4 Land use scenario assumptions in the Hulan River Basin

Table 8 shows the results of multiple linear regression in the research area. From the data, under the Grain Crop Priority Policy, the planting area of rice and maize has reached maximum, and the rice area has increased significantly compared to the other two assumptions and the situation in 2020. Under the Ethanol Crop Priority Policy, the priority of rice yield is reduced, and maize yield is further expanded to reach the maximum value among various assumed types. Under the carbon sequestration priority policy, the area of forest and grassland has been increased to the maximum of the three assumptions, resulting in the farmland area under this assumption reaching the minimum of the three assumptions. Under the three policies, the areas of other crops, unused land, and wetland have all decreased, indicating that these three types of land are relatively unimportant in policy planning.

3.4.1 Grain Crop Priority Policy

Figure 11A shows the land use/cover situation under the Grain Crop Priority Policy in 2030, and Figure 11B shows the land use/cover change situation from 2020 to 2030. The specific area demand value can be found in Table 8. Under this policy, the area of maize, soybean, and rice has all increased. At the same time, while the total farmland area increased by 3255.8 ha, the area of other crops except for maize, soybeans, and rice decreased by 1262.41 ha, and other land use/cover types also had varying degrees of reduction. The area

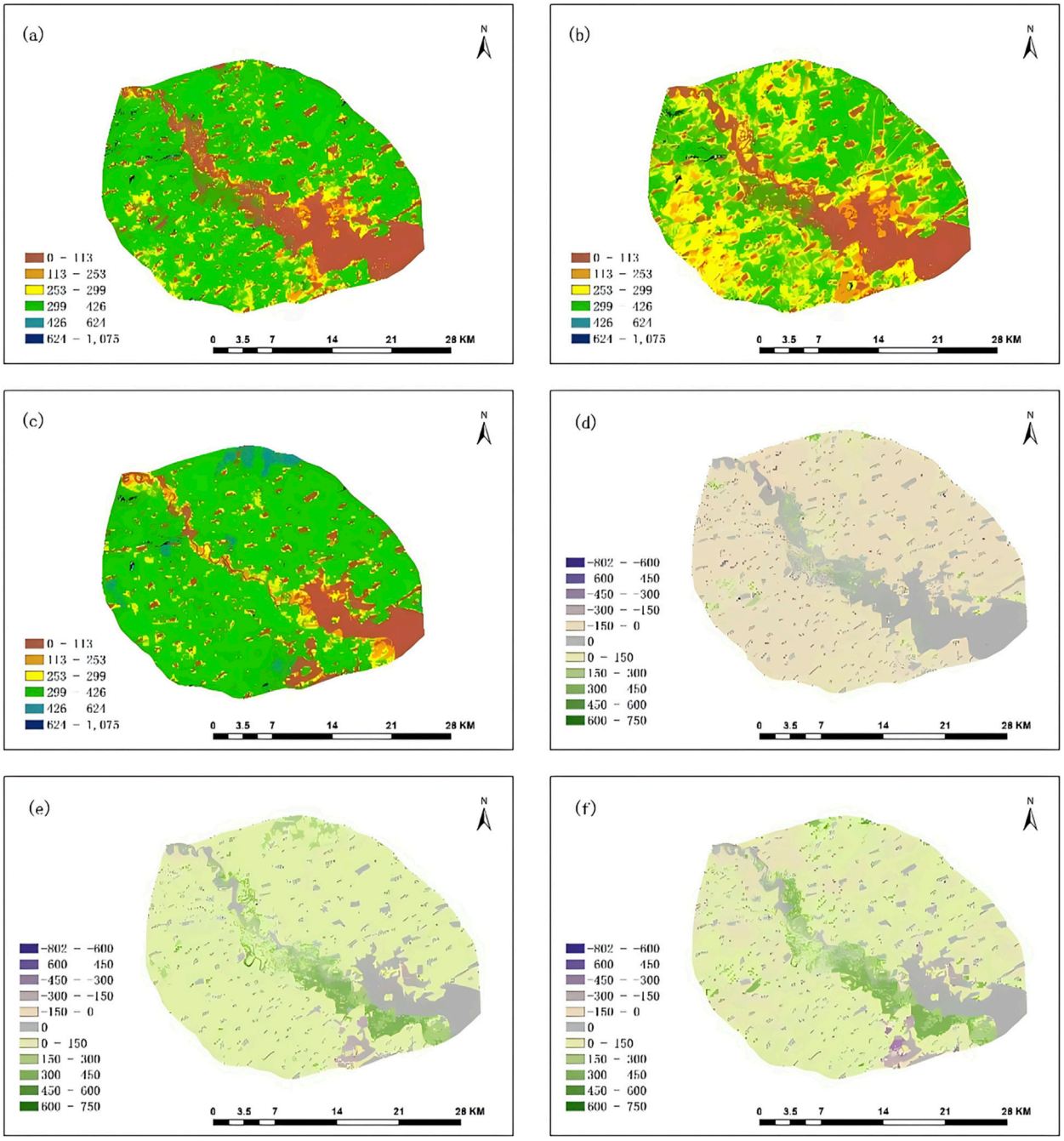

FIGURE 10
Spatial distribution of NEP ($gC \cdot m^{-2} \cdot a^{-1}$) in the Hulan River Basin [**(A)** 2010; **(B)** 2015; and **(C)** 2020]. Spatial distribution of changes in NEP ($gC \cdot m^{-2} \cdot a^{-1}$) in the Hulan River Basin [**(D)** 2010; **(E)** 2015; and **(F)** 2020].

of unused land and wetland on the north bank of the estuary has decreased, while the grassland has increased, having been transferred from water and unused land. This reflects efforts to restore natural habitats or use previously undeveloped land. The transformation of unused land to grassland could indicate a positive trend toward land restoration or a strategy to prevent land degradation. However, the change in water area might raise environmental concerns due to the loss of biodiversity and natural water regulation provided by wetlands. In this situation, the area of maize and rice increases, with the main increase being in the unused land on the south bank of the estuary, while the rice area mainly increases near the existing rice planting area.

3.4.2 Fuel Ethanol Crop Priority Policy

Figure 12A shows the land use/cover situation under the Fuel Ethanol Crop Priority Policy in 2030, and Figure 12B shows the

TABLE 8 Multiple linear regression results in the research area (hectare).

Land use/cover	2020	2030 scenario 1	2030 scenario 2	2030 scenario 3
Maize	35,719.20	38,975.00	39,292.00	38,063.00
Forest	602.91	542.00	542.00	681.00
Grassland	2,209.32	1,988.00	1,988.00	2,631.00
Water	3,168.36	3,168.36	3,168.36	3,168.36
Construction	7,486.11	6,737.00	6,737.00	6,737.00
Unused land	3,322.35	1,662.00	1,662.00	1,662.00
Soybean	2,226.51	2,450.00	2003.00	2,450.00
Rice	3,276.18	3,921.00	2,948.00	2,948.00
Other crops	25,944.93	24,682.52	25,785.52	25,785.52
Wetland	1,700.01	1,530.00	1,530.00	1,530.00
Total	85,655.88	85,655.88	85,655.88	85,655.88

[a]2030 scenario 1: grain crop planting priority; 2030 scenario 2: ethanol crop planting priority; 2030 scenario 3: maximize carbon sequestration priority. Meaning of symbol a: It explains the specific scenarios corresponding to each one.

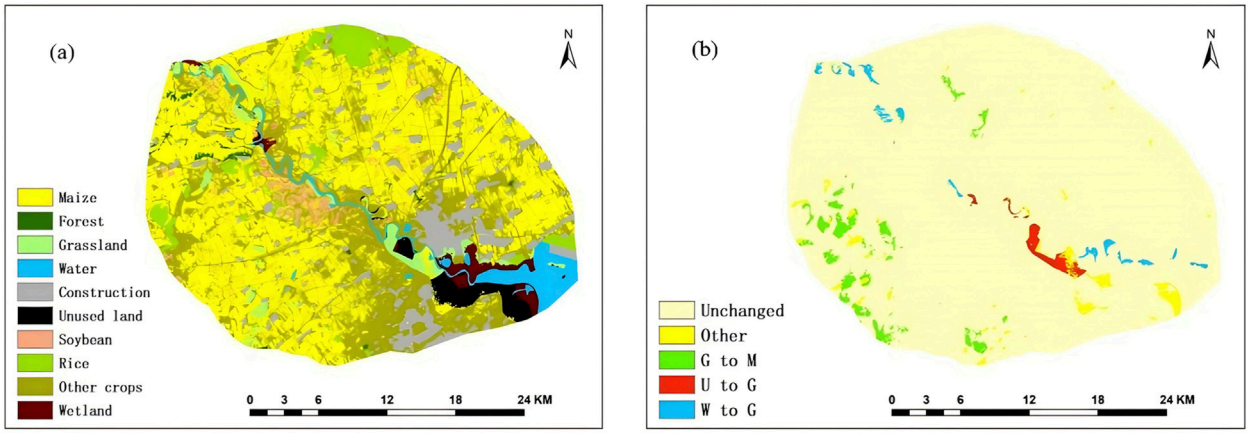

FIGURE 11
Simulation results under the Grain Crop Priority Policy in the research area. **(A)** 2030 **(B)** Change situation from 2020 to 2030.

land use/cover changes from 2020 to 2030. The specific area's demand value can be found in Table 8. In this scenario, the area of maize as the only fuel ethanol crop in the research area has increased by 3572.8 ha, while all other land use/cover areas have decreased, with soybean, rice, and other crops decreasing by 223.51 ha, 328.18 ha, and 159.41 ha, respectively. Under the Fuel Ethanol Crop Priority Policy, the area of maize has significantly increased, like in scenario 1. The main growth point of maize is on the south bank of the estuary. At the same time, due to the reduction in soybean, rice, and other crops, a portion of the farmland near maize has also been converted to maize cultivation. The situation is similar to the Grain Crop Priority Policy, which shows the dual actions of maize in food security and fuel ethanol production promotion. This scenario illustrates a dynamic landscape where agricultural expansion, especially maize cultivation, is prominent, along with significant transitions from natural or unused lands to more productive uses.

3.4.3 Carbon Storage Priority Policy

Figure 13A shows the land use under the Carbon Storage Priority Policy in 2030, and Figure 13B shows the land use/cover change from 2020 to 2030. The specific area demand value can be found in Table 8. In this scenario, the area of forest and grassland, which have the largest carbon sink per unit area, increased by 61.09 ha and 221.68 ha, respectively, and the area of maize increased by 5.44%, with a total area of 1943.97 ha. The same trend appears in soybean cultivation. All other land use/cover

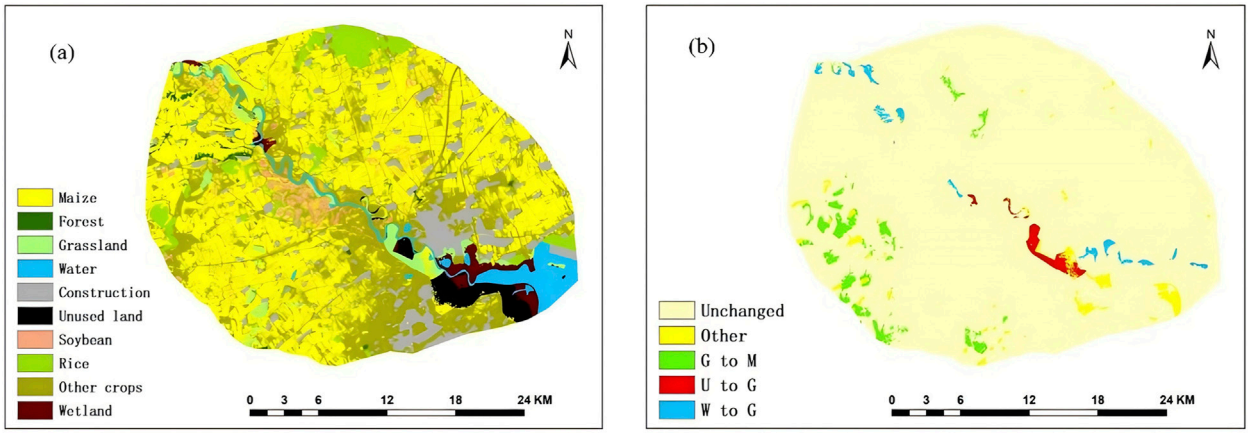

FIGURE 12
Simulation results under the Fuel Ethanol Crop Priority Policy in the research area. **(A)** 2030 **(B)** Change situation from 2020 to 2030.

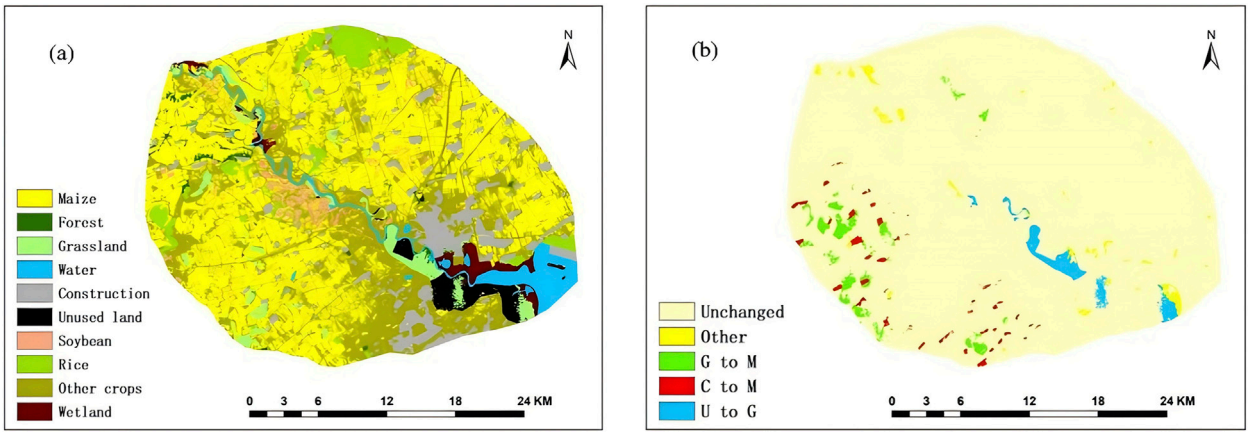

FIGURE 13
Simulation results under the Carbon Storage Priority Policy in the research area. **(A)** 2030 **(B)** Change situation from 2020 to 2030.

areas decreased, including rice and other crops by 328.18 ha and 159.41 ha, respectively. Maize and soybean perform well in carbon storage, especially in Heilongjiang Province where a suitable planting environment is provided. The prominent constraint for maize expansion is the water pollution effect, which reminds the government to pay attention to non-point source pollution prevention while promoting maize planting. In the southern part of the area, construction land is transferred to maize, which may have benefits for water pollution control and carbon sink purposes. In this scenario, the forest area and grassland area have significantly increased, and the main growth point of grassland is still the unused land on the south bank of the estuary. It is speculated that due to the difficulty of converting to forest, the growth rate of grassland in this scenario is even higher than forest. Unused land is relatively easily transferred because of its high elasticity. It transforms grassland near the water body into a transition zone from water to wetland.

3.5 Carbon sinks of different scenario assumptions

The carbon sink status for three scenarios in 2030 was estimated by calculating the average NEP for each land use category based on the NEP values in 2020. The results are shown in Figure 14. Compared to 2020, scenario 1 shows a significant increase in the cultivated areas of maize and rice, with maize having a relatively high carbon sink per unit area. NEP has increased to approximately 4.67×10^3 tC compared to 2020. In scenario 2, NEP has increased by 3.71×10^3 tC compared to 2020. In scenario 3, the primary focus is on maintaining the carbon sink in the study area. Therefore, the forest and grassland areas with higher carbon sink potential have expanded. This has led to an overall improvement in the regional carbon sink capacity. Scenario 3 also has the highest NEP value among the three scenarios simulated. Compared to 2020, scenario 3 shows a substantial increase in the NEP value, with an addition of 8.32×10^3 tC.

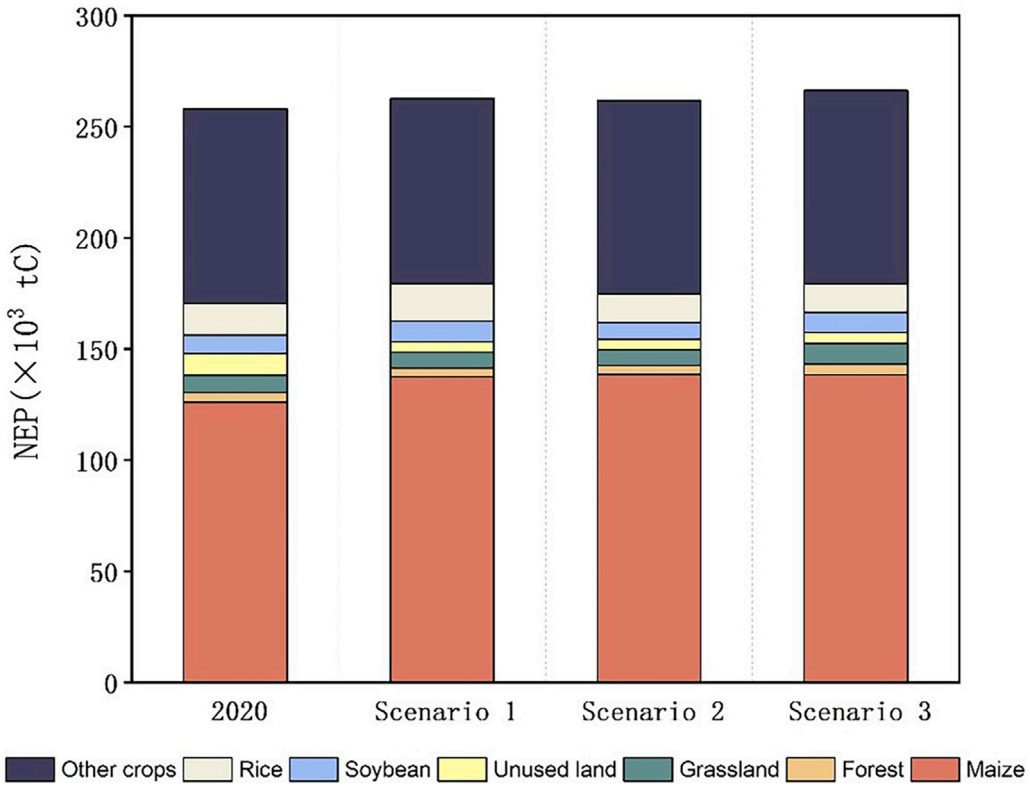

FIGURE 14
Various scenario simulations and 2020 NEP in the Hulan River Basin.

4 Conclusion

NEP in the Hulan River Basin follows a pattern of initial increase followed by a subsequent decrease over the annual cycle. Between 2010 and 2015, NEP decreased by 33.96 g of carbon per square meter per year, whereas from 2015 to 2020, an increase of 55.64 g of carbon per square meter per year was observed. The fluctuations in NEP are intricately linked to climatic conditions and land use practices within the Hulan River Basin. Spanning the decade from 2010 to 2020, areas with low carbon sequestration capabilities were predominantly found in the southeast of the region, showing a notable reduction in their geographic spread. Moderate carbon sink areas were more ubiquitous, with a lower frequency in the northwest. High carbon sink areas were largely situated in the northwest, forming the primary concentration of such zones.

The land demand is simulated within the study area under three distinct policy frameworks: the Grain Crop Priority Policy, the Fuel Ethanol Crop Priority Policy, and the Carbon Storage Priority Policy. This simulation was conducted to translate the developed CLUE-S model and ArcGIS outputs into a visual representation of future land use/cover. The results reveal that under scenario 1, which ensures regional food production, there is an expansion of arable land by 1262.41 ha. Scenario 2, prioritizing regional fuel ethanol output, observes an increase in the area dedicated to maize cultivation by approximately 3572.8 ha. Scenario 3, focused on bolstering the regional carbon sink, leads to substantial growth in both forested and grassland areas. Collectively, these three hypothetical scenarios within the study area effectively fulfill the preset requirements for the corresponding land use/cover categories.

The simulation of land use/cover in the research area in 2030 under four possible future scenarios was visualized based on the secondary classification. The conclusion proves that the land use/cover planning of typical fuel ethanol crop planting areas under different policy orientations can meet the needs of this policy, and its change pattern conforms to the literature description and actual situation, which has practical reference value.

In addition, the study assessed the carbon sequestration performance across a range of hypothetical scenarios, demonstrating a substantial increase in carbon capture for all scenarios compared to the baseline year of 2020. The outcomes highlight the substantial impact of each scenario in enhancing regional carbon sequestration potential, offering substantial empirical data and theoretical support for local policy formulation. Crucially, the study's findings are of considerable importance for shaping future regional land use strategies and refining land use configurations.

Data availability statement

The raw data supporting the conclusions of this article will be made available by the authors, without undue reservation.

Author contributions

GC: writing–original draft, conceptualization, formal analysis, investigation, and methodology. HW: conceptualization, software, visualization, and writing–original draft. XL: data curation, visualization, and writing–original draft. WL: data curation, visualization, and writing–original draft. HL: funding acquisition and writing–review and editing. LD: project administration, supervision, writing–review and editing, and funding acquisition.

Funding

The author(s) declare that financial support was received for the research, authorship, and/or publication of this article. This research was financially supported by the National Natural Science Foundation of China (grant no. 41861124004) and the Social Science Project of Jilin Provincial Department of Education (grant no. JJKH20231248SK).

Conflict of interest

The authors declare that the research was conducted in the absence of any commercial or financial relationships that could be construed as a potential conflict of interest.

Generative AI statement

The author(s) declare that no Generative AI was used in the creation of this manuscript.

Publisher's note

References

Ahmed, N., Wang, G. X., Booij, M. J., Marhaento, H., Pordhan, F. A., Ali, S., et al. (2022). Variations in hydrological variables using distributed hydrological model in permafrost environment. *Ecol. Indic.* 145, 109609. doi:10.1016/j.ecolind.2022.109609

Arunrata, N., Piumijumnong, N., and Hatano, R. (2018). Predicting local-scale impact of climate change on rice yield and soil organic carbon sequestration: a case study in Roi Et Province, Northeast Thailand. *Agric. Syst.* 164, 58–70. doi:10.1016/j.agsy.2018.04.001

Chen, L. D., and Fu, B. J. (2000). Farmland ecosystem management and control of non Point source pollution. *Environ. Sci.* 21 (02), 98–100. doi:10.13227/j.hjkx.2000.02.025

ElNesr, M. N., and Alazba, A. A. (2012). Simple statistical equivalents of Penman–Monteith formula's parameters in the absence of non-basic climatic factors. *Arabian J. Geosciences* 5 (4), 757–767. doi:10.1007/s12517-010-0231-1

Hassan, D. F., Abdalkadhum, A. J., Mohammed, R. J., and Shaban, A. (2022). Integration remote sensing and meteorological data to monitoring plant phenology and estimation crop coefficient and evapotranspiration. *J. Ecol. Eng.* 23 (4), 325–335. doi:10.12911/22998993/146267

He, Y., Yang, A. J., Chen, W. J., Guo, Y., Feng, Y. H., and Song, X. (2022). Agricultural non Point source pollution load and distribution characteristics of typical watershed in southwest Karst Plateau mountain area. *Res. Soil Water Conservation* 29 (01), 148–152. doi:10.13869/j.cnki.rswc.20210803.001

Li, H. Z., and Zhang, M. X. (2019). A review on the calculation of non-point source pollution loads. *IOP Conf. Ser. Earth Environ. Sci.* 344 (1), 012138. doi:10.1088/1755-1315/344/1/012138

Li, J. S., Guo, X. M., Chuai, X. W., Xie, F. J., Yang, F., Gao, R. Y., et al. (2021). Reexamine China's terrestrial ecosystem carbon balance under land use-type and climate change. *Land Use Policy* 102, 105275. doi:10.1016/j.landusepol.2020.105275

Li, W. B., Liang, Y. J., Liu, L. J., He, Q. Q., Huang, J. J., and Yin, Z. C. (2024). Spatio-temporal impacts of land use change on water-energy-food nexus carbon emissions in China, 2011-2020. *Environ. Impact Assess. Rev.* 105, 107436. doi:10.1016/j.eiar.2024.107436

Li, Z. W., Tang, Q., Wang, X., Chen, B. R., Sun, C. M., and Xin, X. P. (2023). Grassland carbon change in northern China under historical and future land use and land cover change. *Agronomy* 13 (8), 2180. doi:10.3390/agronomy13082180

Liang, Y. J., Liu, L. J., and Huang, J. J. (2017). Integrating the SD-CLUE-S and InVEST models into assessment of oasis carbon storage in northwestern China. *PLOS ONE* 12 (2), e0172494. doi:10.1371/journal.pone.0172494

Liu, M., Li, C. L., Hu, Y. M., Sun, F. Y., Xu, Y. Y., and Chen, T. (2014). Combining CLUE-S and SWAT models to forecast land use change and non-point source pollution impact at a watershed scale in Liaoning Province, China. *Chin. Geogr. Sci.* 24 (5), 540–550. doi:10.1007/s11769-014-0661-x

Liu, Y. G., and Wang, L. Y. (2021). Research on simulation and prediction of land use change in Jinan City. *Territ. and Nat. Resour. Study* 190 (01), 47–50. doi:10.16202/j.cnki.tnrs.2021.01.013

Mao, K. Y., Fan, Y. L., Wang, Y., and Wang, Z. H. (2018). Current situation and deep analysis of fuel ethanol industry at home and abroad. *High-Technology and Commer.* 265 (06), 6–13.

Ndegwa Mundia, C., and Murayama, Y. (2009). Analysis of land use/cover changes and animal population dynamics in a wildlife sanctuary in East Africa. *Remote Sens.* 1 (4), 952–970. doi:10.3390/rs1040952

Noppol, A., Sukanya, S., Praeploy, K., and Ryusuke, H. (2022). Soil organic carbon and soil erodibility response to various land-use changes in northern Thailand. *Catena* 219, 106595. doi:10.1016/j.catena.2022.106595

Pei, Z. Y., Ouyang, H., Zhou, C. P., and Xu, X. L. (2009). Carbon balance in an alpine steppe in the qinghai-tibet plateau. *J. Integr. Plant Biol.* 51 (5), 521–526. doi:10.1111/j.1744-7909.2009.00813.x

Peng, K. F., Jiang, W. G., Deng, Y., Liu, Y. H., Wu, Z. F., and Chen, Z. (2020). Simulating wetland changes under different scenarios based on integrating the random forest and CLUE-S models: a case study of Wuhan Urban Agglomeration. *Ecol. Indic.* 117, 106671. doi:10.1016/j.ecolind.2020.106671

Potter, C. S., Randerson, J. T., Field, C. B., Matson, P. A., Klooster, S. A., Mooney, H. A., et al. (1993). Terrestrial ecosystem production: a process model based on global satellite and surface data. *Glob. Biogeochem. Cycles* 7 (4), 811–841. doi:10.1029/93GB02725

Schmidt, N., and Zinkernagel, J. (2017). Model and growth stage based variability of the irrigation demand of onion crops with predicted climate change. *Water* 9 (9), 693. doi:10.3390/w9090693

Su, Y. X., Liu, Y. H., Huo, L. J., and Yang, G. Q. (2024). Research on optimal allocation of soil and water resources based on water-energy-food-carbon nexus. *J. Clean. Prod.* 450, 141869. doi:10.1016/j.jclepro.2024.141869

Wang, H. J., Cao, L., and Feng, R. (2021). Hydrological similarity-based parameter regionalization under different climate and underlying surfaces in ungauged basins. *Water* 13 (18), 2508. doi:10.3390/w13182508

Wang, H. L., He, P., Shen, C., and Y. Wu, Z. (2019). Effect of irrigation amount and fertilization on agriculture non-point source pollution in the paddy field. *Environ. Sci. Pollut. Res.* 26 (10), 10363–10373. doi:10.1007/s11356-019-04375-z

Wang, M. M., Zhao, J., Wang, S. Q., Chen, B., and Li, Z. P. (2021). Detection and attribution of positive net ecosystem productivity extremes in China's terrestrial ecosystems during 2000-2016. *Ecol. Indic.* 132, 108323. doi:10.1016/j.ecolind.2021.108323

Wang, X., Wang, K., Zhang, Y., Gao, J., and Xiong, Y. (2023). Impact of climate on the carbon sink capacity of ecological spaces: a case study from the Beijing–Tianjin–Hebei urban agglomeration. *Land* 12 (8), 1619. doi:10.3390/land12081619

Wei, X. G., Wang, T. L., Li, B., Liu, S. Y., Yao, M. Z., Xie, Y., et al. (2018). Study on the spatiotemporal distribution characteristics of water profit and loss in maize fields and irrigation model zoning in Liaoning Province. *Trans. Chin. Soc. Agric. Eng.* 34 (23), 119–126. doi:10.11975/j.issn.1002-6819.2018.23.014

Wu, D., Zhang, Z. W., Liu, D., Zhang, L. L., Li, M., Khan, M. I., et al. (2024). Calculation and analysis of agricultural carbon emission efficiency considering water-energy-food pressure: modeling and application. *Sci. Total Environ.* 907, 167819. doi:10.1016/j.scitotenv.2023.167819

Wu, H., Yue, Q., Guo, P., and Xu, X. Y. (2025). Exploiting the potential of carbon emission reduction in cropping-livestock systems: managing water-energy-food nexus for sustainable development. *Appl. Energy* 377 (B), 124443. doi:10.1016/j.apenergy.2024.124443

Xu, B. W., Niu, Y. R., Zhang, Y. N., Chen, Z. F., and Zhang, L. (2022). China's agricultural non-point source pollution and green growth: interaction and spatial spillover. *Environ. Sci. Pollut. Res.* 29 (40), 60278–60288. doi:10.1007/s11356-022-20128-x

Xu, X., Liu, J., Jiao, F. S., Zhang, K. S., Ye, X., Gong, H. B., et al. (2023). Ecological engineering induced carbon sinks shifting from decreasing to increasing during 1981–2019 in China. *Sci. Total Environ.* 864, 161037. doi:10.1016/j.scitotenv.2022.161037

Yang, H. Q., Zhang, J., and Yang, Z. G. (2013). Rational land planning utilization structure optimization based on multi-objective linear programming model of foshan. *Adv. Mater. Res.* 616–618, 1243–1248. doi:10.4028/www.scientific.net/AMR.616-618.1243

Yuan, Z., Jiang, Q. Q., and Yin, J. (2023). Impact of climate change and land use change on ecosystem net primary productivity in the Yangtze River and Yellow River Source Region, China. *Watershed Ecol. Environ.* 5, 125–133. doi:10.1016/j.wsee.2023.04.001

Yue, Q., Zhang, F., and Guo, P. (2018). Optimization-based agricultural water-saving potential analysis in minqin county, gansu province China. *Water* 10 (9), 1125. doi:10.3390/w10091125

Zhang, C. L., Huang, N., Wang, L., Song, W. J., Zhang, Y. L., and Niu, Z. (2023). Spatial and temporal pattern of net ecosystem productivity in China and its response to climate change in the past 40 years. *Int. J. Environ. Res. Public Health* 20 (1), 92. doi:10.3390/ijerph20010092

Zhang, P., Liu, Y. H., Pan, Y., and Yu, Z. R. (2013). Land use pattern optimization based on CLUE-S and SWAT models for agricultural non-point source pollution control. *Math. Comput. Model.* 58 (3), 588–595. doi:10.1016/j.mcm.2011.10.061

Zhao, M. M., He, Z. B., Du, J., Chen, L. F., Lin, P. F., and Fang, S. (2019). Assessing the effects of ecological engineering on carbon storage by linking the CA-Markov and InVEST models. *Ecol. Indic.* 98, 29–38. doi:10.1016/j.ecolind.2018.10.052

Zhao, X., Tang, F., Zhang, P. T., Hu, B. Y., and Xu, L. (2019). Dynamic simulation and characteristic analysis of county production life ecological space conflict based on CLUE-S model. *Acta Ecol. Sin.* 39 (16), 5897–5908. doi:10.5846/stxb201901070059

Zhou, F. C., Han, X. Z., Tang, S. H., Song, X. N., and Wang, H. (2021). An improved model for evaluating ecosystem service values using land use/cover and vegetation parameters. *J. Meteorological Res.* 35 (1), 148–156. doi:10.1007/s13351-021-9199-x

Zhou, G. S., Wang, Y. H., Jiang, Y. L., and Yang, Z. Y. (2002). Estimating biomass and net primary production from forest inventory data: a case study of China's Larix forests. *For. Ecol. Manag.* 169 (1), 149–157. doi:10.1016/S0378-1127(02)00305-5

Zhou, S. H., Cao, J. Q., Wang, F., and Chang, Z. D. (2023). Spatio-temporal distribution and influencing factors of carbon source/sink, carbon surplus and deficit in three northeast provinces. *Acta Ecol. Sin.* 43 (22), 9266–9280. doi:10.20103/j.stxb.202212153598

frontiers | Frontiers in Ecology and Evolution

TYPE Original Research
PUBLISHED 31 January 2025
DOI 10.3389/fevo.2025.1513189

OPEN ACCESS

EDITED BY
Chunhui Li,
Beijing Normal University, China

REVIEWED BY
Yurui Fan,
Brunel University London, United Kingdom
Lyuliu Liu,
China Meteorological Administration, China

*CORRESPONDENCE
Ting Hua
thua@nwu.edu.cn

RECEIVED 18 October 2024
ACCEPTED 14 January 2025
PUBLISHED 31 January 2025

CITATION
Tan Q, Hua T, Zhao H and Zhou P (2025) Vegetation greening and climate change respectively regulates the long-term trend and interannual variability in evapotranspiration over the Loess Plateau since the 21st century.
Front. Ecol. Evol. 13:1513189.
doi: 10.3389/fevo.2025.1513189

Vegetation greening and climate change respectively regulates the long-term trend and interannual variability in evapotranspiration over the Loess Plateau since the 21st century

Qiaoyin Tan[1], Ting Hua[1,2]*, Haichen Zhao[1] and Peiye Zhou[3,4]

[1]Shaanxi Key Laboratory of Earth Surface System and Environmental Carrying Capacity, College of Urban and Environmental Sciences, Northwest University, Xi'an, China, [2]Institute of Earth and Surface System and Hazards, College of Urban and Environmental Sciences, Northwest University, Xi'an, China, [3]Key Laboratory of Ecological Safety and Sustainable Development in Arid Lands, Northwest Institute of Eco-Environment and Resources, Chinese Academy of Sciences, Lanzhou, China, [4]College of Resources and Environment, University of Chinese Academy of Sciences, Beijing, China

Since the 21st century, large-scale afforestation projects on the Loess Plateau have resulted in significant vegetation greening, contributing to ecosystem restoration and enhanced soil conservation. However, these efforts have also led to soil aridification, declining groundwater levels, and reduced terrestrial water storage. These negative consequences are primarily attributed to increases in evapotranspiration (ET), which has augmented water consumption. Despite these findings, the underlying mechanisms driving ET variations remain contentious due to the complex interplay of multiple factors. In this study, we employed a logical attribution method, which attributes vegetation changes predominantly to anthropogenic activities (e.g., reforestation or land-use changes), while directly linking changes in climatic factors (e.g., temperature and precipitation) to climate change. We separately examined the contributions of long-term trends and interannual variability in ET to reveal distinct driving forces. Between 2000 and 2022, approximately 80% of areas showing significant changes in ET and its components were directly influenced by vegetation greening, particularly in the central part of the Loess Plateau, where restoration efforts were most prominent. In contrast, only around 20% of these changes were attributable to climate change and other factors. After removing long-term trends, interannual variations in ET were found to be more closely associated with climatic factors (temperature and precipitation), especially in arid and semi-arid regions. This indicates that climate is the dominant factor driving interannual variations in ET across the Loess Plateau. Our findings contribute to a deeper

understanding of the water cycle dynamics in the context of large-scale vegetation restoration on the Loess Plateau. These insights provide a scientific foundation for policymakers to evaluate the environmental impacts and potential water-related risks associated with ecological restoration projects.

KEYWORDS

evapotranspiration, vegetation greening, climatic factors, Loess Plateau, long term trends, interannual variability

1 Introduction

The Loess Plateau is located in the transitional zone between semi-humid and arid climates in China, where the ecosystem has been highly sensitive to climate change and human disturbances (Fu, 1989; Fu et al., 2017; Jiang et al., 2021). Historically, this region was covered by grasslands and forests; however, intense human activities such as deforestation (Zheng et al., 2005) and land reclamation (Guan et al., 2020), combined with climate change, transformed it into one of the most severely eroded regions in the world, which led to a deteriorated ecological environment and significant conflicts between humans and the land (Wu et al., 2019). In recent years, with the implementation of a series of ecological restoration projects (Fu et al., 2017; Li et al., 2019), particularly following the initiation of the Grain to Green Program (GTGP) in 1999, massive greening of vegetation has become the most notable environmental change in the region since the 21st century (Liu et al., 2008; Lü et al., 2012). Vegetation cover increased by 25% between 2000 and 2010 (Feng et al., 2016), and approximately 16,000 km^2 of sloping farmland has been converted into artificial grasslands and forests (Nazarbakhsh et al., 2020). However, such large-scale vegetation restoration has also significantly altered regional energy balance and water cycle processes (Deng et al., 2019), thereby triggering a series of environmental and ecological effects, including some negative impacts. For instance, the newly planted vegetation may have consumed additional water from the soil, leading to soil aridification (Du et al., 2007; Deng et al., 2016; Zhang et al., 2018; Ye et al., 2019), decreased groundwater levels (Han et al., 2020), and ultimately, terrestrial water shortages (Yang et al., 2014; Deng et al., 2019). These issues are closely related to the substantial increases in evapotranspiration (ET) since the implementation of ecological restoration projects.

In the Loess Plateau, which is characterized by a semi-arid to semi-humid climate, a substantial portion of precipitation either evaporates or transpires back into the atmosphere. Consequently, understanding evapotranspiration (ET) is crucial for unraveling the regional water cycle and addressing challenges related to water resource security, particularly within the broader context of ecological restoration and greening initiatives (Reddy, 1996; Williams et al., 2004; Bai et al., 2020). Previous studies have generally identified an increasing trend in ET across the Loess Plateau (Feng et al., 2012; Wang et al., 2020; Jiao et al., 2021; Zhang et al., 2021). However, the driving factors behind this trend—such as vegetation dynamics (Bai et al., 2019; Yue et al., 2019; Wang et al., 2023), climatic variables (e.g., precipitation and temperature) (Gu et al., 2016; Adler et al., 2017), and atmospheric CO_2 concentration (Shi et al., 2013; Mao et al., 2015)—remain inadequately understood. This knowledge gap is particularly critical given the Plateau's transitional climatic conditions and its vulnerability to both natural fluctuations and anthropogenic impacts. Among these factors, precipitation serves as the primary water resource, exerting a direct influence on large-scale ET patterns (Shao et al., 2019). Simultaneously, vegetation exerts a significant influence on ET through mechanisms such as the "pumping effect" of root systems. Nevertheless, fully separating the effects of vegetation dynamics and climate factors to ET remains a topic of considerable debate (Chen et al., 2017; Bai et al., 2019; Jiang et al., 2021). Recent studies have explored the drivers of evapotranspiration (ET) changes in the Loess Plateau region, revealing complex and sometimes divergent findings. Some research has attributed ET trends primarily to climate variability, such as Zhao et al. (2022), who found that rising temperatures and vegetation greening accounted for 45.6% and 31.6% of ET increases, respectively, across the broader Yellow River Basin. In contrast, Wang et al. (2021) utilized high-resolution remote sensing data for the Loess Plateau specifically, and found that vegetation (as indicated by NDVI) explained 61.4% of ET changes, while precipitation showed a surprising negative contribution (−26.3%). Taking a more balanced approach, Li et al. (2021) assigned 68% of ET changes to climate factors (largely precipitation) and 32% to vegetation recovery based on an empirical model. These discrepancies highlight the methodological and spatial-scale challenges in attributing ET trends. Basin-wide analyses may oversimplify regional heterogeneity, as vegetation restoration on the Loess Plateau is concentrated in areas with steeper slopes and bare soil, rather than the flat terrain of the broader Yellow River Basin (Chen et al., 2007). As a result, such differences in topographical and land-cover conditions result in distinct evapotranspiration (ET) response mechanisms across these regions (Fu et al., 2003). Furthermore, even within the Loess

Plateau, localized studies may overemphasize specific conditions or data uncertainties, as demonstrated by Bai et al. (2019), who found that 93% of ET trends could be explained by vegetation (NDVI) in a hilly-gully basin, while attributing only 18.1% to precipitation. These divergent findings reflect the complex, nonlinear interactions between land surface processes and atmospheric conditions in this transitional zone, where both long-term changes and interannual variability play significant roles. Importantly, previous studies have frequently overlooked the distinction between the cumulative effects of long-term trends and the immediate impacts of interannual fluctuations, as well as the separate investigation of the driving mechanisms behind these two types of variability in ET, potentially leading to divergent attribution outcomes. This distinction is critical for characterizing the response of ET to climate and vegetation changes, especially given the temporal dynamics of vegetation recovery, where newly established vegetation may exert a different hydrological influence compared to mature ecosystems.

To address the knowledge gaps identified in previous studies, this research adopted an integrated approach that separately examines long-term trends and interannual variability in evapotranspiration (ET) across the Loess Plateau. The study divided the region into five ecological sub-regions based on different land-use types, and leveraged multiple datasets including the Global Land Evaporation Amsterdam Model (GLEAM) v3 (Miralles et al., 2011; Martens et al., 2017), Normalized Difference Vegetation Index (NDVI) data from the Global Vegetation Health Products (GVHP), and climate reanalysis data from the fifth-generation European Centre for Medium-Range Weather Forecasts (ECMWF) dataset (ERA5) (Hersbach et al., 2023). For long-term trend analysis, the study utilized a simple yet effective method (Huang et al., 2020) to disentangle the respective contributions of vegetation dynamics and climatic factors to ET changes during the growing season. To examine interannual variability, we removed the long-term trends and analyzed the correlations between ET, vegetation activity, and climate factors. By integrating these complementary analytical perspectives, this research provided a comprehensive understanding of the mechanisms driving ET variations in the Loess Plateau. The findings offer valuable insights into the intricate interplay between vegetation restoration and climatic shifts in this transitional climate region.

2 Data and methods

2.1 Data

2.1.1 Evapotranspiration data

This study utilized GLEAM ET data (https://www.gleam.eu/) for the growing season (April to September) from 2000 to 2022 to analyze the spatiotemporal changes in ET on the Loess Plateau. The monthly GLEAM ET data, with a spatial resolution of 0.25° (Miralles et al., 2011; Martens et al., 2017), are subdivided into transpiration (Ec), interception loss (Ei), bare-soil evaporation (Es), snow sublimation (Esn), and open-water evaporation (Ew) (Zhang et al., 2016). For this study, snow sublimation and open-water evaporation were considered negligible for the Loess Plateau during the growing season; thus, only Ec, Ei, and Es were used to calculate ET (Zhang et al., 2019). The GLEAM evapotranspiration data are based on multiple satellite observations, including net radiation, temperature, precipitation, vegetation optical depth, and snow water equivalent. The estimations for Ec and Es are derived from a modified Priestley-Taylor (PT) equation, which calculates them as a function of available energy [net radiation (Rn) minus ground heat flux (G)] and a dimensionless coefficient α representing the parameterized evaporative resistance. Ei is calculated separately using the Gash analytical model of rainfall interception, driven by observations of precipitation and both vegetation and rainfall characteristics. Additionally, this remote-sensing-based dataset accounts for the constraints of soil moisture on evaporation (Priestley and Taylor, 1972) and has been validated as reliable (Song et al., 2023) for assessing the water cycle in semi-arid regions with geographic conditions similar to those of the Loess Plateau.

2.1.2 NDVI data

This study analyzed vegetation changes in the Loess Plateau based on NDVI data with a spatial resolution of 4 km and weekly temporal resolution, obtained from the National Oceanic and Atmospheric Administration (NOAA) Center for Satellite Application and Research (STAR) (https://www.star.nesdis.noaa.gov/smcd/emb/vci/VH/vh_ftp.php). The data have been corrected for atmospheric and geometric distortions to eliminate influences unrelated to vegetation and are widely used in global and regional studies monitoring vegetation dynamics and vegetation responses to climate change (Tang et al., 2020; Zeng et al., 2023). For this study, vegetation changes were analyzed during the same time span as ET, from 2000 to 2022 (April to September). The maximum value compositing (MVC) method was used to synthesize the raw NDVI data into maximum NDVI values (NDVImax) for the growing season, and areas with NDVImax < 0.1 were excluded to avoid potential impacts of soil properties.

2.1.3 Climate data

The monthly precipitation and 2-meter temperature during the growing season (April to September) from 2000 to 2022 were derived from the ERA5 dataset at a resolution of 0.25° × 0.25° (Hersbach et al., 2023). The spatial resolutions of the three aforementioned data sources were aggregated into a common resolution of 0.1° × 0.1° using the bilinear interpolation method.

2.2 Methods

2.2.1 Attribution method of long-term trend in ET

Vegetation changes and climate factors (such as temperature, precipitation, etc.) are the two main driving factors behind the significant trend in ET in the Loess Plateau from 2000 to 2022 (see

Section 3.2). Given the complex interactions among climatic factors, vegetation, and ET, we adopted the method proposed by Huang et al. (2020) to assess the impacts of climate change and vegetation changes on ET and its components. This method assumes that among all pixels showing a significant increasing (or decreasing) trend in ET (or its components), those that also show a significant increasing (or decreasing) trend in vegetation are considered to have their ET changes directly caused by vegetation changes; otherwise, the changes are attributed to other factors. The trends in all variables, including NDVI and ET (and its components), were calculated using two methods: the Mann-Kendall (MK) non-parametric statistical test and least squares estimation. These trends were tested using a T-test to determine the significance level of the trends.

2.2.2 Attribution method of interannual variations in ET

When the long-term trend was removed from the original time series (ET, climatic factors, and NDVI), the detrended time series $y'(i)$ can represent its interannual variability, which can be expressed as:

$$y'(i) = y(i) - (at + b) \quad (1)$$

where $y(i)$ is the original timeseries, i is the time counter (year), a and b are the coefficients using the least square estimation.

After removing the long-term trends, we calculated the interannual correlations between growing season NDVI (or temperature and precipitation) and ET (or its components) at the nearest grid points from 2000 to 2022. The Pearson linear correlation coefficients are expressed as follows:

$$r_{xy} = \frac{\sum_{i=1}^{n}[(x_i - \bar{x})(y_i - \bar{y})]}{\sqrt{\sum_{i=1}^{n}(x_i - \bar{x})^2}\sqrt{\sum_{i=1}^{n}(y_i - \bar{y})^2}} \quad (2)$$

where, x_i is the value of NDVI (or climate factors) for the i th year, and y_i denotes the value of ET (or its components) for the i th year. The significance of the correlation coefficients is test by a T-test (two-tailed).

2.3 Study area

The Loess Plateau (roughly within 34°~41°N, 98°~114°E), with an area of ~632,520 km^2, which accounts for 6.3% of China's total land area (Jiang et al., 2022). The average annual precipitation ranges from 200 mm in the northwest to 800 mm in the southeast, with 60%~70% of the annual precipitation occurring between June and September in the form of high-intensity rainstorms, which often cause extreme soil erosion and drought frequently occurs (Liang et al., 2020). The average annual temperature is 4°C in the northwest and 14°C in the southeast (Peng et al., 2018). Consequently, the region is characterized as a typical transitional zone from an arid to a semi-humid climate, significantly influenced by the East Asian monsoon. The predominant land cover types include grassland, cropland, and forest (Figure 1).

Based on the ecological restoration areas and geographical characteristics of the Loess Plateau, and following the division methods used in previous studies (Jiang et al., 2022; Yang Y. F. et al., 2019), the Loess Plateau is divided into five sub-regions: the Northern Loess Plateau (NLP), the Middle Loess Plateau (MLP), the Eastern Loess Plateau (ELP), the Western Loess Plateau (WLP), and the Southern Loess Plateau (SLP) (Figure 1). Among these, the NLP is a typical semi-arid area with a mean annual precipitation below 400 mm, mostly covered by deserts or desertified land. The MLP is the primary region for vegetation restoration projects (Jiang et al., 2022), while the WLP consists mainly of high tableland and gully regions. The SLP and ELP are primarily composed of broad valley plains and rocky mountain areas.

3 Results

3.1 Climatological pattern of ET on the Loess Plateau

Climatologically, the total growing season ET on the Loess Plateau exhibited a decreasing pattern from southeast to northwest (from > 2 mm/day in the southeast to < 1 mm/day in the northwest), closely mirroring the precipitation pattern and reflecting the limiting role of water resources on the ET process in this semi-humid to semi-arid region (Figure 2A). Among the three components of ET, Ec was the primary contributing component, accounting for ~70% of total ET from 2000 to 2022. Similar to ET, the spatial distribution of Ec (Figure 2B) also showed a decreasing trend from southeast to northwest, with high-value areas exceeding 1.4 mm/day primarily located in semi-humid, forested regions, while low-value areas (<0.6 mm/day) were found in arid to semi-arid regions with precipitation below 200 mm (excluding the Hetao Plain). On the other hand, Ei was substantially lower than Ec (Figure 2C), with rates generally below 0.1 mm/day outside forested areas, contributing minimally to total ET, with values ranging from 3% to 6%.

In contrast to the two vegetation-related ET components (Ec and Ei), the distribution pattern of Es was characterized by low values in the southeast and high values in the northwest (Figure 2D). As the second largest contributor to total ET (~19% to 32%), relatively higher Es values (~1 mm/day) were observed in regions with annual precipitation below 400 mm, where lower vegetation cover allowed Es to dominate the ET process. In comparison, Es in densely vegetated areas was weaker, generally below 0.4 mm/day, indicating a competitive relationship between vegetation water consumption and soil evaporation.

3.2 Change trend in ET on the Loess Plateau from 2000 to 2022

From 2000 to 2022, the regional mean ET time series of the Loess Plateau showed a significant increasing trend ($p < 0.05$)

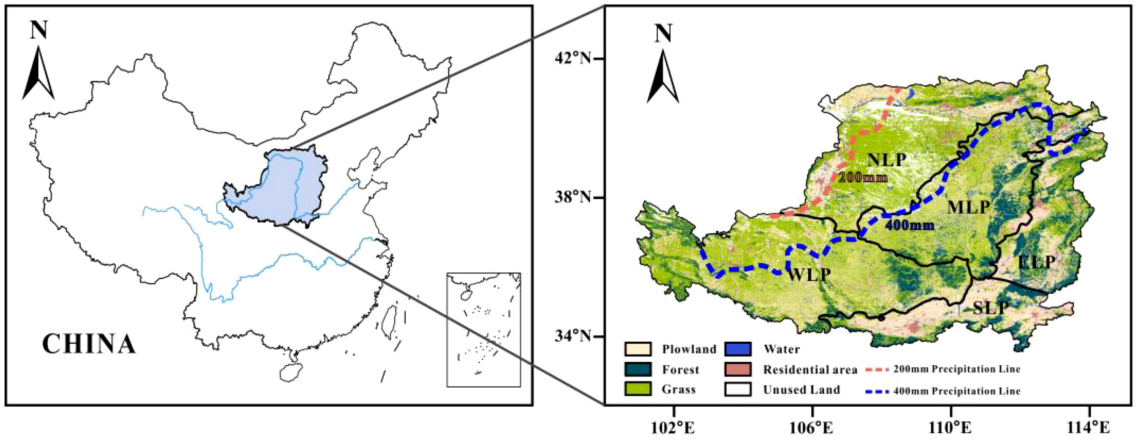

FIGURE 1
Spatial distribution of land use types over the Loess plateau (shading) being divided into five ecological sub-regions (delimited by black lines), and the isolines of mean annual precipitation of 200 mm and 400 mm are also shown in dashed lines. Source: The map was created based on the standard maps provided by the Ministry of Natural Resources Standard Map Service website under GS(2016)1594. No modifications were made to the map boundaries.

(Figure 3A), with an increase rate of 0.164 mm/day per decade (R^2=0.5197). Both vegetation-related components, Ec and Ei, also showed significant increasing trends ($p < 0.05$) with respective increase rates of 0.194 and 0.019 mm/day per decade (Figures 3B, C). In contrast, the regional mean Es demonstrated a significant decreasing trend ($p < 0.05$) over the same period (Figure 3D), with a decrease rate of −0.043 mm/day per decade, partially offsetting the increasing trends of the two vegetation-related components. As a result, the total ET showed a relatively smaller increasing trend compared to Ec.

The distribution of ET change trends indicated that the majority of the Loess Plateau experienced a significant increase in ET from 2000 to 2022, with the exception of marginal areas in the NLP, WLP, SLP, and ELP (Figure 4A). Compared to ET, Ec exhibited a broader area with a significant increasing trend (Figure 4B), particularly in the northwestern and southeastern corners of the

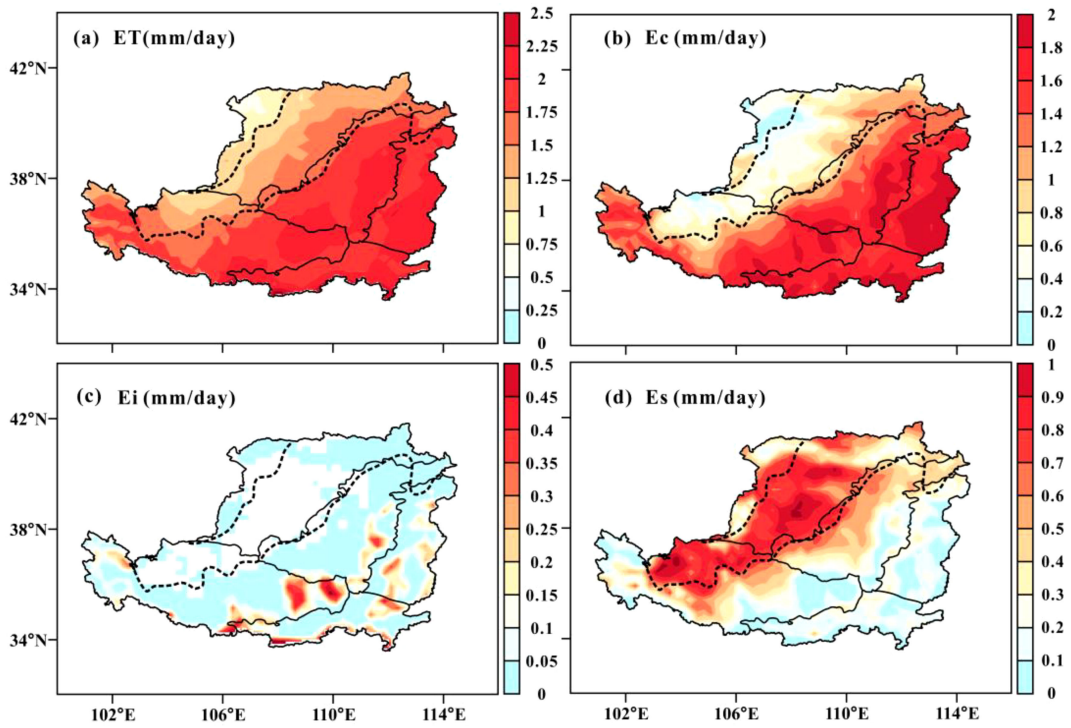

FIGURE 2
Climatological pattern in **(A)** evapotranspiration (ET), **(B)** vegetation transpiration (Ec), **(C)** canopy intercepted water evaporation (Ei), and **(D)** soil evaporation (Es) during the growing season. The dashed and solid lines are the same as that in Figure 1.

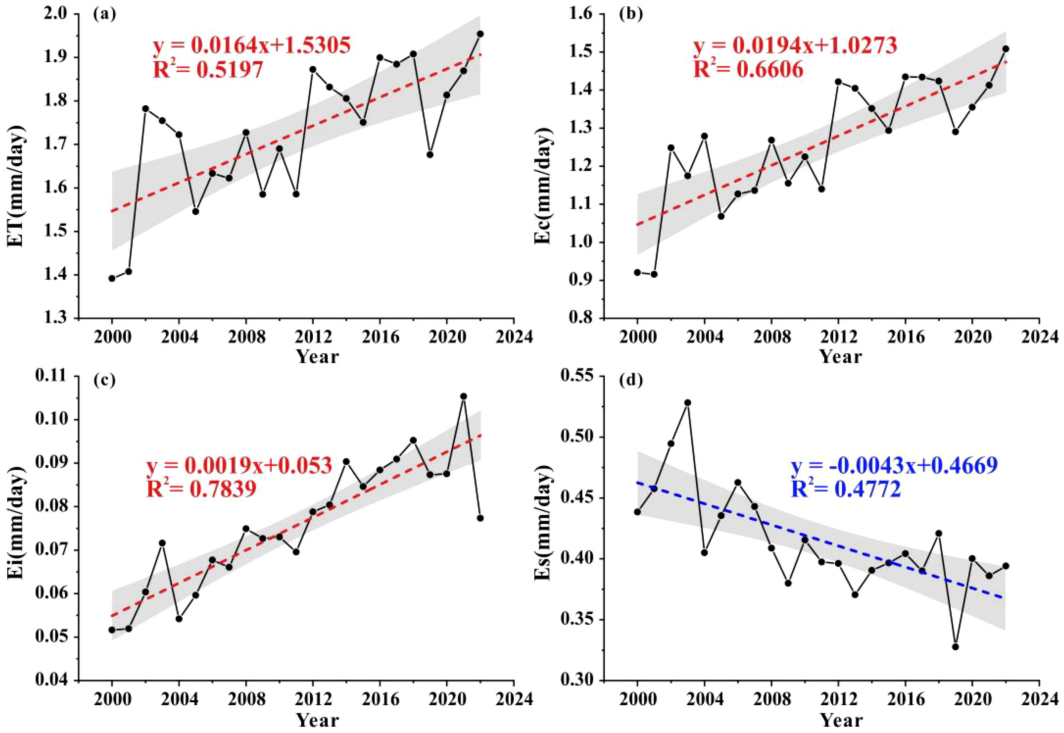

FIGURE 3
Time series of regional mean **(A)** evapotranspiration (ET), **(B)** vegetation transpiration (Ec), **(C)** canopy intercepted water evaporation (Ei), and **(D)** soil evaporation (Es) of the Loess Plateau during the growing season from 2000 to 2022, and their linear regression lines area plotted in dashed lines. The gray shaded area represents the confidence interval for $p < 0.5$.

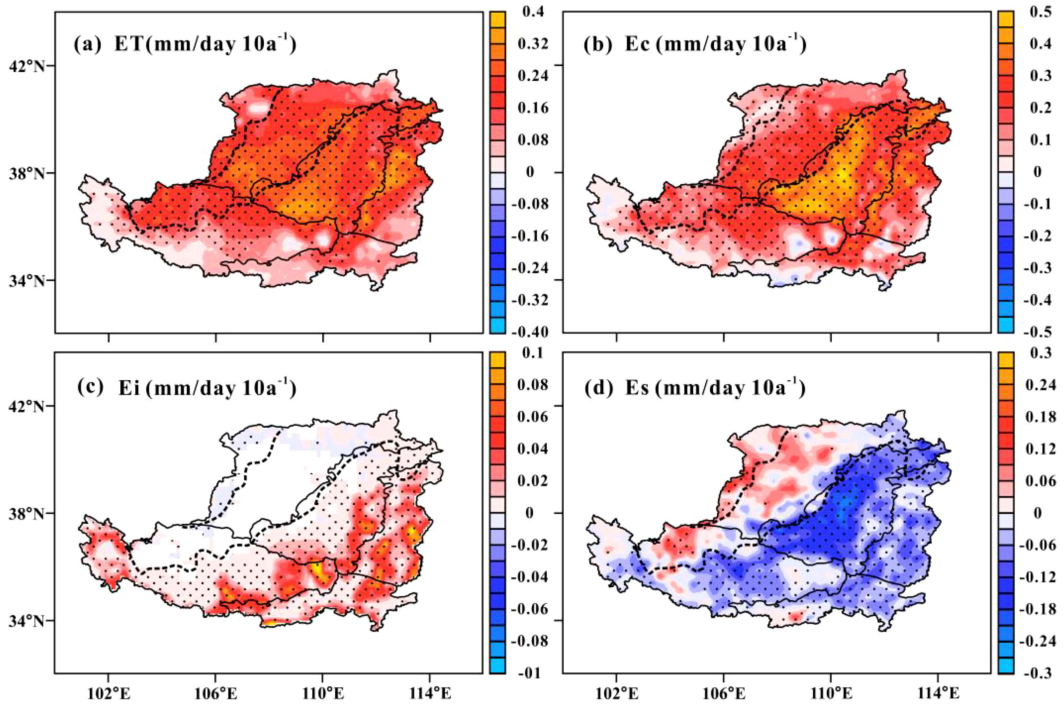

FIGURE 4
Spatial distribution of MK trends in **(A)** evapotranspiration (ET), **(B)** vegetation transpiration (Ec), **(C)** canopy intercepted water evaporation (Ei), and **(D)** soil evaporation (Es) over the Loess Plateau during the growing season from 2000 to 2022. Those areas with significant changes ($p < 0.05$) are stippled.

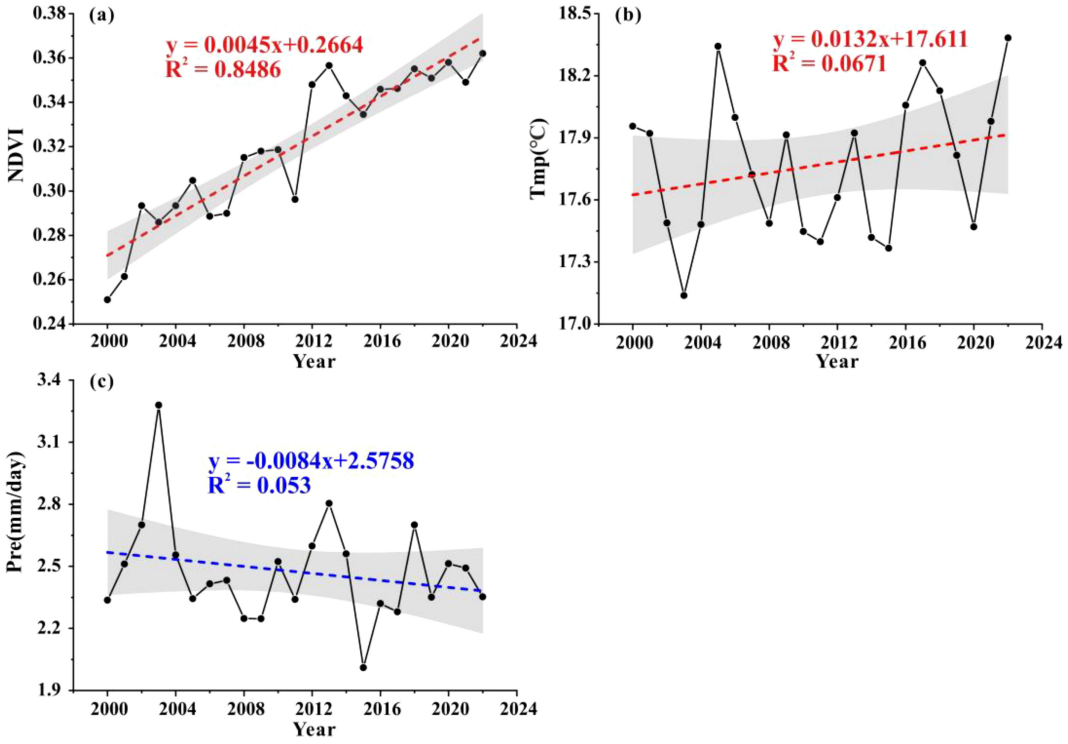

FIGURE 5
Time series of regional mean **(A)** NDVI, **(B)** temperature, and **(C)** precipitation of the Loess Plateau during the growing season from 2000 to 2022. The gray shaded area represents the confidence interval for $p < 0.5$.

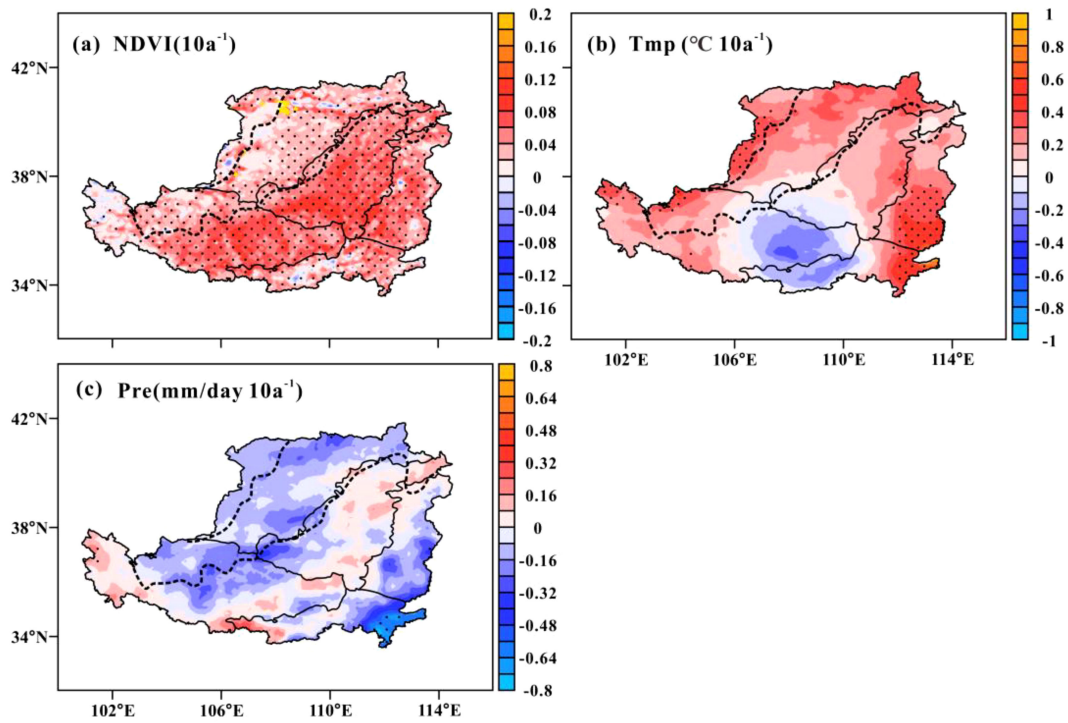

FIGURE 6
MK Trends in **(A)** NDVI, **(B)** temperature, and **(C)** precipitation over the Loess Plateau during the growing season from 2000 to 2022. Stippled areas represent significant changes ($p < 0.05$).

Loess Plateau. In the MLP, where substantial vegetation recovery occurred, the trend in Ec exceeded that of ET (> 0.5 mm/day per decade). The water intercepted by the vegetation canopy showed a marked increase in the southeastern semi-humid region of the Loess Plateau (MLP, WLP, and ELP) (Figure 4C), with particularly pronounced increasing trends (> 0.1 mm/day per decade) in forested areas. In contrast, Es displayed opposite change trends between the northwestern and southeastern parts of the Loess Plateau (Figure 4D). Most of the Loess Plateau exhibited significant decreasing trends in Es, particularly in the semi-humid MLP, WLP, and ELP, while a minority of areas (primarily in the semi-arid and arid NLP and northern WLP) showed significant increasing trends in Es.

3.3 Changes in NDVI and climatic factors over the Loess Plateau from 2000 to 2022

The regional mean NDVI time series of the Loess Plateau exhibited a significant ($p < 0.001$) increasing trend from 2000 to 2022 (Figure 5A), with an increase rate of 0.045 per decade, indicating an overall greening trend for the Loess Plateau since the implementation of large-scale ecological projects. The spatial pattern of NDVI trends revealed that almost the entire Loess Plateau experienced significant increases in NDVI, particularly in the MLP and WLP regions, where the NDVI increase exceeded 0.1 per decade (Figure 6A). During the same period, the Loess Plateau as a whole did not exhibit significant trends in either temperature or precipitation during the growing season (Figures 5B, C), with change rates of 0.132°C per decade and −0.084 mm/day per decade, respectively. Moreover, the spatial distribution of trends in each pixel did not show significant trends in most areas of the Loess Plateau (Figures 6B, C). Most of the Loess Plateau experienced a rise in temperature from 2000 to 2022, with a declining trend observed only in the eastern WLP and western SLP (Figure 6B). Additionally, there were decreasing trends in precipitation across the majority of the Loess Plateau (Figure 6C), with only parts of the eastern MLP and southern WLP showing non-significant increases in precipitation.

3.4 Attribution of long-term trend in ET over the Loess Plateau

By employing the methodology proposed by Huang, we assessed whether vegetation greening is the direct cause of the trends in ET on the Loess Plateau. Among the pixels showing a significant trend in ET (covering approximately 71.4% of the total area of the Loess Plateau),

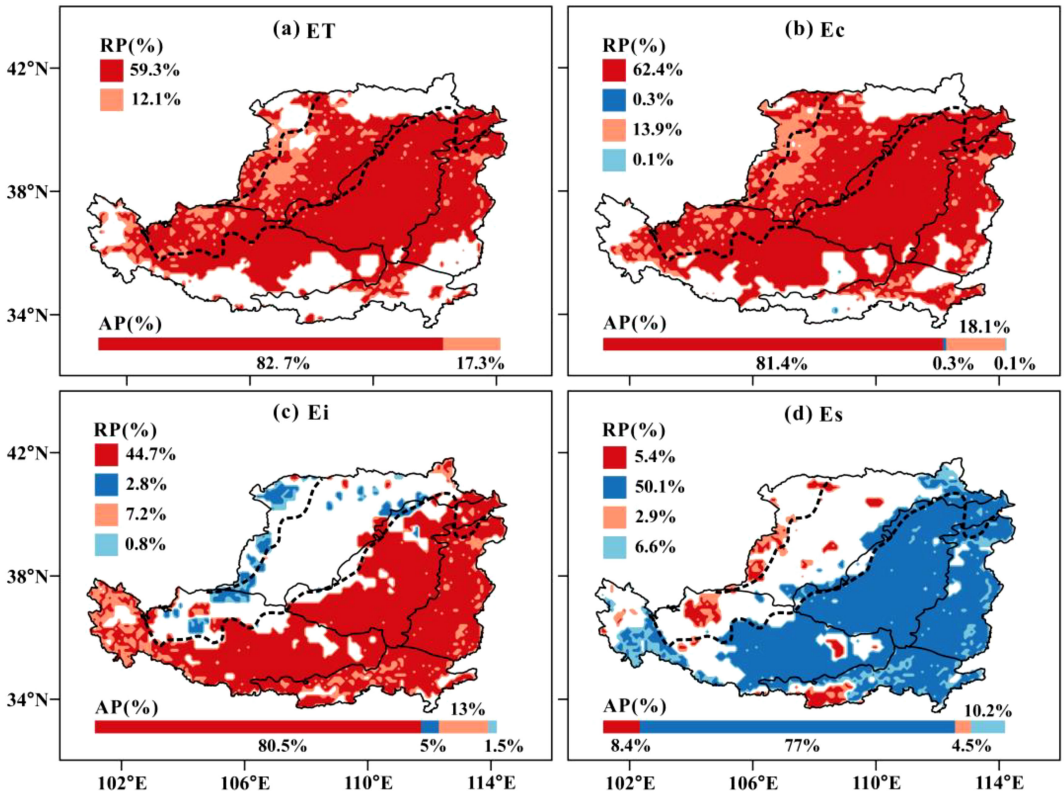

FIGURE 7
The distribution of whether significant trends in **(A)** evapotranspiration (ET), **(B)** vegetation transpiration (Ec), **(C)** canopy intercepted water evaporation (Ei), and **(D)** soil evaporation (Es) are cause directly by NDVI changes: Only pixels with significant increasing (decreasing) ET (and its components) are shown in red (blue), and those also show significant changes in NDVI are shown in dark colors, while those do not show significant NDVI changes are shown in light colors. Absolute Percentage (AP) refers to the percentage of pixels of each color relative to the total number of colored pixels; Relative Percentage (RP) refers to the percentage of pixels of each color relative to the total number of pixels on the Loess Plateau.

around 82.7% also experienced a significant increase in NDVI (Figure 7A), while only about 17.3% did not show any significant change in NDVI. This result indicates that the majority of areas with significant ET changes were directly caused by vegetation greening. Compared to ET, the area with a significant increase in Ec was larger, covering approximately 75.1% of the Loess Plateau (Figure 7B). In areas with significant increases in Ec, over 81.4% of grid points also showed a notable increase in NDVI, suggesting that the rise in Ec is predominantly due to vegetation recovery. Less than 20% of the grid points, primarily located in arid and semi-arid zones, exhibited no significant change in vegetation. There were few pixels with significant decreases in Ec, mainly associated with changes in vegetation cover. Furthermore, approximately 80.5% of all pixels showing a significant increase in Ei also experienced significant rises in vegetation (Figure 7C), indicating that the increase in Ei is mainly driven by vegetation changes. Less than 15% of these areas (primarily in the western WLP and the cropland areas of SLP and ELP) showed Ei enhancement driven by climatic changes. Of the small number of pixels with a significant decrease in Ei in arid and semi-arid regions, about one-fourth of these areas were attributed to vegetation changes.

Between 2000 and 2022, the area with a significant decreasing trend in Es covered approximately 56.7% of the total area of the

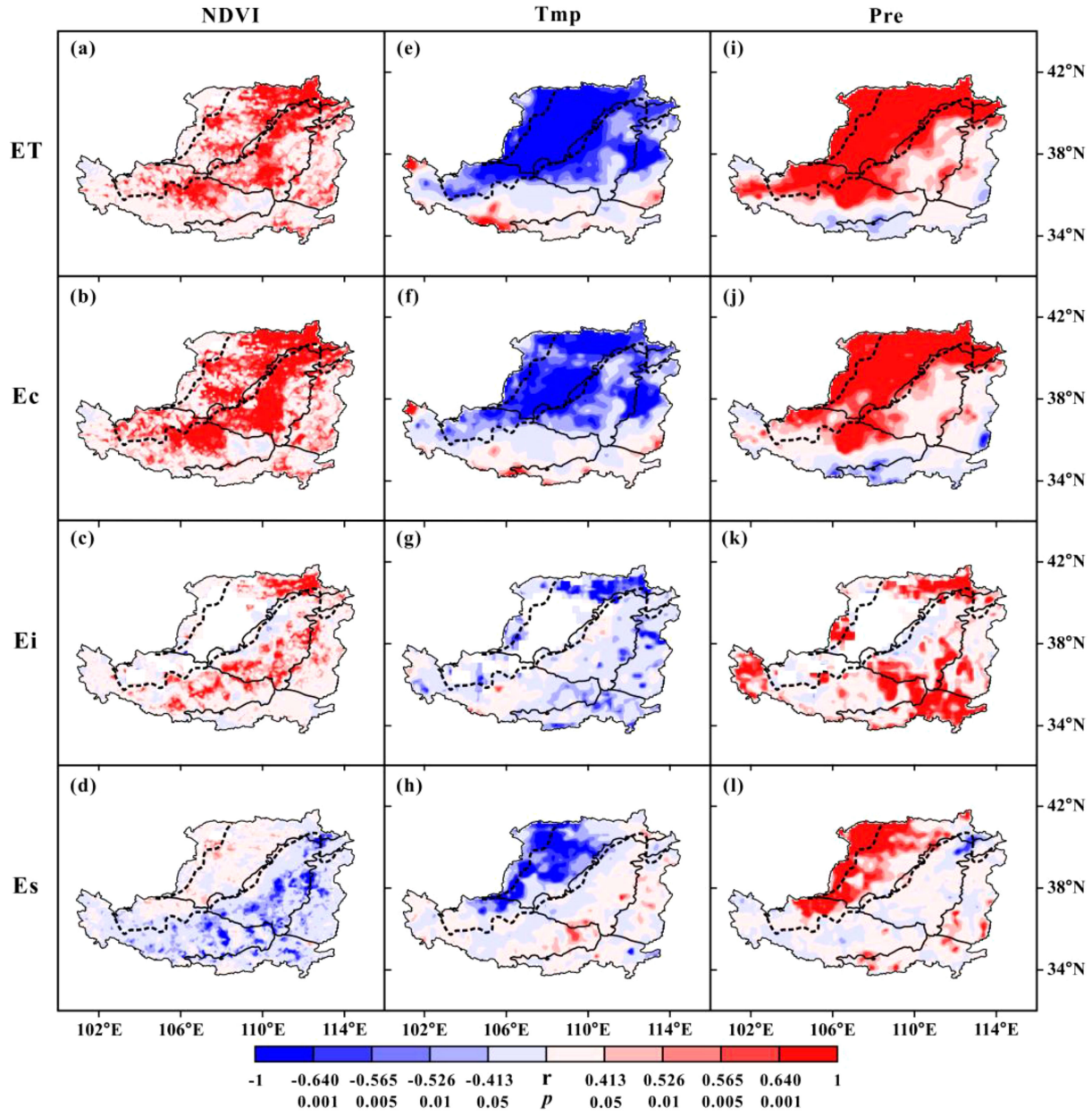

FIGURE 8
Pearson correlation coefficients and their significance levels (two-tailed) between evapotranspiration (ET), vegetation transpiration (Ec), canopy intercepted water evaporation (Ei), and soil evaporation (Es) and (left) NDVI/ (middle) temperature/ (right) precipitation in growing season over the Loess Plateau from 2000 to 2022. The correlation coefficient (*r*) values are shown with the corresponding significance test (*p*-values) below, both sharing the same color bar.

Loess Plateau, primarily distributed across the MLP, ELP, eastern WLP, and parts of the SLP. In these areas, the majority (about 77%) coincided with a significant increase in NDVI (Figure 7D), indicating that the decrease in Es was related to changes in vegetation cover. In addition, about 12.9% of the total area showed a significant increase in Es, sporadically located in arid and semi-arid regions, with approximately 65% of these areas also driven by changes in vegetation cover. Although Es was not directly produced by vegetation, long-term vegetation changes remained a primary cause of the changing trends in Es.

3.5 Attribution of interannual variations in ET over the Loess Plateau

To explore the impact of vegetation conditions and climate factors on ET at an interannual time scale, Pearson correlations between ET (and its components) and NDVI (or climatic factors) were calculated for each pixel after removing their corresponding trend components (Figure 8). The results revealed that ET and Ec were significantly ($p < 0.001$) and positively correlated with NDVI in some areas of the MLP, NLP, and WLP (Figures 8A, B). In contrast, the positive correlation of Ei and the negative correlation of Es were largely insignificant (Figures 8C, D). In comparison, the correlations of ET (Ec and Es) with the two climatic factors were much stronger, particularly in the arid and semi-arid regions ($p < 0.001$, Figures 8E–G, I–K). For instance, there were significantly negative correlations between temperature and ET/Ec/Es, suggesting that in these water-limited areas, increased temperatures and associated drought stress may inhibit the ET process. Additionally, a significantly positive relationship was found between precipitation and ET/Ec/Es over large areas in the northwest, although some negative correlations were observed in the southeastern marginal regions. The correlations between precipitation and temperature indicated that interannual variations in ET were predominantly controlled by water availability in these water-limited regions, rather than energy availability. These findings also suggest that climate is the primary factor influencing the interannual variations in ET and its components in the arid and semi-arid regions of the Loess Plateau.

To verify the robustness of our results, the China meteorological forcing dataset (CMFD) (Yang K. et al., 2019) were also conducted correlation tests with ET with long term trends excluded, this dataset integrates ground observations and satellite data and are widely proven to have good performance in representing the precipitation and temperature pattern (Yang et al., 2010; He et al., 2020). The results of CMFD demonstrate that the spatial patterns in the correlation of ET with both temperature and precipitation are highly consistent with that of ERA5 (Supplementary Figures S1), implying that the dominant role of these climatic factors in regulating interannual variability in ET is relatively robust among different data sources. Although some researches show certain overestimation of ERA5 precipitation over the Loess Plateau (Jiang et al., 2021), our result suggests this potential overestimation of ERA5 precipitation does not undermine the validity of our conclusions.

4 Discussion

4.1 Validation of the GLEAM ET product

In this study, we employed the remote-sensing-based GLEAM ET product to estimate ET changes in the Loess Plateau, as it explicitly considers the impact of soil moisture, which is a critical limiting factor for evapotranspiration in such a relatively water-limited region (Ferguson and Wood, 2010; Vinukollu et al., 2011). Generally, the GLEAM ET dataset has been proven to perform well in representing both the temporal and spatial variations of total ET and its components across China, particularly during the warm months, when compared with *in situ* observations and other products (Li, 2023; Yao, 2023). From the climatological results of ET over the Loess Plateau, GLEAM shows that canopy transpiration tends to be larger than soil evaporation, which contrasts with some other products (Jiang et al., 2022; Zhao et al., 2022). This difference is likely due to the following reasons. The GLEAM ET model uses a multi-layer soil model to capture soil moisture distribution and its effects on vegetation transpiration, limiting soil evaporation in dry regions while increasing Ec (Miralles et al., 2011; Martens et al., 2017). In contrast, other evapotranspiration models, such as PML and VIC models, which are based on the Penman-Monteith equation, focus primarily on vegetation and meteorological factors, emphasizing energy balance over soil moisture (Liang et al., 1994; Zhang et al., 2019). These models estimate transpiration and evaporation separately via remote sensing, potentially overestimating soil evaporation in areas with sparse vegetation. Differences in meteorological inputs also contribute to the variations in their estimates.

4.2 Uncertainty in attribution of long-term trends using Huang's method

To determine whether long-term changes in vegetation are the direct drivers of observed trends in evapotranspiration (ET) and its components, we applied the method proposed by Huang. This approach posits that if both ET (and its components) and NDVI exhibit significant trends at the same grid point, it can be inferred that vegetation changes are the direct drivers of the trends in ET or its components, regardless of the presence of significant changes in climatic factors. Importantly, the trend in NDVI itself may be influenced by significant trends in climatic factors. However, we do not delve further into whether vegetation changes are attributable to anthropogenic activities or climatic factors, nor do we examine the extent to which climate change indirectly influences ET by altering vegetation conditions. Our analysis focuses exclusively on the direct impact of vegetation changes on ET. Conversely, when a significant trend in ET (or its components) occurs without a corresponding significant trend in NDVI, changes in climatic factors are considered the direct cause. Specifically, this method attributes vegetation changes primarily to anthropogenic activities (e.g., reforestation or land-use changes), while linking changes in climatic factors (e.g., temperature or precipitation) directly to

climate change. In reality, the interactions between vegetation, climatic factors (e.g., precipitation and temperature), and ET are highly complex, involving multiple feedback mechanisms, which makes disentangling the relationships among these variables challenging. For example, in the southeastern Loess Plateau, although NDVI exhibited a significant increasing trend, the corresponding increasing trend in Ec may have been offset by the suppressive effects of significantly rising temperatures. Under such stressful conditions, plants may close their stomata, potentially explaining the overall insignificant increase in ET in these areas (Yang Y. et al., 2019). In general, Huang's method provides a robust framework for disentangling the intricate relationships among vegetation dynamics, climatic factors, and ET trends through clear assumptions and logical classification. By avoiding the complexities of deeper causal mechanisms, this method enhances the simplicity and practicality of the analysis. Despite its simplicity, Huang's method effectively evaluates whether vegetation changes are directly responsible for long-term trends in ET.

4.3 Forcing mechanism of vegetation and climatic factors on ET over the Loess Plateau

The growing season of the semi-arid and semi-humid Loess Plateau is characterized by relatively higher temperatures, larger vapor pressure deficits, and abundant solar radiation. Consequently, regional ET is predominantly governed by water availability in the absence of significant human interventions (Magliano et al., 2017). Theoretically, variations in ET are controlled by variations in water supply (i.e., precipitation), given the absence of large river inputs for most areas of the interior Loess Plateau (Jin et al., 2011; Zhang et al., 2017). However, extensive anthropogenic ecological restoration efforts, particularly the annual planting of new vegetation, have increased Ec, resulting in significant upward trends in ET over the past decade. This sustained increase in ET cannot be explained by non-significant trends in climatic factors but is instead attributed to vegetation greening across the plateau. The greening trend has contributed to increasing both total ET and Ec, while simultaneously being associated with a decline in soil evaporation. This decline is not only caused by increased vegetation, which leads to a soil-drying trend through additional water consumption by Ec and Ei (Allen et al., 2017), but also by the diminishing energy available as increased canopy coverage blocks a larger proportion of solar radiation from reaching the soil surface (Duveiller et al., 2018; Jiang et al., 2022).

However, when the linear trends of all variables are removed, climatic factors (precipitation and temperature) exhibit a stronger correlation with the interannual variability in ET and its components across most of the study area, compared to vegetation dynamics. As expected, the positive correlation between precipitation and ET underscores its crucial role in regulating interannual variations in ET in these semi-arid and semi-humid regions. Although rising temperatures can increase potential ET, actual ET tends to decrease. This is likely because, on the one hand, at yearly or shorter time scales, higher temperatures are often associated with lower precipitation and reduced water supply, which in turn limits ET. On the other hand, during the growing season, leaf stomatal conductance tends to close under extreme heat, leading to reduced ET. The interaction and coupling effects of vegetation changes and climate change on ET are complex. Although many studies have attempted to fully disentangle the impacts of vegetation change and climate change on ET, as vegetation also responds to terrestrial ecosystem and climate changes, few studies have focused on the different forcing mechanisms of the long-term trend and interannual variability in ET. Many studies have attempted to disentangle the impacts of vegetation and climate change on evapotranspiration (ET), but few have explored the distinct mechanisms driving its long-term trends and interannual variability. The interactions between vegetation and climate change on ET are inherently complex, as vegetation dynamically responds to changes in ecosystems and climate conditions. These intricate feedbacks among vegetation change, climate change, and ET highlight the need for further research, particularly into the differing drivers of long-term trends and interannual variability.

4.4 Limitations

Although this study separately examined the relative importance of climatic factors and vegetation dynamics on long-term trends and interannual variations in ET, there are still some limitations that should be addressed in future research. First, ET exhibits high spatial heterogeneity due to its strong dependence on underlying surface conditions. However, the available ET product, with its relatively coarse resolution, was not validated against *in situ* ET measurements, which may introduce substantial uncertainties in the ET estimates. Second, the duration of the available data is relatively short (~20 years). While the long-term trend is significant, the attribution results may vary when using data sources with a longer temporal span. Lastly, this study only analyzed the relationship of ET with two primary climatic factors. Other factors, such as atmospheric CO2 concentration, vapor pressure deficit, and sunshine duration, may also influence ET in the Loess Plateau. Although their impacts may be relatively minor, further research is necessary to comprehensively incorporate a broader range of influencing factors in the future.

5 Conclusions

In this study, we investigated the forcing mechanisms of climatic factors and vegetation dynamics in regulating the long-term trends and interannual variations in ET and its components. The results demonstrate that water resources (precipitation) play a fundamental constraining role in the overall distribution pattern of ET on the Loess Plateau. However, precipitation alone does not fully account for the significant increasing trend in total ET and Ec observed since the implementation of vegetation restoration projects. In contrast, the NDVI shows an increasing trend across

most of the Loess Plateau, which may serve as the direct driving force behind the significant trends in ET and its components from 2000 to 2022. Excluding the long-term trend, interannual variability appears to be more closely correlated with climatic factors. The significantly positive relationship between precipitation and ET underscores ET's heavy reliance on water resources in these regions, while the significantly negative correlation with temperature ($p < 0.001$) suggests a warming-induced drought stress effect on ET and its components in the arid and semi-arid regions of the Loess Plateau.

Additionally, our research reveals another intriguing finding: since 2012, the NDVI on the Loess Plateau has plateaued after a period of rapid increase, which aligns with existing studies indicating that the artificial greening of the Loess Plateau may have reached the limits of its environmental carrying capacity. This suggests that as vegetation greening approaches its peak, future ET on the Loess Plateau will be predominantly influenced by climate change. Given the insignificant fluctuations in precipitation, the warming trend is expected to dominate interannual variations in ET, leading to broader soil drying and water resource shortages. These changes will consequently impact the sustainable development of local agriculture and substantially increase the financial investment and costs required by the local government to maintain the current ecosystem. Therefore, it is essential to strike a balance between the limits of vegetation greening and financial investment under future warming scenarios. Our study provides insights into how ET and its components change under current ecological restoration projects on the Loess Plateau and offers a scientific basis for understanding the response processes of the hydrological cycle to large-scale vegetation greening and for regional water resource security assessment.

Data availability statement

The original contributions presented in the study are included in the article/Supplementary Material. Further inquiries can be directed to the corresponding author.

Author contributions

QT: Conceptualization, Data curation, Formal Analysis, Investigation, Methodology, Resources, Software, Validation, Visualization, Writing – original draft, Writing – review & editing. TH: Conceptualization, Data curation, Funding acquisition, Methodology, Project administration, Supervision, Visualization, Writing – review & editing. HZ: Software, Validation, Visualization, Writing – review & editing. PZ: Software, Validation, Writing – review & editing.

Funding

The author(s) declare that financial support was received for the research, authorship, and/or publication of this article. This study was supported by the National Natural Science Foundation of China (No. 42271012).

Conflict of interest

The authors declare that the research was conducted in the absence of any commercial or financial relationships that could be construed as a potential conflict of interest.

Generative AI statement

The author(s) declare that no Generative AI was used in the creation of this manuscript.

Publisher's note

Supplementary material

The Supplementary Material for this article can be found online at: https://www.frontiersin.org/articles/10.3389/fevo.2025.1513189/full#supplementary-material

References

Adler, R. F., Gu, G., Sapiano, M., Wang, J.-J., and Huffman, G. J. (2017). Global precipitation: means, variations and trends during the satellite era, (1979–2014). *Surv. Geophys.* 38, 679–699. doi: 10.1007/s10712-017-9416-4

Allen, S. T., Reba, M. L., Edwards, B. L., and Keim, R. F. (2017). Evaporation and the subcanopy energy environment in a flooded forest. *Hydrol. Process.* 31, 2860–2871. doi: 10.1002/hyp.11227

Bai, M., Mo, X., Liu, S., and Hu, S. (2019). Contributions of climate change and vegetation greening to evapotranspiration trend in a typical hilly-gully basin on the Loess Plateau, China. *Sci. Total Environ.* 657, 325–339. doi: 10.1016/j.scitotenv.2018.11.360

Bai, P., Liu, X., Zhang, Y., and Liu, C. (2020). Assessing the impacts of vegetation greenness change on evapotranspiration and water yield in China. *Water Resour. Res.* 56, e2019WR027019. doi: 10.1029/2019WR027019

Chen, L., Wei, W., Fu, B., and Lü, Y. (2007). Soil and water conservation on the Loess Plateau in China: review and perspective. *Prog. Phys. Geogr. Earth Environ.* 31, 389–403. doi: 10.1177/0309133307081290

Chen, X., Mo, X., Hu, S., and Liu, S. (2017). Contributions of climate change and human activities to ET and GPP trends over North China Plain from 2000 to 2014. *J. Geogr. Sci.* 27, 661–680. doi: 10.1007/s11442-017-1399-z

Deng, L., Kim, D.-G., Li, M., Huang, C., Liu, Q., Cheng, M., et al. (2019). Land-use changes driven by 'Grain for Green' program reduced carbon loss induced by soil erosion on the Loess Plateau of China. *Glob. Planet. Change* 177, 101–115. doi: 10.1016/j.gloplacha.2019.03.017

Deng, L., Yan, W., Zhang, Y., and Shangguan, Z. (2016). Severe depletion of soil moisture following land-use changes for ecological restoration: Evidence from northern China. *For. Ecol. Manage.* 366, 1–10. doi: 10.1016/j.foreco.2016.01.026

Du, F., Shao, H.-B., Shan, L., Liang, Z.-S., and Shao, M.-A. (2007). Secondary succession and its effects on soil moisture and nutrition in abandoned old-fields of hilly region of Loess Plateau, China. *Colloids Surf. B Biointerf.* 58, 278–285. doi: 10.1016/j.colsurfb.2007.04.002

Duveiller, G., Hooker, J., and Cescatti, A. (2018). The mark of vegetation change on Earth's surface energy balance. *Nat. Commun.* 9, 679. doi: 10.1038/s41467-017-02810-8

Feng, X., Fu, B., Piao, S., Wang, S., Ciais, P., Zeng, Z., et al. (2016). Revegetation in China's Loess Plateau is approaching sustainable water resource limits. *Nat. Clim. Change* 6, 1019–1022. doi: 10.1038/nclimate3092

Feng, X. M., Sun, G., Fu, B. J., Su, C. H., Liu, Y., and Lamparski, H. (2012). Regional effects of vegetation restoration on water yield across the Loess Plateau, China. *Hydrol. Earth Syst. Sci.* 16, 2617–2628. doi: 10.5194/hess-16-2617-2012

Ferguson, C. R., and Wood, E. F. (2010). An evaluation of satellite remote sensing data products for land surface hydrology: atmospheric infrared sounder*. *J. Hydrometeorol.* 11, 1234–1262. doi: 10.1175/2010JHM1217.1

Fu, B. (1989). Soil erosion and its control in the loess plateau of China. *Soil Use Manage.* 5, 76–82. doi: 10.1111/j.1475-2743.1989.tb00765.x

Fu, B., Wang, J., Chen, L., and Qiu, Y. (2003). The effects of land use on soil moisture variation in the Danangou catchment of the Loess Plateau, China. *CATENA* 54, 197–213. doi: 10.1016/S0341-8162(03)00065-1

Fu, B., Wang, S., Liu, Y., Liu, J., Liang, W., and Miao, C. (2017). Hydrogeomorphic ecosystem responses to natural and anthropogenic changes in the loess plateau of China. *Annu. Rev. Earth Planet. Sci.* 45, 223–243. doi: 10.1146/annurev-earth-063016-020552

Gu, G., Adler, R. F., and Huffman, G. J. (2016). Long-term changes/trends in surface temperature and precipitation during the satellite era, (1979–2012). *Clim. Dyn.* 46, 1091–1105. doi: 10.1007/s00382-015-2634-x

Guan, Y., Zhou, W., Bai, Z., Cao, Y., Huang, Y., and Huang, H. (2020). Soil nutrient variations among different land use types after reclamation in the Pingshuo opencast coal mine on the Loess Plateau, China. *CATENA* 188, 104427. doi: 10.1016/j.catena.2019.104427

Han, Z., Huang, S., Huang, Q., Bai, Q., Leng, G., Wang, H., et al. (2020). Effects of vegetation restoration on groundwater drought in the Loess Plateau, China. *J. Hydrol.* 591, 125566. doi: 10.1016/j.jhydrol.2020.125566

He, J., Yang, K., Tang, W., Lu, H., Qin, J., Chen, Y., et al. (2020). The first high-resolution meteorological forcing dataset for land process studies over China. *Sci. Data* 7, 25. doi: 10.1038/s41597-020-0369-y

Huang, N., Wang, L., Song, X.-P., Black, T. A., Jassal, R. S., Myneni, R. B., et al. (2020). Spatial and temporal variations in global soil respiration and their relationships with climate and land cover. *Sci. Adv.* 6, eabb8508. doi: 10.1126/sciadv.abb8508

Jiang, Q., Li, W., Fan, Z., He, X., Sun, W., Chen, S., et al. (2021). Evaluation of the ERA5 reanalysis precipitation dataset over Chinese Mainland. *J. Hydrol.* 595, 125660. doi: 10.1016/j.jhydrol.2020.125660

Jiang, F., Xie, X., Liang, S., Wang, Y., Zhu, B., Zhang, X., et al. (2021). Loess Plateau evapotranspiration intensified by land surface radiative forcing associated with ecological restoration. *Agric. For. Meteorol.* 311, 108669. doi: 10.1016/j.agrformet.2021.108669

Jiang, F., Xie, X., Wang, Y., Liang, S., Zhu, B., Meng, S., et al. (2022). Vegetation greening intensified transpiration but constrained soil evaporation on the Loess Plateau. *J. Hydrol.* 614, 128514. doi: 10.1016/j.jhydrol.2022.128514

Jiao, W., Wang, L., Smith, W. K., Chang, Q., Wang, H., and D'Odorico, P. (2021). Observed increasing water constraint on vegetation growth over the last three decades. *Nat. Commun.* 12, 3777. doi: 10.1038/s41467-021-24016-9

Jin, T. T., Fu, B. J., Liu, G. H., and Wang, Z. (2011). Hydrologic feasibility of artificial forestation in the semi-arid Loess Plateau of China. *Hydrol. Earth Syst. Sci.* 15, 2519–2530. doi: 10.5194/hess-15-2519-2011

Li, X., Xu, X., Tian, W., Tian, J., and He, C. (2023). Contribution of climate change and vegetation restoration to interannual variability of evapotranspiration in the agro-pastoral ecotone in northern China. *Ecol. Indic.* 154, 110485. doi: 10.1016/j.ecolind.2023.110485

Li, G., Sun, S., Han, J., Yan, J., Liu, W., Wei, Y., et al. (2019). Impacts of Chinese Grain for Green program and climate change on vegetation in the Loess Plateau during 1982–2015. *Sci. Total Environ.* 660, 177–187. doi: 10.1016/j.scitotenv.2019.01.028

Li, S., Wang, G., Sun, S., Fiifi Tawia Hagan, D., Chen, T., Dolman, H., et al. (2021). Long-term changes in evapotranspiration over China and attribution to climatic drivers during 1980–2010. *J. Hydrol.* 595, 126037. doi: 10.1016/j.jhydrol.2021.126037

Liang, X., Lettenmaier, D. P., Wood, E. F., and Burges, S. J. (1994). A simple hydrologically based model of land surface water and energy fluxes for general circulation models. *J. Geophys. Res. Atmos.* 99, 14415–14428. doi: 10.1029/94JD00483

Liang, W., Zhang, W., Jin, Z., Yan, J., Lü, Y., Li, S., et al. (2020). Rapid urbanization and agricultural intensification increase regional evaporative water consumption of the loess plateau. *J. Geophys. Res. Atmos.* 125, e2020JD033380. doi: 10.1029/2020JD033380

Liu, J., Li, S., Ouyang, Z., Tam, C., and Chen, X. (2008). Ecological and socioeconomic effects of China's policies for ecosystem services. *Proc. Natl. Acad. Sci.* 105, 9477–9482. doi: 10.1073/pnas.0706436105

Lü, Y., Fu, B., Feng, X., Zeng, Y., Liu, Y., Chang, R., et al. (2012). A policy-driven large scale ecological restoration: quantifying ecosystem services changes in the loess plateau of China. *PloS One* 7, e31782. doi: 10.1371/journal.pone.0031782

Magliano, P. N., Giménez, R., Houspanossian, J., Páez, R. A., Nosetto, M. D., Fernández, R. J., et al. (2017). Litter is more effective than forest canopy reducing soil evaporation in Dry Chaco rangelands. *Ecohydrology* 10, e1879. doi: 10.1002/eco.1879

Mao, J., Fu, W., Shi, X., Ricciuto, D. M., Fisher, J. B., Dickinson, R. E., et al. (2015). Disentangling climatic and anthropogenic controls on global terrestrial evapotranspiration trends. *Environ. Res. Lett.* 10, 94008. doi: 10.1088/1748-9326/10/9/094008

Martens, B., Miralles, D. G., Lievens, H., van der Schalie, R., De Jeu, R. A. M., Fernández-Prieto, D., et al. (2017). GLEAM v3: satellite-based land evaporation and root-zone soil moisture. *Geosci. Model. Dev.* 10, 1903–1925. doi: 10.5194/gmd-10-1903-2017

Miralles, D. G., Holmes, T. R. H., De Jeu, R. A. M., Gash, J. H., Meesters, A. G. C. A., and Dolman, A. J. (2011). Global land-surface evaporation estimated from satellite-based observations. *Hydrol. Earth Syst. Sci.* 15, 453–469. doi: 10.5194/hess-15-453-2011

Nazarbakhsh, M., Ireson, A. M., and Barr, A. G. (2020). Controls on evapotranspiration from jack pine forests in the Boreal Plains Ecozone. *Hydrol. Process.* 34, 927–940. doi: 10.1002/hyp.13674

Peng, S., Gang, C., Cao, Y., and Chen, Y. (2018). Assessment of climate change trends over the Loess Plateau in China from 1901 to 2100. *Int. J. Climatol.* 38, 2250–2264. doi: 10.1002/joc.5331

Priestley, C. H. B., and Taylor, R. J. (1972). On the Assessment of Surface Heat Flux and Evaporation Using Large Scale Parameters. *Monthly Weather Rev.* 100, 81–92. doi: 10.1175/1520-0493(1972)100<0081:OTAOSH>2.3.CO;2

Reddy, S. J. (1996). Measurements of soil, plant and total evaporation from millet in Niger [Wallace, J.S., Lloyd, C.R. and Sivakumar, M.V.K., Agric. For. Meteorol., 63 (1993) 149–169. *Agric. For. Meteorol.* 80, 289–294. doi: 10.1016/0168-1923(95)02298-8

Hersbach, H., Bell, B., Berrisford, P., Biavati, G., Horányi, A., Muñoz Sabater, J., et al (2023). Data from: ERA5 monthly averaged data on single levels from 1940 to present. *Copernicus Climate Change Service (C3S) Climate Data Store (CDS)*. doi: 10.24381/cds.f17050d7

Shao, R., Zhang, B., Su, T., Long, B., Cheng, L., Xue, Y., et al. (2019). Estimating the increase in regional evaporative water consumption as a result of vegetation restoration over the loess plateau, China. *J. Geophys. Res. Atmos.* 124, 11783–11802. doi: 10.1029/2019JD031295

Shi, X., Mao, J., Thornton, P. E., and Huang, M. (2013). Spatiotemporal patterns of evapotranspiration in response to multiple environmental factors simulated by the Community Land Model. *Environ. Res. Lett.* 8, 24012. doi: 10.1088/1748-9326/8/2/024012

Song, J., Gao, J., Li, X., Mao, R., and Shi, A. (2023). Changes of evapotranspiration and its driving factors in the Loess Plateau in recent 20 years[J]. *J. Northwest University (Natural Science Edition)*. 53 (6), 974–990. doi: 10.16152/j.cnki.xdxbzr.2023-06-008

Tang, J., Zeng, J., Zhang, Q., Zhang, R., Leng, S., Zeng, Y., et al. (2020). Self-adapting extraction of cropland phenological transitions of rotation agroecosystems using dynamically fused NDVI images. *Int. J. Biometeorol.* 64, 1273–1283. doi: 10.1007/s00484-020-01904-1

Vinukollu, R. K., Wood, E. F., Ferguson, C. R., and Fisher, J. B. (2011). Global estimates of evapotranspiration for climate studies using multi-sensor remote sensing data: Evaluation of three process-based approaches. *Remote Sens. Environ.* 115, 801–823. doi: 10.1016/j.rse.2010.11.006

Wang, S., Cui, C., and Dai, Q. (2021). Contributions of vegetation greening and climate change to evapotranspiration trend after large-scale vegetation restoration on the loess plateau, China. *Water* 13, 1755. doi: 10.3390/w13131755

Wang, C., Fu, B., Lü, Y., and Liu, Y. (2023). Socioeconomic development alters the effects of 'green' and 'grain' on evapotranspiration in China's loess plateau after the grain for green programme. *J. Environ. Manage.* 328, 117013. doi: 10.1016/j.jenvman.2022.117013

Wang, X., Zhang, B., Xu, X., Tian, J., and He, C. (2020). Regional water-energy cycle response to land use/cover change in the agro-pastoral ecotone, Northwest China. *J. Hydrol.* 580, 124246. doi: 10.1016/j.jhydrol.2019.124246

Williams, D. G., Cable, W., Hultine, K., Hoedjes, J. C. B., Yepez, E. A., Simonneaux, V., et al. (2004). Evapotranspiration components determined by stable isotope, sap flow and eddy covariance techniques. *Agric. For. Meteorol.* 125, 241–258. doi: 10.1016/j.agrformet.2004.04.008

Wu, X., Wang, S., Fu, B., Feng, X., and Chen, Y. (2019). Socio-ecological changes on the Loess Plateau of China after Grain to Green Program. *Sci. Total Environ.* 678, 565–573. doi: 10.1016/j.scitotenv.2019.05.022

Yang, K., He, J., Tang, W., Qin, J., and Cheng, C. C. K. (2010). On downward shortwave and longwave radiations over high altitude regions: Observation and

modeling in the Tibetan Plateau. *Agric. For. Meteorol.* 150, 38–46. doi: 10.1016/j.agrformet.2009.08.004

Yang, K., He, J., Tang, W., Lu, H., Qin, J., Chen, Y., et al. (2019). Data from: China meteorological forcing dataset (1979-2018). *National Tibetan Plateau / Third Pole Environment Data Center*. doi: 10.11888/AtmosphericPhysics.tpe.249369.file

Yang, Y., Roderick, M. L., Zhang, S., McVicar, T. R., and Donohue, R. J. (2019). Hydrologic implications of vegetation response to elevated CO2 in climate projections. *Nat. Clim. Change* 9, 44–48. doi: 10.1038/s41558-018-0361-0

Yang, Y. F., Wang, B., Wang, G. L., and Li, Z. (2019). Ecological regionalization and overview of the Loess Plateau. *Acta Ecol. Sin.* 39, 7389–7397. doi: 10.5846/stxb201909031825

Yang, L., Wei, W., Chen, L., Chen, W., and Wang, J. (2014). Response of temporal variation of soil moisture to vegetation restoration in semi-arid Loess Plateau, China. *CATENA* 115, 123–133. doi: 10.1016/j.catena.2013.12.005

Yao, T., Lu, H., Yu, Q., Feng, S., Xue, Y., and Feng, W. (2023). Uncertainties of three high-resolution actual evapotranspiration products across China: Comparisons and applications. *Atmos. Res.* 286, 106682. doi: 10.1016/j.atmosres.2023.106682

Ye, L., Fang, L., Shi, Z., Deng, L., and Tan, W. (2019). Spatio-temporal dynamics of soil moisture driven by 'Grain for Green' program on the Loess Plateau, China. *Agric. Ecosyst. Environ.* 269, 204–214. doi: 10.1016/j.agee.2018.10.006

Yue, P., Zhang, Q., Zhang, L., Li, H., Yang, Y., Zeng, J., et al. (2019). Long-term variations in energy partitioning and evapotranspiration in a semiarid grassland in the Loess Plateau of China. *Agric. For. Meteorol.* 278, 107671. doi: 10.1016/j.agrformet.2019.107671

Zeng, J., Zhou, T., Qu, Y., Bento, V. A., Qi, J., Xu, Y., et al. (2023). An improved global vegetation health index dataset in detecting vegetation drought. *Sci. Data* 10, 338. doi: 10.1038/s41597-023-02255-3

Zhang, Y., Kong, D., Gan, R., Chiew, F. H. S., McVicar, T. R., Zhang, Q., et al. (2019). Coupled estimation of 500 m and 8-day resolution global evapotranspiration and gross primary production in 2002–2017. *Remote Sens. Environ.* 222, 165–182. doi: 10.1016/j.rse.2018.12.031

Zhang, Y., Peña-Arancibia, J. L., McVicar, T. R., Chiew, F. H. S., Vaze, J., Liu, C., et al. (2016). Multi-decadal trends in global terrestrial evapotranspiration and its components. *Sci. Rep.* 6, 19124. doi: 10.1038/srep19124

Zhang, B., Tian, L., Zhao, X., and Wu, P. (2021). Feedbacks between vegetation restoration and local precipitation over the Loess Plateau in China. *Sci. China Earth Sci.* 64, 920–931. doi: 10.1007/s11430-020-9751-8

Zhang, S., Yang, D., Yang, Y., Piao, S., Yang, H., Lei, H., et al. (2018). Excessive afforestation and soil drying on China's loess plateau. *J. Geophys. Res. Biogeosci.* 123, 923–935. doi: 10.1002/2017JG004038

Zhang, W., Zhou, T., and Zhang, L. (2017). Wetting and greening Tibetan Plateau in early summer in recent decades. *J. Geophys. Res. Atmos.* 122, 5808–5822. doi: 10.1002/2017JD026468

Zhao, F., Ma, S., Wu, Y., Qiu, L., Wang, W., Lian, Y., et al. (2022). The role of climate change and vegetation greening on evapotranspiration variation in the Yellow River Basin, China. *Agric. For. Meteorol.* 316, 108842. doi: 10.1016/j.agrformet.2022.108842

Zheng, F., He, X., Gao, X., Zhang, C., and Tang, K. (2005). Effects of erosion patterns on nutrient loss following deforestation on the Loess Plateau of China. *Agric. Ecosyst. Environ.* 108, 85–97. doi: 10.1016/j.agee.2004.12.009

frontiers | Frontiers in Earth Science

TYPE Original Research
PUBLISHED 20 February 2025
DOI 10.3389/feart.2025.1527786

OPEN ACCESS

EDITED BY
Celso Santos,
Federal University of Paraíba, Brazil

REVIEWED BY
Hang Wan,
Southern Marine Science and Engineering Guangdong Laboratory (Guangzhou), China
Jie Zhu,
Chinese Academy of Agricultural Sciences, China

*CORRESPONDENCE
Xuan Wang,
wangx@bnu.edu.cn

RECEIVED 13 November 2024
ACCEPTED 27 January 2025
PUBLISHED 20 February 2025

CITATION
Wei R, Wang X, Hao G, Cai J and Liao Z (2025) An integrated framework for assessing water resource pressure and sustainability based on the total-element agricultural water footprints.
Front. Earth Sci. 13:1527786.
doi: 10.3389/feart.2025.1527786

An integrated framework for assessing water resource pressure and sustainability based on the total-element agricultural water footprints

Rui Wei[1,2], Xuan Wang[1,2]*, Guangling Hao[3], Jianying Cai[1,2] and Zhenmei Liao[1,2]

[1]State Key Laboratory of Water Environment Simulation, School of Environment, Beijing Normal University, Beijing, China, [2]Key Laboratory for Water and Sediment Sciences of Ministry of Education, School of Environment, Beijing Normal University, Beijing, China, [3]Administration of Ecology and Environment of Haihe River Basin and Beihai Sea Area, Ministry of Ecology and Environment, Tianjin, China

The agricultural water footprint (WF) is essential for understanding environmental impacts and managing water resources, especially in water-scarce regions. In this study, an integrated framework for assessing water resource pressure and sustainability based on the total-element agricultural water footprints was developed. Firstly, three types of WFs (i.e., blue, green and grey WFs) of major crops including wheat and maize in the Beijing area were calculated, and spatiotemporal variations were analysed. Subsequently, the water stress index (WSI) of WFs was calculated, and based on this, the reliability-resilience-vulnerability (RRV) indices was established for systematically assessing water resource stress sustainability in agricultural systems. Finally, the driving factors of agricultural WF were analysed using STIRPAT model. The results were as follows. (1) The overall WF decreased from 22.0×10^8 m^3 to 3.9×10^7 m^3, showing a significant downward trend from 1978 to 2018. (2) The WSI values exceeded 1 in 25 out of the 35 years, indicating that the Beijing area continued to experience frequent water shortages. The RRV indices indicated that the sustainability of water resources in the Beijing area had improved in recent years, and the value was 0.35 in 2018, but remained at a low level. (3) Enhancing the effectiveness of irrigation, increasing agricultural machinery density, and reducing the planting area of water-intensive crops can significantly lower the agricultural WF. This study assessed the water resource pressure and sustainability of total-element agricultural WFs by combining the WSI and the RRV indices, from the integrated perspective of both water quantity and quality. This approach is of significant importance for the sustainable utilisation and management of agricultural water resources in water-scarce regions, based on water footprint analysis.

KEYWORDS

agricultural water footprint, agricultural water resource assessment, water stress index, reliability-resilience-vulnerability indices, STIRPAT model

1 Introduction

A critical challenge to economic development is the scarcity of water resources. Agriculture accounts for 70% of global freshwater withdrawals and 90% of freshwater consumption (Dolganova et al., 2019). In China, the agricultural sector was responsible for 63.1% of the country's total water use in 2015 (Beijing Municipal Bureau of Statistics, 2016). As the global population expands and the demand for food intensifies, the research and management of agricultural water resources have become increasingly critical. Consequently, analysing variations in agricultural water use is essential for both regional water resource planning and the implementation of agricultural water conservation strategies, especially for areas with rapid socioeconomic development and serious conflicts between water supply and water use.

The water footprint (WF) method has been widely used to better quantify water resources and to explore the relationship between human production activities and water resource embedded in products and services (Lovarelli et al., 2016; Liu et al., 2023; Mialyk et al., 2024a; Rodriguez et al., 2024). The agricultural WF accounts for water directly consumed during crop production, tillage, and irrigation (Wang et al., 2022), as well as the indirect water associated with the production and consumption of inputs including fertilizers, pesticides, and energy. Thereby the agricultural water footprint can provide a robust basis for agricultural water management. The concept of the WF was first proposed by Dutch water expert Arjen Hoekstra in 2002 (Hoekstra and Hung, 2002). The WF is a multidimensional indicator of water use and pollution (Hogeboom, 2020) and comprises blue, green, and grey WFs. Green water refers to the moisture stored in the unsaturated zone of the soil that is available for evapotranspiration; the green WF reflects the amount of green water consumed in agricultural production. Blue water, commonly understood as water resources, includes rivers, lakes, surface water, and groundwater; the blue WF refers to the amount of blue water consumed during production and consumption. Grey water refers to the volume of water required to dilute pollutants generated by agricultural production to meet water quality standards (Hoekstra, 2011); the grey WF is used to assess the extent of water pollution in terms of water volume (Wang et al., 2019; Elbeltagi et al., 2020). Since its introduction, the WF has been extensively quantified at various scales: global (Mialyk et al., 2024b; Sturla et al., 2024), national (Wang and Ge, 2020; Feng et al., 2022), urban (Cai et al., 2020; Ma and Jiao, 2023), and so on. In previous research, Hoekstra quantified the WF for crop yields in various countries and regions worldwide, establishing the first global benchmarks for crop yield WFs (Mekonnen and Hoekstra, 2014). Xu et al. (2019) quantified the agricultural WF of 207 counties in North China, exploring variations in China's agricultural WF from a county-level perspective.

While quantification of the agricultural WF provides insight into the amount of water resources consumed during crop production, it does not adequately capture the relationship between production activities and regional water resources (Chu et al., 2022). Therefore, building on WF quantification, many studies have analysed the agricultural water stress index (AWSI) (Cao et al., 2017), green water scarcity (WSgreen) (D'Ambrosio et al., 2020), and other indicators to evaluate variations in water resource systems. In previous studies, Xie et al. (2020) considered the impact of irrigation on blue and green water and, on this basis, assessed the scarcity of these water resources in the Yellow River Basin via the WF. Cao et al. (2021) developed the water resource efficiency (WRE) index to assess water use efficiency in crop production. The water stress index (WSI) is a key indicator for assessing regional water stress, as it reflects the pressure on the water system by comparing the ratio of water consumption to the available water resources within the region (Dehghanpir et al., 2024). For instance, Wang Q. et al. (2023) employed the WSI to examine the pressure on water resources resulting from afforestation in the Inner Mongolia Autonomous Region. Typically, only blue and green WFs are used to evaluate the efficiency and scarcity of water resources, with grey WFs rarely included in the evaluation framework. However, the grey WF can assess water resource utilization from a water quality perspective. Addressing agricultural water pollution is also crucial for effective water management and sustainable development. The reliability-resilience-vulnerability (RRV) indices, proposed by Hashimoto, is widely used to evaluate the performance of specific systems (Hashimoto et al., 1982). In water resource studies, the RRV indices has been used to evaluate the performance of water supply systems (Golmohammadi et al., 2021), characterize droughts (Chanda et al., 2014), assess the impacts of water resource allocation (Zeng et al., 2024), analyse the effects of different climatic conditions on water resource systems (Asefa et al., 2014), and assess the sustainability of these systems (Sediqi and Komori, 2024). The WSI reflects the scarcity of agricultural water at a point in time, whereas the RRV indices reflects the sustainability of the system over an extended period. Building on the quantified WF, the WSI and RRV indices are combined to evaluate the pressure and sustainability of local agricultural water resource systems, effectively assessing variations and providing a theoretical basis for the sustainable development of these resources.

This study investigated the spatiotemporal changes and the driving factors of the crop production WF in the Beijing area from 1984 to 2018 while evaluating the shortage and sustainability of the agricultural water resources of the region. As a representative international megacity with high water demand, the Beijing area faces significant challenges in water resource management due to its high population density, dense urban infrastructure, and complex urban governance. This study proposed a framework for assessing water shortages and sustainability based on total-element agricultural WFs (i.e., blue, green, and grey WFs). Compared with previous studies, this research emphasized the critical role of the grey WF in the comprehensive assessment of water resource stress, evaluating agricultural water resources from both the water quantity and water quality perspectives through blue, green, and grey water. Additionally, on the basis of the calculation of the WSI, the RRV indices was constructed to systematically evaluate the pressure on and the sustainability of agricultural water resources. This enhancement can improve the comprehensive water resource evaluation system and provide a theoretical basis for policy formulation and scientific planning for the sustainable development of agricultural water resources.

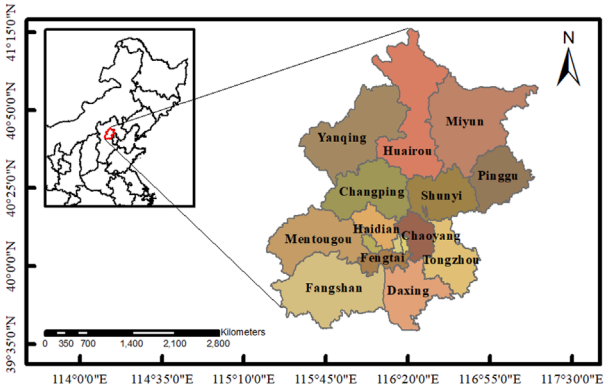

FIGURE 1
Map of administrative divisions of Beijing area, China.

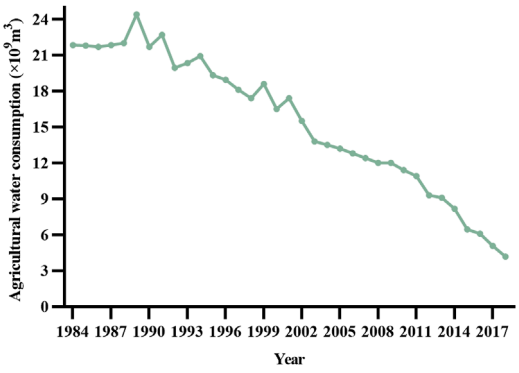

FIGURE 2
Agricultural water consumption in Beijing area, 1984-2018.

2 Materials

2.1 Study area

The Beijing area is situated in the northwest of North China Plain, covering an area of 16,410.54 km^2 (Figure 1), with a semi-humid and semi-arid monsoon climate. The perennial average precipitation is 400–500 mm. The precipitation from June to August accounts for approximately 80% of the annual average throughout the year. In 2018, the total water resources of the Beijing area amounted to 3.546 billion m^3, with the surface water resources accounting for 1.432 billion m^3 and groundwater resources for 2.114 billion m^3. As domestic water demand in the Beijing area increased, agricultural water resources were significantly reduced. Agricultural water consumption decreased year by year. Figure 2 illustrates the change in agricultural water consumption in the Beijing area between 1987 and 2018. It decreased from 2.184 billion m^3 in 1984 to 420 million m^3 in 2018, marking a reduction of nearly 81% over 35 years.

By the end of 2018, the Gross Domestic Product of the Beijing area had reached 3,310.6 billion CNY, with a resident population of 21.542 million, including 2.9 million in agriculture. The plains of the Beijing area were predominantly located in the southeast, offering favourable irrigation conditions. The main soil types of the planting region in the Beijing area were moist soil, brown soil, and brown soil. The primary crops grown included winter wheat, maize, soybeans, and rice. In 2018, the output value of major agricultural products in the Beijing area was 11.47 billion CNY, with an output of 341,000 tonnes of key grain crops. The area sown with major grain crops was 55.6 thousand hectares, which was 89% less than in 1984, when it was 523.1 thousand hectares. As a representative megacity in China, the Beijing area is characterized by high population density, dense urban infrastructure, and complex urban governance challenges. Like many other megacities, the traditional extensive development approach of the Beijing area has led to "urban diseases", such as environmental pollution and resource shortages (Zhu et al., 2022). The situation regarding water resources is particularly critical. In 1984, the *per capita* water availability of the Beijing area was 407 m^3, whereas by 2018, it had dwindled to just 164 m^3. The scarcity of water resources has significantly constrained regional economic development.

2.2 Data sources

The long-term meteorological data used in this study included monthly average temperature, wind speed, relative humidity, precipitation, and sunshine hours. The data covering the period from January 1984 to December 2018 were obtained mainly from Beijing weather stations and the China meteorological data sharing site. The agricultural data included soil data, fertilizer input, the agricultural population and sowing area, output, and the crop coefficient of the main crops, including wheat and maize, in the Beijing area. The data were obtained mainly from the agricultural development statistical bulletin of 30 years of reform and opening up supported by the Beijing Bureau of Statistics website and the Beijing Municipal Bureau of Statistics Information Office. Some data came from *the WF assessment manual setting the global standard* and *the main food crop irrigation water quota of the main food crop in northern China*. The soil data included the total available soil moisture, maximum precipitation infiltration rate, maximum planting depth, initial soil water consumption, etc. No wheat or maize were planted in Dongcheng District or Xicheng District, so these two districts were not considered.

3 Methods

3.1 Research framework

In this study, a comprehensive water resource assessment framework based on the agricultural WF was constructed, as illustrated in Figure 3. The first step involved quantifying the blue, green, and grey WFs in crop production and analysing their spatiotemporal characteristics. The second step involved evaluating the pressure and sustainability of the water resource system from two perspectives: water quantity and water quality, via the WSI and RRV indices. The third step involved analysing the driving factors of the agricultural WF by using the stochastic impacts by regression on population affluence and technology (STIRPAT)

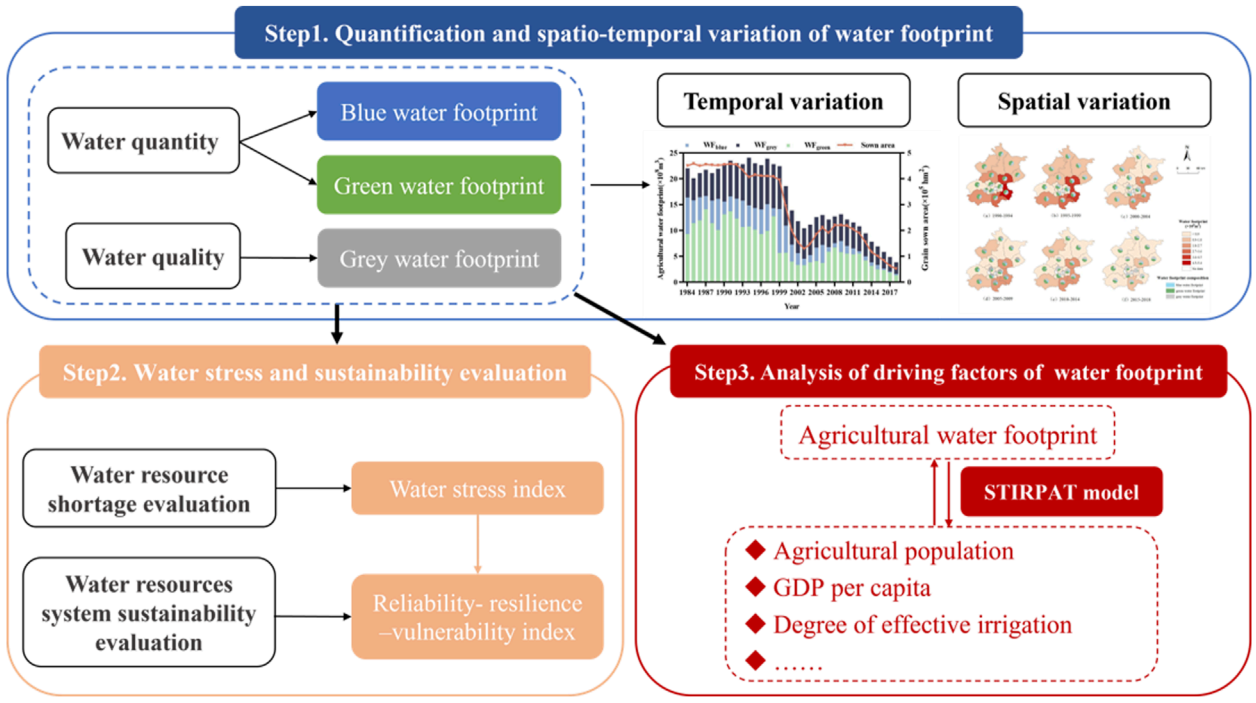

FIGURE 3
Research framework.

model. This framework built upon the use of the WSI to assess the existing pressure on water resources and incorporated the RRV indices to analyse the long-term changes in the sustainability of the water resource system from the perspectives of reliability, resilience, and vulnerability. The framework allowed for a comprehensive evaluation of the agricultural water resource system, enhancing the multi-dimensional assessment of water resources and addressing the limitations of single-method evaluations, thereby providing a theoretical basis for promoting the sustainable development of these resources.

3.2 WF calculation methodology

Blue, green and grey WFs were considered in the measurement of the WF for crop production. The first step in calculating the green WF and blue WF of crop production was the determination of the crop water requirement, which was calculated via the CROPWAT model, which is based on the improved Penman formula recommended by the Food and Agriculture Organization (FAO). The crop water requirement was calculated by the reference evapotranspiration (ET_0), which is based on the Penman formula and considers the influence of climatic factors, can be expressed by Equation 1:

$$ET_0 = \frac{0.408\Delta(R_n - G) + \gamma\frac{900}{T+273}u_2(e_a - e_d)}{\Delta + \gamma(1 + 0.34U_2)} \quad (1)$$

where R_n is the net radiation (MJ·m^{-2} d^{-1}), G is the soil heat flux (MJ·m^{-2} d^{-1}), T is the average air temperature (°C), u_2 is the wind speed at a height of 2 m (m·s^{-1}), e_a is the saturation vapour pressure (kPa), ed is the actual vapour pressure (kPa), Δ is the slope of the saturation vapour pressure versus air temperature curve (kPa·°C^{-1}), and γ is the psychrometric constant (kPa·°C^{-1}).

The crop evapotranspiration (ETc) was estimated by Equation 2:

$$ET_c = K_c * ET_0 \quad (2)$$

where Kc is a crop coefficient that varies with the crop stage.

WF_{blue} and WF_{green} can be calculated based on Equations 3, 4:

$$WF_{blue} = \frac{10\max(0, ET_c - P_e)}{m} \quad (3)$$

$$WF_{green} = \frac{10\min(ET_c, P_e)}{m} \quad (4)$$

where WF_{blue} is the surface water or groundwater consumed in the crop production process, WF_{green} is the precipitation consumed in the crop production process, 10 is the unit conversion coefficient to convert units by mm (depth) into m^3/hm^2 (water amount per unit area), and P_e is the effective precipitation during the crop growth period (mm). On the basis of the WF_{blue} and WF_{green} values of crop production per unit area, corresponding regional crop production can be calculated from the sowing area.

The grey WF (WF_{grey}) of agricultural nonpoint source pollution can be calculated by Equation 5:

$$WF_{grey} = \frac{L}{C_{max} - C_{nat}} = \frac{\alpha \times Appl}{C_{max} - C_{nat}} \quad (5)$$

where Appl is the input of pesticide or fertilizer, α is the proportion of the pollutant in the total pesticide or fertilizer input, C_{max} is

the maximum allowable concentration of pollutants (kg/m^3), and C_{nat} is the initial concentration of pollutants (kg/m^3). According to previous research (Zhang, 2017), 10 mg/L was used for C_{max}.

The Department of Agriculture typically adopts nitrogen (N) and phosphorus (P) as indices reflecting the grey WF. In this case, α is the leaching loss rate of N or P. As nitrogen fertilizer contributes the most to the grey WF in agricultural production in China, nitrogen was taken as the representative index for calculating WF_{grey}.

3.3 Temporal trend analysis

The MK test method was used to analyse the variation trends in crop production WFs. According to the MK test, for the time series $x_1, x_2, \ldots, x_n$, the statistic S is given by Equation 6:

$$S = \sum_{i=1}^{n-1} \sum_{j=i=1}^{n} sgn\left(x_j - x_i\right) \tag{6}$$

where n is the length of the series, x_i and x_j are the sequential data values, and

$$sgn(x) = \begin{cases} 1, x_j - x_i > 0 \\ 0, x_j - x_i = 0 \\ -1, x_j - x_i < 0 \end{cases}$$

when n ≥ 10, the statistic S is approximately normally distributed with a mean of 0, and its standard deviation can be expressed as:

$$\sigma_x = \sqrt{\frac{n(n-1)(2n+5) - \sum_{i=1}^{n} t_i(i-1)(2i+5)}{18}} \tag{7}$$

In Equation 7, where σ_x is the standard deviation of S and t_i is the number of ties of extent i. The MK test statistic Z is expressed as Equation 8:

$$Z_x = \begin{cases} \frac{(S-1)}{\sigma_x}, S > 0 \\ 0, \quad S = 0 \\ \frac{(S+1)}{\sigma_x}, S < 0 \end{cases} \tag{8}$$

The significance trend is tested by comparing the absolute value of Z at the desired significance level α. In this study, a Z value beyond the interval of ±1.96 means that the trend is considered significant at the 95% confidence level. An increasing statistical Z value indicates an increasing trend, and *vice versa*.

3.4 Consideration of water resource scarcity and comprehensive sustainability evaluation of blue, green, and grey WFs

The WSI can reflect agricultural water scarcity in a region and was calculated on the basis of the agricultural WF and agricultural water use as determined by Equations 9–13:

$$WSI = \frac{WF_{total}}{AWR} \tag{9}$$

$$AWR = AWR_{blue} + AWR_{green} \tag{10}$$

where WF_{total} is the sum of the footprints of blue water, green water, and grey water; AWR is the amount of agricultural available water resources; AWR_{green} is the effective precipitation; and AWR_{blue} is the amount of blue water resources used for agricultural production, which is usually the total amount of blue water resources available for agriculture minus the environmental water demand for maintaining the ecosystem. With reference to the study of Hoekstra et al. (2012), it is assumed that the environmental water demand accounts for 80% of the total blue water resources, as shown below:

$$AWR_{blue} = TWR - EWR \tag{11}$$

$$TWR = WR \times \frac{AWU}{WU} \tag{12}$$

$$EWR = 80\% \times TWR \tag{13}$$

where TWR is the total amount of blue water resources available for agriculture; EWR is the demand for environmental water; and WR is the total quantity of available blue water resources within the region. Additionally, AWU is the agricultural water consumption and WU is the total water consumption.

In addition, the footprints of blue water, green water, and grey water are calculated as WSI_{blue}, WSI_{green}, and WSI_{grey}, respectively, and can be expressed by comprehensively considering the water shortage in terms of both water quantity and quality, as represented by Equations 14–16:

$$WSI_{blue} = \frac{WF_{blue}}{AWR_{blue}} \tag{14}$$

$$WSI_{green} = \frac{WF_{green}}{AWR_{green}} \tag{15}$$

where WF_{blue} and WF_{green} are the blue water and green WFs, respectively.

In accordance with the methods of Shu et al. (2021), a water scarcity assessment based on the grey WF was constructed

$$WSI_{grey} = \frac{WF_{grey}}{TWR - \left(WF_{blue} + WF_{green}\right)} \tag{16}$$

where WF_{grey} is the grey WF.

The WSI classified water scarcity into four levels: 0 < WSI < 0.2, no water shortage; 0.2 < WSI < 0.4, slight shortage; 0.4 < WSI < 0.8, moderate shortage; 0.8 < WSI <1, high shortage; WSI > 1, severe shortage.

To further explore the sustainability of agricultural water resources, the RRV indices was used to evaluate the sustainability of agricultural water resources in the Beijing area on the basis of the WSI. First, a standard C was defined. In this study, C was the WSI value when water shortage was under extreme pressure, that is, WSI = 1.0, and X_t can be defined as the WSI of each year:

$$Z_t = \begin{cases} 0, Z_t \in U, \quad X_t \geq 1.0 \\ 1, Z_t \in S, \quad X_t < 1.0 \end{cases}$$

where W_t is the recovery index of the water resource system from severe shortages:

$$W_t = \begin{cases} 1, G_t \in U \; and \; G_{t+1} \in S \\ 0, \quad else \end{cases}$$

The RRV indices includes three indices, namely, reliability, resilience and vulnerability. Reliability refers to the likelihood that the system remains in a satisfactory state, resilience indicates the speed at which the system recovers from an unsatisfactory state, and vulnerability measures the degree to which the system is in its least satisfactory state as represented by Equations 17–19 (Hashimoto et al., 1982).

$$Reliability = \frac{\sum_{t=1}^{T} Z_t}{T} \tag{17}$$

$$Resilience = \left\{ \frac{1}{n} \sum_{j=1}^{n} d(j) \right\}^{-1} \tag{18}$$

$$Vulnerability = \frac{1}{n} \sum_{i=1}^{T} \left\{ \frac{L_{obs}(i) - L_{std}(i)}{L_{std}(i)} \times H\left(L_{obs}(i) - L_{std}(i)\right) \right\} \tag{19}$$

where T is the time step, set to 10 years in this study; n indicates the number of failure events; d(j) is the duration of the j_{th} failure event; $L_{obs}(i)$ is the WF at time i; $L_{std}(i)$ is the amount of agricultural available water resources at time i; and H is the Heaviside function, which is a mathematically discontinuous function with a negative independent variable H = 0 and a positive independent variable H = 1.

The sustainability index was used to evaluate the sustainability of water resources system, and was the geometric average of the reliability, resilience and vulnerability after standardization, as expressed in Equation 20. A higher sustainability index indicates greater sustainability of the water resource system, categorized into five levels: 0-0.20, poor; 0.20–0.40, fair; 0.40–0.60, average; 0.60–0.80, good; and 0.80–1.0, excellent.

$$Sustainability = (Reliability \times Resilience \times Vulnerability)^{\frac{1}{3}} \tag{20}$$

3.5 STIRPAT model for analysing the drivers of WF

The impact of population, affluence and technology (IPAT) model was proposed by Ehrlich and Holden to study the impacts of human socioeconomic activities on the environment and is formulated in Equation 21 (Ehrlich and Holdren, 1971):

$$\mathrm{I} = \mathrm{P} \times \mathrm{A} \times \mathrm{T} \tag{21}$$

where I is the resulting environmental impact, P is the population size, A is the level of affluence, and T is the level of technology.

The proposed IPAT model provides a way to explain the impact of a range of human activities on the environment, but it still has strong limitations, mainly including the simplicity of the interrelationship among parameters and the assumption that the elasticities of P, A, and T are the same, which implies the same contributions of different factors to environmental pressure. This conflicts with the EKC assumption (Liu and Xiao, 2018). Therefore, on the basis of this model, Dietz and Rosa proposed the stochastic impacts by regression on population affluence and technology (STIRPAT) model, which is expressed in Equation 22 (Dietz and Rosa, 1997):

$$\mathrm{I} = a\mathrm{P}^b\mathrm{A}^c\mathrm{T}^d e \tag{22}$$

where a is the intercept term; b, c, and d are the elastic coefficients of P, A and T, respectively; e is the residual error.

The STIRPAT model is usually used in logarithmic posterior form (York et al., 2003; Lohwasser et al., 2020):

$$\ln \mathrm{I} = \ln a + \mathrm{b} \ln \mathrm{P} + c \ln \mathrm{A} + d \ln \mathrm{T} + \ln e \tag{23}$$

The drivers of environmental stress are related not only to population, affluence and technology level but also to various socioeconomic factors, so the STIRPAT model can be analysed by adding more factors according to real needs. To investigate the drivers of the agricultural WF in the Beijing area, we selected six factors, namely, the agricultural population (P), gross output value of agriculture (A1), GDP *per capita* (A2), industrial structure (A3), degree of effective irrigation (T1), agricultural machinery density (T2), and planting structure (PS), as shown in Table 1, and are expressed with Equation 24. Among these factors, the agricultural population (P) represented the number of people engaged in agricultural activities, directly influencing the water demand in the agricultural sector. The gross output value of agriculture (A1) and GDP *per capita* (A2) reflected the level of affluence, the development of the agricultural economy, and the impact of increases in production scale and economic growth on the agricultural WF. The industrial structure (A3) affected the agricultural WF by altering the input of agricultural resources and production methods. The degree of effective irrigation (T1) and agricultural machinery density (T2) reflected advances in agricultural production technology, which in turn influenced the agricultural WF. The adjustment of

TABLE 1 Description of each variable in the STIRPAT model.

Independent variables	Definition	Unit
P	Agricultural population	1×10^4 person
A1	Gross output value of agriculture	1×10^9 CNY
A2	GDP *per capita*	CNY
A3	Industrial structure	%
T1	Degree of effective irrigation	%
T2	Agricultural machinery density	kW/hm^2
PS	Planting structure	%

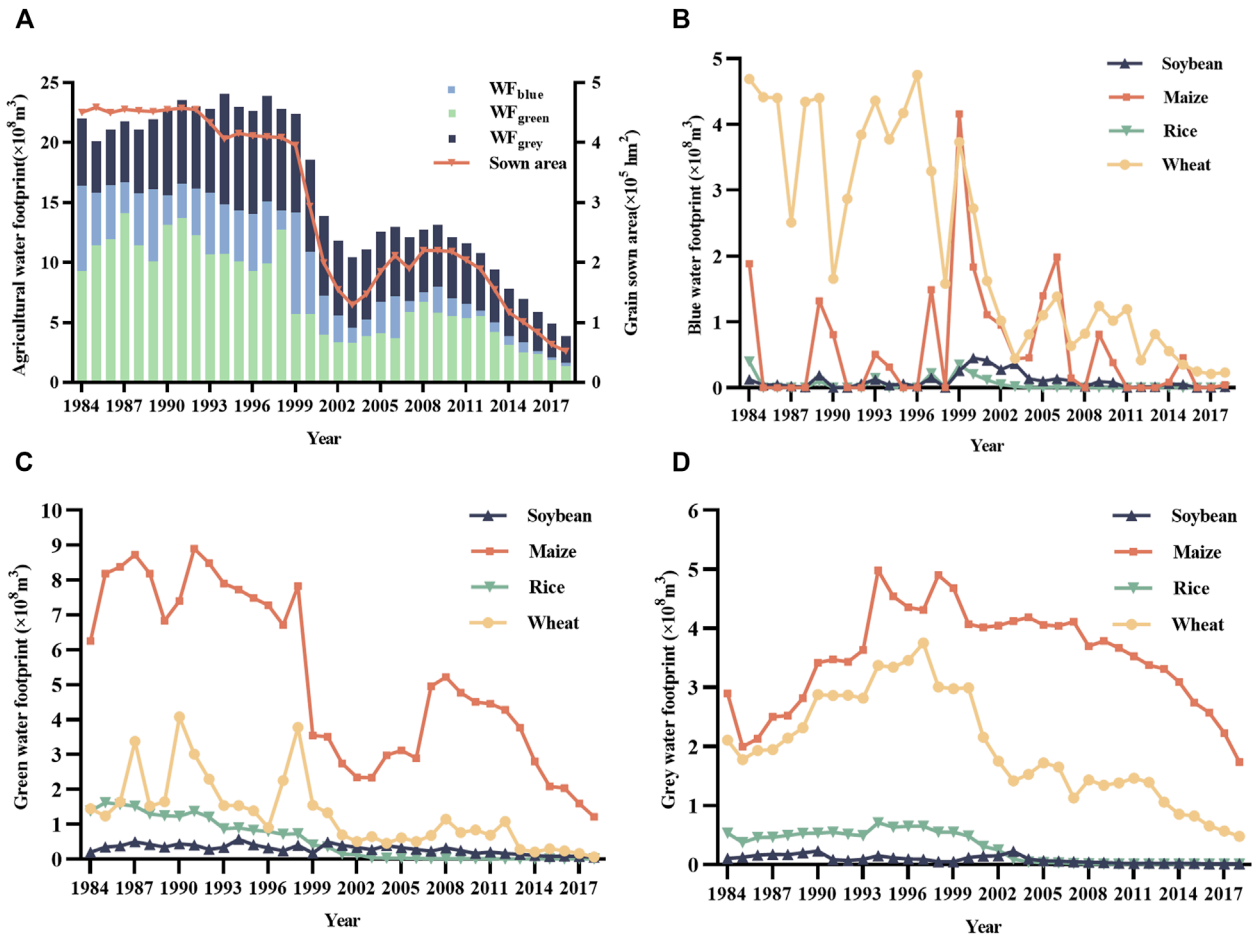

FIGURE 4
(A) Agricultural WF and composition, **(B)** blue WF, **(C)** green WF and **(D)** grey WF of four food crops in Beijing area.

the planting structure (PS) directly affected the total agricultural water demand, making it a key factor representing the production structure.

$$\ln I = \ln a + b \ln P + c \ln A_1 + d \ln A_2 + e \ln A_3 + f \ln T_1 + g \ln T_2 \quad (24)$$

4 Results

4.1 Temporal variations in the agricultural WF in the Beijing area

Equations 1–5 were used to calculate the agricultural WF in the Beijing area from 1984 to 2018. The results of WF and the sown area of main grains are shown in Figure 4A. From 1984 to 2018, the annual average agricultural WF in the Beijing area was 16.0 × 10^8 m^3, decreasing from 22.0 × 10^8 m^3 in 1984 to 3.86 × 10^8 m^3 in 2018, with an average annual variation rate of 4.54%. The absolute Z value from the Mann-Kendall (MK) test was greater than 1.96, indicating a significant downward trend over the study period. The maximum value was 24.1 × 10^8 m^3 in 1994, and the minimum value was 3.86 × 10^8 m^3 in 2018. Between 1984 and 2000, the agricultural WF fluctuated slightly, averaging approximately 22.2 × 10^8 m^3. Starting in 2001, the agricultural WF of the Beijing area began to decrease significantly, although it exhibited an increasing trend from 2004 to 2009, with an average annual growth rate of 4.11%. With an average annual decline of 12.6%, the agricultural WF displayed a continuous downward trend from 2009 to 2018.

The trend in WF variation was consistent with the variation in the crop sowing area, indicating that the crop sowing area was a key factor influencing the WF. In terms of WF composition, the overall pattern observed was green WF > grey WF > blue WF. On average, the green WF accounted for approximately 44% of the total WF, the grey WF accounted for 40%, and the blue WF accounted for 16%. The trend in the variation in the green WF was largely consistent with that in the total WF, with an average annual variation rate of 16.0%. The grey WF initially increased, peaking at 9.21 × 10^8 m^3 in 1994, before continuously decreasing to a minimum of 2.23 × 10^8 m^3 in 2018. The annual variation rate of the blue WF was 52.0%, which was significantly influenced by precipitation and the planting structure.

TABLE 2 MK trend test for WFs.

		Maximum ($\times 10^8 m^3$)	Minimum ($\times 10^8 m^3$)	Average ($\times 10^8 m^3$)	Z value	Variation trend
Total WF		24.07	3.86	16.04	−5.14	Downward trend
Green WF	Wheat	4.08	0.07	1.27	−5.06	Downward trend
	Maize	8.90	1.21	5.19	−5.23	Downward trend
	Soybean	0.57	0.05	0.29	−4.97	Downward trend
	Rice	1.62	0.00	0.53	−8.18	Downward trend
	Total	14.13	1.33	7.27	−5.42	Downward trend
Blue WF	Wheat	4.75	0.21	2.16	−6.11	Downward trend
	Maize	4.16	0.00	0.59	−0.50	No significant trend
	Soybean	0.45	0.00	0.10	−1.01	No significant trend
	Rice	0.40	0.00	0.05	−0.48	No significant trend
	Total	8.50	0.22	2.90	−5.17	Downward trend
Grey WF	Wheat	3.75	0.48	1.98	−4.57	Downward trend
	Maize	4.98	1.74	3.51	−0.80	No significant trend
	Soybean	0.23	0.01	0.09	−5.42	Downward trend
	Rice	0.71	0.01	0.29	−5.17	Downward trend
	Total	9.21	2.23	5.87	−3.86	Downward trend

The green, blue, and grey WFs of the four crops are depicted in Figures 4B–D. The average green WF of the four crops, ranked from largest to smallest, was as follows: maize > wheat > rice > soybean, with a significant decline observed across all crops. The average annual green WF for soybeans was 0.29×10^8 m³. Between 1984 and 1998, the average green WF of maize was approximately 7.75×10^8 m³, but it significantly decreased to 3.55×10^8 m³ in 1999, primarily due to severe drought in the Beijing area, where rainfall was only 36% of that of the previous year. Among the four crops, wheat was the most water intensive, exhibiting the highest blue WF, followed by maize, soybean, and rice. The blue WF of wheat showed a significant fluctuating downward trend, reaching a minimum of 0.21×10^8 m³ in 2017. The blue WF of maize varied significantly from year to year, with an average of 0.59×10^8 m³. When precipitation meets crop growth needs—specifically, when effective precipitation exceeds crop evapotranspiration—the blue WF is zero. The blue WFs of soybeans and rice remained consistently low. The grey WF of maize and wheat accounted for 93.6% of the total footprint among the four crops, initially increasing and then decreasing, whereas that of soybeans and rice remained very low. The MK trend test results are presented in Table 2. From 1984 to 2018, the absolute Z values for the WFs of all crops except for the blue WF and grey WF of maize exceeded 1.96 and were all negative, indicating a significant downward trend.

4.2 Spatial differences in the agricultural WF in the Beijing area

Figure 5 illustrates the spatial distribution and temporal evolution of the agricultural WF across various districts and counties in the Beijing area from 1990 to 2018. Overall, there were considerable variations in the agricultural WF among the districts and counties. Tongzhou District recorded the highest agricultural WF, with an average annual value of 2.71×10^8 m³, followed by Shunyi District and Daxing District, with averages of 2.59×10^8 m³ and 2.44×10^8 m³, respectively. Tongzhou and Shunyi districts were the two largest areas in terms of grain sown area, with an average of 5.4×10^4 m³ and 5.3×10^4 m³ per year. These values were approximately 1.1×10^4 m³ higher than that of Daxing district, which ranked third with 4.2×10^4 m³. The blue and green WFs in Tongzhou and Shunyi districts were relatively similar, with the primary difference lying in the grey WF. Between 1990 and 2018, Tongzhou district had an average fertiliser use of 200 kg per hectare more than Shunyi district. This higher fertiliser application, in the context of similar blue and green WFs, contributed to agricultural WF of Tongzhou district being the highest among all districts and counties in the Beijing area. The agricultural WF in each district decreased by an average of 80.1% from 2015 to 2018 compared to that from 1990 to 1994. Notably, the agricultural

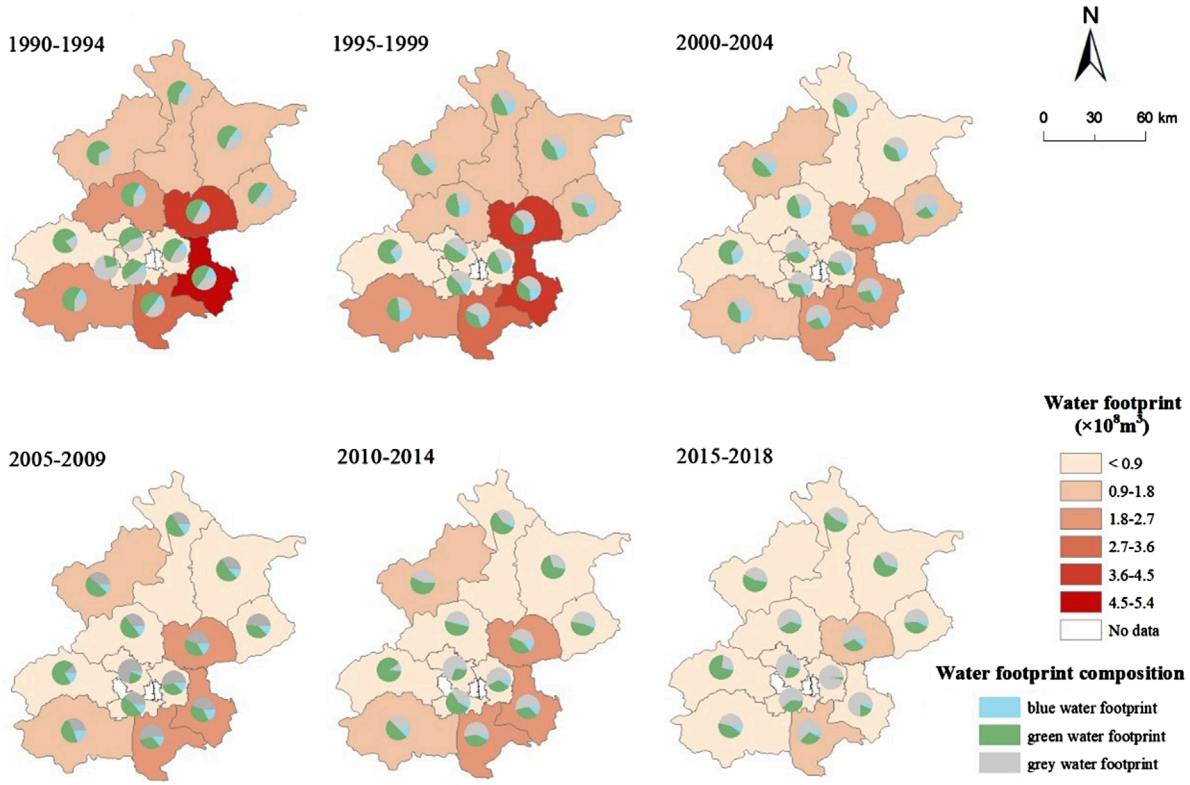

FIGURE 5
Agricultural WFs of Beijing area in different periods.

WFs of the Chaoyang and Fengtai districts exhibited the most significant reductions, each decreasing by more than 98%. In 1992, the actual cultivated land area of the Beijing area was 408,300 hm^2, with 37,900 hm^2 located in the suburban districts of Chaoyang, Fengtai, Shijingshan, and Haidian. By the end of 2018, the cultivated land area of the Beijing area had decreased to 212,800 hm^2, with the four suburban districts reduced to 6,600 hm^2, which was an 82.6% reduction. This significant reduction in arable land was accompanied by a corresponding decrease in the agricultural WF.

In terms of WF composition, the green WF was dominant from 1990 to 1994, accounting for an average of 50%, followed by the grey and blue WFs. The proportion of the grey WF gradually increased thereafter, reaching 55% from 2015 to 2018, whereas the green WF decreased to 39%. The WF composition among different districts and counties showed little variation; however, the green WF in Mentougou District consistently exceeded 70% over many years. This was attributed to the district having the lowest fertilizer usage per unit of cultivated land, resulting in a relatively small grey WF.

4.3 Assessment of agricultural water resource utilization in the Beijing area on the basis of WF variations

Equations 9–19 were employed to calculate the agricultural WSI and RRV indices for the Beijing area from 1984 to 2018. The calculation results of WSI index are shown in Figure 6A. The annual average WSI was 1.21, indicating a severe level of agricultural water resource stress in the Beijing area over the long term, with WSI values exceeding 1 in 25 out of the 35 years. Between 1999 and 2007, the WSI remained above 1 for nine consecutive years, primarily because of significantly lower precipitation than the annual average, marking the most severe drought period in the Beijing area since the 1950s (Shuang-shuan, 2015). WSI_{blue} and WSI_{green} quantified water resource scarcity during crop production from a water quantity perspective. The annual average WSI_{blue} value was 1.37, with a maximum value of 6.70 in 1999; and the annual average WSI_{green} value was 0.60 with a maximum value of 0.73 in 2007. A high WSI_{blue} typically corresponded to a low amount of available water resources, indicating extreme blue water scarcity in the Beijing area, with significant interannual variations. WSI_{grey} quantified the sustainability of water resource use from a water quality perspective (Shu et al., 2021). Between 1984 and 2018, the annual average WSI_{grey} was 0.63, indicating a moderate level of water scarcity. Between 1999 and 2002, WSI_{grey} was greater than 1, coinciding with high WSI_{blue} values and low available water resources, indicating an increased likelihood of agricultural water pollution during this period. To assess the sustainability of agricultural water resources in the Beijing area, RRV index was calculated, as presented in Figure 6B. From 1984 to 2018, the WSI values exceeded 0.8 on 25 occasions, with a multiyear reliability average of 0.25, peaking at 0.60 in 1993 and 1994 and reaching its lowest value of 0.10 between 2001 and 2010. The reliability of agricultural water resources in the

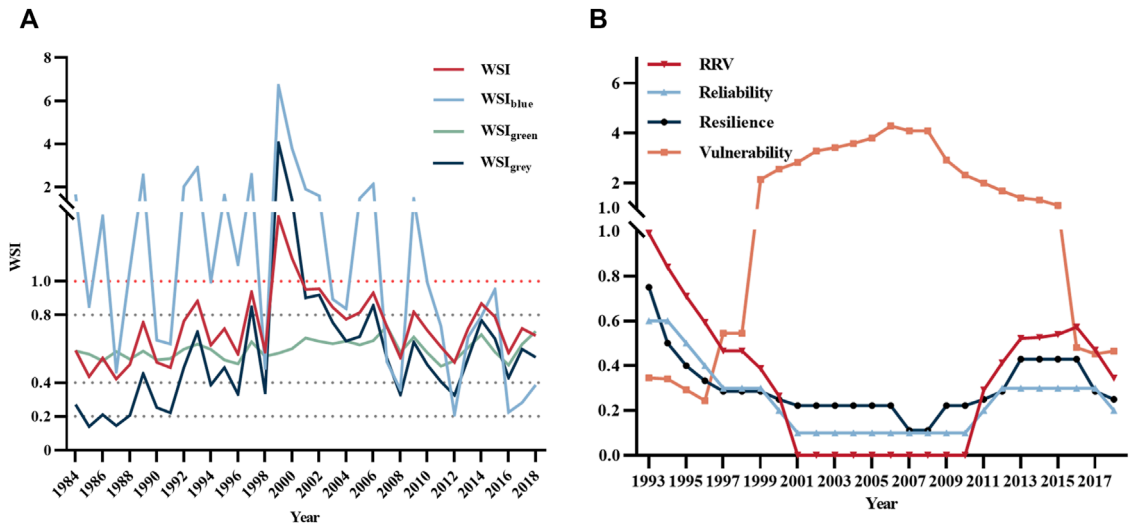

FIGURE 6
(A) WSI of total agricultural WF, blue WF, green WF and grey WF in Beijing area, and **(B)** Reliability-resilience-vulnerability indices.

Beijing area continuously declined from 1994 to 2001, reaching its lowest value of 0.10 before increasing to 0.30 after 2009. In recent years, the reliability of agricultural water resources in the Beijing area had exhibited a downward trend owing to consistently high WSI values exceeding 1. The average annual resilience index was 0.20, reflecting the capacity of water resources to recover from extreme stress to normal levels. The WSI of the Beijing area frequently exceeded 1, suggesting low resilience in agricultural water resources. When pressure becomes too severe, recovery to normal levels is difficult within a short time. Additionally, the average vulnerability index was 1.94, exceeding 1 from 1999 to 2015, reaching a maximum of 4.28 in 2006, and subsequently decreasing from 2016 to 2018. The sustainability index indicated that the sustainability of the agricultural water resource system in the Beijing area peaked in 1993, continued to decline until 2001, and remained in a state of poor sustainability until 2010. After it rose from 2011 to 2018, it decreased again, reaching a fair level in 2018.

4.4 Analysis of the driving factors of the agricultural WF in the Beijing area

The driving factors of the agricultural WF in the Beijing area from 1984 to 2018 were analysed via the extended STIRPAT model. The regression results are shown as Table 3. To address the strong multicollinearity between the dependent and independent variables and prevent interference from their overlapping information, ridge regression was performed by using SPSS 26.0 software. This yielded the regression equation and the corresponding R^2 value with varying asynchronous length k. A smaller k value corresponded to a smaller deviation. The standardized regression coefficients stabilized, leading to the selection of k = 0.02 as the step size. After adjustment, the R^2 value was 0.966, with all seven independent variables passing the significance test and with VIF values less than 10. The equation of the STIRPAT model was obtained as follows:

$$\begin{aligned}\ln I = {} & 0.589 \ln P + 0.245 \ln A_1 - 0.032 \ln A_2 \\ & + 0.164 \ln A_3 - 0.827 \ln T_1 - 0.233 \ln T_2 \\ & + 0.410 \ln PS \end{aligned} \tag{25}$$

Equation 25 revealed that increases in A2, T1, and T2 reduced the agricultural WF of the Beijing area, whereas increases in P, A1, A3, and PS led to an increase in the WF. Among these factors, the most influential on the agricultural WF of the Beijing area was the effective irrigation degree (T1). For every 1% increase in the degree of effective irrigation, the agricultural WF of the Beijing area decreased by 0.827%. Additionally, the agricultural population and planting structure played significant roles. The planting structure emerged as the largest positive driving factor, whereas effective irrigation was the most significant negative driving factor.

5 Discussion

5.1 Temporal and spatial variations in the agricultural WF in the Beijing area

In this study, the agricultural WF across urban and county areas of the Beijing area from 1978 to 2018 was quantified. The agricultural WF in the Beijing area showed slight fluctuations before 1999, a significant decrease from 1999 to 2003, and a trend of an initial increase followed by a decrease from 2004 to 2018; this was consistent with previous research findings (Xu et al., 2015; Jin et al., 2016). From 2000 to 2018, the agricultural WF in the Beijing area showed a trend of first increasing but then decreasing. Nationwide, the agricultural WF exhibited an increasing trend, while the proportion of the agricultural WF in the Beijing area

TABLE 3 Regression results.

Variables	Definition	Non-normalized coefficient	Normalized coefficient	t value	VIF
Constant		10.446	-	12.063	-
P	Agricultural population	−0.589	−0.327	−4.749	8.540
A1	Gross output value of agriculture	0.245	0.350	6.803	4.747
A2	GDP *per capita*	−0.032	−0.085	−2.093	2.963
A3	Industrial structure	0.164	0.334	5.791	5.996
T1	Degree of effective irrigation	−0.827	−0.278	−7.830	2.268
T2	Agricultural machinery density	−0.233	−0.108	−2.690	2.885
PS	Planting structure	0.410	0.237	3.924	6.555

relative to the national total gradually decreased (Wang Z. et al., 2023). This indicated a shift in the industrial structure of the Beijing area, which was characterized by a decline in the proportion of agriculture. The agricultural green WF of the Beijing area accounted for the largest proportion of its WF, with green water being consumed primarily in agricultural production. It played a significant role in both rain-fed crops and irrigated farmland (Cao et al., 2015; Cao et al., 2017). Therefore, improving the utilization rate of green water was crucial for alleviating water resource pressure. Throughout the study period, the proportion of the grey WF showed an increasing trend. The decline in soil fertility in recent years had led to the increased application of chemical fertilizers as the primary means to replenish soil nutrients and improve grain yield. Fertilizer use was the primary source of the grey WF in agricultural production. The fertilizer utilization efficiency in China is low, and the grey WF generated by fertilizer leaching negatively impacts the water environment. Enhancing fertilizer utilization efficiency in grain cultivation is a critical strategy to reduce the grey WF and control agricultural nonpoint source pollution.

The WF of food crops is influenced by natural factors, including crop type, regional climate, and soil type, and social factors, such as agricultural policy, land planning, and economic conditions (Xu et al., 2022). Owing to the relatively small variations in climate types across districts and counties within the Beijing area, the impact of topography is reflected mainly in the differences in cultivated area. The terrain of the Beijing area is characterized by higher elevations in the northwest and lower elevations in the southeast. This study indicated that the southeastern region, which was dominated by plains, featured large and dense crop planting areas, leading to a high and concentrated agricultural WF. According to *Beijing major function-oriented zone planning*, Tongzhou district, Shunyi district, Daxing district, and the plains of the Changping and Fangshan districts have been designated new urban development areas tasked with advancing modern agriculture. For many years, these five districts had accounted for more than 60% of the total WF, necessitating stronger management of agricultural water resources to address the water scarcity in the Beijing area.

5.2 Variations in agricultural water resource scarcity and sustainability in the Beijing area

Rapid population growth and economic development during the urbanization of the Beijing area had significantly increased water demand, leading to severe groundwater overexploitation. The average groundwater depth increased from 6.4 m in 1978 to 25.66 m in 2014, indicating extreme strain on water resources (Liu et al., 2019; Qin, 2021). To further explore the pressure and sustainability of the water resource system in the Beijing area, this study combined the WSI and RRV indices to establish a new comprehensive water resource assessment framework. The WSI results indicated that the regional agricultural water resources had experienced severe shortages for many years, mainly water quantity type water shortage, in which the blue water shortage problem had been particularly frequent. In 1999, a water quality shortage occurred, primarily due to the scarcity of blue water resources. Since the 1960s, the Beijing area had experienced below-average annual precipitation and uneven annual distribution, while the increasing water demand due to population growth had exacerbated agricultural water resource conflicts, significantly restricting the sustainable development of agriculture. This study showed that after 2007, precipitation levels increased compared with those in previous years, leading to a decrease in the WSI and an increase in reliability, resilience, and sustainability, returning to pre-1999 levels. Since 2000, the Beijing Municipal Government had implemented various measures to mitigate water shortages, including increasing reclaimed water irrigation in farmlands, adjusting the agricultural industrial structure, promoting water-saving agriculture and continuously reducing agricultural water consumption. However, further measures are necessary to address the ongoing scarcity of agricultural blue water resources. In particular, under the influence of climate change, it was crucial to strengthen the assessment of and response to natural disaster risks, such as drought. From 2013 to 2018, the WSI remained above 1, and sustainability remained at a poor to average level, indicating that the shortage of agricultural water resources remained severe. The RRV results indicated that, in recent years, the sustainability

of agricultural water resources in the Beijing region showed an improvement relative to the 2000s. However, when compared to the 1990s, there was little improvement, and sustainability levels remained relatively low. While agricultural water consumption in the Beijing area had gradually decreased over the years, further measures, such as the use of advanced water-saving irrigation technology, the development of high-standard farmland, and modernization restructuring, were essential for increasing water resource efficiency and promoting sustainable usage.

This research framework comprehensively considered blue, green, and grey WFs, constructing a comprehensive evaluation system for water resources on the basis of the WSI and RRV indices from the perspectives of both water quantity and quality. Compared with many previous studies, the water stress due to the heavy use of fertilizers was considered, and the grey WF was included into the assessment system in this study. Additionally, by combining the WSI and RRV indices, the RRV indices was proposed as a new systematic approach for assessing water resource in agricultural systems. The agricultural water resource evaluation system was further improved to provide robust and scientific data support for effective water resource management.

5.3 Driving factors of the agricultural WF in the Beijing area

Over the past 35 years, the agricultural WF of the Beijing area had decreased by 82.5%, with the blue WF decreasing by 95.9%, the green WF decreasing by 85.6%, and the grey WF decreasing by 60.4%. From the perspective of water consumption sources, the reduction in the sown area was the primary factor contributing to the decrease in the agricultural WF of the Beijing area. On the one hand, the transformation of the Beijing area into a megacity had led to significant changes in land use due to economic and social development needs; on the other hand, the aggressive promotion of ecological and environmental protection policies, such as returning farmland to forests, reduced the city's cultivated land area. Moreover, as living standards have improved, the demand for fruits and vegetables has increased, leading to a reduction in the area sown with grain. By 2018, the area sown with food crops was only 16.7% of that in 1984.

Variations in crop types significantly impact the amount of water required for irrigation. The WF per unit of wheat and rice was greater than that per unit of corn and soybeans. The driver analysis indicated that a 1% increase in wheat cultivation resulted in a 0.41% increase in the agricultural WF. Given that wheat and corn constituted approximately 90% of the total crop production, cultivating crops such as corn, which had a lower unit WF, can promote more efficient water resource use. Considering the current situation of water shortages in the Beijing area, it is necessary to change the planting structure.

Each 1% increase in the degree of effective irrigation and density of agricultural machinery could reduce the agricultural WF by 0.827% and 0.233%, respectively. This research indicated that agricultural modernization and the continuous progress of water-saving irrigation technology and supportive measures could reduce irrigation water consumption, increase the efficiency of agricultural water resource utilization, and subsequently lower the agricultural WF. Agricultural modernization is an important goal in China, with mechanization serving as its foundation. The growing demand for food crops due to population growth has driven advancements in agricultural machinery. On the one hand, this progress has led to increased crop yield and improved agricultural production efficiency; on the other hand, water-saving agricultural mechanization has improved the utilization efficiency of agricultural water resources.

Population factors significantly influenced the agricultural WF in the Beijing area. The results indicated that a 1% increase in the permanent population corresponded to a 0.589% decrease in the agricultural WF of the Beijing area. Typically, an increase in population led to an increase in the agricultural WF (Huang et al., 2021); however, the context in the Beijing area was contrary to this trend. As a megacity in China, the permanent resident population of the Beijing area in 2018 was 223% of that in 1984, whereas the agricultural population in 2018 was only 75% of that in 1984. Rapid urban development has driven more workers from rural areas to seek employment in cities. This shift had led to the abandonment of cultivated land and a reduction in the agricultural population (Gong et al., 2020). Owing to rapid urbanization and urban planning in the Beijing area, the cultivated land area decreased from 422,000 ha in 1984 to just 21.3 ha in 2018. This drastic reduction in cultivated land area led to a corresponding decrease in the agricultural WF, resulting in a negative impact of population on the agricultural WF of the Beijing area.

Various economic factors exerted distinct impacts on the agricultural WF in the Beijing area. The total agricultural output value was the largest positive driving force of the agricultural WF in the Beijing area; for every 1% increase in the gross output value of agriculture, the agricultural WF increased by 0.245%. From 1984 to 2018, the total agricultural output value of the Beijing area increased from 1.44 billion CNY to 11.47 billion CNY (Beijing Municipal Bureau Of Statistics, 2019). An increase in the gross output value of agriculture indicated an increase in crop production, necessitating significant water resources to support crop growth. The industrial structure was the second most significant positive driver of the agricultural WF in the Beijing area. A 1% increase in the proportion of primary industry resulted in a 0.164% increase in the agricultural WF of the Beijing area. Between 1984 and 2018, the proportion of primary industry in the Beijing area declined from 6.8% to 0.4%. The industrial structure of the Beijing area had been progressively optimized, with primary and secondary industries gradually shifting to the tertiary sector, significantly reducing the agricultural WF. The negative correlation between GDP *per capita* and the agricultural WF of the Beijing area indicated a reduced reliance on agriculture for economic development, with residents increasingly deriving economic benefits from secondary and tertiary industries, in line with the evolving industrial structure.

5.4 Recommendations to ease the pressure on agricultural water resources

The population growth in megacities such as Beijing inevitably increases the demand for food, which in turn drives higher water demand. As a result, the Beijing area imports significant quantities of

food crops to alleviate pressure on water resources. While reducing the crop planting area is the primary strategy for minimizing agricultural water use, the Beijing area must still preserve a certain amount of cultivated land to maintain ecosystem services and ensure a basic level of food self-sufficiency (Huang et al., 2012). To alleviate agricultural water resource pressures and promote regional sustainable water use, the recommendations are proposed as follows. (1) To maximize the efficient use of water resources by considering local climate conditions, selecting suitable crop types, optimizing planting structures, and reducing the planting area of high-water-consuming crops such as wheat. (2) To promote the adoptions of water-saving technologies in agriculture. As of 2020, the effective utilization coefficient of farmland irrigation water in the Beijing area was 75%, leading the nation, although it was still behind the 80%–90% efficiency levels seen in agriculturally developed countries. Advancements in water-saving technology can reduce blue water losses during irrigation, increase the efficiency of green water resource use, and thereby ease agricultural water resource pressures in the Beijing area. Additionally, the government should promote water-saving technologies tailored to the needs of farmers and crop types while encouraging the cultivation of drought-tolerant and water-efficient crops. (3) To continuously promote the applications of formulated fertilizers, organic fertilizers and other scientific fertilizer application methods, such as tailor-made fertilizer formulations according to different soil types and crop varieties along with policy subsidies, strengthen publicity and education on scientific fertilizer application, enhance fertilizer utilization efficiency, reduce grey WF, and control agricultural nonpoint source pollution. At the same time, crop yields have increased, indirectly reducing the WF of crop production.

6 Conclusion

This study analysed the temporal and spatial variations in the agricultural WF from 1978 to 2018, assessing the degree of water resource scarcity from both water quantity and water quality perspectives through blue, green, and grey WFs. On the basis of these assessments, an RRV indices was developed to evaluate the sustainability of agricultural water resources in the Beijing area, further enriching the comprehensive assessment system of water resources. The STIRPAT model was subsequently employed to investigate the driving factors influencing the agricultural WF. The results were as follows. (1) Agricultural WF in the Beijing area decreased significantly from 1978 to 2018. The green WF accounted for 43% of the total WF of the Beijing area. It indicated that the primary requirement for the growth of grain crops in the Beijing area was green water. (2) The WSI revealed that the Beijing area had consistently faced blue water shortages over the years, with water scarcity remaining severe. The RRV results indicated that the sustainability of the water resources system remained at a low level. The Beijing municipal government should continue to increase water resource utilization efficiency to alleviate ongoing water resource pressures. (3) Analysis of the driving factors suggested that reducing the proportion of water-intensive crops such as wheat, enhancing irrigation support measures, and promoting water-saving technologies can effectively reduce the agricultural WF. This study proposed an innovative water resource assessment framework that combined the WSI and the RRV indices. Building on the traditional WSI assessment method, this framework not only analysed the current pressure on water resources but also extended the evaluation to the long-term sustainability of the water resource system. It can provide a more comprehensive and systematic analytical tool for the sustainable management of water resources.

This study has several limitations in quantifying the agricultural WF of the Beijing area, as it considers only the WF of certain crops, does not include the WF of animal husbandry, and does not account for virtual water flows associated with trade. Given that the grain supply for the Beijing area is largely supplied from other regions, future studies should place greater emphasis on the impact of virtual water trade.

Data availability statement

The raw data supporting the conclusions of this article will be made available by the authors, without undue reservation.

Author contributions

RW: Conceptualization, Data curation, Formal Analysis, Investigation, Methodology, Visualization, Writing–original draft, Writing–review and editing. XW: Conceptualization, Project administration, Resources, Supervision, Writing–original draft, Writing–review and editing. GH: Conceptualization, Data curation, Investigation, Methodology, Writing–original draft. JC: Formal Analysis, Methodology, Writing–review and editing. ZL: Formal Analysis, Methodology, Writing–review and editing.

Funding

The author(s) declare that financial support was received for the research, authorship, and/or publication of this article. This research was financially supported by the National Natural Science Foundation of China (52270194, 52070024).

Acknowledgments

We would like to extend special thanks to the editor and the reviewers for their valuable comments in greatly improving the quality of this paper.

Conflict of interest

The authors declare that the research was conducted in the absence of any commercial or financial relationships that could be construed as a potential conflict of interest.

Generative AI statement

The author(s) declare that no Generative AI was used in the creation of this manuscript.

Publisher's note

References

Asefa, T., Clayton, J., Adams, A., and Anderson, D. (2014). Performance evaluation of a water resources system under varying climatic conditions: reliability, Resilience, Vulnerability and beyond. *J. Hydrol. (Amst).* 508, 53–65. doi:10.1016/j.jhydrol.2013.10.043

Beijing Municipal Bureau of Statistics (2016). Beijing statistical yearbook. Available at: https://nj.tjj.beijing.gov.cn/nj/main/2016-tjnj/zk/e/indexch.htm (Accessed October 21, 2016).

Beijing Municipal Bureau of Statistics (2019). Beijing statistical yearbook. Available at: https://nj.tjj.beijing.gov.cn/nj/main/2019-tjnj/zk/e/indexch.htm (Accessed April 28, 2021).

Cai, J., He, Y., Xie, R., and Liu, Y. (2020). A footprint-based water security assessment: an analysis of Hunan province in China. *J. Clean. Prod.* 245, 118485. doi:10.1016/j.jclepro.2019.118485

Cao, X., Wang, Y., Wu, P., Zhao, X., and Wang, J. (2015). An evaluation of the water utilization and grain production of irrigated and rain-fed croplands in China. *Sci. Total Environ.* 529, 10–20. doi:10.1016/j.scitotenv.2015.05.050

Cao, X., Zeng, W., Wu, M., Li, T., Chen, S., and Wang, W. (2021). Water resources efficiency assessment in crop production from the perspective of water footprint. *J. Clean. Prod.* 309, 127371. doi:10.1016/j.jclepro.2021.127371

Cao, X. C., Wu, M. Y., Guo, X. P., Zheng, Y. L., Gong, Y., Wu, N., et al. (2017). Assessing water scarcity in agricultural production system based on the generalized water resources and water footprint framework. *Sci. Total Environ.* 609, 587–597. doi:10.1016/j.scitotenv.2017.07.191

Chanda, K., Maity, R., Sharma, A., and Mehrotra, R. (2014). Spatiotemporal variation of long-term drought propensity through reliability-resilience-vulnerability based Drought Management Index. *Water Resour. Res.* 50 (10), 7662–7676. doi:10.1002/2014WR015703

Chu, Q., Shi, X., Zhao, J., Jia, H., Zhao, J., Lu, J., et al. (2022). Seeking sustainable pathway of crop production by optimizing planting structures and management practices from the perspective of water footprint. *Sci. Total Environ.* 843, 157091. doi:10.1016/j.scitotenv.2022.157091

D'Ambrosio, E., Gentile, F., and De Girolamo, A. M. (2020). Assessing the sustainability in water use at the basin scale through water footprint indicators. *J. Clean. Prod.* 244, 118847. doi:10.1016/j.jclepro.2019.118847

Dehghanpir, S., Bazrafshan, O., Etedali, H. R., Holisaz, A., and Collins, B. (2024). Water scarcity assessment in Iran's agricultural sector using the water footprint concept. *Environ. Dev. Sustain* 26 (11), 28995–29020. doi:10.1007/s10668-023-03852-3

Dietz, T., and Rosa, E. A. (1997). Effects of population and affluence on CO2 emissions. *Proc. Natl. Acad. Sci. U. S. A.* 94 (1), 175–179. doi:10.1073/pnas.94.1.175

Dolganova, I., Mikosch, N., Berger, M., Nunez, M., Mueller-Frank, A., and Finkbeiner, M. (2019). The water footprint of European agricultural imports: hotspots in the context of water scarcity. *Resources-Basel.* 8 (3), 141. doi:10.3390/resources8030141

Ehrlich, P. R., and Holdren, J. P. (1971). Impact of population growth. *Obstet. \& Gynecol. Surv.* 26, 769–771. doi:10.1097/00006254-197111000-00014

Elbeltagi, A., Aslam, M. R., Malik, A., Mehdinejadiani, B., Srivastava, A., Bhatia, A. S., et al. (2020). The impact of climate changes on the water footprint of wheat and maize production in the Nile Delta, Egypt. *Sci. Total Environ.* 743, 140770. doi:10.1016/j.scitotenv.2020.140770

Feng, H., Yang, M., Zeng, P., Liu, Y., Sun, F., Wang, K., et al. (2022). Transprovincial water quality impacts and the environmental inequity of grey water footprint transfer in China. *Resour. Conserv. Recycl* 186, 106537. doi:10.1016/j.resconrec.2022.106537

Golmohammadi, M. H., Safavi, H. R., Sandoval-Solis, S., and Fooladi, M. (2021). Improving performance criteria in the water resource systems based on fuzzy approach. *Water Resour. Manag.* 35 (2), 593–611. doi:10.1007/s11269-020-02739-6

Gong, Y., Li, J., and Li, Y. (2020). Spatiotemporal characteristics and driving mechanisms of arable land in the Beijing-Tianjin-Hebei region during 1990-2015. *Socioecon. Plann Sci.* 70, 100720. doi:10.1016/j.seps.2019.06.005

Hashimoto, T., Stedinger, J. R., and Loucks, D. P. (1982). Reliability, resiliency, and vulnerability criteria for water resource system performance evaluation. *Water Resour. Res.* 18, 14–20. doi:10.1029/wr018i001p00014

Hoekstra, A., and Hung, P. Q. (2002). Virtual water trade: a quantification of virtual water flows between nations in relation to international crop trade. *Water Sci. Technol.* 49, 203–209. doi:10.2166/wst.2004.0456

Hoekstra, A. Y. (2011). *Water footprint assessment manual.*

Hoekstra, A. Y., Mekonnen, M. M., Chapagain, A. K., Mathews, R. E., and Richter, B. D. (2012). Global monthly water scarcity: blue water footprints versus blue water availability. *PLoS One* 7 (2), e32688. doi:10.1371/journal.pone.0032688

Hogeboom, R. J. (2020). The water footprint concept and water's grand environmental challenges. *One Earth* 2 (3), 218–222. doi:10.1016/j.oneear.2020.02.010

Huang, H., La, Z., Wang, R., Shang, K., Li, M., Yang, X., et al. (2021). Agricultural infrastructure: the forgotten key driving force of crop-related water footprints and virtual water flows in China. *J. Clean. Prod.* 309, 127455. doi:10.1016/j.jclepro.2021.127455

Huang, J., Zhang, H., Tong, W., and Chen, F. (2012). The impact of local crops consumption on the water resources in Beijing. *J. Clean. Prod.* 21 (1), 45–50. doi:10.1016/j.jclepro.2011.09.014

Jin, C., Huang, K., Yu, Y., and Zhang, Y. (2016). Analysis of influencing factors of water footprint based on the STIRPAT model: evidence from the Beijing agricultural sector. *Water (Basel)* 8 (11), 513. doi:10.3390/w8110513

Liu, D., and Xiao, B. (2018). Can China achieve its carbon emission peaking? A scenario analysis based on STIRPAT and system dynamics model. *Ecol. Indic.* 93, 647–657. doi:10.1016/j.ecolind.2018.05.049

Liu, L., Hu, X., Zhan, Y., Sun, Z., and Zhang, Q. (2023). China's dietary changes would increase agricultural blue and green water footprint. *Sci. Total Environ.* 903, 165763. doi:10.1016/j.scitotenv.2023.165763

Liu, W., Chen, W., Feng, Q., and Deo, R. C. (2019). Situations, challenges and strategies of urban water management in Beijing under rapid urbanization effect. *Water Sci. Technol. Water Supply* 19 (1), 115–127. doi:10.2166/ws.2018.057

Lohwasser, J., Schaffer, A., and Brieden, A. (2020). The role of demographic and economic drivers on the environment in traditional and standardized STIRPAT analysis. *Ecol. Econ.* 178, 106811. doi:10.1016/j.ecolecon.2020.106811

Lovarelli, D., Bacenetti, J., and Fiala, M. (2016). Water Footprint of crop productions: a review. *Sci. Total Environ.* 548, 236–251. doi:10.1016/j.scitotenv.2016.01.022

Ma, X., and Jiao, S. (2023). Comprehensive analysis of water resources from the perspective of water footprint and water ecological footprint: a case study from Anyang City, China. *Environ. Sci. Pollut. Res. Int.* 30 (1), 2086–2102. doi:10.1007/s11356-022-22139-0

Mekonnen, M. M., and Hoekstra, A. Y. (2014). Water footprint benchmarks for crop production: a first global assessment. *Ecol. Indic.* 46, 214–223. doi:10.1016/j.ecolind.2014.06.013

Mialyk, O., Booij, M. J., Schyns, J. F., and Berger, M. (2024a). Evolution of global water footprints of crop production in 1990-2019. *Environ. Res. Lett.* 19 (11), 114015. doi:10.1088/1748-9326/ad78e9

Mialyk, O., Schyns, J. F., Booij, M. J., Su, H., Hogeboom, R. J., and Berger, M. (2024b). Water footprints and crop water use of 175 individual crops for 1990-2019 simulated with a global crop model. *Sci. Data* 11 (1), 206. doi:10.1038/s41597-024-03051-3

Qin, H. (2021). Numerical groundwater modeling and scenario analysis of Beijing plain: implications for sustainable groundwater management in a region with intense groundwater depletion. *Environ. Earth Sci.* 80 (15), 499. doi:10.1007/s12665-021-09795-0

Rodriguez, C. I., Arrien, M. M., Silva, S. H., and Aldaya, M. M. (2024). Global relevance of Argentinean rainfed crops in a climatic variability context: a water footprint assessment in Buenos Aires province. *Sci. Total Environ.* 927, 171946. doi:10.1016/j.scitotenv.2024.171946

Sediqi, M. N., and Komori, D. (2024). Assessing water resource sustainability in the kabul River Basin: a standardized runoff index and reliability, resilience, and vulnerability framework approach. *Sustainability* 16 (1), 246. doi:10.3390/su16010246

Shu, R., Cao, X., and Wu, M. (2021). Clarifying regional water scarcity in agriculture based on the theory of blue, green and grey water footprints. *Water Resour. Manag.* 35 (3), 1101–1118. doi:10.1007/s11269-021-02779-6

Shuang-shuan, L. (2015). The characteristics of drought-flood variation and its influence factors in Beijing during 1960-2013. *J. Nat. Resour.* doi:10.11849/zrzyxb.2015.06.006

Sturla, G., Ciulla, L., and Rocchi, B. (2024). Estimating the global production and consumption-based water footprint of a regional economy. *Sustain Prod. Consum.* 44, 208–220. doi:10.1016/j.spc.2023.11.023

Wang, L., Zhang, Y., Jia, L., Yang, G., Yao, Y., and Wang, W. (2019). Spatial characteristics and implications of grey water footprint of major food crops in China. *Water (Basel)* 11 (2), 220. doi:10.3390/w11020220

Wang, Q., and Ge, S. (2020). Carbon footprint and water footprint in China: similarities and differences. *Sci. Total Environ.* 739, 140070. doi:10.1016/j.scitotenv.2020.140070

Wang, Q., Zheng, G., Li, J., Huang, K., Yu, Y., and Qu, S. (2023a). Imbalance in the city-level crop water footprint aggravated regional inequality in China. *Sci. Total Environ.* 867, 161577. doi:10.1016/j.scitotenv.2023.161577

Wang, Y., Chen, Y., Duan, W., and Jiao, L. (2022). Evaluation of sustainable water resource use in the tarim River Basin based on water footprint. *Sustainability* 14 (17), 10611. doi:10.3390/su141710611

Wang, Z., Xu, D., Peng, D., and Zhang, X. (2023b). Future climate change would intensify the water resources supply-demand pressure of afforestation in inner Mongolia, China. *J. Clean. Prod.* 407, 137145. doi:10.1016/j.jclepro.2023.137145

Xie, P., La, Z., Yang, X., Huang, H., Gao, X., and Wu, P. (2020). Spatial-temporal variations in blue and green water resources, water footprints and water scarcities in a large river basin: a case for the Yellow River basin. *J. Hydrol. (Amst)* 590, 125222. doi:10.1016/j.jhydrol.2020.125222

Xu, C., Liu, Y., and Fu, T. (2022). Spatial-temporal evolution and driving factors of grey water footprint efficiency in the Yangtze River Economic Belt. *Sci. Total Environ.* 844, 156930. doi:10.1016/j.scitotenv.2022.156930

Xu, Y., Huang, K., Yu, Y., and Wang, X. (2015). Changes in water footprint of crop production in Beijing from 1978 to 2012: a logarithmic mean Divisia index decomposition analysis. *J. Clean. Prod.* 87, 180–187. doi:10.1016/j.jclepro.2014.08.103

Xu, Z., Chen, X., Wu, S. R., Gong, M., Du, Y., Wang, J., et al. (2019). Spatial-temporal assessment of water footprint, water scarcity and crop water productivity in a major crop production region. *J. Clean. Prod.* 224, 375–383. doi:10.1016/j.jclepro.2019.03.108

York, R., Rosa, E. A., and Dietz, T. (2003). STIRPAT, IPAT and ImPACT: analytic tools for unpacking the driving forces of environmental impacts. *Ecol. Econ.* 46 (3), 351–365. doi:10.1016/S0921-8009(03)00188-5

Zeng, Y., Liu, D., Guo, S., Xiong, L., Liu, P., Chen, J., et al. (2024). Assessment of the impacts of water resources allocation on the reliability, resilience and vulnerability of the water-energy-food-society (WEFS) nexus system. *Agric. Water Manag.* 295, 108780. doi:10.1016/j.agwat.2024.108780

Zhang, B. (2017). *The research on the optimization of water usage structure of China*. Hangzhou: Zhejiang University. (in Chinese).

Zhu, Y., Zhang, C., Fang, J., and Miao, Y. (2022). Paths and strategies for a resilient megacity based on the water-energy-food nexus. *Sustain Cities Soc.* 82, 103892. doi:10.1016/j.scs.2022.103892

frontiers | Frontiers in Earth Science

TYPE Original Research
PUBLISHED 19 March 2025
DOI 10.3389/feart.2025.1542367

OPEN ACCESS

EDITED BY
Qiang Liu,
Beijing Normal University, China

REVIEWED BY
Ramanathan Alagappan,
Jawaharlal Nehru University, India
Krzysztof Chudy,
Wrocław University of Technology, Poland
Atulya Kumar Mohanty,
National Geophysical Research Institute (CSIR), India

*CORRESPONDENCE
Weiya Ge,
gewy@mail.cgs.gov.cn

RECEIVED 09 December 2024
ACCEPTED 28 February 2025
PUBLISHED 19 March 2025

CITATION
Zhou X, He S, Sang H and Ge W (2025) Response of groundwater levels to ENSO under the influence of mining.
Front. Earth Sci. 13:1542367.
doi: 10.3389/feart.2025.1542367

Response of groundwater levels to ENSO under the influence of mining

Xiaoping Zhou[1], Shifang He[2], Honghui Sang[3] and Weiya Ge[1]*

[1]Nanjing Center, China Geological Survey, Nanjing, China, [2]Huaihe Energy Group, Huainan, China, [3]School of Soil and Water Conservation, Nanchang Institute of Technology, Nanchang, China

Human activity and climate change have significantly modified the hydrological processes of groundwater. In coal mining areas, dewatering operations have become more influential than climate change, making human activity the primary factor impacting groundwater systems. However, it remains unclear to what extent climate change affects groundwater levels under such strong human influence. This research examines the impact of El Niño Southern Oscillation (ENSO) on groundwater levels, using data from the Pansan Coal Mine in Huainan, China as a case study. We employ wavelet analysis to study four groundwater level time series and investigate the impacts of ENSO and precipitation. The study results indicate that, in cases of groundwater over-exploitation, significant regions in the Continuous Wavelet Transform of groundwater levels decrease significantly. However, despite the substantial drops in groundwater levels caused by mining activities, a distinct resonance period with precipitation and ENSO remains evident in the Cross Wavelet Transform. Human activities have not altered the resonance frequencies between groundwater levels and either precipitation or ENSO. Precipitation correlates with porous groundwater levels on an annual scale and with karst groundwater levels on both annual and inter-annual scales. ENSO significantly impacts Quaternary groundwater levels on annual and inter-annual scales, and it affects Neogene and karst groundwater levels on inter-annual scales. Conducting-water structures serve as the primary pathways for transmitting precipitation and ENSO signals. The findings and methodologies presented in this study can help managers and scientists in enhancing groundwater resource management, sustainable utilization and water disaster prevention amid future climate uncertainties.

KEYWORDS

coal mine groundwater, over-exploited, climate change, Enso, precipitation, wavelet transform

1 Introduction

Groundwater serves as a crucial water resource in coal mining operations, and it is also a disaster that threatens the safe mining of coal (Wang et al., 2012; Xue et al., 2023). Comprehending the fluctuations in groundwater levels, along with their periodic patterns and trends, plays a crucial role in addressing water resource management and disaster prevention effectively. This understanding is instrumental in predicting future variations in groundwater resources (Liesch and Wunsch, 2019). The periodic monitoring of groundwater levels resulting from oscillatory climatic systems serves as a valuable

resource to enhance long-term forecasting capabilities (Rust et al., 2018). While long-term records of groundwater levels are rare, they hold significant importance in supplying the essential data required to assess changes in the resource over time (Liesch and Wunsch, 2019). Consequently, there has been a growing emphasis on studying the influence of long-term periodic fluctuations in groundwater levels attributed to climatic teleconnections. Numerous authors have reported these fluctuations in recent years (Gurdak et al., 2007; Holman et al., 2011; Tremblay et al., 2011; Perez-Valdivia et al., 2012; Dong et al., 2015; Neves et al., 2019).

However, both climate change and human activities have significantly altered hydrological processes (Zhang et al., 2016). The increased magnitude and frequency of climate change since the early 20th century have complicated the relationship between climate change and groundwater systems (IPCC, 2012). El Niño Southern Oscillation (ENSO) is a major interannual climate phenomenon that significantly influences weather and climate patterns around the globe (Brönnimann et al., 2007; Kuss and Gurdak, 2014; Chang et al., 2019). Therefore, ENSO has been selected as the climate change factor in this study.

In numerous locations worldwide, human activities have intensified to the point where they exceed the influence of climate change, making human activity the dominant factor affecting groundwater systems (Hao et al., 2016). Groundwater over-exploitation is the main factor leading to the change of groundwater hydrological process (Salameh, 2008; Li et al., 2013; Pophare et al., 2014; Qian et al., 2018; Li et al., 2022). Groundwater over-exploitation, particularly in areas like China's Yangtze River Delta Plain (Wang et al., 2015; He et al., 2021; Xu et al., 2021), Huaibei Plain (Li and Gao, 2004; Zhu, 2013), and major coal mining areas (Xue and Zhang, 2016; Yin et al., 2016), has led to significant declines in groundwater levels and even land subsidence (Wang et al., 2013; Liu et al., 2019; Xue et al., 2022). The interplay between over-exploitation and climate change further complicates hydrological processes. Despite these challenges, research on the relationship between groundwater levels in such aquifers and climate patterns remains limited. This knowledge gap hampers the government's ability to effectively manage groundwater resources and prevent mine water disasters.

This project aims to investigate the periodicities of four over-exploited groundwater level time-series recorded in various aquifers, and to assess the potential effects of precipitation and climatic teleconnections (ENSO) on groundwater using wavelet analysis. The monitoring wells, situated in the Pansan Coal Mine in Huainan City, China, observe different confined aquifers and types (porous and karst).

2 Materials

2.1 Study area

The study area is situated in the Panji District, northwest of Huainan City, Anhui Province, which comprises Panyi, Paner, Pansan and Zhuji Coal Mines. For this study, Pansan Coal Mine was chosen due to the availability of complete groundwater level data. The area is located in the Huaihe River alluvial plain, with a flat terrain and an elevation ranging from 18 to 22 m and abundant coal resources that have been mined since the 1980s. Stratigraphic sections include Sinian (Z), Cambrian (Є), Ordovician (O), Carboniferous (C), Permian (P, with coal-bearing strata), Palaeogene (E), Neogene (N), and Quaternary (Q) strata. The main outcropping strata is Quaternary deposits, occasionally with Cambrian and Sinian outcrops in the northern region (Figure 1).

Pansan Coal Mine is located on the western part of the southern limb of the Panji Anticline within the Huainan Synclinorium, adjacent to the Panyi Mine. The overall structure is a monocline, with the strata trending in a NWW-SEE direction. The dip angle of the strata generally ranges from 5° to 10°, showing a trend of being steeper near the surface and gentler at greater depths. In some local sections, due to the influence of Fault F1, the dip angle increases to 30°–50°, and in some cases, the strata are even vertical. As a result of regional north-south compressional forces, secondary synclines and anticlines have developed within the coalfield.

The study area is located in the Huaihe River basin with its main water system being the Huaihe River and its tributary, the Mud River. It falls under a subtropical monsoon climate zone characterized by long winters and summers, and short springs and autumns, with distinct four seasons. The average annual temperature is 15.1°C, with an average of 2,298 h of sunshine per year. The annual average precipitation is 905.6 mm, with the highest recorded at 1,558 mm in 1991 and the lowest at 347 mm in 2001. Precipitation is mainly concentrated in the months of June to September. The average frost-free period lasts for 215.5 days per year.

The groundwater system comprises karst groundwater found in Cambrian, Ordovician, and Carboniferous strata, as well as porous groundwater distributed within loose Neogene and Quaternary sediments. These aquifers are distributed throughout the study area. The Quaternary aquifer group primarily receives recharge from vertical infiltration of atmospheric precipitation and surface water, with lateral recharge from rivers during the rainy season. In their natural state, the water levels fluctuate with seasonal variations, with the primary discharge methods being evaporation and artificial extraction. During the dry season, surface river water replenishes the aquifers. The Neogene aquifer is primarily replenished laterally through runoff. In its natural state, there is no hydraulic connection between the upper and lower aquifers. Under the influence of coal mining, groundwater is discharged into the mine through mining-induced fractures and underground boreholes. The development of karst fractures in limestone is uneven; near the outcrop in the northern area, the karst fractures are more developed, and the water-bearing capacity is strong. At the base of the Taiyuan Formation, a mudstone and aluminous mudstone aquitard exists, which under natural conditions limits the hydraulic connection between the Carboniferous and Ordovician aquifer groups. These aquifers primarily receive lateral recharge from runoff, and the discharge occurs through mining operations and drainage to the mine via fault fracture zones. To ensure safe mining operations and prevent water inrush accidents from high water pressure, groundwater is pumped to lower the water level. This process primarily involves extracting Neogene porous groundwater (monitoring well Nw), Carboniferous karst groundwater (monitoring well Cw), and Ordovician karst groundwater (monitoring well Ow), all of which impact the safety of coal mining. Additionally, Quaternary porous groundwater (monitoring well Qw) is extracted for production purposes.

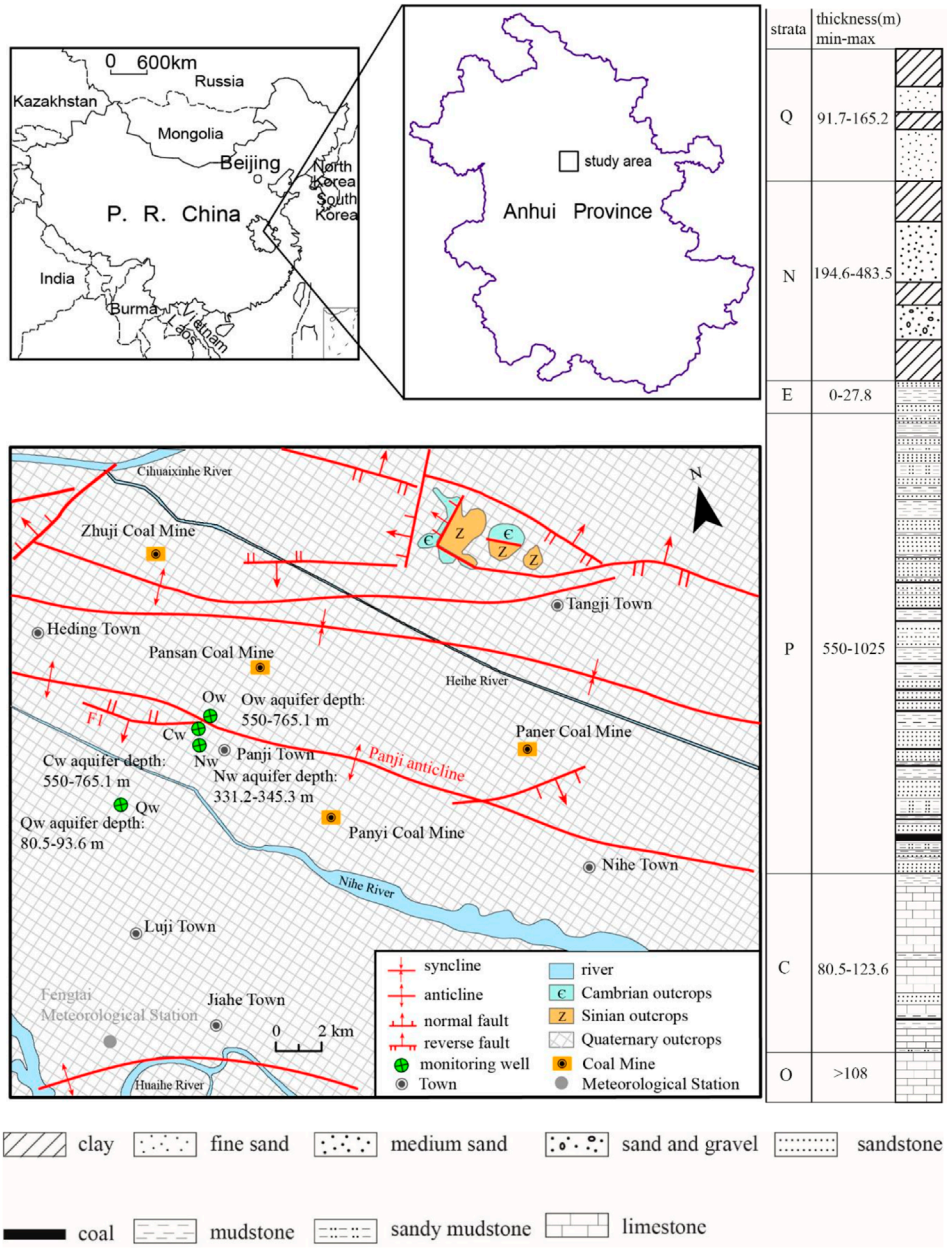

FIGURE 1
Location of groundwater monitoring wells and comprehensive stratigraphic column.

2.2 Data sources

The monthly precipitation data were acquired from the Fengtai meteorological stations of the National Climate Centre (http://data.cma.cn/). Monthly ENSO indices were determined by calculating the average sea surface temperature (SST) anomalies within the region spanning 5°N-5°S and 120–170°W. Monthly data for the ENSO teleconnection pattern were downloaded from the Climate Prediction Center of the National Weather Service website (http://www.cpc.ncep.noaa.gov). The Pansan coal mine began operations in 1992, and groundwater level data from January 2005 to December 2022 was collected. The four monitoring wells with the longest observation periods were selected for this study. The essential details of four monitoring wells are presented in Table 1. The mean monthly groundwater level was calculated by taking the arithmetic average of either three or six observations made during that month (three observations from January to April and October to December; six observations from May to September). Figure 2 displays the monthly precipitation sequences and the data for mean monthly groundwater levels.

Figure 2 depicts a substantial decline in both porous groundwater and karst groundwater levels, with karst aquifers experiencing a maximum groundwater level difference of nearly 80 m. The underlying karst aquifer beneath the A coal seam is

TABLE 1 Groundwater monitoring wells.

Well name	Geology	Aquifer type	Hydraulic conditions	Aquifer depth (m)	Initial water level (m)
Qw	Quarter-nary alluvium	Porous	Confined	80.5–93.6	17.32
Nw	Neogene-nary alluvium	Porous	Confined	331.2–345.3	11.8
Cw	Carboniferous limestone	Karst	Confined	422.7–478.7	17.11
Ow	Ordovician limestone	Karst	Confined	550–765.1	17.73

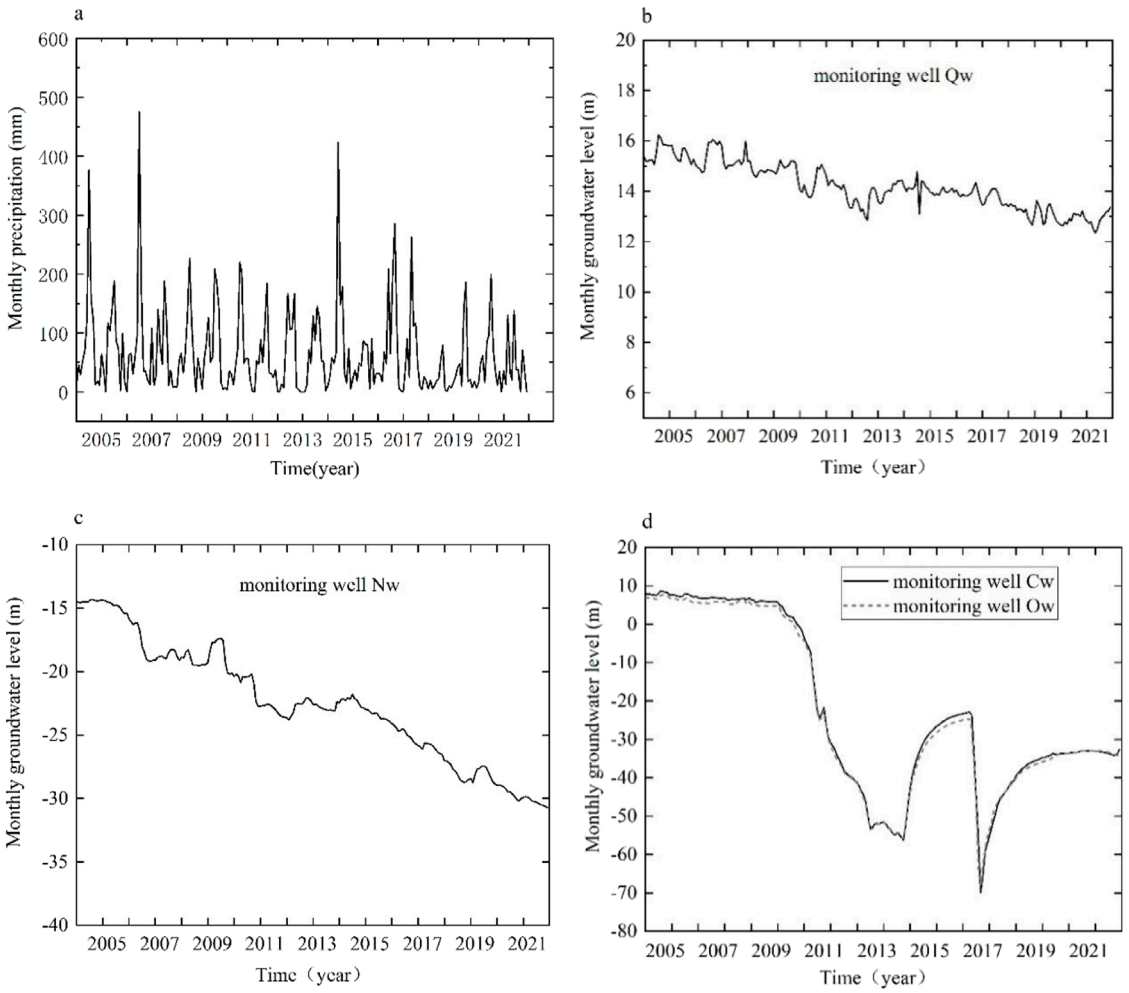

FIGURE 2
Monthly precipitation data and monthly groundwater level data from January 2005 to December 2022. **(a)** Monthly precipitation data, **(b)** Groundwater level in Quaternary pore aquifer (Qw), **(c)** Groundwater level in Neogene pore aquifer (Nw), **(d)** Groundwater levels in Carboniferous and Ordovician karst aquifer (Cw and Ow).

abundant in water, with initial groundwater levels of 17.11 m for the Carboniferous aquifer and 17.73 m for the Ordovician aquifer. The karst water pressure is particularly high. A stable aquiclude, with a thickness ranging from 9 to 21.8 m, separates the A coal seam from the karst water. However, the elevated water pressure and the potential connectivity of mining-induced fractures may lead to a water inrush accident in the coal mine. Therefore, the primary groundwater control measure for karst aquifers in the mine is to reduce water levels and pressure. This is achieved through the construction of underground boreholes for dewatering the karst water, thereby maintaining the water level within a safe range. This measure is a long-term water control strategy, requiring the continuous discharge of large volumes of karst water daily. Due to the lack of data on the volume of water discharged, a quantitative

analysis cannot be performed at present. So human activities, such as groundwater extraction and mine dewatering, these activities greatly disrupt the groundwater flow system.

3 Methods

3.1 Continuous wavelet transform (CWT)

Wavelet analysis is a robust technique widely utilized in various domains for analyzing non-stationary time series like hydrological, atmospheric, other geophysical time series. It provides an efficient method to expand time series into time-frequency space, allowing for the identification of localized intermittent periodicities (Grinsted et al., 2004). A wavelet series represents a square-integrable function by utilizing an orthonormal series based on a wavelet. One of the most frequently applied time-frequency transformations is the Continuous Wavelet Transform (CWT). A wavelet function, represented as $\psi(t)$, meets the requirement $\int_{-\infty}^{+\infty}\psi(t)=0$, which means it is a distinctive waveform with a limited duration and an average value of zero. Unlike traditional Fourier analysis, wavelet analysis is typically more irregular and asymmetrical in the time domain. In this method, the signal is broken down into a sequence of wavelet functions, contrasting with the reliance on trigonometric functions in Fourier analysis (Kriechbaumer et al., 2014). Wavelet functions are created by scaling and shifting a mother wavelet function based on different scales. As a result, they are highly effective in identifying the local characteristics of a signal. Each wavelet function, represented as $\psi_{\alpha,\tau}(t)$, is produced by expanding and translating the mother wavelet $\psi(t)$.

$$\psi_{\alpha,\tau}(t)=\frac{1}{\sqrt{\alpha}}\psi\left(\frac{t-\tau}{\alpha}\right),\alpha,\tau\epsilon R;\alpha>0 \tag{1}$$

In this context (Equation 1), we define the Morlet wavelet function using the following parameters: α for scale expansion, τ for dimensionless time shift, t for dimensionless time, ψ as the mother wavelet function, and R representing the set of real numbers. Numerous mother wavelet functions are at one's disposal, including the Mexican Hat wavelet, Morlet wavelet, and Haar wavelet. For this study's objectives, we chose to utilize the complex non-orthogonal Morlet wavelet function. It has a track record of delivering robust results in the analysis of time series records (Gedalof and Smith, 2001; Grinsted et al., 2004), making it a suitable choice for our research. Here is the definition of the Morlet wavelet function:

$$\psi_0(t)=\pi^{-1/4}e^{i\omega_0 t}e^{-t^2/2} \tag{2}$$

This equation defines the Morlet wavelet function (Equation 2), with ω_0 representing the dimensionless frequency in relation to dimensionless time t. Previous studies have indicated that selecting the Morlet wavelet with $\omega_0=6$ strikes an appropriate balance between time and frequency localization, making it a suitable choice (Gedalof and Smith, 2001; Grinsted et al., 2004). The Continuous Wavelet Transform (CWT) of a time series (x_t), where t ranges from 1 to N with uniform time steps $\triangle t$, is defined as the convolution of x_t with the scaled and transformed wavelet of $\psi_0(t)$:

$$W_x(\alpha,\tau)=\sqrt{\frac{\triangle t}{\alpha}}\sum_{t=1}^{N}x_t\psi_0^*\left[\frac{(t-\tau)\triangle t}{\alpha}\right] \tag{3}$$

In this equation (Equation 3), the symbol "*" represents the complex conjugate. $W_x(\alpha,\tau)$ captures the fundamental features of a time series x_t as it is mapped into a two-dimensional time-frequency space. CWT often exhibits edge artifacts due to the wavelet's incomplete time localization. To address this problem, the concept of the Cone of Influence (COI) can be employed. The Cone of Influence (COI) is defined as the e-folding time for the autocorrelation of wavelet power and represents the region in the wavelet spectrum where edge effects become significant (Torrence and Compo, 1998).

The e-folding time is chosen to ensure that the wavelet power $|W_x(\alpha,\tau)|^2$ for a discontinuity at the edge decreases by a factor e^{-2}, effectively rendering edge effects negligible beyond this threshold. In the case of cyclic series, zero-padding is unnecessary, and the concept of the Cone of Influence (COI) does not apply. The COI's size at each scale serves as an indicator of the decorrelation time for an isolated spike within the time series. By analyzing the width of a peak in the wavelet power spectrum in relation to the decorrelation time, one can distinguish between a transient data spike, possibly caused by random noise, and a harmonic component at the corresponding Fourier frequency (Torrence and Compo, 1998).

3.2 Cross wavelet transform (XWT)

When two Continuous Wavelet Transforms (CWTs) are analyzed together, the result is a Cross Wavelet Transform (XWT), which reveals the common power and represents the continuous wavelet cross-correlation in the time-frequency domain (Gedalof and Smith, 2001; Grinsted et al., 2004). The Cross Wavelet Transform (XWT) for two time series, x_t and y_t is defined as follows:

$$W_{xy}(\alpha,\tau)=W_x(\alpha,\tau)W_y^*(\alpha,\tau) \tag{4}$$

In this equation (Equation 4), the symbol "*" signifies the complex conjugate. The cross-correlation coefficients can be expressed as $W_x(\alpha,\tau)=|W_x(\alpha,\tau)|\exp(\phi_x(\alpha,\tau))$, here $|W_x(\alpha,\tau)|$ represents the wavelet amplitude, while $\phi_x(\alpha,\tau)$ denotes the absolute phase. Additionally, we define the cross wavelet power as $|W_{xy}(\alpha,\tau)|$, representing the cross-covariance between these two time series. You can calculate the relative phase difference between the two time series as follows:

$$\phi_{xy}(\alpha,\tau)=\tan^{-1}\left(\frac{I\left(S\left(a^{-1}W_{xy}(\alpha,\tau)\right)\right)}{R\left(S\left(a^{-1}W_{xy}(\alpha,\tau)\right)\right)}\right)\in[-\pi,\pi] \tag{5}$$

Equation 5, S denotes a smoothing operator, while I and R represent the imaginary and real components of $W_{xy}(\alpha,\tau)$, respectively. It is important to highlight that this definition relies on how the smoothing operator affects the different wavelet spectra. A stable phase relationship suggests a physical causal link between the two time series. When they are in phase, it indicates a perfect positive correlation, whereas being in anti-phase signifies a perfect negative correlation. This study utilizes MATLAB software for program execution and visualization.

4 Results

4.1 CWT for precipitation, ENSO and groundwater level

The study area is located in eastern China, where ENSO (El Niño-Southern Oscillation) significantly influences precipitation patterns by altering the global atmospheric circulation. During the El Niño phase, the West Pacific Subtropical High generally shifts southward, weakening the monsoon and leading to reduced precipitation in eastern China. In contrast, during the La Niña phase, the West Pacific Subtropical High strengthens and moves northward, enhancing the southeast monsoon and bringing more precipitation to eastern China. ENSO also affects the timing and intensity of the monsoon system, further altering the spatial and temporal distribution of precipitation. El Niño events often trigger droughts or floods in the southern regions, while La Niña events are associated with increased drought risk in the north and a higher risk of flooding in the south.

To gain deeper insights into the fluctuations of precipitation, ENSO, and groundwater levels, we conduct an analysis of their oscillations using Continuous Wavelet Transform (CWT), as depicted in Figure 3. In the continuous wavelet plot, the colored shading corresponds to the wavelet magnitude, as illustrated in the color bar. The areas enclosed by thick black contours are designated as significant regions, with the thick black contour indicating the 5% significance level compared to red noise. We also highlight the Cone of Influence (COI), where edge effects remain relevant, using a lighter shade, signifying that wavelet analysis within the COI has been taken into account.

For the precipitation, a typical yearly cycle is observed (Figure 3A). For the ENSO, the periodicities of 1–5 years are observed (Figure 3B). In contrast to the precipitation and the ENSO, the porous groundwater levels cannot be observed with continuous significant region. The periodicities of 0.5-year (2010-2011, 2013 and 2020), 1-year (2011) and 2-year (2012-2015) are observed for Qw and Nw (Figures 3C, D). However, the significant regions are very small and not the global maximum. For the karst aquifers, the power spectra of Cw and Ow are very similar, the periodicities of 1.5- and 5-year are observed for Cw and Ow (Figures 3E, F), with 5-year being the global maximum. The 5-year cycle is consistently present in a significant region, although a substantial portion of it falls outside the Cone of Influence (COI). This is primarily because the recorded time span is relatively short in comparison to the duration of the cycle.

4.2 XWT between precipitation and ENSO

As the dominant mode of global climate change, the ENSO is the primary factor influencing variability in global precipitation patterns (Dai et al., 1997). Groundwater is mainly supplied by atmospheric precipitation. To better understand the effects of how ENSO impacts the groundwater level, it is crucial to comprehend the relationship between ENSO and precipitation.

Figure 4 illustrates the cross-wavelet transform of precipitation and ENSO. In the cross-wavelet plot, the relative phase relationships are indicated by arrows. Arrows pointing to the right represent an in-phase relationship, signifying positive correlation, while arrows pointing to the left represent an anti-phase relationship, indicating negative correlation.

A continuous significant region at the 1-year time scale is observed, enclosed by a thick black contour, except during 2018 and 2019 (Figure 4). Significant regions within the COI during 2012–2018 are observed at a 3-year time scale. In the significant areas of the cross-wavelet plots, the phase angle exhibits quicker changes within the 1-year periodicity band, while it shifts more gradually within the 3-year periodicity band. The findings indicate that precipitation in the study region is correlated with ENSO on both annual and interannual (3-year) time scales.

4.3 XWT between groundwater level and precipitation

Figure 5 illustrates the cross-wavelet transform between groundwater levels and precipitation. In Figure 5A, the cross-wavelet between precipitation and Quaternary groundwater levels (Qw) shows a continuous significant region at the 1-year time scale spanning 2006 to 2018. Figure 5B shows the cross-wavelet transform between precipitation and Neogene groundwater levels (Nw), highlighting a significant region concentrated at the 1-year scale from 2009 to 2013, where an in-phase relationship suggests a complete positive correlation between the variables. In Figure 5C, the cross-wavelet between precipitation and Carboniferous groundwater levels (Cw) displays three intermittent significant regions: at 1-year scales during 2007–2009, 2011–2013, and 2016–2018; at a 3-year scale from 2015 to 2018 with an anti-phase relationship; and at a 5.5-year scale from 2013 to 2015 with an in-phase correlation. Similarly, Figure 5D shows the cross-wavelet between precipitation and Ordovician groundwater levels (Ow), revealing three intermittent significant regions: at 1-year scales during 2007–2008, 2011–2015, and 2016–2018; at a 3-year scale from 2015 to 2018 with an anti-phase correlation; and at a 5.5-year scale from 2013 to 2015 with an in-phase correlation. The results showed that precipitation is correlated with porous groundwater level on annual time scales and with karst groundwater level on annual and inter-annual (3- and 5.5-year) time scales.

4.4 XWT between groundwater level and ENSO

The cross wavelet analyses of ENSO and groundwater levels are shown in Figure 6. The cross-wavelet transform between ENSO and Quaternary groundwater levels (Qw) (Figure 6A) reveals distinct intermittent significant regions at the 1-year time scale during 2007–2008, 2010–2012, and 2014–2016. The periodicities of 2.5- and 3-year are distributed in 2008–2011 and 2011-2016 respectively, with 3-year being the global maximum. The cross-wavelet analysis between ENSO and Neogene groundwater levels (Nw) (Figure 6B) reveals three clusters of significant regions at different time scales: 1.5-year (2007–2017, 2020), 2.8-year (2008–2011) within the COI, and 5-year (2011–2017), with an in-phase correlation. The 5-year time scale represents the global maximum. For the karst groundwater, the significant regions in the power spectra are very similar (Figures 6C, D). The cross-wavelet analysis between ENSO and Carboniferous groundwater levels (Cw) (Figure 6C) reveals significant

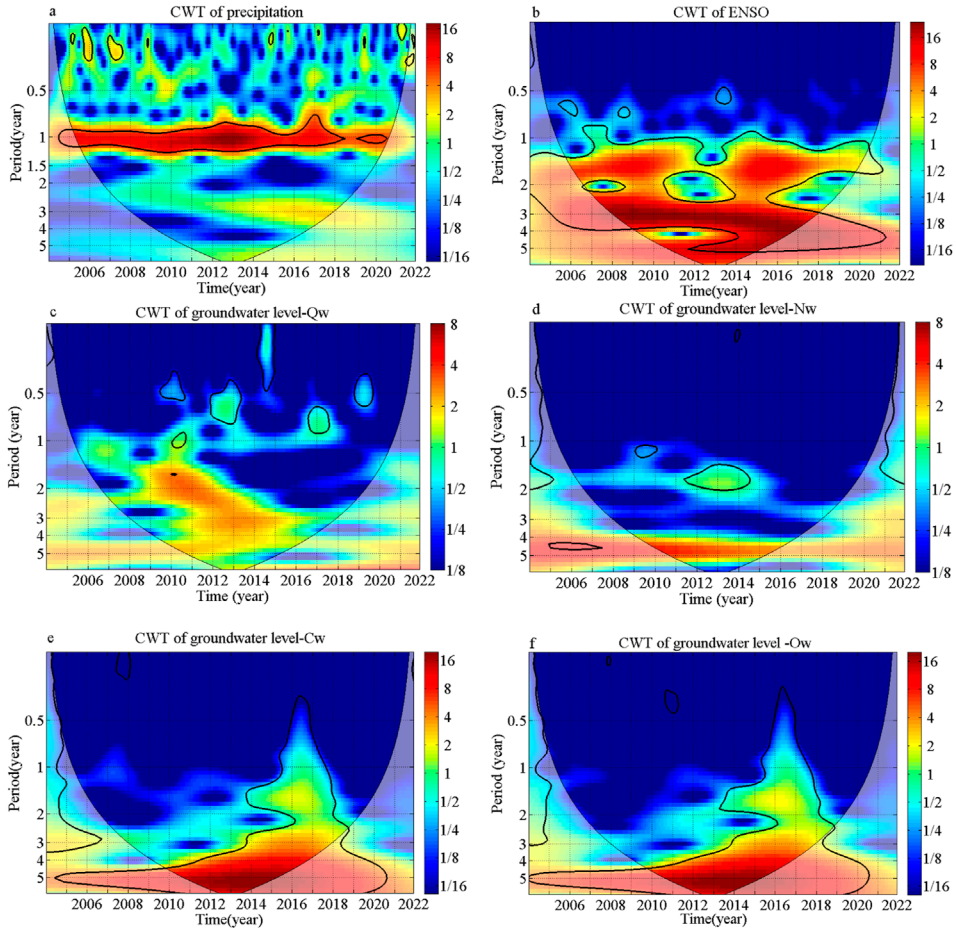

FIGURE 3
The continuous wavelet transform for precipitation, ENSO and groundwater levels: **(a)** CWT plot of precipitation; **(b)** CWT plot of ENSO; **(c)** CWT plot of groundwater level Qw; **(d)** CWT plot of groundwater level Nw; **(e)** CWT plot of groundwater level Cw; **(f)** CWT plot of groundwater level Ow.

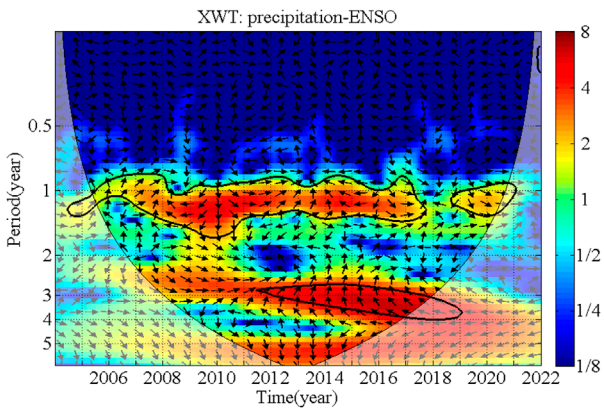

FIGURE 4
The cross wavelet transform between precipitation and ENSO.

regions at a 1.5-year time scale during the periods 2008–2012 and 2014–2019. The periodicities of 3- and 5-year within the COI are distributed in 2009–2018 and 2011-2016 respectively, and 5-year is the global maximum. For the Ordovician groundwater level (Ow), Same as the Carboniferous groundwater level, the wavelet spectrum shows three periods of 1.5-, 3- and 5-year too (Figure 6D). The significant regions are identical to those of the Carboniferous groundwater level, except for the period of 1.5-year (2010–2011, 2014–2019). Thus, ENSO influences Quaternary groundwater levels on both annual and inter-annual time scales, while its impact on Neogene, Carboniferous, and Ordovician groundwater levels occurs primarily on inter-annual time scales.

5 Discussion

The Continuous Wavelet Transform study revealed a significant regions reduction in over-exploited groundwater level (Figure 3). In its natural state, groundwater levels exhibit distinct significant regions and periods in CWT plots (Liesch and Wunsch, 2019; Neves et al., 2019). Cross Wavelet Transform results show that both precipitation and ENSO climate patterns continue to impact groundwater levels at Pansan Coal Mine, with varying effects over different time scales.

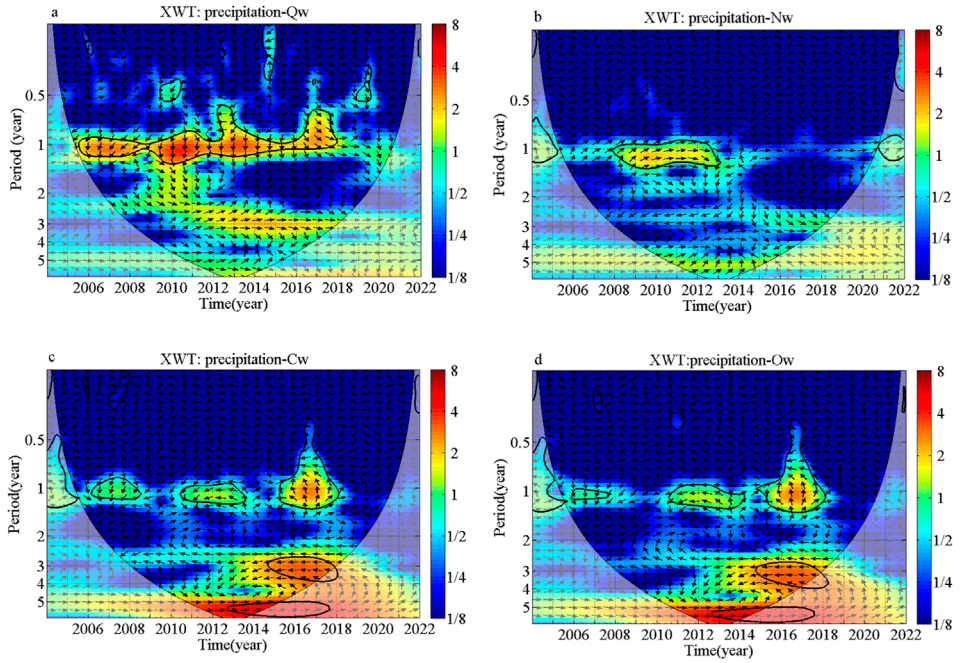

FIGURE 5
The cross wavelet transform between precipitation and groundwater levels: **(a)** XWT plot of precipitation and groundwater level Qw; **(b)** XWT plot of precipitation and groundwater level Nw; **(c)** XWT plot of precipitation and groundwater level Cw; **(d)** XWT plot of precipitation and groundwater level Ow.

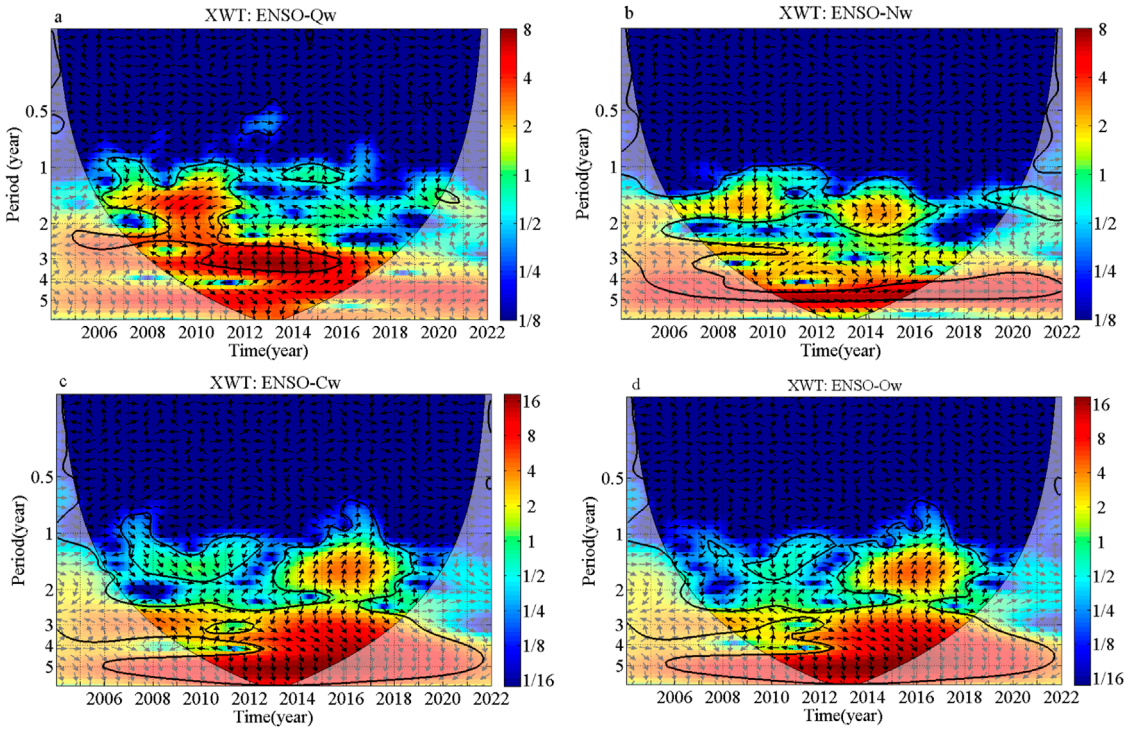

FIGURE 6
The cross wavelet transform between ENSO and groundwater levels: **(a)** XWT plot of ENSO and groundwater level Qw; **(b)** XWT plot of ENSO and groundwater level Nw; **(c)** XWT plot of ENSO and groundwater level Cw; **(d)** XWT plot of ENSO and groundwater level Ow.

Regarding precipitation and groundwater levels, there are noteworthy regions of wavelet correlation at a 1-year time scale for both porous and karst groundwater levels. Additionally, when analyzing the cross-wavelet transform between precipitation and karst groundwater level, intermittent significant regions emerge at 3-year and 5.5-year time scales. Therefore, precipitation significantly impacts porous groundwater levels on an annual time scale and influences karst groundwater levels on both annual and interannual time scales. For the ENSO and groundwater levels, all groundwater levels show resonance period beyond the 1-year cycle, in addition to the 1-year period observed in the Quaternary groundwater level. ENSO has a significant impact on Quaternary groundwater levels at both annual and inter-annual time scales, while it influences Neogene groundwater levels and karst groundwater primarily on inter-annual time scales.

The Cross Wavelet Transform analysis shows similar resonance periods and significant regions between karst groundwater levels and precipitation, ENSO (Figures 5C, D). Considering the geological conditions, monitoring wells Cw and Ow are located in the Panji anticline and F1 fault tectonic belt (Figure 1). Stratigraphic data from boreholes reveal that the water-conducting fault (F1) intersects with Ordovician limestone, indicating a hydraulic connection between the Carboniferous and Ordovician karst groundwater due to tectonic water conduction. Furthermore, the consistent changes in Cw and Ow groundwater levels further support this conclusion (Figure 2D). Consequently, precipitation and ENSO signals can rapidly influence over-exploited karst aquifers through this water-conducting structure.

In summary, excessive groundwater extraction can significantly lower groundwater levels, especially in karst aquifers deeper than 400 m, causing drops of over 80 m. This reduction shrinks the significant regions in Continuous Wavelet Transform plots over the recorded time span. Groundwater levels, however, remain sensitive to precipitation and ENSO signals. Despite the impact of human extraction activities on groundwater, the resonance periods between precipitation, ENSO, and groundwater levels remain unchanged. Even in cases of over-exploited groundwater, precipitation and ENSO signals can infiltrate the aquifer through pores, fractures, and structures.

6 Conclusion

This research utilized wavelet analyses to examine four groundwater level time series from the heavily exploited Pansan Coal Mine. The objective was to evaluate the potential effects of precipitation and the El Niño-Southern Oscillation (ENSO) on long-term variations in groundwater levels. The main findings and conclusions of the study can be summarized as follows:

(1) The Continuous Wavelet Transform reveals that the Quaternary groundwater level exhibits periodicities of 0.5- and 1-year, while the Neogene groundwater level has a 2-year periodicity. However, due to groundwater over-extraction, these periods are only observed in isolated years, with limited significant regions. Karst water exhibits periodicities of 1.5- and 5-year, with the 5-year being the dominant period with the highest power concentration.

(2) Cross Wavelet Transform analysis reveals strong correlations between groundwater and precipitation across various periodicities. Precipitation is correlated with porous groundwater levels annual time scale and with karst groundwater levels on both annual and inter-annual (3- and 5.5-year) time scales.

(3) Cross Wavelet Transform reveals significant correlations between groundwater levels and ENSO at various time scales. The Quaternary groundwater level shows periodicities of 1-, 2.5-, and 3-year, while the Neogene groundwater level exhibits periodicities of 1.5-, 2.8-, and 5-year. The Carboniferous and Ordovician groundwater levels resonate with ENSO at the same periods of 1.5-, 3-, and 5-year. ENSO strongly influences the Quaternary groundwater level annual and inter-annual time scales, and the Neogene and karst groundwater levels at inter-annual time scales.

(4) The Carboniferous and Ordovician aquifers are hydraulically connected, allowing both precipitation and ENSO signals to simultaneously reach these aquifers through conducting-water structure.

Data availability statement

The raw data supporting the conclusions of this article will be made available by the authors, without undue reservation.

Author contributions

XZ: Conceptualization, Software, Validation, Visualization, Writing–original draft, Writing–review and editing. SH: Formal Analysis, Investigation, Writing–review and editing. HS: Validation, Writing–original draft, Writing–review and editing. WG: Funding acquisition, Project administration, Writing–original draft, Writing–review and editing.

Funding

The author(s) declare that financial support was received for the research, authorship, and/or publication of this article. This research was funded by China Geological Survey (Grant No. DD20221732, DD20230116), and by Science and Technology Project of Jiangxi Provincial Water Resources Department, China (Grant No. 202425YBKT19), and by Nanchang Institute of Technology Student Innovation and Entrepreneurship Training Program Projects (Grant No. S202311319006, 202411319004).

Conflict of interest

SH was employed by the Huaihe Energy Group.

The remaining authors declare that the research was conducted in the absence of any commercial or financial relationships that could be construed as a potential conflict of interest.

Generative AI statement

The author(s) declare that no Generative AI was used in the creation of this manuscript.

Publisher's note

References

Brönnimann, S., Xoplaki, E., Casty, C., Pauling, A., and Luterbacher, J. (2007). ENSO influence on Europe during the last centuries. *Clim. Dynam.* 28 (2–3), 181–197. doi:10.1007/s00382-006-0175-z

Chang, X., Wang, B., Yan, Y., Hao, Y., and Zhang, M. (2019). Characterizing effects of monsoons and climate teleconnections on precipitation in China using wavelet coherence and global coherence. *Clim. Dynam.* 52, 5213–5228. doi:10.1007/s00382-018-4439-1

Dai, A., Fung, I. Y., and Genio, A. D. D. (1997). "Surface observed global land precipitation variations during 1900–1988," *J. Clim.*, 10. 2943–2962. doi:10.1175/1520-0442(1997)010<2943:SOGLPV>2.0

Dong, L., Shimada, J., Kagabu, M., and Fu, C. (2015). Teleconnection and climatic oscillation in aquifer water level in Kumamoto plain, Japan. *Hydrol. Process.* 29 (7), 1687–1703. doi:10.1002/hyp.10291

Gedalof, Z., and Smith, D. J. (2001). Interdecadal climate variability and regime-scale shifts in Pacific North America. *Geophys. Res. Lett.* 28, 1515–1518. doi:10.1029/2000GL011779

Grinsted, A., Moore, J. C., and Jevrejeva, S. (2004). Application of the cross wavelet transform and wavelet coherence to geophysical time series. *Nonlinear Proc. geoph.* 11 (5/6), 561–566. doi:10.5194/npg-11-561-2004

Gurdak, J. J., Hanson, R. T., McMahon, P. B., Bruce, B. W., McCray, J. E., Thyne, G. D., et al. (2007). Climate variability controls on unsaturated water and chemical movement, high plains aquifer, USA. *Vadose Zone J.* 6 (2), 533–547. doi:10.2136/vzj2006.0087

Hao, Y., Zhang, J., Wang, J., Li, R., Hao, P., and Zhan, H. (2016). How does the anthropogenic activity affect the spring discharge? *J. Hydrol.* 540, 1053–1065. doi:10.1016/j.jhydrol.2016.07.024

He, L., Hou, M., Chen, S., Zhang, J., Chen, J., and Qi, H. (2021). Construction of a spatio-temporal coupling model for groundwater level prediction: a case study of Changwu area, Yangtze River Delta region of China. *Water Supply* 21 (7), 3790–3809. doi:10.2166/ws.2021.140

Holman, I. P., Rivas-Casado, M., Bloomfield, J. P., and Gurdak, J. J. (2011). Identifying non-stationary groundwater level response to North Atlantic ocean-atmosphere teleconnection patterns using wavelet coherence. *Hydrogeol. J.* 19, 1269–1278. doi:10.1007/s10040-011-0755-9

Intergovernmental Panel on Climate Change (IPCC) (2012). "Summary for policy makers," in *Managing the risks of extreme events and disasters to advance climate change adaptation*. Editor Field, C. B. (Cambridge: Cambridge University Press).

Kriechbaumer, T., Angus, A., Parsons, D., and Casado, M. R. (2014). An improved wavelet-ARIMA approach for forecasting metal prices. *Resour. Policy.* 39, 32–41. doi:10.1016/j.resourpol.2013.10.005

Kuss, A. J. M., and Gurdak, J. J. (2014). Groundwater level response in U.S. principal aquifers to ENSO, NAO, PDO, and AMO. *J. Hydrol.* 519, 1939–1952. doi:10.1016/j.jhydrol.2014.09.069

Li, F., Feng, P., Zhang, W., and Zhang, T. (2013). An integrated groundwater management mode based on control indexes of groundwater quantity and level. *Water Resour. manage.* 27, 3273–3292. doi:10.1007/s11269-013-0346-8

Li, H., Du, X., Lu, X., and Fang, M. (2022). Analysis of groundwater overexploitation based on groundwater regime information. *Ground water* 61 (5), 692–705. doi:10.1111/gwat.13285

Li, Y., and Gao, G. (2004). Ground subsidence in areas of loose porous aquifers. *Acta Geol. Sin. – Engl.* 78, 829–837. doi:10.1111/j.1755-6724.2004.tb00203.x

Liesch, T., and Wunsch, A. (2019). Aquifer responses to long-term climatic periodicities. *J. Hydrol.* 572, 226–242. doi:10.1016/j.jhydrol.2019.02.060

Liu, J., Song, Z., Lu, Y., Bai, Y., Qian, W., Kanungo, D. P., et al. (2019). Monitoring of vertical deformation response to water draining–recharging conditions using BOFDA-based distributed optical fiber sensors. *Environ. Earth Sci.* 78, 406. doi:10.1007/s12665-019-8409-7

Neves, M. C., Jerez, S., and Trigo, R. M. (2019). The response of piezometric levels in Portugal to NAO, EA, and SCAND climate patterns. *J. Hydrol.* 568, 1105–1117. doi:10.1016/j.jhydrol.2018.11.054

Perez-Valdivia, C., Sauchyn, D., and Vanstone, J. (2012). Groundwater levels and teleconnection patterns in the Canadian Prairies. *Water Resour. Res.* 48 (7). doi:10.1029/2011WR010930

Pophare, A. M., Lamsoge, B. R., Katpatal, Y. B., and Nawale, V. P. (2014). Impact of over-exploitation on groundwater quality: a case study from WR-2 Watershed, India. *J. Earth Syst. Sci.* 123, 1541–1566. doi:10.1007/s12040-014-0478-0

Qian, J., Peng, Y., Zhao, W., Ma, L., He, X., and Lu, Y. (2018). Hydrochemical processes and evolution of karst groundwater in the northeastern Huaibei plain, China. *Hydrogeol. J.* 26, 1721–1729. doi:10.1007/s10040-018-1805-3

Rust, W., Holman, I., Corstanje, R., Bloomfield, J., and Cuthbert, M. (2018). A conceptual model for climatic teleconnection signal control on groundwater variability in Europe. *Earth Sci. Rev.* 177, 164–174. doi:10.1016/j.earscirev.2017.09.017

Salameh, E. (2008). Over-exploitation of groundwater resources and their environmental and socio-economic implications: the case of Jordan. *Water Int.* 33 (1), 55–68. doi:10.1080/02508060801927663

Torrence, C., and Compo, G. P. (1998). A practical guide to wavelet analysis. *Bull. Am. Meteorol. Soc.* 79(1), 61–78. doi:10.1175/1520-0477(1998)079<0061:apgtwa>2.0.co;2

Tremblay, L., Larocque, M., Anctil, F., and Rivard, C. (2011). Teleconnections and interannual variability in Canadian groundwater levels. *J. Hydrol.* 410, 178–188. doi:10.1016/j.jhydrol.2011.12.019

Wang, F., Miao, L., and Lu, W. (2013). Sand creep as a factor in land subsidence during groundwater level recovery in the southern Yangtze River delta, China. *Bull. Eng. Geol. Environ.* 72, 273–283. doi:10.1007/s10064-013-0474-7

Wang, G., Zhang, D., Feng, J., Chen, M., and Shan, W. (2015). Land subsidence due to deep groundwater withdrawal in northern Yangtze River Delta area. *Eng. Geol. Soc. Territ.* (5), 125–129. doi:10.1007/978-3-319-09048-1_25

Wang, Y., Yang, W., Li, M., and Liu, X. (2012). Risk assessment of floor water inrush in coal mines based on secondary fuzzy comprehensive evaluation. *Int. J. Rock Mech. Min. Sci.* 52, 50–55. doi:10.1016/j.ijrmms.2012.03.006

Xu, S., Chen, H., Wang, G., Huang, J., Che, Z., Gong, Y., et al. (2021). Analysis on mechanism of geosuture in henglin area, changzhou city, jiangsu Province. *East China Geol.* 42 (1), 93–99. (in Chinese). doi:10.16788/j.hddz.32-1865/P.2021.01.011

Xue, W., Hou, E., Zhao, X., Ye, Y., Tsangaratos, P., Ilia, I., et al. (2023). Discriminant analysis of water inrush sources in the weibei coalfield, shaanxi Province, China. *Water* 15, 453. doi:10.3390/w15030453

Xue, Y., Chen, H., Kong, F., Li, Z., Qiu, D., Chen, Q., et al. (2022). Land subsidence calculation model under the coupling effect of groundwater and coal mining. *Earth Sci. Inf.* 15, 2689–2701. doi:10.1007/s12145-022-00855-y

Xue, Y., and Zhang, Y. (2016). Land subsidence and land fissures in the southern Yangtze River Delta. *East China Geol.* (1), 1–9. (in Chinese). doi:10.16788/j.hddz.32-1865/P.2016.01.001

Yin, S., Han, Y., Zhang, Y., and Zhang, J. (2016). Depletion control and analysis for groundwater protection and sustainability in the Xingtai region of China. *Environ. Earth Sci.* 75, 1246. doi:10.1007/s12665-016-6044-0

Zhang, J., Hao, Y., Hu, B. X., Huo, X., Hao, P., and Liu, Z. (2016). The effects of monsoons and climate teleconnections on the Niangziguan karst spring discharge in North China. *Clim. Dynam.* 48, 53–70. doi:10.1007/s00382-016-3062-2

Zhu, B. (2013). Management strategy of groundwater resources and recovery of over-extraction drawdown funnel in Huaibei city, China. *China. Water Resour. manage.* 27, 3365–3385. doi:10.1007/s11269-013-0352-x

frontiers | Frontiers in Environmental Science

TYPE Original Research
PUBLISHED 09 April 2025
DOI 10.3389/fenvs.2025.1551988

OPEN ACCESS

EDITED BY
Qinghua Cai,
Chinese Academy of Sciences (CAS), China

REVIEWED BY
Yuying Li,
Nanyang Normal University, China
Fangyan Cheng,
Zhejiang Agriculture and Forestry University, China

*CORRESPONDENCE
Yujun Yi,
yiyujun@bnu.edu.cn

RECEIVED 31 December 2024
ACCEPTED 24 March 2025
PUBLISHED 09 April 2025

CITATION
Luo Q, Zhu L, Li D, Zu Z, Chen K, Wang J and Yi Y (2025) Role of hydraulic residence time in shaping phytoplankton community assembly in the upper yellow river cascade reservoirs. *Front. Environ. Sci.* 13:1551988. doi: 10.3389/fenvs.2025.1551988

Role of hydraulic residence time in shaping phytoplankton community assembly in the upper yellow river cascade reservoirs

Qiyong Luo[1,2], Linyu Zhu[1], Daikui Li[1], Zhigang Zu[1,3], Kebin Chen[1], Jia Wang[1] and Yujun Yi[1,3,4]*

[1]State Key Laboratory of Regional Environment and Sustainability, School of Environment, Beijing Normal University, Beijing, China, [2]School of Biological and Chemical Engineering, Guangxi University of Science and Technology, Liuzhou, Guangxi, China, [3]School of Civil Engineering, Yantai University, Yantai, Shandong, China, [4]Ministry of Education Key Laboratory of Water and Sediment Science, School of Environment, Beijing Normal University, Beijing, China

Introduction: Cascade hydropower development significantly alters the structure and function of river ecosystems. Phytoplankton, as primary producers, are highly sensitive to environmental changes, and their diversity and community structure reflect the state of the water environment. While there is extensive research on how changes in river environments affect phytoplankton community structure, studies on the spatial distribution patterns and community assembly mechanisms of phytoplankton in relation to hydraulic residence time (HRT)—a key characteristic of reservoirs—are limited.

Methods: Linear regression analysis was used to examine the relationship between phytoplankton communities and HRT. Additionally, the Neutral Community Model (NCM) combined with the Modified Stochasticity Ratio (MST) was employed to reveal the types of phytoplankton community assembly in these cascade reservoirs. Finally, Mantel tests and stepwise regression analysis assessed the specific impacts of environmental factors on phytoplankton communities.

Results: In the ecosystem of the Yellow River cascade reservoirs, HRT is positively correlated with phytoplankton abundance and diversity across different seasons. In annual regulation hydropower stations (LJX and LYX), phytoplankton species richness, abundance, and diversity indices are higher compared to those in runoff hydropower stations.

Discussion: The phytoplankton community assembly is primarily driven by deterministic processes, with annual regulation hydropower station being more influenced by these processes than runoff hydropower station. HRT, water temperature (WT), and total nitrogen (TN) are the most significant environmental factors affecting the structural differences of phytoplankton in cascade reservoirs. There is a significant positive correlation between phytoplankton and water temperature, especially in short HRT runoff hydropower station where phytoplankton abundance is more significantly impacted by water temperature.

KEYWORDS

phytoplankton, community assembly, hydraulic residence time, cascade reservoir, the upper yellow river

Highlights

- Regression analysis reveals that hydraulic residence time (HRT) is one of the key driving factors influencing phytoplankton community structure changes.
- HRT positively correlates with phytoplankton abundance and diversity in the upper Yellow River cascade reservoirs.
- Deterministic processes play a major role in the assembly of phytoplankton communities in the upper cascade reservoirs of the Yellow River.
- Water temperature positively correlates with phytoplankton abundance, with shorter HRT reservoirs being more influenced by water temperature.

1 Introduction

To meet multiple demands such as hydropower production, flood control, ice jam prevention, transportation, irrigation, and water supply for both industrial and domestic use, 61,988 large reservoirs exceeding 15 m in height have been constructed on rivers worldwide (ICOLD, 2023). Reservoir impoundment alters natural hydrological rhythms (Datry et al., 2023), affects hydrodynamic conditions (Grill et al., 2019; Belletti et al., 2020), and disrupts suspended sediment deposition processes (Maavara et al., 2020), which has a significant nutrient transport and overall health of river ecosystems impacts. Particularly in reservoir areas, there is an increased risk of eutrophication and excessive algal blooms due to slower flow rates and longer water exchange times, all of which pose a threat to the health and stability of river ecosystems.

Phytoplankton are the main primary producers in aquatic ecosystems, playing crucial roles in material cycling, energy flow, and maintaining of aquatic ecosystem balance (Li et al., 2013; Mor et al., 2018; Yi et al., 2023). They are extremely sensitive to environmental changes, and changes in the aquatic environment can cause changes in the diversity and structure of phytoplankton communities (Chen et al., 2020; Salmaso and Tolotti, 2021; Shen et al., 2024). Environmental factors such as nutrient salts and water temperature have important effects on phytoplankton growth (Salmaso and Tolotti, 2021), while hydrodynamic conditions significantly influence phytoplankton community composition (Liu et al., 2021; Ruan et al., 2024), and cascade reservoirs further add to the complexity of the pattern of this effect. Previous studies on the effect of reservoirs on phytoplankton community composition have focused on the effects of changing nutrient concentrations (Zhang et al., 2024), seasonal fluctuations (Ruan et al., 2024), and hydrodynamic conditions (Liu et al., 2021) in single reservoirs on phytoplankton community structure response patterns. In contrast, the impacts of cascade reservoirs on phytoplankton communities are more complex and multidimensional due to their unique cumulative effects (Liu et al., 2021). In the context of climate change, the impacts of terraced development on river ecosystems have become more complex (He et al., 2024). Therefore, clarifying the effects of environmental factors on phytoplankton community composition is crucial to understanding the ecological impacts of cascade reservoirs.

Hydraulic residence time (HRT) is a crucial factor influencing the biogeochemical cycling and physical transformation of nutrients in rivers (Maavara et al., 2020; Zhao et al., 2024). Reservoirs of different scales show significant variations in water quality factors, which are closely linked to their scale and HRT (Wang et al., 2022). The duration of hydraulic residence time significantly affects the structure of phytoplankton communities (Zeng et al., 2006; Yin et al., 2024). HRT affects the retention of nutrients such as nitrogen and phosphorus, altering their composition (Zhao et al., 2024), and ultimately significantly impacts the structure of phytoplankton communities (Li et al., 2013; Znachor et al., 2020). Rivers at high-altitudes are receiving increasing attention due to the impacts of rapid climate change (Xu et al., 2024). These rivers have driven intensive hydropower development activities due to their large slope drop and abundant hydroelectric resources (Li et al., 2018). However, hydropower development may lead to longer or altered HRT in rivers, which in turn pose potential adverse effects on the health and sustainability of river ecosystems. Nevertheless, there is still a lack of clear understanding on the specific effects of hydraulic residence time on phytoplankton community structure and the role it plays in the community assembly process in the context of cascade hydropower development in high-altitude rivers.

In studies analyzing the response of phytoplankton to environmental conditions, ordination analyses such as principal component analysis (PCA) (Xu et al., 2022) and correlation analyses (e.g., Mantel test, Ruan et al., 2024) are often used to compare the effects of different environmental variables on differences in community structure. To gain a deeper understanding of the multifactor-driven mechanisms of phytoplankton community assembly from an ecological perspective, the neutral community model (NCM) was introduced, which distinguishes between deterministic processes (e.g., environmental filtering and species interactions) and stochastic processes (including births, deaths, migrations, dispersal, etc.) (Sloan et al., 2006). In recent years, the model has been widely applied in aquatic ecosystems such as rivers, reservoirs and lakes (Isabwe et al., 2022; Xiao et al., 2022; Zhang et al., 2024). However, regarding the type of dominant drivers of phytoplankton community construction, the results of studies in different water body types are controversial (Xiao et al., 2022; Zhang et al., 2024). Deterministic processes dominate community construction in plain river ecosystems (Isabwe et al., 2022), while stochastic processes are more critical in estuarine and lake ecosystems (Sun et al., 2023; Xiao et al., 2022). Although the above studies have provided insights into the mechanisms of phytoplankton community assembly, the mechanisms and driving factors of phytoplankton community assembly in the cascade ecosystems formed by high-altitude rivers and reservoirs remain unclear.

The Yellow River is the second-longest river in China and the fifth-longest river in the world. The upper reaches of the Yellow River, from Longyangxia to Liujiaxia, are located in the transition zone between the Tibetan Plateau and the Loess Plateau, and belong to the alpine river region, with a unique plateau-alpine climate, which plays an important role in the earth's climate, biodiversity and water cycle (Yang et al., 2023). This section of the river is rich in hydropower resources, and it is the most densely populated area of hydropower stations on the main stream of the Yellow River. Currently, studies on the ecological impacts of hydropower development on the Yellow River gradient on the river mainly focus on reservoir hydrological regulation (Xu et al., 2022), water

temperature change (Ren et al., 2020), carbon emission (Wang et al., 2023), nutrient salts dynamics (Wu et al., 2021), species diversity (Jia et al., 2020) and biological evaluation of water quality (Ding et al., 2021). However, studies on the types of drivers of phytoplankton community aggregation in alpine river terrace reservoirs are still very limited. Given the importance of this reach in exploring the impacts of alpine river terrace development on aquatic ecosystems, this study targeted six reservoirs with different HRT in the upper reaches of the Yellow River, aiming to address the questions of (1) how does the structure of phytoplankton communities change under different HRT conditions? (2) How do environmental factors affect phytoplankton community structure? (3) What are the differences between the contributions of deterministic and stochastic processes in phytoplankton community structure? We hypothesized that terraced hydropower development interferes with the natural process of phytoplankton community construction in alpine rivers, in which HRT plays a key role. This research aims to improve the understanding of the mechanisms of riverine phytoplankton community construction and its drivers.

2 Materials and methods

2.1 Study area

The Yellow River, China's second-longest river spanning 5,464 km, with an annual runoff of 58 billion m^3 and a drainage area of 752,443 km^2, is revered as the "Mother River" of the Chinese nation. The upper Yellow River section from Longyangxia to Liujiaxia (hereafter referred to as the Long-Liu section), is situated on the northeastern fringe of the Qinghai-Tibet Plateau. This region comprises plateaus, wetlands, and valleys, ranging in elevation from 1,800 to 4,800 m. The Long-Liu section experiences a typical plateau continental climate marked by low rainfall, high evaporation, dry air, and cool temperatures. The average annual temperature is 5°C–9°C, with annual precipitation ranging from 194 to 357 mm and evaporation from 1,500 to 2,131 mm. The river section has distinct dry and wet season. The water has high oxygenated, while water temperature and nutrient content remain relatively low. In order to meet the needs of flood control, bulging prevention, irrigation, production and living as well as clean energy supply, 27 reservoirs have been built in the main stream of the Yellow River. Among them, the Long-Liu section is the most concentrated area of reservoirs, with a total of 13. Longyangxia, Laxiwa, Lijiaxia, Gongboxia, Jishixia, and Liujiaxia all have a dam height of more than 100 m, with an annual power generation of more than 1,000 MW (Table 1).

Two surveys were conducted on the cascade reservoirs in the Long–Liu section during the dry season (May 11–26, 2023) and the wet season (September 15–30, 2023). A total of 29 monitoring cross sections were setted, encompassing upstream river reaches, within the reservoirs, in front of the dams and downstream river reaches (Figure 1), to comprehensively characterize the spatial distribution patterns of phytoplankton within the reservoir system. S1-S6 are, in order, the upstream channel, the middle of the reservoir (3 sample sites), the front of the reservoir and the downstream channel of the dam in Longyangxia (LYX) reservoir; S7-S10 are, in order, the upstream channel, the middle of the reservoir, the front of the reservoir and the downstream channel of the dam in Laxiwa (LXW) reservoir; S11-15 are, in order, the upstream channel, the middle of the reservoir (2 sample sites), the front of the reservoir and the downstream channel of the dam in Lijiaxia (LiJX) reservoir; S16- S18 are, in order, the middle, front and downstream channels of Gongboxia (GBX); S19-S22 are, in order, the upstream channel, middle, front and downstream channels of the dam of Jishixia (JSX) reservoir; S23 -S27 are, in order, the upstream channel, middle (2 sample sites), the front of the reservoir and the downstream channel of the dam in Liujiaxia (LYX) reservoir. S28 is a sampling sites in the middle reaches of the Tao River, a tributary, and S29 is where the Tao River tributary joins the Liujiaxia Reservoir area.

2.2 Sample collection and laboratory analyses

Field water quality parameters were measured using the Multiparameter Water Quality Sonde (YSI EXO2, Xylem Inc., United States), including water temperature (WT, °C), pH, electrical conductivity (EC, μS cm^{-1}), salinity (Salt, ng L^{-1}), dissolved oxygen (DO, mg L^{-1}), oxidation-reduction potential (ORP, mV), and chlorophyll-a (Chl-a, μg mL^{-1}). At each sampling site, 2 L of surface water was collected using an organic glass water sampler, sealed, and transported to the laboratory under low-temperature conditions. Following the Chinese *Environmental Quality Standards for Surface Water* (SEPA, 2002), laboratory analyses were conducted to determine total nitrogen (TN, mg L^{-1}), total phosphorus (TP, mg L^{-1}), nitrate nitrogen (NO_3^--N, mg L^{-1}), nitrite nitrogen (NO_2^--N, mg L^{-1}), ammonium nitrogen (NH_4^+-N, mg L^{-1}), and chemical oxygen demand (COD, mg L^{-1}). Total organic carbon (TOC, mg L^{-1}) was measured using a total organic carbon analyzer (TOC-L, Shimadzu Corporation, Japan). Additionally, 5 L of surface water was collected and filtered through a 0.45 μm mixed cellulose membrane (Merck Millipore, United States), and the total suspended solids (TSS, mg L^{-1}) concentration was determined by the gravimetric method. Geographic variables, including longitude, latitude, and altitude, were recorded using the OWI interactive mapping software (V10.1.3).

At each sampling site, qualitative and quantitative phytoplankton samples were collected to analyze phytoplankton community diversity and composition. Qualitative samples were obtained using a No. 25 plankton net (mesh size: 0.064 mm) by towing it in an "∞" pattern at a depth of 50 cm for 1–3 min. The collected samples were transferred into 100 mL sample bottles and fixed with 1%–1.5% (v/v) Lugol's solution for microscopic examination. Quantitative phytoplankton samples were collected by obtaining 1 L of surface water in high-density polyethylene bottles and fixing them with 1%–1.5% (v/v) Lugol's solution. After sedimentation for 24 h, the supernatant was removed using a siphon, and the remaining 20–25 mL of concentrated sediment was transferred into 50 mL sample bottles for further microscopic analysis. For cell counting, the sample was thoroughly mixed, and 0.1 mL was placed into a phytoplankton counting chamber. Species identification and cell enumeration were conducted using a microscope (Olympus BX53, Olympus Corporation, Japan). Each sample was counted twice, and if the mean difference between the

TABLE 1 Basic characteristics of cascade reservoir in the upper Yellow River.

Item	LYX	LXW	LiJX	GBX	JSX	LJX
Reservoir area (km^2)	383	13.94	31.58	22	13.6	131
Total storage capacity (10^8 m^3)	247	10.79	16.5	5.5	2.64	57
Dam height(m)	178	250	155	139	100	147
Average depth(m)	64	77.4	51.6	28.2	19.41	26
Average annual runoff (10^8 m^3)	205	208	213.8	226	221	263
Hydraulic residence time(a)	1.2	0.05	0.08	0.02	0.01	0.25
Reservoir regulation type	Annual	Runoff	Runoff	Runoff	Runoff	Annual

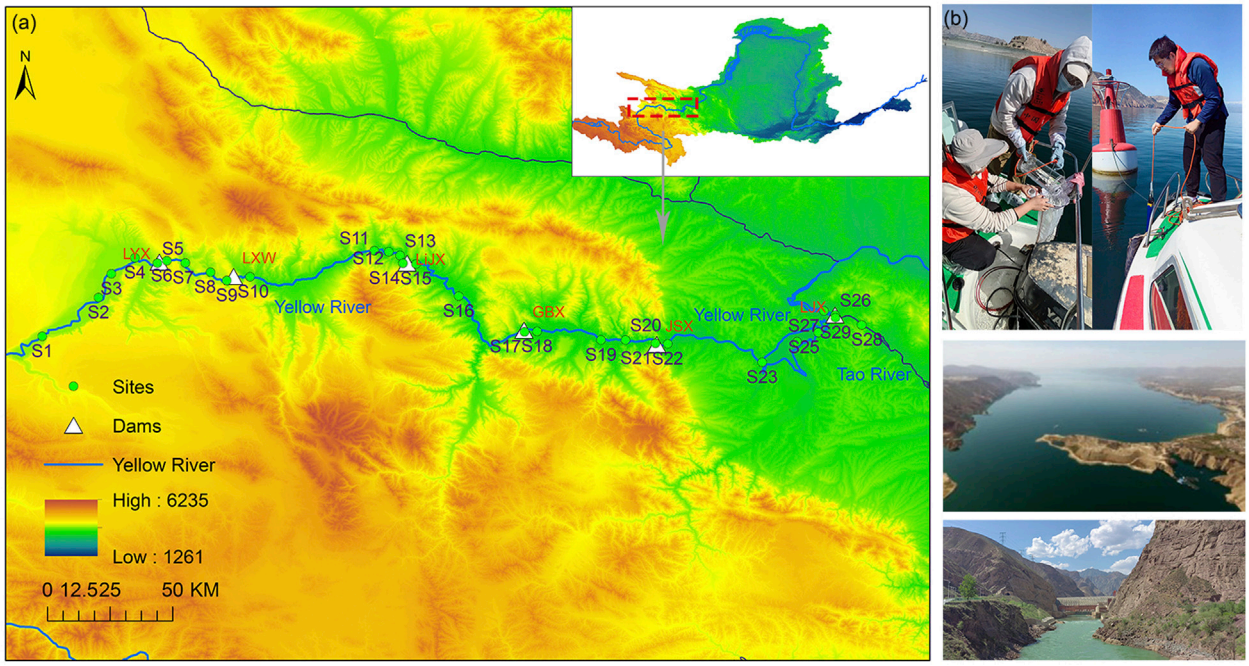

FIGURE 1
Location of cascade reservoirs and sampling sites in the upper Yellow River. **(a)** Study area; **(b)** Photos of field sampling.

two counts was within 15%, the data were considered valid (Zhang et al., 2021). Species identification was based on *Atlas of Common Freshwater Planktonic Algae in China* (Weng and Xu, 2010). Phytoplankton biomass was estimated following the method described by Hillebrand et al. (1999).

2.3 Data statistics and analysis

2.3.1 Types of reservoirs

According to the HRT, reservoirs with an HRT >0.20a are classified as annual regulation hydropower stations, while others are categorized as runoff reservoirs (Yin et al., 2024). LYX and LJX are annual regulation hydropower stations, while LiJX, LXW, GBX, and JSX operate as runoff hydropower stations (Table 1).

$$HRT = V/Q \quad (1)$$

where V is the reservoir capacity (m^3) and Q is the annual runoff volume (m^3).

2.3.2 Biological indices

Alpha diversity analysis: The Shannon-Wiener diversity index (Shannon, 1948) and the Simpson diversity index (Simpson, 1949) were used to analyse the alpha diversity of the phytoplankton. The alpha diversity indices of phytoplankton communities were calculated using the vegan package in R software (version 4.3.2).

Shannon-Wiener diversity index, H':

$$H' = -\sum_{i=1}^{S} P_i \Big/ \ln P_i \quad (2)$$

Simpson diversity index, D:

$$D = 1 - \sum_{i=1}^{S} P_i^2 \quad (3)$$

In the formula, $P_i = N_i/N$, P_i represents the ratio of the number of individuals of species i to the total number of individuals in the sample, N_i denotes the number of individuals of species i, and N represents the total number of individuals in the sample; S represents the total number of species in the sample.

Dominance is an index used to assess the advantageous or disadvantageous status of species within a phytoplankton community. It is determined based on both the occurrence frequency and the individual abundance of each species.

$$Y = (N_i/N) \times f_i \quad (4)$$

Where f_i represents the occurrence frequency of species i across all sampling sites, N_i is the individual count of species i, and N is the total number of individuals in the sample. A species is classified as dominant when $Y > 0.02$ (Lampitt et al., 1993).

2.3.3 Data analysis

This study employed ArcGIS 10.8 for mapping sampling sites. Microsoft Excel 2021 was used for initial data processing. Origin 2023 was utilized for generating chord diagrams, conducting linear regression analysis, and creating corresponding graphs. The NCM, assessed using the Hmisc package, was used to evaluate the relative importance of deterministic and stochastic processes in shaping phytoplankton community structure (Sloan et al., 2006). The NTS package computed the Modified Stochasticity Ratio (MST) to quantitatively assess ecological randomness (Ning et al., 2019). Forward stepwise regression analysis of environmental factors impacting phytoplankton communities was performed using the MASS package (Jiao et al., 2020). To assess the significance of different factors on phytoplankton, Mantel tests were conducted, and the plspm package was employed for partial least squares path modeling (PLS-PM) to explore key driving factors influencing phytoplankton community structure (Liu et al., 2024). Phytoplankton data were transformed using Hellinger transformation during computations, while environmental factors (excluding pH) were log-transformed as log (x+1).

3 Results

3.1 Characteristics of the phytoplankton community composition

A total of 38 species (genera) of phytoplankton were identified across two sampling events, belonging to 7 phyla, 11 classes, 18 orders, and 24 families, with Bacillariophyta, Chlorophyta, and Cyanobacteria being the dominant groups (Figure 2; Table 2). Among them, Bacillariophyta had the highest species richness (14 species), followed by Chlorophyta (13 species) and Cyanophyta (4 species), while Cryptophyta and Chrysophyta had fewer species. The number of phytoplankton species was slightly lower during the dry season (28 species) compared to the wet season (32 species). Annual regulation hydropower station (LJX and LYX), the species richness of phytoplankton was higher compared to other reservoirs. The sequence of phytoplankton richness was LJX > LYX > LiJX > JSX > LXW > GBX.

The chord diagram (Figure 3) illustrates that Bacillariophyta, Chlorophyta, and Cyanobacteria dominate the phytoplankton in the upper Yellow River reservoirs, accounting for over 85% of the total abundance. The seasonal variation in phytoplankton community structure in these reservoirs is pronounced and varies with different HRT levels. Specifically, from the dry to the wet season, Bacillariophyta's relative abundance decreases significantly, while Cyanobacteria and Chlorophyta increase substantially. As HRT increases, especially during the wet season, Bacillariophyta's relative abundance shows a clear downward trend, while Cyanobacteria and Chlorophyta show an upward trend. Particularly in the two reservoirs with longer hydraulic residence times (LJX and LYX), during the wet season, Bacillariophyta's relative abundance decreased by 70.01% and 77.62%, respectively, while Cyanobacteria in LJX and Chlorophyta in LYX increased by 2.16 and 4.31 times, respectively (Figure 3).

3.2 The relationship between phytoplankton community and HRT

The relationship between phytoplankton communities and HRT in six cascade reservoirs in the upper Yellow River is highlighted in the findings (Figure 4). It is evident that HRT significantly influences the structure of phytoplankton communities. Both during the dry and wet seasons, phytoplankton abundance, Chl-a concentration, Shannon-Wiener index, and Simpson index increase with longer HRT. Except for the Simpson index, this increasing trend shows consistent seasonal differences, with a higher rate of increase observed during the wet season compared to the dry season. This difference is particularly notable in phytoplankton abundance. Furthermore, the results indicate that HRT does not alter the characteristic where phytoplankton community structure, Chl-a concentration, and diversity indices are consistently higher during the wet season compared to the dry season in these reservoirs.

3.3 Phytoplankton community assembly

Based on the aforementioned results, it is evident that the richness and diversity of phytoplankton communities in the two annual regulation hydropower station with longer hydraulic residence times (LJX and LYX) are significantly higher compared to the runoff hydropower station. Therefore, this study utilized the NCM and MST to quantitatively the relative importance of deterministic and stochastic processes in the assembly of phytoplankton communities in these two types of reservoirs. The average Modified Stochasticity Ratio is 36.41% in annual regulation hydropower station and 45.18% in runoff hydropower station (Figure 5), both of which are below the 50% threshold. This indicates that deterministic processes predominantly govern phytoplankton community assembly in the upper Yellow River reservoirs. Moreover, as HRT increases, the influence of deterministic processes on phytoplankton community assembly also intensifies. In line with these findings, the study employed

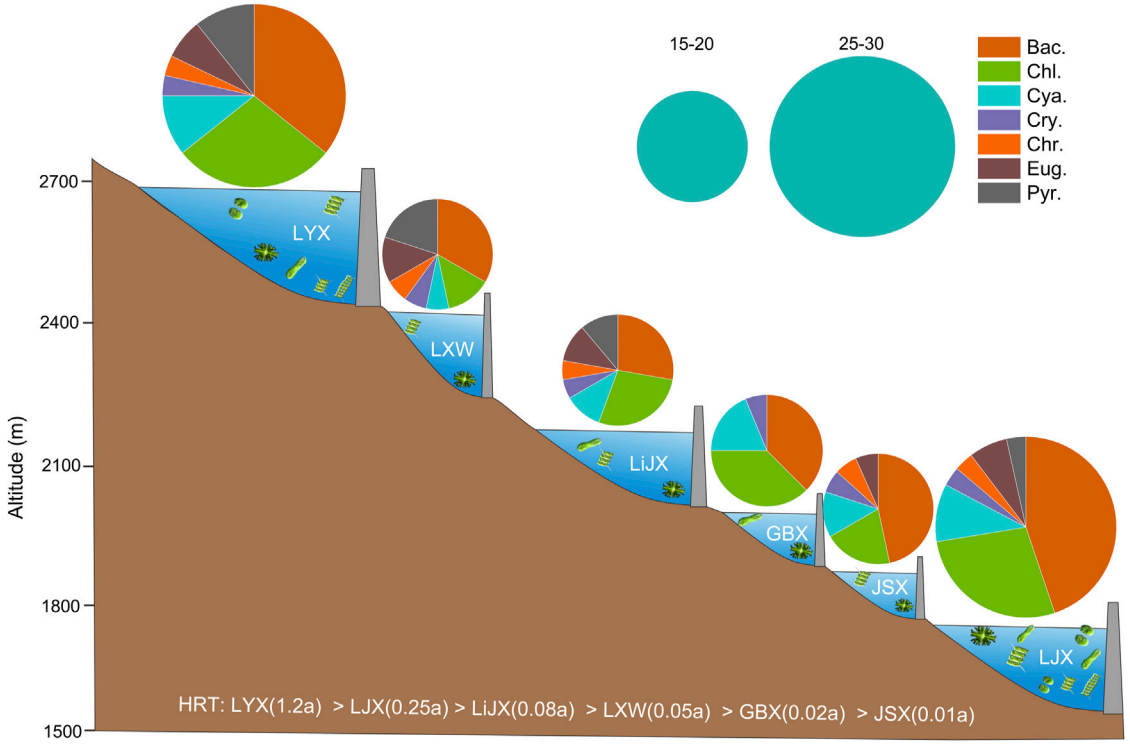

FIGURE 2
Illustrates the distribution of phytoplankton species in the upper Yellow River. The size of the circles represents the number of species, while the pie charts indicate the proportion of each species. Bac: Bacillariophyta; Chl, Chlorothyta; Cya, Cyanobacteria; Cry, Cryptophyta; Chr, Chrysophyta; Eug, Euglenophyta; Pyr, Pyrrothyta.

TABLE 2 Dominant species and dominance of phytoplankton in the cascade reservoirs of the upper Yellow River.

Phylum	Species	Dominance	
		Dry season	Wet season
Bacillariophyta	*Cyclotella* spp.	0.05	0.10
	Fragilaria spp.	0.06	
	Synedra spp.	0.08	0.15
	Navicula spp.	0.07	
	Asterionella sp	0.12	0.36
Chlorothyta	*Scendesmus* sp		0.12
	Cosmarium spp.		0.06
	Chlorella spp.	0.14	0.23
	Pectodictyon spp.		0.03
Cyanobacteria	*Microcystis* spp.		0.11
	Planktothrix sp	0.11	0.23

the NCM to corroborate the MST model results. The migration rate (m) in the NCM reflects the dispersal ability of species. As depicted in the NCM results (Figure 5), the migration rates (m) in annual regulation hydropower station and runoff hydropower station are 0.0010 and 0.0120, respectively, highlighting minimal migration rates for phytoplankton. This suggests that stochastic processes associated with migration and dispersal make negligible contributions to phytoplankton community assembly. Furthermore, the Neutral Community Model explains 20.1% and 46.3% of phytoplankton community variability in annual regulation hydropower station and runoff hydropower station, respectively. This underscores that with increasing HRT, deterministic processes exert a more pronounced influence on phytoplankton community assembly, consistent with the analysis of MST.

3.4 The relationship between phytoplankton and environmental factors

The Mantel test was employed to analyze the significant correlations between phytoplankton communities and environmental factors in different types of reservoirs (Figures 6a, b). In annual regulation hydropower station, the phytoplankton community structure showed a highly significant correlation with WT, TN, COD, and pH (Supplementary Table S3, $P < 0.001$), and a significant correlation with NO_3^--N, EC, salt, and HRT ($P < 0.05$). In runoff hydropower station, changes in the phytoplankton community structure were highly significantly correlated with WT and salt ($P < 0.001$), and significantly correlated with NO_3^--N, COD, DO, and HRT ($P < 0.05$). Employing stepwise multiple regression analysis, this study discerned that phytoplankton abundance within the cascade reservoirs of the upper Yellow

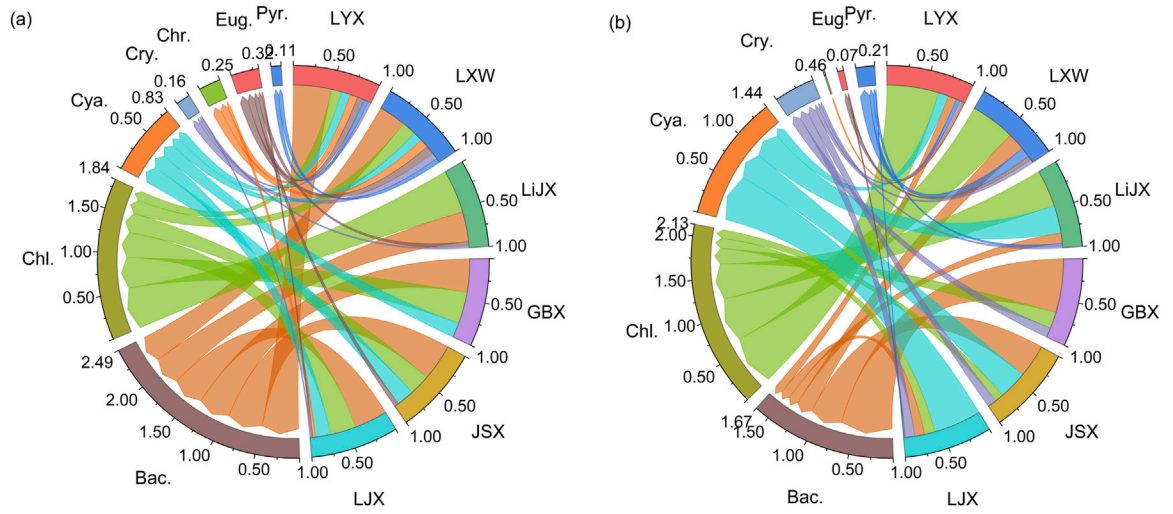

FIGURE 3
Differences in phytoplankton community abundance in the upper Yellow River. **(a)** Dry season **(b)** Wet season. Bac, Bacillariophyta; Chl, Chlorothyta; Cya, Cyanobacteria; Cry, Cryptophyta; Chr, Chrysophyta; Eug: Euglenophyta; Pyr, Pyrrothyta.

River is significantly swayed by HRT, WT and TN than by other environmental factors (Abundance = 2.8919 × TN + 1.2504 × WT + 0.1614 × HRT, R^2 = 0.6121, 3.52 × 10^{-11}). Specifically, as HRT, WT and TN increase, the abundance of phytoplankton significantly rises.

Based on the results of the Mantel test and multiple regression analysis, WT and nutrients are key factors influencing the structure of phytoplankton. Consequently, we established a partial least squares path model (PLS-PM) that includes phytoplankton abundance, zooplankton biomass, and environmental factors to analyze the effects of upstream influences (environmental factors) and downstream influences (zooplankton predation) on phytoplankton abundance (Figure 6). In both annual regulation hydropower station or runoff hydropower station, phytoplankton abundance is significantly positively correlated with water temperature, with this influence being stronger in runoff hydropower station. Additionally, zooplankton and nutrients are positively correlated with phytoplankton abundance. In runoff hydropower station, the predation effect of zooplankton on phytoplankton abundance is more pronounced. However, compared to annual regulation hydropower station, the upstream effect of nutrients on phytoplankton abundance is less significant in runoff hydropower station. Further analysis indicates that under two different HRT conditions, the roles of physicochemical parameters on phytoplankton show significant differences. In annual regulation hydropower station, these parameters exhibit a strong positive influence, whereas in runoff hydropower station, they show a weaker negative influence.

4 Discussion

4.1 The impact of HRT on phytoplankton communities in cascade reservoirs

HRT is one of the key hydrological characteristics of reservoirs and has been shown to play a significant role in shaping phytoplankton communities (Ruan et al., 2024; Yin et al., 2024). This study demonstrates that there are significant differences in the phytoplankton community structures in the cascade reservoirs of the upper Yellow River, with reservoirs having longer HRT exhibiting higher species richness and abundance. The mechanisms underlying this relationship can be attributed to several factors. Firstly, reservoirs with longer HRT have larger water surface areas and greater light penetration, creating favorable conditions for phytoplankton photosynthesis. Secondly, extended HRT increases the interaction time between phytoplankton and available nutrients, thereby enhancing primary productivity and nutrient cycling within the reservoir (Chen et al., 2020; Znachor et al., 2020; Zhao et al., 2024). Thirdly, prolonged HRT promotes nutrient deposition, facilitating nutrient retention in reservoirs and lakes (Maavara et al., 2020; Wu et al., 2022). Notably, when HRT exceeds 5.3 days, the nutrient retention capacity of reservoirs significantly increases (Zhao et al., 2024), further supporting phytoplankton growth. In this study, except for the JSX reservoir, all other reservoirs had HRT exceeding 5.3 days. Among them, the annual regulation reservoirs, LJX and LYX, exhibited exceptionally long HRTs of 80 days and 440 days, respectively—substantially higher than the critical threshold identified by Zhao et al. (2024). The prolonged water retention in these reservoirs allows for greater nutrient accumulation, providing ample resources for phytoplankton development and reproduction. This may explain the higher species richness observed in LYX and LJX compared to other reservoirs.

Beyond its direct impact on nutrient retention, HRT also indirectly shapes phytoplankton community dynamics by influencing water quality. This study found a significant positive correlation between HRT and phytoplankton community structure (Figure 4), as well as with TN, NO_3^--N, salt, TSS, and ORP (Figure 6). This suggests that HRT indirectly affects phytoplankton nutrient uptake by regulating complex physical, chemical, and biological processes. Longer HRT enhances the

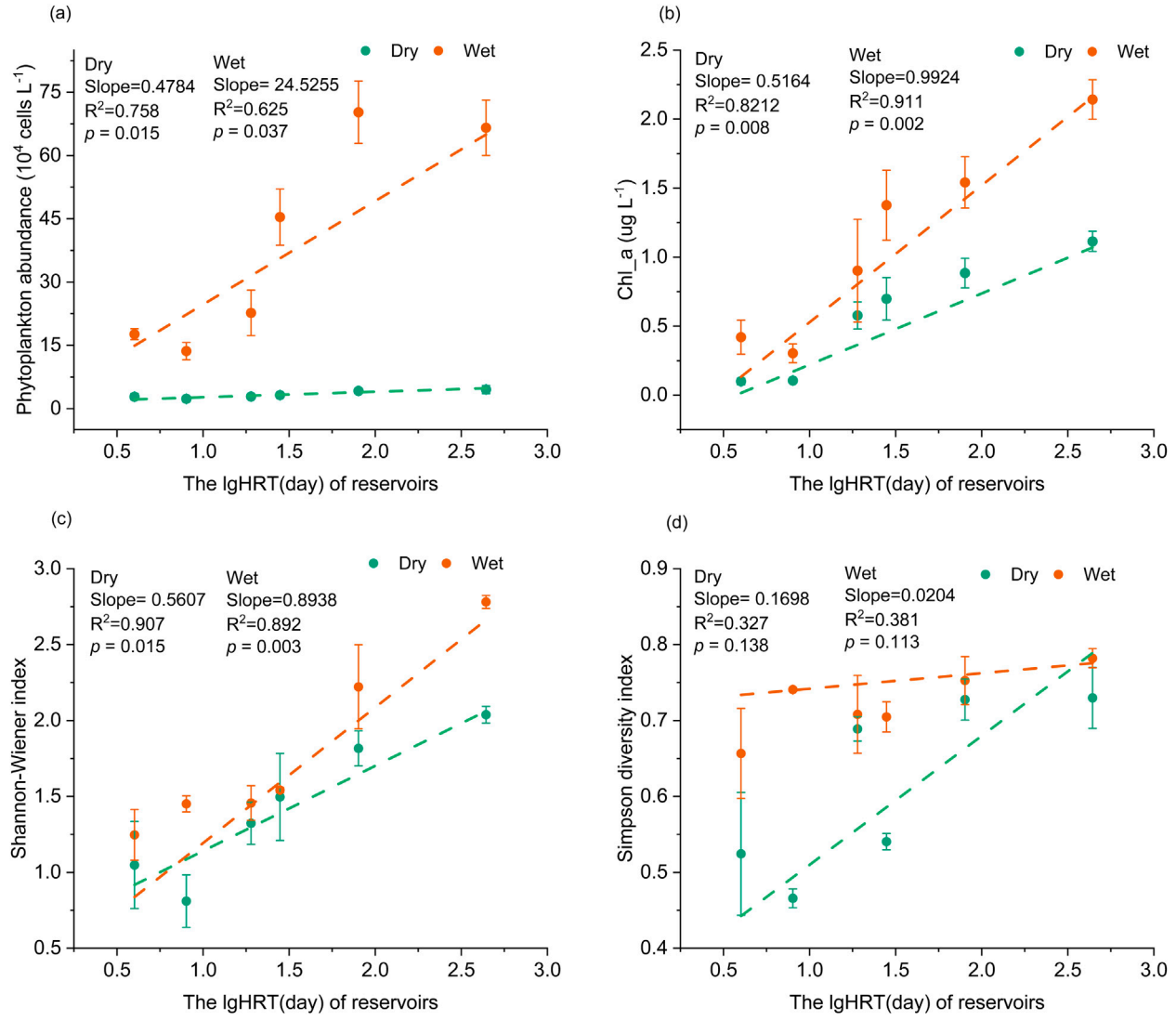

FIGURE 4
The impact of HRT on the phytoplankton community in the upper Yellow River. **(a)** The relationship between HRT and phytoplankton abundance; **(b)** The relationship between HRT and chlorophyll a (Chl-a) concentration **(c–d)** The relationship between HRT and Shannon and Simpson diversity index.

retention of nutrients and particulates (Zhao et al., 2024), improves water transparency, prolongs the interaction time between phytoplankton and nutrients, and strengthens internal nutrient cycling. Furthermore, extended HRT increases the interaction time between phytoplankton and key environmental factors such as nutrient availability and water temperature, thereby influencing their growth patterns and competitive relationships (Yin et al., 2024). Generally, longer HRT is associated with higher phytoplankton abundance and biomass, leading to significant shifts in community structure (Li et al., 2013; Znachor et al., 2020; Liu et al., 2021). These combined factors enable phytoplankton to proliferate rapidly during wet seasons, increasing the risk of eutrophication in reservoirs. Therefore, optimizing reservoir operation to reduce HRT and enhance water exchange can effectively curb excessive algal growth, while releasing ecological flows and flood pulses to lower HRT can increase downstream flow velocity, disrupting algal aggregation and inhibiting their growth. Based on these findings, proper HRT management could be a crucial strategy for controlling phytoplankton overgrowth and maintaining water quality in reservoir ecosystems.

4.2 Environmental drivers of phytoplankton communities in cascade reservoirs

The Long–Liu section is located at the edge of the Qinghai-Tibet Plateau and represents a typical plateau alpine river. Due to the influence of high altitude, this region experiences persistently low temperatures, which significantly inhibit phytoplankton growth, resulting in a strong correlation between altitude and species richness (Ding et al., 2021; Song et al., 2020). Studies have shown that the community characteristics in this area are similar to those of other cold alpine rivers and reservoirs, with diatoms as the dominant

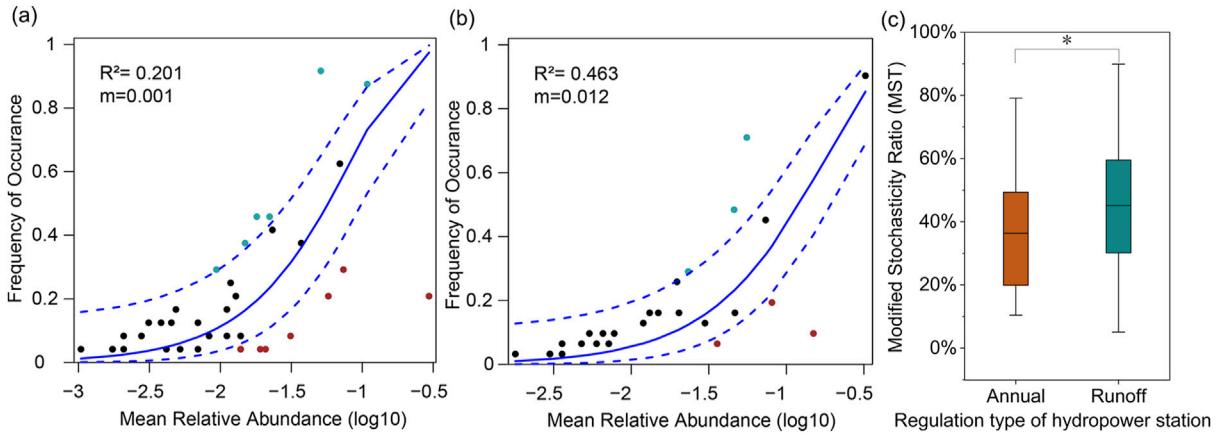

FIGURE 5
Illustrates the Neutral Community Model of phytoplankton communities in the Long-Liu section of the upper Yellow River cascade reservoirs. Species with frequencies higher than the model-predicted values are depicted in green, those with lower frequencies in red, and species falling within the predicted range in black. The solid blue line represents the optimal fit of the Neutral Community Model, while the dashed blue lines indicate the model's 95% confidence intervals. R^2 indicates the overall goodness of fit of the Neutral Community Model, and m denotes the migration rate of phytoplankton communities. **(a)** Annual regulation hydropower station; **(b)** Runoff hydropower station; **(c)** MST for annual regulation hydropower station and runoff hydropower station.

group (Liu et al., 2021). The phytoplankton community composition is relatively simple, with low species richness. A total of 38 species were identified, which is significantly lower than those found in downstream river channels and reservoirs at lower altitudes with higher water temperatures (Song et al., 2020; Ding et al., 2021). During the dry season, diatoms were the dominant group, reflecting their adaptation to low-temperature environments (Liu et al., 2021), with *Cyclotella* spp., *Fragilaria* spp., *Synedra* spp., *Navicula* spp., and *Asterionella* sp. as the dominant species. In the wet season, the dominant species shifted to *Scendesmus* sp., *Cosmarium* spp., *Chlorella* spp., and *Pectodictyon* spp. from the Chlorophyta, as well as *Microcystis* spp. and *Chlorella* spp. from the Cyanophyta. Compared to Bacillariophyta, Chlorothyta and Cyanobacteria are more adapted to high-temperature environments (Chen, 2015; Baker and Geider, 2021). During the wet season, the highest recorded water temperature reached 19.35°C, significantly higher than in the dry season (Supplementary Table S1, S2). This temperature increase created favorable conditions for the proliferation of cyanobacteria and green algae, accelerating their growth and enhancing their competitive advantage over other phytoplankton groups. Consequently, the species richness, abundance, and dominance of cyanobacteria and green algae were significantly higher in the wet season than in the dry season.

The stepwise multiple regression analysis showed that as WT, TN, and HRT increased, the abundance of phytoplankton significantly increased. WT not only directly influences the growth, metabolism, and life cycle of phytoplankton but also indirectly affects their development and reproduction by regulating nutrient decomposition (Ruan et al., 2024). The PLS-PM results further confirmed a stable and significant positive correlation between phytoplankton abundance and WT. However, in annually regulated hydropower stations (LYX and LJX), the influence of WT on phytoplankton communities was weaker compared to runoff-type hydropower stations (LXW, LiJX, GBX, and JSX). This may be attributed to the longer HRT and larger water surface areas of LYX and LJX, which enhance light-heat exchange and result in relatively higher water temperatures. Consequently, the water temperatures in Longyangxia and Liujiaxia reservoirs were notably higher than in other reservoirs, creating more favorable conditions for phytoplankton growth. Additionally, elevated WT may accelerate nutrient mineralization, increasing the availability of essential nutrients for phytoplankton uptake (Zhang et al., 2024), leading to significantly higher algal density and biomass in Longyangxia and Liujiaxia reservoirs compared to other reservoirs. As the largest annually regulated reservoir in the upper Yellow River, the outflow from Longyangxia Reservoir has substantially altered the interannual variation in downstream water temperatures (Ren et al., 2020). Meanwhile, the cumulative effects of cascade reservoirs have exacerbated the negative impacts of temperature fluctuations on phytoplankton survival and reproduction (Liu et al., 2021). Therefore, optimizing reservoir operation strategies to minimize WT fluctuations and mitigate their adverse effects on downstream aquatic ecosystems is crucial for maintaining ecological balance.

Nitrogen is an essential nutrient for phytoplankton growth and a key environmental factor influencing phytoplankton community structure (Reynolds et al., 2006). In the cascade reservoirs of the upper Yellow River, phytoplankton communities exhibit a significant positive correlation with total nitrogen (TN) concentration, likely because higher TN levels promote the proliferation of diatoms and green algae. These groups have high nutrient utilization efficiency, allowing them to gain a competitive advantage in resource competition, dominate ecological niches, and suppress the growth of other algae (Zhang et al., 2024; Ruan et al., 2024). TN is significantly correlated with NO_3^--N, NH_4^+-N, COD, ORP, TSS, pH, WT, and HRT. These environmental factors regulate TN transformation through physical and chemical processes such as sedimentation, nitrification, and denitrification, directly or indirectly altering its bioavailability and influencing phytoplankton nitrogen uptake efficiency (Reynolds et al., 2006).

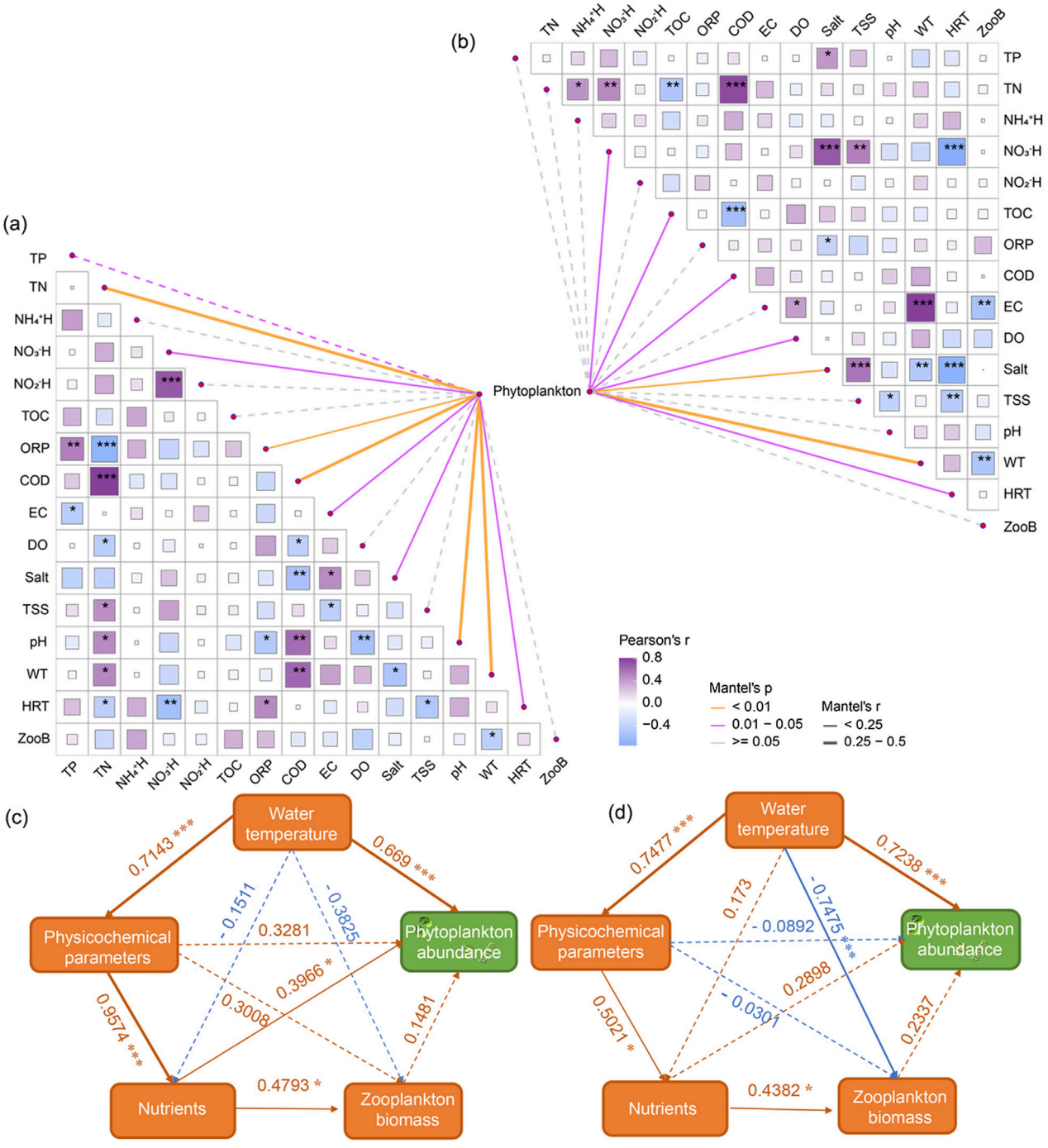

FIGURE 6
Analysis of the correlation between the phytoplankton community and environmental factors. **(a)** The relationship between phytoplankton and environmental factors in annual regulation hydropower station; **(b)** The relationship between phytoplankton and environmental factors in runoff hydropower stations; **(c)** Partial Least Squares Path Modeling (PLS-PM) analysis results for annual regulation hydropower station; **(d)** PLS-PM analysis results for runoff hydropower stations. Parameters included: WT, phytoplankton abundance, zooplankton biomass, nutrient parameters, and physicochemical parameters. Nutrient parameters included: TN, NO_2^--N, NO_3^--N, NH_4^+-N, TP and TOC. Physicochemical parameters included: pH, ORP, DO, EC, Salt, TSS, and COD. Solid lines in **(a, b)** indicate significant correlations ($P < 0.05$), while dashed lines indicate non-significant correlations ($P > 0.05$).

Consequently, this affects their growth and reproduction. Given that phytoplankton are a fundamental resource in the food web, their unhealthy growth may ultimately disrupt the structure and function of the entire ecosystem. Therefore, it is crucial to appropriately adjust hydraulic residence time and adequately regulate nutrient loads and water temperature to ensure the healthy growth of aquatic organisms in reservoirs and downstream rivers.

4.3 The importance of HRT in the construction of phytoplankton communities

The NCM, grounded in neutral theory, is used to infer the roles of stochastic and deterministic processes in community assembly. It has been widely applied in microbial community studies (Dini-Andreote et al., 2015; Yang et al., 2023). In recent years, NCM has also been employed in phytoplankton community research (Liu et al., 2024; Zhang et al., 2024). However, whether the assembly of phytoplankton communities in cascade reservoirs of alpine rivers is primarily driven by deterministic or stochastic processes remains unclear (Yang et al., 2023; Sun et al., 2023). The results of this study indicate that deterministic processes dominate the assembly of phytoplankton communities in the upper Yellow River cascade reservoirs (Figure 5), with a particularly strong influence observed in annually regulated hydropower stations.

Specifically, the results of the NCM show that the explanatory power of the model (R^2 = 0.463) and migration rate (m = 0.012) for phytoplankton communities in runoff hydropower stations are higher than those in annually regulated hydropower stations (R^2 = 0.201, m = 0.0010). Additionally, the MST for phytoplankton in runoff hydropower station is 45.18%, higher than the 36.41% observed in annually regulated hydropower stations. These findings suggest that phytoplankton community assembly in annually regulated hydropower stations is more influenced by deterministic processes compared to runoff hydropower stations. This conclusion aligns with previous research in stepped reservoirs in plains, where phytoplankton community assembly is also primarily shaped by deterministic processes (Isabwe et al., 2022).

The differences in phytoplankton community assembly between annually regulated and runoff-type hydropower stations may be attributed to their respective hydrological characteristics. Runoff-type hydropower stations have a higher water exchange frequency and shorter hydraulic residence time, which enhance connectivity between reservoirs and reduce isolation effects. These hydrological conditions favor increased migration and dispersal of phytoplankton (Liu et al., 2024; Isabwe et al., 2022), potentially explaining why deterministic processes play a lesser role in runoff hydropower stations and a more prominent role in annually regulated hydropower stations.

Similarly, in large lakes with good connectivity, such as Dongting Lake, stochastic processes dominate phytoplankton community assembly (Wu et al., 2022). In contrast, the spatial isolation and limited connectivity of the annually regulated hydropower station at the head and tail of the study area make phytoplankton dispersal more challenging (Zhang et al., 2024). In single-stage reservoirs, the assembly of phytoplankton communities is also dominated by stochastic processes (Liu et al., 2024). The large storage capacity and weak hydrodynamic conditions of annual regulation hydropower stations (Zhao et al., 2024) reduce the ability of phytoplankton to migrate and disperse with water flow. Furthermore, the longer water exchange period and hydraulic residence time increase the interaction time between phytoplankton and environmental factors, thereby strengthening the influence of deterministic processes. While stochastic processes may dominate in lakes (such as Lake Dongting) (Wu et al., 2021) or single-stage reservoirs (Liu et al., 2024), in the upper Yellow River, phytoplankton community assembly is mainly governed by deterministic processes, particularly in annual regulation hydropower stations, where deterministic processes have a greater impact on community assembly than in runoff hydropower stations.

5 Conclusion

This study systematically investigates the spatial distribution patterns and community assembly types of phytoplankton communities in reservoirs with varying HRT. Significant seasonal differences in phytoplankton composition were observed, with these variations differing under different HRT levels. Notably, the richness and diversity of phytoplankton communities in annual regulation hydropower station were much higher than in runoff hydropower stations. From the dry season to the wet season, the relative abundance of diatoms significantly decreased, while the relative abundance of cyanobacteria and green algae greatly increased. In the wet season, the dominant species shifted to *Scendesmus* sp., *Cosmarium* spp., *Chlorella* spp., and *Pectodictyon* spp. from the Chlorophyta, as well as *Microcystis* spp. and *Chlorella* spp. from the Cyanophyta. The neutral community model results indicate that phytoplankton community assembly in upstream cascade reservoirs is primarily governed by deterministic processes. Furthermore, as HRT increases, the influence of these deterministic processes becomes more pronounced, suggesting that in annually regulated hydropower stations, deterministic processes play a more dominant role in community assembly compared to runoff hydropower stations. Stepwise multiple regression analysis further reveals that HRT, WT, and TN are the primary environmental factors driving variations in phytoplankton community structure. Phytoplankton abundance is significantly positively correlated with water temperature, particularly in runoff hydropower stations, where its influence is more pronounced. This study reveals the structure, aggregation characteristics, and influencing factors of phytoplankton communities in the upstream cascade reservoirs of the Yellow River under different HRT conditions, thereby deepening our understanding of the assembly processes of river phytoplankton communities.

Data availability statement

The original contributions presented in the study are included in the article/Supplementary Material, further inquiries can be directed to the corresponding author.

Author contributions

QL: Conceptualization, Data curation, Methodology, Software, Visualization, Writing – original draft. LZ: Investigation, Methodology, Validation, Writing – review and editing. DL: Validation, Writing – review and editing. ZZ: Investigation, Writing – review and editing. KC: Investigation, Writing – review and editing. JW: Investigation, Writing – review and editing. YY: Conceptualization,

Methodology, Funding acquisition, Investigation, Project administration, Writing – review and editing.

Funding

The author(s) declare that financial support was received for the research and/or publication of this article. This research was supported by the Joint Funds of the National Natural Science Foundation of China (U2243236), the Innovative Research Group of the National Natural Science Foundation of China (52221003), and National Science Fund for Distinguished Young Scholars (52025092).

Conflict of interest

The authors declare that the research was conducted in the absence of any commercial or financial relationships that could be construed as a potential conflict of interest.

Generative AI statement

The author(s) declare that no Generative AI was used in the creation of this manuscript.

Publisher's note

Supplementary material

The Supplementary Material for this article can be found online at: https://www.frontiersin.org/articles/10.3389/fenvs.2025.1551988/full#supplementary-material

References

Baker, K., and Geider, R. (2021). Phytoplankton mortality in a changing thermal seascape. *Glob. Change Biol.* 27 (20), 5253–5261. doi:10.1111/gcb.15772

Belletti, B., Garcia de Leaniz, C., Jones, J., Bizzi, S., Börger, L., Segura, G., et al. (2020). More than one million barriers fragment Europe's rivers. *Nature* 588 (7838), 436–441. doi:10.1038/s41586-020-3005-2

Chen, B. (2015). Patterns of thermal limits of phytoplankton. *J. Plankton Res.* 37 (2), 285–292. doi:10.1093/plankt/fbv009

Chen, Q., Shi, W., Huisman, J., Maberly, S. C., Zhang, J., Yu, J., et al. (2020). Hydropower reservoirs on the upper Mekong River modify nutrient bioavailability downstream. *Natl. Sci. Rev.* 7, 1449–1457. doi:10.1093/nsr/nwaa026

Datry, T., Boulton, A., Fritz, K., Stubbington, R., Cid, N., Crabot, J., et al. (2023). Non-perennial segments in river networks. *Nat. Rev. Earth and Environ.* 4 (12), 815–830. doi:10.1038/s43017-023-00495-w

Ding, Y., Pan, B., Zhao, G., Sun, C., Han, X., and Li, M. (2021). Geo-climatic factors weaken the effectiveness of phytoplankton diversity as a water quality indicator in a large sediment-laden river. *Sci. Total Environ.* 792, 148346. doi:10.1016/j.scitotenv.2021.148346

Dini-Andreote, F., Stegen, J. C., Van Elsas, J. D., and Salles, J. F. (2015). Disentangling mechanisms that mediate the balance between stochastic and deterministic processes in microbial succession. *Proc. Natl. Acad. Sci.* 112 (11), E1326–E1332. doi:10.1073/pnas.1414261112

Grill, G., Lehner, B., Thieme, M., Geenen, B., Tickner, D., Antonelli, F., et al. (2019). Mapping the world's free-flowing rivers. *Nature* 569 (7755), 215–221. doi:10.1038/s41586-019-1111-9

He, F., Zarfl, C., Tockner, K., Olden, J. D., Campos, Z., Muniz, F., et al. (2024). Hydropower impacts on riverine biodiversity. *Nat. Rev. Earth and Environ.* 5, 755–772. doi:10.1038/s43017-024-00596-0

Hillebrand, H., Dürselen, C. D., Kirschtel, D., Pollingher, U., and Zohary, T. (1999). Biovolume calculation for pelagic and benthic microalgae. *J. Phycol.* 35 (2), 403–424. doi:10.1046/j.1529-8817.1999.3520403.x

ICOLD, (2023). World Register of Dams: General Synthesis. Available online at: https://www.icold-cigb.org/GB/world_register/general_synthesis.asp (December, 2023)

Isabwe, A., Yang, J., Wang, Y., Wilkinson, D., Graham, E., Chen, H., et al. (2022). Riverine bacterioplankton and phytoplankton assembly along an environmental gradient induced by urbanization. *Limnol. Oceanogr.* 67 (9), 1943–1958. doi:10.1002/lno.12179

Jia, Y., Kennard, M. J., Liu, Y., Sui, X., Li, K., Wang, G., et al. (2020). Human disturbance and long-term changes in fish taxonomic, functional and phylogenetic diversity in the Yellow River, China. *Hydrobiologia* 847 (18), 3711–3725. doi:10.1007/s10750-020-04244-8

Jiao, S., Yang, Y., Xu, Y., Zhang, J., and Lu, Y. (2020). Balance between community assembly processes mediates species coexistence in agricultural soil microbiomes across eastern China. *ISME J.* 14 (1), 202–216. doi:10.1038/s41396-019-0522-9

Lampitt, R. S., Wishner, K. F., Turley, C. M., and Angel, M. V. (1993). Marine snow studies in the Northeast Atlantic Ocean: distribution, composition and role as a food source for migrating plankton. *Mar. Biol.* 116 (4), 689–702. doi:10.1007/BF00355486

Li, J., Dong, S., Liu, S., Yang, Z., Peng, M., and Zhao, C. (2013). Effects of cascading hydropower dams on the composition, biomass and biological integrity of phytoplankton assemblages in the middle Lancang-Mekong River. *Ecol. Eng.* 60, 316–324. doi:10.1016/j.ecoleng.2013.07.029

Li, X., Chen, Z., Fan, X., and Cheng, Z. (2018). Hydropower development situation and prospects in China. *Renew. Sustain. Energy Rev.* 82, 232–239. doi:10.1016/j.rser.2017.08.090

Liu, X., Song, Y., Ni, T., Yang, Y., Ma, B., Huang, T., et al. (2024). Ecological evolution of algae in connected reservoirs under the influence of water transfer: algal density, community structure, and assembly processes. *Sci. Total Environ.* 915, 170086. doi:10.1016/j.scitotenv.2024.170086

Liu, Y., Li, C., Jian, S., Miao, S., Li, K., Guan, H., et al. (2021). Hydrodynamics regulate longitudinal plankton community structure in an alpine cascade reservoir system. *Front. Microbiol.* 12, 749888. doi:10.3389/fmicb.2021.749888

Maavara, T., Chen, Q., Van Meter, K., Brown, L., Zhang, J., Ni, J., et al. (2020). River dam impacts on biogeochemical cycling. *Nat. Rev. Earth and Environ.* 1 (2), 103–116. doi:10.1038/s43017-019-0019-0

Mor, J. R., Ruhí, A., Tornés, E., Valcárcel, H., Muñoz, I., and Sabater, S. (2018). Dam regulation and riverine food-web structure in a Mediterranean river. *Sci. Total Environ.* 625, 301–310. doi:10.1016/j.scitotenv.2017.12.296

Ning, D., Deng, Y., Tiedje, J., and Zhou, J. (2019). A general framework for quantitatively assessing ecological stochasticity. *Proc. Natl. Acad. Sci.* 116 (34), 16892–16898. doi:10.1073/pnas.1904623116

Ren, L., Song, C., Wu, W., Guo, M., and Zhou, X. (2020). Reservoir effects on the variations of the water temperature in the upper Yellow River, China, using principal component analysis. *J. Environ. Manag.* 262, 110339. doi:10.1016/j.jenvman.2020.110339

Reynolds, C. S. (2006). The ecology of phytoplankton. *Camb. Univ. Press*. doi:10.1017/CBO9780511542145

Ruan, Q., Liu, H., Dai, Z., Wang, F., and Cao, W. (2024). Damming exacerbates the discontinuities of phytoplankton in a subtropical river in China. *J. Environ. Manag.* 351, 119832. doi:10.1016/j.jenvman.2023.119832

Salmaso, N., and Tolotti, M. (2021). Phytoplankton and anthropogenic changes in pelagic environments. *Hydrobiologia* 848 (1), 251–284. doi:10.1007/s10750-020-04323-w

SEPA (2002). *Environmental quality standard for surface water (GB3838-2002) state environmental protection administration of China, Beijing of regula (in Chinese)*. Beijing: China Environmental Science Press, 1–10.

Shannon, C. E., and Tolotti, M. (1948). A mathematical theory of communication. *Bell Syst. Tech. J.* 27 (3), 379–423. doi:10.1002/j.1538-7305.1948.tb01338.x

Shen, Y., Zhang, Y., Zhou, X., Li, Q., Zhang, J., Cheng, R., et al. (2024). Environmental DNA metabarcoding revealing the distinct responses of phytoplankton and zooplankton to cascade dams along a river-way. *Ecol. Indic.* 166, 112545. doi:10.1016/j.ecolind.2024.112545

Simpson, E. H. (1949). Measurement of diversity. *Nature*, 163 (4148), 688–688. doi:10.1038/163688a0

Sloan, W., Lunn, M., Woodcock, S., Head, I., Nee, S., and Curtis, T. (2006). Quantifying the roles of immigration and chance in shaping prokaryote community structure. *Environ. Microbiol.* 8 (4), 732–740. doi:10.1111/j.1462-2920.2005.00956.x

Song, J., Hou, C., Liu, Q., Wu, X., Wang, Y., and Yi, Y. (2020). Spatial and temporal variations in the plankton community because of water and sediment regulation in the lower reaches of Yellow River. *J. Clean. Prod.* 261, 120972. doi:10.1016/j.jclepro.2020.120972

Sun, Y., Li, H., Wang, X., Jin, Y., Nagai, S., and Lin, S. (2023). Phytoplankton and microzooplankton community structure and assembly mechanisms in northwestern pacific ocean estuaries with environmental heterogeneity and geographic segregation. *Microbiol. Spectr.* 11 (2), e0492622–22. doi:10.1128/spectrum.04926-22

Wang, J., Wu, W., Zhou, X., and Li, J. (2023). Carbon dioxide (CO_2) partial pressure and emission from the river-reservoir system in the upper Yellow River, northwest China. *Environ. Sci. Pollut. Res.* 30 (7), 19410–19426. doi:10.1007/s11356-022-23489-5

Wang, X., Chen, Y., Yuan, Q., Xing, X., Hu, B., Gan, J., et al. (2022). Effect of river damming on nutrient transport and transformation and its countermeasures. *Front. Mar. Sci.* 9, 1078216. doi:10.3389/fmars.2022.1078216

Weng, J., and Xu, H. (2010). *Atlas of Common freshwater planktonic algae in China*. Shanghai, China: Shanghai Scientific and Technical Publishers. (in Chinese).

Wu, N., Liu, S. M., Zhang, G. L., and Zhang, H. M. (2021). Anthropogenic impacts on nutrient variability in the lower Yellow River. *Sci. Total Environ.* 755, 142488. doi:10.1016/j.scitotenv.2020.142488

Wu, Z., Li, J., Sun, Y., Peñuelas, J., Huang, J., Sardans, J., et al. (2022). Imbalance of global nutrient cycles exacerbated by the greater retention of phosphorus over nitrogen in lakes. *Nat. Geosci.* 15 (6), 464–468. doi:10.1038/s41561-022-00958-7

Xiao, Z., Li, H., Li, X. C., Li, R. H., Huo, S. L., Yu, G. L., et al. (2022). Geographic pattern of phytoplankton community and their drivers in lakes of middle and lower reaches of Yangtze River floodplain, China. *Environ. Sci. Pollut. Res.* 29 (55), 83993–84005. doi:10.1007/s11356-022-21657-1

Xu, M., Wang, G., Wang, Z., Hu, H., Singh, D. K., and Tian, S. (2022). Temporal and spatial hydrological variations of the Yellow River in the past 60 years. *J. Hydrology* 609, 127750. doi:10.1016/j.jhydrol.2022.127750

Xu, S., Li, S. L., Bufe, A., Klaus, M., Zhong, J., Wen, H., et al. (2024). Escalating carbon export from high-elevation rivers in a warming climate. *Environ. Sci. and Technol.* 58 (16), 7032–7044. doi:10.1021/acs.est.3c06777

Yang, Q., Zhang, P., Li, X., Yang, S., Chao, X., Liu, H., et al. (2023). Distribution patterns and community assembly processes of eukaryotic microorganisms along an altitudinal gradient in the middle reaches of the Yarlung Zangbo River. *Water Res.* 239, 120047. doi:10.1016/j.watres.2023.120047

Yi, Y., Zhao, F., Liu, Q., and Song, J. (2023). Runoff from upstream changes the structure and energy flow of food web in estuary. *Front. Mar. Sci.* 10, 1103502. doi:10.3389/fmars.2023.1103502

Yin, Q., Lin, F., Xu, B., Jiang, X., Li, H., Xian, H., et al. (2024). Unveiling the dominant influence of reservoir characteristics over water quality on algal concentrations revealed by qPCR detection. *ACS ES&T Water* 4, 4299–4311. doi:10.1021/acsestwater.3c00831

Zeng, H., Song, L., Yu, Z., and Chen, H. (2006). Distribution of phytoplankton in the Three-Gorge Reservoir during rainy and dry seasons. *Sci. Total Environ.* 367 (2-3), 999–1009. doi:10.1016/j.scitotenv.2006.03.001

Zhang, H., Xu, Y., Liu, X., Ma, B., Huang, T., Kosolapov, D. B., et al. (2024). Different seasonal dynamics, ecological drivers, and assembly mechanisms of algae in southern and northern drinking water reservoirs. *Sci. Total Environ.* 922, 171285. doi:10.1016/j.scitotenv.2024.171285

Zhang, H., Zong, R., He, H., Liu, K., Yan, M., Miao, Y., et al. (2021). Biogeographic distribution patterns of algal community in different urban lakes in China: insights into the dynamics and co-existence. *J. Environ. Sci.* 100, 216–227. doi:10.1016/j.jes.2020.07.024

Zhao, B., Zeng, Q., Wang, J., Jiang, Y., Liu, H., Yan, L., et al. (2024). Impact of cascade reservoirs on nutrients transported downstream and regulation method based on hydraulic retention time. *Water Res.* 252, 121187. doi:10.1016/j.watres.2024.121187

Znachor, P., Nedoma, J., Hejzlar, J., Seďa, J., Komárková, J., Kolář, V., et al. (2020). Changing environmental conditions underpin long-term patterns of phytoplankton in a freshwater reservoir. *Sci. Total Environ.* 710, 135626. doi:10.1016/j.scitotenv.2019.135626

Frontiers in Earth Science

Investigates the processes operating within the major spheres of our planet

Advances our understanding across the earth sciences, providing a theoretical background for better use of our planet's resources and equipping us to face major environmental challenges.

Discover the latest Research Topics

See more →

Frontiers

Avenue du Tribunal-Fédéral 34
1005 Lausanne, Switzerland
frontiersin.org

Contact us

+41 (0)21 510 17 00
frontiersin.org/about/contact